



**HAL**  
open science

# Calcium signature in the pancreatic cancer: role in the activation of the pancreatic stellate cells and in the progression of the pancreatic cancer

Silviya Radoslavova

## ► To cite this version:

Silviya Radoslavova. Calcium signature in the pancreatic cancer: role in the activation of the pancreatic stellate cells and in the progression of the pancreatic cancer. *Tissues and Organs [q-bio.TO]*. Université de Picardie Jules Verne, 2021. English. NNT : 2021AMIE0036 . tel-04051641

**HAL Id: tel-04051641**

**<https://theses.hal.science/tel-04051641>**

Submitted on 30 Mar 2023

**HAL** is a multi-disciplinary open access archive for the deposit and dissemination of scientific research documents, whether they are published or not. The documents may come from teaching and research institutions in France or abroad, or from public or private research centers.

L'archive ouverte pluridisciplinaire **HAL**, est destinée au dépôt et à la diffusion de documents scientifiques de niveau recherche, publiés ou non, émanant des établissements d'enseignement et de recherche français ou étrangers, des laboratoires publics ou privés.



# Thèse de Doctorat

*Mention Biologie-Santé  
Spécialité Physiopathologie Humaine*

présentée à l'Ecole Doctorale en Sciences Technologie et Santé (ED 585)

de l'Université de Picardie Jules Verne

par

**Silviya Radoslavova**

pour obtenir le grade de Docteur de l'Université de Picardie Jules Verne

***Signature calcique dans le cancer du pancréas : Rôle dans  
l'activation des cellules stellaires et dans la progression du  
cancer du pancréas***

Soutenue le 01 juillet 2021, après avis des rapporteurs, devant le jury d'examen :

**M. M. GAUTIER, Professeur des Universités,**  
Université de Picardie Jules Verne

**M<sup>me</sup> C. BOUSQUET, Directeur de Recherche (DR2),**  
Université de Toulouse III Paul Sabatier

**M. A. PENNA, Chargé de Recherche-HDR,**  
Université de Poitiers

**M. A. SCHWAB, Professeur des Universités,**  
Université de Münster

**M. L. LEMONNIER, Chargé de Recherche-HDR,**  
Université de Lille

**M<sup>me</sup> H. OUADID-AHIDOUCH, Professeur des Universités,**  
Université de Picardie Jules Verne

**M<sup>me</sup> N. PREVARSKAYA, Professeur des Universités,**  
Université de Lille

**Président du jury**

**Rapporteur**

**Rapporteur**

**Examineur**

**Examineur**

**Directeur de thèse**

**Co-directeur de thèse**



## ACKNOWLEDGMENTS

First of all, I would like to express my sincere gratitude to Dr Corinne Bousquet and Dr Aubin Penna for honoring me by accepting to be reporters of my thesis jury and, most importantly, for taking the time to evaluate this thesis work. Thank you very much for your attention and critical reading.

I would also like to thank Pr Albrecht Schwab very much for accepting to be a part of my thesis jury and mostly for having the opportunity to work with him, giving rise to a collaborative publication work valorizing these thesis data. I am also grateful to Pr Mathieu Gautier and Dr Loïc Lemmonier for accepting to be part of my thesis jury as well as for being part of my “Comité de suivi de thèse” following the advancing of this work and for their helpful advices.

My heartfelt thanks and gratitude are going to my two thesis directors Pr Halima Ouadid-Ahidouch and Pr Natalia Prevarskaya. Thank you very much for your continuous support, especially during the difficult moments, your guidance, believing in me, trusting, and always encouraging me. You always kept helping me to advance in my work during these three years and a half, and your invaluable supervision, knowledge, and scientific background helped me to progress scientifically and personally.

I would like to thank all the researchers at the LPCM, Pr Ahmed Ahidouch, Pr Mathieu Gautier, Dr Alban Girault, Dr Frédéric Hague, Dr Lise Rodat-Despoix, Dr Isabelle Dhennin, and Dr Philippe Kischel, for their help, advice and for sharing their knowledge each time I needed it.

I would also like to thank all the members of both laboratories, LPCM and PhyCell, especially Antoine, Katya, Mohamed, Julie S, Marie-Sophie, Lucille, Pauline, Hiba, Julie A, Riadh, Madelaine, Lina, Giorgia, Emilie, Valerio, Artem, Thibaut, Alison and Marta for their support, help, advice, for the nice ambiance and all the good moments passing together during this PhD period.

Many thanks go to Stéphanie Guenin, from the CRRBM platform, for her precious help in qPCR experiments and her warm welcoming and good mood.

I would like to express my thanks to Valando and Charalambos, even from far away, you kept supporting, advising, making me laugh, and motivating me during this period. Also,

many thanks to Imane, Aminata, Elodie, Barbara, Meriem and Meidiha for their kindness, patience, support, presence, and advices.

Finally, I would like to dedicate this thesis to my parents, which I will never thank enough for always being on my side, encouraging me in each step, and believing in me, teaching me to never give up, for their unconditional love and support. I also deeply thank my little brother (Martin) and aunty for always being there for me, for their support and advice. Last but not least, no words can express my gratitude and love for the other most important person in my life, Aimen. Thank you for your integral support and love, for keeping me motivated, for listening, understanding, believing, and for your patience, especially during these last months. Thank you for being part of this adventure and making it much easier.

## Table of Contents

<b>Abbreviations</b> .....	<b>8</b>
<b>Introduction</b> .....	<b>10</b>
<b>CHAPTER 1: Anatomy and Function of the pancreas</b> .....	<b>11</b>
<b>I. Anatomy of the pancreas</b> .....	<b>11</b>
<b>II. Functions of the pancreas</b> .....	<b>12</b>
II.1) The endocrine function of the pancreas .....	12
II.2) The exocrine function of the pancreas .....	13
<b>CHAPTER 2: Pancreatic Stellate Cells (PSCs)</b> .....	<b>15</b>
<b>I. Discovery, origin, and characterization of PSCs</b> .....	<b>15</b>
<b>II. Role of PSCs in the healthy pancreas</b> .....	<b>18</b>
<b>III. Role of PSCs in pancreatic fibrosis</b> .....	<b>19</b>
III.1) Phenotypical and functional activation features of PSCs .....	20
III.2) Paracrine and microenvironmental stimulation of PSCs .....	23
III.3) Autocrine stimulation of PSCs .....	27
III.4) Signalling pathways involved in PSC's activation .....	28
III.5) Heterogeneity of activated PSCs .....	33
<b>CHAPTER 3: Role of PSCs in pancreatic diseases</b> .....	<b>36</b>
<b>I. Pancreatitis</b> .....	<b>36</b>
I.1) Chronic pancreatitis (CP) .....	36
I.2) Role of activated PSCs in pancreatitis .....	38
<b>II. Pancreatic ductal adenocarcinoma (PDAC)</b> .....	<b>39</b>
II.1) Development and progression of PDAC .....	39
II.2) Role of activated PSCs in PDAC .....	43
<b>CHAPTER 4: Functional features of activated PSCs: focus on cell proliferation and cytokine secretion</b> .....	<b>48</b>
<b>I. Cell proliferation</b> .....	<b>48</b>
I.1) Cyclin and Cyclin-Dependent Kinases (CDKs) .....	49
I.2) Cyclin-Dependent Kinase Inhibitors (CKIs) .....	50
<b>II. Cell survival</b> .....	<b>51</b>
II.1) Apoptosis .....	52
II.2) Intrinsic apoptosis pathway .....	52
II.3) Extrinsic apoptosis pathway .....	54

<b>III. TGF-<math>\beta</math>1 secretion .....</b>	<b>55</b>
III.1) TGF- $\beta$ 1 signalling in CP and PDAC .....	55
III.1.1) Importance of TGF $\beta$ 1 in pancreatic desmoplasia and cancer .....	55
III.1.2) TGF- $\beta$ 1-induced pancreatic desmoplasia .....	55
III.1.3) TGF- $\beta$ 1-mediated PDAC progression .....	56
III.2) TGF- $\beta$ 1 mechanism in the control of cell proliferation .....	57
III.3) TGF- $\beta$ 1 canonical signalling pathway .....	58
III.4) TGF- $\beta$ 1 non-canonical signalling pathways .....	60
III.4.1) ERK1/2 pathway .....	60
III.4.2) PI3K/AKT pathway .....	62
<b>CHAPTER 5: Ca<sup>2+</sup> signalling in PSC's pathophysiology .....</b>	<b>65</b>
<b>I. Ca<sup>2+</sup> signalling and Ca<sup>2+</sup> ion channels .....</b>	<b>65</b>
I.1) Principal membrane proteins regulating Ca <sup>2+</sup> homeostasis .....	66
I.1.1) Plasma membrane Ca <sup>2+</sup> regulators .....	66
I.1.2) ER membrane Ca <sup>2+</sup> regulators .....	68
I.1.3) Mitochondrial membrane Ca <sup>2+</sup> regulators .....	69
<b>II. Store-Operated Ca<sup>2+</sup> channels (SOCs) .....</b>	<b>70</b>
II.1) Orai channels .....	70
<b>III. TRPC1 channels .....</b>	<b>76</b>
<b>IV. Ca<sup>2+</sup> signalling in PSC's pathophysiology .....</b>	<b>78</b>
<b>Purpose of the thesis .....</b>	<b>84</b>
<b>Material and Methods .....</b>	<b>87</b>
<b>I. Cell culture .....</b>	<b>88</b>
I.1) Cellular models .....	88
I.2) Cell culture conditions .....	88
I.3) Freezing and Thawing procedures .....	89
I.4) Conditioned medium .....	90
I.5) Cell Transfection .....	91
I.6) Cell treatments and stimulations .....	92
<b>II. Cell viability, proliferation, and mortality .....</b>	<b>94</b>
II.1) MTT colorimetric assay .....	94
II.2) Trypan Blue dye exclusion assay .....	94
II.3) Flow cytometry .....	95
II.3.1) Cell cycle analysis .....	95

II.3.2) Apoptosis analysis .....	96
<b>III. Molecular Biology Techniques .....</b>	<b>98</b>
III.1) RNA extraction .....	98
III.2) Reverse transcription-polymerase chain reaction (RT-PCR) .....	99
III.3) Quantitative polymerase chain reaction (qPCR) .....	99
<b>IV. Cell Biology Techniques .....</b>	<b>101</b>
IV.1) Western Blotting .....	101
IV.1.1) Protein extraction .....	101
IV.1.2) Gel electrophoresis .....	102
IV.2) Co-Immunoprecipitation .....	104
IV.3) Immunofluorescence .....	106
IV.4) Enzyme-Linked Immunosorbent Assay (ELISA) .....	107
<b>V. Calcium imaging .....</b>	<b>109</b>
<b>VI. Statistical analysis .....</b>	<b>110</b>
<b>Results and Discussion .....</b>	<b>111</b>
<b>Part N°1: Orai1 channel regulates human activated pancreatic stellate cell's proliferation and TGF<math>\beta</math><sub>1</sub> secretion through the AKT signalling pathway .....</b>	<b>112</b>
Summary .....	112
Article .....	116
Complementary Results .....	145
<b>Part N°2: TRPC1 channels regulate the activation of pancreatic stellate cells through ERK1/2 and SMAD2 pathways and perpetuate their pressure-mediated activation ...</b>	<b>167</b>
Summary .....	167
Article .....	171
Complementary Results .....	192
<b>Conclusion .....</b>	<b>212</b>
<b>Résumé de thèse .....</b>	<b>223</b>
<b>Valorization .....</b>	<b>235</b>
<b>References .....</b>	<b>238</b>
<b>Annexes .....</b>	<b>274</b>
Review: Ion Channels: New Actors Playing in Chemotherapeutic Resistance .....	275
Review-Article: Mammary SLAMF3 Regulates Store-Operated Ca <sup>2+</sup> Entry and Migration Through STIM1 in Breast Cancer Cells and Cell Lines .....	303

Article: Internal structure and remodeling in dystrophin-deficient cardiomyocytes using second harmonic generation ..... 321



## Abbreviations

AKT: protein-kinase B/Akt

AP: acute pancreatitis

Apaf-1: apoptotic protease activating factor-1

ATP: adenosine triphosphate

CAF: cancer-associated fibroblast

CaM: calmodulin

CCK: cholecystokinin

CCL2: chemokine (C-C motif) ligand 2

CDK: cyclin-dependent kinase

CDK: cyclin-dependent kinase

CICD: caspase-independent cell death

CIP/KIP: CDK-interacting protein/kinase inhibitory proteins

CKI: cyclin-dependent kinase inhibitors

CM: conditioned medium

CM: conditioned medium

COX-2: cyclooxygenase-2

CP: chronic pancreatitis

CRAC: Ca<sup>2+</sup> release-activated channels

CTGF: connective tissue growth factor

DAG: diacylglycerol

DMSO: dimethyl sulfoxide

ECM: extracellular matrix

EDTA: ethylenediamine tetraacetic acid

EGF: epidermal growth factor

EGTA: ethylene glycol-bis ( $\beta$ -aminoethyl ether)-*N, N, N', N'*-tetraacetic acid

EMT: epithelial-mesenchymal transition

ER: endoplasmic reticulum

ERK1/2: extracellular signal-regulated kinases 1/2

ET-1: endothelin-1

FBS: fetal bovine serum

FGF: fibroblast-growth factor

GAPDH: glyceraldehyde 3-phosphate dehydrogenase

GTPase: guanosine triphosphate hydrolase enzyme

HGF: hepatocyte growth factor

HPRT1: hypoxanthine phosphoribosyltransferase 1

HSCs: hepatic stellate cells

ICAM-1: intercellular adhesion molecule-1

IL: interleukin

INK4: CDK4/6 inhibitor proteins  
 IP3: inositol 1,4,5-trisphosphate  
 ISCs: islet stellate cells  
 JNK: c-jun N-terminal kinase  
 LPS: lipopolysaccharide  
 MAPK: mitogen activated protein kinases  
 MCP-1: monocyte chemoattractant protein-1  
 MEK: mitogen-activated protein kinase kinase  
 MMP: matrix metalloproteinase  
 MPTP: mitochondrial permeability transition pore  
 MTT: 3-(4,5-Dimethylthiazol-2-yl)-2,5-diphenyltetrazolium bromide  
 M $\beta$ CD: methyl beta cyclodextrin  
 NF- $\kappa$ B: nuclear factor kappa-light-chain-enhancer of activated B cells  
 NO: nitric oxide  
 PACs: pancreatic acinar cells  
 PAMPs: pathogen-associated molecular patterns  
 PanINs: pancreatic intraepithelial neoplasms  
 PBS: phosphate-buffered saline  
 PCC: pancreatic cancer cells  
 PDAC: pancreatic ductal adenocarcinoma  
 PDGF: platelet-derived growth factor  
 PI: Propidium Iodide  
 PI3K: phosphatidylinositol-3-kinase  
 PPAR- $\gamma$ : peroxisome proliferator activated receptor- $\gamma$   
 pRb: protein retinoblastoma  
 PSCs: pancreatic stellate cells  
 RAF: rapidly accelerated fibrosarcoma  
 RAS: rat sarcoma  
 ROS: reactive oxygen species  
 SDF-1: stroma derived factor-1  
 SDS: sodium dodecyl sulphate  
 SOC: store-operated calcium channels  
 SOCE: store-operated calcium entry  
 Stim: stromal interaction molecule  
 Tg: thapsigargin  
 TGF- $\beta$ 1: transform growth factor- $\beta$ 1  
 TIMP: tissue inhibitors of metalloproteinases  
 TNF- $\alpha$ : tumor necrosis factor- $\alpha$   
 TRP: Transient Receptor Potential  
 VASCs: vitamin-A storing cells  
 VEGF: vascular endothelial growth factor  
 $\alpha$ SMA: alpha-smooth muscle actin



---

# INTRODUCTION

---



## **CHAPTER 1: Anatomy and Function of the pancreas**

### **I. Anatomy of the pancreas**

The pancreas is an essential extended digestive gland, considered the second-largest glandular organ in the body (weighing 75-100 g), driving the blood glucose homeostasis and the secretion of enzyme-rich pancreatic juice required for food digestion. It is located retroperitoneally, in the upper left abdomen, posterior to the stomach, surrounded on the right by the duodenum, and on the left by the spleen. The pancreas is divided into four parts connected to several large blood vessels: head, neck, body, and tail. The head is situated at the junction where the stomach communicates with the first part of the small intestine, surrounded by the concave part of the duodenum, lying on the inferior vena cava and renal vein. The neck of the pancreas is situated anterior to the portal vein, containing the superior mesenteric and splenic veins. The body is found anterior to the aorta, the superior mesenteric artery, the left suprarenal gland, the left kidney, and the splenic vein. At last, the tail of the pancreas is extended to the left, close to the spleen, related to the splenic hilum and the left colic flexure (“Anatomy and Functions of the Pancreas,” n.d.; “Anatomy and Histology of the Pancreas,” n.d.; Talathi et al., 2021). Near to the tail, debuts the main pancreatic duct carrying the pancreatic secretions, also called duct of Wirsung, draining the lobules of the gland, continuing until the head of the pancreas, where it joins the common bile duct and releases the pancreatic juice into the descending part of the duodenum. Additionally, in some cases, an accessory pancreatic duct is presented to the main duct called the duct of Santorini, which communicates with the main duct, aiding to release the pancreatic enzymes (Bockman, 1992) (**Figure 1**).

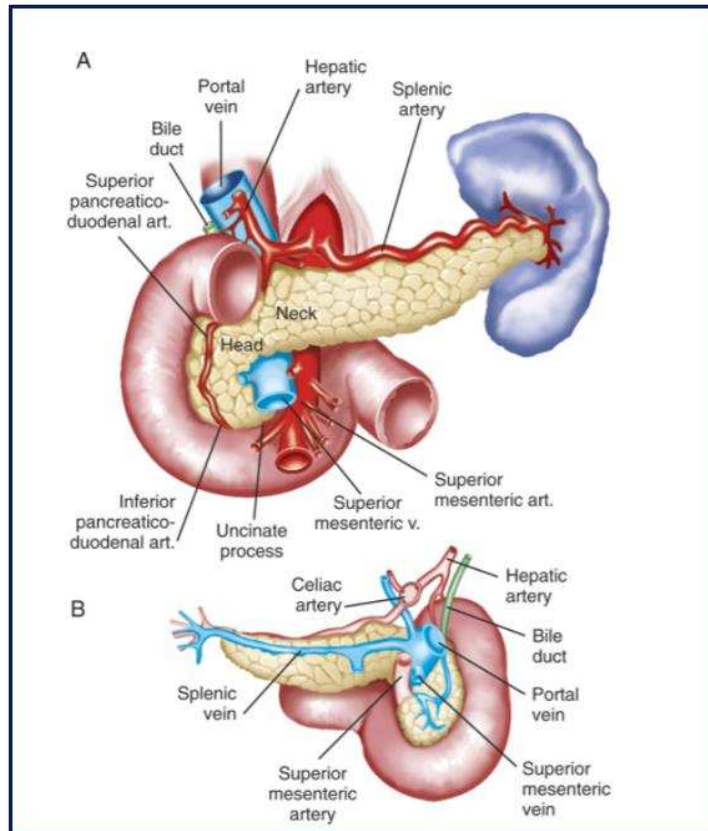


**Figure 1:** The anatomy of the pancreas. **A)** Anterior view, **B)** Posterior view (Longnecker, 2014).

Acting as a mixed gland, the pancreas is functionally divided into two components: the exocrine and endocrine glands.

## **II. Functions of the pancreas**

### **II.1) The endocrine function of the pancreas**

The endocrine compartment of the pancreas represents only 1-2% of the total pancreatic mass. Although its minor repartition compared to the rest of the pancreas, the endocrine pancreas plays a vital role in maintaining the normal blood glucose levels by the secretion of an antagonistic pancreatic hormone pair, including insulin and glucagon. The endocrine part is constituted by the islets of Langerhans, which are highly vascularized to ensure a direct release of the pancreatic hormones into the bloodstream. A healthy pancreas contains between 500 000 to several million islets, each composed of a small cluster of endocrine cells, and each cell type

is responsible for the secretion of a single hormone type. The endocrine cells defining the islet are divided into four categories:  $\alpha$ -cells,  $\beta$ -cells,  $\delta$ -cells, and PP-cells. The  $\beta$ -cells are the major cell type constituting the islet, corresponding to approximately 75% of total cellular islet content, producing and secreting the hypoglycaemic hormone insulin after stimulation by elevated blood glucose levels. Insulin is an anabolic hormone that facilitates glucose uptake converting it into either glycogen through glycogenesis either lipids through lipogenesis. The second most abundant cell type in the islet is the  $\alpha$ -cells, representing 20% of the islet, having as a role to produce and secrete the hyperglycaemic hormone glucagon, after stimulation by low blood glucose levels. Glucagon, contrary to insulin, is a catabolic hormone, stimulating the conversion of glycogen to glucose *via* glycogenolysis to be released in the bloodstream. The other 4% of the islet comprises the  $\delta$ -cells, secreting the pancreatic somatostatin hormone, inhibiting the other two hormones, insulin and glucagon. The resting 1% is composed of the PP-cells, also known as F cells, driving the secretion of pancreatic polypeptide hormone, known to play a role in the appetite by the regulation of the gastric emptying, intestinal motor activity, and glucagon secretion (Da Silva Xavier, 2018; Piro et al., 2018) (**Figure 2**).

## **II.2) The exocrine function of the pancreas**

The major part of the pancreas is comprised of the exocrine gland involved in the secretion of the pancreatic digestive enzymes, ions, and water into the duodenum of the gastrointestinal tract, representing approximately 95% of the total pancreatic mass. The two main components of the exocrine pancreas are the acinar and ductal cells. The acinar cells are organized into clusters named the acini forming pancreatic lobules. The lumen of the acini is linked to the ductal system by small ducts, inter-connecting the lobules by larger intercalated ducts draining into the main pancreatic duct. The acinar cells are synthesizing, storing, and secreting the digestive enzymes that constitute the pancreatic juice into the lumen space. On the apical region of these cells are found the zymogen granules storing the digestive enzymes. In contrast, the basolateral membrane contains the hormonal (e.g., secretin, cholecystokinin) and neurotransmitter (e.g., acetylcholine) receptors involved in the exocytosis of the digestive enzymes into the lumen space. These enzymes fall into four categories: proteases, amylases, lipases, and nucleases, many of them are stored and secreted in their inactive form to avoid acinar cell digestion and cause injuries leading to pancreatitis (Pandolfi, 2015, 2010). Once secreted, the digestive enzymes are carried by the pancreatic main and accessory ducts into the

duodenum of the gastrointestinal tract. To assure the enzymes' transport, the pancreatic duct cells from the ductal system contain carbonic anhydrase, permitting the secretion of bicarbonate ions ( $\text{HCO}_3^-$ ), which create a flux necessary for the transport into the intestine. The high concentration of the secreted bicarbonate ions (up to 140 mM) is important for the neutralization of the acidic gastric chyme delivered to the duodenum from the stomach, providing the optimal pH environment for the digestive enzymes' activity. The secretion of this large  $\text{HCO}_3^-$  amount is initiated by the hormone secretin released in response to the acidic chyme present in the duodenum (Lee et al., 2012; Ogami and Otsuki, 1998). Another cell type of the exocrine pancreas is the centroacinar cells, located at the junction of the acini and the small pancreatic ducts. These cells have ductal and stem cell characteristics, likely implicated in the generation of the different pancreatic cell types (**Figure 2**).

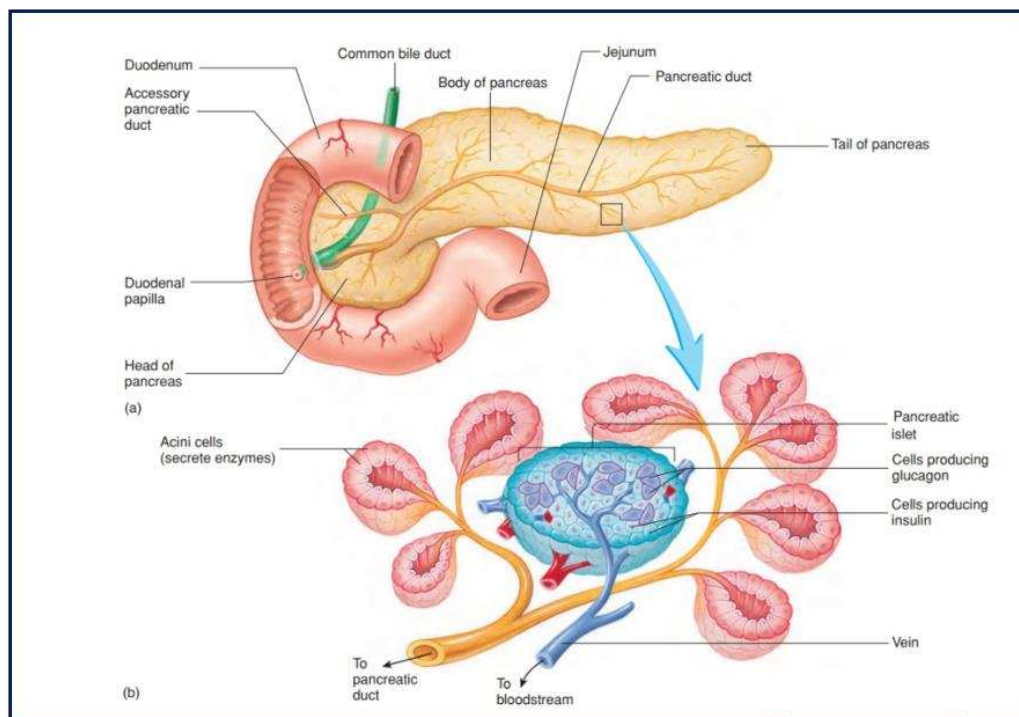


**Figure 2:** Pancreas structure: **a)** Anatomical compartments of the pancreas, **b)** Cellular components of the endocrine and exocrine pancreas (“Anatomy and Functions of the Pancreas,” n.d.).

A minor cell type of the normal pancreas that has received increased interest from the pancreatic research field during the last decades is the pancreatic stellate cells (PSCs). These cells have a star-shaped morphology, located in the periacinar space, encircling the base of the acini with their long cytoplasmic extensions, but they can also be founded in the periductal and

perivascular space (Apte et al., 1998; Bachem et al., 1998; Omary et al., 2007). Moreover, they can be presented in the endocrine pancreas, surrounding the islets of Langerhans (Zha et al., 2014a; Zhou et al., 2019). PSCs participate mainly in maintaining the normal pancreatic tissue architecture (Apte et al., 2012). However, reports from the last several years have shown that their role is much more crucial than that, especially in pancreatic diseases (**Figure 3**).

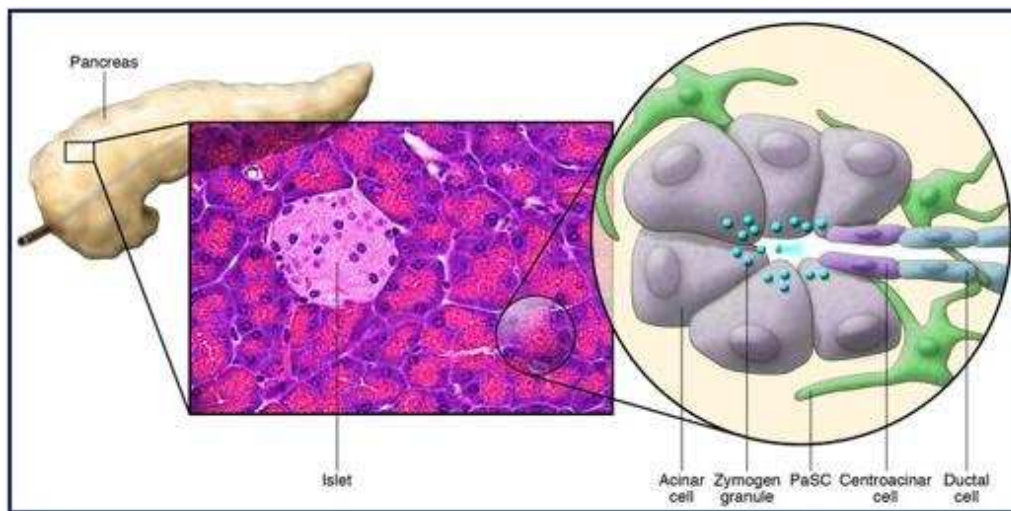


**Figure 3:** Principal localisation of the pancreatic stellate cells in the exocrine pancreas (Omary et al., 2007).

## CHAPTER 2: Pancreatic Stellate Cells (PSCs)

### I. Discovery, origin, and characterization of PSCs

The term “stellate cells” was described for the first time by Karl Wilhelm Von Kupffer in 1876, who observed star-shaped cells in the perisinusoidal spaces of the liver, calling them “Sternzellen” (Wake, 1971). Almost a century later, in 1951, Ito observed that the hepatic stellate cells (HSCs) store lipid droplets in their cytoplasm. A few years after, in 1982, Watari et al. identified a similar cell type in the pancreas of two weeks-vitamin A loaded mice by a blue-green vitamin A emitted autofluorescence followed ultraviolet light excitation at 328nm, naming them vitamin-A storing cells (VASCs) (Watari et al., 1982). Subsequently, Ikejiri found that these cells are present in human and rat pancreatic sections of healthy pancreata, observing a positive but sparse vitamin A autofluorescence. The same author observed that VASCs were also located in fibrotic areas, surrounded by collagen fibers, in human pancreatic specimens of chronic pancreatitis (Ikejiri, 1990). It is only in 1998 that the term of pancreatic stellate cells



was given to these VASCs by Bachem *et al.* This scientific group, together with the Apte-Wilson group, reported a ground-breaking work in the advancement of the pancreatic field, developing a method of PSC's isolation using density gradient centrifugation, culture, and characterization, from human and rat pancreas (Apte et al., 1998; Bachem et al., 1998). Five years later, immortalized rat and human PSC cell lines started to be generated using SV (simian vacuolating virus) 40 large T antigen-induced transformation, followed by the expression of human telomerase for the human PSCs (Jesnowski et al., 2005; Masamune et al., 2003). These cell lines have a phenotype of activated PSCs, providing a tool for better understanding PSC's pathophysiology. The first human immortalized PSC cell line was provided by Jesnowski *et al.* in 2005, almost 20 years after their discovery, originated from patient with chronic pancreatitis, called RLT-PSCs (Jesnowski et al., 2005).

All these reports and tools permitted at a first place to better localized and characterized the PSCs in the healthy pancreas. Under physiological conditions, PSCs exist in an inactive quiescent state, representing only 4-7% of the pancreatic resident cells, and they are found within the periacinar intra- et inter-lobular regions, surrounding the basolateral membrane of the acinar cells (Apte et al., 2012). They can also be situated at the periphery of the blood capillaries, in the perivascular regions surrounding the basal lamina of the endothelial cells, and in periductal regions surrounding the ductal cells. Morphologically, except the perinuclear vitamin A-storing lipid droplets in their cytoplasm, they contain a large nucleus, few mitochondria, a well-developed rough endoplasmic reticulum, and abundant free ribosomes. They have star-shaped bodies, long extending cytoplasmic projections, and show no-detectable expression of alpha-smooth muscle actin ( $\alpha$ SMA). Functionally, they are characterized by a limited proliferation, migration, and extracellular matrix (ECM) and growth factors' synthesis potentials (Apte et al., 1998; Bachem et al., 1998; Ikejiri, 1990; Watari et al., 1982).

Quiescent PSCs can be identified by the expression of the intermediate filament proteins desmin and glial fibrillary acidic protein (GFAP), which along with the lipid droplets, permit to distinguish the quiescent PSCs from the normal pancreatic fibroblasts. Although GFAP is a characteristic protein of astrocytes, its expression has been shown to be specific to quiescent PSCs, using GFAP-*LacZ* transgenic mice model, where GFAP promoter activity was exclusively detected in PSCs within the normal pancreas (Ding et al., 2009). Furthermore, quiescent PSCs can also be defined by the expression of vimentin, nestin, nerve growth factor (NGF) and neural cell adhesion molecule (NCAM) (Apte et al., 2013; Haas et al., 2009; Habisch et al., 2010; Lardon et al., 2002). However, these proteins are expressed by many other cell

types in the organism, including myocytes, neural cells, fibroblasts, and endothelial cells, limiting their use as specific quiescent markers of PSCs. Recently, Nielsen *et al.* have established two others more specific to PSCs quiescent markers, including adipophilin which is located to the vacuole-like structure of quiescent PSC's cytoplasm, and cytoglobin (Nielsen *et al.*, 2017). Despite all the identified markers, the most consistent marker for PSC's quiescence remains their cytoplasmic storage of vitamin A lipid droplets, which participate in maintaining the inactive quiescent phenotype. Vitamin A and all-trans retinoic acid have been demonstrated to inhibit the expression of the principal PSC activation marker, the  $\alpha$ SMA, and diminish the type I collagen synthesis (McCarroll *et al.*, 2006). Nevertheless, the mechanisms implicated in the regulation and accumulation of the lipid droplets remain to be elucidated, even though the study of Kim *et al.* reported a role of albumin in the formation of lipid droplets in the quiescent PSCs. The authors showed that transfection of activated PSCs, which have lost their vitamin A lipid droplets with albumin-expressing plasmids, restored the quiescent PSC phenotype inducing vitamin A lipid droplets formation (Kim *et al.*, 2010, 2009).

Moreover, given the 99.9% gene expression profile shared between PSCs and HSCs, and the fact that PSCs can express both mesenchymal and ectodermal markers as described above, their embryologic origin has been the subject of debate (Buchholz *et al.*, 2005; Paulo *et al.*, 2013). Initially, it was discussed that PSCs might originate from two cell lineages according to their localization, the one being the fibroblast and the other one the pericyte of the blood capillaries. PSCs found in the intra- and inter-lobular spaces were thought to originate from fibroblasts, whereas the ones situated in the perivascular space were originated from pericytes adhered to the endothelial cells (Watari *et al.*, 1982). Other studies have been based on the elevated homology between PSCs and HSCs, suggesting that since HSCs are known to have a mesodermal origin, then PSCs also evolved from the same origin. In addition, in the healthy pancreas but as well as during sustained pancreatic fibrosis, which results in chronic pancreatitis (CP) and pancreatic cancer (PC), PSCs have been demonstrated to derive from the bone marrow (Scarlett *et al.*, 2011). Reports using sex-mismatched bone marrow transplantation from transgenic male mice expressing green fluorescent protein to female wild-type mice revealed the presence of desmin- and lipid droplet-positive bone marrow-derived cells in the pancreas, suggesting that these cells contribute to PSC's quiescent population. The rate of bone marrow-derived PSC cells increased, reaching approximately 20% of the total PSC population, after induction of CP by repeated injections of the cholecystinin analogue, caerulein (Sparmann *et al.*, 2010; Watanabe *et al.*, 2009). The bone marrow-derived PSC population in the CP model

was detected by the presence of the main activator marker of PSC, the  $\alpha$ SMA, and the presence of Y chromosome in their nucleus, indicating that bone marrow is also a source of activated PSCs (Sparmann et al., 2010). However, so far, no direct evidence has been provided identifying the exact origin of PSCs.

Primarily detected within the exocrine pancreas, PSCs were recently identified in the rodent and human pancreatic islets of Langerhans as well and were called islet stellate cells (ISCs) (Zha et al., 2014). Interestingly, ISCs present some morphological and functional differences compared to the typical PSCs. They have less lipid droplets in their cytoplasm, and consequently, they appear to be more easily activated by different stimulators. Nevertheless, once activated, they have lower proliferative and migratory abilities than the activated PSCs (Zha et al., 2014, 2016). Furthermore, single-cell transcriptomics suggested that ISCs could likely be a subtype of PSCs, influencing islet functionality (Zha et al., 2016). Regarding to these recent findings, the characterization and function of ISCs in the healthy and diseased pancreas need to be further elucidated.

## **II. Role of PSCs in the healthy pancreas**

Although most of the research reports have been focusing on the investigation of PSCs' role during pathophysiological conditions, their role in the healthy pancreas should not be overlooked. Under physiological conditions, quiescent PSCs have a moderate capacity of synthesising and secreting matrix metalloproteinases (MMPs) and tissue inhibitors of matrix metalloproteinases (TIMPs), establishing a balance between ECM production and degradation. Through the regulation of this ECM turnover, PSCs maintain the normal architecture of the pancreas (Phillips et al., 2003).

Several studies have revealed a role of quiescent PSCs in innate immunity, demonstrating the expression of Toll-like receptors (TLR) on their surface, known to be involved in the recognition of pathogen-associated molecular patterns (PAMPs). PSCs have been shown to express TLR2, which is implicated in the recognition of PAMPs of gram-positive bacteria, and TLR4 recognising lipopolysaccharides of gram-negative bacteria (Vonlaufen et al., 2007). They also have TLR3 on their surface, responsible for the detection of produced double-stranded RNA during viral replication, and TLR5, involved in the identification of bacterial flagella. These findings indicated that quiescent PSCs might participate in innate immunity by the phagocytosis of exo- and endogenous antigens (Masamune et al., 2008; Nakamura et al., 2011).

However, contrary to their HSCs counterparts, quiescent PSCs have not been demonstrated to express antigen-presenting cell marks, like major histocompatibility complex class II molecules, suggesting that they might not be implicated in the acquired immunity (Shimizu et al., 2012) (**Figure 4**).

Besides their role in ECM turnover and innate immunity, some studies have evoked a role of quiescent PSCs as stem/progenitor cells. Mato *et al.* reported that mitoxantrone-resistant cells isolated and selected from pancreata of lactating rats possessing the ATP binding cassette G2 transporter (ABCG2 transporter), exhibited PSC phenotype (Mato et al., 2009). Indeed, ABCG2 transporter is known now to be one of the stem/progenitor cell markers, playing an important role in innate and acquired multidrug resistance. In this study, ABCG2 transporter was found to be expressed in vitamin A-storing positive and GFAP positive cells, which were able to differentiate into insulin and c-peptide producing cells, conferring to quiescent PSCs a role as stem/progenitor cells (Mato et al., 2009). Moreover, quiescent PSCs are expressing the stem/progenitor marker nestin, which is a type VI intermediate filament protein, acting as essential transcriptional factor for the generation of endocrine cells, initially detected in neural stem cells. Additionally, Zha *et al.* established that activated PSCs and ISCs were able to differentiate into adipocyte-like cells detected by Oil-Red O staining and into osteoblast-like cells identified with Alizarin Red S staining (Zha et al., 2016). Interestingly, Kordes *et al.* supported these findings demonstrating that activated PSCs possess a regenerative potential. The authors transplanted culture-activated PSCs isolated from enhanced green fluorescent protein-expressing rats into wild type rats that have undergone partial liver depletion, and they noted that these PSCs differentiated into functional hepatocytes and cholangiocytes leading to the reconstitution of large host liver areas (Kordes et al., 2012).

### **III. Role of PSCs in pancreatic fibrosis**

Fibrosis is defined as a pathological wound-healing process due to an excessive accumulation of ECM proteins resulted from the interruption of ECM synthesis and degradation balance, leading to the formation of a fibrous connective tissue replacing the normal parenchymal tissue. Hence, progressive pancreatic fibrosis is a main pathological feature of two major pancreatic diseases, including chronic pancreatitis and pancreatic ductal adenocarcinoma (PDAC). One of the key effectors playing a central role in pancreatic fibrogenesis are the activated PSCs (Apte et al., 2011, 2004; Habisch et al., 2010).

### III.1) Phenotypical and functional activation features of PSCs

During pancreatic injury or inflammation, quiescent PSCs undergo morphological and functional transformations acquiring a myofibroblast-like phenotype and become activated. The transition of PSCs from the quiescent to the activated state is morphologically accompanied by the acquisition of a spindle-like shape, nuclear enlargement, enhanced prominence of ER network, loss of vitamin A lipid droplets from the cytosol and an increased  $\alpha$ SMA expression. These changes were first well studied by the culture of primary isolated PSCs. Bachem *et al.*, as many other scientific groups, showed that at the beginning early primary cultured PSCs contained numerous vitamin A lipid droplets, which decreased in size and number within 4-8 days of culture until they completely disappear (Bachem *et al.*, 1998; Omary *et al.*, 2007). Simultaneously PSCs started to express  $\alpha$ SMA, whose expression progressively increased within few days of culture, and they produced large amounts of type I and type III collagen and also of fibronectin and laminin, defining their trans-differentiation to activated PSC. This important ECM protein deposition by activated PSCs contribute to the increase of ECM stiffness (Apte *et al.*, 2013; Bachem *et al.*, 1998).

Functionally, upon activation, PSCs acquire high proliferative and migratory potentials. Additionally, besides the elevated ECM component synthesis, activated PSC excessively secrete MMPs, especially MMP-2, -9 and -13, as well as TIMPs, in particular TIMP-1 and -2, to disrupt the ECM turnover leading to ECM remodelling and promoting pancreatic cancer cell invasiveness *via* the basement membrane degradation (Phillips *et al.*, 2003). Furthermore, activated PSCs synthesise and secrete diverse growth factors, such as PDGF, FGF, TGF- $\beta$ 1, CTGF, activin-A, shown to be involved among others in the ECM remodelling (Shek *et al.*, 2002). In addition, they produce and release various proinflammatory cytokines, including IL-1 $\beta$ , IL-6, IL-15, IL-32, TNF- $\alpha$ , and chemokines, involving the monocyte chemoattractant protein-1 (MCP-1, also called CCL2), neutrophil chemotactic factor IL-8 and RANTES (regulated on activation, normal T cell expressed and secreted) (Andoh *et al.*, 2000; Bynigeri *et al.*, 2017; Erkan *et al.*, 2012; Habisch *et al.*, 2010; Omary *et al.*, 2007). Through the secretion of all these cytokines and chemokines, activated PSCs participate among others to the recruitment of inflammatory cells exacerbating the existent pancreatic inflammation. They are also able to express cell adhesion molecules, such as intercellular adhesion molecule-1 (ICAM-1), promoting the adhesion of the inflammatory recruited cells by the PSCs, or even they can

mediate pancreatic inflammation by the synthesis of cyclooxygenase 2 (COX-2) enzyme (Masamune et al., 2002c). Moreover, along with the augmented  $\alpha$ SMA expression, they produce the vasoconstrictor peptide Endothelin-1 (ET-1) conferring to activated PSCs elasticity and increased contractile potential, contributing to the modulation of the vascular and ductal tones (Masamune et al., 2005b). Activated PSCs could participate in the epithelial-mesenchymal transition (EMT) too during PDAC through the production and secretion of the ECM protein periostin (Fukushima et al., 2008).

A novel function of activated PSCs as proangiogenic factors was reported by the elevated PSC-induced vascular endothelial growth factor (VEGF) expression, as well as some angiogenesis-related molecules' expression. These later included Flt-1 (fms-related tyrosine kinase 1) and Flk-1 (fetal liver kinase 1) VEGF receptors, angiopoietin-1 and its receptor Tie-2 (tyrosine kinase with immunoglobulin and EGF homology domains), as well as vasohibin-1 (Masamune et al., 2008a). Furthermore, PSC-induced VEGF generation has been found to be increased under hypoxia conditions, while conditioned media from hypoxia-treated activated PSCs induced angiogenesis in vitro and in vivo, reflecting the synergistic relationship between activated PSCs and its surrounding microenvironment (Erkan et al., 2009). Indeed, during CP and PDAC, pancreatic tissue is characterized by a chronic hypoxia and increased pancreatic ductal hypertension, suggesting a role of activated PSCs in the maintenance of this pathological microenvironment and thus the exacerbation of pancreatic fibrosis. Beyond this function, very recently Shao *et al.* reported a role of activated PSC in the metabolism of glucose, and particularly in glycolysis, mediated by the caveolin-1-reactive oxygen species (ROS) signalling. The authors demonstrated an up-regulated expression of the glucose transporter Glut1, and the glycolytic enzymes hexokinase-2, 6-phosphofructokinase, and pyruvate kinase isozyme type M2 leading to lactate increased production, which in turn is up taken by the PCCs (Shao et al., 2020).

Another proposed function of activated PSCs is their capacity to internalize by phagocytosis necrotic and apoptotic acinar cells, as well as apoptotic neutrophils, using a WBN/Kob model of spontaneous CP and a bile-duct ligation model of acute pancreatitis. Shimizu et al. demonstrated that additionally to this mechanism, necrotic acinar cells' engulfment promotes in turn PSCs necrotic death themselves, suggesting that activated PSCs might play a protective role in early stages of pancreatic injury inhibiting disease progression (Shimizu et al., 2005).

Following these findings, it is believed that activated PSCs might have two fates during pancreatic injury and inflammation. When the inflammation and injury are limited or single, activated PSCs aid to the restoration of pancreas integrity through ECM protein synthesis, and then they might undergo apoptosis or revert to their quiescent state. However, the extended or repeated inflammation and injury perpetuates PSCs activation resulting to an excessive ECM protein deposition accompanied by loss of cellular components, including acinar cells, and thus to pancreatic fibrosis development (Masamune and Shimosegawa, 2009).

Besides the above-mentioned functions of activated PSCs, these multifunctional cells seem to also affect the endocrine part of the pancreas, during CP and type 2 diabetes, since their number was found to be increased within the islets of Langerhans, contributing to islets fibrosis. Zang *et al.* characterized these activated PSCs within the Langerhans islets, as ISCs, highly expressing  $\alpha$ SMA and producing type I and III collagen as well as fibronectin. Furthermore, the same authors established that activated PSCs cause  $\beta$ -cells dysfunction, decreasing insulin mRNA expression and secretion, and inducing  $\beta$ -cells apoptosis (Zang et al., 2015). In addition, it has been demonstrated that hyperglycaemia, a central feature of diabetes, resulted usually by decreased insulin production from  $\beta$ -cells, aggravates the noxious effects of activated PSCs on  $\beta$ -cells, revealing a positive feedback loop between activated PSCs and dysfunctional  $\beta$ -cells (Lee et al., 2017; Zha et al., 2014). In contrast, another study presented that activated PSCs increase insulin secretion from mice  $\beta$ -cells, and that culture supernatants from INS-1 (rat insulinoma cell line used for  $\beta$ -cell dysfunction studies) cells reduced PSC-induced proinflammatory cytokines and ECM proteins. However, more studies are required to determine the exact role of activated PSCs within the Langerhans islets, and thus in pancreas' endocrine function under fibrosis-induced conditions (Li et al., 2014) (**Figure 4**).

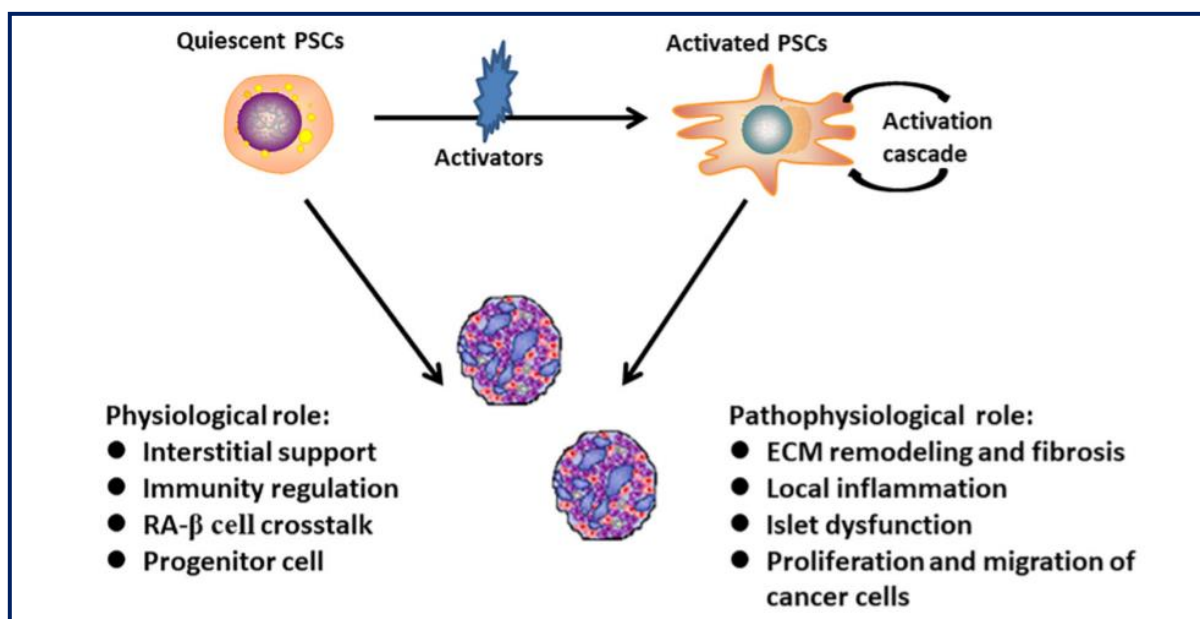


**Figure 4:** Illustrative summary of quiescent and activated PSC's functions (Zhou et al., 2019).

### III.2) Paracrine and microenvironmental stimulation of PSCs

Activation of PSCs is triggered among others by various cytokines and growth factors produced during pancreatic injury and inflammation by the neighbour cells, including acinar, inflammatory, platelets, endothelial, ductal and cancer cells, exacerbating pancreatic fibrosis development (Apte et al., 2011, 2004). The most common identified growth factors and cytokines showed to be involved in PSC's activation through the modulation of at least one of PSC's activation features are presented below (**Figure 5**).

#### ➤ Transforming growth factor- $\beta$ 1 (TGF- $\beta$ 1):

TGF- $\beta$ 1 is defined as the most important factor involved in PSC's activation and thereby in pancreatic fibrosis, known to induce PSC's profibrogenic phenotype, stimulating PSC-induced ECM proteins, including type I and III collagen, fibronectin, and laminin, promoting PSC-induced ECM synthesis (Apte et al., 1999; E. Schneider et al., 2001; Shek et al., 2002). Moreover, it increases  $\alpha$ SMA expression, the main activation marker of PSCs and MMP2 production by the PSCs (Haber et al., 1999). Other studies have showed that TGF- $\beta$ 1 is involved in the enhancement of PSC's proliferation through the TGF- $\beta$ 1-induced platelet-derived growth



factor (PDGF) secretion (Kordes et al., 2005). More about TGF- $\beta$ 1 role in the activation of PSCs and the related signalling pathways will be discussed in Chapter 4.

➤ **Platelet derived-growth factor (PDGF):**

PDGF has been referred as the most potent mitogenic factor for PSCs since it induces their proliferation but also stimulates their migration and type I collagen as well as fibronectin synthesis (Apte et al., 1999; E. Schneider et al., 2001). Furthermore, PDGF stimulates the activation of the nicotinamide adenine dinucleotide phosphate oxidase (NADPH) which is involved in the reactive oxygen species (ROS) generation, shown, as reported below, to be another stimulator of PSC's activation (Hu et al., 2007). Another demonstrated function of PDGF is its ability to stimulate PSC-induced MMP-3 and MMP-13 expression (Kordes et al., 2005).

➤ **Interleukin 1 $\beta$  (IL-1 $\beta$ ):**

IL-1 $\beta$  is principally secreted by the inflammatory leukocytes in the inflamed pancreas, but it can also be released by the acinar cells during pancreatitis, leading to PSC-increased  $\alpha$ SMA expression and thus PSCs activation (Manohar et al., 2017).

➤ **Interleukin 6 (IL-6):**

IL-6 is a proinflammatory cytokine, often produced by many cell types in response to IL-1 $\beta$  and TNF- $\alpha$  stimulation, shown to be detected in high levels within the serum of patients with CP or PDAC. It has been found to stimulate PSC's activation modulating  $\alpha$ SMA expression and promoting TGF- $\beta$ 1 expression and secretion (Shimada et al., 2002; Zheng et al., 2021).

➤ **Tumor necrosis factor-  $\alpha$  (TNF- $\alpha$ ):**

TNF- $\alpha$  is another proinflammatory cytokine, produced during the early stages of CP, detected in high amounts in patient's blood and pancreatic inflamed tissue, and its level in the serum was correlated to the severity of pancreatitis. It has been established by in vitro and in vivo studies that TNF- $\alpha$  participates in the stimulation of PSC's proliferation,  $\alpha$ SMA expression and PSC-induced type I collagen synthesis (Mews et al., 2002; Michalski et al., 2007).

Moreover, microenvironmental factors presented in the inflamed fibrotic pancreatic tissue during CP and PDAC are also capable to activate PSCs, either by synergetic or competitive effects, either independently of each other. Among them, the most important factors are described below.

➤ **Ethanol:**

Ethanol and its metabolite acetaldehyde are recognized as one of the major risk factors causing CP (Apte et al., 2011). Indeed, it has been demonstrated that ethanol can directly activate PSCs by promoting  $\alpha$ SMA expression and increasing type I collagen synthesis (Casini et al., 2000). This direct responsiveness of PSCs to ethanol is due to PSC's capacity to metabolize ethanol into acetaldehyde through the alcohol dehydrogenase activation, resulting to oxidative stress generation, that subsequently induces lipid peroxidation (Apte et al., 2000). In turn, as described below, oxidative stress also perpetuates PSC's activation (Casini et al., 2000). Additionally, ethanol can upregulate the PDGF-induced NADPH oxidase activity leading to the increase of PSC's proliferation (Hu et al., 2007). Moreover, it has been suggested that ethanol intake from PSCs might favour their survival, since it has been reported to inhibit PSC's apoptosis enhancing thus their activation. Ethanol can also act in a synergistic way with the lipopolysaccharide (LPS) increasing further the inhibitor effect on PSC's apoptosis, suggesting that both together exacerbate PSC's activation (Vonlaufen et al., 2011). Interestingly, McCarroll *et al.* have demonstrated that vitamin A is unable to fully maintain PSC's quiescence in the presence of ethanol, proposing a role of ethanol in PSC's quiescent-activated transition (McCarroll et al., 2006). Additionally, Masamune et al. have shown that the nonoxidative ethanol metabolite, palmitic acid ethyl ester can also influence PSC's activation stimulating PSC-induced IL-8 secretion (Masamune et al., 2010).

➤ **Oxidative stress and reactive oxygen species (ROS):**

Another proposed stimulator of PSC's activation is the exogenous hydrogen peroxide ( $H_2O_2$ ), a principal cellular ROS inducer leading to oxidative stress generation within PSCs, found to promote  $\alpha$ SMA expression and PSC's migration. Moreover, exposure to the iron sulphate/ascorbic acid pro-oxidant complex induced increase of  $\alpha$ SMA and type I collagen expression contributing to PSC's activation, whereas these effects were reduced by the application of the antioxidant chemical DA-9601 (Apte et al., 2000; Kikuta et al., 2006, 2004; Yoo et al., 2005).

➤ **Pressure:**

During CP and PDAC, pancreatic tissue pressure is much more elevated than in the healthy pancreas (Jalleh et al., 1991). Asami *et al.* established that externally elevated applied pressure (80 mmHg) resulted to PSC's activation by increasing  $\alpha$ SMA, type I collagen et TGF- $\beta$ 1 expression. Furthermore, the authors have shown that elevated pressure generates ROS, also

reported to be involved in PSC's activation, illustrating an example of synergetic interaction between different stimulating factors in order to perpetuate PSC's activation (Asaumi et al., 2007). The study of Watanabe *et al.* supported these findings, demonstrating that additionally to these effects, high pancreatic pressure can stimulate PSC's proliferation, as well PSC-induced TGF- $\beta$ 1 and type I collagen secretion (Watanabe et al., 2004).

➤ **Hyperglycemia:**

Several studies have reported that PSC's exposure to high glucose led stimulation of PSC's proliferation, increase of  $\alpha$ SMA expression and of the ECM protein connective tissue growth factor (CTGF) (Nomiya et al., 2007). Hyperglycemia also participates in the exacerbation of PDAC favouring the interaction between activated PSCs and PCCs. In addition, Hong *et al.* demonstrated that hyperglycemia induces ISC's activation as well, promoting islet fibrosis (Hong et al., 2007).

➤ **Hypoxia inducible factor-1 $\alpha$  (HIF-1 $\alpha$ ):**

The hypoxic microenvironment is a characteristic feature of pancreatic tissue during CP and PDAC (Koong et al., 2000; Patel et al., 1995). These oxygen changes surrounding PSCs microenvironment are sensed by the PSC-produced HIF-1 $\alpha$  factor, which then translocates to PSCs nucleus inducing VEGF transcription (Ide et al., 2006). HIF-1 $\alpha$  has also been found to upregulate the hepatoma-derived growth factor gene preventing PSC's apoptosis, promoting indirectly PSC's activation. Therefore, PSC-produced HIF-1 $\alpha$  suggests that activated PSCs might serve as oxygen-sensing cells in the inflamed pancreas (Masamune et al., 2008).

➤ **Angiotensin II (Ang II):**

Except its presence in the cardiovascular system, Ang II was found to be highly expressed in the pancreas under pathological conditions, including CP and PDAC. PSCs are able to respond to Ang II by the expression of angiotensin II receptor (AT1) on their surface, but they do not produce Ang II themselves (Reinehr et al., 2004). Ang II binding to AT1 stimulates PSC's proliferation on the one side through epidermal growth factor receptor transactivation and on the other side *via* the inhibition of SMAD3 and SMAD4 nuclear accumulation by stimulating SMAD7 expression (Hama et al., 2006) (this mechanism will be better described in Chapter 4). Moreover, PSC treatment with losartan, an AT1 antagonist, caused PSC's apoptosis, suggesting a role of Ang II through its AT1 in PSC's survival, and consequently in sustaining PSC's activation (Liu et al., 2005).

### III.3) Autocrine stimulation of PSCs

Besides PSC's activation by paracrine and microenvironmental signals, PSCs themselves can mediate and sustain their own activation through autocrine loops, implying that even in the absence of external stimuli, PSCs can remain in their activated state (**Figure 5**).

Aoki et al. have revealed the presence of two autocrine loops preserving the activation of PSCs, the one loop formed between PSC induced -TGF- $\beta$ 1 and -IL-6 secretion, and the other loop between PSC induced -TGF- $\beta$ 1 and -IL-1 $\beta$  secretion. Using TGF- $\beta$ 1, IL-6 or IL-1 $\beta$ -neutralizing antibodies independently, the authors have demonstrated that the expression and secretion of one of the cytokines stimulates the expression and secretion of the other one, but through different signalling pathways. This mutual stimulation is achieved through the expression of TGF- $\beta$ 1, IL-6, and IL-1 $\beta$  receptors on the cell surface of activated PSCs. TGF- $\beta$ 1/IL-6 autocrine loop is driven by the SMAD2/3 and ERK1/2-dependent pathways, respectively, while TGF- $\beta$ 1/IL-1 $\beta$  autocrine loop is mediated by the SMAD3 and ERK1/2-dependent pathways, respectively (Aoki et al., 2006, 2006).

Another autocrine stimulation that might occur is through PSC-induced PDGF secretion. Activated PSCs are characterized by an increased PDGF receptor expression on their cell surface, suggesting that in addition to the PDGF-paracrine stimulation, secreted PDGF from PSC can bind to its receptor, further promoting PSC's proliferation and migration, through an autocrine manner. Moreover, activated PSCs express endothelin type A receptors (ET<sub>A</sub>), indicating that secreted ET-1 from activated PSCs is able to bind to its own receptor located on the cell surface, stimulating PSC's contraction and migration (Jonitz et al., 2009; Masamune et al., 2005). Additionally, secreted activin A from PSCs, a member of the TGF- $\beta$  family has been also reported to proceed autocrine properties, by binding to the expressed TGF- $\beta$  receptors on activated PSC's surface leading to the augmentation of TGF- $\beta$ 1 and type I collagen expression and secretion (Ohnishi et al., 2003). Interestingly, Masamune *et al.* have been shown that activated PSCs express NADPH (nicotinamide adenine dinucleotide phosphate) oxidase, a major enzyme involved in the production of ROS, implying that activated PSCs themselves can be a source of ROS, further stimulating  $\alpha$ SMA and type I collagen expression and PSC's migration (Apte et al., 2000; Masamune et al., 2008).

This capacity of activated PSCs to maintain their own activation through an autocrine stimulation, even in the absence of initial paracrine or microenvironment stimuli, could in part

explain the persistence of CP progression even when the pathogenic stimulus is eliminated. Subsequently, CP persistence constitute one of the major risk factors for PDAC development.

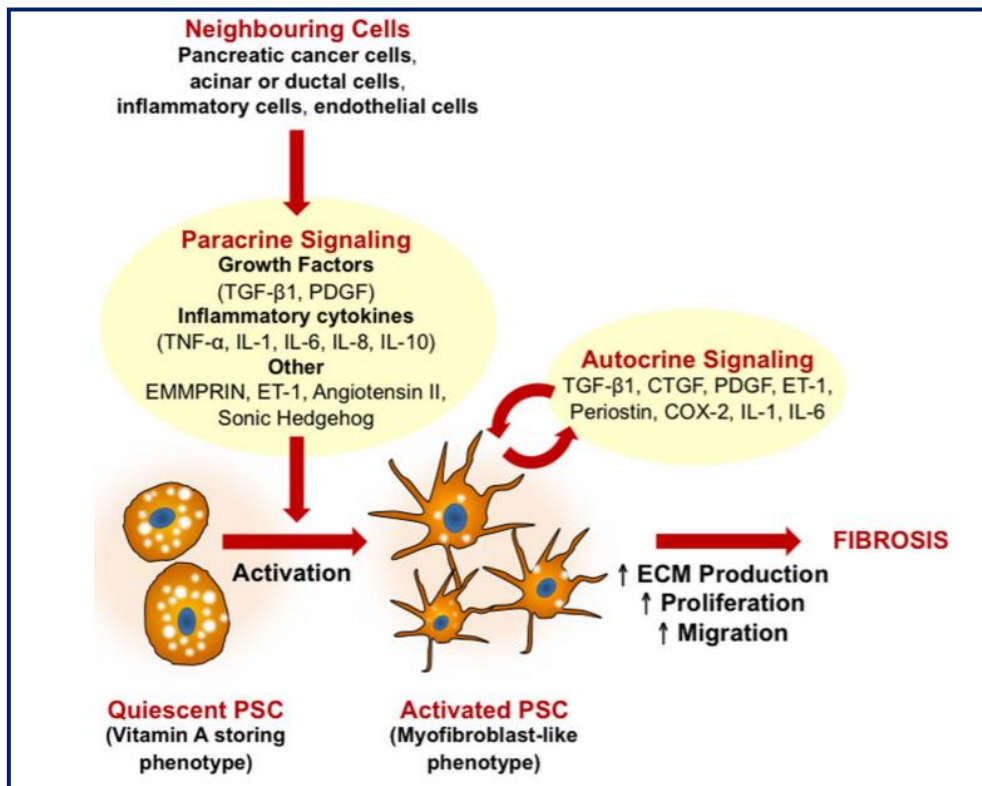


**Figure 5:** Recapitulative scheme of PSC's activation through paracrine and autocrine stimulations (McCarroll et al., 2014).

#### III.4) Signalling pathways involved in PSC's activation

Since the discovery of PSC's crucial role in pancreatic fibrosis development, multiple signalling pathways and molecules have been identified to drive the occurred dynamic and orchestrated changes during PSC's activation, following paracrine, microenvironmental (e.g., pressure) or autocrine stimulation. Cross-talks between the different signalling pathways aid to sustain the activation of PSCs (**Figure 6**).

One of the major signalling pathways by which mammalian cells respond to extracellular stimuli, that has received the most attention from PSC's research is the mitogen-activated protein kinase (MAPK) pathway. This signalling pathway, known to regulate numerous cell functions including cell division, survival, apoptosis and protein synthesis or

secretion, is composed of three MAPK members, the extracellular signal-regulated kinase 1/2 (ERK1/2), the c-jun N-terminal kinase (JNK) and the p38 MAP kinase, found to be activated during CP and PDAC (Apte et al., 2007; Chang and Karin, 2001; Sahin et al., 2016). In response to extracellular stimuli, these kinases are activated by phosphorylation, translocating to the nucleus where they phosphorylate and activate transcription factors. It has been reported that all of the three MAPK are implicated in PSC's activation processes, each MAPK regulating different PSC's functions. However, all of them can be activated in response to ethanol, acetaldehyde, and oxidant stress (Kikuta et al., 2004, 2006; Masamune et al., 2002).

The ERK1/2 kinase has been found to be phosphorylated from the early stage of PSC's activation preceding  $\alpha$ SMA expression increase (Jaster et al., 2002; Watanabe et al., 2004). Moreover, ERK1/2 has been demonstrated to stimulate PSC's proliferation and migration in response to PDGF, defined as the most potent mitogen in PSCs (Jaster et al., 2002; Masamune et al., 2003). Except PDGF, ERK1/2 drives PSC's proliferation also in response to other microenvironment stimuli, including pressure, trypsin, galectin-1, and angiotensin II (Hama et al., 2004; Masamune et al., 2006, 2005; Watanabe et al., 2004). This latter stimulates ERK1/2-mediated proliferation through the transactivation of EGFR. In addition, ERK1/2 is implicated in the modulation of PSC-induced MMP production, and particularly of MMP-1 synthesis, in response to IL-1 $\beta$  and TNF- $\alpha$  stimulation (Tasaki et al., 2003). Activation of ERK1/2 has been also shown to drive rodent PSC-induced TGF- $\beta$ 1 expression, in response to exogenous TGF- $\beta$ 1 stimulation, suggesting the involvement of a stimulatory TGF- $\beta$ 1 autocrine loop (Ohnishi et al., 2004), and also in response to IL-6 (Aoki et al., 2006) and IL-1 $\beta$  (Aoki et al., 2006) resulting to PSC sustained activation and TGF- $\beta$ 1-induced ECM deposition. Another study have investigated this hypothesis, demonstrating an activation of ERK1/2 after TGF- $\beta$ 1 stimulation and a decrease of TGF- $\beta$ 1-induced  $\alpha$ SMA and fibronectin expression when ERK1/2 pathway is inhibited, implying an indirect role of ERK1/2 kinase in the modulation of  $\alpha$ SMA and fibronectin expression (Xu et al., 2018).

The second member of the MAPK family, the JNK, has been reported to respond to PDGF, TGF- $\beta$ 1 and to IL-1 $\beta$  stimulation, as ERK1/2 (Masamune et al., 2004). Indeed, inhibition of JNK curbed PDGF-mediated PSC proliferation, and reduced TGF- $\beta$ 1-induced  $\alpha$ SMA and fibronectin expression. Whereas the third member of the MAPK, the p38 MAP kinase has been suggested by Masamune *et al.* to induce the activation of quiescent PSCs through the modulation of  $\alpha$ SMA expression. The authors have used freshly isolated quiescent rat PSCs that they cultivate in the presence and absence of the SB 203580 p38 MAP kinase

pharmacological inhibitor. After 7 days of treatment, they noted that inhibition of p38 MAP kinase prevented the activation of cultivated PSCs defined by weak  $\alpha$ SMA expression and the persistence of the lipid droplets, while withdrawing of the inhibitor triggered PSC's activation increasing  $\alpha$ SMA expression (Masamune et al., 2003). Furthermore, as for the other two MAPK members, IL-1 $\beta$  and PDGF activate the p38 MAP kinase, and thus implying a role in the stimulation of PDGF-induced PSC's proliferation, whereas inhibition of p38 MAP kinase reduced  $\alpha$ SMA expression, and PSC-induced MCP-1 and type I collagen expression. In addition, p38 MAP kinase increases the expression of  $\alpha$ SMA and stimulates type I collagen production in response to ethanol, acetaldehyde, and oxidative stress (Kikuta et al., 2004, 2006; Masamune et al., 2002; McCarroll et al., 2003).

Another essential signalling pathway known to drive multiple cells processes, demonstrated to modulate PSC's activation is the phosphatidylinositol-3-kinase (PI3K) /protein-kinase B (AKT) pathway (McCarroll et al., 2004). Masamune *et al.* have established that PDGF triggers PI3K/AKT phosphorylation leading to the stimulation of PSC's migration but not proliferation (Masamune et al., 2003). AKT phosphorylation drives PSC's migration also following periostin stimulation (Erkan et al., 2007). Whereas Schwer *et al.* have demonstrated that blockage of PI3K/AKT activation, using carbon monoxide releasing molecule-2 inhibited PSC's proliferation, inducing a cell cycle arrest in G0/G1 phase through the down-regulation of cyclin D1 and E expression (Schwer et al., 2013). Additionally, Zhang *et al.* have reported that the tumor suppressor PTEN (phosphatase and tensin homolog), which has the ability to inhibit AKT activity, induced cyclin D1 down-regulation resulting to the diminution of PSC's proliferative potential, suggesting an indirect role of AKT pathway in the promotion of PSC's proliferation (Zhang et al., 2018). Furthermore, AKT phosphorylation mediates the proinflammatory PSC-induced IL-32 expression in response to IL-1 $\beta$ , TNF- $\alpha$  or IFN- $\gamma$  (interferon- $\gamma$ ) stimulation (Nishida et al., 2008). Supplementary to these findings, Duluc *et al.* have shown that activation of one of the AKT downstream effectors, namely mTOR activation stimulates the capacity of activated PSCs (also called cancer-associated fibroblasts) to synthesize and secrete various proteins, notably IL-6 production and secretion, during PDAC (Duluc et al., 2015).

A third crucial signalling pathway implicated in the modulation and perpetuation of PSC's activation is the TGF- $\beta$ 1 pathway, shown to be the most potent profibrotic factor causing pancreatic fibrosis. Ohnishi *et al.* have studied the role of SMAD2 and SMAD3, two principal downstream effectors of TGF- $\beta$ 1 signalling in rodent PSCs. Using dominant-negative

SMAD2/3 mutant, the authors revealed an inhibition of PSC's activation reflected by the reduction of  $\alpha$ SMA expression, and paradoxically by the enhancement of PSC's proliferation. When they co-expressed SMAD2 with the dominant-negative mutant, they noted that  $\alpha$ SMA expression increased, and thus that PSC's activation was restored, implying a role of SMAD2 in the regulation of  $\alpha$ SMA expression. Whereas, when they co-expressed SMAD3 with the dominant negative mutant, they observed an attenuation of PSC's proliferation, suggesting that SMAD3 regulates negatively PSC's proliferation (Ohnishi et al., 2004). In addition, TGF- $\beta$ 1-mediated SMAD2/3 pathway has been shown to induce the expression of COX-2 by activated PSCs (Aoki et al., 2007). Interestingly, TGF- $\beta$ 1-mediated SMAD3 pathway stimulates IL-1 $\beta$  expression, which in turn through the ERK1/2 pathways induces TGF- $\beta$ 1 expression, forming a TGF- $\beta$ 1/IL-1 $\beta$  autocrine loop (Aoki et al., 2006). Another existing autocrine loop is the one between TGF- $\beta$ 1 and IL-6 mediated by the SMAD2/3 and ERK1/2 pathways. Indeed, TGF- $\beta$ 1 stimulates IL-6 expression and secretion through the SMAD2/3 pathway, and in turn IL-6 induces TGF- $\beta$ 1 expression and secretion through the ERK1/2 pathway (Aoki et al., 2006). The involvement of TGF- $\beta$ 1 signalling pathways, including the canonical SMAD pathway and non-canonical pathway, in PSC's activation, and thus pancreatic fibrogenesis will be presented in Chapter 4.

Other studies have provided evidence of Ras homolog gene family (Rho) and Rho-associated protein kinase (ROCK/Rho kinase) importance in PSC's activation processes, and particularly in cytoskeleton reorganization. Indeed, during PSC activation the formation of stress fibers increases permitting the recruitment of  $\alpha$ SMA which is an isoform of the cytoskeletal protein actin (Takai et al., 1995). The role of Rho and its downstream effector, Rho kinase, in this process has been demonstrated using the Y-27632 Rho kinase inhibitor (Masamune et al., 2003). Treatment of activated PSCs with Y-27632 caused stress fibers disassembly resulting to morphological changes, reflected by the obtention of an elongated, fusiform shape, and consequently inhibited PSC's activation. Furthermore, Y-27632 treatment of activated PSCs led to the reduction of  $\alpha$ SMA expression, proliferation, type I collagen synthesis, and chemotaxis (Masamune et al., 2003). These findings reported the important role of Rho/Rho kinases in PSC's activation processes as well as in actin cytoskeleton and actin stress fibers organization and consequently in PSC's morphology. In addition, inhibition of Rho/Rho kinase pathway has been shown to diminish ET-1-induced contraction and migration in activated PSCs, suggesting an indirect involvement of Rho/Rho kinase in these activation processes (Masamune et al., 2005).



Shinozaki *et al.* have established a role of the indian hedgehog (IHH), one of the three members constituting the hedgehog pathway, in the promotion of PSC's migration *via* a chemotactic and chemokinetic manner, without affecting PSC's proliferation,  $\alpha$ SMA expression nor type I collagen expression (Shinozaki *et al.*, 2008). Indeed, after IHH binding to its receptors, smoothed and patched-1, found to be expressed on PSC's surface, it augments MMP-1 expression and permits MMP-1 transport to the plasma membrane leading to ECM degradation (Shinozaki *et al.*, 2008). In parallel, MMP-1 activates other MMPs, such as MMP-2, MMP-3, and MMP-13, expanding ECM degradation (Yana and Seiki, 2002). This remodelling aid to facilitate cell movements and so to enhance PSC's migration. On the other side IHH-mediated PSC migration has been demonstrated to be attenuate by TIMP2 (Shinozaki *et al.*, 2008).

Another signalling molecule presenting a role in the regulation of PSC's activation is the transcription nuclear factor- $\kappa$ B (NF- $\kappa$ B), known to control, among others, cytokine production and cell survival. However, an alteration of NF- $\kappa$ B activity leads to development of pathologies, including cancer, inflammation, and autoimmune disease. The activity of NF- $\kappa$ B has been shown to be elevated and to persist in activated PSCs compared to quiescent PSCs, indicating that the regulation of its activity is disrupted. This high persistent NF- $\kappa$ B activity was induced by TNF- $\alpha$ , IL-1 $\beta$  and galectin-1 (a  $\beta$ -galactoside-binding protein) stimulations, which are soluble factors presented in the inflamed microenvironment surrounding the activated PSCs (Masamune *et al.*, 2006). In response to these stimulation, NF- $\kappa$ B promotes the expression of IL-6, IL-8, MCP-1 and ICAM-1, all of them being a characteristic of activated PSC secretory potential (Andoh *et al.*, 2000; Masamune *et al.*, 2002; Shimada *et al.*, 2002).

Nevertheless, signalling molecules that inhibit PSC's activation have also been identified. Among them, the most studied is the peroxisome proliferator activated receptor- $\gamma$  (PPAR- $\gamma$ ). PPAR- $\gamma$  is nuclear hormone receptor which heterodimers with the retinoic acid X nuclear receptor, mainly found to be expressed in adipose tissue regulating the lipid metabolism (Tontonoz and Spiegelman, 2008). Reports using PPAR- $\gamma$  ligands, such a troglitazone, have revealed a reduction of PSC's proliferative capacity,  $\alpha$ SMA expression, type I collagen synthesis and MCP-1 production, implying that PPAR- $\gamma$  negatively regulates PSCs activation maintaining them into their quiescent state (Jaster *et al.*, 2005; Kulkarni *et al.*, 2011; Masamune *et al.*, 2002; Shimizu *et al.*, 2002; van Westerloo *et al.*, 2005).

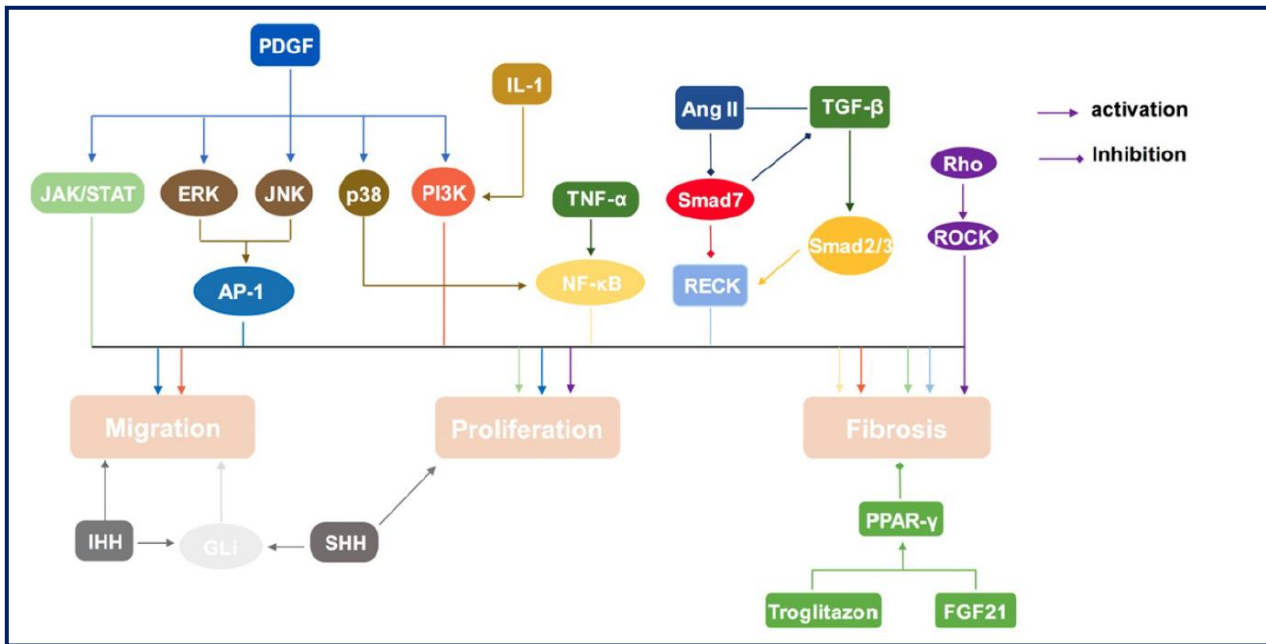


**Figure 6:** Representation of the principal signalling pathways found to be involved in PSC's activation or inhibition (Jin et al., 2020).

### III.5) Heterogeneity of activated PSCs

During PDAC, activated PSCs constitute the major source of cancer-associated fibroblasts (CAF), participating in the formation of the dense desmoplastic stroma surrounding PCCs. Therefore, a lot of research studies are referring activated PSCs as CAFs in pancreatic carcinogenesis, revealing the existence of more than one distinct subtype of activated PSCs, or so called CAFs in PDAC. The discovery of different activated PSCs subpopulation underlines their intra- and inter-tumor heterogeneity (Norton et al., 2020; Pereira et al., 2019).

According to their spatial localization within the tumor, Öhlund *et al.* have revealed in mouse and human PDAC tissue, the existence of two different activated PSCs subpopulation. The one subtype, called myCAF is located in the periglandular region, in tight contact with the PCCs and found to become activated *via* juxtacrine interactions with the PCCs, having myofibroblastic features. myCAFs are characterized by high  $\alpha$ SMA expression and an up-regulation of TGF- $\beta$ 1 responding genes, including type I collagen and CTGF but by low expression of inflammatory mediators, possessing mostly contractile and stroma remodelling potentials. The second subtype, called iCAF is situated distantly of PCCs and becomes activated through the secreted paracrine factors from PCCs. iCAFs have an inflammatory and secretory

phenotype, defined by increased cytokine and chemokine expression, particularly of IL-6 and IL-11, but also by low levels of  $\alpha$ SMA expression. Interestingly the authors have demonstrated that both myCAFs and iCAFs can dynamically transit from myofibroblastic to inflammatory phenotype and vice versa, highlighting the plasticity of activated PSCs (Öhlund et al., 2017) (**Figure 7**). Additionally, Bernard *et al.* have established that iCAFs are involved in PDAC development and progression through the promotion of an immunosuppressive microenvironment, whereas myCAFs are implicated in the high-grade intraductal papillary mucinous neoplasms precursors of PDAC (Bernard et al., 2019).

Furthermore, Neuzillet *et al.* have identified four other subtypes of activated PSCs associated with PDAC prognosis and classify according to their ability to express  $\alpha$ SMA and vimentin, to produce ECM components, to proliferate and to their immune-related signature. The PSC subtype shown to correlate with a good prognosis of PDAC, was determined by the expression of podoplanin in PSC's plasma membrane and characterized by an immunogenic profile and ECM synthesis, named subtype C. The second PSC subpopulation, called subtype B, was defined by myosin-11 expression within PSC's cytoplasm, which is a member of the myosin heavy chain family. The subtype B presents low proliferative potential but increased  $\alpha$ SMA and vimentin expression, as well as ECM synthesis, and is associated to an intermediate PDAC prognosis. The other PSC subtype linked to an intermediate to poor PDAC prognosis is depicted by periostin secretion and is found at the invasive front of the tumour. Contrary to subtype B, this subtype, named subtype A, has a high proliferative ability, produces ECM components, but has low  $\alpha$ SMA and vimentin expression. The last identified subpopulation, correlated to a poor PDAC prognosis, called subtype D, is mainly characterized by elevated  $\alpha$ SMA and vimentin expression, ECM remodelling and low proliferative capacity (Neuzillet et al., 2019) (**Figure 8**).

These findings highlighted the dynamic complexity of activated PSCs in PDAC, suggesting that some PSC's subtypes promote PDAC progression and spreading, resulting to shorter patient survival and thus poor PDAC prognosis. Whereas other PSC's subtypes might have mostly a "protective" role enhancing PDAC prognosis. However, the intra et inter-tumour heterogeneity of activated PSCs might not be limited only to the above cited subpopulations. Other subtypes might exist and be distinguished regarding to the cytokine production, cell surface marker expression, cell signalling, gene expression profile and their interaction with PCCs or the other cell types of the tumour microenvironment.

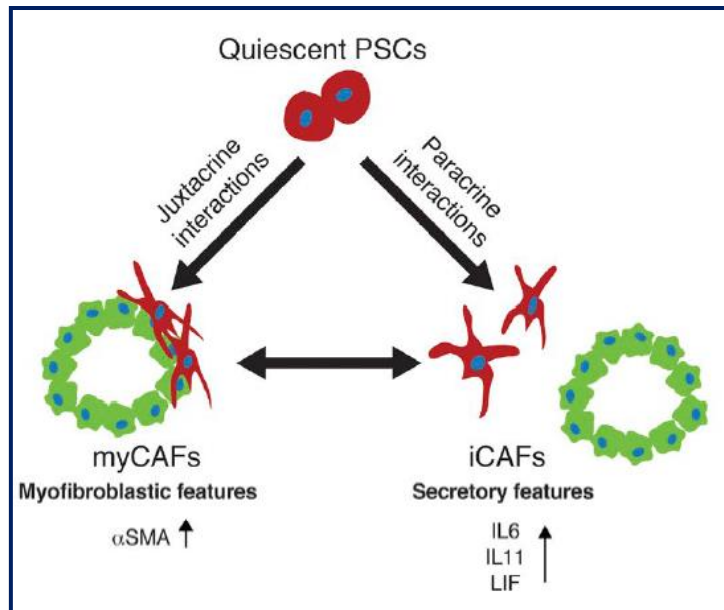


**Figure 7:** Conclusive scheme of Öhlund *et al.* work showing the two major discovered phenotypes of activated PSCs, called myCAFs for the PSCs having a myofibroblastic phenotype and iCAFs for that having an inflammatory phenotype (Öhlund *et al.*, 2017).

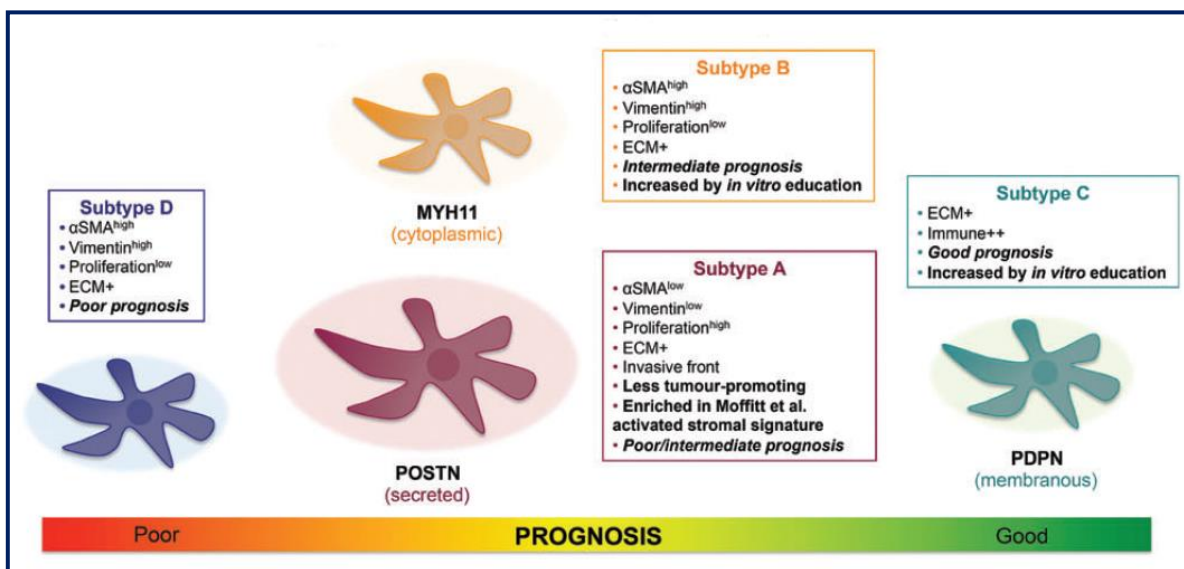


**Figure 8:** Illustration of the other four major activated PSC's subpopulations, classified depending on their influence in PDAC prognosis (Neuzillet *et al.*, 2019).

## **CHAPTER 3: Role of PSCs in pancreatic diseases**

### **I. Pancreatitis**

#### **I.1) Chronic pancreatitis (CP)**

Excessive pancreatic fibrogenesis, known now to be principally mediated by the activated PSCs, is the main consequence of chronic pancreatitis development and progression (Apte et al., 2011; Klöppel et al., 2004). Indeed, CP is a progressive necro-inflammatory pancreatic disease causing an irreversible destruction of the exocrine and endocrine pancreatic tissues accompanied by loss of pancreatic acinar and islets cells, which are consequently replaced by fibrous tissue disrupting pancreatic normal functions. Initially CP development is in general asymptomatic and then is manifested by recurrent episodes of acute pancreatitis, followed at a later stage by intermittent or constant pain, ductal dilatation, and pancreatic calcification. At the final stage of CP, most of patients present exocrine and endocrine insufficiency accompanied by maldigestion and diabetes, respectively. However, despite intensified research studies, CP treatment remains a challenge since no effective therapy other than supportive care has been found to stop pancreatic fibrosis progression (Spanier et al., 2008).

In the developed countries, the principal etiological factor causing CP is alcohol abuse, accounting for approximately for 70-80% of all CP cases. Nevertheless, in approximately 20% of the cases the real cause is unknown, and thereby are considered as idiopathic CP. In addition, there are other risk factors leading to CP development, all classified according to the TIGAR-O system into six categories, including toxic-metabolic (T), idiopathic (I), genetic (G), autoimmune (A), recurrent acute pancreatitis (R), and obstructive (O) aetiologies (Etemad and Whitcomb, 2001). Moreover, another classification system divided CP into 7 categories based on the prevalence of each risk factor, the clinical stage and the severity of the disease, named the M-ANNHEIM system (Schneider et al., 2007). This system subclassified the multiple (M) risk factors inducing CP into alcohol consumption (A), nicotine consumption (N), nutritional factors (N), hereditary factors (H) efferent pancreatic duct factors (E), immunological factors (I), and miscellaneous and metabolic factors (M) (Schneider et al., 2007).

At the molecular level, CP pathogenesis can be explained in part by the generated free radicals within pancreatic acinar cells (PACs) due to the alcohol- or its metabolites-induced oxidative stress, resulting to lipid oxidation. Therefore, this promotes the activation of transcription factors, such as NF- $\kappa$ B, involved in the expression and secretion of

proinflammatory cytokines and chemokines causing PAC death. Furthermore, the non-oxidative alcohol metabolism can induce the accumulation of fatty acid ethyl esters in PAC, found to provoke organelle damages, like lysosome fragility, leading to acinar cell dysfunction (Haber et al., 2004, 1993). Another cause responsible for CP pathogenesis is the ductal obstruction induced by the increased protein concentration and viscosity of the pancreatic juice. Indeed, alcohol modifies PAC's secretory function resulting to protein hypersecretion, and thus to the formation of protein plugs within the pancreatic duct. These proteins plugs can induce the formation of calculi, containing  $\text{Ca}^{2+}$  carbonate precipitates, contributing to pancreatic duct's obstruction (Tsujimoto et al., 2008).

However, besides alcoholic CP, repetitive episodes of acute pancreatitis (AP) characterized by pancreatic tissue autogestion can lead to severe CP. During AP, there is a dysregulated activation of pancreatic enzymes secreted by the PAC, including aberrant trypsin activation, resulting to PAC' auto-destruction and loss by necrosis and apoptosis (Bateman et al., 2002) but also to inflammatory cell infiltration. Therefore, recurrent episodes of AP cause a replacement of the cellular component by non-cellular fibrous tissue and an induction of sustained inflammation, corresponding to CP development. In fact, the divers liberated cytokines in response to the inflammatory injury will stimulate PSC's activation setting the stage for pancreatic fibrogenesis, and consequently promoting ECM deposition (Apte et al., 2016).

Additionally, sustained CP-induced inflammation can alter the ductal epithelium microenvironment increasing the risk of neoplastic transformations due to an augmentation of the ductal cell proliferation and genomic damages, defining CP as predisposing factor for pancreatic cancer development (Binkley et al., 2004; Raimondi et al., 2010). This CP-induced inflammation can also contribute to the development of pancreatic cancer through the formation of preneoplastic pancreatic intraepithelial lesions (mPanINs) triggered from PACs' dedifferentiation and increase of their sensitivity to *K-RAS* mutation-induced transformations by inhibition of the senescence process (Guerra et al., 2011).

## I.2) Role of activated PSCs in pancreatitis

Activation of PSCs occurs as an early event of AP- and CP-induced necro-inflammation and it has been shown that activated PSCs communicate with their neighbour PACs participating in the amplification of the necro-inflammatory reaction and thereby destruction of PACs (Masamune et al., 2009).

Besides the previous-cited activation properties, it has been reported that once activated PSCs express both, type 1 and 2 of cholecystokinin (CCK) receptors (CCK1 and CCK2) (Berna et al., 2010; Phillips et al., 2010). Indeed, upon CCK exposure, activated PSCs produce and secrete acetylcholine, which then binds to PACs' muscarinic receptors stimulating digestive enzymes release, such as amylase, implying a CCK-elicited acetylcholine release mechanism mediated by activated PSCs and stimulating PAC's secretion (Phillips et al., 2010). However, a maintained PSC's activation will trigger an enhanced acinar secretory activity leading to protein hypersecretion and thus protein plugs formation obstructing the pancreatic ducts.

Another study conducted by Gryshchenko *et al.* identified a necrotic amplification loop between activated PSCs and PAC (Gryshchenko et al., 2018). The authors have demonstrated that ethanol, fatty acid ethyl esters, or certain bile acids generate excessive  $Ca^{2+}$  signals in PACs which activate PAC intracellular trypsin inducing PAC autodigestion and consequently PAC necrosis. This process permits trypsin's release from the zymogen granules into the interstitial fluid, where it acts on the neighbour activated PSCs generating  $Ca^{2+}$  signals which stimulate nitric oxide (NO) synthase activation leading to NO formation (Jakubowska et al., 2016). In turn, the PSC-generated NO diffuses into the adjacent PACs promoting PAC necrosis which provokes additional trypsin release, by mechanisms not yet known, and thus creating a vicious destructive circle (Gryshchenko et al., 2018) (**Figure 9**). This necrotic loop mediated in part by the activated PSC-generated NO could explain the observed high serum nitrite/nitrate levels in patients with pancreatitis responsible for the decreased velocity of pancreatic microcirculation (Hegyí and Rakonczay, 2011). This suggests that the elevated NO synthesis by activated PSCs might participate in duct's vascular tone modification resulting to blood capillaries vasodilation, known in general to be regulated by endothelial-produced NO (Rees et al., 1989). Thereafter, PSC-induced PAC necrosis will recruit the inflammatory cells which in turn will produce and secrete high amounts of proinflammatory cytokines conducting from the one side to further PSC's activation and from the other side increasing pancreatic inflammation, and hence further exacerbating pancreatic fibrogenesis.

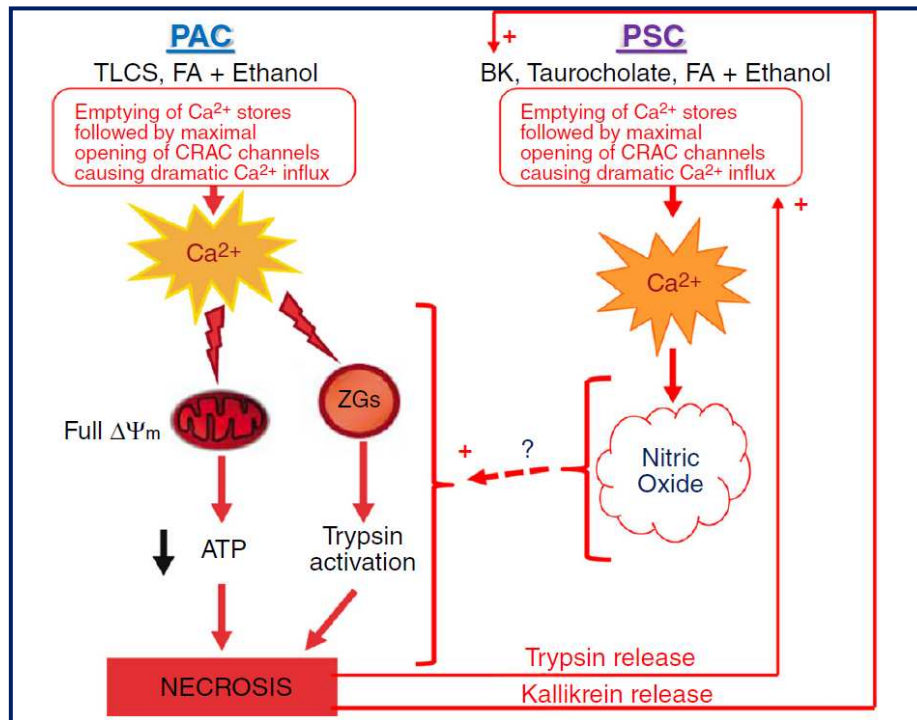


**Figure 9:** Activated PSCs' interaction with pancreatic acinar cells creates a necro-inflammatory amplification loop exacerbating pancreatic acinar cells' necrosis, promoting thus their replacement by an acellular fibrotic tissue. FA, ethanol and/or bile acids trigger excessive Ca<sup>2+</sup> signals in PACs leading, on the one side, to mitochondria depolarization followed by a diminution of ATP production, and, on the other side, to trypsin activation, both resulting to PACs' necrosis. This is manifested by the release of trypsin and kallikrein from the necrotic PACs, which in turn will stimulate Ca<sup>2+</sup> signal generation in PSCs. The generated from PSCs Ca<sup>2+</sup> signals will then induce nitric oxide production, which in turn will act on PACs promoting their necrosis. TLCS: taurolithocholic acid sulphate; FA: fatty acids, ZGs: zymogen granules; ATP: adenosine triphosphate; BK: bradykinin; (Gryshchenko et al., 2018).

## II. Pancreatic ductal adenocarcinoma (PDAC)

### II.1) Development and progression of PDAC

Among all types of pancreatic cancer, pancreatic ductal adenocarcinoma (PDAC) is the most common type, representing 90% of all pancreatic malignancies (Hidalgo, 2010; Kleeff et al., 2016). PDAC constitute one of the most lethal cancers, currently representing the 4<sup>th</sup> cause of cancer-related deaths in the world, with a 5-year survival rate less than 8% ("Cancer Facts



& Figures 2019 | American Cancer Society,” n.d.). Its genesis can be triggered by multiple risk factors, including smoking, alcohol abuse, diabetes, age, and CP. Actually, it has been shown that patients with more than 5 years of CP have 14-fold increased risk to develop PDAC, implying that CP progression represents a precancerous lesion for PDAC development (Pandol et al., 2012). Besides environmental factors, genetic predispositions related to gene mutations (e.g.: *BRCA1* for breast cancer 1, *BRCA2* or *PRSSI* for serine protease 1 gene mutations) can also conduct to PDAC development. It is expected that PDAC-related cases and deaths will increase by more than two-fold within the next ten years (Bray et al., 2018). Its poor prognosis is mainly due to PDAC asymptomatic progression, associated with an early-stage metastatic spread and strong chemoresistance (Hidalgo, 2010; Oettle, 2014).

PDAC principally occurs in the head of the pancreas, and rapidly infiltrates the surrounding tissues, including the spleen, the lymphatic tissues and peritoneal cavity. This PDAC infiltration is accompanied by early metastasis into the lungs and liver, even when the primary tumour is still approximately 10 mm in size, decreasing patient’s survival rate. Furthermore, what renders PDAC treatment even harder is its heterogeneity within the same tumour, since according to the tumour region, the tumour grade or differentiation degree the lesion varies. Indeed, PDAC arises from three types of non-invasive precursor lesions, followed by genetic alterations, resulting to the development of a fully invasive tumour. These lesions include pancreatic intraepithelial neoplasms (PanINs), mucinous cystic neoplasms (MCN), and intraductal papillary mucinous neoplasms (IPMN), and they have different origins. PanINs have been shown to mostly originate from acinar or centroacinar cells, particularly from the transdifferentiation of those cells into cells with ductal identity, but in some cases PanINs can also originate directly from ductal cells. While IPMNs arise mostly from the ductal epithelium, and especially from the progenitor niche of the ductal epithelium (Yamaguchi et al., 2018). Among these lesions, PanINs are the most common lesion found in the intralobular pancreatic ducts, presenting approximately 90% of the cases. Moreover, according to the severity of the induced architectural disorganization and nuclear atypia by the lesions as well as the aberrant cell proliferation, PanINs are classified into three grades from I to III, where grade I is the less severe and grade III ultimately transforms into invasive PDAC (**Figure 10**). PanINs are accompanied by genetic abnormalities, with the *K-RAS* gene mutation being the most frequent, presented in 90% of PDAC tumors (Hezel et al., 2006).

However, despite the early metastatic and invasive fate of PDAC, the therapeutic treatment inefficiency arises essentially from the dense fibrotic stroma (desmoplasia), which can account

for 90% of the total tumour volume, surrounding the pancreatic cancer cells (PCC), thus preventing the drug delivery (Norton et al., 2020; Vennin et al., 2018). The cellular component of pancreatic desmoplasia is essentially constituted by cancer-associated fibroblasts (CAFs) or so-called activated pancreatic stellate cells (PSCs), which are in permanent dialogue with the PCCs providing them with an optimal heterogeneous microenvironment that aids the tumour's development and progression (Tang et al., 2013; Thomas and Radhakrishnan, 2020; von Ahrens et al., 2017). Therefore, reducing PSC-induced activation factors might be the key for improving PDAC chemotherapeutic efficiency.

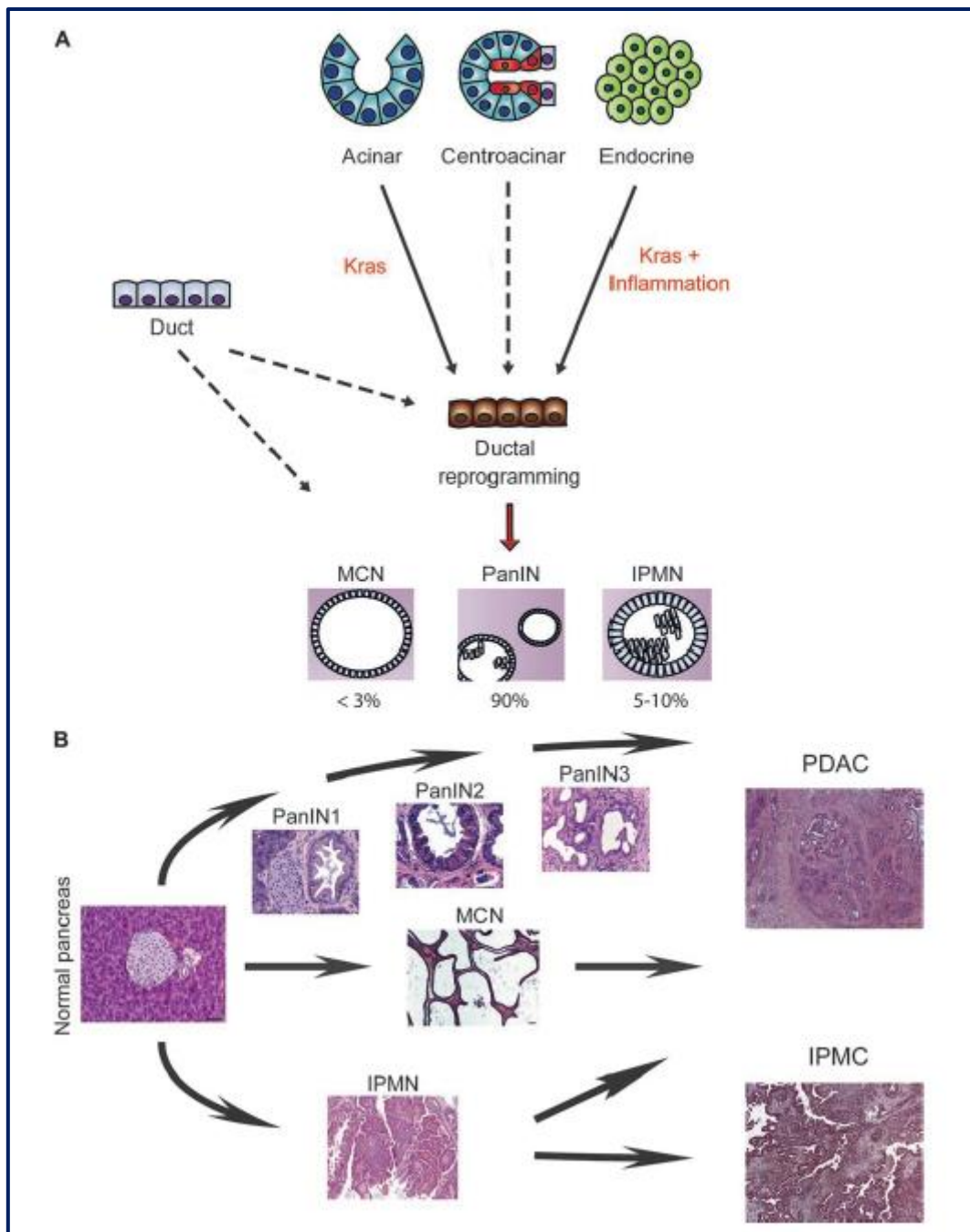


**Figure 10:** Stages of PDAC development, including the precancerous non-invasive precursor lesions (PanINs, IPMN and MCN) and their origins. PanIN: pancreatic intraepithelial neoplasia; IPMN: intraductal papillary mucinous neoplasm; MCN: mucinous cystic neoplasm; IPMC: intraductal papillary mucinous carcinoma (Modified from Mazur and Siveke, 2012).

## II.2) Role of activated PSCs in PDAC

Activated PSCs are well known now to be involved in a dynamic dialogue with the PCCs, promoting PDAC's initiation, progression, aggressiveness, and chemoresistance (Apte and Wilson, 2012; Hanahan and Weinberg, 2011; Vonlaufen et al., 2008). In fact, co-cultures of PCCs and PSCs have demonstrated that activated PSCs stimulate the proliferation and migration of the PCCs, and consequently they reduce PCC's apoptosis (Hwang et al., 2008; Vonlaufen et al., 2008a; Xu et al., 2010). Other reports using a sex mismatch mouse model or engineered fluorescent PCC and PSC cell lines, have established that activated PSCs not only accompany the migrating PCCs but they also favour the development of metastatic colonies (Suetsugu et al., 2015, 2012). These findings reveal that activated PSC's potential is not limited only to their enhanced proliferative and migratory capacities, but they can also travel in the blood circulation together with the PCCs, intravasating or extravasating blood vessels, and hence disseminating into distant organs (Xu et al., 2010).

Moreover, the excessive ECM deposition induced by activated PSC-produced type I collagen, fibronectin, or laminin, reflected by an increase of ECM stiffness, influences PCCs phenotype (Lu et al., 2014). For example, increased type I collagen secretion from activated PSCs have been shown to promote PCC's migratory, metastatic, adhesive abilities as well as their survival *via* the  $\beta 1$  integrin-focal adhesion kinase (FAK) signalling pathway (Drifka et al., 2016). Additionally, the  $\beta 1$  integrin-FAK pathway drives PSC's radio-protective effect on PCCs irradiation decreasing PCC's sensitivity to fractionated radiotherapy, as observed by  $\beta 1$  integrin and FAK knocking down in PCCs co-cultured with PSCs (Cabrera et al., 2014; Mantoni et al., 2011). At the same time, PSC-mediated exorbitant ECM deposition augments the interstitial pressure, restricting the blood flow, inflammatory cell infiltration and oxygen availability, and thus providing the ideal environment for PDAC development and progression, but also preventing chemotherapeutic agents' delivery to PCCs. Another protein implicated in ECM remodelling established to enhance PDAC spreading, is the secreted MMP-2 from activated PSCs. Indeed, the assessment of observed xenograft tumor formations in an immunodeficient mouse host has demonstrated that ECM degradation mediated by MMP-2 stimulates PCCs migration and invasion (Koikawa et al., 2018) (**Figure 11**).

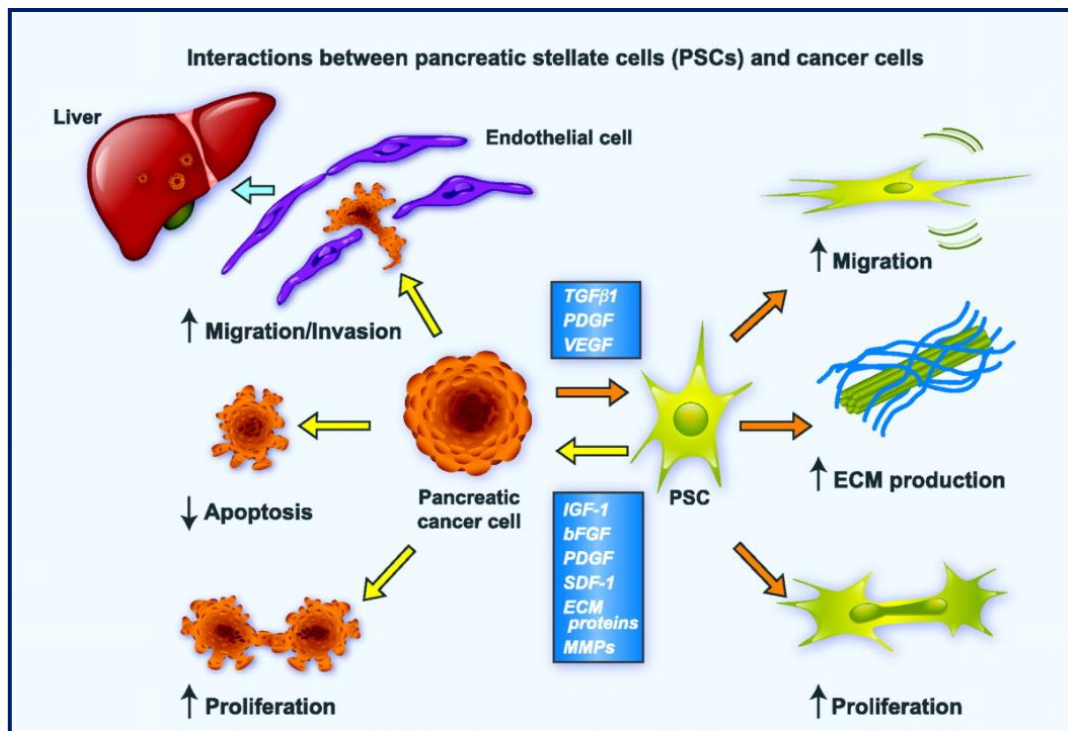


**Figure 11:** Dynamic bidirectional communication between activated PSCs and pancreatic cancer cells, influencing each other's behaviour (Vonlaufen et al., 2008).

Besides these effects on PCCs behaviour, activated PSCs can also induce epithelial-mesenchymal transition (EMT) in PCCs, reflected by a diminution of epithelial markers expression, such as E-cadherin and consequently an augmentation of mesenchymal markers expression, like N-cadherin and vimentin (Kikuta et al., 2010; Tian et al., 2016). Therefore, the acquisition of a mesenchymal phenotype in PCCs following the EMT further promotes their migratory and invasive properties as well as increases their resistance to apoptosis (Thiery et al., 2009). Furthermore, it has been reported that activated PSC favour the acquisition of stem-cell like phenotype in PCCs, illustrated by the expression of stem cell markers in PCCs, such as nestin and ATP-binding cassette sub-family G member 2 (ABCG2), and their enhanced ability to form spheroids, when co-cultured with PSCs *in vitro*, implying that PSCs might constitute a niche for PC stem cells (Hamada et al., 2012). Along with these capacities, activated PSCs promote T lymphocytes apoptosis and thereby inhibit their infiltration in the tumor microenvironment, and in parallel they activate mast cells and myeloid-derived suppressor cell's differentiation, aiding PCCs to escape the host immunosurveillance (Ene-Obong et al., 2013; Ino et al., 2013).

This dynamic dialogue between activated PSCs and PCCs promoting PDAC spreading is notably modulated by PSC-secreted cytokines and growth factors. For instance, activated PSCs secrete hepatocyte growth factor (HGF), which binds and activates its protooncogenic tyrosine kinase c-Met receptor located at PCC's membrane, rising their proliferative, migratory, and invasive potential, as well as their apoptosis resistance (Patel et al., 2014). Another example is the secretion of the chemokine stroma derived factor-1 (SDF-1) from activated PSCs, which acts through its canonical receptor CXCR4 expressed in PCCs, participating in the evasion of gemcitabine-induced apoptosis in PCCs, further supporting their survival (Gao et al., 2010; Wei et al., 2018; Zhang et al., 2015). Indeed, gemcitabine administration is the principal conventional agent used for PDAC treatment. This mechanism was found to be mediated by the activation of ERK1/2, AKT and FAK pathways in PCCs, followed by an upregulation of IL-6 secretion from PCCs (Zhang et al., 2015). In addition to SDF-1, fibronectin release from activated PSCs has also been demonstrated to be involved in PCC's gemcitabine resistance *via* the activation of the ERK1/2 pathway. Furthermore, it has been demonstrated that PSC-induced T lymphocyte apoptosis is driven by the PSC-secreted galectin-1, a  $\beta$ -galactoside-binding protein, providing an immunosuppressive tumor microenvironment (Tang et al., 2015). Moreover, secreted proangiogenic factors from activated PSC, such as IL-8, VEGF, PDGF, FGF and periostin, have been established to stimulate endothelial cells' growth and thus angiogenesis (Erkan et al., 2009; Xu et al., 2010). Periostin has also been established to participate in the augmentation of PCC's chemoresistance and in the enhancement of their metastatic capacity through the ERK/c-Myc and EGF receptor/AKT pathways (Fukushima et al., 2008). Other studies have reported an important role of PSC-secreted IL-6 in the transformation of non-invasive PanIN cells into invasive PCCs through the activation of the STAT3 (Signal Transducer and Activator of Transcription 3) signalling pathway, indicating that activated PSCs trigger PDAC genesis even from the early precursor stage (Mace et al., 2013). Another report highlighting the involvement of PSCs from the very early stage of PDAC development, has demonstrated that inhibition of PSC-secreted COX-2 declines the progression of non-invasive PanINs lesions to neoplastic lesions, in a mouse model of PDAC (Yoshida et al., 2005, 2004).

However, the interaction between activated PSCs and PCCs is bidirectional, and therefore PCCs also influence PSC's behaviour (Apte et al., 2015; Bachem et al., 2005). Indeed, PCC-secreted cytokines increase PSC's proliferation, migration, ECM and MMP synthesis, and their inflammatory profile, hence promoting and sustaining PSC's activation (Apte et al., 2012,

1999; Ferdek and Jakubowska, 2017; Jaster and Emmrich, 2008). For instance, PCC-secreted PDGF and COX-2 stimulate PSC's proliferation, whereas PCC-secreted TGF- $\beta$ 1 and FGF stimulate PSC-induced ECM production and secretion (Bachem et al., 2005; Königer et al., 2004; Tjomsland et al., 2016; Vonlaufen et al., 2008a). Moreover, PSC's proliferation and MMP expression has been found to increase from the precancerous stage, as shown by PSC's exposure to conditioned medium from PanINs cells (Pandol et al., 2012).

Within sight of activated PSC's primordial role in PDAC genesis and the exacerbation of pancreatic fibrosis, or so-called desmoplastic reaction in PDAC, a stromal activity index has been developed as a prognostic tool for PDAC severity reflected by PSC's activation, and thus the grade of fibrotic process activity. This stromal activity index is defined by the ratio of  $\alpha$ SMA expression to the density of type I collagen deposition. Therefore, a high stromal activity index is associated with a weaker patient prognosis (Erkan et al., 2008).

All these properties and potentials defined activated PSCs not only as pro-fibrogenic cells implicated in pancreatic stroma development but as multifunctional cells, indispensable for CP and PDAC development, progression, and aggressiveness (**Figure 12**).

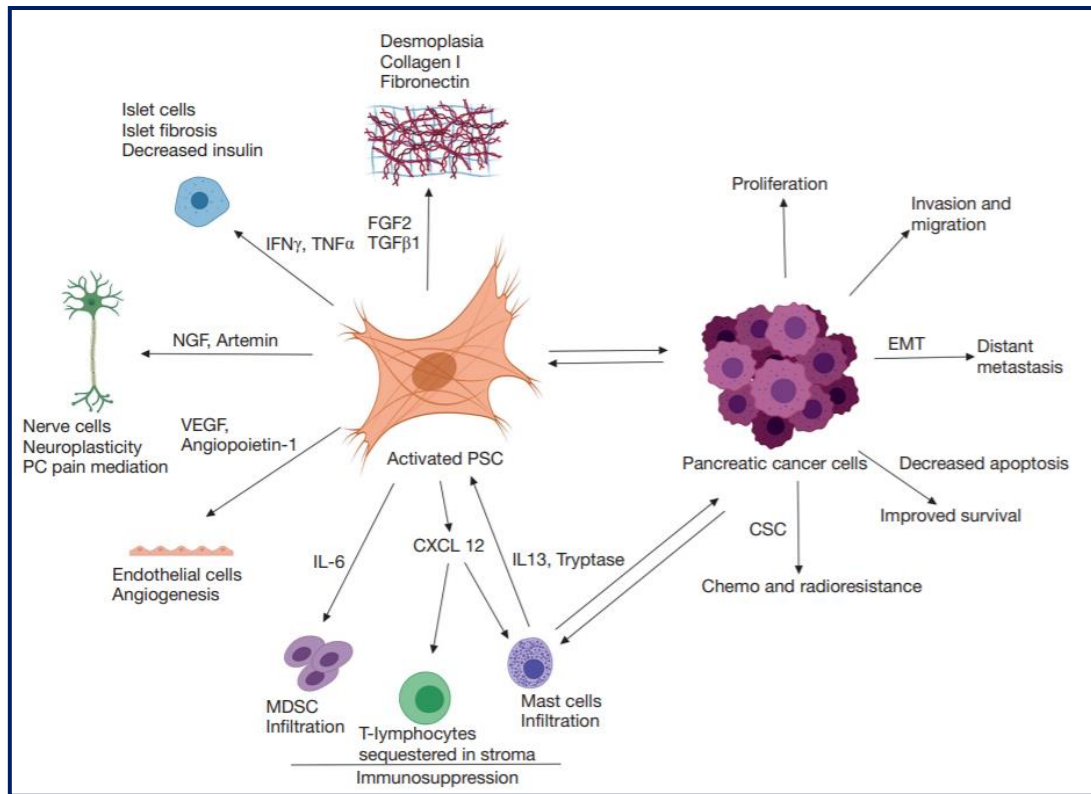


**Figure 12:** Brief illustration of activated PSC’s crucial role in the development and progression of PDAC. Indeed once activated, PSCs communicate tightly with the pancreatic cancer cells (PCCs) through the secretion of various cytokines and growth factors leading among others to the promotion of PCCs’ proliferation, migration, invasion but also chemo- and radioresistance. In turn, PCCs stimulate/exacerbate PSCs’ activation promoting their proliferative, migratory, and secretory abilities, and notable the secretion of type I collagen and fibronectin. Moreover, activated PSCs participate in PDAC development and progression through their communication with the nerve cells, the endothelia cells and the immune cells *via* the secretion of neurotrophic factors (e.g., NGF), angiogenic factors (e.g., VEGF) and cytokines (e.g., IL-6), respectively. CSC: cancer stem cells; CXCL: chemotactic chemokine ligand; CXCR: chemotactic chemokine receptor; EMT: epithelial mesenchymal transition; FGF: fibroblast growth factor;  $IFN\gamma$ : interferon gamma, IL: interleukin, NGF: nerve growth factor, MDSC: myeloid derived suppressor cells,  $TGF\beta$ : transforming growth factor beta;  $TNF\alpha$ : tumor necrosis factor alpha; VEGF: vascular endothelial growth factor (Mekapogu et al., 2019).



## **CHAPTER 4: Functional features of activated PSCs: focus on cell proliferation and cytokine secretion**

### **I. Cell proliferation**

One of the main functional characteristics of activated PSCs is their enhanced capacity to proliferate. However, a disruption of the balance between cell proliferation and cell death leads to tissue homeostasis interruption, causing different pathologies, including fibrosis and cancer (Feitelson et al., 2015; Fukumoto et al., 2019; Johnson and DiPietro, 2013). Therefore, together with the ECM remodelling, the high proliferative potential of PSCs could partially explain why once activated, PSCs lose their ability to maintain pancreatic tissue homeostasis.

Cell proliferation is defined as the process leading to the generation of an increased number of cells, through the ability of a mother cell to divide into two daughter cells under the tight control of cell cycle. This latter is composed of four major distinct phases, namely G1, S, G2 and M phase. G1 phase, also called first gap phase, corresponds to the most important phase of the cell cycle, since during this step a cell undergo G1/S checkpoint, which determines whether the cell will continue or exit from the cell cycle (Norbury and Nurse, 1992). During G1 phase, the cell prepares its entry to the S phase, increasing its size, becoming metabolically active, and replicating its centrosomes. However, if the cell is not ready to proceed to the S phase, either it rests in G1 until it passes the restriction point, known also as G1/S checkpoint, either it exits the cell cycle entering in the G0 resting phase. Once the G1/S checkpoint is passed, extracellular signals, such as mitogenic factors are no longer necessary for stimulating the cell cycle progression, and thus proliferation (Pardee, 1974). The cell then enters the S phase where it completes the centrosome replication started during G1 phase, playing a role in DNA separation during the M phase, and synthesizes and replicates its DNA to give 4N chromosomes at the end of the phase. Afterwards, the cell moves to the G2 phase or in other words second gap phase, where it continues to grow synthesizing proteins and organelles, preparing its division in the M phase. Actually, the G2 phase contains the second checkpoint of the cell cycle, named G2/M DNA damage checkpoint, assuring that the entirety of the cell DNA has been properly replicated without any damages, before permitting the cell mitosis. These three phases constitute the interphase, where the cell pass the most time of the cell cycle, undergoing controls and reparations before entering in the last phase, named M phase. During this highly regulated phase, also called mitosis, the cell divides its duplicated DNA and cytoplasm to produce two daughter cells containing the same genetic material as their mother cell (Novák et al., 2003).

For a proper cell division, five types of checkpoints have been described to occur during the cell cycle progression (Barnum and O'Connell, 2014). A checkpoint controlling the cell size, arising at the first and second gap phase (G1 and G2), ensuring an adequate cell growth indispensable for regulation of the genetic and nutrient distribution. A checkpoint monitoring DNA replication during the S phase, followed by a DNA damage responses checkpoint occurring during the G2/M transition, verifying, and repairing any detected DNA lesions. Additionally, a S-M dependency checkpoint arises repairing post-replication errors that have not been corrected by the previous checkpoints, assuring that mitosis is not initiated until the DNA is correctly and completely replicated. Last, a mitotic spindle checkpoint takes place during mitosis checking that each chromosome is properly attached to the spindle before permitting the separation of the duplicated chromosomes (Barnum and O'Connell, 2014). However, if the detected damages and errors during the cell cycle progression are irreparable, the cell undergo a programmed cell death, most of the times through the apoptosis pathway.

### **I.1) Cyclin and Cyclin-Dependent Kinases (CDKs)**

In addition to the checkpoints, there are two groups of intracellular regulatory molecules that either promote either interrupt cell cycle progression. The cyclins and cyclin-dependent kinases are the molecules responsible for the cell progression through the checkpoints. Indeed, the CDKs are part of the serine/threonine kinase family, forming complexes with their regulatory cyclin subunit to become activated. Among the 21 identified CDKs within the human genome, the most related to the cell cycle regulation are CDK1-6. The CDKs are constitutively expressed but their activation depends on the availability of their binding regulatory cyclin subunit, and also on the induced phosphorylation of the cyclin/CDK complex in response to mitogenic stimuli (Malumbres, 2014; Whittaker et al., 2017). Therefore, the first CDKs involved in the cell cycle progression after mitogenic stimulation occurring in G1 phase are the CDK4 and CDK6, which bind to cyclin D forming the cyclin D/CDK4/6 complex, inducing the phosphorylation of the tumor suppression protein retinoblastoma (pRb). Indeed, in resting/quiescent cells pRb is found in its dephosphorylated state, associated to the E2F (Eucaryotic Elongation Factor 2) transcription factor, blocking E2F translocation to the nucleus and thus its transcriptional activity (Duronio and Xiong, 2013). Consequently, pRb phosphorylation by the cyclin D/CDK4/6 complex induces the dissociation of the pRb-E2F complex, promoting E2F nuclear translocation and gene transcription indispensable for the

G1/S transition, including genes encoding for cyclin E. In turn, pRb is further phosphorylated by the cyclin E/CDK2 complex occurring during the G1/S checkpoint. However, a dysregulation of this restriction checkpoint results to developmental and pathological disorders due to the uncontrolled cell division, including fibrosis and cancer. Furthermore, E2F also stimulates the transcription of genes encoding for cyclin A, which accumulates during S phase binding to the CDK2, whereas it binds to CDK1 during the S/G2 transition. During G2 phase, cyclin B mRNA and protein levels increase, which allows CDK1 binding to cyclin B, stimulating the expression of genes implicated in mitosis progression preparing the M phase and thus promoting the G2/M transition (Malumbres, 2014; Whittaker et al., 2017) (**Figure 13, Figure 14**).

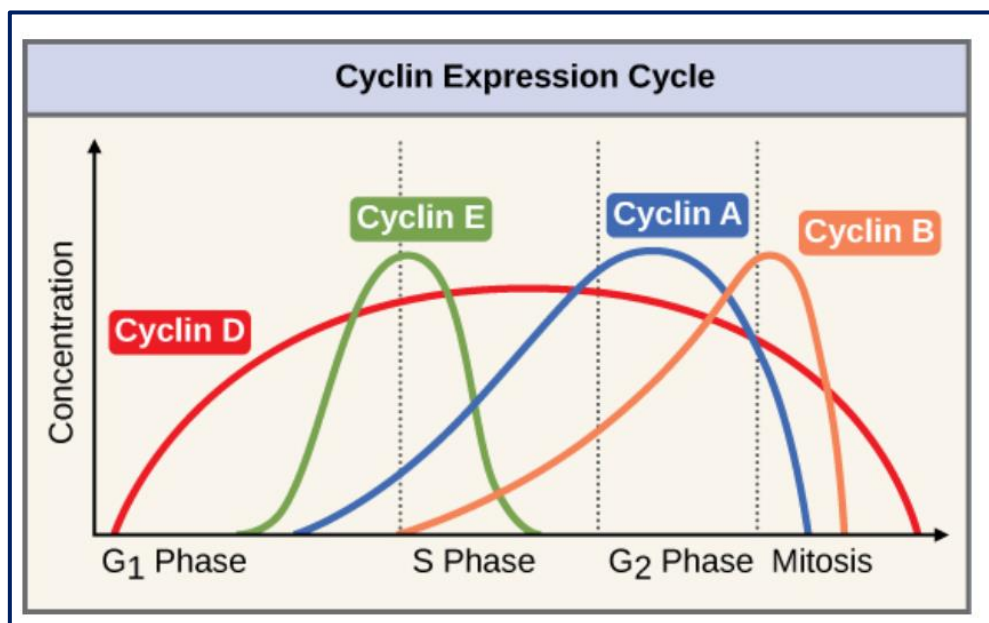


**Figure 13:** Variation of cyclins’ expression according to their role and implication in the cell cycle phases (“Cell Cycle Checkpoints | Biology for Majors I,” n.d.).

## I.2) Cyclin-Dependent Kinase Inhibitors (CKIs)

Besides the cyclin/CDK complexes responsible for the promotion of cell cycle progression, molecules preventing cell division until problematic conditions are resolved, also play an essential role. These molecules, called cyclin-dependent kinase inhibitors (CKI) block cell cycle progression principally in G<sub>1</sub> phase reducing the activity of the cyclin/CDK complexes. They intervene among others in response to cellular stress, absence of growth

factors, DNA mutations or to stimulate the cell differentiation, limiting an aberrant cell proliferation. CKIs are divided into two main families, containing the CDK4/6 inhibitor proteins (INK4) and the CDK-interacting protein/kinase inhibitory proteins (CIP/KIPs). The INK4 family is constituted by p16<sup>INK4a</sup>, p15<sup>INK4b</sup>, p18<sup>INK4c</sup> and p19<sup>INK4d</sup>, occurring during the G1 phase (Cánepa et al., 2007; Malumbres and Barbacid, 2009). The CIP/KIP family is composed of p21<sup>CIP1</sup>, p27<sup>KIP1</sup> and p52<sup>KIP2</sup>, negatively regulating cyclin E/CDK2, cyclin A/CDK2, cyclin A/CDK1 and cyclin B/CDK1 complexes, and thus participating in all four cell cycle phases (Harper et al., 1993; Sherr and Roberts, 1995; Xiong et al., 1993). On the other side, these proteins positively modulate the cyclin D/CDK4/6 complex, promoting cell cycle progression in the early G1 phase (Malumbres and Barbacid, 2009) (**Figure 14**).

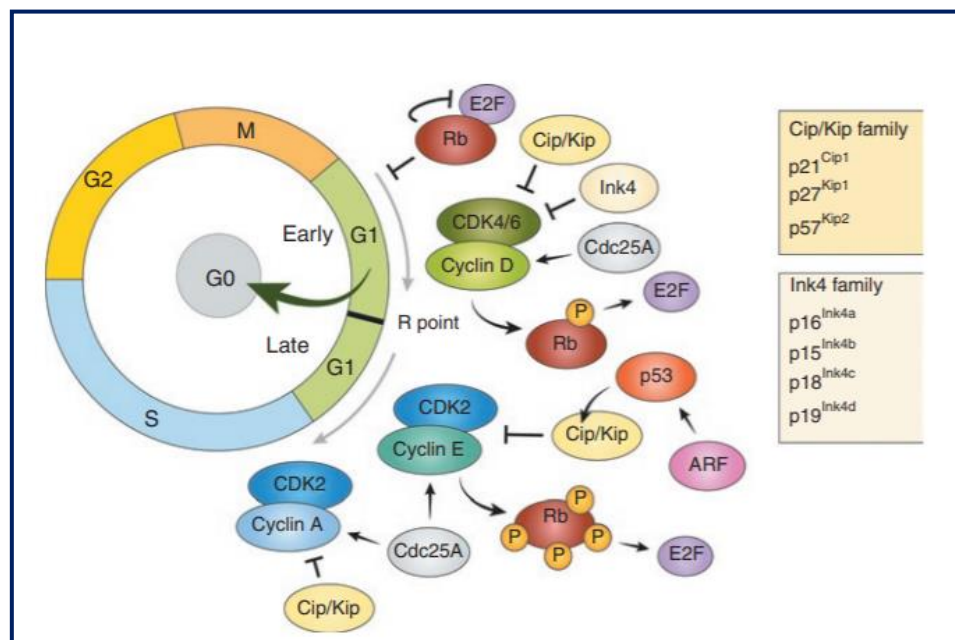


**Figure 14:** Summary of cyclin/cyclin-dependent kinases (CDK) and cyclin dependent kinase inhibitors (CKI) involvement during the cell cycle progression (Strauss et al., 2012).

## II. Cell survival

Tissue homeostasis is not only relying on an adequate controlled proliferation but also on a proper cell death permitting to eliminate old and dysfunctional or harmed cells. In general, there are three major types of cell death: apoptosis (type I), autophagy (type II) and necrosis (type III). Apoptosis and autophagy are considered as programmed cell deaths whereas necrosis is a sudden non-programmed cell death. Among these types of cell death, apoptosis has been linked to the development of various pathologies. Indeed, resistance to apoptosis has been found to

exacerbate the severity of the fibrotic outcomes (Johnson and DiPietro, 2013; Kisseleva and Brenner, 2008) and to promote cancer development and progression (Cory and Adams, 2002; Hamacher et al., 2008).

## **II.1) Apoptosis**

Under physiological conditions, apoptosis is a finely controlled process, responsible for the elimination of mutated, damaged, or useless cells, occurring during embryogenesis and in any other step of human's life. This genetically programmed cell death is characterized by an exposure of phosphatidylserine to the outer layer of the plasma membrane, a diminution of the cellular volume caused by nucleus and chromatin's condensation but also to membrane's blebbing, followed by a nuclear fragmentation and DNA cleavage by caspases. Moreover, during apoptosis, cytochrome C is released from mitochondria in the cytoplasm where it activates caspases. This is due to a perturbation of the mitochondrial membrane reflected by depolarization of the mitochondrial potential and consequently permeabilization of the mitochondrial membrane with opening of the mitochondrial permeability transition pore (MPTP). Together these events induce cell fragmentation into several apoptotic bodies, which will be then eliminated by macrophages (Jin and El-Deiry, 2005; Kroemer et al., 2009; Wyllie et al., 1984).

Apoptosis activation can be induced through two different pathways, an intrinsic pathway, and an extrinsic pathway (Fulda and Debatin, 2006). Both pathways activate proteins basically not functional, namely initiator caspases 8 and 9, which act as precursors for the effector caspases 3,6 and 7, leading to the cleavage of target proteins such as proteins of the Bcl2 family or even cell cycle regulators like p21, p27 or Rb, and thus inducing apoptotic cell death (Jin and El-Deiry, 2005).

## **II.2) Intrinsic apoptosis pathway**

The intrinsic or also known as mitochondrial pathway is triggered mainly by the mitochondria in response to death stimuli, such as oxidative stress (ROS), ER stress and DNA damage. These death stimuli induce a depolarization of the mitochondrial potential resulting to MPTP opening which leads to the release of pro-apoptotic proteins like cytochrome C, pro-caspase 9 and Apaf-1 (apoptotic protease activating factor-1) from the mitochondrial

intermembrane space into the cytoplasm (Kwong and Molkenin, 2015; Li and Yuan, 2008). Once in the cytoplasm cytochrome C and Apaf-1 interact forming a complex called “apoptosome” which induces the cleavage of the inactive pro-caspase 9 to active caspase 9, cleaving and activating in turn the effector pro-caspases 3 and 7. In addition, MPTP opening releases also pro-apoptotic and anti-apoptotic proteins of the Bcl-2 family sharing Bcl-2 homology domains, shown to regulate apoptosome’s formation. The pro-apoptotic proteins include the Bax, BID and Bak proteins, while the anti-apoptotic proteins contain the Bcl-2, Bcl-xl and Mcl-1 proteins (Hengartner, 2000; Jin and El-Deiry, 2005; Suhaili et al., 2017). Pro-apoptotic proteins like Bax are recruited at the outer mitochondrial membrane promoting cytochrome C release in the cytoplasm, whereas anti-apoptotic proteins such as Bcl-2 block Bax inhibiting the mitochondrial permeabilization (Crompton, 2000; Wei et al., 2001). Consequently, apoptosis depends on the ratio between pro- and anti-apoptotic protein expression since high expression of Bax promotes apoptosis, while elevated expression of Bcl-2 prevents apoptosis (**Figure 15**).

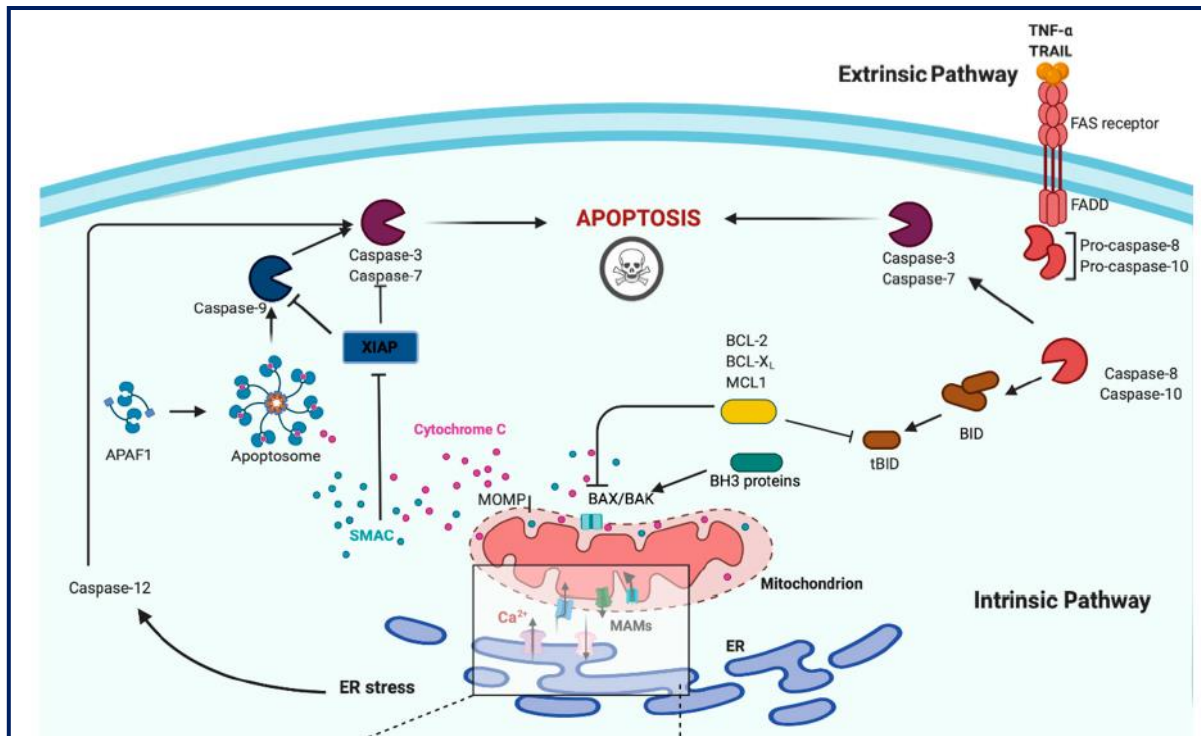


**Figure 15:** Representation of the two principal apoptotic pathways, including the intrinsic or mitochondrial pathway and the extrinsic pathway (Patergnani et al., 2020).

### II.3) Extrinsic apoptosis pathway

The extrinsic pathway mediates apoptosis through the activation of specific death receptors belonging to the TNFR (tumor necrosis factor receptor) family, carrying the death signal inside the cell. The TNFR family is composed of the TNFR1 and TNFR2 receptors which are activated after binding of TNF- $\alpha$ , of the Fas receptors, activated after FasL binding, and of the TRAIL (TNF-related apoptosis-inducing ligand) receptors, activated after TRAIL binding. Once the receptor is activated, adaptor proteins such as FADD (Fas-associated death domain) and TRADD (TNF receptor-associated death domain) are recruited from the receptor activating the initiator caspases 8 which in turn will activate the effector caspases 3,6 and 7 by cleavage. Moreover, caspase 8 is able to active by cleavage the BID factor, a pro-apoptotic Bcl-2 protein that once activated interacts with Bax, another protein of Bcl-2 family permitting its translocation from the cytoplasm to the outer mitochondrial membrane where it triggers the intrinsic apoptosis pathway (Ashkenazi, 2008; Li et al., 1998). Therefore, the extrinsic apoptosis pathway can also induce the activation of the intrinsic apoptosis pathway (**Figure 15**).

### **III. TGF- $\beta$ 1 secretion**

#### **III.1) TGF- $\beta$ 1 signalling in CP and PDAC**

The most potent fibrogenic cytokine known to be involved in PSC's activation and PSC-induced fibrosis and pancreatic tumorigenesis and desmoplasia is the transforming growth factor- $\beta$ 1 (TGF- $\beta$ 1) (Kim et al., 2018; Kulkarni et al., 2011; Eric Schneider et al., 2001).

##### **III.1.1) Importance of TGF- $\beta$ 1 in pancreatic desmoplasia and cancer**

TGF $\beta$  mammalian family is composed of three different isoforms, TGF- $\beta$ 1, - $\beta$ 2, and - $\beta$ 3, sharing 75% sequence homology and structural similarity (Wakefield and Hill, 2013). Amongst these, TGF- $\beta$ 1 has been found to be the most abundantly expressed and secreted isoform, controlling a plethora of cellular processes, including cell proliferation, protein expression, biosynthesis, and turnover of the ECM, as well as apoptosis (Massagué, 2012). Most importantly, TGF- $\beta$ 1 signalling has been shown to be a critical regulator of pancreatic fibrosis development and PDAC evolution, acting as a linking factor in PSC-PCC crosstalk (Löhr et al., 2001; Satoh et al., 1998).

##### **III.1.2) TGF- $\beta$ 1-induced pancreatic desmoplasia**

TGF- $\beta$ 1-induced fibrotic processes are well demonstrated now to be mainly targeted by the activated PSCs within the pancreatic tumor microenvironment (Pickup et al., 2013). This is due to the potential of TGF- $\beta$ 1 to transform the quiescent PSCs into activate PSCs, principally by inducing an increase of  $\alpha$ SMA expression. After TGF- $\beta$ 1 stimulation, activated PSCs strengthen their ability to synthesize all ECM important proteins, especially type I collagen, fibronectin, and proteoglycans, conferring a strong rigidity to the tumour stroma (Lee et al., 1995; Shek et al., 2002). For example, in cultured PSCs, TGF- $\beta$ 1 exposure augmented up to 10-fold fibronectin gene expression and up to 8-fold its protein secretion. Whereas Vogelmann *et al.* have found that TGF- $\beta$ 1 overexpressing transgenic mice present morphological features of chronic pancreatitis, the major precursor of PDAC, since the 14<sup>th</sup> day after birth, developing a pancreatic fibrous tissue mainly composed of PSC-induced type I collagen (Vogelmann et al., 2001). At the same time, TGF- $\beta$ 1-induced PSC's fibrosis inhibits ECM degradation by decreasing the expression and secretion of MMPs, particularly of MMP1, MMP3 and MMP9 (Tjomsland et al., 2016). Moreover, TGF- $\beta$ 1-mediated pancreatic fibrosis downregulates



MMPs by inhibiting their enzymatic activity through TIMPs' expression and secretion, leading to the regulation of ECM turnover. Furthermore, TGF- $\beta$ 1 is involved in the enhancement of PSC's proliferation through the stimulation of mitogenic factors' expression and secretion, such as PDGF (Masamune et al., 2003). However, where TGF- $\beta$ 1 has a significant direct effect on the promotion of PSC's proliferation still an unresolved issue, contrarily to hepatic stellate cells, the counterparts of PSCs, where it clearly increases their cell proliferation (Shen et al., 2003).

Once activated, in turn, PSCs trigger TGF- $\beta$ 1 synthesis and secretion, creating an autocrine stimulatory feedback loop to sustain their activation but also to perpetuate TGF- $\beta$ 1-induced ECM deposition (Apte et al., 1999; Kruse et al., 2000). This vicious cycle between TGF- $\beta$ 1-mediated PSC's activation and PSC-induced TGF- $\beta$ 1 secretion exacerbates the desmoplastic reaction, responsible for the formation of the dense fibrotic tissue. These mechanisms could partially explain the elevated mRNA and protein levels of TGF- $\beta$ 1, observed during PDAC, notably in the fibrotic areas. In addition, high TGF- $\beta$ 1 expression has been associated to a poorer patient's survival and spreading of PCCs (Park et al., 2019).

### **III.1.3) TGF- $\beta$ 1-mediated PDAC progression**

PCCs express and secrete high amounts of TGF- $\beta$ 1, and this overexpression becomes strongest in the most advanced stages of PDAC. Therefore, chronic elevated PCC-derived TGF- $\beta$ 1 expression correlates with tumor progression, aggressiveness, and poorer prognosis (Friess et al., 1993; Javle et al., 2014). In contrast, it has been shown that low circulating levels of TGF- $\beta$ 1 extend patient's survival. The tumorigenic effect of TGF- $\beta$ 1 results from TGF- $\beta$ 1-enhanced PCC proliferation, migration, invasion, and survival, particularly during later stages of PDAC (Glazer et al., 2017; Gupta and Maitra, 2016). Moreover, PCC-induced TGF- $\beta$ 1 overexpression stimulates the production of other mitogenic growth signals, including PDGF, and FGF, leading to further promotion of tumorigenesis and progression. Additionally, it promotes the EMT of PCC, occurring to enhanced PCC's migratory ability (Morrison et al., 2013). In cooperation with the high PSC-derived TGF- $\beta$ 1, it participates to the exacerbation of PDAC development through the excessive PSC/TGF- $\beta$ 1-induced ECM deposition and tissue fibrosis, the perpetuation of immune and inflammatory functions, and the increased chemoresistance (Löhr et al., 2001).

However, TGF- $\beta$ 1 has a dichotomous effect on pancreatic tumour initiation and progression. In non-neoplastic epithelial cells and in the earliest stages of PDAC, TGF- $\beta$ 1 acts

as a tumour growth suppressor *via* the inhibition of cellular proliferation. Whereas, during PDAC progression, it becomes a tumour growth promoter by stimulating PCCs oncogenic properties, including PCC proliferation and inducing EMT (Ellenrieder et al., 2001). The complexity and dual role of TGF- $\beta$ 1 vary regarding the tumour microenvironment, PSC-PCCs crosstalk, and PCCs behaviour. Hence, the multiple aberrations of TGF- $\beta$ 1 signalling observed in PCCs, could partially explain why TGF- $\beta$ 1 loses its anti-tumoral and antiproliferative properties during pancreatic tumorigenesis. Indeed, several mutations of the TGF- $\beta$ 1 transduction pathway have been identified in PDAC. The most well-characterized detected mutation is the loss of *SMAD4*, one of the downstream effectors of TGF- $\beta$ 1 signalling cascade, shown to be deleted in at least 50% of PDAC, and thus leading to TGF- $\beta$ 1-diminished inhibition of cell cycle progression (Fan et al., 2016). It has been established that *SMAD4* can be either homozygously deleted or inactivated by an allelic loss of counterparts in PDAC (Cicenas et al., 2017). Besides, *SMAD4* gene alteration, mutations in the gene of type I and type II TGF $\beta$ 1 receptors have also been found, most of which are frameshift resulting in the production of a truncated protein with absented intracellular and transmembrane domains, observed in approximately 5% of cases (Subramanian et al., 2004; Wagner et al., 1998). Therefore, the suppressed TGF- $\beta$ 1 capacities to decrease tumour cell growth and proliferation are due on the one hand, to disruptions of its own transduction signalling pathway, and on the other hand, to TGF- $\beta$ 1 ability to promote PCC-secreted mitogenic factors and so PCC proliferation. However, it is still less elicited where TGF- $\beta$ 1 can directly promote PCCs as well as activated PSCs proliferation.

### **III.2) TGF- $\beta$ 1 mechanism in the control of cell proliferation**

To date, the molecular mechanisms driving the proliferative potential of TGF- $\beta$ 1 remain less defined than those leading to cytostasis. TGF- $\beta$ 1 exerts its antiproliferative effect principally through two sets of mechanisms, involving stimulation of cyclin-dependent kinase inhibitors and eliminating growth-promoting transcription factors during cell cycle progression. This latter is composed mainly of four distinct phases, including G1 phase, DNA synthesis corresponding to S phase, G2 phase, and cell division controlled by M phase. The cell cycle process from G1 to S phase is controlled by the activation of cyclin-dependent kinases (CDKs), including CDK2, 4 and 6, and cyclins, as cyclin D and E. CDK2 needs to bind cyclin E to

phosphorylate its substrates, while CDK4 or CDK6 binds to cyclin D, permitting the G1/S transition. Nevertheless, CDK inhibitors disrupt CDK-cyclin complexes resulting in a cell cycle arrest in G1 phase. TGF- $\beta$ 1 interferes in cell cycle arrest blocking G1/S transition by inducing the expression of p15, p21, and p27- CDK inhibitors. Additionally, TGF- $\beta$ 1 can also augment p27 activity without modifying its expression, in part because TGF- $\beta$ 1-increased p15 disrupts the existing p27-CDK4/6-cyclin D complex, releasing p27. Indeed, p27 is inactive within the p27-CDK4/6-cyclin D complex, but when it is released, it binds to the CDK2-cyclin E complex inhibiting its activity. Furthermore, TGF- $\beta$ 1 can also directly suppress the expression of mitogenic transcriptional factors, particularly of c-myc, and cell differentiation inhibitors, as Id1, 2 and 3. It is known that c-myc promotes cell growth and proliferation by its binding to the promoters of CDK inhibitors, e.g., p15 and p21, blocking thus their activation. Therefore, TGF- $\beta$ 1-induced c-myc downregulation prevents cells from entering a growth-promoting state. The Id1 cell differentiation suppressor decreases p21 expression and simultaneously increases the inactivation of the retinoblastoma protein through its phosphorylation, abolishing the repression CDK2-cyclin E activity, which is inverse by TGF- $\beta$ 1 stimulation. Besides these mechanisms, TGF- $\beta$ 1 represses the expression and activity of the CDK tyrosine phosphatase Cdc25A, involved in promoting G1/S and G2/M transitions. Hence, all these multiple TGF- $\beta$ 1-induced mechanisms are due to TGF- $\beta$ 1's ability to activate distinct downstream signalling pathways (Kim et al., 2018b; Morikawa et al., 2016; Truty and Urrutia, 2007; Zhang et al., 2017).

### **III.3) TGF- $\beta$ 1 canonical signalling pathway**

The classic signalling pathway of TGF- $\beta$ 1, or so-called TGF- $\beta$ 1 canonical signalling pathway, consists of TGF- $\beta$ 1 assembling into specific functional ligand-receptor complexes. Initially, latent circulating TGF- $\beta$ 1 undergo proteolytic cleavage and dissociation to become activated and form a TGF- $\beta$ 1 dimer complex to bind the type II TGF- $\beta$ 1 receptor (TGFRII) homodimer. The association of TGF- $\beta$ 1 to TGFRII allows the recruitment of type I TGF- $\beta$ 1 receptor (TGFRI) dimer. Both TGFs are cell surface receptors possessing an intracellular serine/threonine kinase activity, and the TGFRII-induced phosphorylation of TGFRI on multiple serine residues in its glycine-serine domain leads to its activation. Moreover, TGF- $\beta$ 1 possesses a high affinity for TGFRII and cannot bind to isolated TGFRI. Thus, a functional, active signalling complex requires an activated TGF- $\beta$ 1 dimer ligand associated with two TGFRI and

two TGFRII, forming a heterotetrameric complex. After that, the active complex phosphorylates specific SMAD transcription factors playing a pivotal role in TGF- $\beta$ 1-related signal transduction to modulate the transcription of defined genes. The SMADs family is classified into three functional groups: the receptor-regulated Smad (R-Smad) (Wu et al., 2001), the common-mediator Smad (Co-SMAD) (Shi et al., 1997), and the inhibitory Smad (I-Smad) (Itoh et al., 2001). The activated TGFRI specifically phosphorylates the R-Smads (especially Smads-2 and -3), which then oligomerize with the Co-Smad, Smad4 to form a functional transcriptional complex, and subsequently, translocate to the nucleus where it regulates the transcription of the target genes. In activated PSCs, phosphorylated Smad2 and Smad3 combine with Smad4, forming a dynamic complex that enters PSC's nucleus, inducing the transcription of type I collagen and fibronectin through its interaction with coactivators and/or corepressors, and thus promoting PSC-induced desmoplasia in PDAC. However, the last category of Smads, the I-Smads (Smad 7), acts as an attenuator of inhibitor of TGF- $\beta$ 1 signalling. Indeed, TGF- $\beta$ 1 stimulation results in Smad7 translocates from the nucleus to the plasma membrane, where it directly binds to TGFRI, competing with Smad2/Smad3 resulting in the inhibition of TGFRI-induced phosphorylation, and so to the association with Smad4. Under transient TGF- $\beta$ 1 stimulation, Smad7 undergoes ubiquitination to be degraded, ending hence the negative feedback loop, but the continued TGF- $\beta$ 1 stimulation will further activate Smad7 preventing its degradation (Finsson et al., 2020; Liu et al., 2018; Truty and Urrutia, 2007).

Furthermore, TGF- $\beta$ 1/Smad canonical signalling pathway has been demonstrated to play a predominant role in PDAC development and progression. David *et al.* have established that PDAC cell phenotypes depend on the presence of Smad4 factor (David et al., 2016). They have shown from the one side that Smad4-positive PCCs expressing Smad2/3/4 complex promotes the EMT by the TGF- $\beta$ 1/Smad-mediated EMT-associated transcription factors, such as Snail. On the other side, Smad4-positive PCCs repress Krüppel-like transcription factor 5 (KLF5), known to promote the activation of Smad2/3 pathway resulting in tumor progression. Additionally, in the absence of KLF5, the same Smad2/3 pathway drives PCC's apoptosis preventing tumour development (He et al., 2018).

Moreover, in transgenic mutant *Kras*-driven PDAC mouse models, loss of Smad4 by homozygous or heterozygous gene deletion was correlated with a more aggressive tumour phenotype. Taken together, these findings suggest that SMAD4 negatively controls PCC's behaviour at the late stages of PDAC, thus limiting PDAC's progression (Leung et al., 2013).

In accordance with these data, it has been demonstrated that reduced levels of TGFRII also led to a more aggressive form of PDAC (Lu et al., 1997).

However, TGF- $\beta$ 1/Smad signalling influences activated PSC's behaviour as well. Contrary to PCCs, Smad4 positively regulates activated PSCs by initiating the transcription of the plasminogen activator inhibitor 1 (PAI-1), leading to the production of ECM proteins. It has also been illustrated that the I-Smad7 plays an inhibitory role in PSC's activation by its association to TGFRI, and subsequently blocking the phosphorylation of Smad2/3 and TGF- $\beta$ 1 signal translocation to the nucleus, preventing PSC's activation (Lee et al., 2008; Qian et al., 2010). This factor can also decrease the TGF- $\beta$ 1-mediated overexpression of TIMPs, abolishing TGF- $\beta$ 1/PSC-induced type I collagen synthesis and ECM deposition (He et al., 2009). Nevertheless, Smad7 mRNA expression has been shown to be decreased by angiotensin II through the protein kinase C pathways, promoting TGF- $\beta$ 1-mediated PSC proliferation (Hama et al., 2006).

#### **III.4) TGF- $\beta$ 1 non-canonical signalling pathways**

Although TGF- $\beta$ 1 canonical transduction pathway through the activated TGF- $\beta$ 1/TGFRII/TGFRI complex and the transcription factors Smad2/3/4 has received the most attention, this activated complex can also lead to activation of Smad-independent, non-canonical pathways. Activation of these TGF- $\beta$ 1 non-canonical pathways can induce stand-alone signalling responses but can also directly or indirectly synergize or antagonize with the Smad canonical pathway and broaden the diversity of TGF- $\beta$ 1 signalling responses. Among them, MAPK, especially ERK1/2 and PI3K/AKT pathways, have been shown to play a critical role in pancreatic fibrosis and cancer development (Finsson et al., 2020; Zhang, 2017, 2009).

##### **III.4.1) ERK1/2 pathway**

Initially, TGF- $\beta$ 1 has been thought to activate ERK1/2 pathway through the observed rapid TGF- $\beta$ 1-induced activation of Ras GTPase, leading to the recruitment of Raf kinase to the plasma membrane, and therefore to the activation of ERK1/2 through MEK1/2. ERK1/2 phosphorylation requires activation of receptor tyrosine kinases RTK, which, once activated by their binding growth factors (e.g., EGF), recruits the Grb2/Sos complex bringing Sos to the plasma membrane. Growth factor receptor-binding protein 2 (Grb2) is a docking adaptor

protein that binds to the guanine nucleotide exchange factor Sos, which becomes activated by phosphorylated RTK, and in its turn, it activates Ras leading to GDP-GTP exchanges. The Grb2/Sos complex binds to the phosphorylated tyrosine residues of RTK either through the SH2 domain of Grb2 either through the RTK-phosphorylated Shc (Src homology domain 2 containing) adaptor protein, permitting Ras binding to Raf, which then initiates the MAPK/ERK1/2 cascade. Moreover, TGFRI and TGFRII can also phosphorylate Shc directly and recruit the Shc/Grb2/Sos complex or indirectly after Src phosphorylation (proto-oncogene tyrosine-protein kinase Src), respectively, resulting in sequential activation of Ras/Raf/MEK/ERK cascade. TGFRII and TGFRI can undergo autophosphorylation on tyrosine residues at a much lower level than serine/threonine autophosphorylation. Hence, TGF- $\beta$ 1 is involved in ERK1/2 non-Smad signalling pathway through the tyrosine phosphorylation of Shc, even though it has been established that TGF- $\beta$ 1-induced ERK1/2 phosphorylation kinetic vary according to the cell type and context. Indeed, TGF- $\beta$ 1 stimulation can rapidly activate ERK1/2 within 5-10 min, a time frame comparable to ERK1/2 phosphorylation by mitogenic growth factors, such as EGF, suggesting a direct TGF- $\beta$ 1-induced mechanism. However, it can also induce a delayed ERK1/2 response, with ERK1/2 phosphorylation peak occurring hours after TGF- $\beta$ 1 stimulation, involving an indirect TGF- $\beta$ 1-mediated mechanism. The direct and indirect TGF- $\beta$ 1-mediated ERK1/2 phosphorylation mechanisms remain to be elucidated.

In turn, ERK1/2 can directly phosphorylate Smad2 and Smad3 occurring to their inhibition, partially explaining how the oncogenic Ras overrides TGF- $\beta$ 1-mediated growth arrest in cancer cells, including PCCs. Furthermore, ERK1/2 modulates TGF- $\beta$ 1-induced biological functions *via* the phosphorylation of its substrates, as AP-1 (activator protein-1) or p53 (tumor protein 53) transcription factors, which interact and cooperate with Smads factors to regulate gene's expression (Truty and Urrutia, 2007; Zhang, 2017, 2009) (**Figure 16**).

These mechanisms could explain how TGF- $\beta$ 1-induced ERK1/2 activation promotes TGF- $\beta$ 1-mediated EMT and thus tumor growth in the late stages of pancreatic tumorigenesis. Besides, TGF- $\beta$ 1-mediated PCC's adherens junction disassembly and PCCs motility require ERK1/2 phosphorylation. Therefore, TGF- $\beta$ 1-induced Shc-Grb2 activation of ERK1/2 is a crucial component for TGF- $\beta$ 1 pro-oncogenic activity, enhancing PCC's migration and invasion.

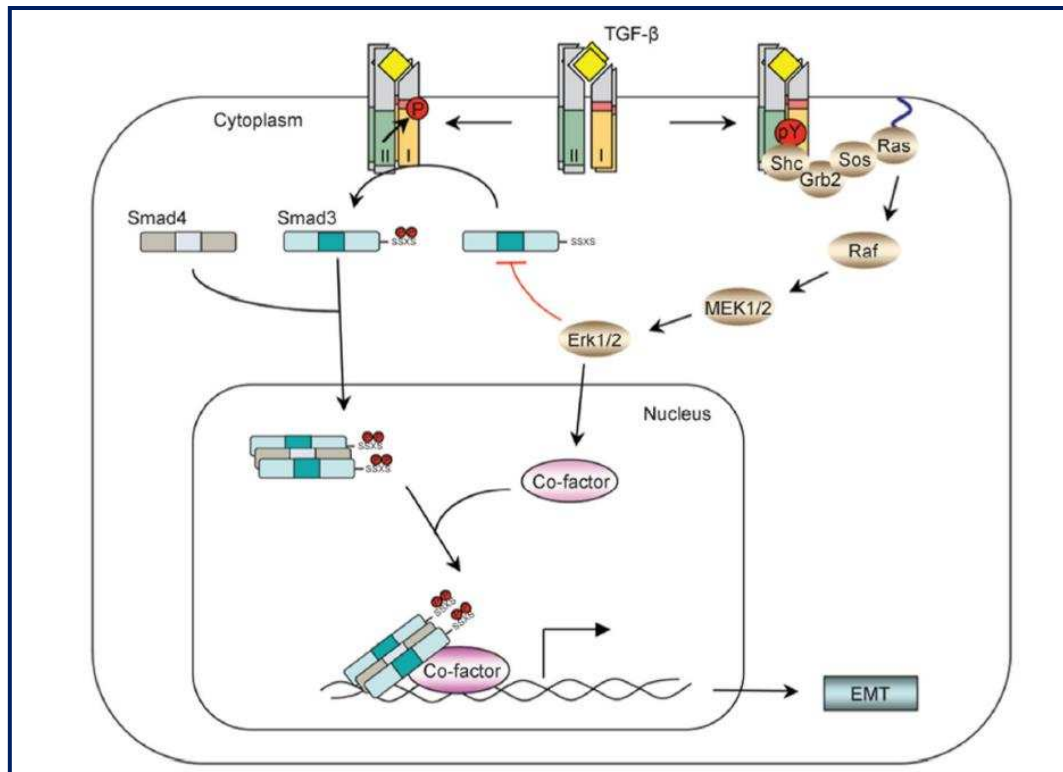


**Figure 16:** Illustration of TGF- $\beta$ 1-mediated ERK1/2 non-canonical signalling pathway (Zhang, 2009).

### III.4.2) PI3K/AKT pathway

Besides ERK1/2, TGF- $\beta$ 1 activates PI3K/AKT non-canonical pathway through both Smad-dependent and Smad-independent mechanisms. The TGF- $\beta$ 1-Smad2/3 independent-induced PI3K/AKT activation necessitates the kinases activities of TGFRI and TGFRII, which were found to be indirectly associated with the p85 regulatory subunit of PI3K. This latter was reported to be constitutively associated with TGFRII while requires TGF- $\beta$ 1 stimulation to bind TGFRI. Additionally, TGF- $\beta$ 1 is able to directly activate PI3K, by the phosphorylation of its downstream effector AKT, and indirectly through TGF- $\alpha$  expression and subsequently EGF receptor signalling activation. Moreover, TGF- $\beta$ 1 induces activation of an AKT downstream effector, the mammalian target of rapamycin (mTOR) which phosphorylates the S6 kinase (S6K) and the eukaryotic initiation factor 4E-binding protein 1 (4E-BP1) to regulate proteins' synthesis involved in TGF- $\beta$ 1-induced EMT of PCCs. Supplementary to this effect, TGF- $\beta$ 1 activates the mTOR complex 2 (mTORC2), enhancing cytoskeletal reorganization, RhoA (Ras homologous protein A) activation, and cell migration. In turn, the activated mTORC2 promotes

AKT activation at a late stage of TGF- $\beta$ 1-induced EMT of PCCs. Conversely, TGF- $\beta$ 1-Smad dependent pathway leads to PI3K/AKT signalling downregulation by expressing the phosphoinositide lipid phosphatase SHIP.

On the other hand, activated AKT can antagonize Smad-mediated effects, as reported by the direct physical interaction between AKT and Smad3. The formation of this complex prevents TGFRI-induced Smad3 phosphorylation and nuclear translocation and hence protects cells from TGF- $\beta$ 1-Smad induced growth inhibition and apoptosis. Besides its association with Smad3, AKT can abolish TGF- $\beta$ 1-Smad mediated growth inhibition *via* the phosphorylation of forkhead transcription factor (FoxO). Indeed, FoxO has been demonstrated to form a complex with Smad3 and Smad4, indispensable for TGF- $\beta$ 1-mediated p21 and p15 CDK inhibitors expression, leading to cytostasis in G1 phase. However, FoxO phosphorylation by AKT suppresses its activity by inhibiting FoxO translocation to the nucleus and thereby preventing FoxO/Smad3/Smad4 complex formation (**Figure 17**). This mechanism suggests that the ratio of activated Smads and activated Akt determines whether within the same cell type, TGF- $\beta$ 1 stimulation will promote cell proliferation, cell-cycle arrest, or apoptosis, partially explaining the dual role of TGF- $\beta$ 1 during pancreatic tumorigenesis. All these pieces of evidence indicate a crucial role of PI3K/AKT non-canonical pathway, not only in TGF- $\beta$ 1-mediated EMT of PCCs but also in TGF- $\beta$ 1-induced cytoskeleton reorganization and cell migration of PCCs. Furthermore, the cooperation between TGF- $\beta$ 1-mediated Smad canonical pathway and TGF- $\beta$ 1-induced AKT non-canonical pathway defines PCC's behaviour leading either to their growth inhibition or promotion. However, although PI3K/AKT pathway is known to play an essential role in TGF- $\beta$ 1-mediated fibroblast proliferation and morphological transformation to myofibroblast, to date, there is no clear evidence of its role in PSC's activation and proliferation (Finsson et al., 2020; Kim et al., 2018b; Morikawa et al., 2016; Truty and Urrutia, 2007; Zhang et al., 2017; Zhang, 2017, 2009).



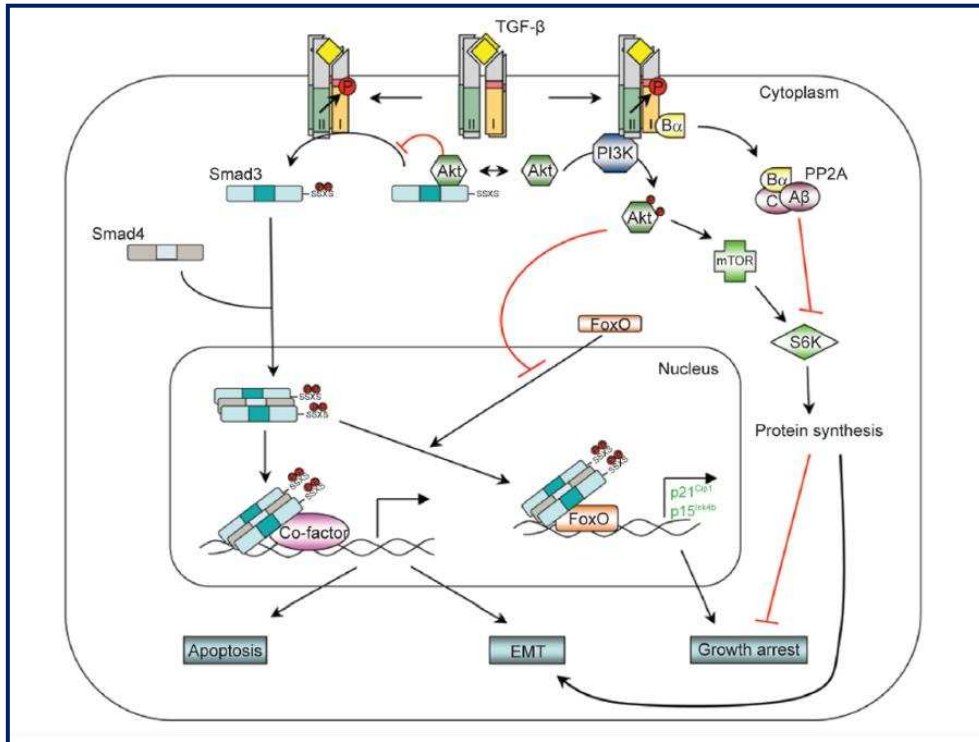


**Figure 17:** Illustration of TGF- $\beta$ 1-mediated PI3K/AKT non-canonical signalling pathway (Zhang, 2009).

Due to TGF- $\beta$ 1's signalling complexity, the autocrine and paracrine mechanisms by which TGF- $\beta$ 1 regulates PCCs and PSCs, promoting PDAC and desmoplasia progression, require further studies to define the most effective way to target TGF- $\beta$ 1 or its downstream effectors therapeutically. However, several strategies have already been employed to block TGF- $\beta$ 1 signalling pathways in fibrosis. These ones consist of using molecules that inhibit the activation of latent TGF- $\beta$ 1, neutralizing anti-TGF- $\beta$ 1 antibodies, antisense oligonucleotides directed against TGF- $\beta$ 1, decorin, which is an ECM protein blocking TGF- $\beta$ 1 signalling, adenoviral expressed Smad7, and soluble TGFRII. Unfortunately, the dual role of TGF- $\beta$ 1 during pancreatic tumorigenesis and its unclear yet role in PSC's proliferation requires more caution in using these strategies, highlighting the necessity to better understand the involved molecular mechanism.

## CHAPTER 5: Ca<sup>2+</sup> signalling

### I. Ca<sup>2+</sup> signalling and Ca<sup>2+</sup> ion channels

Ca<sup>2+</sup> is one of the most abundant ions in our body, acting as a universal versatile intracellular second messenger involved in the regulation of various signalling pathways controlling diverse physiological processes including cell proliferation, cell death, gene expression, protein secretion, cellular metabolism and so on (Berridge et al., 1998; Carafoli et al., 2001; Giorgi et al., 2012; Roderick and Cook, 2008). To coordinate all these processes, Ca<sup>2+</sup> functions through a Ca<sup>2+</sup> signalling toolkit permitting to amplify and regulate Ca<sup>2+</sup> signals in terms of space, time, frequency, and amplitude, representing together what we call the Ca<sup>2+</sup> signature (Berridge et al., 1998).

Under resting physiological conditions in eukaryotic cells, the intracellular free Ca<sup>2+</sup> concentration is approximately 100 nM, whereas the extracellular Ca<sup>2+</sup> concentration is higher, varying between 1 and 2 mM (Berridge, 2003; Petersen, 2002). To maintain this cellular Ca<sup>2+</sup> homeostasis, the cell uses two sources to control the intracellular Ca<sup>2+</sup> concentrations. It either uses the extracellular Ca<sup>2+</sup> which enters the cell through different Ca<sup>2+</sup> channels and/or transporters present at the plasma membrane, either utilizes the stored intracellular Ca<sup>2+</sup> which is released from the organelles, particularly from the ER, the Golgi apparatus, or mitochondria. However, in response to external or internal stimuli, the intracellular Ca<sup>2+</sup> concentration is modified by Ca<sup>2+</sup>-induced influx through the plasma membrane Ca<sup>2+</sup> channels and transporters, or through a Ca<sup>2+</sup> store released mechanism. This modification results to an increase of the intracellular Ca<sup>2+</sup> concentration, indispensable for the regulation of Ca<sup>2+</sup>-mediated cellular processes either inducing their activation or inhibition (Clapham, 2007; Parkash and Asotra, 2010). However, to preserve cell's Ca<sup>2+</sup> physiological concentration, the Ca<sup>2+</sup> augmentation is counteracted by Ca<sup>2+</sup> outflux *via* Ca<sup>2+</sup> exchangers, Ca<sup>2+</sup> ATPase pumps or Ca<sup>2+</sup>-buffering proteins.

A sustained increase of intracellular Ca<sup>2+</sup> concentration or alteration of Ca<sup>2+</sup> signature can be lethal for the cell or cause carcinogenesis. To avoid this cellular fate, Ca<sup>2+</sup> signals are often delivered as brief transients illustrated by Ca<sup>2+</sup> spikes, or even with low signal amplitude. In addition, when the activation or inhibition of a cellular process requires a longer period of Ca<sup>2+</sup> signals transmission, then repetitive Ca<sup>2+</sup> signals occur reflected by Ca<sup>2+</sup> oscillations having a different frequency or duration according to the cellular process (Dolmetsch et al., 1997; Pande et al., 1996; Porter et al., 1998; Stewart et al., 2015). For instance, spontaneous Ca<sup>2+</sup> oscillations

are essential for the cell cycle progression, during the G1/S and G2/M phase transition, promoting the activation of transcription factors such as activator protein 1 or the nuclear factor of activated T-cell (NFAT) (Patergnani et al., 2020; Rao, 2009). Nevertheless, the regulation of  $\text{Ca}^{2+}$  signals is much more complex than that and necessity a coordinated  $\text{Ca}^{2+}$  signalling toolkit, ensuring adequate  $\text{Ca}^{2+}$  signal management. An escapement of  $\text{Ca}^{2+}$  signals' regulation provoking an alteration of the  $\text{Ca}^{2+}$  signature due most of the times to an aberrant expression or function of at least one component of the  $\text{Ca}^{2+}$  signalling toolkit causes various pathologies including fibrosis and cancer (Marchi and Pinton, 2016; Prevarskaya et al., 2014; Radoslavova et al., 2020).

### **I.1) Principal membrane proteins regulating $\text{Ca}^{2+}$ homeostasis**

Intracellular  $\text{Ca}^{2+}$  homeostasis is maintained and regulated by  $\text{Ca}^{2+}$  permeable channels, pumps, exchangers, and transporters, located at the plasma membrane or at the ER and mitochondrial membrane, mediating either the  $\text{Ca}^{2+}$  influx either the  $\text{Ca}^{2+}$  outflow. Among these  $\text{Ca}^{2+}$  regulators, the most important are described below (**Figure 18**).

#### **I.1.1) Plasma membrane $\text{Ca}^{2+}$ regulators**

##### **➤ PMCA (Plasma Membrane $\text{Ca}^{2+}$ ATPase) pumps**

PMCA pumps function with the energy obtained from ATP (adenosine triphosphate) hydrolysis, extruding  $\text{Ca}^{2+}$  from the cell, against its electrochemical gradient, and therefore permitting to restore the physiological intracellular  $\text{Ca}^{2+}$  concentration. Indeed, for each ATP hydrolysed molecule one  $\text{Ca}^{2+}$  ion is transported into the extracellular milieu. In mammalian cells, there are 4 isoforms of PMCA, namely PMCA1-4, with PMCA1 and 4 to be ubiquitously expressed, whereas PMCA2 and 3 are more specifically expressed. Structurally, these pumps are constituted of 10 transmembrane segments, cytoplasmic N- and C- terminal regions and two large cytoplasmic loops. These latter contain binding sites for ATP, as well as acidic phospholipid binding domain (PL) and calmodulin binding domain (CaMBD) (Bobe et al., 2005; Strehler et al., 2007; Strehler and Zacharias, 2001).

### ➤ **Na<sup>+</sup>/ Ca<sup>2+</sup> exchangers (NCX)**

NCX exchangers are antiporter membrane proteins, which using the energy of Na<sup>+</sup> electrochemical gradient permit to export one Ca<sup>2+</sup> ion outside the cell in exchange of 3 Na<sup>+</sup> that are imported inside the cell, rapidly decreasing the intracellular Ca<sup>2+</sup> concentration. In contrast to PMCAs, they have a lower affinity for Ca<sup>2+</sup> and when the intracellular Na<sup>+</sup> concentration increases they switch their activity driving Na<sup>+</sup> flow outside the cell and hence allowing Ca<sup>2+</sup> entry in the cell. These exchangers are ubiquitously expressed but more abundantly expressed in the cardiac and neural cells and exist in three isoforms (Beaugé and DiPolo, 2005; Blaustein and Lederer, 1999; Carafoli et al., 2001, 1999; Philipson and Nicoll, 2000).

### ➤ **Ca<sup>2+</sup> channels**

There are two main types of Ca<sup>2+</sup> plasma membrane channels, the voltage-dependent Ca<sup>2+</sup> channels (VDCCs), which are activated by the membrane potential depolarization and the voltage-independent Ca<sup>2+</sup> channels. The VDCCs or also known as voltage-gated Ca<sup>2+</sup> channels (VGCCs) are classified in two categories based on their threshold of activation (Simms and Zamponi, 2014), including the low voltage-activated channels (LVA) and the high voltage-activated channels (HVA). The LVA channels are activated following small depolarizations of approximately -60 mV, while HVA need increased depolarizations to become activated, superior of -30 mV (Ertel et al., 2000; Simms and Zamponi, 2014). On the other side, the voltage-independent Ca<sup>2+</sup> channels can be activated by neurotransmitters or hormone agonist such as acetylcholine or glutamate constituting the ROCs (Receptor-Operated Channels), or by intracellular second messenger like diacylglycerol or arachidonic acid composing the SMOCs (Second Messenger-Operated Channels). Other voltage-independent Ca<sup>2+</sup> channels can be activated by the depletion of ER Ca<sup>2+</sup> stores, which once released it generates Ca<sup>2+</sup>-release activated Ca<sup>2+</sup> currents (CRAC) through the SOCs (Store-Operated Channels) (McFadzean and Gibson, 2002; Parekh and Putney, 2005; Tsien and Tsien, 1990). Among these channels, SOCs represent one of the major Ca<sup>2+</sup> entry pathways in non-excitabile cells and therefore are so far the best studied in the field of cancer.

## **I.1.2) ER membrane Ca<sup>2+</sup> regulators**

### **➤ SERCA (Sarco-Endoplasmic Reticulum Calcium ATPase) pumps**

SERCA pumps are transporting Ca<sup>2+</sup> ions against their electrochemical gradient from the cytoplasm into the ER, through ATP hydrolysis. For each hydrolysed ATP molecule, 2 Ca<sup>2+</sup> ions enter into the ER lumen, permitting to fill the ER stores in Ca<sup>2+</sup>. They thus belong to the ATPase family, located at the ER membrane, and encoded by 3 different genes (*SERCA1-3*), each of which produces various isoforms. Moreover, these pumps have been shown to be irreversibly inhibited by Thapsigargin, which is widely used in experimental protocols in order to induce a depletion of the ER Ca<sup>2+</sup> stores by blocking the refuelling of ER in Ca<sup>2+</sup> through the SERCA pumps (Lytton et al., 1991; Martonosi and Pikula, 2003; Misquitta et al., 1999).

### **➤ Inositol 1,4,5-trisphosphate receptors (IP3R)**

IP3R, contrary to SERCA pumps, are acting as Ca<sup>2+</sup> release channels, driving Ca<sup>2+</sup> influx from the ER into the cytoplasm upon inositol IP3 stimulation. Indeed, activation of the plasma membrane G protein-coupled receptors (GPCRs) after ligand binding activates the phospholipase C enzyme (PLC), which then hydrolyses PIP2 (phosphatidylinositol-4,5-bisphosphate) into DAG (diacylglycerol) and IP3. Thereafter IP3 will bind to its IP3R located at the ER triggering Ca<sup>2+</sup> release from the ER. IP3R are homotetrameric channel complexes where their C-terminal portion corresponds to the channel function domain, they are ubiquitously expressed and contain 3 isoforms (IP3R1-3) (Wright and Wojcikiewicz, 2016).

### **➤ Ryanodine receptors (RyRs)**

RyRs act like IP3R, releasing Ca<sup>2+</sup> from the ER into the cytoplasm. RyRs are homotetrameric proteins, existing in three isoforms (RyR1-3), and as their name indicates, they are sensitive and activated by ryanodine at nanomolar concentrations, while higher concentrations (>100 μM) of ryanodine have an inhibitory effect on RyRs. These receptors also contain a cytoplasmic Ca<sup>2+</sup> binding sites, which in response to low cytoplasmic Ca<sup>2+</sup> levels induce a RyR-mediated Ca<sup>2+</sup> release, whereas a rise of the intracellular cytoplasmic Ca<sup>2+</sup> concentration lead to RyR closing, preventing thus ER Ca<sup>2+</sup> store depletion (Buck et al., 1992; Fill and Copello, 2002; Lanner et al., 2010; Sárközi et al., 2017; Seidel et al., 2015).

### I.1.3) Mitochondrial membrane $\text{Ca}^{2+}$ regulators

#### ➤ Mitochondrial $\text{Ca}^{2+}$ Uniporter (MCU)

MCU represents the major  $\text{Ca}^{2+}$  regulator in mitochondria, situated at the inner mitochondrial membrane allowing  $\text{Ca}^{2+}$  uptake from the cytoplasm into the mitochondria, which is mediated by mitochondrial membrane potential. In resting cells, the mitochondrial  $\text{Ca}^{2+}$  concentration remains the same as in the cytoplasm (~100 nM), and it increases to trigger cellular biological processes like apoptosis and ATP production (Arnaudeau et al., 2001; Patron et al., 2014).

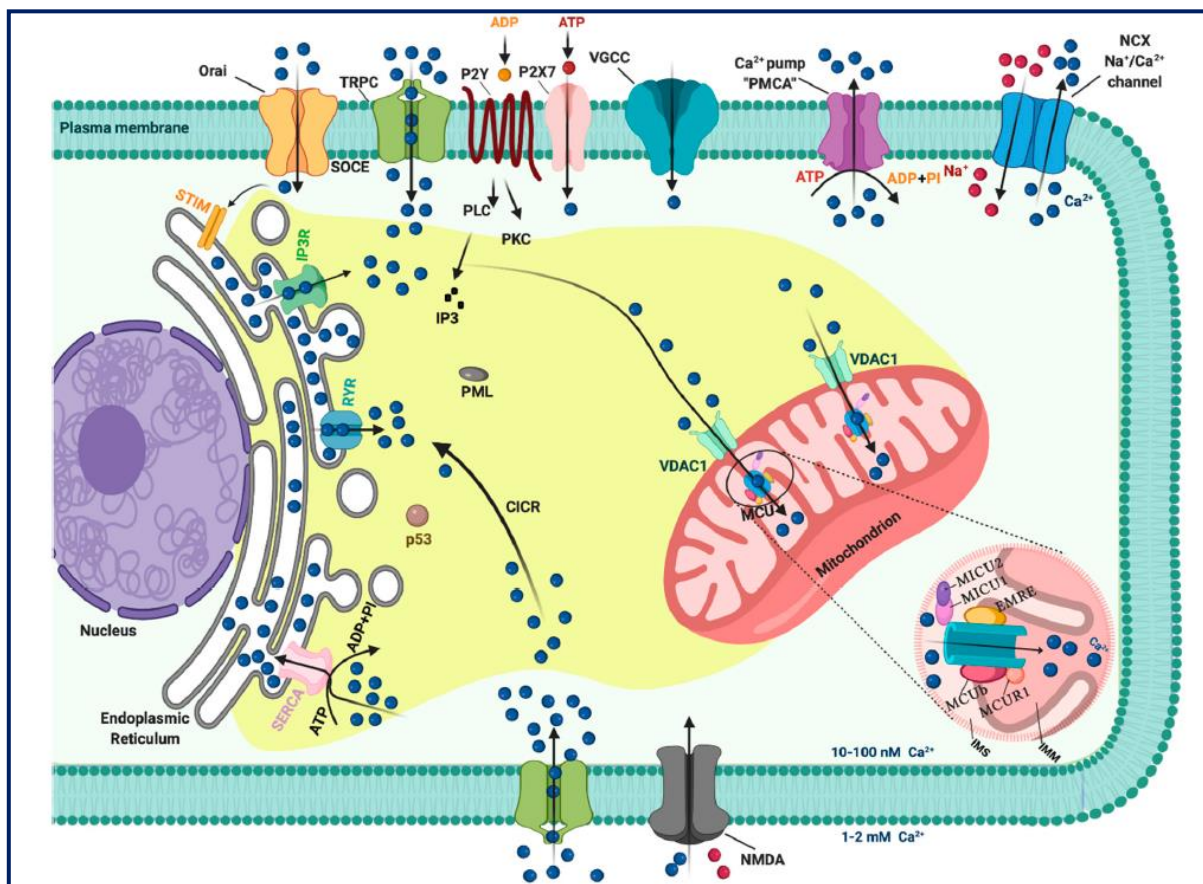


Figure 18: Illustration of  $\text{Ca}^{2+}$  signalling toolkit actors (Patergnani et al., 2020).

## **II. Store-Operated Ca<sup>2+</sup> channels (SOCs)**

One of the most common mechanisms driving Ca<sup>2+</sup> entry within the non-excitabile cells occurs after activation of the plasma membrane G protein-coupled receptors (GPCRs) which then activates the phospholipase C (PLC) enzyme. Once activated PLC cleave the phosphatidylinositol 4,5-bisphosphate (PIP<sub>2</sub>) into DAG and IP<sub>3</sub>. The produced IP<sub>3</sub> then binds to its IP<sub>3</sub>R at the ER membrane triggering Ca<sup>2+</sup> outflow from the ER to the cytoplasm. Subsequently the decreased ER Ca<sup>2+</sup> content promotes extracellular Ca<sup>2+</sup> influx through the activation of plasma membrane Ca<sup>2+</sup> channels named Store-Operated Ca<sup>2+</sup> Channels (SOCs) in a process known as Store-Operated Ca<sup>2+</sup> entry (SOCE). This latter involves principally two types of protein, the Orai proteins forming the pore of the channel and the Stim (Stromal Interaction Molecule) proteins sensing the ER Ca<sup>2+</sup> depletion (Berridge and Irvine, 1984; Prakriya and Lewis, 2015; Srikanth and Gwack, 2012).

### **II.1) Orai channels**

Orai channels are highly selective Ca<sup>2+</sup> channels, comprised of 3 Orai protein isoforms, namely Orai1, Orai2 and Orai3. The three isoforms are closely related and share sequence homologies, but they differ in their N- and C-terminal regions. Indeed, Orai1 and Orai2 share 60.3% sequence homology, while Orai1 and Orai3 share 63.2% homology, and Orai2 with Orai3 have 66.4% homology (Feske et al., 2006; Lis et al., 2007; Prakriya and Lewis, 2015). These channels have been firstly discovered in 2006 by Feske and co-workers in T lymphocytes, studying the molecular mechanisms of severe combined immunodeficiency disorder (SCID) (Feske et al., 2006). The authors have found that this genetic disorder was characterized by a dysregulation of T lymphocyte activation which was associated to a diminution of the Ca<sup>2+</sup> entry through the CRAC (Ca<sup>2+</sup> release-activated channels) due to a mutation (R91W) of Orai1 protein (Feske, 2011; Feske et al., 2006). Even though, more and more studies have started to be interested on the role and functionality of the other 2 Orai isoforms (Orai2 and Orai3), Orai1 channel remains so far, the best- and most- studied CRAC channel, shown to be one of the major SOCE actors in different cell types (Guzman et al., 2014). For these reasons, during our study, we have mostly focused on Orai1 channel.

Orai1 Ca<sup>2+</sup> channel is a protein composed of 303 amino acids, encoded by the FLJ14466, located at the chromosome 12q24, having 4 transmembrane segments, as well as cytoplasmic N- and C- terminal regions. The C-terminus contains the “coiled-coil” domain, driving the

interaction of Orai1 with its activation protein STIM, while the N-terminus contains a proline/arginine- rich domain, unlike Orai2 and Orai3, which they do not have this domain in their N-terminus (Frischauf et al., 2008; Gwack et al., 2007; McNally et al., 2009). Additionally, Orai3 presents a significantly shorter C-terminal region, compared to Orai1 and Orai2. Another particularity of Orai1 channel, compared to its two other homologues, is the possession of glycosylation sites at the asparagine residues (Asp223) (Gwack et al., 2007) and phosphorylation sites at the serine residues (Ser27-30) (Kawasaki et al., 2010). To become functional Orai1 form an homo- or hetero-tetramer complex, and recently shown also to form an homo-or hetero-hexamer complex with other Orai1 proteins or it can associate with its other two homologues, Orai2 and Orai3, participating in SOCE (Cai et al., 2016; Frischauf et al., 2008; Gwack et al., 2007) (**Figure 19**).

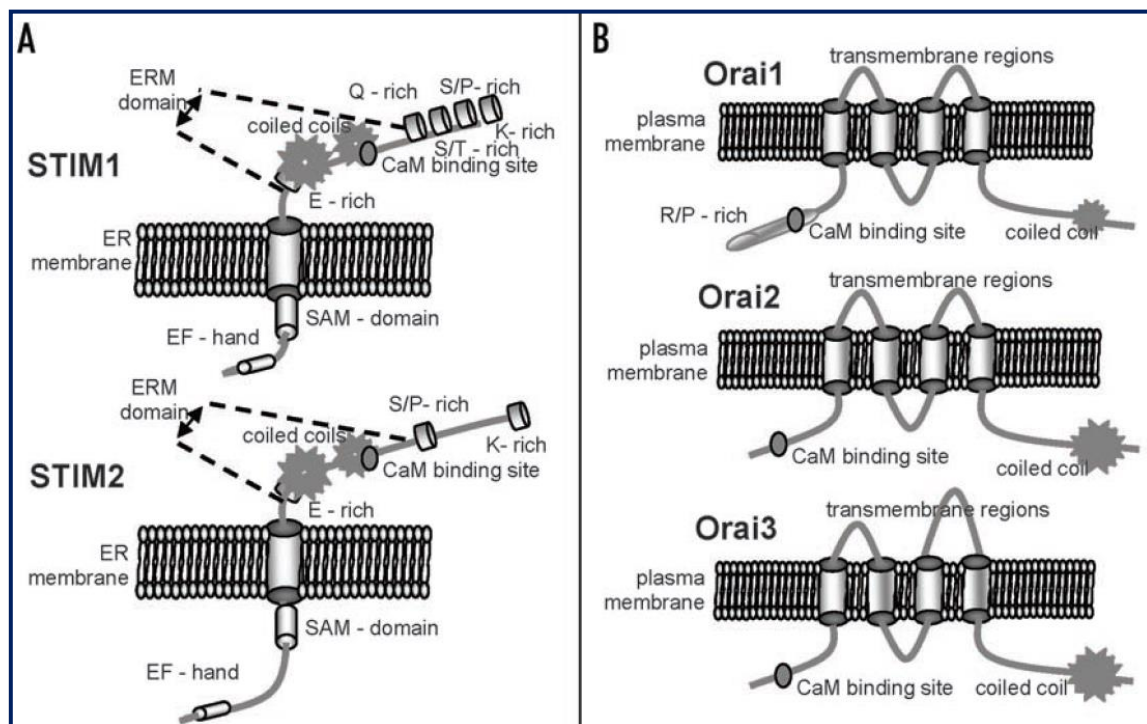


**Figure 19:** Structure of STIM proteins (STIM1, STIM2) and of the three Orai isoforms (Orai1, Orai2, Orai3) forming the Store-Operated Channels (Frischauf et al., 2008).

Orai1 channel activity was identified by their capacity to generate  $\text{Ca}^{2+}$  release-activated  $\text{Ca}^{2+}$  (CRAC) currents inducing SOCE. Orai1-mediated CRAC current is generated after ER  $\text{Ca}^{2+}$  depletion sensed by its activation protein STIM located generally at the ER membrane.



However, 15-25% of STIM proteins can also be expressed at the plasma membrane (Spassova et al., 2006; Zhang et al., 2005). These proteins are composed of a unique transmembrane domain, an intra-ER N-terminal region which contains a “EF-Hand” domain detecting the variations of the ER  $\text{Ca}^{2+}$  concentration, and a cytoplasmic C-terminal region having two “coiled-coil” domains permitting its interaction with Orai1 (Johnstone et al., 2010; Muik et al., 2008). In addition, STIM proteins include two isoforms, STIM1 and STIM2, with STIM1 and STIM1-Orai1 interaction being the best-studied hitherto and with STIM2 having two times less affinity for  $\text{Ca}^{2+}$  (Brandman et al., 2007). Indeed, ER  $\text{Ca}^{2+}$  concentration decrease induces a release of the fixed  $\text{Ca}^{2+}$  at the “EF-Hand” domain allowing STIM1 oligomerization with four STIM1 proteins through their N-terminus, forming “puncta” near to the plasma membrane (Liou et al., 2005; Luik et al., 2008). This mechanism is reversible once ER  $\text{Ca}^{2+}$  stores are refilled. The formed STIM1 “puncta” interact physically through their C-terminus with the C-terminus of Orai1, activating thus Orai1 channel, which once activated it generates CRAC current permitting  $\text{Ca}^{2+}$  ions passage through Orai1 channel and thus a  $\text{Ca}^{2+}$  influx, and all this process is called SOCE (Soboloff et al., 2006; Wang et al., 2010) (**Figure 20**). In fact, electrophysiologically, CRAC current is characterized by a high selectivity for  $\text{Ca}^{2+}$ , exhibiting an inward rectification and elevated intracellular  $\text{Ca}^{2+}$  concentration inhibit CRAC current (Li et al., 2007; Lis et al., 2007; Mercer et al., 2006). Nevertheless, it is the interaction between Orai1 and STIM1 that is the crucial element for SOCE, since the inhibition of one and/or both actors abolish SOCE, even when ER  $\text{Ca}^{2+}$  depletion occurs (Soboloff et al., 2006).

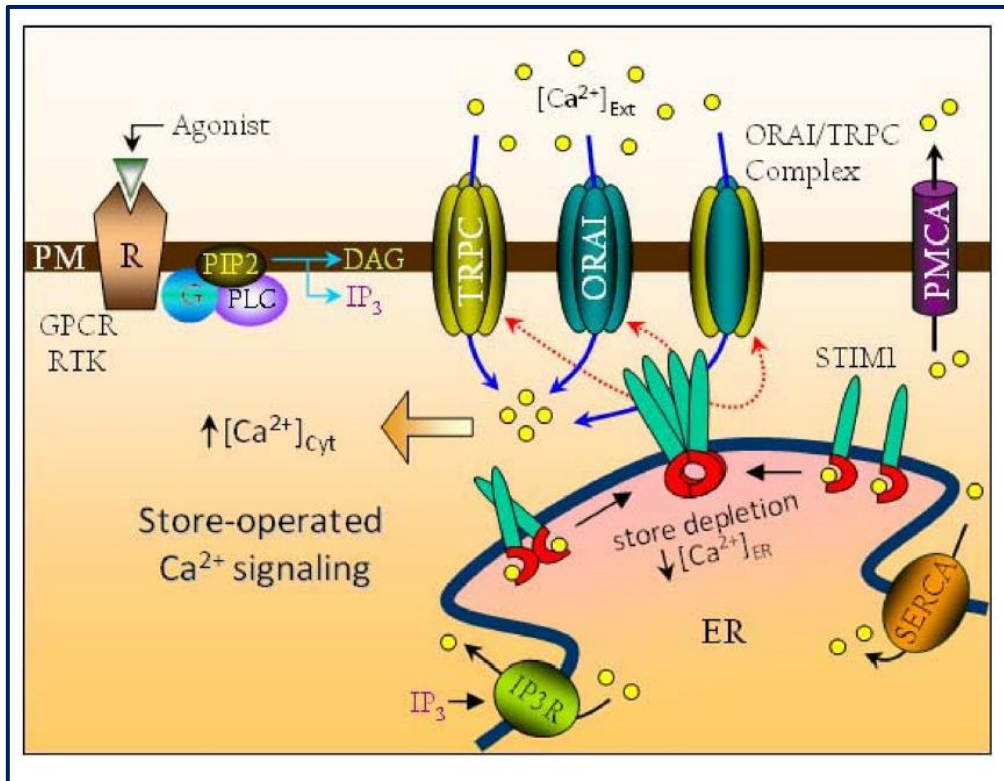


**Figure 20:** Representation of Orai1/STIM1- and TRPC1-mediated SOCE process (B et al., 2012).

Furthermore, CRAC currents have been reported to also be generated by Orai2 and Orai3, but with lower current peak, with Orai2 generating only 50% and Orai3 generating 20% of Orai1-generated CRAC current (DeHaven et al., 2007; Lis et al., 2007; Yoast et al., 2020). Indeed, studies have demonstrated that Orai2 and Orai3 can heteromerize with Orai1, regulating CRAC current generation, and consequently SOCE (Yoast et al., 2020). This interaction was supported by Gwack *et al.* work, showing a physical interaction between all three Orai isoforms by co-immunoprecipitation experiments using tagged overexpressed Orai proteins. Other studies utilizing the FRET (Fluorescence Resonance Energy Transfer) approach have shown that the physical interaction between the three Orai isoforms is not stimulated by the ER  $Ca^{2+}$  depletion (Gwack et al., 2007). Moreover, the functional involvement of Orai2 and Orai3 has been suggested measuring the SOCE of mast cells from Orai1 knockout mice, which showed only 50% reduction of SOCE, implying that the other two Orai isoforms might interfere and regulate SOCE (Vig et al., 2008). Additionally to these findings, other works have established

that when Orai1 isoform expression is altered, then the other two isoforms take over the SOCE regulation. For instance, T lymphocytes from Orai1 knockout mice expressed high Orai2 mRNA levels and presented an intact cell proliferation (Vig et al., 2008). These data indicate that Orai2 might regulate SOCE in the absence of Orai1 expression, as well as the Orai1-mediated cellular processes, acting as a negative modulator of SOCE. Conversely, Tsvilovskyy *et al.* have measured an increased SOCE in mast cells from Orai2 knockout mouse, suggesting that in the absence of Orai2, Orai1 increases its capacity to generate CRAC currents and thus SOCE (Tsvilovskyy et al., 2018). On the other side, using DNA constructs that express different combinations of Orai1/Orai3 subunits, Kappel *et al.* have showed that depending on the number and position of Orai3 units within the Orai1/Orai3 complex, CRAC current properties are not the same (Kappel et al., 2020). These few non-exhaustive cited examples, as well as other studies not mentioned here, showing the interaction between Orai1 and Orai3 or Orai2, indicate that depending on the relative expression levels of each of the three Orai isoforms, they might possess different stoichiometric properties mediating their ability to heteromerize with each other, within a specific cell type (Yoast et al., 2020) (**Figure 21**).

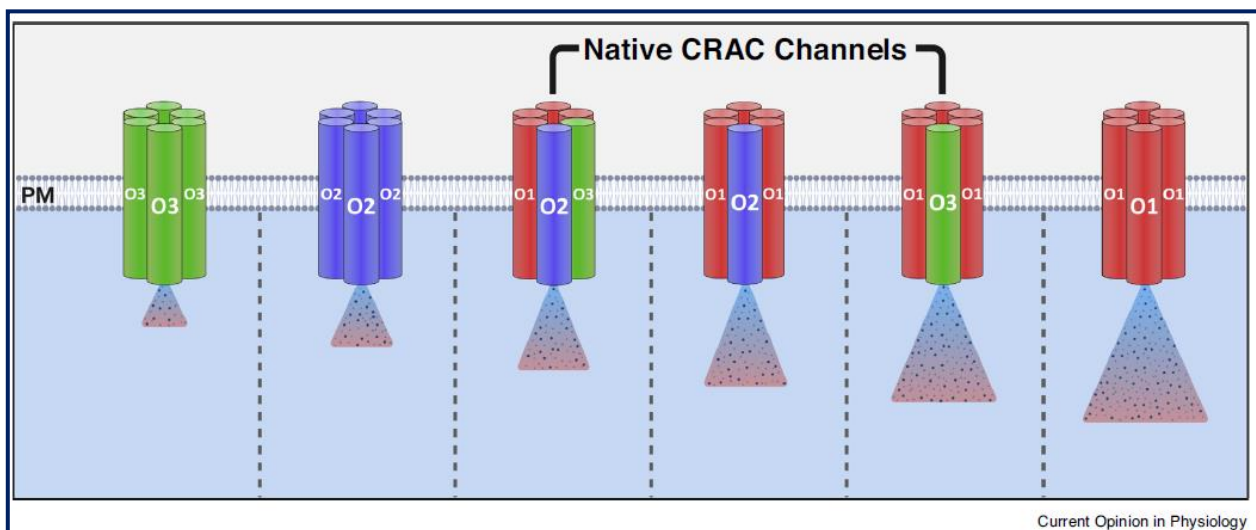


**Figure 21:** Suggested Orai isoforms homo and/or heterohexamers depending on their stoichiometry (Yoast et al., 2020).

### III. TRPC1 channels

TRPC1 channels are part of the TRP (Transient Receptor Potential) channel superfamily initially identified in drosophila (Wes et al., 1995; Zhu et al., 1995). The TRP channels contain three major subfamilies including the TRPC (canonical), TRPV (vanilloid) and TRPM (melastatin) (Ramsey et al., 2006). The TRPC subfamily is comprised of four groups depending on channel's sequence homology, including TRPC1 group, TRPC2 group, TRPC3/6/7 group, and TRPC4/5 group. Among all TRP channels, TRPC1 has been up until now the most studied (Ramsey et al., 2006).

TRPC1 channel functions as a non-selective  $\text{Ca}^{2+}$  channel, inducing  $\text{Ca}^{2+}$  and  $\text{Na}^{+}$  influx. Structurally, it is constituted of four subunits, each subunit having six transmembrane segments, and intracellular N- and C-terminal regions. The pore of the channel is found between the fifth and sixth transmembrane segment, forming a P loop, containing an extracellular putative cation selectivity filter (Beech, 2005; Dohke et al., 2004; Ramsey et al., 2006). In general, TRPC1 channel requires four proteins coming together around a central selectivity cation filter and gate, forming a homotetrameric structure. Moreover, TRPC1 can also associated with other isoforms of its subfamily, such as TRPC4 and TRPC5, constituting heterotetrameric structures (Brownlow and Sage, 2005; Goel et al., 2002; Hofmann et al., 2002; Strübing et al., 2001). In its C-terminus, TRPC1 contains a highly conserved TRP box (EWKFAR TRP box), a calmodulin (CaM) binding domain and an IP3R binding domain, while, Brazer *et al.* have identified a caveolin-1 binding domain in its N-terminus (**Figure 22**) (Boulay et al., 1999; Brazer et al., 2003; Rosado and Sage, 2000; Singh et al., 2002). In addition, TRPC1 channel has mostly been found in compartments of the plasma membrane with close apposition to the superficial ER structures (Golovina, 2005; Wang et al., 1999; Xu and Beech, 2001). Other reports have localized TRPC1 in lipid raft domains rich in cholesterol, suggesting a role of TRPC1 in the regulation of lipid rafts' integrity and phosphatidylserine transmembrane distribution (Bergdahl et al., 2003; Brownlow et al., 2004; Kunzelmann-Marche et al., 2002; Lockwich et al., 2000). However, TRPC1 can also be found in intracellular membranes, such as in the membrane of ER or Golgi apparatus (Chen and Barritt, 2003; Goel et al., 2006, 2002; Uehara, 2005; Wang et al., 1999).

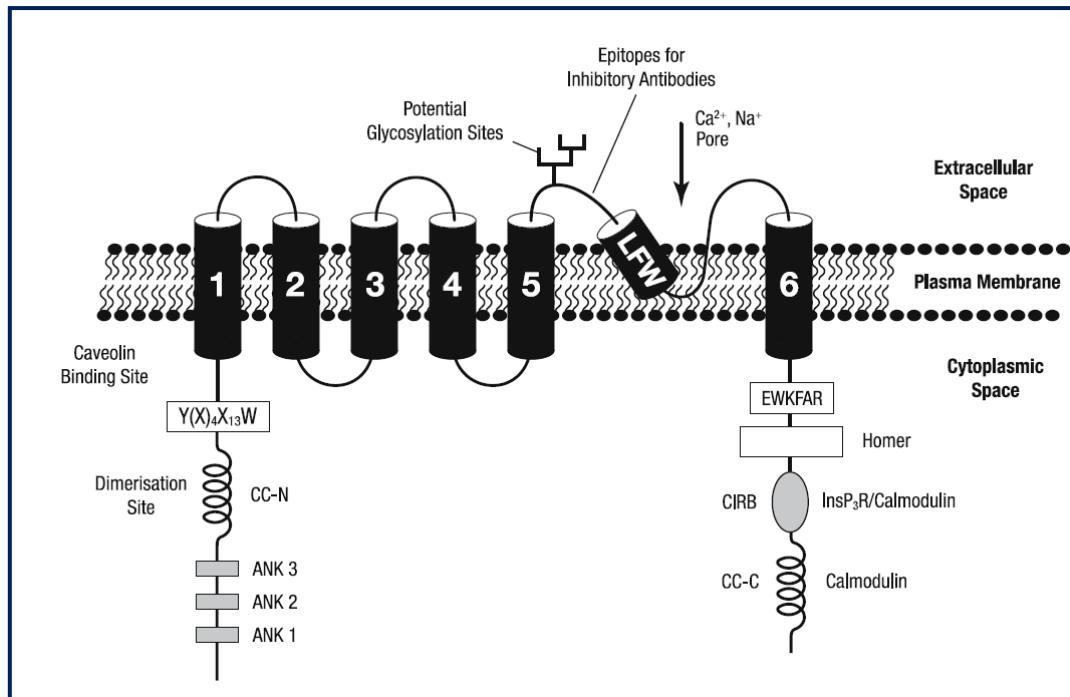


**Figure 22:** TRPC1 channel structure (Rychkov and Barritt, 2007).

Functionally, TRPC1 has been proposed to be involved in two  $\text{Ca}^{2+}$  entry mechanisms, either through a TRPC1-related SOCE mechanism either through a mechanical stretch-induced TRPC1 activation mechanism triggering a  $\text{Ca}^{2+}$  influx. Therefore, TRPC1 can act both as SOCE-mediated channel and as a mechanosensitive channel, even though its dual functional role remains debated (Dietrich et al., 2014; Rychkov and Barritt, 2007).

So far, the most attention has been given to TRPC1 involvement in SOCE. Liu *et al.* have reported that TRPC1 silencing decreased SOCE in human salivary gland cells, suggesting a contribution of TRPC1 in this process (Liu et al., 2003). Additionally, Worley *et al.* have established an interaction between TRPC1 and STIM1 following ER  $\text{Ca}^{2+}$  depletion (Lee et al., 2014; Shi et al., 2017; Worley et al., 2007; Yuan et al., 2007), while Cheng *et al.* have demonstrated that Orai1 through SOCE-generated  $\text{Ca}^{2+}$  signals mediates TRPC1 activation and its interaction with STIM1 in human salivary gland cells (Cheng et al., 2011). Other reports have also established an interaction of TRPC1 with the IP3R after ER  $\text{Ca}^{2+}$  depletion (Lockwich et al., 2000; Rosado et al., 2002; Rosado and Sage, 2001, 2000). In addition to this finding, Yuan *et al.* have reported that indeed TRPC1-IP3R association is prior to ER  $\text{Ca}^{2+}$  depletion, and that the interaction between these two actors is mediated by the homer adaptor protein

(Yuan et al., 2003). Furthermore, it has been established that as for Orai1-STIM1-mediated SOCE, high intracellular  $\text{Ca}^{2+}$  concentration inactivates TRPC1 channel through a mechanism involving CaM, as shown using the CaM inhibitor calmidazolium (Rosado et al., 2002; Singh et al., 2002; Tang et al., 2001; Vaca and Sampieri, 2002).

However, there are also some evidences demonstrating that TRPC1 permits  $\text{Ca}^{2+}$  influx in response to mechanical stretch. Maroto *et al.* have revealed a fraction giving high mechanosensitive cation channel (MscCa) activity, containing TRPC1 channels, recorded by patch-clamp, after sub-fractionating frog oocyte plasma membrane proteins (Maroto et al., 2005). The same authors have showed that TRPC1 inhibition injecting TRPC1-specific antisense RNA abolished MscCa current, whereas human TRPC1 expression in CHO-K1 (chinese hamster ovary) cells which normally do not present MscCa activity, showed an increased MscCa current. More recent studies have reported a role of TRPC1 as a mechanosensitive channel driving  $\text{Ca}^{2+}$  in response to stretch in MDCK-F (madin-darby canine kidney) cells, synoviocytes and mouse PSCs modulating the migratory cell behaviour (Fabian et al., 2012; Fels et al., 2016).

Nevertheless, further experiments are required to understand how the two above-cited activation mechanisms converge on the same channel, and whether the choice of one of the two proposed TRPC1-mediated  $\text{Ca}^{2+}$  influx mechanisms depend on the given physiological context or on the cell type.

# Ca<sup>2+</sup> signaling is critical for pancreatic stellate cell's pathophysiology : from fibrosis to cancer hallmarks

Silviya Radoslavova<sup>1,2</sup>, Halima Ouadid-Ahidouch<sup>1,3</sup> and Natalia Prevarskaya<sup>2,3</sup>



Known as the key effector of pancreatic fibrosis and pancreatic cancer's desmoplastic stromal reaction development, activated pancreatic stellate cells (aPSCs) are attracting more and more the attention of pancreatic research. Since a few years, a crucial role of Ca<sup>2+</sup> signaling in PSC's activation processes has emerged. Although most of the work on PSCs and Ca<sup>2+</sup> signaling has been carried on aPSCs, because once seated in culture, they become activated within 2–5 days, there are also some studies focusing on the role of Ca<sup>2+</sup> in quiescent pancreatic stellate cells (qPSCs). In this mini-review, we reported all findings on Ca<sup>2+</sup> signaling in qPSCs and aPSCs, in relation to pancreatic fibrosis and cancer promotion.

## Addresses

<sup>1</sup> Laboratory of Cellular and Molecular Physiology, UR 4667, University of Picardie Jules Verne, Amiens, France

<sup>2</sup> Laboratory of Cell Physiology, INSERM U1003, Laboratory of Excellence, Ion Channels Science and Therapeutics, University of Lille 1, Villeneuve d'Ascq, France

## Corresponding authors:

Ouadid-Ahidouch, Halima ([halima.ahidouch-ouadid@u-picardie.fr](mailto:halima.ahidouch-ouadid@u-picardie.fr)), Prevarskaya, Natalia ([natacha.prevarskaya@univ-lille.fr](mailto:natacha.prevarskaya@univ-lille.fr))

<sup>3</sup> These authors contributed equally to this work.

**Current Opinion in Physiology** 2020, **17**:255–260

This review comes from a themed issue on **Calcium signaling**

Edited by **Indu S Ambudkar** and **Aldebaran M Hofer**

For a complete overview see the [Issue](#) and the [Editorial](#)

Available online 4th September 2020

<https://doi.org/10.1016/j.cophys.2020.08.018>

2468-8673/© 2020 Elsevier Ltd. All rights reserved.

## Introduction

Pancreatic stellate cell's research is receiving, since several years, increased attention due to the crucial role of PSCs in the development of pancreatic fibrosis (PF) and cancer (PC) [1]. Initially characterized as resident quiescent vitamin A storing cells of the exocrine pancreas, they undergo transformations during pancreatic injury in order to become activated [2]. The aPSCs are responsible for the extracellular matrix (ECM) deposition, leading to the creation of a dense fibrotic stroma, presented during PF and PC [2,3]. Despite, the well studied hitherto mechanisms participating in PSC's activation, still much has to

be learned, especially regarding the processes triggering their transition from the quiescent to the activated state.

Ca<sup>2+</sup> acts as a universal intracellular second messenger implicated in the regulation of myriad biological processes, including protein secretion, gene expression, cell proliferation, migration, contraction and cell death, as well as cell differentiation [4,5]. Several studies have already elucidated the importance of Ca<sup>2+</sup> signals in PSCs pathophysiology, suggesting its role in the modulation of PSC's phenotype transition. Here, we summarized what is already known about Ca<sup>2+</sup> signaling in qPSCs and aPSCs, focusing on extracellular agents and ion channel's mediated-Ca<sup>2+</sup> signals, in PF and PC context.

## How important pancreatic stellate cells are for pancreatic pathophysiology?

The role of PSCs in the healthy and diseased pancreas has been underestimated for a long time. In the normal healthy pancreas, PSCs represent only 4–7% of the pancreas' total cell number, existing in a so-called quiescent state [6]. Under physiological conditions, qPSCs are characterized by their ability to store retinoid-containing cytoplasmic lipid droplets, having periacinar space location but also founded in perivascular and periductal regions [2,6]. The presence of retinoids participates in their quiescent state maintenance by inhibiting  $\alpha$ -SMA expression [7]. Even though to be in an inactive state, qPSCs play a crucial role in maintaining pancreatic tissue architecture by modulating the ECM turnover though ECM protein degradation and synthesis [8]. Furthermore, the expression of toll-like receptors (TLRs 2-5) in rat qPSCs, suggests that they are also implicated in innate immunity [9]. However, it is still unknown whether human qPSCs possess TLRs as well since they are hardly accessible.

Nevertheless, in response to pancreatic injury or inflammation, qPSCs undergo morphological and functional transformations to become activated. This transition is highlighted by the acquisition of a myofibroblast-like phenotype. This latter is characterized by an increased expression of  $\alpha$ -SMA and excessive ECM component's production and secretion, especially type I collagen synthesis, as well as intensive proliferative, migratory, and contractile abilities. All these properties define aPSCs as the major actor involved in the development of PF, resulting from the presence of ECM large protein amount

[10]. PF is the main feature of three pancreatic diseases : acute (AP), chronic pancreatitis (CP) and pancreatic ductal adenocarcinoma (PDAC), and is caused by the exacerbated activation of PSCs, inducing an increased deposition and reduced degradation of ECM [11,12]. Nonetheless, during pancreatic damage, a variety of extracellular stimuli including cytokines (e.g. : interleukin [IL]-1, IL-6, IL-8 and tumor necrosis factor- $\alpha$ ), and growth factors (e.g. : platelet-derived growth factor [PDGF] and transforming growth factor  $\beta$  [TGF $\beta$ ]) trigger PSC activation [13–16]. Alcohol metabolites [17], trypsin, thrombin, fatty and bile acids [18\*,19\*,20\*,21\*\*], endothelin-1 (ET-1) [22], angiotensin II (ATII) [23] and hypoxic conditions [24] participate in PSC's activation as well. In turn, aPSCs are capable of an autocrine stimulation by secreting cytokines and growth factors, to maintain their activated state [10,13,14,25]. Moreover, aPSCs are in permanent dialogue with their neighbor cells, involving pancreatic acinar cells (PACs) during pancreatitis [18\*] and pancreatic cancer cells (PCCs) during PDAC [26]. PSC's interplay with PACs and PCCs strengthens the poor prognosis of pancreatitis and PDAC, respectively. Throughout AP, aPSCs are responsible for the perpetual PACs necrosis leading to the replacement of the pancreatic cellular component by non-cellular fibrotic tissue, caused by the necrotic amplification loop between PACs and aPSCs [27]. This phenomenon conducts to extended AP resulting in CP, that significantly increases the risk of PDAC development [18\*,19\*,20\*,28,29]. Furthermore, in PDAC, and in hepatocellular carcinoma, activated stellate cells have the particularity of constituting the chief source of Cancer-Associated Fibroblasts (CAFs). During PDAC, the pancreatic CAFs (pCAF) or aPSCs are liable for more than 80% of the pancreatic tumor mass, representing the main component of the dense fibrotic stroma leading to the desmoplastic reaction, tightly surrounding the PCCs [30]. aPSCs enhance PDAC spreading by raising PCCs proliferation, migration and invasion to form early distant metastases. In this line, aPSCs not only provide the ideal microenvironment for pancreatic tumor development and progression, but they also feed the tumor by the paracrine stimulation of PCCs through cytokines and growth factors secretion. Since recently, few studies have identified the existence of more than one distinct aPSC/pCAF subtypes, underlining their inter- and intra-tumor heterogeneity. This latter is defined from the cell surface marker expression, cell signaling, cytokine production, aPSC-PCC interactions, and gene expression, which differs between each subtype [31]. Among others, Öhlund *et al.*'s study, is of important interest, proposing two main aPSC subpopulations according to their spatial location. One subpopulation that interacts directly with the PCCs, characterized by high  $\alpha$ -SMA expression, called myofibroblastic CAFs, and one located more distantly from the PCCs, defined by high IL-6, IL-11 and leukemia inhibitory factor expression and low  $\alpha$ -SMA expression, called

inflammatory CAFs [32]. Neuzillet *et al.* highlighted the importance of such aPSC heterogeneity by identifying four more pCAF subpopulations, classified depending on their :  $\alpha$ -SMA and vimentin expression, ECM production, proliferation rate, immunogenic profile and role in PDAC prognosis [33]. All these recent studies brought a new feature of aPSC functioning, showing that according to the subtype, they can promote more or less PDAC progression. In addition, they restrict oxygen availability maintaining the ideal hypoxic conditions for the tumor, as well as they limit inflammatory infiltration and delivery of chemotherapeutic agents increasing PDAC chemoresistance. Contrary to PACs, there is a positive amplification loop between aPSCs and PCC in order to stimulate PDAC propagation [34–38]. It seems that aPSCs are the key link between these three pancreatic diseases and therefore understanding and limiting PSC's activation may be the key for their medical treatment.

### Distinguished Ca<sup>2+</sup> signaling between quiescent and activated PSCs

Impaired Ca<sup>2+</sup> homeostasis is one of the critical events triggering pancreatic failure, leading to AP, CP, or PDAC. However, the involvement of Ca<sup>2+</sup> signaling in PSC's pathophysiology remains relatively little explored hitherto. Won *et al.* [21\*\*] were the first to investigate the Ca<sup>2+</sup> signature in mouse PSCs from healthy pancreas and a model of chronic pancreatitis, showing evidence of distinguished intracellular Ca<sup>2+</sup> signaling between qPSCs and aPSCs.

Believed for a longtime to exist in a « quiescent » state under physiological conditions, qPSCs are far away from being really « inactive », since they can generate Ca<sup>2+</sup> signals in response to extracellular stimuli. Won *et al.* [21\*\*] nicely demonstrated that qPSCs can produce Ca<sup>2+</sup> signals in response to the muscarinic agonist carbachol, ATII, ATP, and bradykinin (BK). This latter finding was supported by Gryshchenko *et al.* [19\*], showing that, qPSCs can respond to BK concentrations (100 pM), close to the ones present during AP (140 pM), through the activation of BK type 2 receptor. Once linked to its receptor, BK generates a biphasic Ca<sup>2+</sup> response, in qPSCs, represented by an initial large cytosolic Ca<sup>2+</sup> transient signal followed by a sustained Ca<sup>2+</sup> plateau. The Ca<sup>2+</sup> transient signal is caused by Ca<sup>2+</sup> release from the endoplasmic reticulum (ER) stores, after phospholipase C (PLC) and inositol trisphosphate receptor (InsP3R) activation, while the Ca<sup>2+</sup> plateau is induced by Ca<sup>2+</sup> entry through Ca<sup>2+</sup> release-activated Ca<sup>2+</sup> (CRAC) channels. BK-elicited Ca<sup>2+</sup> signals in qPSCs may play a key role in PSC transformation into the activated state, since once activated, they respond to a much higher concentration of BK, involving BK type 1 receptor, which is a hallmark of inflammatory diseases, such as pancreatitis [18\*,19\*]. Moreover, BK-mediated Ca<sup>2+</sup> signaling changes in aPSCs, inducing only a single cytosolic Ca<sup>2+</sup> transient signal. Furthermore, qPSCs but also aPSCs, are capable of producing sustained toxic cytosolic Ca<sup>2+</sup> signals in response



to bile acids (BAs), such as sodium cholate and taurocholate, activating intracellular InsP3R-Ca<sup>2+</sup> release and thus Ca<sup>2+</sup> entry via CRAC channels [20<sup>\*</sup>]. In turn, BK and BAs-induced cytosolic Ca<sup>2+</sup> and hydrogen peroxide-mediated Ca<sup>2+</sup>, activates the Ca<sup>2+</sup>/calmodulin-dependent enzyme nitric oxide synthase in order to produce a diffusible nitric oxide-mediated inflammatory response, acting on the PAC neighbor cells. This phenomenon triggers an amplification loop by promoting PAC's death and increasing PSC-stimulating factor's secretion from dying PACs and therefore aggravate AP, rising the risk to transform into CP [39<sup>\*</sup>]. Another example of different Ca<sup>2+</sup> signaling toolkit between qPSCs and aPSCs, is their responsiveness to ATP. Indeed, aPSCs are approximately threefold more sensitivities to ATP than qPSCs. Won *et al.* [21<sup>\*\*</sup>] established that ATP-mediated Ca<sup>2+</sup> signals are initiated near to the nucleus and propagated into it, increasing nucleoplasmic Ca<sup>2+</sup> concentrations in aPSCs, which stimulates their proliferation during CP. In accordance with these data, some other authors reported that ATP but also UTP and UDP-induced intracellular Ca<sup>2+</sup> signals through several types of purinergic receptors P2X and P2Y in aPSCs. Hennigs *et al.* [40] demonstrated that P2X<sub>4</sub> and P2Y<sub>2</sub> (shown to be upregulated in CP) are the most abundantly expressed isoforms in aPSCs. Interestingly, Haanes *et al.* [41] completed these findings, by reporting the importance of ATP-induced Ca<sup>2+</sup> signals mediated by P2X<sub>7</sub>, shown to be overexpressed and playing an important role in aPSCs proliferation, in CP. The authors concluded that depending on ATP concentration, P2X<sub>7</sub> can drive PSC's proliferation (at low ATP concentration) or death (at high ATP doses). These could explain, in part, the high sensitivity of aPSCs to ATP compared to qPSCs, so they can maintain their activated state by promoting their proliferation in a Ca<sup>2+</sup>-dependent manner, leading to pancreatic fibrosis development. Giannuzzo *et al.* [42] highlighted the significance of P2X<sub>7</sub> also in collagen's deposition during the desmoplastic reaction in PDAC. Nevertheless, contrary to qPSCs, only aPSCs produce prominent nuclear Ca<sup>2+</sup> signals in response to protease-activated receptors 1 driven by thrombin and PDGF, stimulating PSC proliferation [21<sup>\*\*</sup>]. Furthermore, ET-1 and ATII, have been reported to be implicated in fibrosis progression by increasing Ca<sup>2+</sup>-dependent contractility and proliferation of aPSCs. Moreover, only aPSCs can evoke intracellular Ca<sup>2+</sup> signals in response to ET-1 through ET<sub>A</sub> receptor [22], while both qPSCs and aPSCs respond to ATII *via* AT<sub>1</sub> receptor [23]. In contrast, some other agents, like melatonin [43,44] or the pesticide dimethoate [45], impair PSC's viability even though they promote Ca<sup>2+</sup> mobilization from the ER.

### Ca<sup>2+</sup> signaling and ion channels in aPSCs

Ca<sup>2+</sup> entry is controlled by a large number of Ca<sup>2+</sup>-permeable ion channels localized at the plasma membrane and PSCs have been shown to also express a number of Ca<sup>2+</sup> channels.

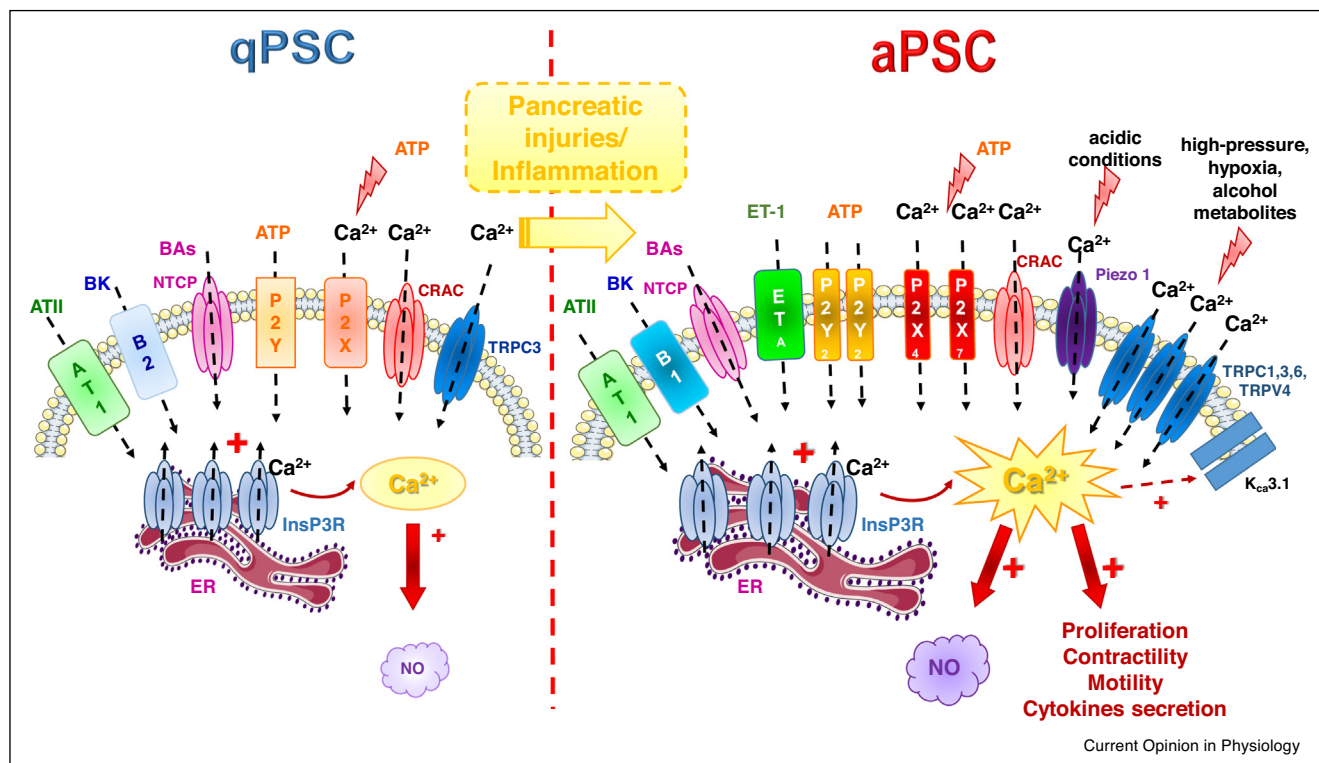
### Ion channels and pancreatitis

Zhang *et al.* [46<sup>\*\*</sup>] were the first to report the presence of transient receptor potential (TRP) channels, particularly TRPV4 in aPSCs from rat model of CP. The authors found an upregulated TRPV4 expression in CP compared to control, which is in concordance with the observed increased and sustained intracellular Ca<sup>2+</sup> mobilization. Their study revealed that TRPV4-mediated Ca<sup>2+</sup> mobilization is enhanced by tumor necrosis factor- $\alpha$  stimulation, showing the importance of cytokines in Ca<sup>2+</sup> signaling modulation in the aPSCs activation. A few years after, Gryshchenko *et al.* [19<sup>\*</sup>], pharmacologically identified the presence of CRAC channels, suggesting a CRAC-mediated Ca<sup>2+</sup> entry in both qPSCs and aPSCs. Their findings were clearly supported by Waldron *et al.* [47<sup>\*\*</sup>], who highlighted the expression of Orai1, Orai2, and Stim1 proteins, the main constituent of CRAC channels, in aPSCs of AP model. Using a CRAC channel inhibitor, they observed an inhibition of TLR-mediated fibro-inflammatory signals, leading to a decrease expression, among others, of IL-6, TGF $\beta$ <sub>1</sub>, type I collagen, and  $\alpha$ -SMA, proposing a crucial role of CRAC-mediated Ca<sup>2+</sup> entry in cytokine expression from aPSCs in AP.

### Ion channels and PDAC

Several reports have been focusing on the role of PSC-expressed ion channels in the context of PDAC as well. Fels *et al.* [48<sup>\*\*</sup>] firstly established a role of TRPC1 ion channel in the activation of PSCs, under high-pressure application, which is one of the PDAC microenvironment features and one of PSC's activator stimuli, thereby perpetuating fibrosis formation. They demonstrated that pressure induces TRPC1 activation allowing Ca<sup>2+</sup> influx into PSCs in order to regulate their migration and enhance their activated behaviour. Similar to pressure, it has been shown by Nielsen *et al.* [49<sup>\*\*</sup>] that hypoxia, another hallmark of PDAC microenvironment, known to activate PSCs, induces activation of TRPC6 leading to an increase of Ca<sup>2+</sup> influx, which promotes aPSC's migration and promigratory factor's secretion by aPSCs. The report of Storck *et al.* [50<sup>\*\*</sup>] brought evidence of cooperative regulation of PSC's migration, mediated by TRPC3 (shown to be upregulated in the PDAC stroma) and the calcium-activated potassium channel K<sub>Ca</sub>3.1, under PDGF stimulation, known to activate PSCs. The authors demonstrated that Ca<sup>2+</sup> entry through TRPC3 is involved in neighboring K<sub>Ca</sub>3.1 channel's activation, resulting in increased PDGF-stimulated migration of PSCs. These data confirm, once more, the importance of cytokines in the regulation of PSC's Ca<sup>2+</sup> signaling. The key role of PDAC microenvironment on PSC's ion channels-mediated Ca<sup>2+</sup> influx in the perpetuation of cancer progression, was also documented by Kuntze *et al.* [51<sup>\*\*</sup>]. Their work determined the impact of Piezo1-mediated Ca<sup>2+</sup> influx on PSC's pathophysiology, under acidification conditions, also characteristic of PDAC microenvironment. Indeed Piezo1 activity is reduced upon acidification leading to

Figure 1



Concluding model that distinguish the  $\text{Ca}^{2+}$  signature between quiescent (qPSCs) and activated PSCs (aPSCs). In response to pancreatic injury or inflammation qPSC undergo transformations to become activated. During this transition, the cell surface expression and function of several receptors and ion channels are modified. qPSCs are characterized by bradykinin type 2 receptor activation, while in aPSCs, bradykinin activates type 1 receptor. Moreover, aPSCs are defined by an overexpression of  $\text{P2Y}_2$  receptor,  $\text{P2X}_4$  and  $\text{P2X}_7$  channels, as well as TRPC3 and TRPV4 channels. However, both qPSCs and aPSCs express AT1 receptors, NTCP transporters and CRAC channels but only aPSCs express  $\text{ET}_A$  receptor.

ATII = angiotensin II, AT1 = angiotensin II type 1 receptor, BK = bradykinin, B1 = bradykinin type 1 receptor, B2 = bradykinin type 2 receptor, BAs = bile acids, CRAC =  $\text{Ca}^{2+}$ -release-activated  $\text{Ca}^{2+}$  channels, ER = endoplasmic reticulum, ET-1 = endothelin-1,  $\text{ET}_A$  = endothelin type A receptor, InsP3R = inositol trisphosphate receptor, NO = nitric oxide, NTCP = sodium-taurocholate cotransporting polypeptide,  $\text{P2Y}$  = purinergic receptors,  $\text{P2X}$  = purinergic channels, TRPC = transient receptor potential-canonical channels, TRPV = transient receptor potential-vanilloid channels.

$\text{Ca}^{2+}$  influx decrease. The reduction of Piezo 1 activity would be due to the protonation in order to protect aPSCs from cell death and promote their migration into well-perfused invasive tumor regions where Piezo1 can be fully functional. Therefore, under physiological pH, the increased Piezo1 mediated- $\text{Ca}^{2+}$  influx enhances PSC's migration and myosin light chain isoform 9 phosphorylation, leading to aPSC's cytoskeletal architecture modification, which, in turn, increases aPSC's motility.

## Conclusion

To summarize, pancreatic injury or inflammation induces a disequilibrium in PSC's composition, leading to an increased number of aPSCs, due to the transition of qPSCs to aPSCs. Taken together, it seems that in both qPSCs and aPSCs,  $\text{Ca}^{2+}$  signaling is initiated through the canonical pathway, involving InsP3R-mediated  $\text{Ca}^{2+}$  release from the ER, under diverse extracellular stimuli.

Moreover, in aPSCs, ion channels-mediated  $\text{Ca}^{2+}$  influx appears to be a key effector for the development and progression of PF and PDAC, as summarized in the conclusion scheme (Figure 1). Hence, controlling the transition of qPSCs to aPSCs will limit pancreatic fibrosis formation and so PF and PDAC promotion. May the answer to this challenge is laying on the management of PSC's intracellular  $\text{Ca}^{2+}$  by using a combination of two or more ion channel inhibitors.

## Conflict of interest statement

Nothing declared.

## Acknowledgements

SR is grateful for the funding by the Région Hauts-de-France (Picardie), the FEDER (Fonds Européen de Développement Économique Régional), the Université Picardie Jules Verne, and the Ministère de l'Enseignement Supérieur et de la Recherche.

## References and recommended reading

Papers of particular interest, published within the period of review, have been highlighted as:

- of special interest
- of outstanding interest

1. Apte M, Pirola R, Wilson J: **Pancreatic stellate cell: physiologic role, role in fibrosis and cancer.** *Curr Opin Gastroenterol* 2015, **31**:416-423.
2. Bachem MG, Schneider E, Gross H, Weidenbach H, Schmid RM, Menke A, Siech M, Beger H, Grünert A, Adler G: **Identification, culture, and characterization of pancreatic stellate cells in rats and humans.** *Gastroenterology* 1998, **115**:421-432.
3. Apte MV, Park S, Phillips PA, Santucci N, Goldstein D, Kumar RK, Ramm GA, Buchler M, Friess H, McCarroll JA *et al.*: **Desmoplastic reaction in pancreatic cancer: role of pancreatic stellate cells.** *Pancreas* 2004, **29**:179-187.
4. Berridge MJ, Bootman MD, Lipp P: **Calcium - a life and death signal.** *Nature* 1998, **395**:645-648.
5. Petersen OH, Michalak M, Verkhratsky A: **Calcium signalling: past present and future.** *Cell Calcium* 2005, **38**:161-169.
6. Apte MV, Haber PS, Applegate TL, Norton ID, McCaughan GW, Korsten MA, Pirola RC, Wilson JS: **Periacinar stellate shaped cells in rat pancreas: identification, isolation, and culture.** *Gut* 1998, **43**:128-133.
7. McCarroll JA, Phillips PA, Santucci N, Pirola RC, Wilson JS, Apte MV: **Vitamin A inhibits pancreatic stellate cell activation: implications for treatment of pancreatic fibrosis.** *Gut* 2006, **55**:79-89.
8. Phillips PA, Yang L, Shulkes A, Vonlaufen A, Poljak A, Bustamante S, Warren A, Xu Z, Guilhaus M, Pirola R *et al.*: **Pancreatic stellate cells produce acetylcholine and may play a role in pancreatic exocrine secretion.** *Proc Natl Acad Sci U S A* 2010, **107**:17397-17402.
9. Masamune A, Kikuta K, Watanabe T, Satoh K, Satoh A, Shimosegawa T: **Pancreatic stellate cells express toll-like receptors.** *J Gastroenterol* 2008, **43**:352-362.
10. Ferdek PE, Jakubowska MA: **Biology of pancreatic stellate cells—more than just pancreatic cancer.** *Pflugers Arch* 2017, **469**:1039-1050.
11. Jaster R, Emmrich J: **Crucial role of fibrogenesis in pancreatic diseases.** *Best Pract Res Clin Gastroenterol* 2008, **22**:17-29.
12. Apte MV, Pirola RC, Wilson JS: **Pancreatic stellate cells: a starring role in normal and diseased pancreas.** *Front Physiol* 2012, **3**.
13. Apte M, Haber P, Darby S, Rodgers S, McCaughan G, Korsten M, Pirola R, Wilson J: **Pancreatic stellate cells are activated by proinflammatory cytokines: implications for pancreatic fibrogenesis.** *Gut* 1999, **44**:534-541.
14. Schneider E, Schmid-Kotsas A, Zhao J, Weidenbach H, Schmid RM, Menke A, Adler G, Waltnerberger J, Grünert A, Bachem MG: **Identification of mediators stimulating proliferation and matrix synthesis of rat pancreatic stellate cells.** *Am J Physiol-Cell Physiol* 2001, **281**:C532-C543.
15. Vogelmann R, Ruf D, Wagner M, Adler G, Menke A: **Effects of fibrogenic mediators on the development of pancreatic fibrosis in a TGF- $\beta$ 1 transgenic mouse model.** *Am J Physiol-Gastrointest Liver Physiol* 2001, **280**:G164-G172.
16. Shimada M, Andoh A, Hata K, Tasaki K, Araki Y, Fujiyama Y, Bamba T: **IL-6 secretion by human pancreatic periacinar myofibroblasts in response to inflammatory mediators.** *J Immunol Baltim Md 1950* 2002, **168**:861-868.
17. Apte MV, Phillips PA, Fahmy RG, Darby SJ, Rodgers SC, McCaughan GW, Korsten MA, Pirola RC, Naidoo D, Wilson JS: **Does alcohol directly stimulate pancreatic fibrogenesis? Studies with rat pancreatic stellate cells.** *Gastroenterology* 2000, **118**:780-794.
18. Gryshchenko O, Gerasimenko JV, Peng S, Gerasimenko OV, Petersen OH: **Calcium signalling in the acinar environment of the exocrine pancreas: physiology and pathophysiology.** *J Physiol* 2018, **596**:2663-2678  
In this work, the authors highlight the change to bradykinin responsiveness between quiescent and activated pancreatic stellate cells, in acute pancreatitis models.
19. Gryshchenko O, Gerasimenko JV, Gerasimenko OV, Petersen OH: **Ca<sup>2+</sup> signals mediated by bradykinin type 2 receptors in normal pancreatic stellate cells can be inhibited by specific Ca<sup>2+</sup> channel blockade.** *J Physiol* 2016, **594**:281-293  
Bradykinin type 2 receptor mediates bradykinin-induced Ca<sup>2+</sup> signals leading to Ca<sup>2+</sup> release from endoplasmic reticulum stores and so Ca<sup>2+</sup> release-activated Ca<sup>2+</sup> channel's activation, in normal pancreatic stellate cells.
20. Ferdek PE, Jakubowska MA, Gerasimenko JV, Gerasimenko OV, Petersen OH: **Bile acids induce necrosis in pancreatic stellate cells dependent on calcium entry and sodium-driven bile uptake.** *J Physiol* 2016, **594**:6147-6164  
This report shows that sodium cholate and taurocholate bile acid salts entry induces Ca<sup>2+</sup> release through the inositol triphosphate receptor from the endoplasmic reticulum stores, in quiescent and activated pancreatic stellate cells.
21. Won JH, Zhang Y, Ji B, Logsdon CD, Yule DI: **Phenotypic changes in mouse pancreatic stellate cell Ca<sup>2+</sup> signaling events following activation in culture and in a disease model of pancreatitis.** *Mol Biol Cell* 2011, **22**:421-436  
Quiescent and activated pancreatic stellate cells are characterized by a different Ca<sup>2+</sup> signature. In activated pancreatic stellate cells, nuclear Ca<sup>2+</sup> signals promote cell proliferation.
22. Klonowski-Stumpe H, Reinehr R, Fischer R, Warskulat U, Lüthen R, Häussinger D: **Production and effects of endothelin-1 in rat pancreatic stellate cells.** *Pancreas* 2003, **27**:67-74.
23. Reinehr R, Zoller S, Klonowski-Stumpe H, Kordes C, Häussinger D: **Effects of angiotensin II on rat pancreatic stellate cells.** *Pancreas* 2004, **28**:129-137.
24. Masamune A, Kikuta K, Watanabe T, Satoh K, Hirota M, Shimosegawa T: **Hypoxia stimulates pancreatic stellate cells to induce fibrosis and angiogenesis in pancreatic cancer.** *Am J Physiol Gastrointest Liver Physiol* 2008, **295**:G709-717.
25. Luttenberger T, Schmid-Kotsas A, Menke A, Siech M, Beger H, Adler G, Grünert A, Bachem MG: **Platelet-derived growth factors stimulate proliferation and extracellular matrix synthesis of pancreatic stellate cells: implications in pathogenesis of pancreas fibrosis.** *Lab Invest J Tech Methods Pathol* 2000, **80**:47-55.
26. Allam A, Thomsen AR, Gothwal M, Saha D, Maurer J, Brunner TB: **Pancreatic stellate cells in pancreatic cancer: i focus.** *Pancreatol Off J Int Assoc Pancreatol IAP AI* 2017, **17**:514-522.
27. Hegyi P: **Necrotic amplification loop in acute pancreatitis: pancreatic stellate cells and nitric oxide are important players in the development of the disease.** *J Physiol* 2018, **596**:2679-2680.
28. Gerasimenko JV, Peng S, Tsugorka T, Gerasimenko OV: **Ca<sup>2+</sup> signalling underlying pancreatitis.** *Cell Calcium* 2018, **70**:95-101.
29. Gerasimenko JV, Gryshchenko O, Ferdek PE, Stapleton E, Hébert TOG, Bychkova S, Peng S, Begg M, Gerasimenko OV, Petersen OH: **Ca<sup>2+</sup> release-activated Ca<sup>2+</sup> channel blockade as a potential tool in antipancreatitis therapy.** *Proc Natl Acad Sci U S A* 2013, **110**:13186-13191.
30. Norton J, Foster D, Chinta M, Titan A, Longaker M: **Pancreatic cancer associated fibroblasts (CAF): under-explored target for pancreatic cancer treatment.** *Cancers* 2020, **12**.
31. Pereira BA, Vennin C, Papanicolaou M, Chambers CR, Herrmann D, Morton JP, Cox TR, Timpon S: **CAF subpopulations: a new reservoir of stromal targets in pancreatic cancer.** *Trends Cancer* 2019, **5**:724-741.
32. Öhlund D, Handly-Santana A, Biffi G, Elyada E, Almeida AS, Ponz-Sarvise M, Corbo V, Oni TE, Hearn SA, Lee EJ *et al.*: **Distinct populations of inflammatory fibroblasts and myofibroblasts in pancreatic cancer.** *J Exp Med* 2017, **214**:579-596.

33. Neuzillet C, Tijeras-Raballand A, Ragulan C, Cros J, Patil Y, Martinet M, Erkan M, Kleeff J, Wilson J, Apte M *et al.*: **Inter- and intra-tumoural heterogeneity in cancer-associated fibroblasts of human pancreatic ductal adenocarcinoma.** *J Pathol* 2019, **248**:51-65.
34. Habisch H, Zhou S, Siech M, Bachem MG: **Interaction of stellate cells with pancreatic carcinoma cells.** *Cancers* 2010, **2**:1661-1682.
35. Vonlaufen A, Joshi S, Qu C, Phillips PA, Xu Z, Parker NR, Toi CS, Pirola RC, Wilson JS, Goldstein D *et al.*: **Pancreatic stellate cells: partners in crime with pancreatic cancer cells.** *Cancer Res* 2008, **68**:2085-2093.
36. Sousa CM, Biancur DE, Wang X, Halbrook CJ, Sherman MH, Zhang L, Kremer D, Hwang RF, Witkiewicz AK, Ying H *et al.*: **Pancreatic stellate cells support tumour metabolism through autophagic alanine secretion.** *Nature* 2016, **536**:479-483.
37. Schneiderhan W, Diaz F, Fundel M, Zhou S, Siech M, Hasel C, Möller P, Gschwend JE, Seufferlein T, Gress T *et al.*: **Pancreatic stellate cells are an important source of MMP-2 in human pancreatic cancer and accelerate tumor progression in a murine xenograft model and CAM assay.** *J Cell Sci* 2007, **120**:512-519.
38. Hwang RF, Moore T, Arumugam T, Ramachandran V, Amos KD, Rivera A, Ji B, Evans DB, Logsdon CD: **Cancer-associated stromal fibroblasts promote pancreatic tumor progression.** *Cancer Res* 2008, **68**:918-926.
39. Jakubowska MA, Ferdek PE, Gerasimenko OV, Gerasimenko JV, Petersen OH: **Nitric oxide signals are interlinked with calcium signals in normal pancreatic stellate cells upon oxidative stress and inflammation.** *Open Biol* 2016, **6**
- Bradykinin mediated-Ca<sup>2+</sup> signals, sodium cholate and taurocholate-induced Ca<sup>2+</sup> signals stimulate nitric oxide generation in quiescent and activated pancreatic stellate cells.
40. Hennigs J, Seiz O, Spiro J, Berna M, Baumann H, Klose H, Pace A: **Molecular basis of P2-receptor-mediated calcium signaling in activated pancreatic stellate cells.** *Pancreas* 2011, **40**:740-746.
41. Haanes KA, Schwab A, Novak I: **The P2X7 receptor supports both life and death in fibrogenic pancreatic stellate cells.** *PLoS One* 2012, **7**.
42. Giannuzzo A, Saccomano M, Napp J, Ellegaard M, Alves F, Novak I: **Targeting of the P2X7 receptor in pancreatic cancer and stellate cells.** *Int J Cancer* 2016, **139**:2540-2552.
43. Santofimia-Castaño P, Garcia-Sanchez L, Ruy DC, Sanchez-Correa B, Fernandez-Bermejo M, Tarazona R, Salido GM, Gonzalez A: **Melatonin induces calcium mobilization and influences cell proliferation independently of MT1/MT2 receptor activation in rat pancreatic stellate cells.** *Cell Biol Toxicol* 2015, **31**:95-110.
44. Estaras M, Moreno N, Santofimia-Castaño P, Martínez-Morcillo S, Roncero V, Blanco G, Lopez D, Fernandez-Bermejo M, Mateos JM, Iovanna JL *et al.*: **Melatonin induces reactive oxygen species generation and changes in glutathione levels and reduces viability in human pancreatic stellate cells.** *J Physiol Biochem* 2019, **75**:185-197.
45. Martínez-Morcillo S, Pérez-López M, Soler-Rodríguez F, González A: **The organophosphorus pesticide dimethoate decreases cell viability and induces changes in different biochemical parameters of rat pancreatic stellate cells.** *Toxicol In Vitro* 2019, **54**:89-97.
46. Zhang LP, Ma F, Abshire SM, Westlund KN: **Prolonged high fat/ alcohol exposure increases TRPV4 and its functional responses in pancreatic stellate cells.** *Am J Physiol - Regul Integr Comp Physiol* 2013, **304**:R702-R711
- TRPV4 expression and TRPV4-mediated Ca<sup>2+</sup> mobilization increase within pancreatic stellate cells during chronic pancreatitis. The latter is stimulated by the TNF- $\alpha$  cytokine in activated pancreatic stellate cells.
47. Waldron RT, Chen Y, Pham H, Go A, Su H-Y, Hu C, Wen L, Husain SZ, Sugar CA, Roos J *et al.*: **The Orai Ca<sup>2+</sup> channel inhibitor CM4620 targets both parenchymal and immune cells to reduce inflammation in experimental acute pancreatitis.** *J Physiol* 2019, **597**:3085-3105
- This is the first study identifying Orai1, Orai2 and STIM1 expression in mouse activated pancreatic stellate cells. The authors demonstrate pharmacologically that Orai-Ca<sup>2+</sup> channels regulate fibro-inflammatory gene expression in mouse activated pancreatic stellate cells.
48. Fels B, Nielsen N, Schwab A: **Role of TRPC1 channels in pressure-mediated activation of murine pancreatic stellate cells.** *Eur Biophys J* 2016, **45**:657-670
- High pressure stimulates TRPC1-mediated Ca<sup>2+</sup> influx in order to regulate pancreatic stellate cell's migration, within pancreatic ductal adenocarcinoma microenvironment.
49. Nielsen N, Kondratska K, Ruck T, Hild B, Kovalenko I, Schimmelpfennig S, Welzig J, Sargin S, Lindemann O, Christian S *et al.*: **TRPC6 channels modulate the response of pancreatic stellate cells to hypoxia.** *Pflug Arch - Eur J Physiol* 2017, **469**:1567-1577
- Pancreatic stellate cell's migration and promigratory factor' secretion is modulated by TRPC6-induced Ca<sup>2+</sup> influx under hypoxic conditions.
50. Storck H, Hild B, Schimmelpfennig S, Sargin S, Nielsen N, Zaccagnino A, Budde T, Novak I, Kalthoff H, Schwab A: **Ion channels in control of pancreatic stellate cell migration.** *Oncotarget* 2016, **8**:769-784
- This work reveals a functional cooperation between TRPC3 and K<sub>Ca</sub>3.1 channels in order to regulate pancreatic stellate cell's migration in pancreatic ductal adenocarcinoma stroma.
51. Kuntze A, Goetsch O, Fels B, Najder K, Unger A, Wilhelmi M, Sargin S, Schimmelpfennig S, Neumann I, Schwab A *et al.*: **Protonation of Piezo1 impairs cell-matrix interactions of pancreatic stellate cells.** *Front Physiol* 2020, **11**
- Piezo1 mechanosensitive channel participate in the modulation of pancreatic stellate cell's migration through the Ca<sup>2+</sup> influx. However Piezo1-mediated Ca<sup>2+</sup> influx is modified under acidic conditions, in the pancreatic tumor stroma.



---

# **PURPOSE OF THE THESIS**

---



The impact of PSC's activation in pancreas pathophysiology has been disregarded for a long time. Currently, activated PSCs are well known for their prominent role in pancreatic fibrogenesis, representing a key pathological feature of CP and PDAC, two major pancreatic diseases having a poor prognosis. Additionally, CP is defined as one of the main risk factors leading to PDAC development.

PSCs reside in an inactive-quiescent state in the healthy pancreas, having a vitamin-A lipid-storing phenotype, accounting only for 4-7% of the pancreas total cell population. In their quiescent state, PSCs participate in the maintenance of pancreatic tissue architecture, sustaining the ECM turnover. However, upon pancreatic injury or inflammation, PSCs undergo transformations to become activated, obtaining a myofibroblast-like phenotype. PSC's activation is principally characterized by vitamin A lipid droplets disappearance, increased  $\alpha$ SMA expression, excessive ECM protein synthesis, acquisition of high proliferative and migratory abilities, and an abundant cytokine and growth factors secretion, including TGF- $\beta$ 1 and IL-6 (Ferdek and Jakubowska, 2017; Masamune and Shimosegawa, 2009). Moreover, external environmental stimuli, such as high pressure or hypoxia, and soluble paracrine factors, including cytokines, can induce PSC activation. Therefore, sustained pancreatic lesions or microenvironmental stimulations perpetuate PSC's activation leading to the development of dense fibrotic tissue, observed during both CP and PDAC. Moreover, throughout PDAC, activated PSCs are liable for more than 80% of the pancreatic tumor mass and are in permanent communication with the PCCs. This dynamic dialogue between activated PSCs and PCCs affects importantly PCC's behavior resulting in PDAC spreading and consequently promoting treatment inefficiency. In this line, activated PSCs not only provide the ideal microenvironment for PDAC development and progression, but they also feed the tumor by PCC's paracrine stimulation via the secretion of diverse cytokines and growth factors, including TGF- $\beta$ 1 and IL-6 (Habisch et al., 2010).

Furthermore, it has been well established that intracellular  $Ca^{2+}$  acts as a second messenger that mediates multiple biological processes, such as cell proliferation, survival, migration, protein secretion, and gene expression. However, disruption of  $Ca^{2+}$  homeostasis results in the development of various pathologies, including fibrosis and cancer. Several studies have revealed that  $Ca^{2+}$  signature is modified in activated PSCs compared to quiescent PSCs, suggesting an essential role of intracellular  $Ca^{2+}$  signalling in the regulation of PSC's activation (Won et al., 2011). This observation indicates that plasma membrane  $Ca^{2+}$  channels permitting  $Ca^{2+}$  entry within PSCs might be tightly related to the  $Ca^{2+}$ -altered signature in activated PSCs,

and, thus in the modulation of PSC's activation processes. In this line, our collaborators have previously shown that  $\text{Ca}^{2+}$  influx through the stretch-activated  $\text{Ca}^{2+}$  channel TRPC1 is implicated in the regulation of PSC's migration (Fels et al., 2016). Additionally, another study pharmacologically identified the presence of Store-Operated  $\text{Ca}^{2+}$  channels in PSCs, known as one of the major  $\text{Ca}^{2+}$  entry pathways in non-excitable cells, but without reporting their role in PSC's activation. Consequently, up until now, the involvement of  $\text{Ca}^{2+}$  and  $\text{Ca}^{2+}$  channels in the modulation of the molecular and cellular mechanisms characterizing PSC's activation remains poorly known due to the limited existing data.

Hence, the aims of the present work were divided into two main parts:

- 1) Evaluating the role Store-Operated  $\text{Ca}^{2+}$  Channels and particularly Orai1 channel in PSC's activation processes, focusing on cell proliferation, survival, and cytokine secretion, as well as the related signalling pathways.
- 2) Understanding the role of the mechanosensitive  $\text{Ca}^{2+}$ -permeable TRPC1 channel in PSC's activation and the underlying mechanisms during normal and elevated pressure conditions.



---

# **MATERIAL AND METHODS**

---





## **I. Cell culture**

### **I.1) Cellular models**

We have used two different cell lines of human-activated PSCs from different origins, the PS-1 cell line and the RTL-PSC cell line, during this thesis work.

The PS-1 cell line was isolated from the pancreas of a healthy donor by the group of Pr Hemant M. Kocher from the Queen Mary University of London (Froeling et al., 2009). This cell line was immortalized using a retrovirus containing cDNA encoding human telomerase reverse transcriptase (hTERT), followed by a cell selection using the antibiotic puromycin. Although PS-1 cells originate from a normal healthy pancreas, they present *in vitro* all the characteristics of activated PSCs, and they are so considered activated (Froeling et al., 2009).

The RLT-PSC cell line was the first immortalized human cell line of activated PSCs to be generated (Jesnowski et al., 2005). This cell line derives from the pancreas of a patient with chronic pancreatitis, immortalized using the SV40 large T antigen in conjunction with the hTERT, and the cell selection was realized using the antibiotic geneticin G418 for four weeks.

The third used cellular model is the pancreatic cancer cell line MIA PaCa-2, provided by ATCC (ATCC CRL-1420<sup>TM</sup>) and initially originated from the pancreas' tail and body of a 65-year-old Caucasian male with pancreatic ductal adenocarcinoma, that had also infiltrated the periaortic area (Yunis et al., 1977). This cell line was used to study the interaction between pancreatic stellate cells and pancreatic cancer cells using the conditioned medium of PSCs, as described further below.

### **I.2) Cell culture conditions**

Both human-activated PSC cell lines were cultured in Dulbecco's Modified Eagle Medium/ Nutrient Mixture F-12 (DMEM/F12, Gibco, Thermo Fischer Scientific, France) supplemented with 10% of Fetal Bovine Serum (FBS, Pan Biotech, Dominique Dutscher, France) without any antibiotics, in T75 (surface of 75 cm<sup>2</sup>) plastic culture flasks. PS-1 cells were used up to a maximum of passage 55, while RLT-PSCs were used not more than passage 28 for the different experiments.

MIA PaCa-2 cells were cultured in DMEM high glucose medium (DMEM, Gibco, Thermo Fischer Scientific, France), supplemented with 10% FBS (Gibco, Thermo Fischer

Scientific, France) and 2 mM of L-Glutamine (Gibco, Thermo Fischer Scientific, France), without any antibiotics, in T25 ( surface of 25 cm<sup>2</sup>) plastic culture flasks. These cells were used until maximum passage 30 for the different experiments.

All cell lines were maintained at 37°C in a humidified atmosphere with 5% CO<sub>2</sub>, under normoxic conditions, in pre-treated plastic flasks facilitating their cell adhesion, and the cell culture medium was changed every 48 hours renewing the nutrient intake. Furthermore, the FBS utilized for each cell culture medium was previously decomplexed at 56°C for 30 minutes.

Once the cells had reached 80% of their confluency within the flask, they were split into a new flask to maintain them in culture. All the manipulations of cell culture, as well as all the cell treatments, were performed under a cell culture hood of class II (Faster BH-EN-2003-S) in order to ensure sterile conditions and avoid any potential contaminations. The culture medium of the confluent flask was then removed, cells were rinsed with PBS (Phosphate Buffered Saline, Sigma, France) solution ( 5 ml for the T75 flask and 2.5 ml for the T25 flask), and thereafter a trypsin-EDTA (Ethylenediaminetetraacetic acid) (0.05%, Gibco, Thermo Fischer Scientific, France ) solution (1.5 ml for the T75 flask and 1 ml for the T25 flask) was added to the cells placing the flask in the incubator at 37°C. The trypsin solution will permit the cell dissociation since trypsin is a proteolytic enzyme hydrolyzing the esters of basic amino acids (lysine and arginine), cleaving hence the adhesion transmembrane proteins. RLT-PSCs and MIA PaCa-2 cells were kept for 5 minutes in trypsin at 37°C to be detached and dissociated, while PS-1 needed 7 minutes. The effect of trypsin was then neutralized by adding a complete culture medium (3.5 ml for the T75 flask and 3 ml for the T25 flask) as the FBS contains trypsin inhibitors and resuspending the cells by ten repetitive pipettings to dissociate mechanically better the cells. After dissociation, the cells were counted using the Malassez counting chamber and seeded into new flasks until they reached 80% of confluency again. 2\*10<sup>5</sup> cells were seeded in a T75 flask for PS-1 and 8\*10<sup>4</sup> cells for RLT-PSCs since they have a higher proliferative potential than PS-1, and 6\*10<sup>4</sup> cells were plated in a T25 flask for MIA PaCa-2 in order to be confluent after one week of culture.

### **I.3) Freezing and Thawing procedures**

When they reached 80% of confluency, cells were detached using the trypsin-EDTA solution and counted as described above. 2\*10<sup>6</sup> cells were transferred into a sterile tube and

centrifuged at 1100 rpm for 7 minutes to pellet the cells, then the supernatant was removed, and the cells were resuspended in 1 ml of freezing medium containing 95% of FBS and 5% of DMSO (Dimethyl sulfoxide, Sigma-Aldrich, France) per cryogenic freezing vial. The vials were next placed in the freezing container CoolCell™ (Biocision, Dutscher, Thermo Fischer Scientific, France) at -80°C for 48 hours, permitting slow and progressive freezing of the cells, and after they were placed in the storage boxes in -80°C for long term conservation.

To thaw the cells, the freezing vial was heated either in the water bath at 37°C or manually until the cells were thawed, and then 1 ml of DMEM/F12 for PSCs and of DMEM for MIA PaCa-2 (without FBS) was added to the vial dissociating the cells with gentle and slow pipetting. Thereafter the totality of the vial volume was transferred into a 50 ml tube containing 20 ml of DMEM/F12 for PSCs and DMEM for MIA PaCa-2 (without FBS) to dilute the DMSO contained in the freezing medium, and cells were centrifuged at 1100 rpm for 7 minutes. After centrifugation, the supernatant was discarded, the cells were resuspended with complete culture medium and seeded into a T75 flask for PSCs and T25 flask for MIA PaCa-2 containing their complete medium, and placed in the incubator at 37°C. The day after, the medium was changed to eliminate any not attached cells. Cells were maintained in culture and they were used for experiments only two weeks after their thawing.

#### **I.4) Conditioned medium**

The dialogue between activated PSCs and pancreatic cancer cells (PCCs) and the role of  $\text{Ca}^{2+}$  in this inter-communication has been assessed using the conditioned medium (CM) produced by the activated PSCs. To obtain this conditioned medium which contains all the factors secreted by the activated PSCs, PS-1 cells and RLT-PSCs have been cultivated in their classic complete culture medium in T75 flasks until reaching 80% of confluency. Subsequently, the media was removed, cells were washed with PBS to eliminate any resting of FBS, and a new medium was added to the PSCs. This new medium corresponds to the culture medium of MIA PaCa-2 cells, namely to DMEM medium but without FBS, so the secreted from PSCs' factors can be distinguished from the factors contained in the FBS and in which PSCs were cultivated for 48 hours. Afterward, the so-called conditioned medium (CM) from the PS-1 cells and RLT-PSCs is collected, filtered using a 0.22  $\mu\text{m}$  pore size sterile filter, and stored at -80°C until usage. We will call this latter CM with a physiological  $\text{Ca}^{2+}$  concentration since the  $\text{Ca}^{2+}$  concentration of the commercial DMEM media is 1.8 mM. To evaluate the role of  $\text{Ca}^{2+}$  in the

interplay between activated PSCs and PCCs, we simultaneously generated a low  $\text{Ca}^{2+}$  (0.2 mM  $\text{Ca}^{2+}$ ) CM from PSCs using the  $\text{Ca}^{2+}$  chelator EGTA (Ethylene glycol-bis( $\beta$ -aminoethyl ether)-N,N,N', N'-tetraacetic acid)). We calculated the optimal concentration of EGTA (1.6 mM of EGTA) to add in the DMEM medium in order to decrease the media  $\text{Ca}^{2+}$  concentration to 0.2 mM using the max-chelator software [somapp.ucdmc.ucdavis.edu/pharmacology/bers/maxchelator/CaMgATPEGTA-NIST.htm](http://somapp.ucdmc.ucdavis.edu/pharmacology/bers/maxchelator/CaMgATPEGTA-NIST.htm).

Similarly, we cultivated the 80% PS-1 and RLT-PSCs confluent cells in this FBS free-DMEM medium with low  $\text{Ca}^{2+}$  concentration (0.1 mM) for 48 hours and then collected the low  $\text{Ca}^{2+}$  CM as described previously. After that, these CMs with physiological and low  $\text{Ca}^{2+}$  concentrations from PSCs were used to cultivate MIA PaCa-2 cells for 48 hours and 72 hours to study the effect of the PSCs secreted factors in physiological and low  $\text{Ca}^{2+}$  concentration on PCCs behavior. Before replacing the classic complete medium of MIA PaCa-2 with the PSC-CM, the cells were washed with PBS to eliminate any trace of resting FBS.

### **I.5) Cell Transfection**

Transient silencing of the protein-coding genes of interest was performed with the most commonly used RNA interference, namely the small (or short) interfering RNA (siRNA). This latter is a synthetic RNA duplex designed to specifically target a particular messenger ribonucleic acid (mRNA) for degradation, thus leading to the inhibition of the protein of interest. To introduce the specific siRNA for each target gene and hence protein into cells, we used the electroporation method consisting of generating an electrical pulse which creates temporary pores in the cell membrane allowing the passage of siRNA into the cell. The electroporation was performed using nucleofection technology (Nucleofector™ II, Amaxa Biosystems, Lonza, Aubergenville, France) and according to the manufacturer's protocol. All cell lines (PSCs and MIA PaCa-2) were efficiently transfected with the Nucleofector Kit L from Lonza (reference: VVCA-1005). Indeed, after trypsinization,  $1 \times 10^6$  or  $1.5 \times 10^5$  cells were transferred into a 2 ml Eppendorf tube and were pellet after 7 minutes of centrifugation at 1500 rpm or 200g. The supernatant was then removed, and 100  $\mu$ l of supplemented transfection kit L was added in each Eppendorf tube, as well as 4  $\mu$ g of scrambled siRNA (negative duplex control used as control, Eurogentec, France) or of siRNA directed against the protein of interest (Eurogentec, France or Dharmacon Research, Chicago). However, for siStim1 2  $\mu$ g of siRNA was sufficient to obtain an efficient protein inhibition. The initial concentration of all used

siRNAs was 40  $\mu$ M, and all of their sequences are listed in **Table 1**. The whole mix (cells with transfection buffer and siRNA) was transferred into the transfection cuvette, and the electroporation was carried out using the nucleofector device cited above. Moreover, the transfection efficiency depends also on an adequate transfection program. The adapted program for PSCs was the BHK-21 (X-031), and for MIA PaCa-2, the program Panc-1 (X-005). Once the electroporation was done, 400  $\mu$ l of culture medium was added to each transfection cuvette. Thereafter the whole volume was transferred into a 2 ml Eppendorf tube, in which 500  $\mu$ l or 1 ml (depending on the number of transfected cells, for  $1 \times 10^6$  cells, 500  $\mu$ l of medium were added, while for  $1.5 \times 10^6$  cells, 1 ml was added) more were added and incubated for 10 minutes at 37°C before seeding the transfected cells into the Petri dishes. All the carried-out experiments were performed 72 hours after the siRNA transfection.

**Table 1: siRNA sequences used for transfection.**

No	siRNA name	Sequence (all in the 5'-to-3'direction)
1	siCtrl	duplex negative control, Eurogentec # SQ-SIRNA-20007
2	siOrai1	CG UG CA CA AU CU CA AC UC G
3	siOrai2	GG AC UG GA UG AC UU CU CC U
4	siOrai3	GG GU CA AG UU UG UG CC CA U
5	siStim1	GG AG GA UA AU GG CU CU AU U
6	siTRPC1	ON-TARGET plus SMART pool siRNA, Dharmacon Research, Chicago, IL # L-004191-000005
7	si $\alpha$ SMA	GG GC UG UU UU CC CA UC CA U
8	siSmad2	GU CC CA UG AA AA GA CU UA A

### **I.6) Cell treatments and stimulations**

All the applied cell treatments or stimulations during the different experimental procedures of this thesis work are listed in the below table (**Table 2**). For the long-term treatments (48 hours or 72 hours), cells were first seeded into the Petri dishes for 24 hours to adhere to the plastic support before treating them with different chemicals. 24 hours after

plating the cells, the culture medium was changed and replaced by a fresh medium containing the corresponding treatment with the corresponding concentration indicated in the below table for the treatment-indicated time. All the cell treatments and cell stimulations were realized within the classic culture medium of PSCs (DMEM/F12 supplemented with 10% FBS) except for the TGF- $\beta$ 1 treatment, where cells were cultivated and treated in DMEM/F12 medium supplemented with 1% FBS. Furthermore, for all the studies performed to investigate the phosphorylated form of a protein, cells were FBS-starved overnight and stimulated with 10% FBS-containing media and/or with the corresponding chemical the day of the carried-out experiment.

**Table 2: Chemicals used for the experiments.**

No	Chemical name	Solvent	Stock solution	Used concentration	Treatment time	Chemical reference and supplier
1	TGF- $\beta$ 1	DMEM F12	1 $\mu$ g/ml	20 ng/ml	48h	Sigma, #H8541
1bis	TGF- $\beta$ 1	DMEM F12	1 $\mu$ g/ml	5 ng/ml	30 min	Sigma, #H8541
2	LY 294002	DMSO	20 mM	20 $\mu$ M	72h	Sigma, #L9908
3	SB 431542	DMSO	100 mM	80 $\mu$ M	72h	Sigma, #616464
4	U 0126	DMSO	10 mM	10 $\mu$ M	72h	Sigma, #U120
5	EGTA	Culture medium	0.5 M	1.3 mM	30min and 72h	Sigma, #324626
6	W 7	H2O	5 mM	20 $\mu$ M	72h	Tocris, # 61714-27-0
7	Thapsigargin	DMSO	10 mM	1 $\mu$ M	2-3 min	Sigma, # T9033
8	SKF 96365	DMSO	10 mM	10 $\mu$ M	72h	Sigma, # S7809-5MG
8bis	SKF 96365	DMSO	10 mM	5 $\mu$ M	10 min	Sigma, # S7809
9	2 APB (2-Aminoethoxy-diphenyl borate)	H2O	20 mM	50 $\mu$ M	10min and 72h	Sigma, #100065
10	M $\beta$ CD	Culture medium	powder	5 ng/ml	24h	Sigma, #C4555

## **II. Cell viability, proliferation, and mortality**

### **II.1) MTT colorimetric assay**

The MTT test for 3-(4,5-dimethylthiazol-2-yl)-2,5-diphenyltetrazolium bromide is a colorimetric assay permitting the assessment of the cell viability by measuring the cellular metabolic activity. The yellow tetrazolium salt of MTT is reduced to purple insoluble formazan crystals by the mitochondrial succinate dehydrogenase reflecting the mitochondrial respiratory activity and thus the cellular energy capacity, characteristic only of the viable cells. The MTT (Sigma-Aldrich, France) powder used for the experiments was solubilized in the culture medium (0.5 mg/ml). To perform this assay, cells were seeded in 6-well plates ( $8 \times 10^4$  per well for PS-1 cells and  $6 \times 10^4$  for RLT-PSCs and MIA PaCa-2 cells), and the cell viability was assessed 72 hours after siRNA transfection or treatment with the different chemicals. The culture medium of the cells was discarded, and cells were incubated with 800  $\mu$ l per well of the dissolved in the media MTT, for 45 minutes, at 37°C, in the dark because the MTT is a photosensitive molecule, to be converted into formazan. After 45 minutes of incubation, the purple formazan crystals were dissolved by replacing the medium with 800  $\mu$ l of DMSO per well, resulting in a more or less colored solution. The volume of DMSO was then divided into 4 and placed in the wells (200  $\mu$ l per well) of a 96-well plate, and the absorbance of the obtained colored solution was measured at 550 nm using the spectrophotometer Infinite P200 PRO™ TECAN. Consequently, the optical density obtained using the Tecan-i-control software reflects the proportion of living cells.

### **II.2) Trypan Blue dye exclusion assay**

The Trypan Blue staining assay is used to quantify the number of viable and dead cells within a cell suspension. This is due to the capacity of the trypan blue dye to penetrate the cells through porous membranes, characteristic of dead cells, and color the cytoplasm in blue, whereas it cannot cross the intact membrane of the living cells. Hence the number of blue-stained cells reflects the number of dead cells, while the uncolored cells correspond to the viable and proliferative cells within a cell population. This exclusion assay was carried out on PSCs plated in 35 mm Petri dishes ( $8 \times 10^4$  cells per dish for PS-1 cells and  $6 \times 10^4$  for RLT-PSCs) for 72 hours after siRNA transfection or after cell treatment with the different chemicals. The cell medium was removed and kept in a 2 ml Eppendorf tube to preserve the possible dead cells contained in the media, and cells were detached using 400  $\mu$ l of trypsin-EDTA for 5 and 7

minutes for PS-1 cells and RLT-PSCs respectively, at 37°C. The trypsin activity was then neutralized using the conserved cell medium corresponding to each condition, and cells were kept in suspension. Next, 200 µl of cell suspension was added in 50 µl of trypan blue solution (0.4%, Sigma-Aldrich, France), in the volume ratio of 4:1, and after homogenization, dead and alive cells were counted using the Malassez counting chamber. For each condition, cells were counted six times to determine the rate of cell death and cell proliferation for each condition. Firstly, the total cell number was quantified using the formula: Total cell number = number of cells \* 4 \* 1900 (which corresponds to the 400 µl of the added trypsin-EDTA and to the 1.5 ml of the collected, conserved cell medium). After that, the cell mortality rate was obtained using the formula: Percentage of dead cells = (number of blue-stained cells/number of total cells) \* 100 (normalized or not to the control condition), and the cell proliferation rate using the formula: Rate of cell proliferation = number of alive cells \* 4 \* 1900, normalized to the control condition.

### **II.3) Flow cytometry**

#### **II.3.1) Cell cycle analysis**

Flow cytometry is a laser-based technique utilized to detect and measure several biophysical and biochemical parameters of a cell population or particles in suspension, such as the granularity, size, number, profile, function, and phenotype. This technique also can measure the optical and fluorescence characteristics of a cell population or particles in suspension, for example, by using fluorescent antibodies or dyes. The flow cytometer contains an optical detection system and a laser beam in front of which the cells pass one by one in a constant flow. The light scattering from the cells which is linked to their structural and morphological properties, and the emitted fluorescence coming from the amount of the fluorescent probe bound to the cells, are then measured by sensors which transmit the information to a computer for analysis. Based on this principle, we used flow cytometry to assess the cell proliferation. Indeed, we utilized the Propidium Iodide (PI), a fluorescent stoichiometric DNA-binding dye that intercalates between adjacent DNA base pairs to determine the cell distribution of a population in the different cell cycle phases (G0/G1, S, and G2/M). PI is excited by a laser of 488 nm wavelength, and its emitted fluorescence is detected at 631 nm. After the excitation of PI (FL2 filter), the intensity of the emitted fluorescence is represented in graphic form according to the number of cells passed in front of the optical detector (Count). Hence, the intensity of the



fluorescence detected at 631 nm is proportional to the DNA content of the cell, which varies from one phase of the cell cycle to the other, permitting to quantify the percentage of cells in each phase. Notably, the G2/M phase contains two times more DNA than the G0/G1 phase. To evaluate the cell cycle distribution,  $1 \times 10^6$  PS-1 cells were transfected with siCtrl, siOrai1, siStim1, siTRPC1 or si $\alpha$ SMA independently, and plated in 100 mm dishes for 72 hours. After 72 hours of post-transfection, cells were rinsed with 3 ml of PBS and detached using 1 ml of trypsin-EDTA solution per dish for 7 minutes at 37°C. The trypsin activity was then stopped by adding 3 ml of complete culture medium per dish, and cells were collected in a 15 ml tube, following centrifugation of 7 minutes at 1000 rpm. Thereafter, the supernatant was removed, the cell pellet was resuspended in PBS, and cells were centrifuged again for 7 minutes at 1000 rpm. This procedure was repeated one more time before the supernatant was definitively eliminated. Cells were next resuspended in 150  $\mu$ l of PBS containing 5 mM EDTA, to which 350  $\mu$ l of cold absolute ethanol (99.8%, Sigma-Aldrich, France) was added drop by drop to fix the cells. The whole suspension was gently vortexed and stored at 4°C for at least 6 hours and not more than 2 weeks. After the cell fixation step, necessary for the permeabilization of the cell membrane facilitating afterwards the PI entry within the cells, the cell suspension was pelleted by centrifugation of 7 minutes at 1000 rpm. Cells were then resuspended in 100  $\mu$ l of PBS-5 mM EDTA and treated with 2  $\mu$ l of RNase A (20 mg/ml, Sigma-Aldrich, France) for 30 minutes at ambient temperature to avoid any PI binding to presented RNAs. Before analyzing the samples by the flow cytometer (Accuri® C6 BD), 100  $\mu$ l of PBS-5 mM EDTA solution containing 50  $\mu$ g/ml of PI was added to each sample and the emitted from the PI fluorescence was measured after excitation at 488 nm with the FL-2 laser filter. The obtained cell cycle profiles were after analyzed by calculating the cell percentage in each phase with the Cyflogic software.

### **II.3.2) Apoptosis analysis**

Apoptosis, a programmed cell death process, can be assessed using specific markers of apoptotic cells that are conjugated to a fluorophore by flow cytometry. Such a specific marker is Annexin V, an intracellular protein that binds to the phospholipid phosphatidylserine in a calcium-dependent manner. In healthy cells, phosphatidylserine is found on the inner leaflet of the plasma membrane. However, during early apoptosis, this phospholipid translocates to the outer leaflet of the plasma membrane, making its detection possible by using fluorochrome-labeled Annexin V. To distinguish the apoptotic from the necrotic cells, another marker is

needed to be used, such as the Propidium Iodide (PI) that binds to DNA. Indeed, during apoptosis analysis, cells are either fixed or permeabilized, thus, the PI will be able to penetrate and stain only cells that have lost their plasma membrane integrity, a phenomenon that occurs during late-stage apoptosis and necrosis. Hence the early apoptotic cells will be labeled only with Annexin V, whereas the late apoptotic cells and the necrotic cells will be stained with PI.

We performed our experiments using the fluorochromes FITC (fluorescein) Annexin V and PI from the PE Annexin V Apoptosis Detection Kit (BD Biosciences Pharmingen, France). Before analyzing the apoptosis,  $1 \times 10^6$  PS-1 cells were transfected with siCtrl, siOrai1, siTRPC1 or si $\alpha$ SMA independently and seeded in 100 mm Petri dishes for 72 hours. Thereafter, the culture medium from each condition containing the detached cells was removed and conserved in a 15 ml tube. Cells were washed with 3 ml of PBS (also collected in the 15 ml tube corresponding to each condition) and detached using 1 ml of trypsin-EDTA for 7 minutes at 37°C. The trypsin activity was neutralized, and cells were resuspended using the collected from each 15 ml tube medium of the corresponding condition. The cells were then pelleted by centrifugation of 7 minutes at 1000 rpm, and the supernatant was discarded. The pelleted cells were resuspended in 1 ml of PBS, transferred to a 1.5 ml Eppendorf tube, and centrifuged again at 1000 rpm for 7 minutes. This washing step with PBS was repeated one more time. After the last centrifugation, the pelleted cells were resuspended in 100  $\mu$ l of 1x apoptosis binding buffer (diluted 1:10 in PBS) and 2.5  $\mu$ l of FITC Annexin V, and 2.5  $\mu$ l of PI (50  $\mu$ g/ml) staining solutions were added to each Eppendorf tube. The whole mix was incubated for 15 minutes in a dark place at room temperature, then 400  $\mu$ l of 1x apoptosis binding buffer was added to each tube, and samples were directly analyzed by flow cytometry (Accuri® C6 BD). During the analysis, each detected cell by the cytometer was classified according to its fluorescence labeling to viable, apoptotic or necrotic. The cells stained either with Annexin V or PI (Annexin V -/ PI -) correspond to the viable cell population, while the ones labeled only with Annexin V but not with PI (Annexin V+/PI-) correspond to the early apoptotic cell population. In addition, the cells stained only with PI (Annexin V-/PI+) correspond to the necrotic cell population, whereas the ones labeled with both Annexin V and PI (Annexin V+/PI+) correspond to the cells in late-stage apoptosis and/or in necrosis.

### **III. Molecular Biology Techniques**

#### **III.1) RNA extraction**

PSCs (PS-1 and RLT-PSCs) were seeded in 60 mm Petri dishes at the density of  $5 \times 10^5$  cells for PS-1 and  $2 \times 10^5$  cells for RLT-PSCs (for 72 or 96 hours of culture) until the end of the transfection time-point or the cell treatment. Petri dishes were then placed on ice and brought under the fume hood where the workspace was cleaned with RNase AWAY Reagent solution (Molecular Bioproducts) to avoid any RNA degradation from the existing on the work surface RNases. The culture medium was after that removed, cells were rinsed with PBS and 1 ml of Trizol solution (TRI-Reagent<sup>®</sup> solution, Sigma-Aldrich, France) was added per dish to lyse the cells. After 2 minutes of cell lysis, the Trizol solution containing the lysed cells was transferred to a 1.5 ml Eppendorf tube, to which 200  $\mu$ l of 1-Bromo-3-Chloropropane (Sigma-Aldrich) was added to separate the nucleic acids (RNA and DNA) from the proteins. To mix the 2 solutions, the Eppendorf tubes were vortexed for 3 minutes at room temperature and then centrifuged at 12 000 g for 15 minutes at 4°C. After the centrifugation, 3 distinguished phases were formed inside the tube, an upper clear aqueous phases containing the nucleic acids, an intermediate white phase containing the proteins and a lower organic phase containing the lipids. The upper phase was carefully collected and transferred into a new Eppendorf tube, whereas the rest of the mix was discarded. Thereafter, 500  $\mu$ l of isopropanol (Sigma-Aldrich) was added in each tube to collect the RNAs by alcohol-based precipitation, followed by a slow manual shaking. After that tubes were kept for 10 minutes at room temperature before being centrifuged again at 12 000 g for 10 minutes at 4°C. At the end of the centrifugation, a pellet was formed corresponding to the RNAs, thus the supernatant was discarded, and 500  $\mu$ l of 70% ethanol were carefully added (without disrupting the pellet). The tubes were centrifuged at 7500 g for 7 minutes and the ethanol was then discarded. This washing step was repeated one more time before letting the RNA pellet to dry completely under the fume hood. Once the pellet was completely dry, 22  $\mu$ l of RNase free sterile water was added to each tube to dilute the RNA pellet. After that, the RNA concentration was quantified by measuring its absorbance at 260 nm (wavelength of nucleic acids absorbance) with the NanoDrop 2000 spectrophotometer. Simultaneously the absorbance at 280 nm (corresponding to the wavelength of protein absorbance) and at 230 nm (corresponding to the wavelength of solvent absorbance) was measured. The purity then of the extracted RNA was determined using the ratios A260/A280 reflecting the protein contamination, and A260/230 reflecting the solvent contamination. Only

the samples having ratios higher than 1.8 were considered as pure and thus used for the experiments.

### **III.2) Reverse transcription-polymerase chain reaction (RT-PCR)**

After the RNA extraction, the obtained and quantified RNA was retro-transcribed into complementary DNA (cDNA) using the High-Capacity cDNA Reverse Transcription kit (Applied Biosystems). For our experiments 2 µg of RNA per sample diluted in RNase free water to a final volume of 13.2 µl and transferred into a 0.2 ml heat-resistant tube, was retro-transcribed into cDNA. To each sample was then added 6.8 µl of RT mix containing 2 µl of RT buffer, 2 µl of Random primers, 0.8 µl of deoxynucleotide triphosphates (dNTPs), 1 µl of RNase inhibitor and 1 µl of the reverse transcriptase Multiscribe™. The heat-resistant tubes containing a final volume of 20 µl each were placed into the thermocycler for the reverse transcription of the RNA to cDNA. This procedure was performed in 3 steps, a first step of primers' hybridization for 10 minutes at 25°C, then a step of retro-transcription for 2 hours at 37°C and a final step of the reverse transcriptase deactivation for 5 minutes at 85°C. After that step, the obtained cDNAs were stored at -20°C until use.

### **III.3) Quantitative polymerase chain reaction (qPCR)**

The quantification of the genes of interest in our samples was realized with the quantitative PCR (qPCR) technique. qPCR permits the amplification and quantification of specific DNA sequences using fluorescent probes and specific forward and reverse primers for each gene of interest (all the primers used for our experiments are listed in **Table 3**). All the qPCR experiments were performed at the Regional Resource Center in Molecular Biology (CRRBM) in Amiens. The obtained from the RT-PCR cDNA were diluted 1:20 in RNase free water before being used for the qPCR experiments. Then 2 µl of each cDNA sample was added in a 384 well plate, followed by the addition of 0.5 µl of forward primer and 0.5 µl of reverse primer, both concentrated at 10 µM, and 1.6 µl of RNase free water, per well. Thereafter, 4.6 µl of the SYBR green buffer, containing the fluorescent SYBR green probe (ABsolute™ QPCR SYBR® Green Mixes kit, ABgene), was added to each well to reach a total volume of 9.2 µl per well. Indeed, SYBR green is a fluorescent probe having the ability to intercalate between the double-strands of DNA emitting a fluorescence at 550 nm. Hence, the intensity of the emitted

fluorescence is proportional to the produced number of amplicons during the qPCR, and it is measured at the end of the extension phase of each cycle. Once the wells were filled, the 384 well plate was sealed using a heat sealer device, then centrifuged for 60 seconds and placed in the thermocycler Light Cycler (LightCycler® 480, Roche Molecular System) for 40 amplification cycles. Each cycle contained 3 phases, a first phase of denaturation at 95°C (10-15 minutes) to melt the double-stranded DNA into single strands, followed by a hybridization phase at 60°C (2-60 seconds) where the primers bind to DNA and a last phase of elongation at 72°C (4-120 seconds) where the PCR enzymes synthesize the complementary strand of the exposed single-stranded DNA. After the end of the qPCR, the gene expression was quantified based on the cycle threshold (Ct) corresponding to the number of cycles at which the fluorescent probe SYBR linked to the PCR amplification was detected. The Ct level, thus, is inversely proportional to the amount of the targeted nucleic acids (genes) in the sample (for example the lower the Ct lever the greater the expression of the target gene). At the end, the transcriptional expression of the genes of interest was normalized to the expression of the housekeeping gene HPRT1 (hypoxanthine phosphoribosyl transferase 1) using the Pfaffl method (Pfaffl et al., 2002).

**Table 3: Human primers sequences used for the qPCR experiments.**

No	Primer name	Forward	Reverse
1	HPRT1	AG TT CT GT GG CC AT CT GC TT	CA AT CC GC CC AA AG GG AA CT
2	$\beta$ -actin	CA GA GC AA GA GA GG CA TC CT	AC GT AC AT GG CT GG GG TG
3	ORAI1	AG GT GA TG AG CC TC AA CG AG	CT GA TC AT GA GC GC AA AC AG
4	ORAI2	AC CT GG AA CT GG TC AC CT CT	AT GG CC AC CA TG GC AA AG C
5	ORAI3	CC AA GC TC AA AG CT TC CA GC C	CA AA GA GG TG CA CA GC CA CC A
6	STIM1	CT TC AG CA CA GT CC CT GT CA	TG TG GA GC TG CC TC AG TA TG
7	TRPC1	GA GG TG AT GG CG CT GA AG G	GC AC GC CA GC AA GA AA AG C

8	IL-6	AG AC AG CC AC TC AC CT CT TC AG	TT CT GC CA GT GC CT CT TT GC TG
9	IL-11	CT GT GG GG AC AT GA AC TG TG	AG GG TC TG GG GA AA CT CG
10	TGF- $\beta$ 1	AC AT CA AC GC AG GG TT CA CT	GA AG TT GG CA TG GT AG CC CT
11	ColA1	TC TG CG AC AA CG GC AA GG TG	GA CG CC GG TG GT TT CT TG GT
12	$\alpha$ SMA	CC GA CC GA AT GC AG AA GG A	AC AG AG TA TT TG CG CT CC GA A
13	SMAD2	GT TC CT GC CT TT GC TG AG AC	TC TC TT TG CC AG GA AT GC TT

#### IV. Cell Biology Techniques

##### IV.1) Western Blotting

##### IV.1.1) Protein extraction

PSCs (PS-1 and RLT-PSCs) or pancreatic cancer cells (MIA PaCa-2) were cultured in 60 mm Petri dishes ( $5 \times 10^5$  cells for PS-1, and  $2 \times 10^5$  cells for RLT-PSCs or MIA PaCa-2) or in 100 mm Petri dishes for the Co-immunoprecipitation experiments ( $1.5 \times 10^6$  for PS-1 cells) for 72 or 96 hours. Cells were then placed on ice; the culture medium was removed, and cells were washed twice with cold PBS (3 ml per 60 mm Petri dish and 5 ml per 100 ml dish). Thereafter cells were incubated with complete RIPA buffer (60  $\mu$ l of RIPA for the 60 mm Petri dishes and 110  $\mu$ l for the 100 mm dishes) for 30 minutes on ice. The RIPA buffer was composed of 1 % Triton X-100, 1 % sodium deoxycholate, 0.1 % SDS (Sodium Dodecyl Sulphate), 150 mM sodium chloride and 20 mM  $\text{PO}_4\text{Na}_2/\text{K}$  (pH 7.2), and it was supplemented before cell incubation with protease inhibitor cocktail (Sigma-Aldrich), 0.5 mM sodium orthovanadate (phosphatase inhibitor) and 2 mM EDTA. After 30 minutes of incubation, the Petri dishes were scratched on ice using scrapers to detach the cells, and then the whole cell lysate was transferred into 1.5 ml Eppendorf tube. The tubes were centrifuged for 15 minutes at 15 000 rpm at 4°C to separate the proteins (found in the supernatant) from the cellular debris. After centrifugation

the supernatant was collected to a new Eppendorf tube and proteins were dosed using the Bradford colorimetric method (Bio-Rad DC Protein Assay Kit) in 96 well plates. Before the dosage, proteins were diluted 1:5 into water and 5 µl of the diluted proteins was added per well, followed by the addition of 25 µl of a reagent mixture (1 ml of reagent A for 20 µl of reagent S) and 200 µl of reagent B. The 96 well plate was then protected from light and incubated under slow agitation for 20 minutes at room temperature. After that the optical densities of the obtained coloration of each sample were measured using a plate reader (spectrophotometer, Infinite P200 PRO™ TECAN) at 620 nm and the Tecan i-control software. The protein concentration was determined using a standard curve established from known BSA (Bovine Serum Albumin) concentrations. All proteins were stored at -20 °C until use.

#### **IV.1.2) Gel electrophoresis**

All the Western Blotting experiments were performed using 30 µg of proteins per condition, except for the Co-immunoprecipitation experiments where 500 µg of proteins per condition were used. The protein lysates containing 30 µg of proteins were completed with 5x Laemmli (62.5 mM Tris-base, 10 % glycerol, 2.3 % SDS, 5 % β-mercaptoethanol and bromophenol blue) and 1x Laemmli (diluted in water) buffer to reach a final volume of 39 µl. Samples were then denatured for 10 min at 95°C. After denaturation the whole sample volume was loaded into the wells (39 µl per well) of a polyacrylamide gel (PAG), followed by an one-dimensional electrophoresis performed into a Bio-Rad system according to the SDS-PAGE method (Sodium Dodecyl Sulphate – Polyacrylamide Gel Electrophoresis). For our experiments, PAGs with different percentages (10 % and 12 %) were made by the chemical polymerization of an acrylamide / bis-acrylamide mixture to separate the proteins according to their molecular weight, covered on the top with a 5 % stacking gel. Simultaneously with the protein loading, a molecular weight marker (Bio-Rad) was also loaded in a separate well in each PAG to follow the protein migration. The SDS-PAGE was then completed using a migration running buffer (10 % Tris-glycine, 1 % SDS at 10 % and 18 MΩ water) during 1 hour at 200 Volts permitting the migration of the negatively charged proteins and their separation according to their molecular weight.

After the end of the migration, proteins were transferred from the PAG to a nitrocellulose membrane through a liquid transfer during 2 hours at 60 Volts on ice. This step was realized using a transfer buffer that contained 10 % Tris-glycine, 20 % methanol and 18

MΩ water. Once the transfer was terminated, the nitrocellulose membrane containing the transferred proteins was incubated for 5 minutes in 1x Ponceau S staining solution under slow agitation to label in red the proteins. This step was done to verify whether the protein transfer was efficiently performed. The nitrocellulose membrane was then incubated with 3 % BSA diluted in TBS (Tris Buffered Saline) containing 0.1 % Tween-20 (TBS-T), for 1 hour under slow agitation in room temperature to prevent the non-specific binding of the antibodies. Thereafter, the nitrocellulose membrane was incubated with the primary antibody (which was diluted in 3% BSA + TBS-T) overnight at 4°C or during 2 hours at room temperature, under slow agitation. All the primary antibodies used for our experiments as well as their dilution are listed in **Table 4**.

The day after or after 2 hours of incubation at room temperature, the primary antibody was removed, and the membrane was washed at least 3 times with TBS-T, with 7 minute high agitation between each washing. The membrane was next incubated with the suitable secondary antibody anti-IgG (diluted in 3 % BSA + TBS-T, table 4) coupled to a horseradish peroxidase enzyme (HRP), for 1 hour under slow agitation at room temperature. Afterwards, the membrane was washed again 3 times with TBS-T (7 minutes each) under high agitation and with a 4<sup>th</sup> last wash only with TBS. The recognized by the secondary antibody proteins were then revealed by chemiluminescence using the ECL reagent (Enhanced ChemiLuminescence, Ozyme) with the ChemiDoc XRS device (Bio-Rad). Indeed, the ECL contains luminol and hydrogen peroxide which interact with the HRP conjugated to the secondary antibody permitting hence the signal emission of the target protein, which is then captured by the ChemiDoc and analysed by the Quantity One<sup>®</sup> software. Protein expression was quantified by densitometry analysing and measuring the emission signal intensity using the Quantity One<sup>®</sup> software. After quantification, the expression level of each protein of interest was normalized to the housekeeping protein expression GAPDH (Glyceraldehyde 3-phosphate dehydrogenase) or tubulin.



**Table 4: Antibodies used for Western Blot and Co-immunoprecipitation experiments.**

No	Antibody name	Primary antibody dilution	Primary antibody reference and supplier	Secondary antibody dilution
1	pAKT	1/500	Cell signalling, #9271S	1/2000
2	AKT	1/500	Cell signalling, #92725S	1/2000
3	pERK1/2	1/500	Cell signalling, #9101S	1/2000
4	ERK1/2	1/500	Cell signalling, #9102S	1/2000
5	pSMAD2	1/1000	Abcam, #ab188334	1/3000
6	SMAD2	1/1000	Abcam, #ab40855	1/3000
7	ORAI1	1/250	Sigma, # O8264	1/3000
8	ORAI3	1/200	Sigma Prestige, #HPA015022	1/3000
9	STIM1	1/1000	Cell signalling, #5668S	1/3000
10	TRPC1	1/1000	Abcam, #ab51255	1/3000
11	$\alpha$ SMA	1/1000	Abcam, # ab7817	1/3000
12	GAPDH	1/4000	Abcam, #ab8245	1/5000
13	Tubulin	1/1000	Sigma, #SAB4500087	1/3000

#### IV.2) Co-Immunoprecipitation

Co-Immunoprecipitation is a method utilized to reveal the physical interaction between two proteins through the recognition of a target protein antigen using a specific antibody. The formed antibody-protein complex is precipitated out of a solution by binding to a solid substrate, such as magnetic or agarose beads. For all the co-immunoprecipitation experiments we used protein A magnetic beads (PureProteome™, Millipore), which were pre-cleaned using complete RIPA buffer (containing protease inhibitor cocktail, sodium orthovanadate and EDTA) and with the help of the magnetic rack (Millipore). For each sample 100  $\mu$ l of pre-cleaned protein A magnetic beads were used, 50  $\mu$ l for the pre-fixation step and 50  $\mu$ l for

the antibody binding step. After calculating the total volume of the magnetic beads needed for all the experimental conditions, beads were washed twice with complete RIPA using the equivalent volume of the total beads' volume (for example for 300  $\mu$ l of beads 300  $\mu$ l of complete RIPA are added). After the last wash, beads were kept into complete RIPA on ice, in an equivalent volume of the initial total beads' volume. Simultaneously, protein samples were prepared with a volume corresponding to 500  $\mu$ g of proteins per condition and completed with RIPA (complete) buffer to reach a final volume of 300  $\mu$ l per sample. Thereafter, each protein sample was incubated with 50  $\mu$ l of precleaned magnetic beads for 90 minutes at 4°C under slow agitation. This step corresponds to the non-specific protein pre-fixation to the beads in the absence of the specific antibody. After the 90 minutes of incubation, the beads were removed, and the specific antibody was added to each sample (all the used antibodies are listed in **Table 5**). However, each time a control sample without the specific antibody was made to confirm the specificity of the beads. The samples were the incubated overnight at 4°C under slow agitation. The next day the formed antigen-antibody complex was precipitated by adding 50  $\mu$ l of precleaned magnetic beads to each sample, followed by an incubation of 1 hour at 4°C under slow agitation. The supernatant was then removed, and the beads of each sample were washed twice with 100  $\mu$ l of complete RIPA buffer. After that, the beads were resuspended in 50  $\mu$ l of 1x Laemmli and proteins were denatured for 10 minutes at 95°C. At the end, the beads were discarded, and the protein samples were loaded in SDS-PAGE for standard Western Blot.

**Table 5: Antibodies used as Co-immunoprecipitation antibody.**

No	Antibody name	Co-immunoprecipitation (Co-IP) antibody dilution	Primary antibody dilution	Co-IP and primary antibody reference and supplier	Secondary antibody dilution
1	SMAD2	1/100	1/500	Abcam, #ab40855	1/2000
2	pSMAD2	1/100	1/500	Abcam, #ab188334	1/2000
3	ORAI1	1/100	1/250	Sigma, # O8264	1/2000
4	TRPC1	1/100	1/500	Abcam, #ab51255	1/2000
5	$\alpha$ SMA	1/200	1/1000	Abcam, # ab7817	1/3000

No	Secondary antibody name	Reference and supplier	Type
1	Anti-Mouse IgG	Cell signalling #7076S	HRP-linked
2	Anti-Rabbit IgG	Cell signalling #7074P2	HRP-linked

### IV.3) Immunofluorescence

Immunofluorescence is another technique of protein detection based on the use of antibodies conjugated to fluorescent dyes. These experiments were carried out on PSCs cultured on glass coverslips to avoid any autofluorescence emission.  $2 \times 10^4$  non-transfected PS-1 cells and  $1 \times 10^4$  non-transfected RLT-PSCs were plated on 14 mm autoclaved glass coverslips for 72 hours, priorly placed in a 12 well plate. After 72 hours of culture, the medium was removed, and cells were gently rinsed twice with filtered PBS (500  $\mu$ l per well). Cells were then fixed using 4 % of paraformaldehyde diluted in filtered PBS for 20 min at room temperature. The fixation solution was after that removed and cells were carefully washed twice with PBS followed by 1 minute of slow agitation. Cells were next permeabilized using 0.1 % of saponin diluted in filtered PBS for 10 minutes at room temperature, followed by 3 successive washes with filtered PBS of 1-minute gentle shaking. After the last wash, the coverslips were transferred to a humidified protected from light chamber, where cells were incubated with 5 % of BSA diluted in filtered PBS (blocking solution) for 45 minutes at room temperature to prevent the non-specific binding of the antibodies. Thereafter, the blocking solution was removed, and cells were incubated with the primary antibody diluted in 5 % BSA+ filtered PBS (60  $\mu$ l per coverslip) overnight at 4°C (all the used antibodies are detailed in **Table 6**). The next day the primary antibody was removed, the coverslips were washed 3 times with filtered PBS (100  $\mu$ l per coverslip) and cells were incubated with the secondary antibody (diluted in 5 % BSA + filtered PBS) conjugated to a fluorophore for 45 minutes at room temperature in the dark. The secondary antibodies utilized for our experiments were the secondary AlexaFluor<sup>®</sup> 550 conjugated antibody (IgG DyLight, Thermo Fischer Scientific) and the secondary AlexaFluor<sup>®</sup> 488 conjugated antibody (Invitrogen). AlexaFluor<sup>®</sup> 550 was used for all the anti-rabbit primary antibodies, while AlexaFluor<sup>®</sup> 488 was used for all the anti-mouse primary antibodies. All the double labelings were made in a sequential manner incubating the following primary antibody after the washing of the first secondary antibody. Afterwards, cells were rinsed 3 times with filtered PBS (100  $\mu$ l per coverslip) and then the nucleus was labelled using

a DAPI (4',6-diamidino-2-phenylindole) solution (1 µg/ml, 60µl per coverslip, Sigma-Aldrich) for 10 minutes at room temperature in the dark. DAPI solution was after that removed, cells were washed twice with filtered PBS (100 µl per coverslip) and the coverslips with the labelled cells were then mounted on glass slides using the mounting medium ProLong® Gold Antifade Mountant (Thermo Fisher Scientific). After drying of the mounting medium, the glass slides were analyzed by confocal microscopy where the fluorescence image acquisition was made using the LSM710 confocal microscope and the ZEN software (Carl Zeiss MicroImaging). The acquired images were after that analyzed with the Fiji Image J software.

**Table 6: Antibodies used for immunofluorescence staining.**

No	Antibody name	Primary antibody dilution	Primary antibody reference and supplier	Secondary antibody dilution
1	TRPC1(rabbit)	1/200	Alomone, #ACC-010	1/200
2	TRPC1 (mouse)	1/50	Santa Cruz, # sc-133076	1/50
3	ORAI1	1/100	ProSciΨ, # 3F6H5	1/100
4	pSMAD2	1/100	Abcam, #ab188334	1/100
5	αSMA	1/1000	Abcam, # ab7817	1/1000

#### **IV.4) Enzyme-Linked Immunosorbent Assay (ELISA)**

ELISA dosage is a high-sensitive quantitative method used to measure the amount of proteins or antibodies presented in a biological sample, such as the cell culture supernatant, the serum plasma, and cell/tissue lysates, based on an antigen-antibody reaction (like the immunoprecipitation principle). For our experiments we utilized two ELISA kits, one for the detection of the secreted TGF-β1 in the cell culture supernatant, and one for the detection of the secreted IL-6. The TGF-β1 ELISA kit was supplied by Sigma-Aldrich (reference: RAB0460) while the IL-6 ELISA kit was provided by Invitrogen (# 88-7066-86). The whole experimental procedure was strictly realized according to the technical protocol provided by the supplier.

All the ELISA dosages were performed on cell culture supernatants from transfected or treated PS-1 cells for 72 or 96 hours. Cells were plated in 100 mm Petri dishes ( $1 \times 10^6$  cells) or 60 mm dishes ( $5 \times 10^5$ ) for 72 or 96 hours, and then the supernatant from each condition was collected in 15 ml tubes and centrifuged for 5 minutes at 1100 rpm to eliminate all the cellular debris. The collected supernatant was then aliquoted in 2 ml Eppendorf tubes and stored at  $-80^\circ\text{C}$  until use. Before performing the experiments, a “test” dosage for each cytokine was done in order to determine the appropriated dilution of each cytokine to use according to the detection sensitivity of each kit. After testing several dilutions (cascade dilutions) for TGF- $\beta$ 1 and IL-6, we determined a supernatant dilution of 1:16 as optimal for TGF- $\beta$ 1 dosage (Sigma-Aldrich) and of 1:800 for IL-6 (Invitrogen). These dilutions can vary with the use of different ELISA kits but also with the cellular density. Briefly after determining the optimal dilution to use, 100  $\mu\text{l}$  of the diluted supernatant was added, per well, in a specific capture antibody coated (with TGF- $\beta$ 1 or IL-6) 96 well plate, and then the plate was incubated overnight at  $4^\circ\text{C}$  under gentle agitation. During this step the target protein (TGF- $\beta$ 1 or IL-6) present in the supernatant will bind to the wells by the immobilized antibody. However, for TGF- $\beta$ 1 dosage, a supplementary step was done before incubation of the diluted supernatant. All the samples were treated with 1 N HCl for 10 minutes at room temperature to activate the latent TGF- $\beta$ 1 to its immunoreactive form, and then were neutralized with 1.2 N NaOH/0.5 N HEPES, followed by the sample incubation in the pre-coated 96 well plate. The next day, wells were carefully washed (4 washes) and then incubated with 100  $\mu\text{l}$  (per well) of diluted biotinylated detection antibody specific for the target protein for 1 hour at room temperature under slow agitation. Thereafter, wells were carefully washed (4 washes) and incubated with 100  $\mu\text{l}$  (per well) of HRP (horseradish peroxidase) -conjugated streptavidin solution which will detect the biotinylated bound antibody for 45 minutes at room temperature under gentle agitation. The wells were then again washed (6 times) and 100  $\mu\text{l}$  of TMB (3, 3', 5, 5'-tetramethylbenzidine) substrate solution which will detect the HRP was added to each well for 30 minutes at room temperature under slow agitation. The detection of HRP by the TMB substrate will permit the obtention of a blue coloration that is proportional to the amount of the target protein (TGF- $\beta$ 1 or IL-6) bound to the streptavidin-biotinylated HRP complex. At the end, 50  $\mu\text{l}$  of stop solution was added to each well to stop the reaction changing the blue coloration to yellow, and the absorbance of this yellow coloration was measured at 450 nm with a plate reader (spectrophotometer, Infinite P200 PRO™ TECAN). TGF- $\beta$ 1 and IL-6 concentrations were then quantified taking in consideration the dilution factor of each cytokine and using the obtained equation from each standard curve.

Indeed, for each used 96 well plate, a standard curve was done following the technical protocol given by the supplier.

## V. Calcium imaging

Calcium imaging is a technique used to measure in real-time the fluctuations of the intracellular  $\text{Ca}^{2+}$  levels in living non-fixed cells using  $\text{Ca}^{2+}$ -sensitive fluorescent probes. One of the most utilized probes is the Fura2 probe coupled to an acetoxymethyl ester group (Fura2-AM) permitting to the dye to cross the cell plasma membrane. Once Fura2-AM is inside the cell, the acetoxymethyl ester group will be cleaved by cellular esterases forming the pentacarboxylate  $\text{Ca}^{2+}$  indicator Fura2 which cannot anymore exit the cell. The particularity of Fura2 is that it is a ratiometric  $\text{Ca}^{2+}$  fluorescent sensor having 2 excitation wavelengths, at 340 nm and at 380 nm, and a same emission wavelength at 510 nm. The binding of Fura2 to free- $\text{Ca}^{2+}$  induces an increase of the excitation wavelength fluorescence at 340 nm while the non-binding to  $\text{Ca}^{2+}$  induces an augmentation of the excitation wavelength fluorescence at 380 nm, both measured at the same emission wavelength. Hence, the ratio of both excitation wavelength fluorescence ( $F_{340}/F_{380}$ ) emitted at the same wavelength (510 nm) reflects the intracellular  $\text{Ca}^{2+}$  concentration.

To perform this type of experiment, PS-1 cells ( $8 \times 10^4$  cells) and RLT-PSCs ( $6 \times 10^4$  cells) were seeded on 30 mm autoclaved glass coverslips priorly placed in 35 mm Petri dishes each. The use of glass coverslips is important for the  $\text{Ca}^{2+}$  imaging measurements to avoid any possible emitted autofluorescence from the plastic material of the Petri dishes. After 72 hours post-transfection or post-proliferation, the culture medium was removed and cells were loaded with 3  $\mu\text{M}$  Fura2-AM (Sigma-Aldrich) in extracellular saline solution (ECSS) (145 mM NaCl, 5 mM KCl, 10 mM HEPES, 5 mM D-glucose, 2 mM  $\text{CaCl}_2$  and 1 mM  $\text{MgCl}_2$ ) at pH 7.4, for 45 minutes at 37°C in the dark. After Fura2 incubation, the extracellular saline solution (ECSS) containing the probe was discarded and cells were washed 3 times and kept in ECSS at pH 7.4 until the beginning of the fluorescence measurement. The washed coverslips were then removed from the culture Petri dishes and were placed onto pierced bottom Petri dishes using silicone grease. Thereafter, the coverslips were transferred into a perfusion chamber on a Zeiss inverted microscope equipped for fluorescence and Fura2 fluorescence was excited alternatively at 340 nm and 380 nm using the monochromator polychrome IV (TILL Photonics, Planegg, Germany). Fluorescence fluctuations were then captured using a Cool SNAP HQ camera

(Princeton Instruments) after filtration through a long-pass filter (510 nm emission wavelength) and were analyzed using the Metafluor software (version 7.1.7.0, Molecular Devices). During the whole experimental procedure, cells were continuously perfused with ECSS at room temperature in the dark, maintaining a stable flow rate of 1 ml/min and a chamber volume of 700  $\mu$ l.

The SOCE of PSCs was measured by a 2 minute-perfusion of ECSS (containing 2 mM  $\text{CaCl}_2$  and 1 mM  $\text{MgCl}_2$ ) which was after removed by an aspiration pump, followed by 2-minute perfusion of  $\text{Ca}^{2+}$ -free ECSS (containing only 1 mM  $\text{MgCl}_2$ ). Thereafter, the  $\text{Ca}^{2+}$ -free ECSS was replaced by  $\text{Ca}^{2+}$ -free ECSS containing 1  $\mu$ M Thapsigargin (Sigma-Aldrich), perfused until to reach a peak of the fluorescence ratio, and then replaced again with only  $\text{Ca}^{2+}$ -free ECSS until the 15<sup>th</sup> minute of the signal acquisition. Indeed, Thapsigargin is an irreversible inhibitor of the sarco-/endoplasmic reticulum  $\text{Ca}^{2+}$ -ATPase (SERCA) pump inducing indirectly a  $\text{Ca}^{2+}$  release from the endoplasmic reticulum. After the  $\text{Ca}^{2+}$  depletion, a 2mM  $\text{Ca}^{2+}$ -ECSS solution (also containing 1 mM  $\text{MgCl}_2$ ) was perfused for 10 minutes in order to measure the Thapsigargin-induced SOCE, and then a  $\text{Ca}^{2+}$ -free ECSS was again perfused as a control for 10 minutes. At the end of the experiments, we were able to obtain 2 types of information, one on the basal  $\text{Ca}^{2+}$  concentration of the cells which was reflected by the measurement of the basal fluorescence ratio obtained during the first 2 minutes of the ECSS (2 mM  $\text{CaCl}_2$  + 1mM  $\text{MgCl}_2$ ) perfusion, and another information on the SOCE. These informations were obtained after analyzing the acquired signals using the Origin 7.0 software (OriginLabs Corporation).

## VI. Statistical analysis

All the presented data within this work are illustrated as mean  $\pm$  SEM (Standard Error of Mean), followed by the number of the used cell passages (referred as N) and the total number of the used cells (referred as n). All the experiments were carried out with at least 3 different cell passages, except of some preliminary illustrated data. The mean values of the different experimental groups were analyzed by Student's *t*-test, one-way ANOVA or two-way ANOVA performed with Bonferroni or Tukey's post hoc test, for multiple comparison and depending to the compared conditions, using the GraphPad Prism software (version 5 and 7). Differences between the values were considered as significant when p-value was less than 0.05 ( $p < 0.05$ ). The p-values  $< 0.05$ ,  $< 0.01$ ,  $< 0.001$  and  $< 0.0001$  are represented as \*, \*\*, \*\*\*, and \*\*\*\*, respectively.



---

# **RESULTS AND DISCUSSION**

---





## **Part N°1:**

### **Orai1 channel regulates human activated pancreatic stellate cell's proliferation and TGF $\beta$ 1 secretion through the AKT signalling pathway**

#### **Summary:**

PDAC is characterized by an excessive dense desmoplastic stroma surrounding the PCCs, which accounts for up to 80% of the total tumour volume, liable for the early tumour spreading and resistance to existing treatments. The major cellular component of this fibrotic tissue is the activated PSCs, found to be in permanent communication with the PCCs, providing them with the ideal microenvironment leading to PDAC development and progression. Even though these cells exist in a quiescent state in the normal pancreas, during pancreatic carcinogenesis, they become activated acquiring, among others, an increased  $\alpha$ SMA expression and ECM synthesis, high proliferative and migratory capacities, and they also abundantly secrete diverse cytokines (Ferdeik and Jakubowska, 2017). Among the PSC-secreted cytokines, TGF- $\beta$ 1 has been demonstrated to play a crucial role in pancreatic fibrous tissue development and in PSC's activation through existing autocrine loops (Kruse et al., 2000).

In addition, most of the above-cited cellular processes are known to be controlled by the intracellular second messenger Ca<sup>2+</sup> in various cell types. Indeed, one of the principal Ca<sup>2+</sup> entry pathways in non-excitabile cells is the SOCs, mainly constituted of the channel pore-forming Orai1 protein and the Ca<sup>2+</sup>-sensing stromal interaction molecule STIM1. However, so far, the role of SOC-mediated Ca<sup>2+</sup> entry in the regulation of PSC's activation processes has not yet been elucidated. We thus aimed to investigate, at a first place, the role of SOC-mediated Ca<sup>2+</sup> entry, mainly focusing on Orai1-mediated Ca<sup>2+</sup> entry, in activated PSC's proliferation, TGF- $\beta$ 1 synthesis, and secretion, as well as the associated signalling mechanisms. We evaluated these activation processes using two human activated PSC cell lines of different origin, namely PS-1 and RLT-PSCs. Indeed, the PS-1 cell line is isolated from a healthy donated human pancreas (Froeling et al., 2009), whereas RLT-PSC cell line is originated from a pancreatic tissue resection of patient with chronic pancreatitis (Jesnowski et al., 2005). Simultaneously, we wondered whether Orai1 and Orai1-mediated Ca<sup>2+</sup> entry could be involved in TGF- $\beta$ 1-mediated autocrine PSCs stimulation using the PS-1 cells.

We firstly evaluated the functional expression of the Orai1 channel in both used human cellular models of activated PSCs, PS-1 and RLT-PSCs, after Orai1 silencing for 72h, using the siRNA approach. We then measured Orai1-mediated Ca<sup>2+</sup> entry by Ca<sup>2+</sup>-imaging, applying a

Tg-induced SOCE protocol, and we found that Orai1 channel mediates SOCE in both PS-1 and RLT-PSCs. We thereafter sought to know whether the functionally expressed Orai1 channel plays an important role in PSC's activation, assessing two main PSC's activation processes, the cell proliferation, and cytokine expression and secretion. Among the known PSC-expressed and secreted cytokines, we chose to focus on TGF- $\beta$ 1 since it is the major profibrotic cytokine, shown to have a crucial role in PSC's activation and in the dialogue between activated PSCs and PCCs. On the one hand, the invalidation of Orai1 for 72h resulted in a similar decrease of the proliferation rate in PS-1 and RLT-PSCs, quantified by MTT colorimetric assay, demonstrating a role of Orai1 in the modulation of activated PSC's proliferation. Moreover, we wanted to know by which cell cycle phase Orai1 mediates PSC proliferation. To address this question, we assessed the cell cycle phase distribution by flow cytometry in 72h siCtrl and siOrai1 PS-1 transfected cells, and we revealed a cell cycle arrest illustrated by a cell accumulation in G0/G1 phase. On the other hand, Orai1 knocking induced a similar decrease of TGF- $\beta$ 1 mRNA expression in both PS-1 and RLT-PSCs, as quantified by qPCR, and diminished TGF- $\beta$ 1 secretion measured by Elisa assay in PS-1 cells, indicating that Orai1 mediates TGF- $\beta$ 1 expression and secretion in activated PSCs.

We then wondered by which signalling pathway Orai1 could regulate these two PSC's activation processes. Based on the already well-defined signalling pathways shown to drive PSC's activation, we chose to evaluate three of the major pathways, namely the AKT, ERK1/2, and SMAD2 pathway (Masamune and Shimosegawa, 2009). Among them, Orai1 was able to only activate the AKT signalling pathway in PS-1 and RLT-PSCs, suggesting that Orai1 is probably implicated in the regulation of activated PSC's proliferation and TGF- $\beta$ 1 expression and secretion through the AKT pathway. To further assess this hypothesis, we treated PS-1 non-transfected cells with the AKT pharmacological inhibitor LY 294002, and as for siOrai1 transfected cells, we noted a reduction of their proliferation rate, as well as TGF- $\beta$ 1 expression and secretion. However, to determine whether all these mechanisms are driven by the Orai1-mediated  $\text{Ca}^{2+}$  influx in activated PS-1 cells, we reduced the extracellular  $\text{Ca}^{2+}$  concentration, and we first evaluated the impact on AKT phosphorylation, observing a decrease of its activation in the low  $\text{Ca}^{2+}$ -conditions (0.1 mM) compared to the physiological  $\text{Ca}^{2+}$ -conditions (1.4 mM). We then investigated the impact of siOrai1 transfected cells under 0.1 mM  $\text{Ca}^{2+}$  conditions on PSC's proliferation, revealing an additive effect in siOrai1-reduced proliferation in low  $\text{Ca}^{2+}$ -conditions compared to siOrai1-decreased proliferation in 1.4 mM  $\text{Ca}^{2+}$  conditions, due to an increase of the cell mortality. At the same time, we did not observe any difference in

TGF- $\beta$ 1 secretion between siOrai1 cells under low  $\text{Ca}^{2+}$  -conditions and the ones in physiological  $\text{Ca}^{2+}$  -conditions, indicating that Orai1-mediated  $\text{Ca}^{2+}$  influx mediates PSC-induced TGF- $\beta$ 1 secretion and in part PSC's proliferation.

Interestingly, we identified that Orai1-induced TGF- $\beta$ 1 secretion in PS-1 cells is involved in an autocrine feedback loop promoting Orai1-mediated PSC's proliferation. Additionally, we also found that TGF- $\beta$ 1 activates the Orai1-mediated AKT pathway and increases the Orai1-mediated  $\text{Ca}^{2+}$  influx. We could associate the stimulatory effect of TGF- $\beta$ 1 on Orai1/AKT-dependent proliferation to TGF- $\beta$ 1-induced Orai1 mRNA and protein expression increase, and consequently to TGF- $\beta$ 1-promoted Orai1 functional expression.

Taken together, these data revealed a novel role of Orai1 channel in the regulation of PSC's activation processes and highlighted the importance of TGF- $\beta$ 1 in the maintenance of PSC's activation, summarized in the below scheme (**Figure 23**) and better detailed in the following publication: Radoslavova S., Folcher A., Lefebvre T., Kondratska K., Guénin S., Dhennin-Duthille I., Gautier M., Prevarskaya N., and Ouadid-Ahidouch H. (2021). **Orai1 Channel Regulates Human-Activated Pancreatic Stellate Cell Proliferation and TGF $\beta$ 1 Secretion through the AKT Signaling Pathway.** *Cancers* 13, 2395.

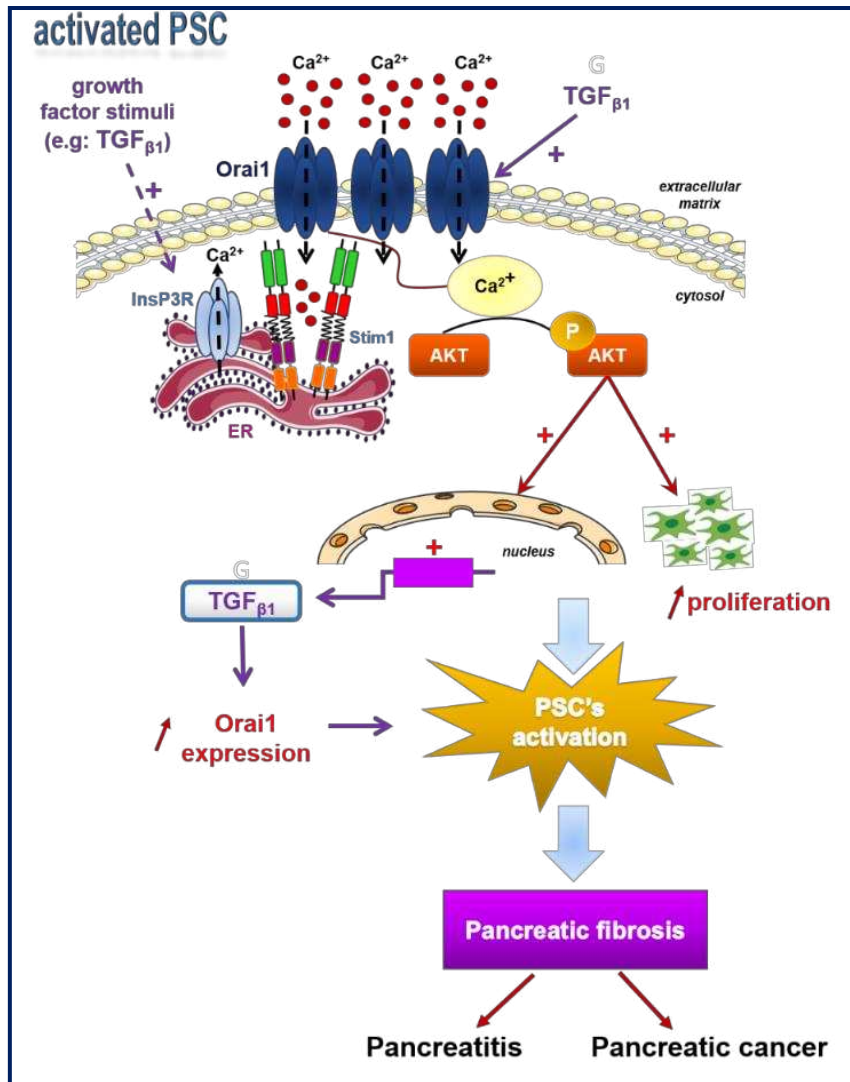


Figure 23: Summarized scheme of Orai1 role in PSC's activation processes.

## Article

# Orai1 Channel Regulates Human-Activated Pancreatic Stellate Cell Proliferation and TGF $\beta$ <sub>1</sub> Secretion through the AKT Signaling Pathway

Silviya Radoslavova<sup>1,2</sup>, Antoine Folcher<sup>2</sup> , Thibaut Lefebvre<sup>1</sup>, Kateryna Kondratska<sup>2</sup>, Stéphanie Guénin<sup>3</sup>, Isabelle Dhennin-Duthille<sup>1</sup> , Mathieu Gautier<sup>1</sup> , Natalia Prevarskaya<sup>2,†</sup> and Halima Ouadid-Ahidouch<sup>1,\*,†</sup>

<sup>1</sup> Laboratory of Cellular and Molecular Physiology, UR-UPJV 4667, University of Picardie Jules Verne, 80039 Amiens, France; silviya.radoslavova@etud.u-picardie.fr (S.R.); th.lefebvre27@gmail.com (T.L.); isabelle.dhennin@u-picardie.fr (I.D.-D.); mathieu.gautier@u-picardie.fr (M.G.)

<sup>2</sup> University of Lille, Inserm U1003-PHYCEL-Cellular Physiology, 59000 Lille, France; antoine.folcher@inserm.fr (A.F.); kateryna.kondratska@inserm.fr (K.K.); natacha.prevarskaya@univ-lille.fr (N.P.)

<sup>3</sup> Centre de Ressources Régionales en Biologie Moléculaire, UFR des Sciences, 80039 Amiens, France; stephanie.vandecasteele@u-picardie.fr

\* Correspondence: halima.ahidouch-ouadid@u-picardie.fr; Tel.: +33-3-22-82-7646; Fax: +33-3-2282-7550

† These authors contributed equally to this work.



**Citation:** Radoslavova, S.; Folcher, A.; Lefebvre, T.; Kondratska, K.; Guénin, S.; Dhennin-Duthille, I.; Gautier, M.; Prevarskaya, N.; Ouadid-Ahidouch, H. Orai1 Channel Regulates Human-Activated Pancreatic Stellate Cell Proliferation and TGF $\beta$ <sub>1</sub> Secretion through the AKT Signaling Pathway. *Cancers* **2021**, *13*, 2395. <https://doi.org/10.3390/cancers13102395>

Academic Editor: Alexander Arlt

Received: 30 March 2021

Accepted: 12 May 2021

Published: 15 May 2021

**Publisher's Note:** MDPI stays neutral with regard to jurisdictional claims in published maps and institutional affiliations.



**Copyright:** © 2021 by the authors. Licensee MDPI, Basel, Switzerland. This article is an open access article distributed under the terms and conditions of the Creative Commons Attribution (CC BY) license (<https://creativecommons.org/licenses/by/4.0/>).

**Simple Summary:** Activated pancreatic stellate cells (aPSCs), the main source of cancer-associated fibroblasts in pancreatic ductal adenocarcinoma (PDAC), are well known as the key actor of the abundant fibrotic stroma development surrounding the tumor cells. In permanent communication with the tumor cells, they enhance PDAC early spreading and limit the drug delivery. However, the understanding of PSC activation mechanisms and the associated signaling pathways is still incomplete. In this study, we aimed to evaluate the role of Ca<sup>2+</sup>, and Orai1 Ca<sup>2+</sup> channels, in two main PSC activation processes: cell proliferation and cytokine secretion. Indeed, Ca<sup>2+</sup> is a versatile second messenger implicated in the regulation of numerous biological processes. We believe that a better comprehension of PSC Ca<sup>2+</sup>-dependent activation mechanisms will bring up new crucial PDAC early prognostic markers or new targeting approaches in PDAC treatment.

**Abstract:** Activated pancreatic stellate cells (aPSCs), the crucial mediator of pancreatic desmoplasia, are characterized, among others, by high proliferative potential and abundant transforming growth factor  $\beta$ <sub>1</sub> (TGF $\beta$ <sub>1</sub>) secretion. Over the past years, the involvement of Ca<sup>2+</sup> channels in PSC pathophysiology has attracted great interest in pancreatic cancer research. We, thus, aimed to investigate the role of the Orai1 Ca<sup>2+</sup> channel in these two PSC activation processes. Using the siRNA approach, we invalidated Orai1 expression and assessed the channel functionality by Ca<sup>2+</sup> imaging, the effect on aPSC proliferation, and TGF $\beta$ <sub>1</sub> secretion. We demonstrated the functional expression of the Orai1 channel in human aPSCs and its implication in the store-operated Ca<sup>2+</sup> entry (SOCE). Orai1 silencing led to a decrease in aPSC proliferation, TGF $\beta$ <sub>1</sub> secretion, and AKT activation. Interestingly, TGF $\beta$ <sub>1</sub> induced a higher SOCE response by increasing Orai1 mRNAs and proteins and promoted both AKT phosphorylation and cell proliferation, abolished by Orai1 silencing. Together, our results highlight the role of Orai1-mediated Ca<sup>2+</sup> entry in human aPSC pathophysiology by controlling cell proliferation and TGF $\beta$ <sub>1</sub> secretion through the AKT signaling pathway. Moreover, we showed a TGF $\beta$ <sub>1</sub>-induced autocrine positive feedback loop by promoting the Orai1/AKT-dependent proliferation via the stimulation of Orai1 expression and function.

**Keywords:** activated pancreatic stellate cells; Orai1 channel; TGF $\beta$ <sub>1</sub>; cell proliferation; AKT activation

## 1. Introduction

Extensive desmoplastic stroma is the central pathological feature of pancreatic ductal adenocarcinoma (PDAC), responsible for the tumor's development, progression, metastasis, and treatment resistance. This fibrotic stroma is mainly composed of cancer-associated fibroblasts (CAFs), also called pancreatic stellate cells (PSCs). Indeed, activated PSCs are the orchestrators of fibrotic desmoplasia development and the major source of CAFs in PDAC [1–4].

In the healthy pancreas, PSCs are stromal vitamin A lipid-storing cells residing in an inactive-quiescent state that accounts for 4–7% of the organ. Quiescent PSCs are known to maintain pancreatic tissue architecture by sustaining the balance between extracellular matrix (ECM) secretion and degradation. However, in response to pancreatic injury, inflammation, or carcinogenic processes, PSCs undergo morphological and functional modifications to acquire a myofibroblast-like phenotype and become activated. This transition is followed by a loss of vitamin A-containing lipid droplets, an increase in alpha-smooth muscle actin ( $\alpha$ SMA) expression, and ECM secretion, such as type I collagen. PSC activation induces the enhancement of their proliferative and migratory potentials, leading to the development of the dense fibrotic tissue surrounding the pancreatic cancer cells (PCCs) and disrupting the drug delivery [5–8]. Indeed, during PDAC, this desmoplastic reaction formed by the PSC-induced fibrotic tissue accounts for 80% of the tumor's total volume. In fact, it is well known that activated PSCs establish a dynamic dialogue with the PCCs, and profoundly affect the tumor cell behavior by promoting PCCs proliferation, migration, and invasion to enhance PDAC early spreading [4,9].

PSC activation is also characterized by abundant secretion of various cytokines, chemokines, and growth factors, such as the transforming growth factor  $\beta_1$  (TGF $\beta_1$ ) [10,11]. TGF $\beta_1$  is well known now as the profibrotic critical regulator of pancreatic fibrosis, which drives PSC activation through the regulation of  $\alpha$ SMA expression, cell proliferation, and ECM synthesis, mainly by type I collagen synthesis [12–14]. This TGF $\beta_1$ -mediated autocrine loop contributes to the sustained activation of PSCs [15–17].

All these cellular processes implicated in PSC activation are controlled by intracellular signal transduction pathways [10,18,19]. Among these pathways, the serine-threonine kinase AKT has been reported to regulate PSC proliferation and cell cycle progression. Schwer et al. have demonstrated that blockade of the PI3K/AKT pathway with carbon monoxide releasing molecule-2 (CORM-2) inhibited PSC proliferation and induced the cell cycle arrest in the G0/G1 phase [20]. Moreover, Zhang et al. highlighted the effect of the tumor suppressor PTEN (phosphatase and tensin homolog), known to reduce AKT phosphorylation, on the inhibition of PSC proliferation and apoptosis [21]. Furthermore, Nishida et al. have shown the involvement of PI3K/AKT in the regulation of platelet-derived growth factor-induced PSC migration [10,18].

Moreover, most of the biological processes, including cell proliferation, survival, migration, or protein secretion, are driven by intracellular Ca<sup>2+</sup>, which acts as a universal second messenger. A few studies have revealed that intracellular Ca<sup>2+</sup> signaling is also crucial for the regulation of PSC physiology. Won et al. were the first to demonstrate that Ca<sup>2+</sup> signaling is different between quiescent and activated PSCs. Activated PSCs were characterized by transient elevations of intracellular Ca<sup>2+</sup> in response to thrombin or trypsin, which were absent in quiescent PSCs. They have also reported that nuclear Ca<sup>2+</sup> signals are essential for promoting activated PSC proliferation [22]. Therefore, one of the major Ca<sup>2+</sup> entry pathways in non-excitabile cells is the store-operated calcium channels (SOCs), also known as Ca<sup>2+</sup> release-activated Ca<sup>2+</sup> (CRAC) channels. SOCs are mainly composed of the pore-forming Orai1 protein and the Ca<sup>2+</sup>-sensing stromal interaction molecule STIM1, and they become activated after endoplasmic reticulum (ER) Ca<sup>2+</sup> depletion [23]. A recent study has pharmacologically identified the presence of CRAC channels in mice PSCs [24]. These data were supported by Waldron et al., who demonstrated the expression of Orai1, Orai2, and STIM1 in mice PSCs [25].

Although many studies have been focused on the molecular and cellular mechanisms of PSC activation, a very limited number of data is available on the role of  $\text{Ca}^{2+}$  and SOCs channels in the regulation of PSC activation and the associated signaling pathways. In the present study, we focused on two principal PSC activation hallmarks, (i) cell proliferation and (ii) cytokine secretion, particularly  $\text{TGF}\beta_1$  secretion. We aimed to investigate the role of  $\text{Ca}^{2+}$  entry through the Orai1 channel in the regulation of these two processes and the associated molecular mechanisms. We showed, for the first time, that the Orai1 channel is expressed and functional in human-activated PSCs. Moreover, we demonstrated that Orai1- $\text{Ca}^{2+}$  entry is essential for human-activated PSC proliferation and  $\text{TGF}\beta_1$  secretion by triggering the activation of the AKT signaling pathway. Interestingly,  $\text{TGF}\beta_1$  treatment induced an autocrine positive feedback loop, which led to the enhancement of PSC Orai1/AKT-dependent proliferation through the regulation of Orai1 activity and expression.

## 2. Results

### 2.1. Functional Expression of Orai1 Channel in PS-1 and RLT Human-Activated PSCs

At first, the activated state of PS-1 and RLT human immortalized PSCs was determined by the presence of  $\alpha\text{SMA}$  expression, the main activation marker of PSCs, using Western blot experiments (Figure 1(Aa, Da), respectively). We, therefore, investigated Orai1 channel expression, also by Western blotting, which revealed its presence in the PS-1 (Figure 1(Ab)) and RLT (Figure 1(Db)) human-activated PSCs, and by immunofluorescence staining for PS-1 (Figure S1A).

To establish whether Orai1 channels are functional too in PS-1 and RLT cells, we performed  $\text{Ca}^{2+}$  - imaging experiments using Fura2/AM fluorescent probe. Since, it is well known that Orai1 is one of the key players of store-operated  $\text{Ca}^{2+}$  entry (SOCE) in the majority of cell types, we evaluated this possibility by using the siRNA approach. Orai1 protein expression was decreased by  $60.54 \pm 4.40\%$  in PS-1 cells ( $N = 3, p < 0.001$ , Figure 1(Ba, Bb)), and by  $38.38 \pm 13.26\%$  in RLT cells ( $N = 3, p < 0.05$ , Figure 1(Ea, Eb)), 72 h post-transfection. We then measured the SOCE after an endoplasmic reticulum (ER)  $\text{Ca}^{2+}$  depletion induced by thapsigargin (Tg), which acts as an irreversible inhibitor of the sarco/endoplasmic reticulum  $\text{Ca}^{2+}$ -ATPase (SERCA) pump. Orai1 silencing reduced SOCE by 67.81% (siCtrl:  $100 \pm 2.52\%$ , siOrai1:  $32.19 \pm 1.36\%$ ,  $N = 5, p < 0.001$ , Figure 1(Ca, Cb)) in PS-1 cells, and by 72.65% (siCtrl:  $100 \pm 3.54\%$ , siOrai1:  $27.35 \pm 1.55\%$ ,  $N = 3, p < 0.001$ , Figure 1(Fa, Fb)) in RLT cells. Moreover, in both, PS-1 and RLT cells, Orai1 knocking down decreased the  $\text{Ca}^{2+}$  basal fluorescence ratio, by 5.93% (siCtrl:  $100 \pm 1.25\%$ , siOrai1:  $94.07 \pm 0.84\%$ ,  $N = 5, p < 0.001$ , Figure S1(Ba)) and by 17.17% (siCtrl:  $100 \pm 1.42\%$  siOrai1:  $82.83 \pm 1.51\%$ ,  $N = 3, p < 0.001$ , Figure S1(Bb)), respectively. However, contrary to PS-1 cells (siCtrl:  $100 \pm 4.21\%$ , siOrai1:  $101.35 \pm 3.53\%$ ,  $N = 5$ , Figure 1(Ca, Cc)), Orai1 inhibition led to 21.80% reduction in the  $\text{Ca}^{2+}$  ER depletion induced by Tg, in RLT cells (siCtrl:  $100 \pm 2.61\%$ , siOrai1:  $78.20 \pm 5.60\%$ ,  $p < 0.001$ ,  $N = 3$ , Figure 1(Fa, Fc)).

These results showed that the Orai1 channel is functionally expressed, and it participates in the SOCE as well as the regulation of  $\text{Ca}^{2+}$  basal concentration in human-activated PSCs.

To investigate whether SOCE is already induced by the PS-1 cell culture conditions (with cell medium containing 10% fetal bovine serum (FBS)), we performed  $\text{Ca}^{2+}$  imaging experiments after overnight FBS deprivation. Indeed, it is well known that FBS can induce a  $\text{Ca}^{2+}$  ER depletion by acting on the inositol triphosphate receptor, which will promote STIM1 translocation to the cell membrane in order to activate Orai1 protein and so permit the SOCE [26–29]. We so measured SOCE after perfusion of  $1 \mu\text{M}$  Tg and 10% FBS, and we observed that both Tg and FBS-induced  $\text{Ca}^{2+}$  ER depletion triggering a SOCE. However, FBS stimulation led to a lower SOCE (30% decrease) compared to Tg stimulation (Tg:  $100 \pm 2.94\%$ , FBS:  $73.41 \pm 2.37\%$ ,  $N = 3, p < 0.001$ , Figure S1(Ca, Cb)). These data revealed that, in our culture conditions, Orai1 is activated and leads to SOCE that regulates  $\text{Ca}^{2+}$  basal concentration.

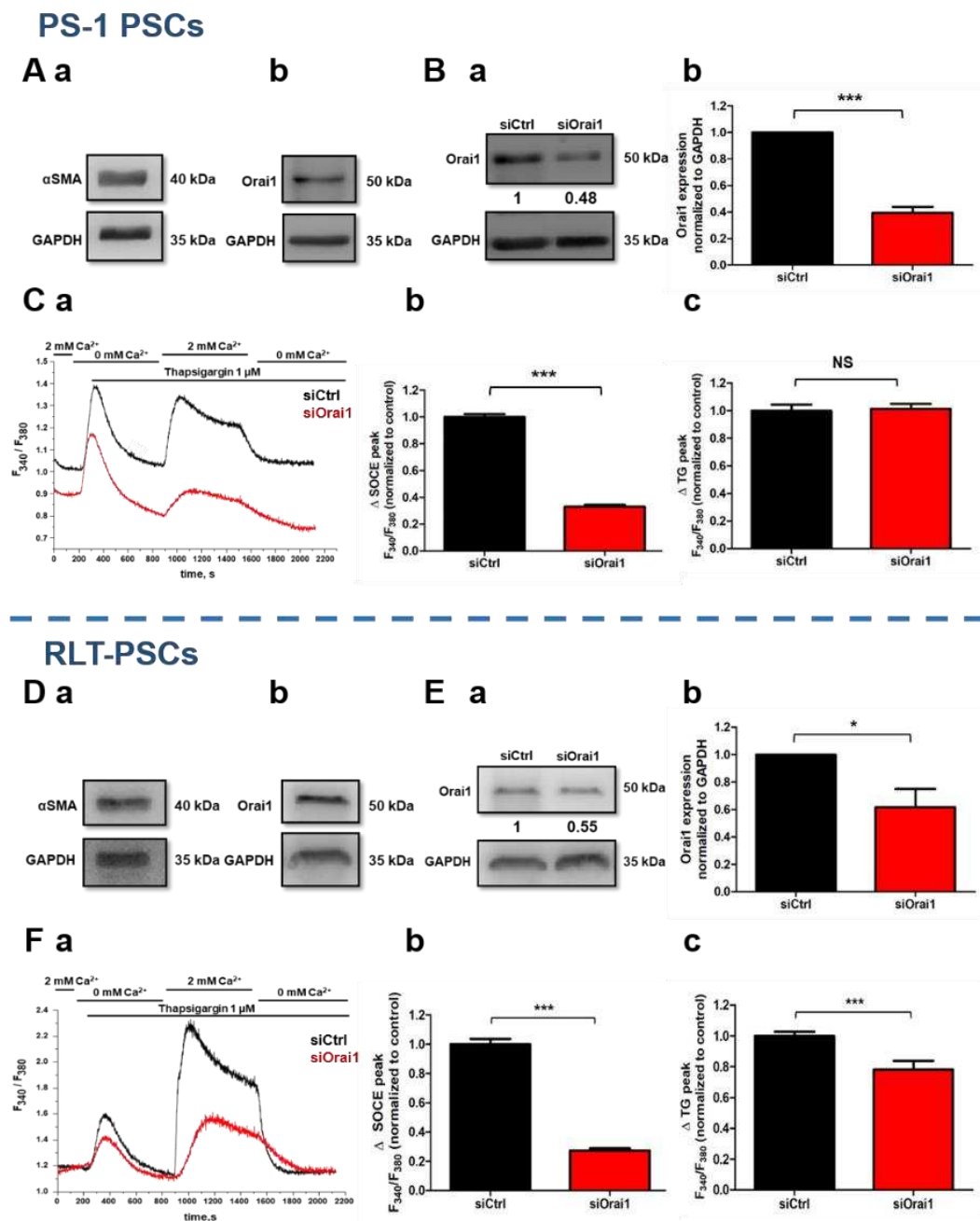


**Figure 1.** Orai1 channel is functionally expressed in human-activated PSCs by regulating the store-operated  $\text{Ca}^{2+}$  entry (SOCE). (A,D) Protein expression of  $\alpha\text{SMA}$ , the principal marker of PSC activation (Aa, Da), and Orai1 channel (Ab, Db), by Western blot, 72 h post-proliferation, in PS-1 (A) and RLT (D) human-activated PSCs. (B,E) Evaluation of Orai1 siRNA 72 h post-transfection efficiency by Western blot. Illustrative Western blot of Orai1 protein inhibition (Ba, Ea), with the quantification (Bb, Eb), in both PS-1 (B) and RLT (E) PSCs. Western blotting results were first normalized to the referent protein GAPDH and then to the control ( $N = 3$ , \*  $p < 0.05$ , \*\*\*  $p < 0.001$ , Student's  $t$ -test). (C,F) Assessment of Orai1 channel's function in siOrai1 transfected PS-1 (C) and RLT (F) cells, using calcium imaging, 72 h post-transfection. SOCE was measured after endoplasmic reticulum release induced by  $1 \mu\text{M}$  of thapsigargin, illustrated by representative traces (Ca, Fa) of SOCE measurements in both cell lines. All histograms are represented as the average  $\pm$  SEM normalized to the control, of SOCE (siCtrl:  $n = 210$ , siOrai1:  $n = 189$ ,  $N = 5$  for PS-1 cells, (Cb)) (siCtrl:  $n = 91$ , siOrai1:  $n = 80$ ,  $N = 3$  for RLT cells, (Fb)), and of endoplasmic reticulum release induced by  $1 \mu\text{M}$  Thapsigargin (siCtrl:  $n = 210$ , siOrai1:  $n = 184$ ,  $N = 5$  for PS-1 cells, (Cc)) (siCtrl:  $n = 91$ , siOrai1:  $n = 80$ ,  $N = 3$  for RLT cells, (Fc)) (\*  $p < 0.001$ , NS: no significant, Student's  $t$ -test,  $n$ : number of cells,  $N$ : number of passage).



## 2.2. *Orai1* Is Involved in Human-Activated PSC Proliferation and $TGF\beta_1$ Secretion

We next wondered whether the *Orai1* channel could drive some of PSCs activation processes. We chose to focus on PSC proliferation and cytokine secretion, which are two of the main activation hallmarks of PSCs. After 72h of *Orai1* silencing, we assessed PS-1 and RLT's cell proliferation by MTT colorimetric assay and we found that *Orai1* knock-down decreased by 37.12% PS-1's cell proliferation rate (siCtrl:  $100 \pm 4.89\%$ , si*Orai1*:  $62.88 \pm 2.04\%$ ,  $N = 4$ ,  $p < 0.001$ , Figure 2A), and by 31.39% RLT's cell proliferation (siCtrl:  $100 \pm 3.80\%$ , si*Orai1*:  $68.61 \pm 6.21\%$ ,  $N = 3$ ,  $p < 0.001$ , Figure 2A). We next performed cell cycle analysis on PS-1 cells using flow cytometry (Figure 2(Ba,Bb)). *Orai1* silencing induced a cell cycle arrest in G0/G1 phase (siCtrl:  $77.18 \pm 0.65\%$ , si*Orai1*:  $82.10 \pm 1.06\%$ ,  $N = 3$ ,  $p < 0.001$ ), followed by a decrease in cell number in S phase (siCtrl:  $8.37 \pm 0.37\%$ , si*Orai1*:  $5.12 \pm 0.46\%$ ,  $N = 3$ ,  $p < 0.01$ ), without affecting the G2/M phase (siCtrl:  $14.44 \pm 0.61\%$ , si*Orai1*:  $12.76 \pm 0.80\%$ ,  $N = 3$ , Figure 2(Ba,Bb)). Simultaneously, we checked if the observed effect may be caused by an increase of cell mortality, which was evaluated by Trypan blue colorimetric assay. In both PS-1 and RLT PSCs, we did not reveal any significant effect on cell mortality (Figure S2C,D). In accordance with this data, apoptosis analysis on PS-1 cells, using the Annexin V/IP staining, confirmed the absence of any effect on cell mortality (Figure S2(Ea,Eb)).

Another characteristic of PSC activation is the abundant secretion of  $TGF\beta_1$  multifunctional cytokine [6,30]. To test whether *Orai1* could be involved in the modulation of  $TGF\beta_1$  expression and secretion, we first quantified  $TGF\beta_1$  mRNA expression after 72 h of *Orai1* protein inhibition in both PS-1 and RLT cells. *Orai1* knock-down led to 69.71%  $TGF\beta_1$  mRNA decrease in PS-1 cells (siCtrl:  $100 \pm 24.45\%$ , si*Orai1*:  $30.29 \pm 10.25\%$ ,  $N = 3$ ,  $p < 0.05$ , Figure 2(Ca)), and to 53.95% mRNA decrease in RLT cells (siCtrl:  $100 \pm 16.87\%$ , si*Orai1*:  $46.05 \pm 12.59$ ,  $N = 3$ ,  $p < 0.05$ , Figure S2B). We then evaluated the impact of *Orai1* in the  $TGF\beta_1$  secretion process by ELISA assay (Figure 2D) in PS-1 cells. We observed no effect on  $TGF\beta_1$  secretion 72 h after *Orai1* silencing, but we found a 41.31% decrease in  $TGF\beta_1$  secretion after 96 h of si*Orai1* transfection (siCtrl:  $100 \pm 9.49\%$ , si*Orai1*:  $58.69 \pm 12.30\%$ ,  $N = 3$ ,  $p < 0.05$ , Figure 2D). Simultaneously, we have also looked at  $TGF\beta_1$  mRNA expression to see whether the effect of *Orai1* silencing persists 96 h post-transfection. However, even though we observed a tendency of  $TGF\beta_1$  mRNA decrease, it remained no significant (siCtrl:  $100 \pm 20.95\%$ , si*Orai1*:  $58.67 \pm 14.19\%$ ,  $N = 3$ , Figure 2(Cb)).

These results demonstrated the involvement of the *Orai1* channel in human-activated PSC proliferation by regulating cell cycle progression in the G1 phase and G1/S transition and  $TGF\beta_1$  secretion.

## 2.3. *Orai1* Regulates the Activation of AKT But Not of ERK1/2 and SMAD2 in Human-Activated PSCs

Since the discovery of PSCs, accumulating studies have been focused on the investigation of the signal transduction pathways implicated in PSC activation [10,18]. AKT, ERK1/2, and SMAD2 phosphorylation have been reported to be three of the main signaling pathways involved in PSC activation processes [18,31–33]. Hence, we sought to determine whether *Orai1* regulates one of these signaling pathways. We, therefore, evaluated AKT, ERK1/2, and SMAD2 phosphorylation levels after 72 h of si*Orai1* transfection, by Western blotting, in both PS-1 (Figure 3) and RLT cells (Figure S4). Silencing of *Orai1* induced a 61.4% decrease in AKT phosphorylation after 10% FBS stimulation (Figure 3(Aa,Ab)), without affecting the AKT total protein amount (Figure S3A) in PS-1 cells. Similar experiments performed on ERK1/2 and SMAD2 activation showed that *Orai1* silencing failed to affect ERK1/2 (Figure 3(Ba,Bb)) and SMAD2 (Figure 3(Ca,Cb)) phosphorylation as well as ERK1/2 total protein amount (Figure S3B). However, under 0% FBS conditions, the SMAD2 total protein amount was decreased in the si*Orai1* transfected cells, without any alteration in 10% FBS conditions (Figure S3C). Interestingly, 72 h *Orai1* knocking down led to a 46.8% reduction of AKT phosphorylation, in RLT cells, without modifying ERK1/2 and SMAD2 activation, and either the total protein amount of each one (Figure S4A–C).

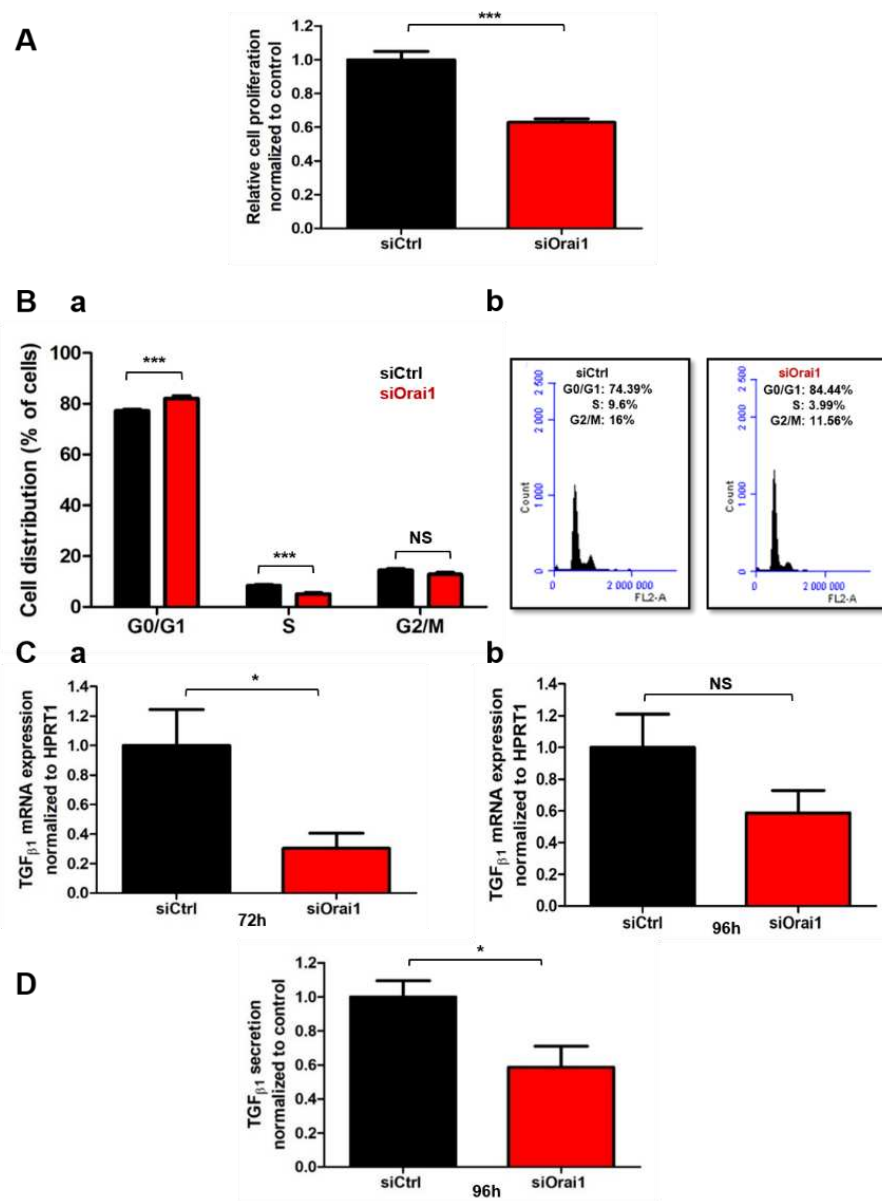


**Figure 2.** Orai1 modulates human-activated PSC proliferation and TGF $\beta_1$  secretion. **(A)** Effect of Orai1 silencing on PS-1 cell proliferation, assessed 72 h post-transfection by MTT assay (\*\* $p < 0.001$ ,  $N = 4$ , Student's  $t$ -test). **(B)** Implication of Orai1 in PS-1 cell cycle progression. Cell distribution (G0/G1, S and G2/M phase) was examined by flow cytometry 72 h after transfection, with propidium iodide staining (\*\* $p < 0.001$ , NS: no significant,  $N = 3$ , two-way ANOVA followed by Bonferroni *post hoc* test, **(Ba)** and represented by an illustrative cell cycle profile 72 h after Orai1 inhibition **(Bb)**. **(C)** Impact of Orai1 knocking down on TGF $\beta_1$  mRNA expression, evaluated by qPCR, 72 h **(Ca)** and 96 h **(Cb)** post-transfection. **(D)** Role of Orai1 inhibition on TGF $\beta_1$  secretion, assessed by ELISA assay, 96 h post-transfection (\* $p < 0.05$ ,  $N = 3$ , Student  $t$ -test). Values were normalized to control and reported as mean  $\pm$  SEM.

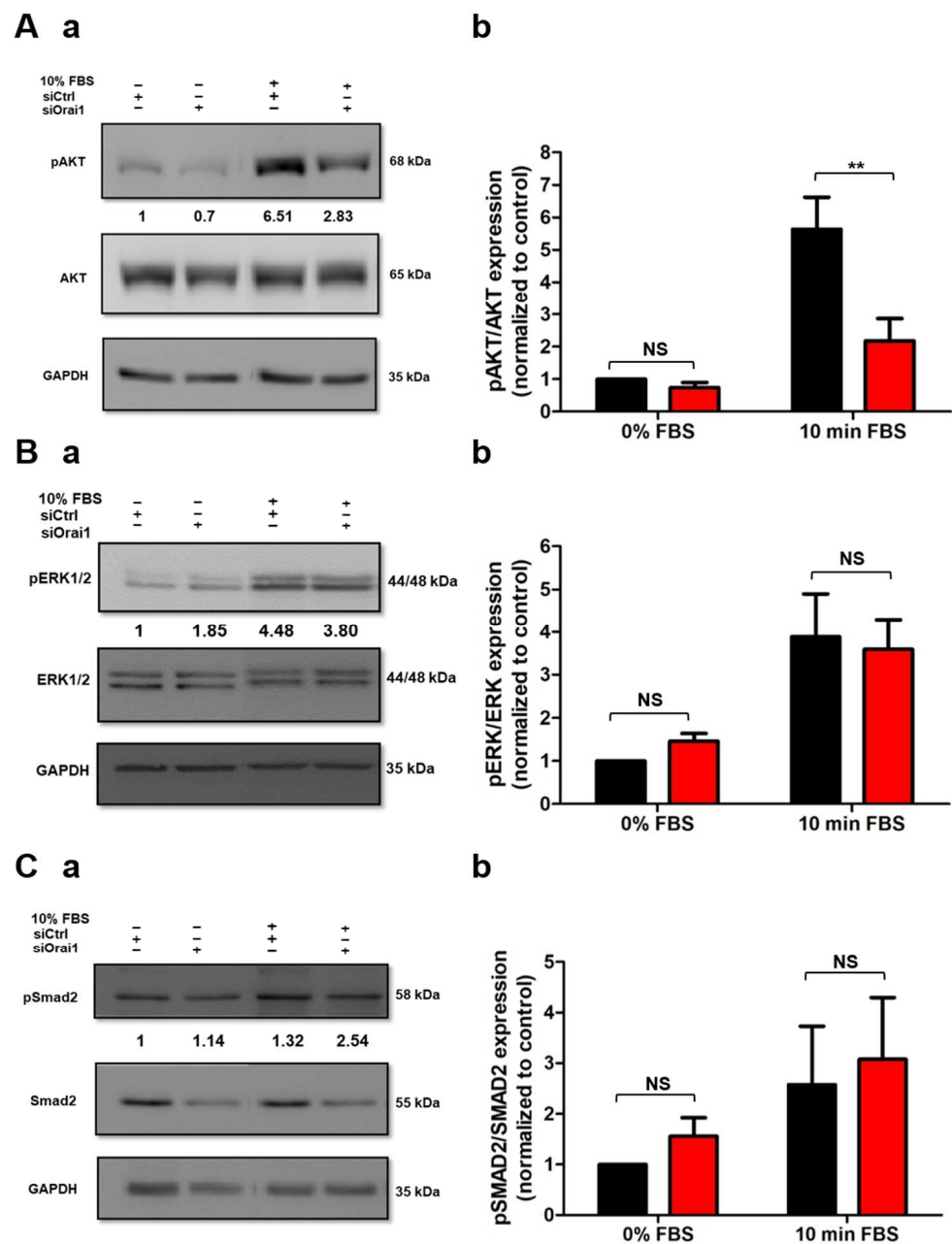


**Figure 3.** Orai1 mediates AKT activation but not ERK1/2 nor SMAD2 phosphorylation in human-activated PSCs. **(A)** Involvement of Orai1 in AKT phosphorylation in PS-1 cells. Representative Western blot showing the effect of Orai1 inhibition after FBS starvation of transfected cells overnight. Cells were then stimulated 10 min with FBS to evaluate the impact of Orai1 on AKT activation (**Aa**). AKT phosphorylation was quantified by the ratio of phosphorylated AKT form/total AKT protein (siCtrl + 10 min FBS:  $5.63 \pm 0.99$ -fold, siOrai1 + 10 min FBS:  $2.18 \pm 0.69$ -fold, (**Ab**). **(B)** Assessment of ERK1/2 activation after Orai1 knocking down in PS-1 cells. Representative Western blot showing the effect of Orai1 silencing on ERK1/2 activation, using the protocol described above (**Ba**). ERK1/2 phosphorylation was quantified by the ratio of phosphorylated ERK1/2 form/total ERK1/2 protein (**Bb**). **(C)** Evaluation of Orai1 silencing on SMAD2 phosphorylation. Representative Western blot showing the effect of siOrai1 transfected cells on SMAD2 activation (**Ca**), with the quantification using the ratio of phosphorylated SMAD2 form/total SMAD2 protein (**Cb**). All values were first normalized to the referent protein GAPDH and then to the 0% FBS control condition. All experiments were realized 72 h post-transfection. Values were reported as mean  $\pm$  SEM (\*\*  $p < 0.01$ , NS, at least  $N = 3$ , two-way ANOVA followed by Bonferroni *post hoc* test).

#### 2.4. AKT Signaling Pathway Mediates Human-Activated PSC Proliferation and TGF $\beta_1$ Secretion

Up until now, very few studies have demonstrated the involvement of the PI3K/AKT signaling pathway in PSC proliferation, without showing a direct role in the regulation of this process [21]. We thus investigated the potential direct implication of the AKT pathway in the modulation of PS-1 proliferation. To determine this, we treated PS-1 for 72 h with the pharmacological inhibitor of PI3K/AKT pathway LY 294002 and evaluated the effect on both AKT phosphorylation and cell proliferation. LY 294002 treatment drastically reduced AKT activation by  $83.68 \pm 3.20\%$  ( $N = 3$ ,  $p < 0.001$ , Figure 4(Aa,Ab)). PS-1 treatment with LY 294002 induced a 59.58% decrease in the proliferation rate, revealing that AKT pathway mediates PS-1 cell proliferation (Ctrl:  $100 \pm 4.60\%$ , LY 294002:  $40.42 \pm 2.06\%$ ,  $N = 4$ ,  $p < 0.001$ , Figure 4B).

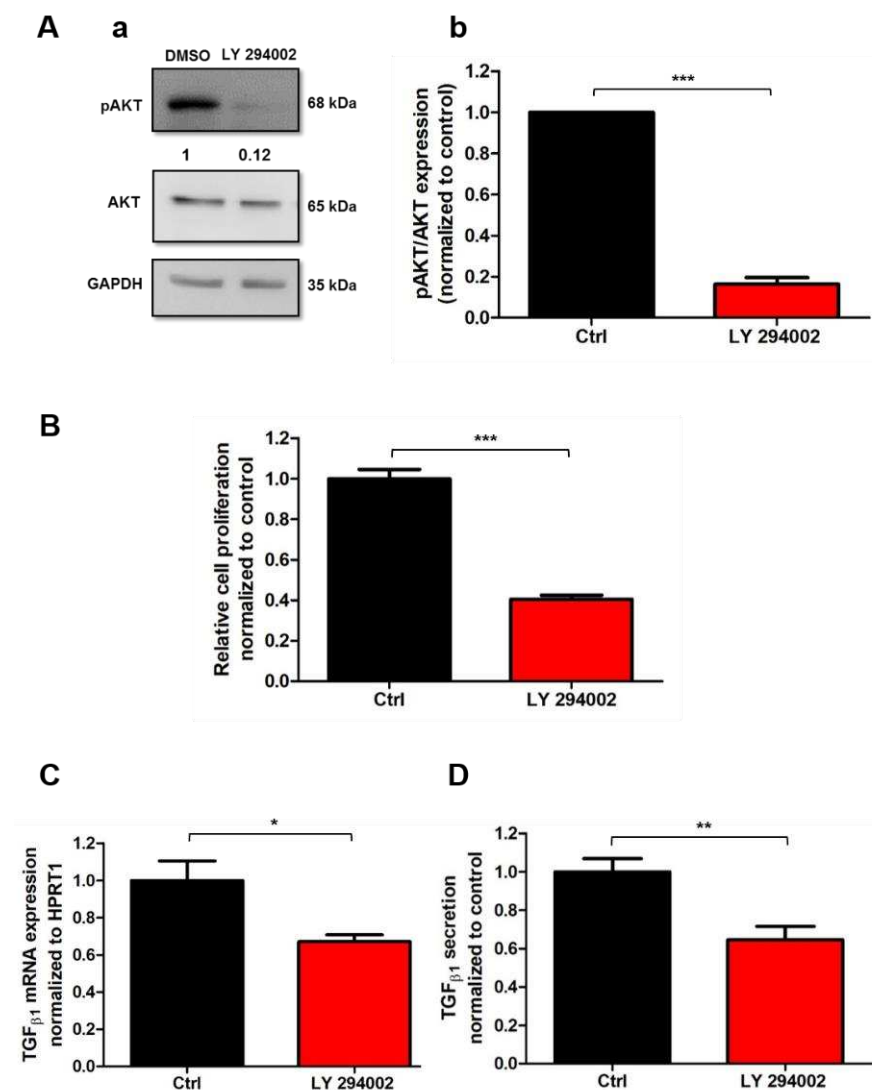


**Figure 4.** AKT signaling pathway controls PSC proliferation and TGF $\beta_1$  secretion. (A,B) Inhibition of AKT activation after 72 h cell treatment with the PI3K/AKT pharmacological inhibitor LY 294002 (20  $\mu$ M) decreased PS-1 cell proliferation. Representative Western blot of AKT reduced phosphorylation by LY 294002 treatment (Aa) and the quantification as previously described (Ab) ( $N = 3$ ,  $*** p < 0.001$ , Student  $t$ -test). All values were first normalized to the referent protein GAPDH and then to the control condition, reported as mean  $\pm$  SEM. Cell proliferation was evaluated after 72 h of treatment by MTT assay ( $N = 4$ ,  $*** p < 0.001$ , Student  $t$ -test) (B). (C,D) Effect of AKT inhibition on TGF $\beta_1$  mRNA expression (C) and secretion (D) after 72 h LY 294002 treatment ( $* p < 0.05$ ,  $** p < 0.01$ ,  $N = 3$ , Student  $t$ -test). Values were normalized to control and reported as mean  $\pm$  SEM.

Moreover, some studies established the involvement of the AKT pathway in TGF $\beta_1$  mRNA and protein expression in hepatic stellate cells, suggesting that TGF $\beta_1$  might be regulated by the AKT pathway [34]. However, there is no evidence yet of this mechanism in PSCs. We then assessed whether the AKT pathway plays a role in TGF $\beta_1$  mRNA expression and secretion using the pharmacological inhibitor LY 294002. We observed a 32.96% reduction in TGF $\beta_1$  mRNA (Ctrl:  $100 \pm 10.44\%$ , LY 294002:  $67.04 \pm 3.75\%$ ,  $N = 3$ ,  $p < 0.05$ ) after the pharmacological inhibition of AKT pathway (Figure 4C). These results were completed with the evaluation of TGF $\beta_1$  secretion using the ELISA assay. In accordance with the mRNA transcripts, LY 294002 treatment induced 35.41% decrease in TGF $\beta_1$  secretion (Ctrl:  $100 \pm 6.83\%$ , LY 294002:  $64.59 \pm 6.92\%$ ,  $N = 3$ ,  $p < 0.01$ , Figure 4D).

Taken together, these data suggested that Orai1 regulates PSC proliferation and TGF $\beta_1$  secretion, probably through the activation of the AKT signaling pathway.

### 2.5. TGF $\beta_1$ Promotes Orai1-Mediated Ca $^{2+}$ Entry and Increases Both Orai1 mRNA and Protein Expression in Human-Activated PSCs

TGF $\beta_1$  has been reported to be involved in the fibrosis mediated by PSC activation [35] and the autocrine regulation of PSCs [15]. Several reports have already demonstrated the involvement of TGF $\beta_1$  in the regulation of some cell types' intracellular mechanisms, including lung, embryonic fibroblasts, and pancreatic cancer cells, through a Ca $^{2+}$ -dependent pathway [36–38]. Indeed, it has been shown for a long time that TGF $\beta_1$  can modulate Ca $^{2+}$  signaling by stimulating the Ca $^{2+}$  influx and thus by increasing the cytoplasmic Ca $^{2+}$  concentration [36]. According to these findings, we wondered whether TGF $\beta_1$  could also mediate the Ca $^{2+}$  influx in PS-1 human-activated PSCs by promoting Orai1-mediated Ca $^{2+}$  entry. To evaluate this hypothesis, we performed Ca $^{2+}$  imaging experiments where we perfused TGF $\beta_1$  on siCtrl and siOrai1 transfected cells and measure the SOCE response. Interestingly, we noted a 14% increase in SOCE after TGF $\beta_1$  perfusion on siCtrl transfected cells compared to the siCtrl non-perfused with TGF $\beta_1$  cells. However, we did not remark any difference in Orai1 knock-down cells, perfused and non-perfused with TGF $\beta_1$ , inferring an effect of TGF $\beta_1$  on Orai1-mediated Ca $^{2+}$  entry (siCtrl:  $100 \pm 3.33\%$ , siCtrl+ TGF $\beta_1$ :  $114.14 \pm 3.07\%$ , siOrai1:  $21.74 \pm 1.19\%$ , siOrai1+ TGF $\beta_1$ :  $24.96 \pm 0.92\%$ ,  $N = 3$ ,  $p < 0.001$ ,  $p > 0.05$ , Figure 5(Aa,Ab)). We then supposed that the short-term effect of TGF $\beta_1$  on Orai1-mediated Ca $^{2+}$  entry might be due to a long-term effect of this cytokine on Orai1 mRNA and protein expression. We thus treated PS-1 cells for 48 h with TGF $\beta_1$ , in the presence of low-FBS conditions (1%), and we observed that both, Orai1 mRNA and protein expression were increased following TGF $\beta_1$  treatment. qPCR experiments revealed a 2.87-fold increase in Orai1 mRNA transcripts in TGF $\beta_1$  treated cells (Ctrl:  $1 \pm 0.36$ -fold, TGF $\beta_1$ :  $2.87 \pm 0.66$ -fold,  $N = 3$ ,  $p < 0.05$ , Figure 5(Ba)). Furthermore, it is known that the store-operated Orai1-mediated Ca $^{2+}$  entry is promoted by the intracellular STIM1 protein. Consequently, we quantified in parallel the impact of TGF $\beta_1$  treatment on STIM1 mRNA expression, finding a comparable increase in STIM1 mRNAs as for Orai1 (Ctrl:  $1 \pm 0.34$ -fold, TGF $\beta_1$ :  $2.94 \pm 0.68$ -fold,  $N = 3$ ,  $p < 0.05$ , Figure 5(Bb)). These data suggest that TGF $\beta_1$  stimulates store-operated Orai1-mediated Ca $^{2+}$  entry modulating the expression of both main SOCE actors, Orai1 and STIM1. Similarly, Western blotting experiments showed a  $1.52 \pm 0.15$ -fold rise of Orai1 protein level in treated compared to non-treated with TGF $\beta_1$  cells ( $N = 3$ ,  $p < 0.05$  Figure 5(Ca,Cb)).

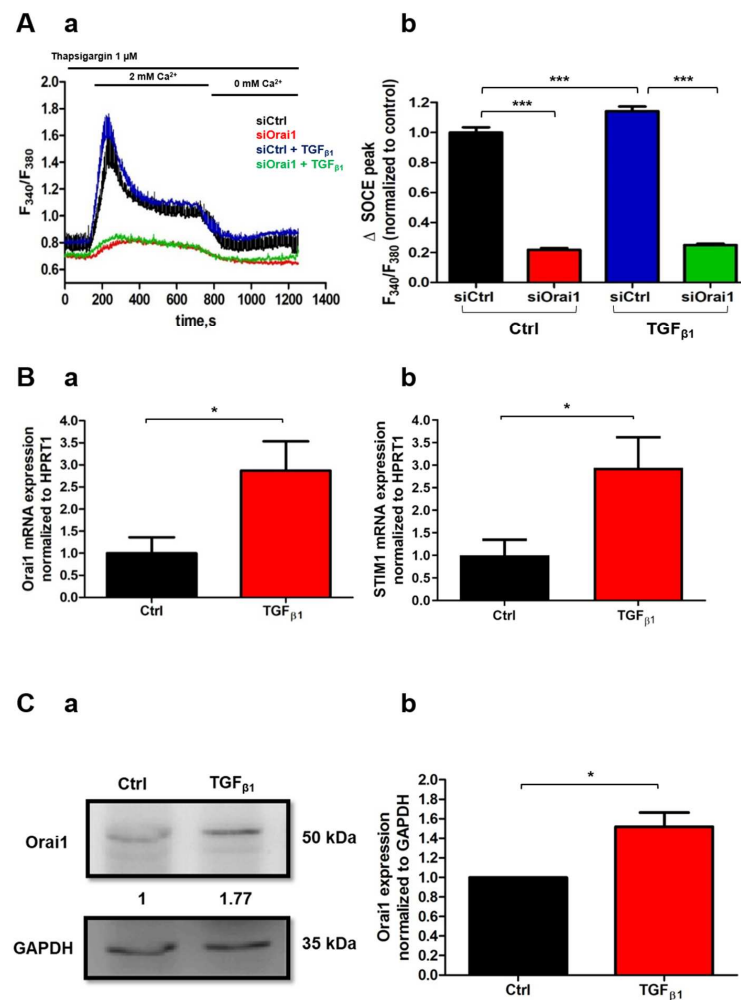


**Figure 5.** TGF $\beta_1$  enhances Orai1-mediated  $Ca^{2+}$  entry and increases both Orai1 mRNA and protein expression. (A) TGF $\beta_1$  (5 ng/mL) perfusion was applied to investigate the effect of TGF $\beta_1$  on Orai1 activity. siCtrl and siOrai1 72 h-transfected cells were pre-treated for 5 min with 1  $\mu$ M of Thapsigargin before use for SOCE measurements in  $Ca^{2+}$  - imaging. Illustrative traces of SOCE measurements (Aa) and the quantification of perfused and non-perfused siCtrl and siOrai1 transfected cells (siCtrl: n = 133, siCtrl + TGF $\beta_1$ : n = 163, siOrai1: n = 102, siOrai1 + TGF $\beta_1$ : n = 122, N = 3, \*\*\*  $p < 0.001$ , one-way ANOVA followed by Bonferroni multiple comparison test, n: number of cells, N: number of passages, (Ab). All values were normalized to siCtrl non-treated with TGF $\beta_1$  condition and reported as mean  $\pm$  SEM. (B,C) Impact of 48 h TGF $\beta_1$  treatment (20 ng/mL) in the presence of low-FBS conditions (1%) on Orai1 and STIM1 (B) mRNA and Orai1 protein expression (C). Quantification of Orai1 (Ba) and STIM1 (Bb) mRNA transcripts 48 h post-TGF $\beta_1$  treatment (\*  $p < 0.05$ , N = 3, Student *t*-test) (B). Representative Western blot showing the effect of TGF $\beta_1$  treatment on Orai1 expression (Ca) with the quantification (Cb) (\*  $p < 0.05$ , N = 3, Student *t*-test). All values were first normalized to the referent protein GAPDH and then to the control condition, reported as mean  $\pm$  SEM.

## 2.6. TGF $\beta_1$ Enhances Orai1/AKT-Dependent Proliferation Through an Autocrine Positive Feedback Loop in Human-Activated PSCs

We thereafter wondered whether TGF $\beta_1$  could also be involved in the promotion of the Orai1/AKT-dependent proliferation. Indeed, TGF $\beta_1$  is known to have a dual role in cell proliferation, since according to the cell type, it can induce an inhibition or stimulation of cell proliferation. Furthermore, it has been shown to enhance the hepatic stellate cell's proliferation, known as counterparts of PSCs [34]. However, its role in PSC proliferation and proliferation-related signaling pathways remains little known. We hence started by assessing the impact of TGF $\beta_1$  on Orai1-mediated AKT activation after inhibiting Orai1 expression. For that, we FBS-starved siCtrl and siOrai1 cells overnight and then stimulated

them 30 min with TGF $\beta_1$  (Figure 6(Aa,Ab)). As expected, TGF $\beta_1$  stimulation increased by  $1.68 \pm 0.23$ -fold ( $N = 4, p < 0.05$ , Figure 6(Ab)) the AKT phosphorylation in the siCtrl cells compared to the no-stimulated siCtrl cells. Moreover, we revealed a 42.37% decrease in AKT activation in siOrai1 ( $0.97 \pm 0.18$ -fold) compared to siCtrl stimulated with TGF $\beta_1$  cells ( $N = 4, p < 0.05$ , Figure 6(Ab)), whereas no significant effect was observed in siOrai1 stimulated and no-stimulated with TGF $\beta_1$  cells. These results inferred the involvement of TGF $\beta_1$  in the stimulation of Orai1-mediated AKT phosphorylation.

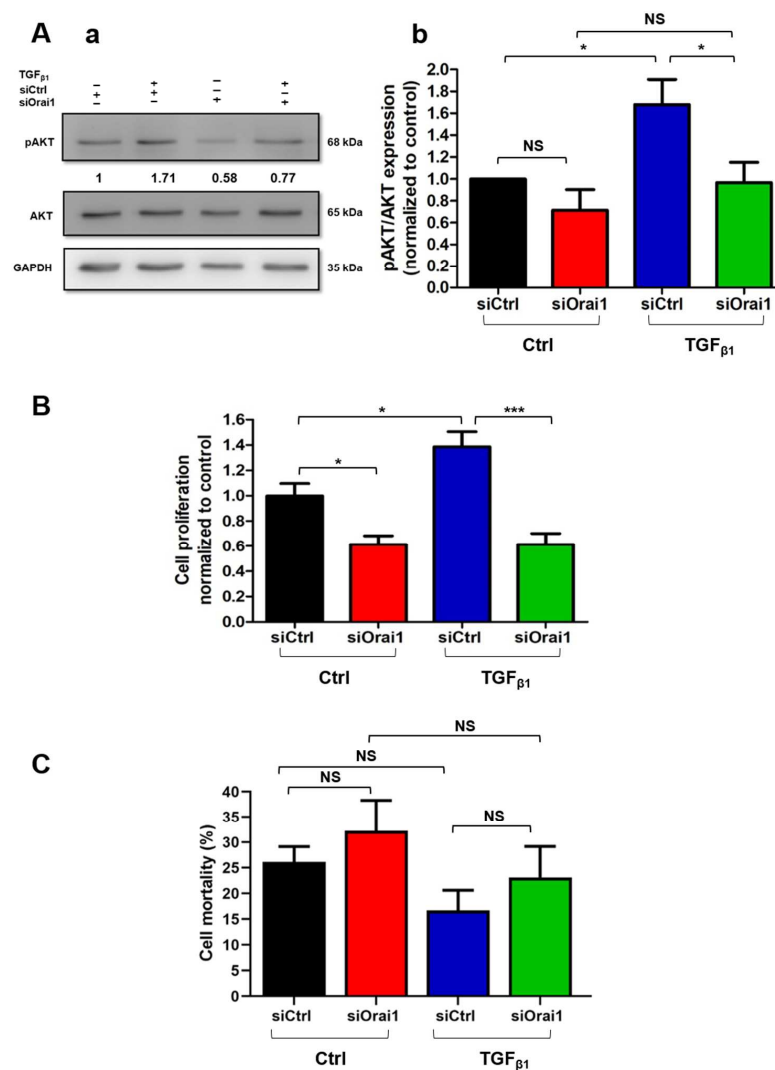


**Figure 6.** TGF $\beta_1$  promotes Orai1/AKT-dependent proliferation through an autocrine positive feedback loop in human-activated PSCs. (A) TGF $\beta_1$  stimulation decreased AKT phosphorylation in Orai1 knocked-down cells. Orai1 knocked-down cells were FBS-starved overnight and then stimulated 30 min with TGF $\beta_1$ , 72 h post-transfection. Representative Western blot of TGF $\beta_1$  stimulation on Orai1 knocked-down mediated AKT activation (Aa) and the quantification (\*  $p < 0.05$ , at least  $N = 3$ , two-way ANOVA followed by Bonferroni *post hoc* test, (Ab)). All values were first normalized to the referent protein GAPDH and then to siCtrl non-treated with TGF $\beta_1$  condition and reported as mean  $\pm$  SEM. (B,C) Involvement of TGF $\beta_1$  in PS-1 cell proliferation and survival. Transfected cells were treated 48 h with TGF $\beta_1$  (20 ng/mL) within an FBS-free medium, and the proliferation rate, as well as the mortality rate, were evaluated by Trypan blue assay, 72 h post-transfection (\*  $p < 0.05$ , \*\*\*  $p < 0.001$ , NS,  $N = 3$ , one-way ANOVA followed by Bonferroni multiple comparison tests). All values were normalized to siCtrl non-treated with TGF $\beta_1$  condition and reported as mean  $\pm$  SEM. Cell mortality was calculated using the formula: % of cell death = number of dead cells/number of total cells, reported as mean  $\pm$  SEM for each condition.

Therefore, we wanted to evaluate if TGF $\beta_1$  promotion of Orai1-mediated AKT activation regulates PS-1 cell proliferation or survival. After treating siCtrl and siOrai1 transfected cells 48 h with TGF $\beta_1$ , we found that TGF $\beta_1$  enhanced by 38.55% the cell proliferation of siCtrl cells compared to the non-treated ones (N = 3,  $p < 0.05$ , Figure 6B). In addition, TGF $\beta_1$  treatment did not reveal any effect on the proliferation rate of siOrai1 cells compared to the non-treated siOrai1 cells (siCtrl:  $100 \pm 9.63\%$ , siCtrl + TGF $\beta_1$ :  $138.55 \pm 11.91\%$ , siOrai1:  $61.45 \pm 6.85\%$ , siOrai1 + TGF $\beta_1$ :  $61.45 \pm 8.81$ , N = 3,  $p > 0.05$ , Figure 6B). Simultaneously, the Trypan blue colorimetric assay showed the no involvement of TGF $\beta_1$  in PS-1's cell mortality and so in cell survival (siCtrl:  $26.18 \pm 2.97\%$ , siCtrl + TGF $\beta_1$ :  $16.70 \pm 3.92\%$ , siOrai1:  $32.22 \pm 6.05\%$ , siOrai1 + TGF $\beta_1$ :  $23.11 \pm 6.07$ , N = 3,  $p > 0.05$ , Figure 6C). It should be noted that the impact of TGF $\beta_1$  on these two cellular processes was investigated under 0% FBS conditions since the 1% FBS was still preventing its action on cell proliferation and survival. Hence, 0% FBS conditions induced an elevation of the basal cell death.

TGF $\beta_1$  is also known to be an important profibrotic factor due to its ability to regulate  $\alpha$ SMA expression, the main activation marker of PSCs [15]. Furthermore, it has been shown that ion channels, particularly TRPC6, can regulate  $\alpha$ SMA expression as well, in human-activated hepatic stellate cells, counterparts of PSCs [39], and human intestinal myofibroblasts [40]. In these later, TRPC6 interacts with  $\alpha$ SMA, too, to form a protein complex. According to these data, we hypothesized that Orai1 could modulate  $\alpha$ SMA expression or form a complex with it. However, Orai1 silencing failed to induce any significant decrease in  $\alpha$ SMA protein expression ( $p > 0.05$ , N = 3, Figure S5(Aa,Ab)), and neither to interact with  $\alpha$ SMA (N = 3, Figure S5(Ba,Bb)). To confirm these findings, we next investigated whether Orai1-mediated TGF $\beta_1$  expression and secretion might be involved in the regulation of  $\alpha$ SMA expression. We thereby treated siCtrl and siOrai1 transfected cells 48h with TGF $\beta_1$ , in the presence of low-FBS conditions. As expected, TGF $\beta_1$  treatment of siCtrl cells induced a  $3.82 \pm 0.54$ -fold increase in  $\alpha$ SMA expression, as quantified by Western blotting, compared to siCtrl non-treated cells ( $p < 0.05$ , N = 4, Figure S5(Ca,Cb)). However, treatment of siOrai1 transfected cells with TGF $\beta_1$  did not reveal any significant difference in  $\alpha$ SMA expression compared to the siCtrl TGF $\beta_1$  treated cells ( $p > 0.05$ , N = 4, Figure S5(Ca,Cb)), indicating that Orai1-induced TGF $\beta_1$  expression and secretion is not implicated in the modulation of  $\alpha$ SMA expression.

Based on these data, we can conclude that TGF $\beta_1$  is involved in an autocrine positive feedback loop by the promotion of Orai1-dependent AKT phosphorylation, leading to PS-1 cell proliferation enhancement through the stimulation of Orai1-mediated Ca $^{2+}$  entry and the increase in Orai1 mRNA and protein expression.

### 2.7. Ca $^{2+}$ Entry Through Orai1 Regulates AKT-Dependent Proliferation and TGF $\beta_1$ Secretion in PS-1 Human-Activated PSCs

It is well known that most of the signaling pathways are regulated by the Ca $^{2+}$  second messenger. Moreover, it has been demonstrated that Ca $^{2+}$  modulates a myriad of biological processes, including cell proliferation or cytokine secretion [41,42]. To determine whether Ca $^{2+}$  and, more specifically, Ca $^{2+}$  entry through Orai1 regulates AKT activation, as well as Orai1/AKT-dependent proliferation and TGF $\beta_1$  secretion in PS-1 cells, we reduced the physiological extracellular Ca $^{2+}$  concentration. We started by evaluating the impact of extracellular Ca $^{2+}$  modification on AKT phosphorylation after overnight FBS starvation of PS-1 non-treated cells. As expected, 30 min treatment with low Ca $^{2+}$  -conditions (0.1 mM Ca $^{2+}$ ) led to 65.60% decrease in AKT activation, compared to the physiological Ca $^{2+}$  -conditions (1.4 mM Ca $^{2+}$ ) (N = 3,  $p < 0.05$ , Figure 7(Aa,Ab)).



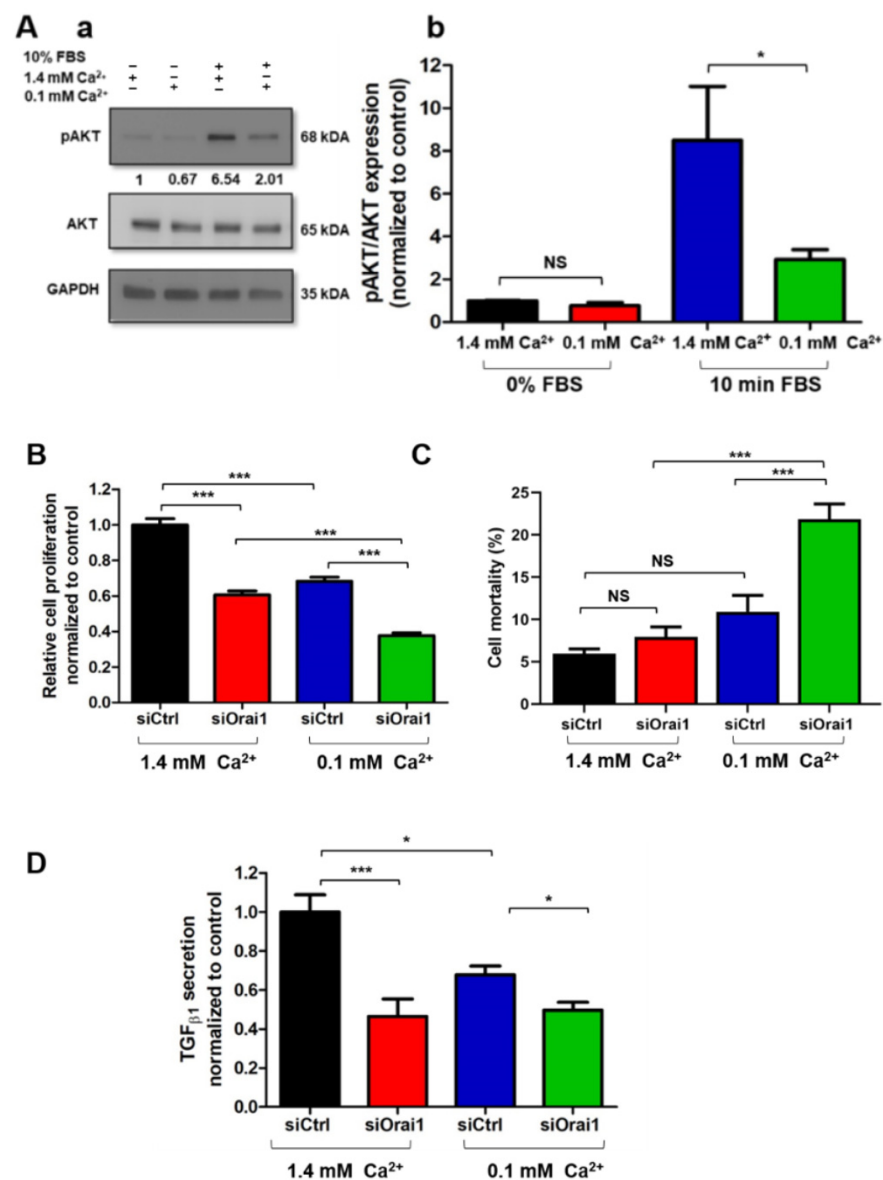


**Figure 7.** Ca<sup>2+</sup> entry through Orail regulates AKT-dependent proliferation and TGF $\beta$ <sub>1</sub> secretion in PS-1 human-activated PSCs. (A) Effect of extracellular Ca<sup>2+</sup> decrease on AKT activation, 72 h post-proliferation, after overnight FBS starvation of no transfected cells. Then PS-1 cells were pre-treated for 30 min with 1.3 mM EGTA in order to reduce the extracellular Ca<sup>2+</sup> concentration (0.1 mM Ca<sup>2+</sup>), with (+) and without (-) 10 min of 10% FBS stimulation. Representative Western blot of low extracellular Ca<sup>2+</sup> concentration impact on AKT phosphorylation (Aa). AKT activation was evaluated as described previously, by the ratio of phosphorylated AKT form/total AKT protein (1.4 mM Ca<sup>2+</sup> + 10 min FBS: 8.5 ± 2.52-fold, 0.1 mM Ca<sup>2+</sup> + 10 min FBS: 2.92 ± 0.46-fold, N = 3, \* p < 0.05, NS, two-way ANOVA followed by Bonferroni *post hoc* test, (Ab). Values were first normalized to the referent protein GAPDH and then to the 0% FBS + 1.4 mM Ca<sup>2+</sup> condition, reported as mean ± SEM. (B) Evaluation of siOrai1 transfected PS-1 cells' proliferation after 72 h of 1.3 mM EGTA treatment by MTT assay. (C) Impact of Orail knocked-down cells, treated with low Ca<sup>2+</sup> condition, on cell survival, assessed by Trypan blue assay. Cell mortality was calculated using the formula: % of cell death = number of dead cells/number of total cells, reported as mean ± SEM for each condition. (D) Similarly, TGF $\beta$ <sub>1</sub> secretion was measured in Orail knocked-down PS-1 cells, in the presence of low-Ca<sup>2+</sup> conditions, by ELISA assay. All values were normalized to 1.4 mM Ca<sup>2+</sup> control condition (except for the mortality rate) and reported as mean ± SEM (\*\*\*) p < 0.001, \* p < 0.05, NS, N = 3, one-way ANOVA followed by Bonferroni multiple comparison test).

We thereafter wanted to establish whether Orai1-mediated  $\text{Ca}^{2+}$  entry is involved in the modulation of PS-1 cell proliferation and  $\text{TGF}\beta_1$  secretion. We thus incubated siCtrl and siOrai1 transfected cells for 72 h with low and physiological  $\text{Ca}^{2+}$  -conditions. Interestingly, we noticed a more important effect on the proliferation rate of siOrai1 cells treated with low  $\text{Ca}^{2+}$  -conditions compared to the ones in physiological  $\text{Ca}^{2+}$  -conditions (siCtrl 1.4 mM  $\text{Ca}^{2+}$ :  $100 \pm 3.45\%$ , siCtrl 0.1 mM  $\text{Ca}^{2+}$ :  $68.29 \pm 2.27\%$ , siOrai1 1.4 mM  $\text{Ca}^{2+}$ :  $60.58 \pm 2.19\%$ , siOrai1 0.1 mM  $\text{Ca}^{2+}$ :  $37.69 \pm 1.59$ ,  $N = 3$ ,  $p < 0.001$ , Figure 7B). We could explain this result, in part, by the increased mortality, due to the low  $\text{Ca}^{2+}$  -conditions in the siOrai1 transfected cells, quantified by Trypan blue colorimetric assay (siCtrl 1.4 mM  $\text{Ca}^{2+}$ :  $5.97 \pm 0.55\%$ , siCtrl 0.1 mM  $\text{Ca}^{2+}$ :  $10.91 \pm 1.93\%$ , siOrai1 1.4 mM  $\text{Ca}^{2+}$ :  $7.93 \pm 1.18\%$ , siOrai1 0.1 mM  $\text{Ca}^{2+}$ :  $21.84 \pm 1.83$ ,  $N = 3$ ,  $p < 0.001$ , Figure 7C). Moreover,  $\text{TGF}\beta_1$  secretion remained similar, between Orai1 knocked-down cells treated with low  $\text{Ca}^{2+}$  -conditions and with physiological  $\text{Ca}^{2+}$  -conditions (siCtrl 1.4 mM  $\text{Ca}^{2+}$ :  $100 \pm 8.77\%$ , siCtrl 0.1 mM  $\text{Ca}^{2+}$ :  $67.79 \pm 4.43\%$ , siOrai1 1.4 mM  $\text{Ca}^{2+}$ :  $46.43 \pm 8.91\%$ , siOrai1 0.1 mM  $\text{Ca}^{2+}$ :  $49.66 \pm 3.96\%$ ,  $N = 3$ ,  $p > 0.05$ , Figure 7D).

Together, these data suggested that  $\text{Ca}^{2+}$  entry through Orai1 mediates AKT activation in order to regulate PS-1 cell proliferation and  $\text{TGF}\beta_1$  secretion.

### 3. Discussion

Since, Won et al. first characterized the  $\text{Ca}^{2+}$  signaling events present in PSCs in 2011, relatively few reports have continued to investigate the importance of  $\text{Ca}^{2+}$  and  $\text{Ca}^{2+}$  channels in PSC activation hallmarks [22]. While it is well known that PSC activation mediates pancreatic tumor's desmoplastic reaction, this study is one of the first pieces of evidence showing the functional expression and role of the Orai1- $\text{Ca}^{2+}$  channel in human PSCs' activation processes. We demonstrated, for the first time, that  $\text{Ca}^{2+}$  entry through the Orai1 channel promotes activated PSC proliferation by controlling cell cycle progression in G0/G1 phase, as well as G1/S transition and  $\text{TGF}\beta_1$  secretion, via the activation of the AKT signaling pathway. Moreover, we found that  $\text{TGF}\beta_1$  enhances PSC proliferation via an autocrine positive feedback loop, which involves  $\text{TGF}\beta_1$  mediated Orai1-dependent AKT activation through the increase of Orai1 expression.

Whereas there is a very limited number of studies focusing on the importance of Orai1-CRAC channels in pancreatic cancer, we have previously demonstrated the functional expression of Orai1 in several pancreatic ductal adenocarcinoma cell lines [43]. However, the Orai1-CRAC channel has only recently been identified in PSCs [24,25]. CRAC channels were initially discovered in mouse quiescent PSCs by Gryshchenko et al., using the 2APB and GSK-7975A SOC pharmacological inhibitors, where they have shown that SOCs mediate bradykinin-elicited  $\text{Ca}^{2+}$  signals [24]. The same authors have then investigated the effect of GSK-7975A inhibitor in mouse activated PSCs in acute pancreatitis conditions, which seemed to prevent the increased responsiveness of PSCs to trypsin, known to be involved in PSC activation [24]. A year later, Waldron et al. have highlighted the presence of CRAC channels in mouse immortalized activated PSC cell line by demonstrating a marked expression of Orai1 and STIM1, the key actors of SOCs [25]. Our study strengthened these data by using a more specific approach leading to Orai1 protein silencing by siRNA transfection, showing Orai1 channel involvement in SOCE but also in the regulation of the  $\text{Ca}^{2+}$  basal concentration in human-activated PSCs. Nevertheless, there is no direct evidence of Orai1 function in PSC activation hallmarks so far.

Our results demonstrated an essential role of Orai1-mediated  $\text{Ca}^{2+}$  entry in the regulation of human-activated PSC proliferation, known to be involved in fibrotic desmoplasia development. The relationship between  $\text{Ca}^{2+}$  entry through the SOCs and cell proliferation has been demonstrated for a long time in many cell types, such as neural progenitor cells, osteoblasts, kidney cells, endothelial cells, and cancer cells, but not in PSCs [41,44–47]. Indeed, a decrease in SOCE amplitude is related to cell cycle arrest [48–50]. However, although the involvement of the Orai1 channel in cell proliferation is well established, most of the research evidence has shown that Orai1 mediates the G2/S phase of the cell cycle,

especially in cancer cells [51–54]. Nevertheless, some other studies have proven that Orai1 can control G1/S transition in several cell types by downregulating the Cyclin E-CDK2 complex, known to be involved in this cell cycle phase transition, but not necessarily the G2/M transition [55]. These findings are in agreement with our data, showing that the knocking down of Orai1 in activated PSCs induced a cell number accumulation in G0/G1 phase and thus a decrease in G1/S transition, without affecting the G2/M phase.

Activated PSCs are also characterized by their ability to produce and secrete a variety of cytokines and growth factors, such as TGF $\beta$ <sub>1</sub>, leading to the perpetuated activation of PSCs but also participating in the permanent dialogue with the pancreatic cancer cells [5]. Although the implication of Orai1-mediated Ca<sup>2+</sup> entry has been well illustrated in immune cell's cytokine production and secretion, some other studies showed the involvement of Orai1 in cytokine synthesis in bronchial cells, spinal astrocytes, and microglia [42,56,57]. However, the first study of Orai1-mediated Ca<sup>2+</sup> entry involvement in fibro-inflammatory gene expression in activated PSCs emerged only in 2019. In this report, the researchers used the SOCE inhibitor CM4620 ( $\geq 10$ -fold selectivity for Orai1 vs. Orai2), providing novel data on SOCE mediated fibro-inflammatory gene expression, including TGF $\beta$ <sub>1</sub>, within mouse activated PSCs, after lipopolysaccharide (LPS) stimulation [25]. This later is known to induce Orai1-mediated SOCE and cytokine production in mesenchymal cells. In agreement with these data, we demonstrated in the current work that Ca<sup>2+</sup> entry through Orai1 mediates TGF $\beta$ <sub>1</sub> expression and secretion, the main profibrotic cytokine implicated in the desmoplastic reaction, in human-activated PSCs.

Furthermore, PSCs' activation and cell functions are under the control of multiple signaling pathways and molecules, entraining dynamic cellular modifications [18]. One of the key intracellular pathways shown to be crucially involved in the regulation of PSC activation processes is the PI3K/AKT pathway [31]. Indeed, AKT is a serine-threonine kinase, initiator of PI3K cascade, described to play an important role in the development of pancreatic fibrosis by modulating PSC proliferation, migration, collagen production as well as growth factors and cytokine secretion [58–60]. Schwer et al. have reported that inhibition of the AKT pathway, using carbon monoxide releasing molecule-2, disrupted PSC activation by inducing a translational inhibition. This phenomenon caused inhibition of PSC proliferation due to the down-regulation of cyclin D1 and E protein expression and the interruption of G1/S cell phase progression [20]. In addition, Zhang et al. have shown that reduction in AKT activity by the tumor suppressor PTEN led to cyclin D1 down-regulation and inhibition of cell proliferation in human and rodent activated PSCs [21].

Moreover, according to the literature, AKT pathway activation requires Ca<sup>2+</sup> influx. It has been demonstrated that Ca<sup>2+</sup> entry through Orai1 induces AKT phosphorylation in order to stimulate cell proliferation in several cell types, such as esophageal squamous cancer cells, colorectal and non-small lung cancer cells [46,61,62]. Furthermore, it has recently been established that Orai1 inhibition, using the RP4010 CRAC channel inhibitor, decreased pancreatic cancer cell proliferation through the down-regulation of the AKT/mTOR signaling pathway [63]. However, we were the first to illustrate activation of the AKT pathway via Orai1-mediated Ca<sup>2+</sup> entry resulting in cell proliferation enhancement in human-activated PSCs. In our study, on the one hand, Orai1 silencing decreased AKT phosphorylation without affecting ERK1/2 and SMAD2 activation, which are two of the main pathways modulating PSC activation. On the other hand, low extracellular Ca<sup>2+</sup> concentration led to an inhibition of AKT phosphorylation and PSC proliferation, suggesting that Orai1-mediated Ca<sup>2+</sup> entry is indispensable for AKT activation in order to stimulate PSC proliferation. This data, on the primordial role of the AKT pathway in the regulation of PSC proliferation, was also confirmed using the known PI3K/AKT pharmacological inhibitor LY294002.

However, the high mitotic index of activated PSCs alone is insufficient to induce pancreatic fibrogenesis during chronic pancreatitis and pancreatic cancer, leading to dense fibrotic desmoplasia development. To date, the most potent fibrogenic factor involved in PSC-mediated fibrosis, as well as in the interaction with the pancreatic cancer cells, is the

TGF $\beta_1$ . This pleiotropic cytokine promotes PSC activation by regulating  $\alpha$ -SMA expression, type I collagen synthesis, and cell proliferation in an autocrine manner. Indeed, in turn, activated PSCs trigger TGF $\beta_1$  auto-synthesis to maintain their activation. Ohnishi et al. have reported that TGF $\beta_1$  expression and secretion are mediated through the activation of the ERK1/2 pathway in rat-activated PSCs [32,64]. In contrast, TGF $\beta_1$  mRNA and protein expression are regulated by the PI3K/AKT pathway in human-activated hepatic stellate cells, counterparts of PSCs, which is in line with our findings in human-activated PSCs [34]. We have shown that PSC treatment with LY294002 significantly decreases TGF $\beta_1$  mRNA expression and secretion, suggesting that TGF $\beta_1$  synthesis and secretion in human-activated PSCs is AKT-dependent. Interspecies differences could explain TGF $\beta_1$  synthesis and secretion-dependent pathway discordance between rat and human-activated PSCs. Besides AKT-dependent TGF $\beta_1$  secretion, we have demonstrated that Ca $^{2+}$  is essential for this process since extracellular Ca $^{2+}$  reduction led to decreased-TGF $\beta_1$  secretion. In addition, we proposed in this study a mechanism by which Ca $^{2+}$  influx through Orai1 regulates TGF $\beta_1$  secretion via an AKT-dependent pathway. When we inhibited Orai1 expression under low extracellular Ca $^{2+}$  concentrations, we did not observe any additional effect on TGF $\beta_1$  secretion compared to Orai1 knocked-down cells under physiological extracellular Ca $^{2+}$  concentrations. These findings suggested that Ca $^{2+}$  entry through Orai1 induces AKT phosphorylation to promote TGF $\beta_1$  secretion in human-activated PSCs.

The most interesting finding in this report is the identification of a TGF $\beta_1$ -mediated autocrine positive feedback loop, promoting PSC Orai1/AKT-dependent proliferation through Orai1 activity and expression increase, leading to a perpetuated PSC activation. A link between TGF $\beta_1$  and Orai1 has previously been reported in airway smooth muscle cells, showing a SOCE stimulation due to Orai1 mRNA expression increase, promoted by TGF $\beta_1$  long-term exposure [65]. Following these findings, we were the first to illustrate that TGF $\beta_1$  treatment induced a rise of Orai1 mRNA and protein amounts in human-activated PSCs, leading to Orai1-mediated Ca $^{2+}$  entry promotion. Indeed, the TGF $\beta_1$  effect on Orai1 activity was observed only by TGF $\beta_1$  perfusion in our cellular model. Furthermore, several studies have demonstrated a stimulatory role of TGF $\beta_1$  on Ca $^{2+}$  entry in a context-dependent manner. For example, TGF $\beta_1$  long- but not short-term treatment has been shown to increase voltage-operated channel-mediated Ca $^{2+}$  entry in hepatic stellate cells [66], whereas TGF $\beta_1$  short treatment was sufficient to promote Ca $^{2+}$  influx through TRPC6 in intestinal myofibroblasts [40]. Additionally, TGF $\beta_1$  perfusion raised Ca $^{2+}$  release from the endoplasmic reticulum and so the SOCE in pancreatic cancer cells, suggesting its crucial involvement in pancreatic cancer as well [38]. Furthermore, we have provided evidence that TGF $\beta_1$ -mediated Orai1-Ca $^{2+}$  entry and expression stimulate Orai1/AKT activation and proliferation. Cell treatment with exogenous TGF $\beta_1$  increased AKT phosphorylation in siCtrl transfected cells, while this rise of AKT activity was partially absent in Orai1-knocked-down cells under TGF $\beta_1$  treatment. It has already been established by Tsang et al. that TGF $\beta_1$  can activate the AKT pathway by increasing its phosphorylation in rat-activated PSCs [67], and these data were confirmed here in human-activated PSCs. Moreover, we have reported a role of TGF $\beta_1$  in the promotion of PSC proliferation through Orai1-mediated AKT activation. Indeed, PSC proliferation increased after TGF $\beta_1$  treatment compared to non-treated cells, while Orai1 silencing abolished the stimulatory effect of TGF $\beta_1$  on PSC proliferation. Unlike our results, most of the studies conducted on PSCs have shown an inhibitory effect of TGF $\beta_1$  on PSC proliferation. These reports have been realized on rat-activated PSCs, demonstrating that TGF $\beta_1$  inhibits PSC proliferation through a Smad3-dependent pathway and by an accumulation of the G1 phase inhibitors p21 and p27, inducing G0/G1 cell cycle arrest [68]. TGF $\beta_1$  has been shown to induce both growth promotion and inhibition within the same cell type, depending on the context but also on the abundance or activity of extracellular TGF $\beta_1$  ligands, which could partly explain TGF $\beta_1$  promoted proliferation in our human-activated PSCs [13,69,70]. Elsner et al. have reported an indirect stimulatory effect of TGF $\beta_1$  on rat-activated PSC proliferation through the AKT pathway, using the multi-kinase inhibitor sorafenib [71]. TGF $\beta_1$  has been

shown to regulate cell growth through a Smad-dependent and Smad-independent pathway. The latter consisted of AKT activation [17]. Indeed, it has been reported that TGF $\beta$ <sub>1</sub>-induced AKT phosphorylation inhibits Smad3-mediated growth inhibition by binding to and sequestering Smad3 in the cytosol, leading to growth promotion, a mechanism that could justify our present results [72,73].

#### 4. Conclusions

Taken together, this is the first study revealing the important role of the Orai1 channel in PSC physiology, suggesting a role in fibrotic desmoplasia development, the main feature of PDAC. We suggest in this report that Orai1 can be involved in maintaining PSC activation to perpetuate pancreatic fibrosis by promoting PSC proliferation and TGF $\beta$ <sub>1</sub> expression and secretion through an AKT-dependent pathway. More importantly, we show that secreted TGF $\beta$ <sub>1</sub> from activated PSCs induces an autocrine positive feedback loop by stimulating Orai1-mediated Ca<sup>2+</sup> entry and increasing Orai1 expression. This later results in the promotion of Orai1-dependent AKT phosphorylation and thus to PSC proliferation enhancement to exacerbate pancreatic fibrosis development (Figure 8). Therefore, compounds that inhibit PSC proliferation by targeting Orai1 activity directly or the downstream effectors by inhibiting PI3K/AKT pathway or TGF $\beta$ <sub>1</sub> synthesis and/or secretion may have the potential to become a new approach for PDAC treatment or limit the drug resistance.

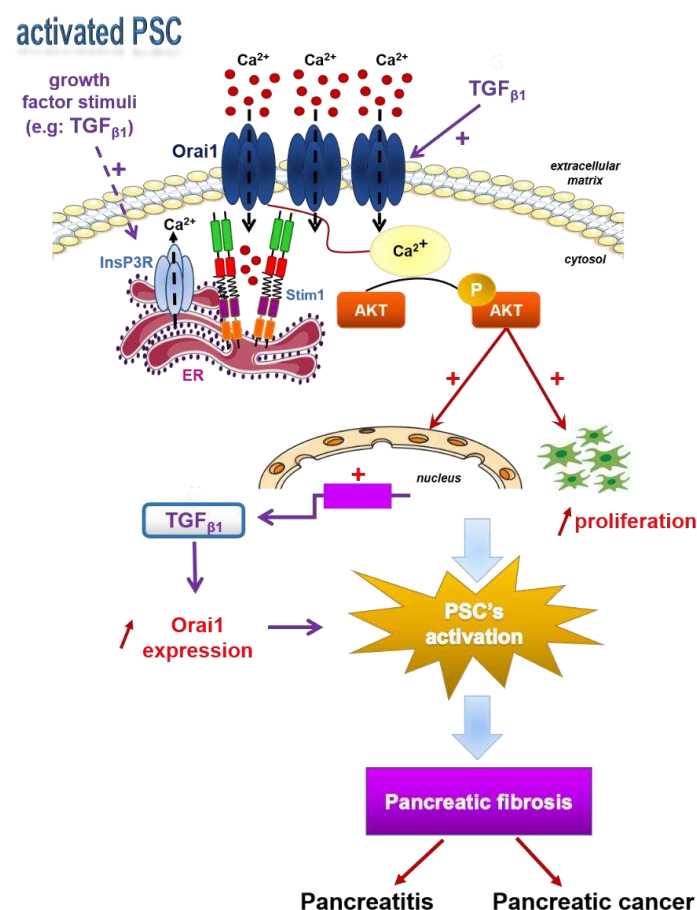


**Figure 8.** Conclusive scheme: Endoplasmic reticulum Ca<sup>2+</sup> store depletion activates Orai1 channel permitting SOCE. Ca<sup>2+</sup> entry through Orai1 activates AKT phosphorylation, which stimulates human-activated PSC proliferation and TGF $\beta$ <sub>1</sub> expression and secretion, enhancing PSC activation to promote pancreatic fibrosis, and so pancreatitis and pancreatic cancer. In turn, TGF $\beta$ <sub>1</sub> secretion stimulates Orai1-mediated Ca<sup>2+</sup> entry by simultaneously increasing Orai1 mRNA and protein expression in order to stimulate Orai1/AKT-dependent proliferation, maintaining PSC activation.

## 5. Materials and Methods

### 5.1. Cell Culture

The PS-1 pancreatic human stellate cell line was generously given by Pr Hemant M. Kocher from the Queen Mary University of London. PS-1 cells were isolated from a healthy donated human pancreas and immortalized with retroviruses containing cDNA encoding human telomerase reverse transcriptase (hTERT) and selected with puromycin, as previously described [74]. RLT PSCs were established from a chronic pancreatic tissue resection and immortalized with SV40 large T antigen and the catalytic subunit of hTERT, as previously described [75]. PS-1 and RLT PSCs were grown in Dulbecco's Modified Eagle Medium/Nutrient Mixture F-12 (DMEM/F12, Gibco, Thermo Fischer Scientific, Illkirch, France) supplemented with 10% Fetal Bovine Serum (FBS, Pan Biotech, Dominique Dutscher, Brumath, France). Cells were maintained at 37 °C in a humidified atmosphere containing 5% CO<sub>2</sub>, and the cell culture medium was changed every 48 h.

### 5.2. Cell Transfection and RNA Interference

Cells were transfected with small interfering RNA (siRNA) by electroporation, using the nucleofection technology (Amaxa Biosystems, Lonza, Aubergenville, France). PS-1 and RLT cells (10<sup>6</sup>) were transiently nucleofected according to the manufacturer's protocol with 4 µg of scrambled siRNA as a control (siCtrl: duplex negative control, Eurogentec) or with siRNA directed against Orai1 (siOrai1: 5'-CGUGCACAAUCUCAACUCG-3', Eurogentec). All the experiments were performed 72 h after the siRNA transfection.

### 5.3. Chemicals and Reagents

Pharmacological inhibitors and cytokines used to study the signaling pathways were the following: LY-294002 (20 µM, 72 h, Sigma-Aldrich, St. Quentin Fallavier, France), and transforming growth factor-β<sub>1</sub> human (20 ng/mL for 48 h treatment and 30 min stimulation, 5 ng/mL for perfusion, Sigma-Aldrich). The chemical ethylene glycol-bis (β-aminoethyl ether)-N,N,N',N'-tetraacetic acid (EGTA, 1.3 mM, 72 h treatment and 30 min stimulation, Sigma-Aldrich) was used to chelate extracellular Ca<sup>2+</sup>. The optimal EGTA concentration in order to reach 0.1 mM of extracellular Ca<sup>2+</sup> was determined using the max-chelator software (<https://somapp.ucdmc.ucdavis.edu/pharmacology/bers/maxchelator/CaMgATPEGTA-TS.htm>, accessed on 10 October 2019)

### 5.4. Cell Proliferation Assay

PS-1 and RLT cells were seeded in 6-well plates (8 × 10<sup>4</sup> cells per well for PS-1, 6 × 10<sup>4</sup> cells per well for RLT), and cell proliferation was assessed 72 h after siRNA transfection or treatment with pharmacological inhibitors or TGFβ<sub>1</sub> cytokine, as described above, by MTT assay. Cells were incubated with the 3-(4,5-dimethylthiazol-2-yl)-2,5-diphenyltetrazolium bromide (MTT, Sigma-Aldrich, Inc.) solubilized in culture medium (0.5 mg/mL), for 45 min at 37 °C in the dark, to be converted to an insoluble formazan. To dissolve the formazan crystals, the culture medium was replaced by dimethyl sulfoxide (DMSO, Sigma-Aldrich, Inc.), and the absorbance was measured at 550 nm using an Infnite<sup>®</sup> 200 Pro reader (Tecan Trading AG, Männedorf, Switzerland).

### 5.5. Cell Cycle Analysis

DNA cellular content quantitation by flow cytometry was used for cell cycle evaluation. Cells transfected (1 × 10<sup>6</sup>) with siOrai1 or siCtrl, were firstly fixed with cold absolute ethanol (≥99.8%, Sigma-Aldrich) for at least 6 h at 4 °C. Then, cells were pelleted, resuspended in PBS-5 mM EDTA, treated with 20 mg/mL RNaseA (Sigma-Aldrich) for 30 min at ambient temperature, and stained with 50 mg/mL of propidium iodide (Sigma-Aldrich, St. Quentin Fallavier, France). Samples were then analyzed by flow cytometer (Accuri<sup>®</sup>, Dominique Dutscher, Brumath, France), and the cell percentage in different phases was calculated using Cyflogic software.

### 5.6. Cell Mortality

PS-1 cells were grown in 35 mm Petri-dishes at a density of  $8 \times 10^4$  cells, and RLT cells at a density of  $6 \times 10^4$ , for 72 h, after siRNA transfection, and then cell death was measured by trypan blue assay. Cells were removed by trypsinization, diluted in trypan blue solution (Sigma-Aldrich), and counted six times using the standard Malassez cell method. The number of cell mortality was obtained using the formula: rate of cell death = number of dead cells/number of total cells, normalized to control. This colorimetric assay also provided us the number of cell proliferation, obtained using the formula: rate of cell proliferation = number of alive cells \* 4 \* 1900, normalized to control.

### 5.7. Apoptosis Analysis

The apoptosis process was assessed by studying the cell surface of phosphatidylserine exposure on the outer leaflet of the plasma membrane, an early marker of apoptotic cell death. Both detached and adherent cells were collected, washed twice in ice-cold PBS, and resuspended in  $1 \times$  binding buffer (BD Biosciences Pharmingen, Le Pont de Claix, France). Apoptotic cells were determined using a PE Annexin V Apoptosis Detection Kit staining (BD Biosciences Pharmingen), which consisted of adding FITC Annexin V and propidium iodide (PI) to the cell preparations and incubating them for 15 min at 25 °C in the dark. Binding buffer was then added to each tube, and the samples were analyzed by a flow cytometer (Accuri®). Compensation and quadrants were set up using the following controls: unstained cells, cells stained only with FITC Annexin V, and cells stained only with PI.

### 5.8. Calcium Imaging

Store-operated calcium entry (SOCE) was measured by calcium imaging using the ratiometric probe Fura-2/AM. Transfected cells ( $8 \times 10^4$  for PS-1 and  $6 \times 10^4$  for RLT) were plated on glass coverslips in 35 mm Petri-dishes and loaded with 3  $\mu$ M Fura-2/AM (Sigma-Aldrich) in extracellular saline solution for 45 min at 37 °C before  $\text{Ca}^{2+}$  measurement. After Fura-2 incubation, cells were washed three times and kept in the extracellular saline solution containing 145 mM NaCl, 5 mM KCl, 10 mM HEPES, 5 mM glucose, 2 mM  $\text{CaCl}_2$ , and 1 mM  $\text{MgCl}_2$ , at pH 7.4. The coverslip was transferred onto a perfusion chamber on a Zeiss microscope equipped for fluorescence. Fura-2 fluorescence was excited alternatively at 340 and 380 nm using a monochromator (polychrome IV, TILL Photonics, Planegg, Germany) and captured by a Cool SNAPHQ camera (Princeton Instruments, Evry, France) after filtration through a long-pass filter (510 nm emission wavelength). Signal acquisition and analysis were obtained with Metafluor software (version 7.1.7.0, Molecular Devices, St. Grégoire, France). The intracellular  $\text{Ca}^{2+}$  concentration was derived from the ratio of the fluorescence intensities for each of the excitation wavelengths ( $F_{340}/F_{380}$ ). Cells were continuously perfused with the saline solution, and all recordings were performed at room temperature. SOCE was induced after 1  $\mu$ M Thapsigargin (Sigma-Aldrich) stimulation in  $\text{Ca}^{2+}$ -free solution for 11 min, followed by 2 mM  $\text{Ca}^{2+}$  perfusion for 10 min. The flow rate of the whole-cell chamber perfusion system was set to 1 mL/min, and the chamber volume was 700  $\mu$ L.

### 5.9. qRT-PCR

Total cellular RNA was extracted by the standard Trizol reagent (Sigma-Aldrich) method, and RNA concentration and purity were determined by using a spectrophotometer (NanoDrop 2000, Wilmington, NC, USA). Then, cDNA was synthesized with a MultiScribe™ Reverse Transcriptase kit (Applied Biosystems, Carlsbad, CA, USA) from 2  $\mu$ g of RNA. For the real-time PCR, sense, and antisense PCR primers specific to Orai1 (forward 5'-AGGTGATGAGCCTCAACGAG-3' and reverse 5'-CTGATCATGAGCGCAAACAG-3'),  $\text{TGF}\beta_1$  (forward 5'-ACATCAACGCAGGGTTCCTACT-3' and reverse 5'-GAAGTTGGCATGGTAGCCCT-3'), and HPRT1 (forward 5'-AGTTCTGTGGCCATCTGCTT-3' and reverse 5'-CAATCCGCCCAAAGGGAACCT-3') were used. Real-time PCR was performed on a

LightCycler System (Roche, Basel, Switzerland) using LightCycler 480 SYBR Green I PCR master mix (Life Science, Roche). *Orai1* and  $TGF\beta_1$  mRNA expression were normalized to the endogenous gene control (*HPRT1*) and compared to the *siCtrl* sample, using the Pfaffl method [76].

#### 5.10. $TGF\beta_1$ Dosage Assay

Enzyme-Linked Immunosorbent Assay kit for  $TGF\beta_1$  quantitative measurement from cell culture supernatant was realized according to the technical protocol provided by the supplier (Sigma-Aldrich). All samples dosed for  $TGF\beta_1$  were treated 10 min with 1 N HCl at room temperature to activate latent  $TGF\beta_1$  to the immunoreactive form and then neutralized with 1.2 N NaOH/0.5 N HEPES. The absorbance from the colorimetric reaction corresponding to the  $TGF\beta_1$  quantity contained in the supernatant was read at 450 nm.

#### 5.11. Western Blotting and Co-Immunoprecipitation

Cells were lysed in RIPA buffer (1% Triton X-100, 0.1% sodium deoxycholate, 150 mM NaCl, 10 mM  $PO_4Na_2/K$ , pH = 7.4) containing protease inhibitor cocktail (Sigma-Aldrich), 5 mM sodium orthovanadate and 2 mM EDTA. Protein concentration was determined by the Bicinchoninic Acid protein assay (Bio-Rad, Marnes-La-Coquette, France). For standard Western blotting, 30  $\mu$ g of denatured protein lysate from each sample was loaded in SDS-PAGE, separated by the denaturing SDS-PAGE, and transferred onto a nitrocellulose membrane (Dominique Dutscher, Brumath, France). The primary antibodies used were: anti-*Orai1* (1:250, Sigma-Aldrich), anti- $\alpha$ SMA (1:1000, Abcam), anti-GAPDH (1:4000, Abcam), anti-SMAD2 (1:1000, Abcam), anti-p-SMAD2 (phospho S255) (1:1000, Abcam), anti-ERK1/2 (1:500, Cell Signaling), anti-p-ERK1/2 (Thr202/Tyr204) (1:500, Cell Signaling), anti-Akt (1:500, Cell Signaling) and anti-p-Akt (Ser473) (1:500, Cell Signaling). The secondary antibodies used were coupled to horseradish peroxidase, which permitted protein band detection through an enhanced chemiluminescence kit (Ozyme). Protein bands were quantified using the densitometric analysis option in the Bio-Rad image acquisition software (Quantity One), and all experiments results were normalized to the GAPDH, used as a control referent protein.

Co-immunoprecipitation experiments were realized with 500  $\mu$ g of protein lysates, precleared for 1 h 30 with protein A sepharose magnetic beads (Millipore, PureProteome™) and then incubated overnight with the primary antibody. The dilution of primary antibodies used for the co-immunoprecipitation experiments was anti-*Orai1* 1:100 (Sigma-Aldrich) and anti- $\alpha$ SMA 1:200 (Abcam). Then, the antigen-antibody complex was precipitated with protein A sepharose magnetic beads (Millipore, PureProteome™) for 1 h. After denaturation, proteins were used for a standard Western blot, as described above.

#### 5.12. Statistical Analysis

All data are presented as mean  $\pm$  SEM (standard error of the mean), n corresponds to the number of cells, and N refers to the number of cell passages. All experiments were performed at least with three different cell passages. Statistically significant differences were determined with paired or unpaired *t*-test or with one-way or two-way ANOVA and post hoc Bonferroni test for multiple comparisons, depending on the compared conditions, using GraphPad Prism version 5 (GraphPad Software, La Jolla, CA, USA). Differences between the values were considered significant when  $p < 0.05$ . The  $p$ -values  $< 0.05$ ,  $< 0.01$ , and  $< 0.001$  are represented as \*, \*\*, and \*\*\*, respectively.

**Supplementary Materials:** The following are available online at <https://www.mdpi.com/article/10.3390/cancers13102395/s1>, Figure S1: (A) Localization of *Orai1* channel in PS-1 visualized by confocal microscopy, 72h post-proliferation. (B) *Orai1* channel mediates the  $Ca^{2+}$  basal concentration in both, PS-1 and RLT human activated PSC cell lines. (C) SOCs channels are opened in cell culture conditions due to the permanent ER- $Ca^{2+}$  depletion induced by FBS. Figure S3: *Orai1* knocking-down impacts SMAD2 total protein expression without affecting AKT and ERK1/2 in PS-1 human activated PSCs, Figure S4: *Orai1* modulates AKT activation but not ERK1/2 nor SMAD2 phosphorylation in RLT



human activated PSCs, without affecting their total protein amount. Figure S5: Orai1 channel neither regulates  $\alpha$ SMA expression nor colocalizes with  $\alpha$ SMA in human activated PSCs.

**Author Contributions:** S.R.: experiment's performance (cell culture, treatments, cell proliferation, and mortality, cytometry, qPCR, ELISA assay, calcium imaging, Western blot, co-immunoprecipitation, and immunofluorescence), interpretation of data, statistical analysis, and manuscript preparation. A.F.: calcium imaging and qPCR experiments. T.L.: cell culture and cytometry experiments. K.K.: confocal microscopy experiments. S.G.: qPCR experiments. I.D.-D. and M.G.: interpretation of data. N.P.: design and supervised the project, interpretation of data and manuscript preparation. H.O.-A.: design and supervised the project, interpretation of data and manuscript preparation. All authors have read and agreed to the published version of the manuscript.

**Funding:** This research was funded by the Cancéropôle Nord-Ouest (CNO) for the project entitled "SICASTE", 2016-2018.

**Institutional Review Board Statement:** Not applicable.

**Informed Consent Statement:** Not applicable.

**Data Availability Statement:** Data are contained within the article or supplementary material.

**Acknowledgments:** We acknowledge the Région Hauts-de-France (Picardie), the FEDER (Fonds Européen de Développement Économique Régional), the Université Picardie Jules Verne, and the Ministère de l'Enseignement Supérieur et de la Recherche for supporting this study. We thank the H.M. Kocher and his laboratory members from the Queen Mary University of London, for kindly providing us the PS-1 cell line, used for this study. We also thank the platform of Centre de Ressources Régionales en Biologie Moléculaire for the equipment availability.

**Conflicts of Interest:** The authors declare that they have no interest of any kind affecting this study.

## References

1. Jaster, R.; Emmrich, J. Crucial role of fibrogenesis in pancreatic diseases. *Best Pract. Res. Clin. Gastroenterol.* **2008**, *22*, 17–29. [[CrossRef](#)]
2. Apte, M.V.; Pirola, R.C.; Wilson, J.S. Pancreatic stellate cells: A starring role in normal and diseased pancreas. *Front. Physiol.* **2012**, *3*, 344. [[CrossRef](#)] [[PubMed](#)]
3. Norton, J.; Foster, D.; Chinta, M.; Titan, A.; Longaker, M. Pancreatic Cancer Associated Fibroblasts (CAF): Under-Explored Target for Pancreatic Cancer Treatment. *Cancers* **2020**, *12*, 1347. [[CrossRef](#)] [[PubMed](#)]
4. Thomas, D.; Radhakrishnan, P. Pancreatic Stellate Cells: The Key Orchestrator of the Pancreatic Tumor Microenvironment. In *Advances in Experimental Medicine and Biology*; Birbrair, A., Ed.; Springer Science and Business Media LLC: Berlin/Heidelberg, Germany, 2020; Volume 1234, pp. 57–70.
5. Ferdek, P.E.; Jakubowska, M.A. Biology of pancreatic stellate cells—more than just pancreatic cancer. *Pflügers Arch. Eur. J. Physiol.* **2017**, *469*, 1039–1050. [[CrossRef](#)] [[PubMed](#)]
6. Masamune, A.; Shimosegawa, T. Pancreatic stellate cells—Multi-functional cells in the pancreas. *Pancreatology* **2013**, *13*, 102–105. [[CrossRef](#)] [[PubMed](#)]
7. Bynigeri, R.R.; Jakkampudi, A.; Jangala, R.; Subramanyam, C.; Sasikala, M.; Rao, G.V.; Reddy, D.N.; Talukdar, R. Pancreatic stellate cell: Pandora's box for pancreatic disease biology. *World J. Gastroenterol.* **2017**, *23*, 382–405. [[CrossRef](#)]
8. Masamune, A.; Watanabe, T.; Kikuta, K.; Shimosegawa, T. Roles of Pancreatic Stellate Cells in Pancreatic Inflammation and Fibrosis. *Clin. Gastroenterol. Hepatol.* **2009**, *7*, S48–S54. [[CrossRef](#)] [[PubMed](#)]
9. Pereira, B.A.; Vennin, C.; Papanicolaou, M.; Chambers, C.R.; Herrmann, D.; Morton, J.P.; Cox, T.R.; Timpon, P. CAF Subpopulations: A New Reservoir of Stromal Targets in Pancreatic Cancer. *Trends Cancer* **2019**, *5*, 724–741. [[CrossRef](#)]
10. Jin, G.; Hong, W.; Guo, Y.; Bai, Y.; Chen, B. Molecular Mechanism of Pancreatic Stellate Cells Activation in Chronic Pancreatitis and Pancreatic Cancer. *J. Cancer* **2020**, *11*, 1505–1515. [[CrossRef](#)]
11. Schneider, E.; Schmid-Kotsas, A.; Zhao, J.; Weidenbach, H.; Schmid, R.M.; Menke, A.; Adler, G.; Waltenberger, J.; Grünert, A.; Bachem, M.G. Identification of mediators stimulating proliferation and matrix synthesis of rat pancreatic stellate cells. *Am. J. Physiol. Physiol.* **2001**, *281*, C532–C543. [[CrossRef](#)]
12. Kulkarni, A.A.; Thatcher, T.H.; Olsen, K.C.; Maggirwar, S.B.; Phipps, R.P.; Sime, P.J. PPAR- $\gamma$  Ligands Repress TGF $\beta$ -Induced Myofibroblast Differentiation by Targeting the PI3K/Akt Pathway: Implications for Therapy of Fibrosis. *PLoS ONE* **2011**, *6*, e15909. [[CrossRef](#)] [[PubMed](#)]
13. Kim, K.K.; Sheppard, D.; Chapman, H.A. TGF- $\beta$ 1 Signaling and Tissue Fibrosis. *Cold Spring Harb. Perspect. Biol.* **2018**, *10*, a022293. [[CrossRef](#)]
14. Omary, M.B.; Lugea, A.; Lowe, A.W.; Pandol, S.J. The pancreatic stellate cell: A star on the rise in pancreatic diseases. *J. Clin. Investig.* **2007**, *117*, 50–59. [[CrossRef](#)] [[PubMed](#)]

15. Apte, M.V.; Haber, P.S.; Darby, S.J.; Rodgers, S.C.; McCaughan, G.W.; Korsten, M.; Pirola, R.C.; Wilson, J.S. Pancreatic stellate cells are activated by proinflammatory cytokines: Implications for pancreatic fibrogenesis. *Gut* **1999**, *44*, 534–541. [[CrossRef](#)]
16. Kruse, M.-L.; Hildebrand, P.B.; Timke, C.; Fölsch, U.R.; E Schmidt, W. TGF $\beta$ 1 autocrine growth control in isolated pancreatic fibroblastoid cells/stellate cells in vitro. *Regul. Pept.* **2000**, *90*, 47–52. [[CrossRef](#)]
17. Finnson, K.W.; Almadani, Y.; Philip, A. Non-canonical (non-SMAD2/3) TGF- $\beta$  signaling in fibrosis: Mechanisms and targets. *Semin. Cell Dev. Biol.* **2020**, *101*, 115–122. [[CrossRef](#)] [[PubMed](#)]
18. Masamune, A.; Shimosegawa, T. Signal transduction in pancreatic stellate cells. *J. Gastroenterol.* **2009**, *44*, 249–260. [[CrossRef](#)]
19. Kusiak, A.A.; Szopa, M.D.; Jakubowska, M.A.; Ferdek, P.E. Signaling in the Physiology and Pathophysiology of Pancreatic Stellate Cells—A Brief Review of Recent Advances. *Front. Physiol.* **2020**, *11*, 78. [[CrossRef](#)]
20. Schwer, C.I.; Stoll, P.; Rospert, S.; Fitzke, E.; Schallner, N.; Bürkle, H.; Schmidt, R.; Humar, M. Carbon monoxide releasing molecule-2 CORM-2 represses global protein synthesis by inhibition of eukaryotic elongation factor eEF2. *Int. J. Biochem. Cell Biol.* **2013**, *45*, 201–212. [[CrossRef](#)]
21. Zhang, X.; Jin, T.; Huang, X.; Liu, X.; Liu, Z.; Jia, Y.; Hao, J. Effects of the tumor suppressor PTEN on biological behaviors of activated pancreatic stellate cells in pancreatic fibrosis. *Exp. Cell Res.* **2018**, *373*, 132–144. [[CrossRef](#)]
22. Won, J.H.; Zhang, Y.; Ji, B.; Logsdon, C.D.; Yule, D.I. Phenotypic changes in mouse pancreatic stellate cell Ca<sup>2+</sup> signaling events following activation in culture and in a disease model of pancreatitis. *Mol. Biol. Cell* **2011**, *22*, 421–436. [[CrossRef](#)]
23. Son, A.; Park, S.; Shin, D.M.; Muallem, S. Orai1 and STIM1 in ER/PM junctions: Roles in pancreatic cell function and dysfunction. *Am. J. Physiol. Physiol.* **2016**, *310*, C414–C422. [[CrossRef](#)] [[PubMed](#)]
24. Gryshchenko, O.; Gerasimenko, J.V.; Gerasimenko, O.V.; Petersen, O.H. Ca<sup>2+</sup> signals mediated by bradykinin type 2 receptors in normal pancreatic stellate cells can be inhibited by specific Ca<sup>2+</sup> channel blockade. *J. Physiol.* **2015**, *594*, 281–293. [[CrossRef](#)] [[PubMed](#)]
25. Waldron, R.T.; Chen, Y.; Pham, H.; Go, A.; Su, H.; Hu, C.; Wen, L.; Husain, S.Z.; Sugar, C.A.; Roos, J.; et al. The Orai Ca<sup>2+</sup> channel inhibitor CM4620 targets both parenchymal and immune cells to reduce inflammation in experimental acute pancreatitis. *J. Physiol.* **2019**, *597*, 3085–3105. [[CrossRef](#)] [[PubMed](#)]
26. Fu, T.; Xu, Y.; Jiang, W.; Zhang, H.; Zhu, P.; Wu, J. EGF receptor-mediated intracellular calcium increase in human hepatoma BEL-7404 cells. *Cell Res.* **1994**, *4*, 145–153. [[CrossRef](#)]
27. Wang, L.; Wormstone, I.M.; Reddan, J.R.; Duncan, G. Growth factor receptor signalling in human lens cells: Role of the calcium store. *Exp. Eye Res.* **2005**, *80*, 885–895. [[CrossRef](#)] [[PubMed](#)]
28. Davis, F.M.; Peters, A.A.; Grice, D.M.; Cabot, P.J.; Parat, M.-O.; Roberts-Thomson, S.J.; Monteith, G.R. Non-Stimulated, Agonist-Stimulated and Store-Operated Ca<sup>2+</sup> Influx in MDA-MB-468 Breast Cancer Cells and the Effect of EGF-Induced EMT on Calcium Entry. *PLoS ONE* **2012**, *7*, e36923. [[CrossRef](#)] [[PubMed](#)]
29. Azimi, I.; Bong, A.H.; Poo, G.X.H.; Armitage, K.; Lok, D.; Roberts-Thomson, S.J.; Monteith, G.R. Pharmacological inhibition of store-operated calcium entry in MDA-MB-468 basal A breast cancer cells: Consequences on calcium signalling, cell migration and proliferation. *Cell. Mol. Life Sci.* **2018**, *75*, 4525–4537. [[CrossRef](#)]
30. Aoki, H.; Ohnishi, H.; Hama, K.; Shinozaki, S.; Kita, H.; Yamamoto, H.; Osawa, H.; Sato, K.; Tamada, K.; Sugano, K. Existence of autocrine loop between interleukin-6 and transforming growth factor- $\beta$ 1 in activated rat pancreatic stellate cells. *J. Cell. Biochem.* **2006**, *99*, 221–228. [[CrossRef](#)]
31. Masamune, A.; Kikuta, K.; Satoh, M.; Kume, K.; Shimosegawa, T. Differential Roles of Signaling Pathways for Proliferation and Migration of Rat Pancreatic Stellate Cells. *Tohoku J. Exp. Med.* **2003**, *199*, 69–84. [[CrossRef](#)]
32. Ohnishi, H.; Miyata, T.; Yasuda, H.; Satoh, Y.; Hanatsuka, K.; Kita, H.; Ohashi, A.; Tamada, K.; Makita, N.; Iiri, T.; et al. Distinct roles of Smad2-, Smad3-, and ERK-dependent pathways in transforming growth factor-beta1 regulation of pancreatic stellate cellular functions. *J. Biol. Chem.* **2004**, *279*, 8873–8878. [[CrossRef](#)]
33. Jaster, R.; Sparmann, G.; Emmrich, J.; Liebe, S. Extracellular signal regulated kinases are key mediators of mitogenic signals in rat pancreatic stellate cells. *Gut* **2002**, *51*, 579–584. [[CrossRef](#)]
34. Yu, D.-K.; Zhang, C.-X.; Zhao, S.-S.; Zhang, S.-H.; Zhang, H.; Cai, S.-Y.; Shao, R.-G.; He, H.-W. The anti-fibrotic effects of epigallocatechin-3-gallate in bile duct-ligated cholestatic rats and human hepatic stellate LX-2 cells are mediated by the PI3K/Akt/Smad pathway. *Acta Pharmacol. Sin.* **2015**, *36*, 473–482. [[CrossRef](#)] [[PubMed](#)]
35. Xu, M.; Wang, G.; Zhou, H.; Cai, J.; Li, P.; Zhou, M.; Lu, Y.; Jiang, X.; Huang, H.; Zhang, Y.; et al. TGF- $\beta$ 1-miR-200a-PTEN induces epithelial–mesenchymal transition and fibrosis of pancreatic stellate cells. *Mol. Cell. Biochem.* **2017**, *431*, 161–168. [[CrossRef](#)] [[PubMed](#)]
36. Alevizopoulos, A.; Dusserre, Y.; Rüegg, U.; Mermoud, N. Regulation of the Transforming Growth Factor  $\beta$ -responsive Transcription Factor CTF-1 by Calcineurin and Calcium/ Calmodulin-dependent Protein Kinase IV. *J. Biol. Chem.* **1997**, *272*, 23597–23605. [[CrossRef](#)] [[PubMed](#)]
37. Chow, J.Y.C.; Dong, H.; Quach, K.T.; Van Nguyen, P.N.; Chen, K.; Carethers, J.M. TGF- $\beta$  mediates PTEN suppression and cell motility through calcium-dependent PKC- $\alpha$  activation in pancreatic cancer cells. *Am. J. Physiol. Liver Physiol.* **2008**, *294*, G899–G905. [[CrossRef](#)]
38. Dong, H.; Shim, K.-N.; Li, J.M.J.; Estrema, C.; Ornelas, T.A.; Nguyen, F.; Liu, S.; Ramamoorthy, S.L.; Ho, S.; Carethers, J.M.; et al. Molecular mechanisms underlying Ca<sup>2+</sup>-mediated motility of human pancreatic duct cells. *Am. J. Physiol. Physiol.* **2010**, *299*, C1493–C1503. [[CrossRef](#)]

39. Iyer, S.C.; Kannan, A.; Gopal, A.; Devaraj, N.; Halagowder, D. Receptor channel TRPC6 orchestrate the activation of human hepatic stellate cell under hypoxia condition. *Exp. Cell Res.* **2015**, *336*, 66–75. [[CrossRef](#)]
40. Kurahara, L.H.; Sumiyoshi, M.; Aoyagi, K.; Hiraishi, K.; Nakajima, K.; Nakagawa, M.; Hu, Y.; Inoue, R. Intestinal Myofibroblast TRPC6 Channel May Contribute to Stenotic Fibrosis in Crohn's Disease. *Inflamm. Bowel Dis.* **2015**, *21*, 496–506. [[CrossRef](#)]
41. Hodeify, R.; Yu, F.; Courjaret, R.; Nader, N.; Dib, M.; Sun, L.; Adap, E.; Hubrack, S.; Machaca, K.; Kozak, J.A.; et al. Regulation and Role of Store-Operated Ca<sup>2+</sup> Entry in Cellular Proliferation. In *Calcium Entry Channels in Non-Excitable Cells*; Kozak, J.A., Putney, J.W., Eds.; CRC Press: Boca Raton, FL, USA, 2017; pp. 215–240.
42. Gao, X.; Xia, J.; Munoz, F.M.; Manners, M.T.; Pan, R.; Meucci, O.; Dai, Y.; Hu, H. STIMs and Orai1 regulate cytokine production in spinal astrocytes. *J. Neuroinflamm.* **2016**, *13*, 126. [[CrossRef](#)]
43. Kondratska, K.; Kondratskyi, A.; Yassine, M.; Lemonnier, L.; Lepage, G.; Morabito, A.; Skryma, R.; Prevarskaya, N. Orai1 and STIM1 mediate SOCE and contribute to apoptotic resistance of pancreatic adenocarcinoma. *Biochim. Biophys. Acta (BBA) Bioenerg.* **2014**, *1843*, 2263–2269. [[CrossRef](#)] [[PubMed](#)]
44. Somasundaram, A.; Shum, A.K.; McBride, H.J.; Kessler, J.A.; Feske, S.; Miller, R.J.; Prakriya, M. Store-Operated CRAC Channels Regulate Gene Expression and Proliferation in Neural Progenitor Cells. *J. Neurosci.* **2014**, *34*, 9107–9123. [[CrossRef](#)] [[PubMed](#)]
45. Liu, H.; Hughes, J.D.; Rollins, S.; Chen, B.; Perkins, E. Calcium entry via ORAI1 regulates glioblastoma cell proliferation and apoptosis. *Exp. Mol. Pathol.* **2011**, *91*, 753–760. [[CrossRef](#)] [[PubMed](#)]
46. Zhu, H.; Zhang, H.; Jin, F.; Fang, M.; Huang, M.; Yang, C.S.; Chen, T.; Fu, L.; Pan, Z. Elevated Orai1 expression mediates tumor-promoting intracellular Ca<sup>2+</sup> oscillations in human esophageal squamous cell carcinoma. *Oncotarget* **2014**, *5*, 3455–3471. [[CrossRef](#)] [[PubMed](#)]
47. Choi, D.; Park, E.; Jung, E.; Seong, Y.J.; Hong, M.; Lee, S.; Burford, J.; Gyarmati, G.; Peti-Peterdi, J.; Srikanth, S.; et al. ORAI1 Activates Proliferation of Lymphatic Endothelial Cells in Response to Laminar Flow through Krüppel-Like Factors 2 and 4. *Circ. Res.* **2017**, *120*, 1426–1439. [[CrossRef](#)]
48. Capiod, T. Cell proliferation, calcium influx and calcium channels. *Biochimie* **2011**, *93*, 2075–2079. [[CrossRef](#)]
49. Kim, J.-H.; Lkhagvadorj, S.; Lee, M.-R.; Hwang, K.-H.; Chung, H.C.; Jung, J.H.; Cha, S.-K.; Eom, M. Orai1 and STIM1 are critical for cell migration and proliferation of clear cell renal cell carcinoma. *Biochem. Biophys. Res. Commun.* **2014**, *448*, 76–82. [[CrossRef](#)] [[PubMed](#)]
50. Capiod, T. The Need for Calcium Channels in Cell Proliferation. *Recent Pat. Anti-Cancer Drug Discov.* **2012**, *8*, 4–17. [[CrossRef](#)]
51. El Boustany, C.; Katsogiannou, M.; Delcourt, P.; Dewailly, E.; Prevarskaya, N.; Borowiec, A.-S.; Capiod, T. Differential roles of STIM1, STIM2 and Orai1 in the control of cell proliferation and SOCE amplitude in HEK293 cells. *Cell Calcium* **2010**, *47*, 350–359. [[CrossRef](#)]
52. Abdullaev, I.F.; Bisailon, J.M.; Potier, M.; Gonzalez, J.C.; Motiani, R.K.; Trebak, M. Stim1 and Orai1 Mediate CRAC Currents and Store-Operated Calcium Entry Important for Endothelial Cell Proliferation. *Circ. Res.* **2008**, *103*, 1289–1299. [[CrossRef](#)]
53. Borowiec, A.-S.; Bidaux, G.; Tacine, R.; Dubar, P.; Pigat, N.; Delcourt, P.; Mignen, O.; Capiod, T. Are Orai1 and Orai3 channels more important than calcium influx for cell proliferation? *Biochim. Biophys. Acta (BBA) Mol. Cell Res.* **2014**, *1843*, 464–472. [[CrossRef](#)] [[PubMed](#)]
54. Wang, L.; Hao, J.; Zhang, Y.; Yang, Z.; Cao, Y.; Lu, W.; Shu, Y.; Jiang, L.; Hu, Y.; Lv, W.; et al. Orai1 mediates tumor-promoting store-operated Ca<sup>2+</sup> entry in human gastrointestinal stromal tumors via c-KIT and the extracellular signal-regulated kinase pathway. *Tumor Biol.* **2017**, *39*, 1010428317691426. [[CrossRef](#)] [[PubMed](#)]
55. Chen, Y.-W.; Chen, Y.-F.; Chen, Y.-T.; Chiu, W.-T.; Shen, M.-R. The STIM1-Orai1 pathway of store-operated Ca<sup>2+</sup> entry controls the checkpoint in cell cycle G1/S transition. *Sci. Rep.* **2016**, *6*, 1–13. [[CrossRef](#)]
56. Jairaman, A.; Yamashita, M.; Schleimer, R.P.; Prakriya, M. Store-Operated Ca<sup>2+</sup> Release-Activated Ca<sup>2+</sup> Channels Regulate PAR2-Activated Ca<sup>2+</sup> Signaling and Cytokine Production in Airway Epithelial Cells. *J. Immunol.* **2015**, *195*, 2122–2133. [[CrossRef](#)] [[PubMed](#)]
57. Heo, D.K.; Lim, H.M.; Nam, J.H.; Lee, M.G.; Kim, J.Y. Regulation of phagocytosis and cytokine secretion by store-operated calcium entry in primary isolated murine microglia. *Cell. Signal.* **2015**, *27*, 177–186. [[CrossRef](#)] [[PubMed](#)]
58. Murthy, D.; Attri, K.S.; Singh, P.K. Phosphoinositide 3-Kinase Signaling Pathway in Pancreatic Ductal Adenocarcinoma Progression, Pathogenesis, and Therapeutics. *Front. Physiol.* **2018**, *9*, 335. [[CrossRef](#)]
59. Cui, L.-H.; Li, C.-X.; Zhuo, Y.-Z.; Yang, L.; Cui, N.-Q.; Zhang, S.-K. Saikosaponin d ameliorates pancreatic fibrosis by inhibiting autophagy of pancreatic stellate cells via PI3K/Akt/mTOR pathway. *Chem. Interact.* **2019**, *300*, 18–26. [[CrossRef](#)]
60. Ramakrishnan, P.; Loh, W.M.; Gopinath, S.C.B.; Bonam, S.R.; Fareez, I.M.; Mac Guad, R.; Sim, M.S.; Wu, Y.S. Selective phytochemicals targeting pancreatic stellate cells as new anti-fibrotic agents for chronic pancreatitis and pancreatic cancer. *Acta Pharm. Sin. B* **2020**, *10*, 399–413. [[CrossRef](#)]
61. Deng, W.; Wang, J.; Zhang, J.; Cai, J.; Bai, Z.; Zhang, Z. Orai1, a Direct Target of microRNA-519, Promotes Progression of Colorectal Cancer via Akt/GSK3 $\beta$  Signaling Pathway. *Dig. Dis. Sci.* **2016**, *61*, 1553–1560. [[CrossRef](#)]
62. Zhan, Z.-Y.; Zhong, L.-X.; Feng, M.; Wang, J.-F.; Liu, D.-B.; Xiong, J.-P. Over-expression of Orai1 mediates cell proliferation and associates with poor prognosis in human non-small cell lung carcinoma. *Int. J. Clin. Exp. Pathol.* **2015**, *8*, 5080–5088.
63. Khan, H.Y.; Mpilla, G.B.; Sexton, R.; Viswanadha, S.; Penmetsa, K.V.; Aboukameel, A.; Diab, M.; Kamgar, M.; Al-Hallak, M.N.; Szlaczky, M.; et al. Calcium Release-Activated Calcium (CRAC) Channel Inhibition Suppresses Pancreatic Ductal Adenocarcinoma Cell Proliferation and Patient-Derived Tumor Growth. *Cancers* **2020**, *12*, 750. [[CrossRef](#)] [[PubMed](#)]

64. Xu, X.-F.; Liu, F.; Xin, J.-Q.; Fan, J.-W.; Wu, N.; Zhu, L.-J.; Duan, L.-F.; Li, Y.-Y.; Zhang, H. Respective roles of the mitogen-activated protein kinase (MAPK) family members in pancreatic stellate cell activation induced by transforming growth factor- $\beta$ 1 (TGF- $\beta$ 1). *Biochem. Biophys. Res. Commun.* **2018**, *501*, 365–373. [[CrossRef](#)] [[PubMed](#)]
65. Gao, Y.-D.; Zheng, J.-W.; Li, P.; Cheng, M.; Yang, J. Store-Operated Ca<sup>2+</sup>-Entry is Involved in Transforming Growth Factor- $\beta$ 1 Facilitated Proliferation of Rat Airway Smooth Muscle Cells. *J. Asthma* **2013**, *50*, 439–448. [[CrossRef](#)] [[PubMed](#)]
66. Roth-Eichhorn, S.; Eberheim, A.; Bode, H.-P.; Gressner, A.M. Transformation-dependent calcium influx by voltage-operated calcium channels in stellate cells of rat liver. *J. Hepatol.* **1999**, *30*, 612–620. [[CrossRef](#)]
67. Tsang, S.W.; Bian, Z.-X. Anti-fibrotic and Anti-tumorigenic Effects of Rhein, a Natural Anthraquinone Derivative, in Mammalian Stellate and Carcinoma Cells. *Phytother. Res.* **2014**, *29*, 407–414. [[CrossRef](#)]
68. Berna, M.J.; Seiz, O.; Nast, J.F.; Bente, D.; Bläker, M.; Koch, J.; Lohse, A.W.; Pace, A. CCK1 and CCK2 Receptors Are Expressed on Pancreatic Stellate Cells and Induce Collagen Production. *J. Biol. Chem.* **2010**, *285*, 38905–38914. [[CrossRef](#)]
69. Morikawa, M.; Derynck, R.; Miyazono, K. TGF- $\beta$  and the TGF- $\beta$  Family: Context-Dependent Roles in Cell and Tissue Physiology. *Cold Spring Harb. Perspect. Biol.* **2016**, *8*, a021873. [[CrossRef](#)]
70. Zhang, Y.; Alexander, P.B.; Wang, X.-F. TGF- $\beta$  Family Signaling in the Control of Cell Proliferation and Survival. *Cold Spring Harb. Perspect. Biol.* **2016**, *9*, a022145. [[CrossRef](#)] [[PubMed](#)]
71. Elsner, A.; Lange, F.; Fitzner, B.; Heuschkel, M.; Krause, B.J.; Jaster, R. Distinct antifibrogenic effects of erlotinib, sunitinib and sorafenib on rat pancreatic stellate cells. *World J. Gastroenterol.* **2014**, *20*, 7914–7925. [[CrossRef](#)]
72. Zhang, Y.E. Non-Smad Signaling Pathways of the TGF- $\beta$  Family. *Cold Spring Harb. Perspect. Biol.* **2016**, *9*, a022129. [[CrossRef](#)]
73. Zhang, Y.E. Non-Smad pathways in TGF- $\beta$  signaling. *Cell Res.* **2009**, *19*, 128–139. [[CrossRef](#)]
74. Froeling, F.E.; Mirza, T.A.; Feakins, R.M.; Seedhar, A.; Elia, G.; Hart, I.R.; Kocher, H.M. Organotypic Culture Model of Pancreatic Cancer Demonstrates that Stromal Cells Modulate E-Cadherin,  $\beta$ -Catenin, and Ezrin Expression in Tumor Cells. *Am. J. Pathol.* **2009**, *175*, 636–648. [[CrossRef](#)] [[PubMed](#)]
75. Jesnowski, R.; Fürst, D.; Ringel, J.; Chen, Y.; Schrödel, A.; Kleeff, J.; Kolb, A.; Schareck, W.D.; Löhr, M. Immortalization of pancreatic stellate cells as an in vitro model of pancreatic fibrosis: Deactivation is induced by matrigel and N-acetylcysteine. *Lab. Invest.* **2005**, *85*, 1276–1291. [[CrossRef](#)] [[PubMed](#)]
76. Pfaffl, M.W.; Horgan, G.W.; Dempfle, L. Relative expression software tool (REST) for group-wise comparison and statistical analysis of relative expression results in real-time PCR. *Nucleic Acids Res.* **2002**, *30*, e36. [[CrossRef](#)] [[PubMed](#)]

Article

# Orai1 Channel Regulates Human-Activated Pancreatic Stellate Cell Proliferation and TGF $\beta$ <sub>1</sub> Secretion through the AKT Signaling Pathway

Silviya Radoslavova, Antoine Folcher, Thibaut Lefebvre, Kateryna Kondratska, Stéphanie Guénin, Isabelle Dhennin-Duthille, Mathieu Gautier, Natalia Prevarskaya and Halima Ouadid-Ahidouch

Supplementary Figures

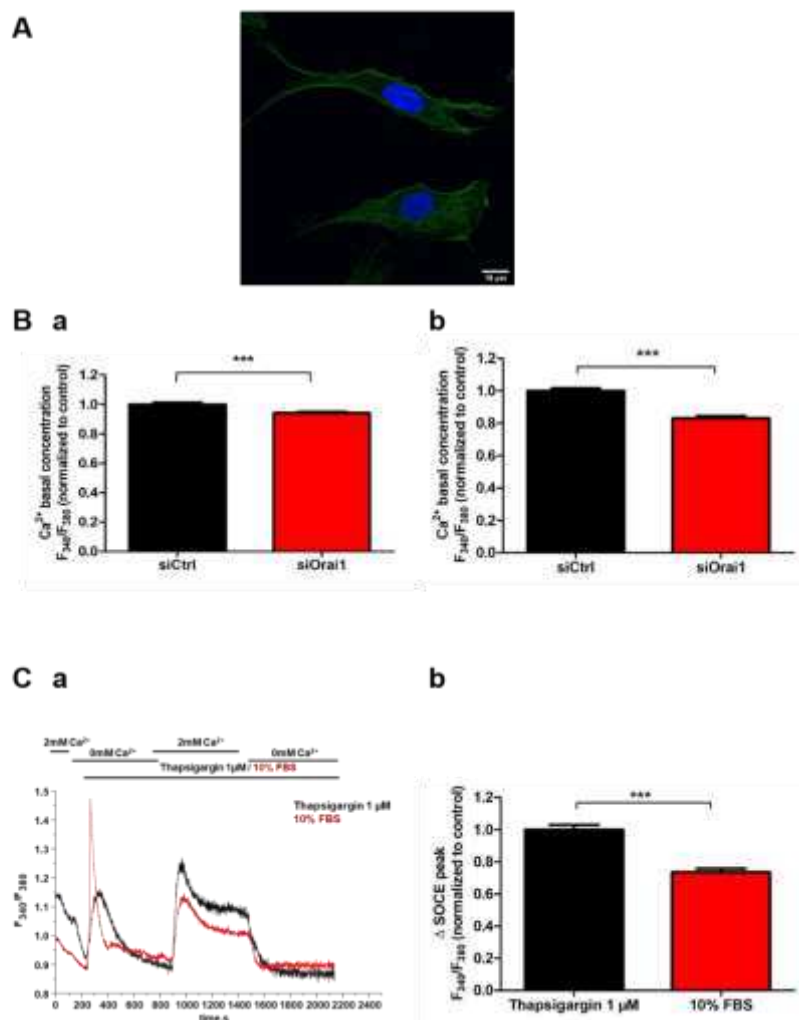


**Figure S1.** (A) Localization of Orai1 channel in PS-1 visualized by confocal microscopy, 72h post-proliferation. (B) Orai1 channel mediates the Ca<sup>2+</sup> basal concentration in both, PS-1 and RLT human activated PSC cell lines. Quantification of Ca<sup>2+</sup> basal concentration in PS-1 cells (B-a) (siCtrl: n = 210, siOrai1: n = 189, N = 5) and RLT cells (B-b) (siCtrl: n = 92, siOrai1: n = 80, N = 3), after 72h of Orai1 inhibition. Histograms are represented as the average ± SEM normalized to the control. (C) SOCs channels are opened in cell culture conditions due to the permanent ER-Ca<sup>2+</sup> depletion induced by FBS. Illustration of representatives SOCE measurement traces, after perfusion of 1 μM Thapsigargin and 10% FBS, in PS-1 no-treated cells, 72h post-proliferation (C-a). Cells were starved overnight, the day before the experiments. SOCE

quantification was normalized to the control condition (Thapsigargin) (C-b). FBS perfusion induced a lower SOCE than Thapsigargin perfusion (Thapsigargin:  $n = 87$ , FBS:  $n = 78$ ,  $N = 3$ ). All values were reported as mean  $\pm$  SEM. (\*\* $p < 0.001$ , Student's  $t$ -test,  $n$ : number of cells,  $N$ : number of passage).

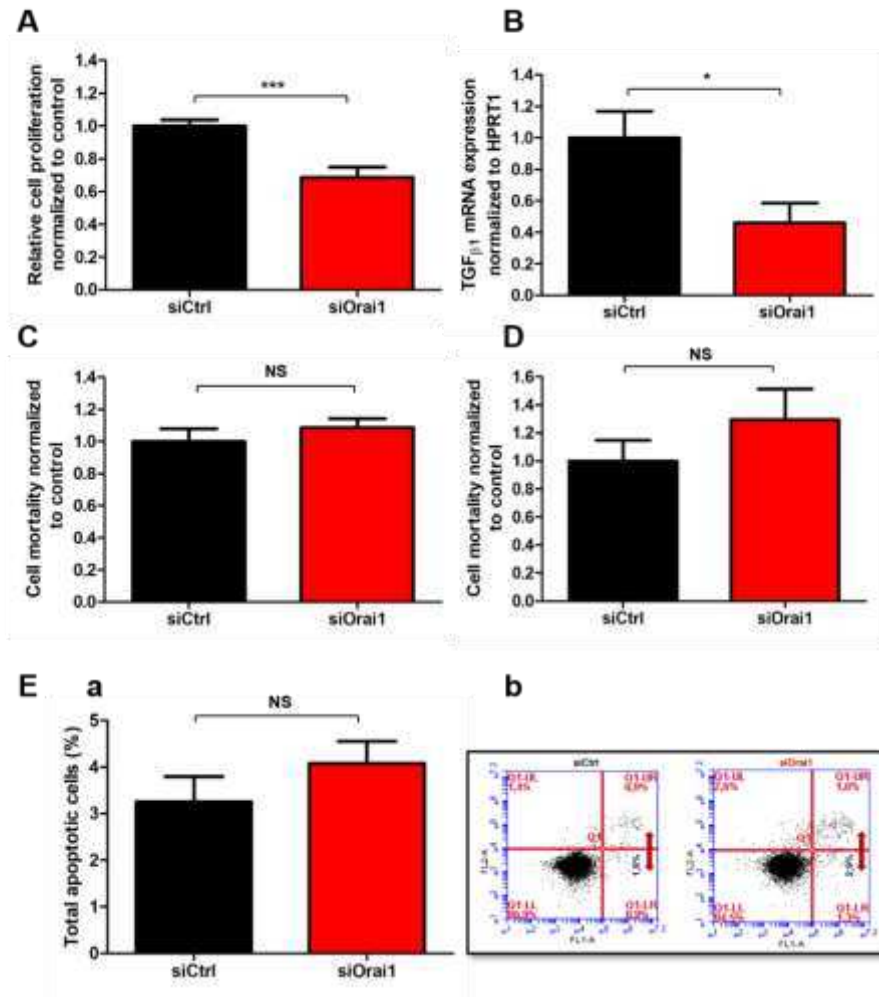


**Figure S2.** Orai1 is involved in the regulation of RLT-PSC's proliferation and TGF $\beta$ 1 expression without affecting the human activated PSC's survival. (A) Effect of Orai1 inhibition on RLT cell proliferation, 72 h post-transfection, evaluated by MTT assay. (B) Involvement of Orai1 in the modulation of TGF $\beta$ 1 mRNA expression in RLT cells, assessed by qPCR, after 72 h of siOrai1 transfection. (C,D) Impact of Orai1 inhibition on PS-1 and RLT cell mortality, evaluated by Trypan Blue assay, 72h post-transfection. (E) Measurement of total apoptosis rate using annexin V staining in PS-1 siOrai1 transfected cells (E-a), with a representative apoptosis profile after 72h of Orai1 silencing (E-b). Values were normalized to control and reported as mean  $\pm$  SEM, each experiment was performed at least in triplicate. (\*\* $p < 0.001$ , \*  $p < 0.05$ , NS,  $N = 3$ , Student  $t$ -test).

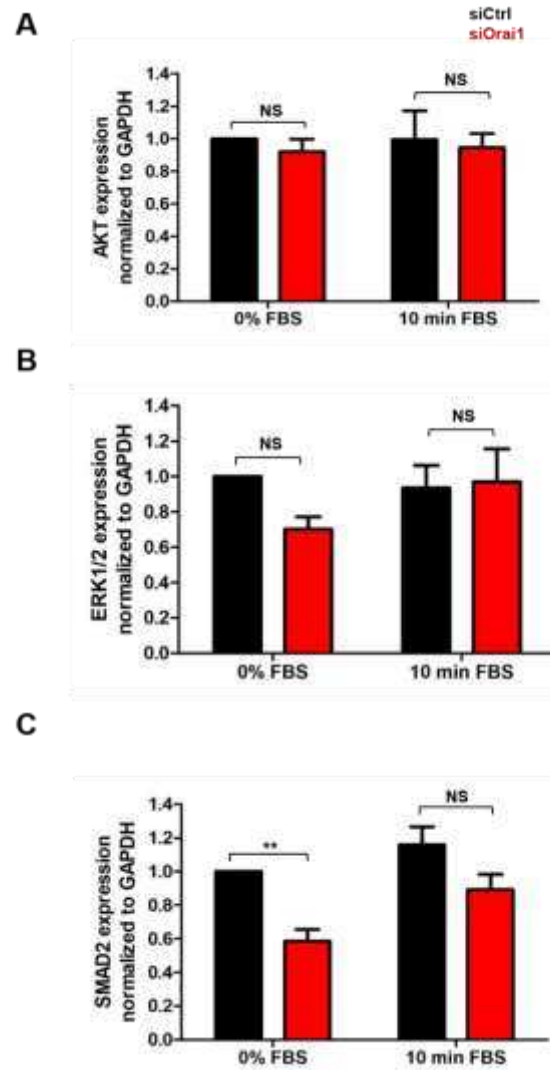


**Figure S3.** Orail knocking-down impacts SMAD2 total protein expression without affecting AKT and ERK1/2 in PS-1 human activated PSCs. Quantification of AKT (A), ERK1/2 (B), and SMAD2 (C) total protein expression in siOrai1 transfected cells. All values were first normalized to the referent protein GAPDH and then to the 0% FBS control condition. All experiments were performed 72 h post-transfection. Values were reported as mean  $\pm$  SEM (\*\*  $p < 0.01$ , NS, at least  $N = 3$  two-way ANOVA followed by Bonferroni *post hoc* test).

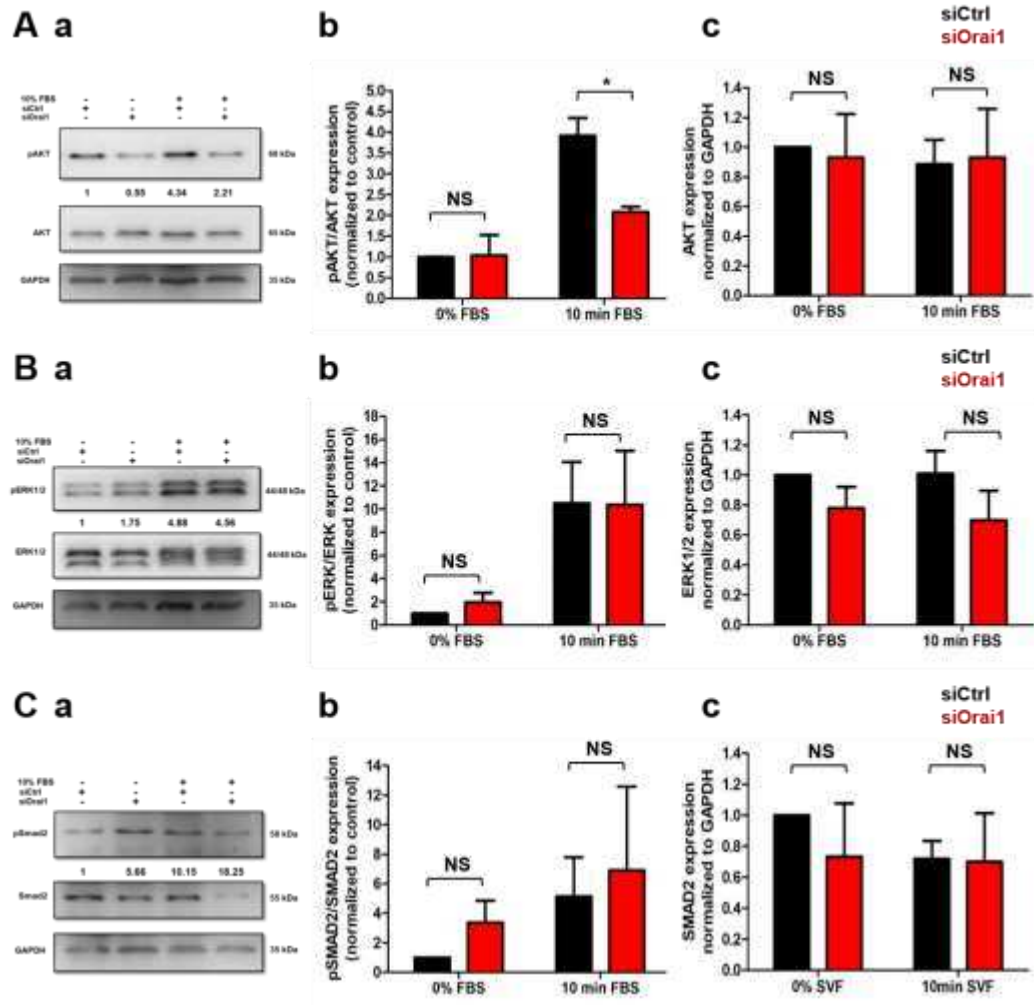


**Figure S4.** Orai1 modulates AKT activation but not ERK1/2 nor SMAD2 phosphorylation in RLT human activated PSCs, without affecting their total protein amount. **(A)** Implication of Orai1 in AKT phosphorylation in RLT cells. Representative Western blot showing the effect of Orai1 inhibition after FBS starvation of transfected cells overnight (**A-a**). Cells were then stimulated 10 min with FBS to evaluate the impact of Orai1 on AKT activation. AKT phosphorylation was quantified by the ratio of phosphorylated AKT form/total AKT protein (siCtrl+10 min FBS:  $3.92 \pm 0.43$ -fold, siOrai1+10 min FBS:  $2.09 \pm 0.13$  fold, **A-b**) and in parallel, the effect on the total protein expression was measured (**A-c**). **(B)** Assessment of ERK1/2 activation and total protein amount after Orai1 knocking down in RLT cells. Representative Western blot showing the effect of Orai1 silencing on ERK1/2 activation, using the protocol described above (**B-a**). ERK1/2 phosphorylation was quantified by the ratio of phosphorylated ERK1/2 form/total ERK1/2 protein (**B-b**), as well as the total protein expression (**B-c**). **(C)** Evaluation of Orai1 silencing on SMAD2 phosphorylation (**C-b**) and SMAD2 total protein expression (**C-c**). Representative Western blot showing the effect of siOrai1 transfected cells on SMAD2 activation (**C-a**), with the quantification using the ratio of phosphorylated SMAD2 form/total SMAD2 protein (**C-b**). All values were first normalized to the referent protein GAPDH and then to the 0% FBS control condition. All experiments were realized 72 h post-transfection. Values were reported as  $\pm$  SEM (\*  $p < 0.05$ , NS,  $N = 3$ , two-way ANOVA followed by Bonferroni *post hoc* test).



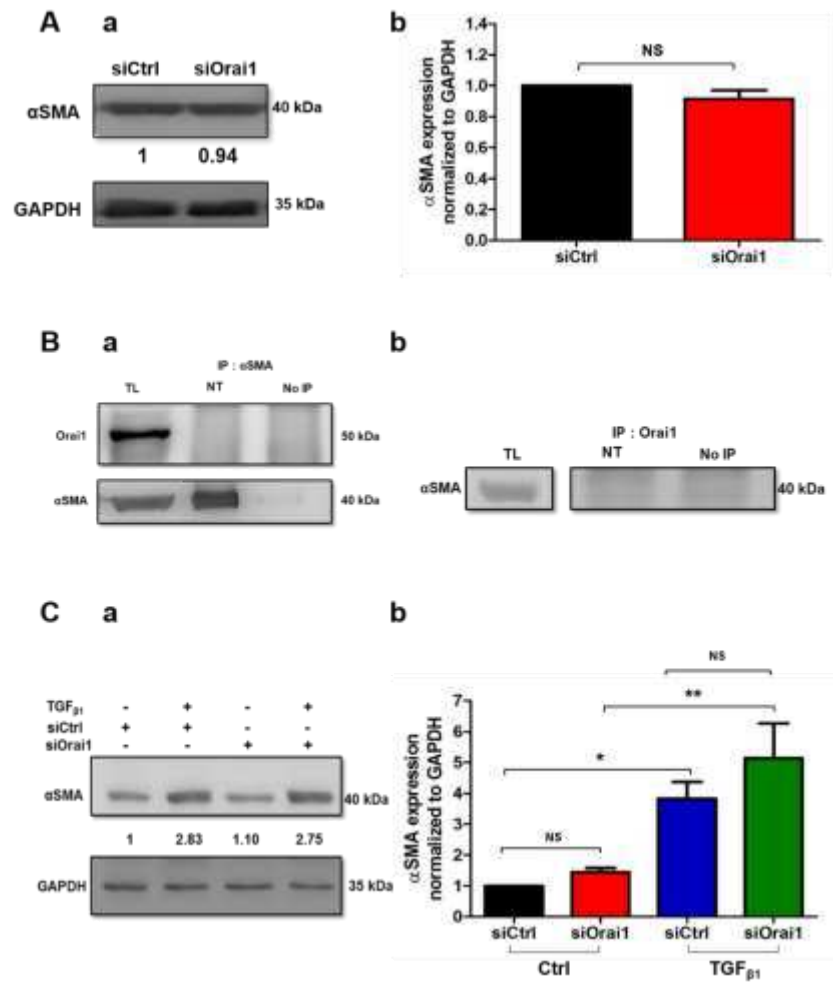


**Figure S5.** Orai1 channel neither regulates  $\alpha$ SMA expression nor colocalizes with  $\alpha$ SMA in human activated PSCs. (A) Orai1 silencing did not affect  $\alpha$ SMA protein expression. Representative Western blot showing the impact of 72h Orai1 inhibition on  $\alpha$ SMA expression (A-a) and the quantification (A-b) (NS, N = 3, Student *t*-test). The values were first normalized to the referent protein GAPDH and then to the control condition, reported as mean  $\pm$  SEM. (B) Representatives Western blot of Orai1 and  $\alpha$ SMA expression after immunoprecipitation experiments using anti- $\alpha$ SMA (B-a) and anti-Orai1 antibodies (B-b) (N = 3), showing the absence of physical interaction between the two proteins. (C) Effect of 72 h Orai1 knocked-down cells, treated 48h with TGF $\beta_1$  (20 ng/mL), in the presence of low-FBS conditions (1%), on  $\alpha$ SMA expression. Representative Western blot of  $\alpha$ SMA expression (a) and the quantification (b) (\*  $p < 0.05$ , \*\*  $p < 0.01$ , NS, N = 4, one-way ANOVA followed by Bonferroni multiple comparison test). The values were first normalized to the referent protein GAPDH and then to the control condition, reported as mean  $\pm$  SEM.

## Complementary Results:

### I. Role of Orai1 channel in activated PSC cell lines

#### 1) PS-1 cell line

##### 1.1) Physical interaction between Orai1 and STIM1 in lipid rafts

We have established above that SOCE in PS-1 cells is in part mediated by Orai1. Indeed, it is well known that in most of the non-excitabile cells, SOCE is driven by the translocation of STIM1 to the plasma membrane where it interacts with Orai1 in order to activate Orai1 channel and permit the  $\text{Ca}^{2+}$  entry (Prakriya and Lewis, 2015). To investigate whether Orai1 interacts physically with STIM1 in PS-1 cells as well, triggering SOCE, and whether this association takes place in the lipid rafts of the plasma membrane, we performed co-immunoprecipitation experiments treating the cells 24h with M $\beta$ CD, known to destabilize the plasma membrane cholesterol. In fact, it has been previously reported that lipid rafts domains are indispensable for the formation of heteromultimeric complexes between STIM1 proteins and Orai1 channels, modulating SOCE activation, in human platelets (Dionisio et al., 2011; Jardin et al., 2008). According to these findings, we used Orai1 immunoprecipitation antibody to assess the association between STIM1 and Orai1. We found that the two SOCE partners interacted physically, and that this association is partially located in the lipid rafts (M $\beta$ CD:  $27.30 \pm 5.25\%$  decrease of STIM1-Orai1 interaction, N=3, **Figure 24**). To validate this data, co-immunoprecipitation experiments using this time a STIM1 immunoprecipitation antibody are required, and also  $\text{Ca}^{2+}$  imaging experiments to investigate whether disruption of lipid rafts perturbs partially the SOCE in PS-1 cells.

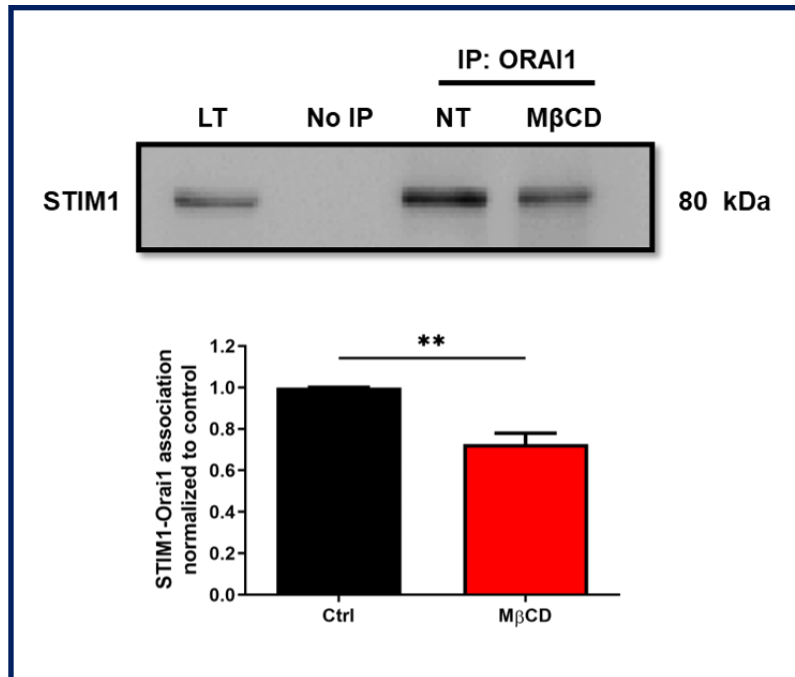


**Figure 24: Orai1 channel interacts with STIM1 protein, and this interaction partially occurs in the lipid rafts, in PS-1 cells.** 24h treatment of non-transfected PS-1 cells with 5 ng/ml of MβCD, used for destabilizing the plasma membrane cholesterol, partially interrupted Orai1-STIM1 interaction in the lipid rafts, as quantified using anti-Orai1 immunoprecipitation antibody and revealed subsequently by Western blot (\*\* $p < 0.01$ ,  $N = 3$ , Student's *t*-test). All values were normalized to the control condition and reported as mean  $\pm$ SEM.

### 1.2) Orai1 modulates IL-6 secretion

We have demonstrated in the current publication that Orai1 through the Orai1-mediated  $\text{Ca}^{2+}$  entry is involved in the modulation of TGF- $\beta$ 1 expression and secretion, in PS-1 cells. Additionally, to TGF- $\beta$ 1, we investigated the role of Orai1 in the regulation of IL-6, which is another crucial proinflammatory cytokine implicated in activated PSC-mediated desmoplasia (Apte et al., 1999; Shimada et al., 2002). Moreover, IL-6 has been found to be elevated in the serum of PDAC patients and mostly detected in advanced tumor stage, and also in CP patients, correlating with patient's poor prognosis (Holmer et al., 2014)(R et al., 2008). Therefore, despite being an important PDAC and CP marker, IL-6 could become a potential therapeutic target. Interestingly, we observed that 72h Orai1 knocking down diminished by 41.09% IL-6 secretion assessed by Elisa assay (siCtrl:  $100 \pm 12.16\%$ , siOrai1:  $58.91 \pm 8.51\%$ ,  $p < 0.05$ ,  $N = 4$ ,

**Figure 25 B**), but did not modify IL-6 mRNA expression (siCtrl:  $100 \pm 38.42\%$ , siOrai1:  $91.11 \pm 24.63\%$ ,  $p > 0.05$ ,  $N=4$ , **Figure 25 A**). According to the effect of 96h Orai1 inhibition on TGF- $\beta$ 1 secretion, it appears that Orai1 regulates with the same importance both, TGF- $\beta$ 1 and IL-6 secretion, implying that Orai1 inhibition might attenuate PSC-mediated TGF- $\beta$ 1 and IL-6 secretion in CP and PDAC patients. In contrast it seems that there is a time-lapse in Orai1-mediated TGF- $\beta$ 1 and IL-6 secretion, suggesting that Orai1 firstly drives IL-6 secretion and lately TGF- $\beta$ 1 secretion. In consistence with our data, Waldron *et al.* have demonstrated that inhibition of Orai proteins, using the Orai inhibitor CM4620 significantly decreased lipopolysaccharide-mediated IL-6 and TGF- $\beta$ 1 mRNA expression in mouse PSCs, supporting our hypothesis of using Orai1 inhibitors in order to decrease these cytokines' production in CP and PDAC patients (Waldron *et al.*, 2019).

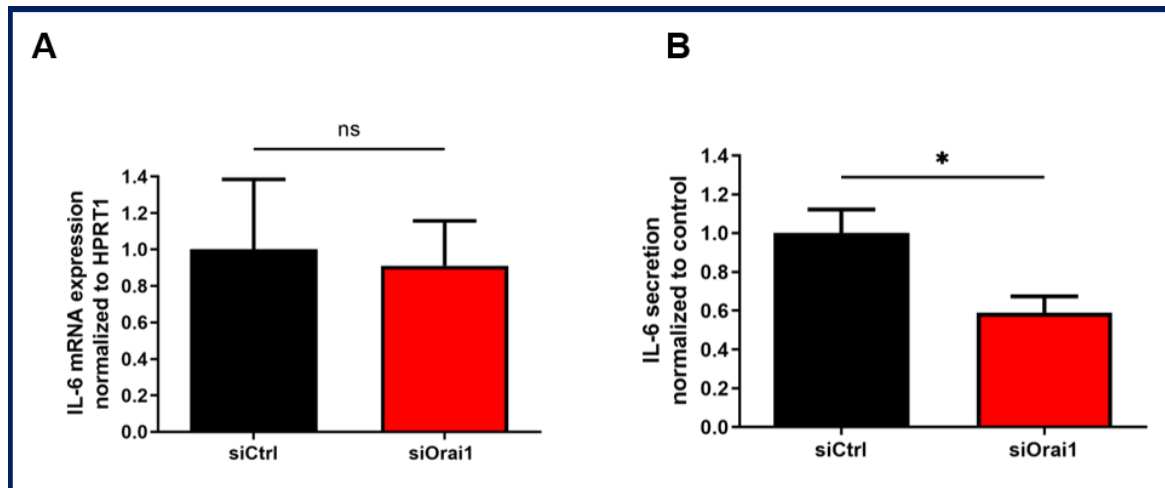


**Figure 25: Orai1 modulates IL-6 secretion but not mRNA expression in PS-1.** A) Effect of Orai1 silencing on PS-1's IL-6 mRNA expression, assessed 72h post-transfection by qPCR (NS: no significant,  $N=4$ , Student's *t*-test). B) Evaluation of Orai1 impact on IL-6 secretion by Elisa assay ( $*p < 0.05$ ,  $N=4$ , Student *t*-test), 72h post-transfection. Values were normalized to control and reported as mean  $\pm$  SEM. qPCR values were first normalized to the referent gene HPRT1.

### **1.3) External TGF- $\beta$ 1 stimulation activates AKT non-canonical signalling pathway, without affecting ERK1/2 non-canonical nor Smad canonical pathways in PS-1 cells**

As described in the introduction, TGF- $\beta$ 1 can drive its cellular responses through Smad-dependent and -independent pathways. We have demonstrated that in PS-1 cells, TGF- $\beta$ 1 promotes Orail-mediated proliferation through the AKT non-canonical pathway. To exclude the hypothesis that TGF- $\beta$ 1 might also modulate the other common Smad independent pathway, ERK1/2, but also the classical Smad dependent pathway, we treated PS-1 cells for 48h under low FBS conditions (1%) and then assessed the phosphorylation of AKT, ERK1/2 and SMAD2. As expected, TGF- $\beta$ 1 treatment induced a  $1.42 \pm 0.17$ -fold increase of AKT activation ( $p < 0.05$ ,  $N=4$ , **Figure 26 A-B**), but it did not lead to the phosphorylation of ERK1/2 (TGF- $\beta$ 1:  $0.81 \pm 0.13$ -fold,  $p > 0.05$ ,  $N=4$ , **Figure 26 A, C**) nor of SMAD2 (TGF- $\beta$ 1:  $0.97 \pm 0.3$ -fold,  $p > 0.05$ ,  $N=4$ , **Figure 26 A, D**), indicating that in PS-1 cells TGF- $\beta$ 1 long-term stimulation acts mainly through the AKT pathway. However, it has been shown that the phosphorylated AKT can form a complex with Smad3, the other Smad factor known to be phosphorylated by TGFRI triggering TGF- $\beta$ 1 cytostatic effect. The direct interaction between the phosphorylated AKT and Smad3, induces a diminution of Smad3 phosphorylation and hence nuclear accumulation, consequently decreasing TGF- $\beta$ 1/Smad3-mediated cytostatic effect and indirectly promoting cell proliferation (Conery et al., 2004; Remy et al., 2004). In our above publication we have demonstrated that TGF- $\beta$ 1 stimulates AKT phosphorylation, promoting PS-1 cell proliferation. But what if the observed effect is due to subsequent inhibition of Smad3 mediated TGF- $\beta$ 1 cytostatic effect by the activation of AKT pathway? To determine this, it would be interesting to evaluate whether AKT and the phosphorylated form of AKT interacts with Smad3 in PS-1 cells, performing co-immunoprecipitation experiments, and simultaneously evaluate whether AKT inhibition influences Smad3 phosphorylation.

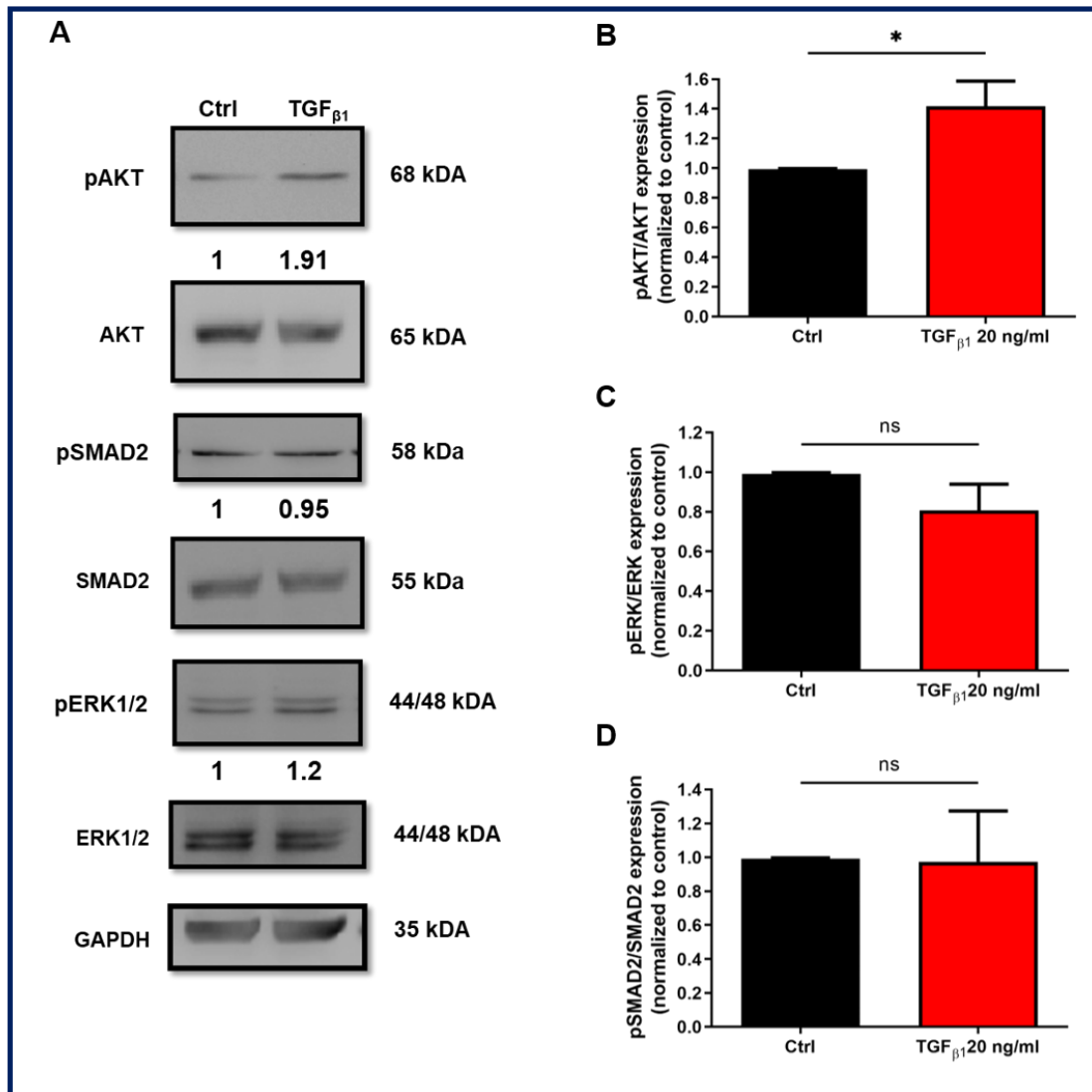


**Figure 26: Impact of 48h TGF- $\beta_1$  treatment (20 ng/ml) in the presence of low-FBS conditions (1%) on AKT, ERK1/2 and SMAD2 activation.** A) Representative Western blot showing the effect of TGF- $\beta_1$  treatment on AKT, SMAD2 and ERK1/2 phosphorylation. Each protein's phosphorylation was quantified using the ratio phosphorylated protein form/total protein. The quantification of AKT, ERK1/2, and SMAD2 activation are represented respectively in (B), (C) and (D) (\* $p < 0.05$ ,  $N = 4$ , Student  $t$ -test). All values were firstly normalized to the referent protein GAPDH, and then to the 1% FBS control condition. All experiments were realized 72h post-proliferation. Values were reported as mean  $\pm$  SEM.

#### **1.4) TGF- $\beta$ 1 treatment increases $\alpha$ SMA, IL-6, type I collagen and TGF- $\beta$ 1 mRNA in PS-1 cells**

We have also established in the current report that TGF- $\beta$ 1 through an autocrine positive feedback loop stimulates Orai1 mRNA expression. However, simultaneously, we investigated whether TGF- $\beta$ 1 impacts the mRNA expression of  $\alpha$ SMA and type I collagen in the human PS-1, known to be upregulated under TGF- $\beta$ 1 treatment in rodent PSCs (Apte et al., 1999). Indeed, TGF- $\beta$ 1 increased by  $24.1 \pm 8.21$ -fold  $\alpha$ SMA mRNA expression ( $p < 0.05$ ,  $N=3$ , **Figure 27 A**) and by  $50.63 \pm 40.23$ -fold the type I collagen mRNA expression ( $p < 0.05$ ,  $N=3$ , **Figure 27 B**). Moreover, it has been reported that external TGF- $\beta$ 1 promotes its own mRNA production, and that it is involved in an autocrine loop promoting IL-6 mRNA expression, in rodent PSCs (Aoki et al., 2006; Ohnishi et al., 2004). Hence, we assessed whether this was the case in human PSCs too, by quantifying IL-6 and TGF- $\beta$ 1 mRNAs in PS-1 48h treated with TGF- $\beta$ 1 cells. We found an  $8.34 \pm 1.6$ -fold increase of IL-6 mRNA expression ( $p=0.0012$ ,  $N=3$ , **Figure 27 C**) and  $12.42 \pm 1.86$ -fold augmentation of TGF- $\beta$ 1 mRNAs ( $p=0.0001$ ,  $N=3$ , **Figure 27 D**), suggesting that TGF- $\beta$ 1 stimulates its own synthesis in human PSCs, as in the rodent PSCs, as well as IL-6 production. However, to determine whether it exist an autocrine loop between TGF- $\beta$ 1 and IL-6, within which the production of each cytokine stimulates the synthesis and secretion of the other cytokine, experiments with IL-6 treatment are required in order to assess the impact on TGF- $\beta$ 1 mRNA expression and secretion. Moreover, the impact of TGF- $\beta$ 1 treatment on IL-6 secretion is needed to be quantified. The usage of TGF- $\beta$ 1 and IL-6 neutralizing antibodies could strengthen these data. To complete our results, it would be worth to evaluate the related signalling pathways starting from what its already demonstrated in rodent PSCs, namely the evaluation of SMAD2/3 and ERK1/2 pathway (Aoki et al., 2006). Even though these data won't provide novel evidence of PSC-mediated autocrine regulation, they will confirm that this mechanism can be extrapolated to human PSCs or maybe reveal the involvement of further signalling pathways.

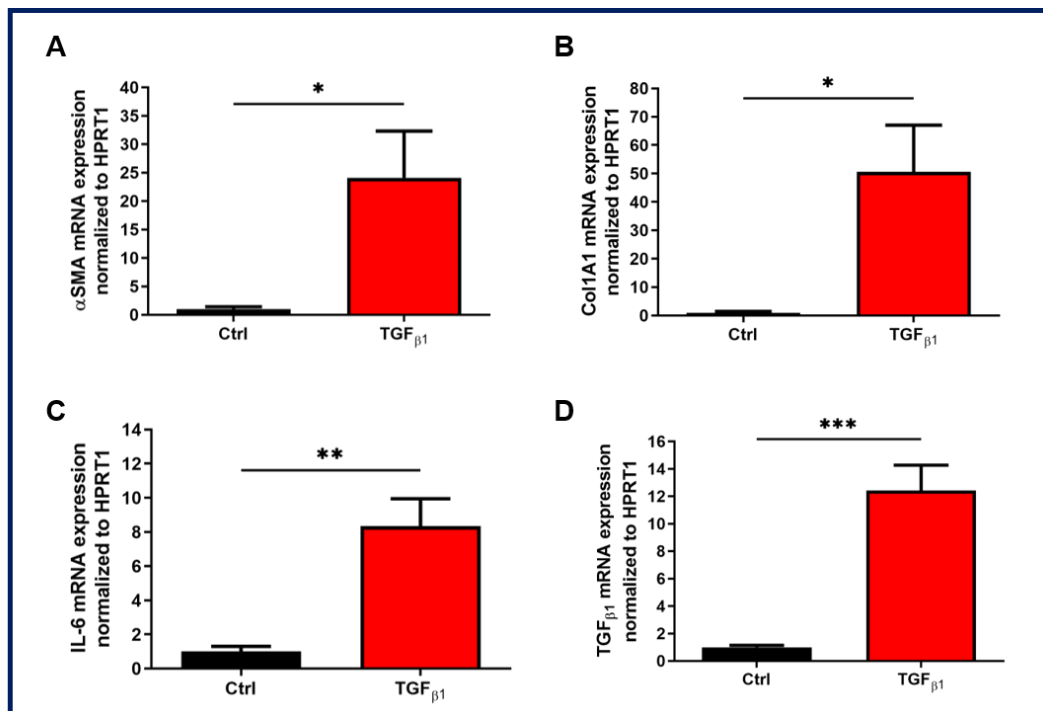


**Figure 27: External TGF- $\beta$ 1 stimulates  $\alpha$ SMA, type I collagen, IL-6 and TGF- $\beta$ 1 mRNA expression in PS-1 cells.** The effect of PS-1 48h treatment with 20 ng/ml TGF- $\beta$ 1 in low FBS conditions (1% FBS) on  $\alpha$ SMA (A), type I collagen (B), IL-6 (C), and TGF- $\beta$  (D) mRNA expression was quantified by qPCR, respectively, (\*p<0.05, \*\* p=0.0012, \*\*\* p=0.0001, N=3, Student *t*-test). All values were first normalized to the referent gene HPRT1, and then to the control condition, reported as mean  $\pm$  SEM.

### 1.5) Pharmacological inhibition of AKT by LY 294002 does not affect Orai1 and $\alpha$ SMA protein expression in PS-1 cells

The main finding of the above study was the involvement of Orai1 in the regulation of activated PSC's proliferation and TGF- $\beta$ 1 expression and secretion through the AKT pathway. Consequently, we wondered whether AKT pathway could induce a positive feedback loop by modulating Orai1 protein and mRNA expression in order to enhance PS-1's proliferation and TGF- $\beta$ 1 expression and secretion. Thus, we treated PS-1 cells for 72h with the AKT pharmacological inhibitor LY294002, and then investigate its effect on Orai1 protein and mRNA expression. We observed that either Orai1 protein (LY294002:  $0.65 \pm 0.15$ -fold, p>0.05, N=3, **Figure 28 A-B**) nor mRNA expression (Ctrl:  $100 \pm 12.10\%$ , LY294002:  $95.29 \pm 12.71\%$ , p>0.05, N=4, **Figure 28 D**) was modified following the LY294002 treatment, although there was a slight tendency of Orai1 protein decrease. In parallel, knowing from our data that Orai1



does not mediate  $\alpha$ SMA expression in PS-1 cells, and that Orai1 activates the AKT signalling, we wanted to confirm that this pathway was not involved in the regulation of  $\alpha$ SMA expression either. As expected, Western blotting and qPCR experiments did not reveal any significant effect in the protein (LY294002:  $1.18 \pm 0.08$ -fold,  $p > 0.05$ ,  $N=3$ , **Figure 28 A, C**) and mRNA (Ctrl:  $100 \pm 11.42\%$ , LY294002:  $75.19 \pm 12.41\%$ ,  $N=4$ ,  $p > 0.05$ , **Figure 28 E**)  $\alpha$ SMA expression PS-1 treated with LY294002 cells. Therefore, these data, indicates that TGF- $\beta$ 1-induced Orai1 mRNA and protein expression is mediated through an AKT-independent pathway, which remains to be elucidated.

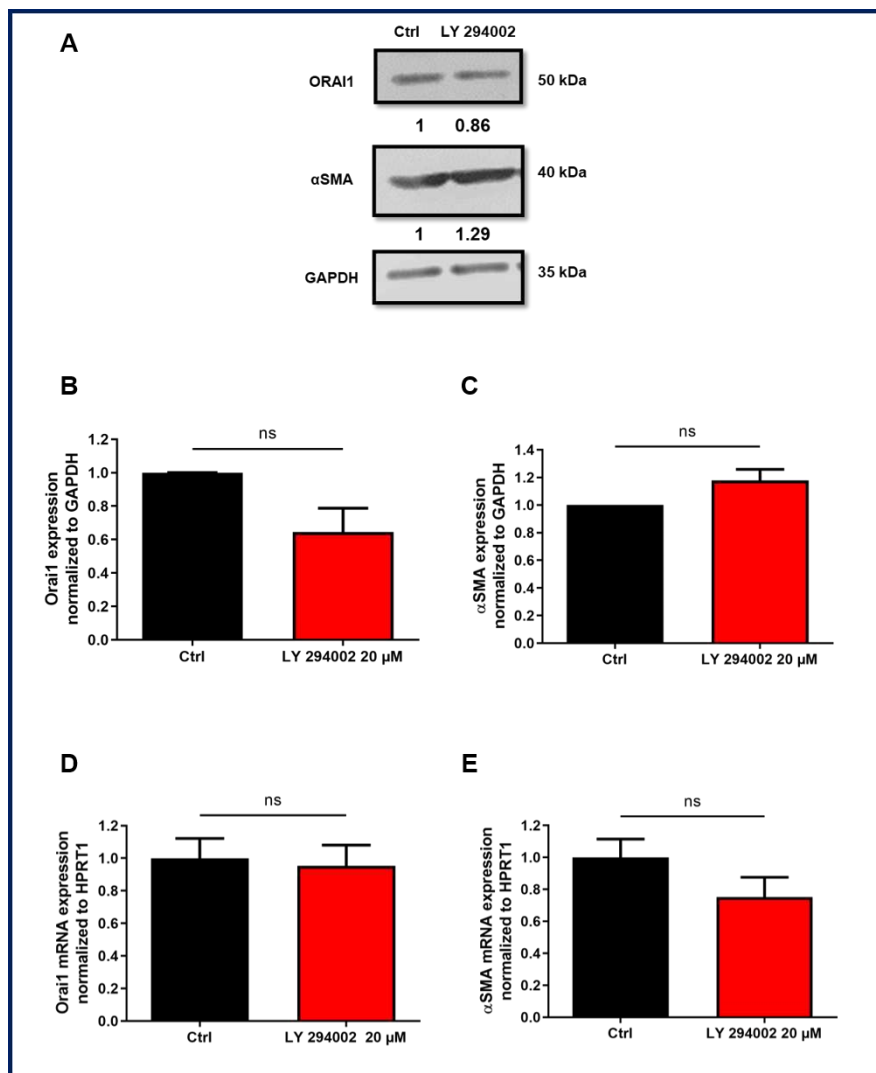


**Figure 28: AKT signalling pathway does not modulate PS-1 Orai1 and  $\alpha$ SMA mRNA and protein expression.** A-C) Inhibition of AKT activation, after 72h cell treatment with the PI3K/AKT pharmacological inhibitor LY 294002 (20  $\mu$ M), did not impact Orai1 (B)

and  $\alpha$ SMA expression (C), as evaluated by Western blot, respectively (NS: no significant, N=4, Student *t*-test). D-E) Decrease of AKT phosphorylation applying 72h treatment with LY 294002 did not influence Orai1 (D) and  $\alpha$ SMA (E) mRNA expression, quantified by qPCR, respectively (NS: no significant, N=4, Student *t*-test). All values were first normalized to the referent protein GAPDH or referent gene HPRT1, and then to the control condition, reported as mean  $\pm$  SEM.

## 2) RLT-PSC cell line

### 2.1) Orai1 drives IL-6 mRNA expression

Since, we have demonstrated that Orai1 modulates IL-6 secretion in PS-1 cell, we wanted to investigate whether this is the case in RLT-PSCs. We thus started by evaluating the mRNA expression of IL-6 in 72h siOrai1 transfected RLT-PSCs cells compared to the siCtrl ones. The almost complete Orai1 mRNA abolished expression (siCtrl:  $100 \pm 14.47\%$ , siOrai1:  $4.48 \pm 0.65\%$ , N=3,  $p < 0.0001$ , **Figure 29 A**) led to 70.83% decrease of IL-6 mRNA expression (siCtrl:  $100 \pm 22.56\%$ , siOrai1:  $29.17 \pm 5.07\%$ ,  $p = 0.0057$ , N=3, **Figure 29 B**), suggesting an important role of RLT-PSCs in the regulation of IL-6 mRNA expression.

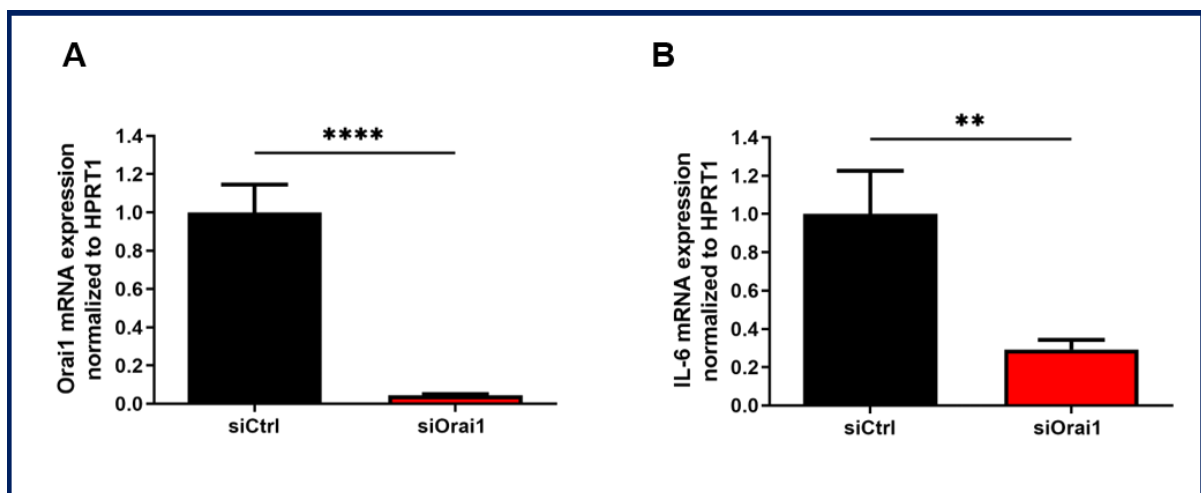


**Figure 29: Orai1 channel modulates IL-6 mRNA expression in RLT-PSCs.** A) Quantification of Orai1 invalidation efficiency by qPCR (\*\*\*\* $p < 0.0001$ , N=3, Student *t*-test). Evaluation of Orai1 silencing in IL-6 mRNA expression by qPCR (\*\* $p = 0.0057$ , N=3, Student *t*-test). All values were reported as mean  $\pm$  SEM normalized first to the HPRT1 referent gene and then to the control condition.

## 2.2) Orai1 negatively regulates $\alpha$ SMA expression

We have shown in PS-1 cells that Orai1 does not influence the expression of  $\alpha$ SMA, but what about its effect in RLT-PSCs cells? In contrast to PS-1, we detected a  $2.74 \pm 0.44$ -fold augmentation of  $\alpha$ SMA expression followed the 72h invalidation of Orai1 in RLT-PSCs ( $p < 0.05$ ,  $N=3$ , **Figure 30 A-B**). We, therefore, wondered whether Orai1 could mostly drive the acquisition of an inflammatory profile in RLT-PSCs by modulating the expression of IL-6 (shown above), and when it is down-regulated RLT-PSCs revert mostly to a myofibroblastic phenotype by increasing their expression of  $\alpha$ SMA. Actually, Öhlund *et al.* have reported that there are two principal subtypes of PSCs, one subtype having a myofibroblastic phenotype expressing abundantly  $\alpha$ SMA and other subtype presenting mostly an inflammatory profile with an abundant secretion of IL-6. Importantly, both subtypes are capable to revert from a myofibroblastic to inflammatory subtype and vice-versa, depending on the microenvironmental factors (Öhlund *et al.*, 2017). Consequently, to determine whether Orai1 drives mostly activated RLT-PSCs to the acquisition of an inflammatory phenotype, further experiments are needed to be performed, including measurement of IL-6 secretion in siOrai1 RLT-PSCs but also other inflammatory cytokines known to participate in the inflammatory phenotype acquisition such as IL-11, or chemokines as CXCL1 and CXCL2 (Öhlund *et al.*, 2017).

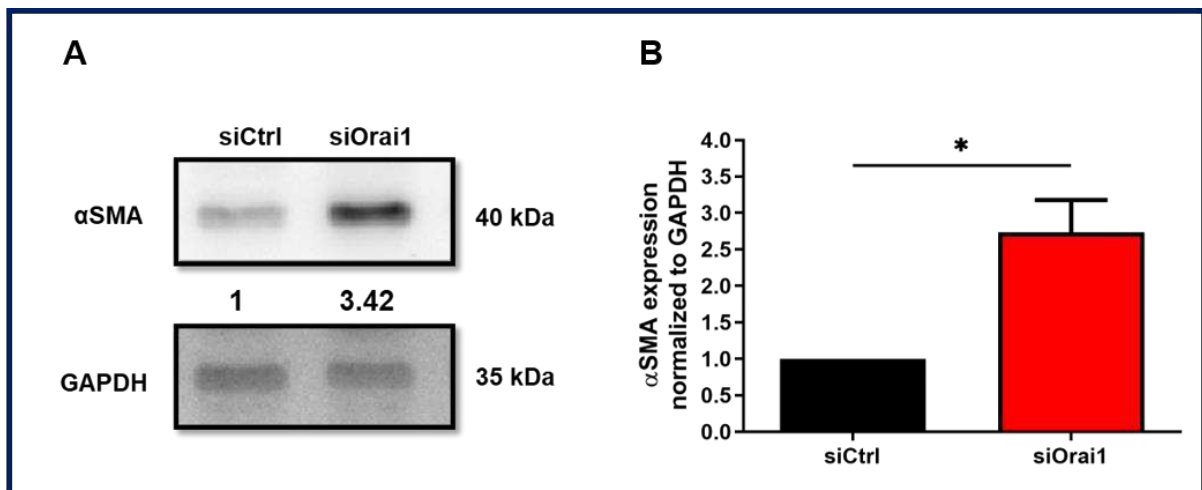


**Figure 30: Orai1 channel regulates negatively  $\alpha$ SMA expression in RLT-PSCs.** A) Representatives Western blot of 72h Orai1 knocked-down RLT-PSC cells effect on  $\alpha$ SMA expression with the quantification (B) (\* $p < 0.05$ ,  $N=3$ , Student *t*-test). All values were reported as mean  $\pm$  SEM normalized first to the GAPDH referent protein and then to the control condition.

## **II. Role of Orai2, Orai3, and STIM1 in human activated PSC's SOCE, proliferation, and survival**

We have highlighted in the above study the functional expression of Orai1 and Orai1-mediated SOCE, and its crucial role in the regulation of human activated PSC's proliferation without affecting cell survival. But what about the other SOC actors' involvement in this PSC activation process?

### **1) Expression profile of SOC in PS-1 and RLT-PSC cell lines**

Waldron *et al.* were the first to clearly demonstrated the mRNA expression of Orai1, Orai2, and STIM1 in mouse activated PSCs, but since then, nothing has been reported about SOCs expression in human activated PSCs (Waldron et al., 2019). Hence, we looked at the mRNA and protein expression profile of SOCs, focusing on Orai1, Orai2, Orai3 and STIM1 expression, in both of our cell line models PS-1 and RLT-PSCs, 72h post-proliferation. We showed the mRNA and protein expression of Orai1 and STIM1, the main regulators of SOCE, in both PS-1 and RLT-PSCs (**Figure 31 A-D**). Indeed, they seem to be the most expressed compared to Orai2 and Orai3 in PS-1 cells (**Figure 31 A-B**) and compared to Orai3 in RLT-PSCs (**Figure 31 D**). However, the mRNA and protein expression of STIM2 need to be elicited in both cell lines, as well as Orai2 expression in RLT-PSCs. We then proceeded to the evaluation of each actor's function independently, 72h following their silencing.

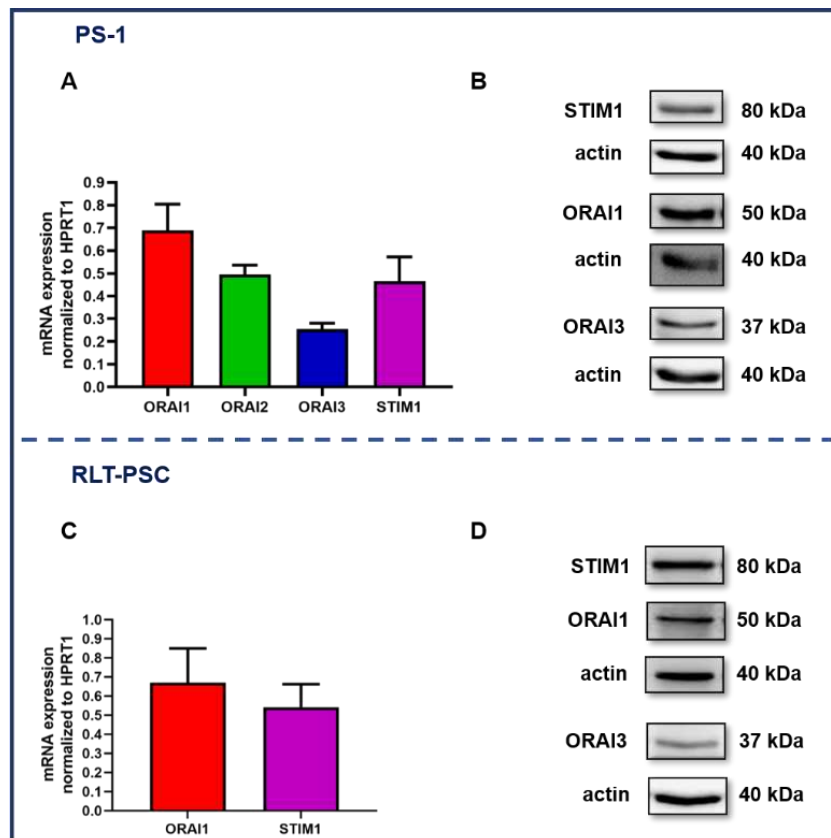


**Figure 31:** Evaluation of Orai isoforms and STIM1 expression profile in both PS-1 and RLT-PSCs by qPCR (A and C, respectively, N=3) and Western blot (B and D, respectively, N=3). mRNA values were normalized to the referent gene HPRT1 and Western blot values to the referent protein actin.

## 2) Role of STIM1 in PS-1 and RLT-PSC cell lines

### 2.1) Effect of STIM1 silencing in PS-1 and RLT-PSC SOCE

Using the siRNA approach, we inhibited STIM1 expression for 72h and performed after that  $\text{Ca}^{2+}$  imaging experiments using the Fura2/AM fluorescent probe. STIM1 was almost fully knocked down at the protein level in PS-1 (**Figure 32 A**, N=1) and RLT-PSC (siSTIM1:  $85.79 \pm 2.66\%$ , N=2, **Figure 32 E**) cells. Similarly, its expression was almost completely abolished at the mRNA level as well in both, PS-1 (siCtrl:  $100 \pm 11.56\%$ , siSTIM1:  $6.96 \pm 0.26\%$ , N=2, **Figure 32 B**) and RLT-PSC (siCtrl:  $100 \pm 15.79$ , siSTIM1:  $14.21 \pm 2.66\%$ , N=2, **Figure 32 F**) cells. We then measured the SOCE by using the classical protocol with Tg. STIM1 inhibition decreased SOCE by 63.53% in PS-1 cells (siCtrl:  $100 \pm 2.26\%$ , siSTIM1:  $36.47 \pm 2.70\%$ ,

p<0.0001, N=3, **Figure 32 C-D**) and by 50.39% in RLT-PSC cells (siCtrl: 100 ± 4.05%, siSTIM1: 49.61 ± 4.77%, p<0.0001, N=3, **Figure 32 G-H**). Interestingly, the siSTIM1-induced SOCE diminution in PS-1 was comparable to the siOrai1-induced SOCE decrease (67.81% diminution), suggesting that SOCE in these cells is mainly mediated by the Orai1-STIM1 association. Whereas in RLT-PSCs, the SOCE decrease resulted from STIM1 silencing was less important than the siOrai1-induced SOCE diminution (72.65% reduction), suggesting that in these cells, Orai1 probably mediates SOCE by its interaction also to STIM2. This latter has been demonstrated to form hetero-oligomers with its homologue STIM1 to trigger SOCE, but it can also promote SOCE independently to STIM1 (Brandman et al., 2007; Dziadek and Johnstone, 2007; Ong et al., 2015; Subedi et al., 2018). However, other studies have established that STIM2 acts as a negative regulator of SOCE by inhibiting STIM1 activity (Soboloff et al., 2006). Consequently, to evaluate whether STIM2 mediates SOCE in RLT-PSCs but also in PS-1 either by interacting with STIM1, either by having STIM1-independent effect or either by negatively modulating SOCE, a simultaneous invalidation of both STIM1 and STIM2 is required, as well as a STIM2 independent knocking down, to assess the impact on SOCE in both cell lines. Furthermore, co-immunoprecipitation experiments are needed to assess if STIM2 interacts physically with Orai1 and STIM1, and whether this interaction is interrupted when one of the proteins is silenced.

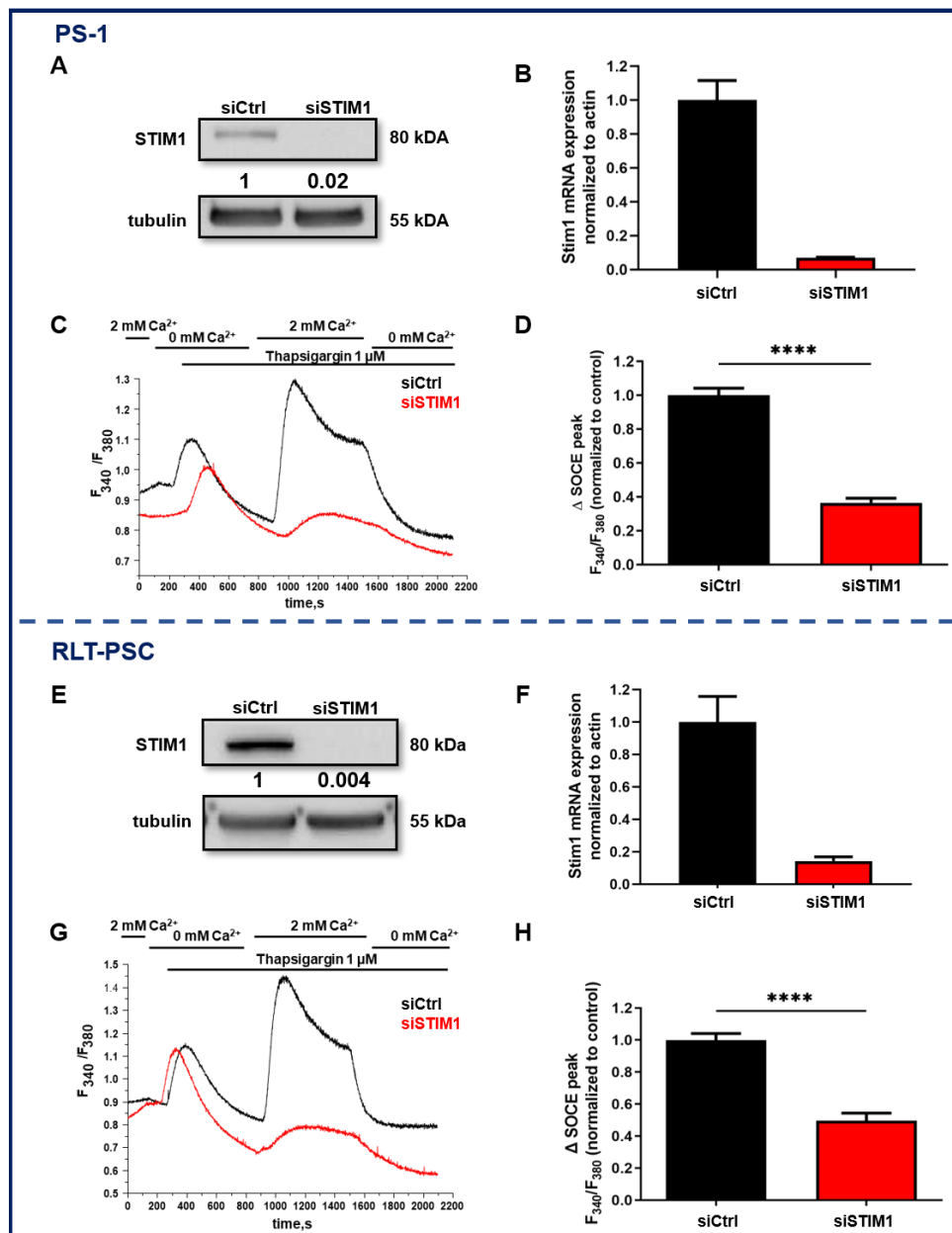


**Figure 32: STIM1 decreases SOCE in both PS-1 and RLT-PSCs.** A-D) Assessment of STIM1 role in SOCE, using STIM1 knocked down PS-1 cells, 72h post-transfection. STIM1 silencing efficiency was determined by Western blot (N=1) (A) and qPCR (B) (N=2) respectively. C) SOCE was measured after endoplasmic reticulum release induced by 1 μM of Thapsigargin, as described previously. Representative traces of SOCE measurements (C) and SOCE quantification (D) (siCtrl: n=107, siSTIM1: n=99, N=3, \*\*\*\*p<0.0001, Student *t*-test). E-H) Involvement of STIM1 protein in SOCE, in 72h siSTIM1 transfected RLT-PSC cells. STIM1 inhibition efficiency was determined by Western blot (E) and qPCR (F) (N=2). G-H) SOCE was measured as described previously. Representative traces of SOCE measurements

(G) and SOCE quantification (H) (siCtrl: n=32, siOrai3: n=46, N=1). All values were reported as mean  $\pm$  SEM normalized to the control (n: number of cells, N: number of passage). Western blot values were first normalized to the referent protein tubulin and then to the control condition.

## 2.2) Impact of STIM1 knocking-down in PS-1 and RLT-PSC' s proliferation, survival and $\alpha$ SMA expression

We next aimed to assess whether STIM1 could play a role in one of the principal PSCs activation processes we are interested in, the cell proliferation, regarding in parallel the PSC's survival. We evaluated both processes by Trypan Blue colorimetric assay, 72h after STIM1 knocking down, in PS-1 and RLT-PSC cells. Unfortunately, STIM1 invalidation did not reveal any significant effect either in PS-1 (siCtrl:  $100 \pm 11.86\%$ , siSTIM1:  $81.43 \pm 8.29\%$ ,  $p > 0.05$ , N=3, **Figure 33 A**) nor RLT-PSC's (siCtrl:  $100 \pm 6.78\%$ , siSTIM1:  $93.37 \pm 4.88\%$ ,  $p > 0.05$ , N=3, **Figure 33 F**) proliferation. We, moreover, used the flow cytometry approach to analyse the cell cycle progression in case there was an effect that we could miss with the Trypan Blue assay in PS-1 cells. Consisting with the Trypan Blue results, we did not observe a significant difference in the cell cycle phases when cells were transfected with siSTIM1 (G0/G1 phase: siCtrl:  $77.83 \pm 1.16\%$ , siSTIM1:  $75.27 \pm 1.44\%$ , S phase: siCtrl:  $6.95 \pm 0.65\%$ , siSTIM1:  $8.61 \pm 1.08\%$ , G2/M phase: siCtrl:  $15.21 \pm 0.72\%$ , siSTIM1:  $16.11 \pm 0.61\%$ ,  $p > 0.05$ , N=3, **Figure 33 B-C**). In accordance with these data, the simultaneous investigation of cell mortality did not show any effect, either in PS-1 (siCtrl:  $100 \pm 7.87\%$ , siSTIM1:  $78.98 \pm 9.77\%$ ,  $p > 0.05$ , N=3, **Figure 33 D**) either in RLT-PSC cells (siCtrl:  $100 \pm 10.13\%$ , siSTIM1:  $96.51 \pm 9.11\%$ ,  $p > 0.05$ , N=3, **Figure 33 G**). Nevertheless, these findings are in contradiction with our data showing that Orai1-mediated  $Ca^{2+}$  entry drives both PS-1 and RLT-PSCs' proliferation. Indeed, we were expecting to observe an effect on activated PSC's proliferation when STIM1 is invalidated, indicating that Orai1/STIM1-mediated SOCE is responsible for the regulation of this process in both PSC cell lines. Therefore, the absence of STIM1 effect on PSC's proliferation following its invalidation might be compensated by STIM2 expression, since it has been demonstrated that the ratio of STIM1/STIM2 expression could play a role in STIM1 activity. Precisely, a low STIM1/STIM2 expression ratio, with an increased STIM2 expression has been reported to partially compensate STIM1 function and generates a small SOCE (Liou et al., 2005; Stanisiz et al., 2014). Consequently, it would be interesting to evaluate the STIM1/STIM2 ratio in both PS-1 and RLT-PSCs, as well as the impact of STIM2 in both PSC cell lines' proliferation, in order to clarify whether the prevented STIM1 effect following its inhibition on PSC's is due to



a compensatory effect of STIM2. Moreover, a double STIM1/STIM2 silencing will permit to reveal whether there is an additive effect on PSC's proliferation when inhibiting both STIM isoforms compared to their independent knocking down, and thus confirm or not this hypothesis.

Furthermore, consistent with our findings on Orai1, we wondered whether STIM1 could be implicated in the modulation of  $\alpha$ SMA expression, the main activation marker of PSCs. As for Orai1 silencing, we did not observe any effect on the protein expression of  $\alpha$ SMA after 72h inhibition of STIM1, in PS-1 cells (**Figure 33 E**, N=1), either in RLT-PSCs (siSTIM1:  $0.94 \pm 0.32$ -fold, N=2, **Figure 33 H**), although more experiments are needed to be performed to confirm this result.

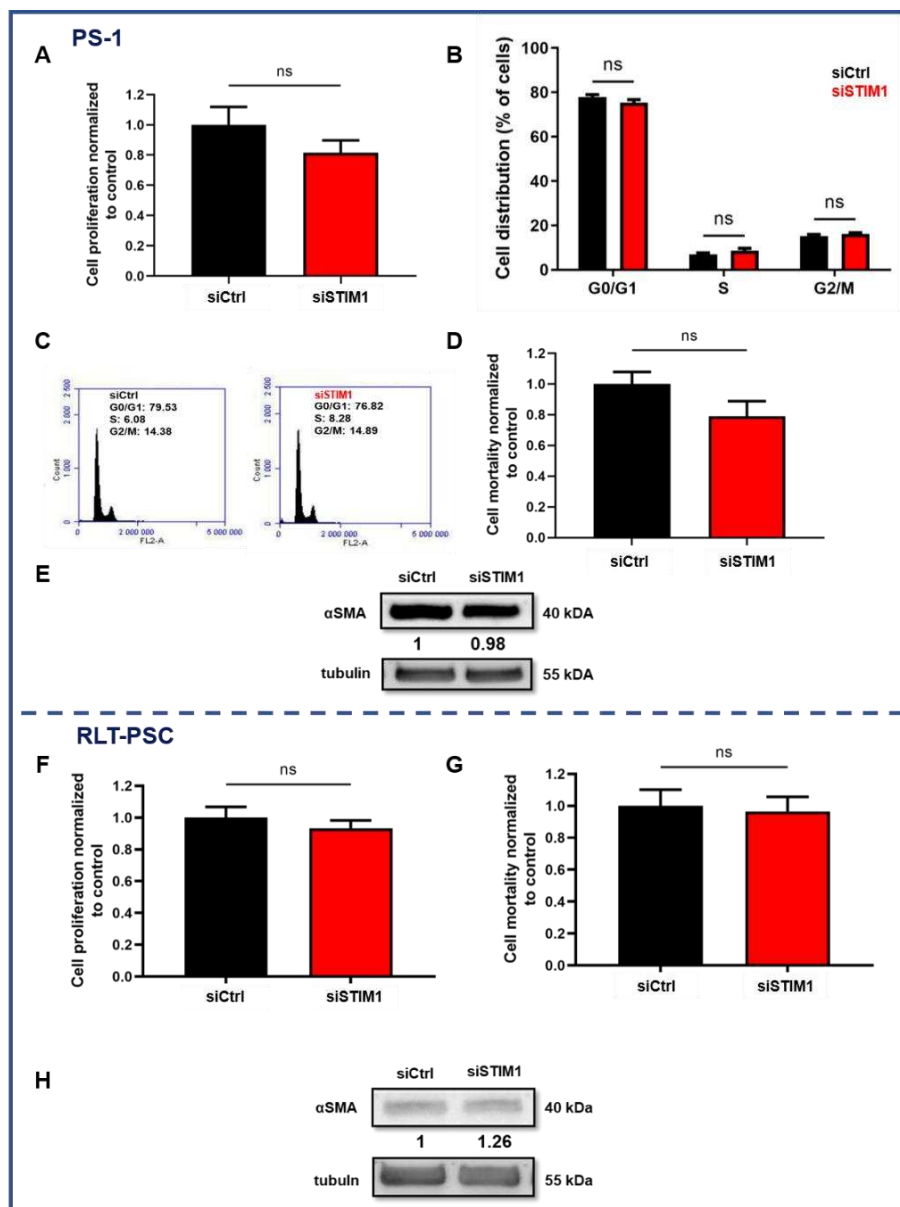


**Figure 33: STIM1 does not mediate human activated PSC's proliferation nor survival.** A) Effect of STIM1 silencing on PS-1 cell proliferation, assessed 72h post-transfection by Trypan blue assay (NS: no significant, N=3, Student's *t*-test). B) Assessment of STIM1 knocking down in PS-1 cell cycle progression. Cell distribution (G0/G1, S and G2/M phase) was examined by flow cytometry 72h after transfection, with propidium iodide staining (NS: no significant, N=3, two-way ANOVA followed by Bonferroni *post hoc* test). C) Illustrative representation of cell cycle profile 72h after Orai1 inhibition. D) Impact of STIM1 knocking down on PS-1 survival measured by Trypan blue assay (NS: no significant, N=3, Student's *t*-test). E) Quantification of STIM1 involvement in  $\alpha$ SMA expression by Western blot (N=1). F-G) Evaluation of STIM1 role in RLT-PSCs' proliferation (F) and survival (G) by Trypan blue assay (NS: no significant, N=3, Student's *t*-test). H) Impact of STIM1 silencing on  $\alpha$ SMA expression quantified by Western blot (N=2). Values were normalized to control and reported mean as  $\pm$  SEM. Western blotting values were first normalized to the referent protein tubulin and then to the control condition.

### 3) Role of Orai3 in PS-1 and RLT-PSC cell lines

#### 3.1) Effect of Orai3 invalidation in PS-1 and RLT-PSC SOCE

We performed the same type of experiments to assess whether Orai3, the second most studied isoform of Orai channels, is involved in SOCE in PS-1 and RLT-PSC cells since it has been reported to often participate in this process in different cell types, including cancer cells and in particular breast cancer cells (Ay et al., 2013; Bhattacharya et al., 2018; Faouzi et al., 2016; Motiani et al., 2010). Thus, we invalidated Orai3 for 72h, evaluated the efficiency of this silencing, and measured the SOCE, as described above in both cell lines. At the mRNA level, Orai3 was inhibited by 52.84% in PS-1 cells (siCtrl:  $100 \pm 23.43\%$ , siOrai3:  $47.16 \pm 6.94\%$ , N=3,  $p < 0.05$ , **Figure 34 B**) and by 63.36% in RLT-PSC cells (N=1, **Figure 34 H**). At the protein level, the knockdown efficiency was more important in PS-1 cells, inducing a 76% decrease of Orai3 (N=1, **Figure 34 A**) compared to RLT-PSCs where only 30% of Orai3 protein were inhibited (N=1, **Figure 34 G**). Nevertheless, more experiments are required to validate Orai3 inhibition efficiency in RLT-PSCs. We then quantified the SOCE response, and we found that Orai3 acts similarly in both cell lines, as its silencing induced approximately 17% increase of SOCE in PS-1 (siCtrl:  $100 \pm 3.11\%$ , siOrai3:  $118.70 \pm 4.66\%$ , N=3,  $p < 0.001$ , **Figure 34 E-F**) and RLT-PSCs (siCtrl:  $100 \pm 4.33\%$ , siOrai3:  $116.80 \pm 3.22\%$ , N=1, **Figure 34 I-J**). To

eliminate the hypothesis that the observed effect may be due to an upregulation of the other two Orai isoforms, we checked the mRNA levels of Orai1 and Orai2 in PS-1, without observing any alteration (Orai1: siCtrl:  $100 \pm 11.58\%$ , siOrai3:  $76.90 \pm 9.72\%$ ,  $p > 0.05$ ,  $N=3$ , **Figure 34 C**) (Orai2: siCtrl:  $100 \pm 19.08\%$ , siOrai3:  $114.80 \pm 19.36\%$ ,  $p > 0.05$ ,  $N=3$ , **Figure 34 D**). Together, these results brought the first evidence that Orai3 might act as a SOCE negative regulator in activated PSCs. Indeed, very recent published studies have demonstrated a similar effect of Orai3 in PDAC and lung cancer cell lines (Daya et al., 2021; Dubois et al., 2021).

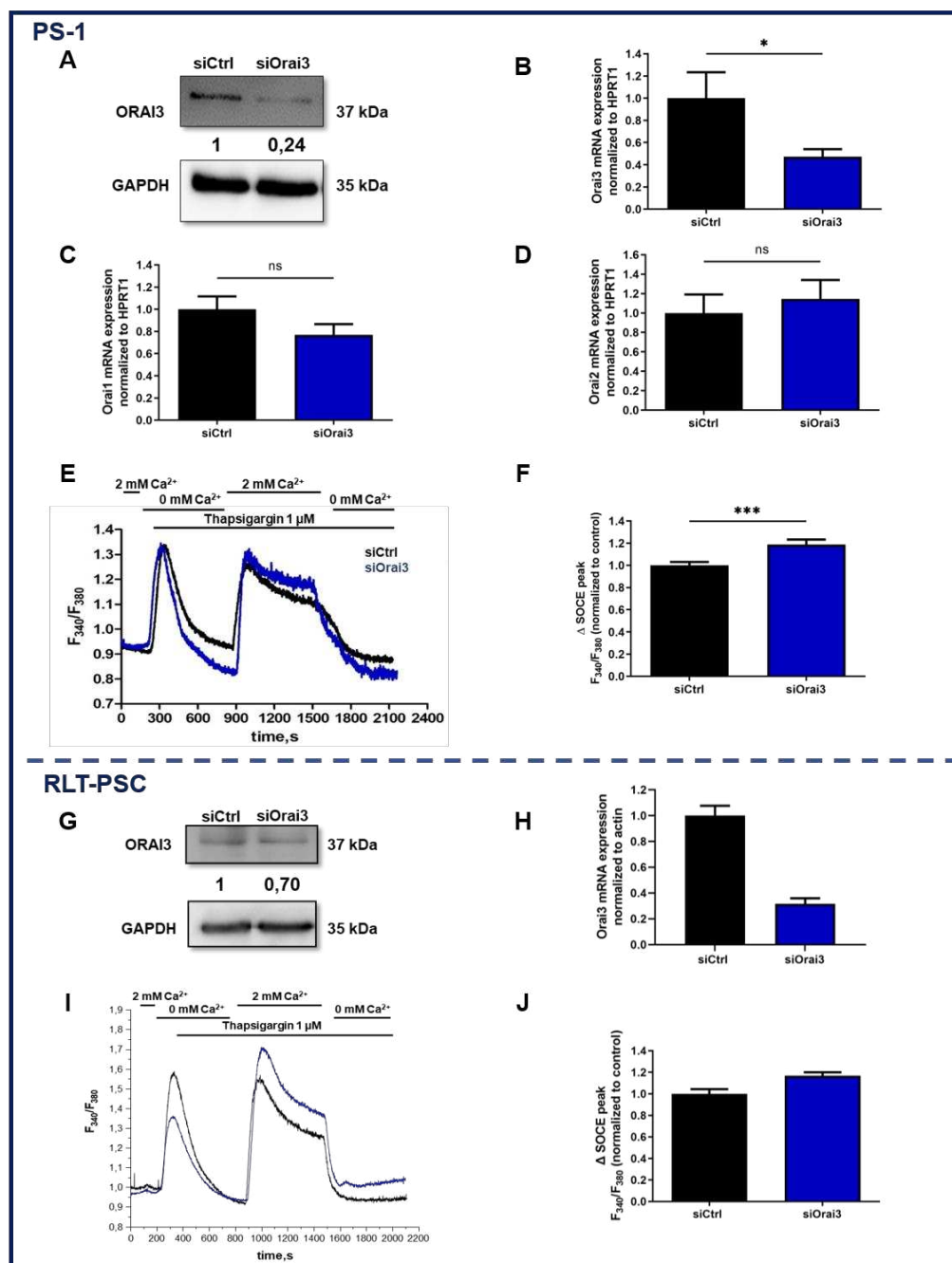


**Figure 34: Orai3 channels are not involved in SOCE in human activated PSCs.** **A-F)** Assessment of Orai3 channel in SOCE, in Orai3 knocked down PS-1 cells, 72h post-transfection. Orai3 silencing efficiency was determined by Western blot (N=1) (A) and qPCR (B) respectively. Simultaneously Orai1 (C) and Orai2 (D) mRNA expression was evaluated in siOrai3 PS-1 cells (\* $p < 0.05$ , NS: no significant, N=3, Student *t*-test). SOCE was measured after endoplasmic reticulum release induced by 1  $\mu$ M of Thapsigargin, as described previously. Representative traces of SOCE measurements (E) and SOCE quantification (F) (siCtrl: n=99, siOrai3: n=93, N=3, \*\*\* $p < 0.001$ , Student *t*-test). **G-J)** Involvement of Orai3 channel in SOCE, in 72h siOrai3 transfected RLT-PSC cells. Orai3 inhibition efficiency was determined by Western blot (G) and qPCR (H) (N=1). SOCE was measured as described previously. Representative traces of SOCE measurements (I) and SOCE quantification (J) (siCtrl: n=32, siOrai3: n=46, N=1). All values were reported as mean  $\pm$  SEM normalized to the control (n: number of cells, N: number of passage).

### 3.2) Role of Orai3 in PS-1 and RLT-PSC's proliferation and survival

As for STIM1, we next investigated the impact of Orai3 knocking down in the modulation of cell proliferation and survival. By Trypan Blue colorimetric assay, we quantified the proliferation and the mortality rate of PS-1 siOrai3 transfected cells and compared them to the PS-1 siCtrl transfected cells. We noticed that Orai3 silencing induced 39.33% decrease of PS-1 proliferation (siCtrl:  $100 \pm 5.47\%$ , siOrai3:  $60.67 \pm 3.83\%$ ,  $p < 0.0001$ , N=3, **Figure 35 A**), without any significant modification in the cell survival (siCtrl:  $100 \pm 11.92\%$ , siOrai3:  $87.75 \pm 17.10\%$ ,  $p > 0.05$ , **Figure 35 B**). In accordance with these data, a recent study from our lab reported that Orai3 knocking down impairs PCC's proliferation blocking the cell cycle progression in G2/M phase, but it also induces an increase of PCC's death (Dubois et al., 2021). Furthermore, we observed that Orai3 silencing changed PS-1 cell shape, giving them an elongated morphology (**Figure 35 C**), mostly noted during the migration process, contrary to the observed flattening morphology of siOrai3 transfected PCCs (Dubois et al., 2021), supporting that Orai3 is involved in PS-1 cell survival. Moreover, the percentage of siOrai3-decreased PS-1 proliferation was comparable to the one found after Orai1 inhibition, suggesting that the two Orai isoforms might have a competitive effect on PS-1. However, Orai3 does not seem to have the same impact on RLT-PSC's proliferation, extrapolated by the measured cell metabolic activity using MTT colorimetric assay. It appears that Orai3 inhibition either slightly increases either does not regulate RLT-PSC's proliferation (N=1, **Figure 35 D**), needing further

experiments to clarify its effect. Moreover, visually, in contrast to PS-1 cells, we did not note any modification in the morphology of siOrai3 transfected RLT-PSCs.

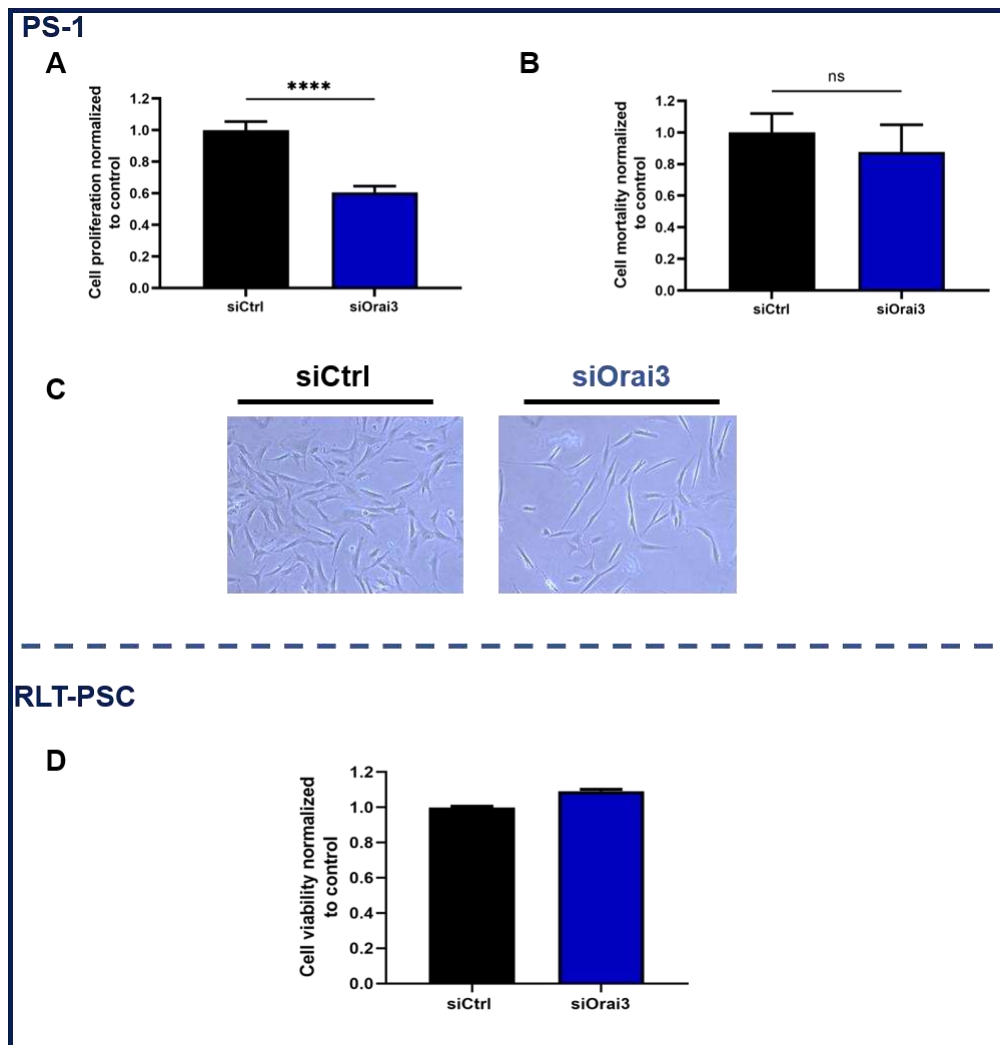


**Figure 35: A-C) Orai3 modulates PS-1 cells' proliferation and morphology but not survival.** A) Impact of Orai3 inhibition on PS-1 cell proliferation, assessed 72h post-transfection by Trypan Blue assay (\*\*\*\* $p < 0.0001$ ,  $N=3$ , Student  $t$ -test). B) Effect of Orai3 silencing in PS-1 mortality, evaluated by Trypan Blue assay, 72h post-transfection. C) Influence of Orai3 knocking down in PS-1 cell morphology. D) Orai3 does not seem to effect RLT-PSCs' proliferation, assessed by MTT colorimetric assay ( $N=1$ ). Values were normalized to control and reported as mean  $\pm$  SEM, each experiment was performed at least in triplicate. (\*\*\*\* $p < 0.0001$ , NS: no significant,  $N=3$ , Student  $t$ -test).

#### 4) Effect of Orai2 silencing in PS-1 SOCE

Lastly, we assessed the impact of the less common Orai isoform, Orai2 in PS-1 SOCE. Following the validation of siOrai2 mRNA transfection efficiency, we proceeded to quantify the SOCE response. qPCR experiments showed a 69.22% diminution of Orai2 mRNA, 72h post-transfection in PS-1 (siCtrl:  $100 \pm 8.66\%$ , siOrai2:  $30.78 \pm 20.28$ ,  $p < 0.05$ , N=3, **Figure 36 A**). Surprisingly, SOCE measurement in siOrai2 transfected cells revealed a more than 2-fold increase of  $\text{Ca}^{2+}$  entry than the control cells (siCtrl:  $100 \pm 2.32\%$ , siOrai2:  $233.80 \pm 6.95\%$ ,  $p < 0.0001$ , N=3, **Figure 36 C-D**). This might be due to the observed important Tg-induced ER  $\text{Ca}^{2+}$  release in siOrai2 transfected PS-1 cells (siCtrl:  $100 \pm 4.83\%$ , siOrai2:  $255.34 \pm 8.52\%$ ,  $p < 0.0001$ , N=3, **Figure 36 E**). We thought that the important observed effect might be due to an upregulation of Orai1 expression since it is the only Orai isoform among the three that mediates SOCE in PS-1. We so checked the Orai1 mRNA levels in siOrai2 cells compared to the siCtrl cells, but we did not reveal any significant effect, although there was a slight tendency to Orai1 mRNA increase (siCtrl:  $100 \pm 13.05\%$ , siOrai2:  $121.40 \pm 24.27\%$ , N=3, **Figure 36 B**). However, it is also worth to verify whether there is any modification in Orai3 mRNAs.

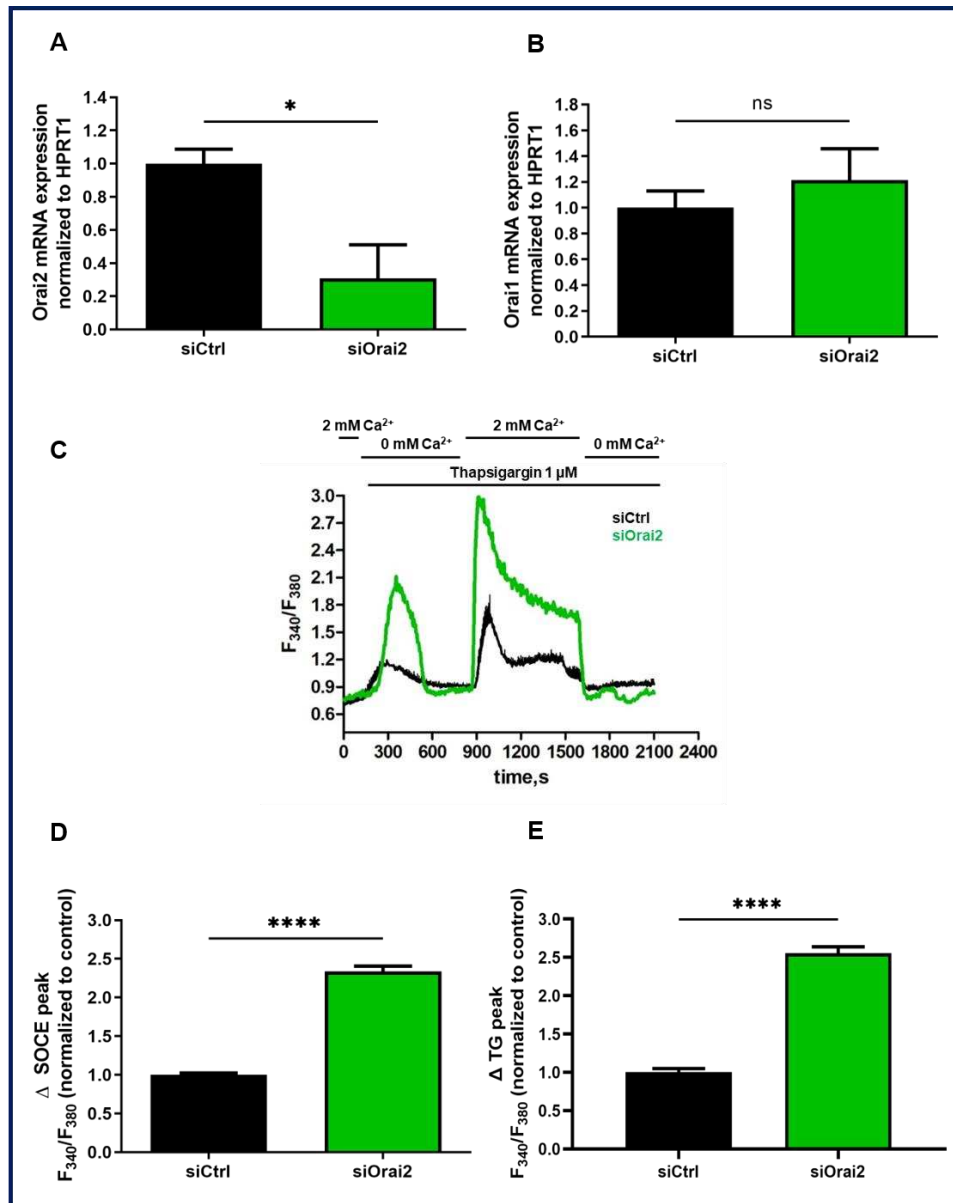


**Figure 36: Orai2 channels are not involved in SOCE in human activated PS-1.** A) Orai2 silencing efficiency was determined by qPCR (\* $p < 0.05$ ,  $N = 3$ , Student  $t$ -test). B) In parallel the impact on Orai1 mRNA expression was assessed (NS: no significant,  $N = 3$ , Student  $t$ -test) C) SOCE was measured after endoplasmic reticulum release induced by 1  $\mu$ M of Thapsigargin (Tg), as described previously. Representative traces of SOCE measurements (C), SOCE quantification (D) (siCtrl:  $n = 169$ , siOrai2:  $n = 145$ ,  $N = 3$ , \*\*\*\* $p < 0.001$ , Student  $t$ -test) and Tg response quantification (E) (siCtrl:  $n = 106$ , siOrai2:  $n = 121$ ,  $N = 3$ , \*\*\*\* $p < 0.001$ , Student  $t$ -test). All values were reported as mean  $\pm$  SEM normalized to the control ( $n$ : number of cells,  $N$ : number of passage).

## **Part N°2:**

### **TRPC1 channels regulate the activation of pancreatic stellate cells through ERK1/2 and SMAD2 pathways and perpetuate their pressure-mediated activation**

#### **Summary:**

Overlooked for too long, activated PSCs are well notorious now for their orchestrator role in pancreatic fibrogenesis, constituting a central pathological feature of two major pancreatic diseases, chronic pancreatitis and pancreatic cancer. Indeed, in the normal pancreas, PSCs are in a quiescent state, but under pancreatic injury, inflammation, or external environmental stimuli, such as elevated pressure and cytokine stimulation, they become activated. This activation is accompanied, among others, by the acquisition of an enhanced proliferative and migratory potential, as well as induced abundant cytokine and growth factors secretion, like IL-6 and TGF- $\beta$ 1 (Ferdek and Jakubowska, 2017; Masamune and Shimosegawa, 2009). Once activated, PSCs are phenotypically characterized by an increased level of  $\alpha$ SMA expression.

Furthermore, we have previously demonstrated that ion channels, particularly the mechanosensitive  $\text{Ca}^{2+}$  channel TRPC1, can participate in the modulation of pressure-induced PSC activation by regulating their migratory abilities. Indeed, TRPC1 senses the mechanical forces induced by the elevated environmental pressure present during chronic pancreatitis and pancreatic cancer, which activates its channel function, permitting the  $\text{Ca}^{2+}$  influx into PSCs to modulate their migration (Fels et al., 2016). Based on these promising findings, we aimed in this study to better understand the role of TRPC1 in PSC's activation processes and the underlying mechanisms, using mouse primary TRPC1-KO PSCs and a human cell line of activated PSCs where we transiently inhibited TRPC1.

We have firstly demonstrated that TRPC1 expression is required for the pressure-mediated PSC's activation, as reflected by the expression degree of the main PSC's activation marker,  $\alpha$ SMA. We noted that TRPC1-KO PSCs present significantly lower  $\alpha$ SMA expression levels under high-pressure conditions than the wild-type PSCs, suggesting that TRPC1 might play an essential role in the modulation of  $\alpha$ SMA. To clarify this aspect, we used a human cell line model of activated PSCs where we observed that the transient knocked down of TRPC1 using the siRNA approach decreased  $\alpha$ SMA expression. We then wanted to investigate how TRPC1 could drive this process, and knowing that TRPC channels have the ability to modulate  $\alpha$ SMA expression as a consequence of their physical association with  $\alpha$ SMA (Kurahara et al.,



2015), we performed co-immunoprecipitation experiments to assess this possibility. We found that TRPC1 interacts directly or indirectly with  $\alpha$ SMA in human activated PSCs and the phosphorylated active form of SMAD2 transcription factor (pSMAD2), shown to drive  $\alpha$ SMA expression in rodent PSCs (Ohnishi et al., 2004), modulating human PSC's activation. Moreover, we revealed a strong regulatory link between TRPC1,  $\alpha$ SMA, and pSMAD2 within the formed complex, since the silencing of each actor independently interrupted the physical association of the other two partners.

Simultaneously, we determined whether TRPC1 functional expression is crucial for human pressure-induced PSC's activation, as so far, its function was established only in mouse-activated PSCs. In accordance with our previous results in mouse pressure-induced PSC's activation (Fels et al., 2016), we detected an increased  $Ca^{2+}$  influx measured by  $Mn^{2+}$  quench imaging in siCtrl transfected cells under pressurization, whereas this influx was significantly diminished in siTRPC1 transfected cells. Moreover, the difference in the  $Ca^{2+}$  influx between TRPC1 knocked down and siCtrl cells persist even under physiological pressure conditions, suggesting that TRPC1 is basally activated in human activated PSCs, and its activity is promoted by pressurization. This result could be explained by the observed augmentation of pressure-induced TRPC1 protein expression.

We subsequently sought to know through which signalling pathways TRPC1 could mediate PSC's activation, and thus  $\alpha$ SMA expression. After overnight FBS starvation of siTRPC1 and siCtrl transfected cells, followed by 10 min stimulation with 10% FBS, we evaluated the phosphorylation of three majors signalling pathways involved in PSC's activation (Masamune and Shimosegawa, 2009). We observed that TRPC1 can activate the ERK1/2 and SMAD2 pathways, this latter probably through its interaction within the formed protein complex. Based on this hypothesis, we have also noted that only the pharmacological inhibition of SMAD2 but not ERK1/2 affected  $\alpha$ SMA expression, highlighting the strong link between TRPC1,  $\alpha$ SMA, and pSMAD2.

Once we established the TRPC1-mediated signalling pathways, we wanted to know in which PSC's cellular activation responses TRPC1 was involved, probably through the regulation of ERK1/2 and SMAD2 pathways. We then focused on investigating three principal PSC activation potentials, including i) the cell proliferation, ii) the IL-6 secretion, and iii) PSC's stiffness. We, therefore, demonstrated that TRPC1 invalidation significantly reduced activated PSC's proliferation assessed by MTT colorimetric assay, eliciting a cell cycle arrest in G0/G1 phase defined by flow cytometry without affecting their survival as confirmed by Trypan Blue

colorimetric assay and apoptosis measurement. In addition, evaluation of IL-6 secretion by Elisa assay revealed that TRPC1 is involved in IL-6 secretion as well, as TRPC1 silencing decreased its secretion. TRPC1 modulates these two mechanisms probably by both ERK1/2, and SMAD2 pathways since the pharmacological inhibition of each pathway independently led to the diminution of activated PSC's proliferation and IL-6 secretion.

Moreover, PSC-induced IL-6 secretion was four times higher under pressurization and importantly abolished in TRPC1-KO PSCs. Indeed, pressure-induced PSC's activation enhanced not only IL-6 secretion but also increased PSC's stiffness, which was restored in TRPC1-KO PSCs under pressurization.

Together all these findings brought new evidence of TRPC1's role in PSC's mechanosignalling and activation processes, summarized in the below scheme (**Figure 37**) and better detailed in the following published report: Radoslavova S. \*, Fels B. \*, Pethö Z., Gruner M., Ruck T., Meuth S., Folcher A., Prevarskaya N., Schwab A., and Ouadid-Ahidouch H. (2022). **TRPC1 channels regulate the activation of pancreatic stellate cells through ERK1/2 and SMAD2 pathways and perpetuate their pressure-mediated activation.** *Cell Calcium* 106 (2022) 102621.

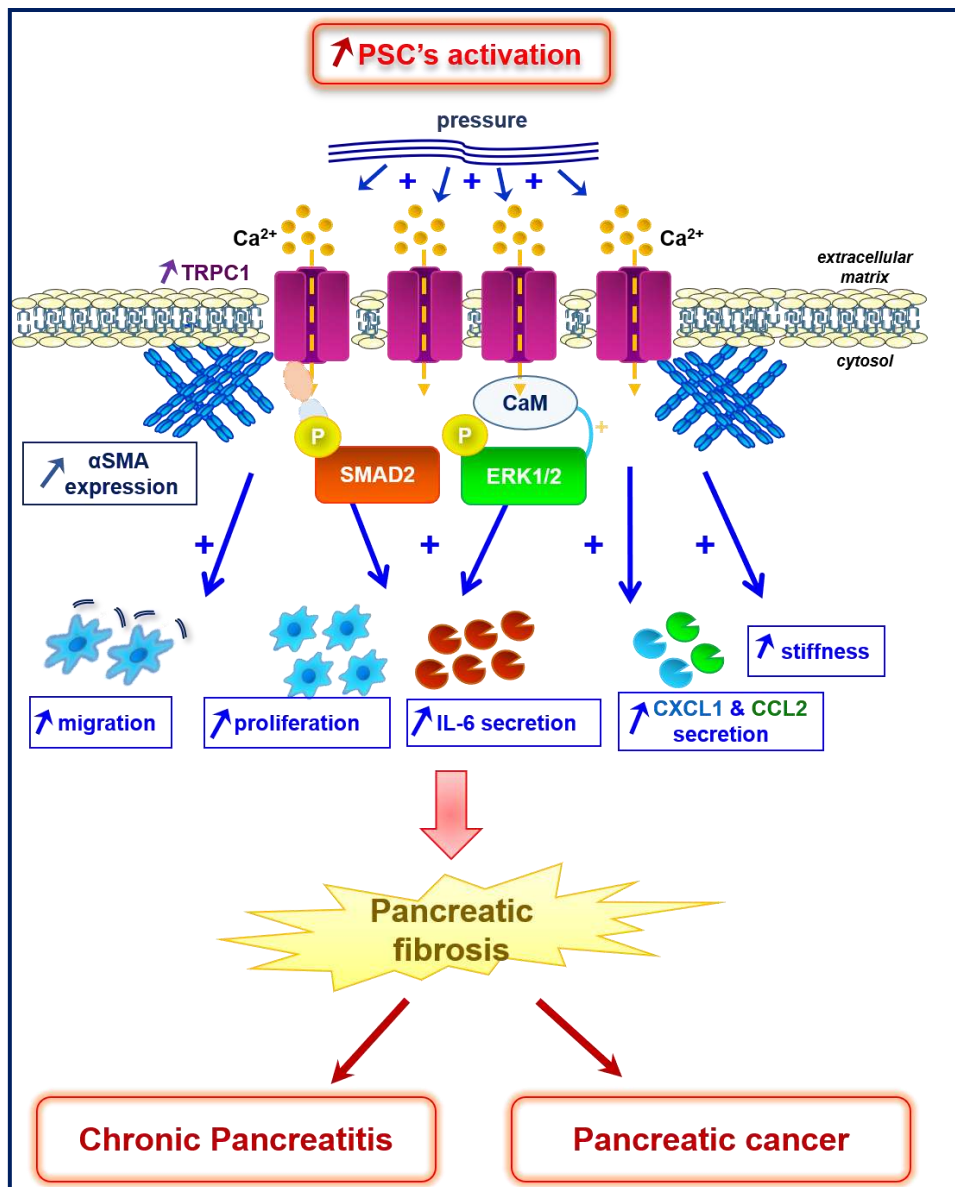
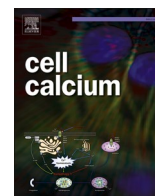


Figure 37: Illustrative scheme of TRPC1 channels' role in PSC's activation processes.



## TRPC1 channels regulate the activation of pancreatic stellate cells through ERK1/2 and SMAD2 pathways and perpetuate their pressure-mediated activation

Silviya Radoslavova<sup>a,b,§</sup>, Benedikt Fels<sup>c,f,§</sup>, Zoltan Pethö<sup>d</sup>, Matthias Gruner<sup>d</sup>, Tobias Ruck<sup>e</sup>, Sven G. Meuth<sup>e</sup>, Antoine Folcher<sup>b</sup>, Natalia Prevarskaya<sup>b,\*</sup>, Albrecht Schwab<sup>d,\*</sup>, Halima Ouadid-Ahidouch<sup>a,\*</sup>

<sup>a</sup> Laboratory of Cellular and Molecular Physiology, UR-UPJV 4667, University of Picardie Jules Verne, 80039 Amiens, France

<sup>b</sup> University of Lille, Inserm U1003 - PHYCEL - Cellular Physiology, F-59000 Lille, France

<sup>c</sup> Institute of Physiology, University Lübeck, Lübeck, Germany

<sup>d</sup> Institute of Physiology II, University Münster, Münster, Germany

<sup>e</sup> Klinik für Neurologie, Medical Faculty, Universitätsklinikum Düsseldorf, Düsseldorf, Germany

<sup>f</sup> DZHK (German Research Centre for Cardiovascular Research), Partner Site Hamburg/Lübeck/Kiel, Lübeck, Germany

### ARTICLE INFO

#### Keywords:

TRPC1 channels  
Pancreatic stellate cells  
Activation  
Pancreatic ductal adenocarcinoma  
High-pressure

### ABSTRACT

Pancreatic stellate cell (PSC) activation is a major event occurring during pancreatic ductal adenocarcinoma (PDAC) development. Up to now mechanisms underlying their activation by mechanical cues such as the elevated tissue pressure in PDAC remain poorly understood. Here we investigate the role of one potential mechano-transducer, TRPC1 ion channel, in PSC activation. Using pre-activated human siTRPC1 and murine TRPC1-KO PSCs, we show that TRPC1 promotes  $\alpha$ SMA ( $\alpha$ -smooth muscle actin) expression, the main activation marker, in cooperation with the phosphorylated SMAD2, under normal and elevated pressure. Functional studies following TRPC1 silencing demonstrate the dual role of TRPC1 in the modulation of PSC proliferation and IL-6 secretion through the activation of ERK1/2 and SMAD2 pathways. Moreover, pressurization changes the mechanical behavior of PSCs by increasing their cellular stiffness and emitted traction forces in a TRPC1-dependent manner. In summary, these results point to a role of TRPC1 channels in sensing and transducing the characteristic mechanical properties of the PDAC microenvironment in PSCs.

### 1. Introduction

Activated pancreatic stellate cells (PSCs) are the main source of the extensive fibrotic stroma that characterizes pancreatic ductal adenocarcinoma (PDAC). It accounts for up to 90% of the total tumor mass [1–3]. Therefore, PSCs have become the subject of intensive research in order to elucidate their therapeutic potential in the improvement of PDAC treatment.

In the healthy pancreas, PSCs exist in a quiescent vitamin-A lipid-storing state. They are involved in the maintenance of pancreatic tissue architecture by regulating the extracellular matrix (ECM) turnover [4]. However, during PDAC development PSCs become activated which

leads to a change of their phenotypical and functional properties. They transform to a more myofibroblast-like phenotype, defined by a high expression of  $\alpha$ -smooth muscle actin ( $\alpha$ SMA) and loss of Vitamin A-containing lipid droplets [5]. Activated PSCs are also characterized by increased proliferative and migratory activity as well as by enhanced secretion of cytokines, growth factors and ECM proteins [5–7]. PSCs can maintain their activation through autocrine positive feedback loops and paracrine interactions with the pancreatic cancer cells [3,8,9]. The intense mutual communication between PSCs and pancreatic cancer cells leads to the perpetuation of PSC activation as well as to the promotion of the tumorigenic potential of the cancer cells [3,10,11].

PSCs can also be activated by the PDAC microenvironment which

\* Corresponding authors.

E-mail addresses: [natacha.prevarskaya@univ-lille.fr](mailto:natacha.prevarskaya@univ-lille.fr) (N. Prevarskaya), [aschwab@uni-muenster.de](mailto:aschwab@uni-muenster.de) (A. Schwab), [halima.ahidouch-ouadid@u-picardie.fr](mailto:halima.ahidouch-ouadid@u-picardie.fr) (H. Ouadid-Ahidouch).

§ Co-first authors

<https://doi.org/10.1016/j.ceca.2022.102621>

Received 25 May 2022; Received in revised form 4 July 2022; Accepted 5 July 2022

Available online 9 July 2022

0143-4160/© 2022 Elsevier Ltd. All rights reserved.

contains an abundant amount of cytokines and growth factors secreted from stromal cells including PSCs as well as from cancer cells [12–14]. Among these, interleukin-6 (IL-6) has been shown to be overexpressed in PDAC microenvironment [15]. IL-6 levels correlate with patients' poor survival rate [16]. In addition, the altered mechanical properties of the PDAC microenvironment strongly contribute to PSC activation. This includes the elevated tissue pressure which is up to 10 times higher than

in the healthy pancreas [17–19].

However, the activation of PSCs by mechanical cues is not yet well understood. There is evidence that ion channels implicated in mechanosensation may be involved in the activation cascade of PSCs [20]. These ion channels are sensors that transduce mechanical forces into intracellular biochemical signals, mainly via the conduction of  $Ca^{2+}$  ions. This results in different cellular responses including cell

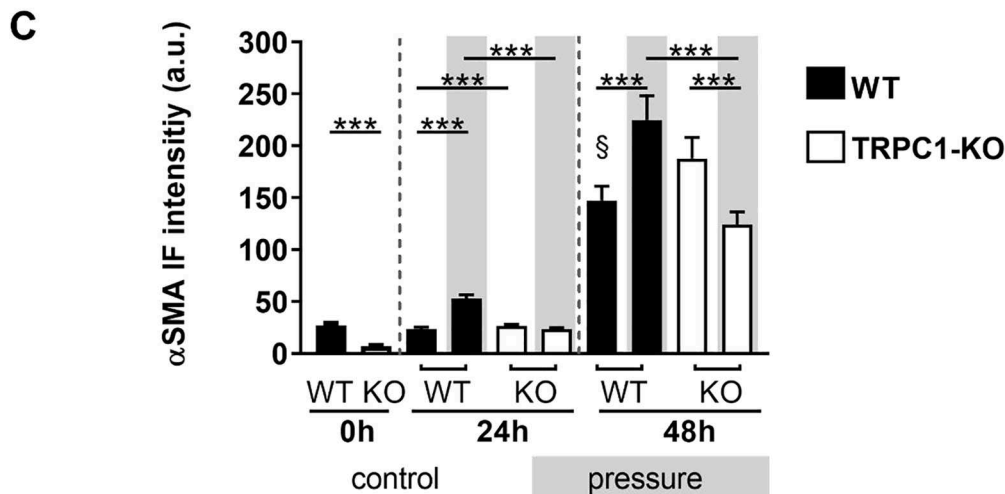
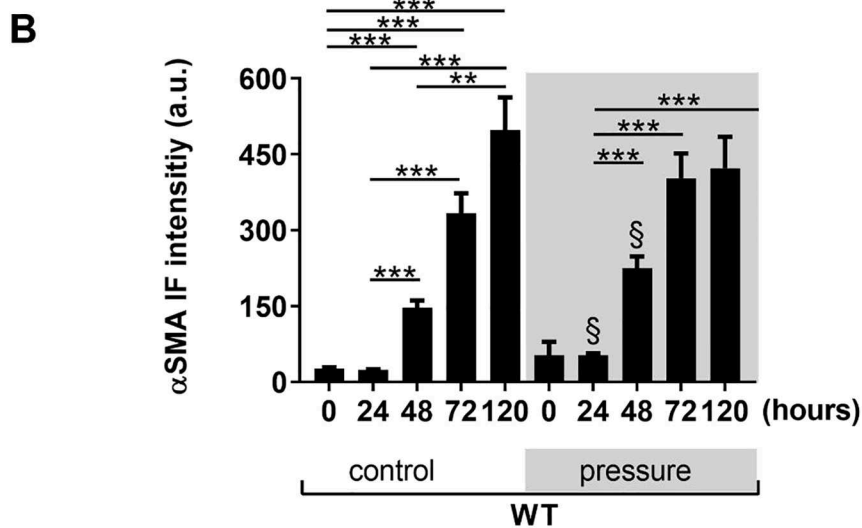
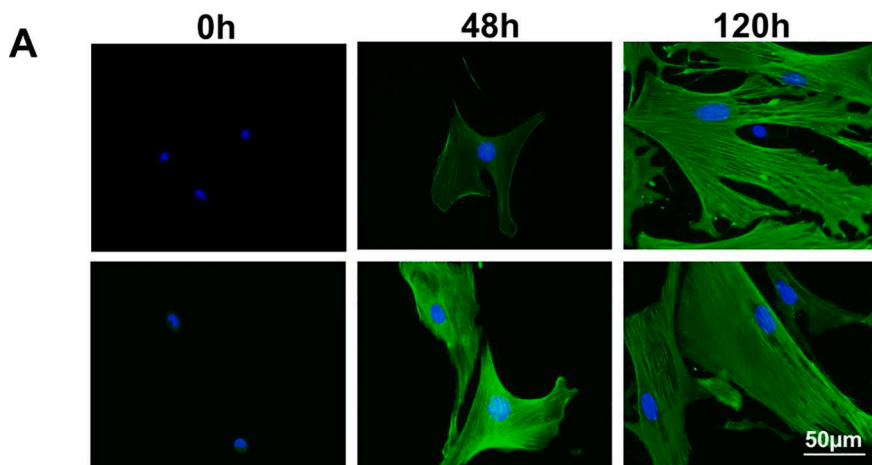


**Fig. 1.** Pressure accelerates mouse PSC activation TRPC1-dependently. A) Typical  $\alpha$ SMA staining in freshly isolated, quiescent WT-PSCs directly after isolation (t = 0h), at t = 48h and t = 120h. Upper panel: control conditions; lower panel: pressure ( $\Delta$ +100 mmHg). Pressure incubation leads to earlier and more pronounced  $\alpha$ SMA expression. B) Quantification of the time course of  $\alpha$ SMA expression in PSCs under control conditions and upon culturing them at an elevated ambient pressure. PSC activation is accelerated by an increased ambient pressure during the first 48h after isolation (indicated by §; N(0-48h) = 4-5, N(72-120h) = 3, n = 104-347; §, \*p<0.05, control vs. pressure). C) Pressurization (indicated by the grey shading) accelerates the increase of  $\alpha$ SMA in WT but not in TRPC1-KO PSCs within the first 48h (N(WT) = 4-5, N(KO) = 3; n = 183-347; \*p<0.05, control vs. pressure).

proliferation, migration, apoptosis or protein expression, and secretion [21]. One of the candidate channels involved in mechanosensation is TRPC1 (canonical transient receptor potential), a member of the large family of TRP channels [22]. We have previously demonstrated that mechanical forces generated by high pressure augment  $\text{Ca}^{2+}$  influx into murine PSCs via TRPC1 activation. This in turn leads to the increase of migration which reflects PSC activation [19].

Several signal transduction pathways such as the extracellular signal-regulated kinases (ERK1/2) or the mothers against decapentaplegic homolog 2 (SMAD2) pathway have been linked to PSC activation in response to environmental stimuli [17,23–25]. However, so far, the role of mechanical forces transduced by TRPC1 into intracellular signals in the modulation of PSC activation as well as the underlying mechanisms are by and large unknown.

Here we demonstrate the role of TRPC1-dependent mechanisms in PSC activation by an elevated pressure. We identify signaling pathways by which TRPC1 channels regulate  $\alpha$ SMA expression, cell proliferation, IL-6 secretion and shape the mechanical properties of PSCs themselves.

## 2. Results

### 2.1. Pressure accelerates initial activation of murine PSCs

The transition of PSCs from a quiescent to an activated state is triggered among others by mechanical stimuli such as pressure [17,19]. We, therefore, first started by using primary PSCs from murine WT and TRPC1-KO PSCs and tested whether increased pressure is able to accelerate the initial activation of freshly isolated, quiescent PSCs. PSC activation can be monitored by an increase of  $\alpha$ SMA expression (Fig. 1 A). When PSCs are cultured in the presence of an elevated ambient pressure,  $\alpha$ SMA expression rises faster than under control conditions (24h: Ctr  $23.7 \pm 1.8$  a.u. vs. pressure  $53.1 \pm 3.5$  a.u.; 48h: Ctr  $147.3 \pm 13.7$  a.u. vs. pressure  $225.0 \pm 23.4$  a.u., Fig. 1 B). PSCs under pressurization remain activated when cultured for a time period of 5 days as evidenced by an increased  $\alpha$ SMA expression at  $t = 120$ h (Fig. 1 A-B). However, the accelerated activation in response to an elevated ambient pressure is absent in TRPC1-KO PSCs after 24h (TRPC1-KO control  $26.4 \pm 1.8$  a.u. vs pressure  $23.7 \pm 1.1$  a.u.; Fig. 1 C). It is strongly attenuated after 48h (TRPC1-KO control  $188.0 \pm 20.2$  a.u. vs pressure  $124.3 \pm 12.0$  a.u.). These data suggest that pressure-induced PSC activation is in part TRPC1-dependent.

During activation PSCs typically lose Vitamin A-containing lipid droplets, which can be stained with NileRed [1]. Activation of quiescent freshly isolated PSCs is at least in part due to culturing them on unphysiologically stiff tissue culture plastic [26]. This activation leads to a steady decrease of NileRed positive cells within the first days of culture (Supplementary Figure 1 A). Their relative number is reduced from  $60.5 \pm 5.0$  % ( $t = 24$ h) to  $27.5 \pm 2.8$  % ( $t = 120$ h, Supplementary Figure 1 A). When PSCs are cultured at an increased atmospheric pressure, the decrease of NileRed positive cells is markedly accelerated during the first 24h ( $t = 24$ h:  $42.2 \pm 5.2$  %). It reaches the same low level as control cells after 120h ( $27.6 \pm 3.2$  %).

Furthermore, the mechanical properties of the PDAC microenvironment are modulated by the excessive ECM deposition resulting in the increase of PDAC tissue stiffness, which consequently leads to the increase of PDAC tissue pressure [27]. Such an unphysiologically high stiffness is also observed on the cell culture plastic support. This phenomenon induces and maintains PSCs in an activated state [26]. We therefore wondered whether TRPC1 silencing could also influence  $\alpha$ SMA expression in already pre-activated human PSC cell line (PS-1) when they are cultured in cell culture plastic dishes. Indeed, knocking down of TRPC1 for 72h leads to a decrease of  $\alpha$ SMA expression by  $58.4 \pm 10.8$  % (Supplementary Figure 1 B-D). This finding suggests that  $\alpha$ SMA expression is also partly TRPC1-dependent in pre-activated human PSCs.

### 2.2. Physical association and colocalization between TRPC1, $\alpha$ SMA and pSMAD2 in pre-activated human PSCs

After showing a link between TRPC1 and  $\alpha$ SMA expression in pressure-induced activation of murine PSCs and pre-activated human PSCs, we wondered whether TRPC1 channels could be colocalized with  $\alpha$ SMA. Furthermore, knowing that  $\alpha$ SMA expression is mediated by the SMAD2 pathway [25], we simultaneously sought to know whether TRPC1 channels could be linked to  $\alpha$ SMA through the phosphorylated active form of SMAD2 (pSMAD2). To determine this, we used the pre-activated human PSC cell line PS-1 and analyzed the colocalization of TRPC1,  $\alpha$ SMA and pSMAD2 by immunofluorescence. We quantified the colocalization degree of these three proteins with Pearson's correlation coefficient using Fiji ImageJ software. Indeed, when the coefficient value lies between 1 and 0.5, this reflects an important colocalization between the two proteins. According to this and as shown in Fig. 2 A-C we noted a "partial" colocalization between TRPC1,  $\alpha$ SMA and pSMAD2, suggesting that they might be interacting with each other. To confirm this hypothesis, we performed co-immunoprecipitation followed by Western blot experiments using anti-TRPC1, anti- $\alpha$ SMA and anti-pSMAD2 antibodies to evaluate the interaction between the three partners. We found that TRPC1,  $\alpha$ SMA and pSMAD2 form a direct or indirect physical interaction network within pre-activated human PSCs (Fig. 2 D).

### 2.3. Mutual regulation between TRPC1, $\alpha$ SMA and pSMAD2 within the formed protein complex in pre-activated human PSCs

We then wanted to determine whether TRPC1- $\alpha$ SMA-pSMAD2 association in pre-activated human PSCs depends on the protein expression level of each partner. To this end, we silenced each actor independently for 72h, using the siRNA approach and evaluated the interaction level between the two other partners by co-immunoprecipitation and Western blot experiments. 72h of TRPC1 silencing decreases the interaction between  $\alpha$ SMA and pSMAD2 by  $41.8 \pm 14.9$  % (Fig. 3 A) and by  $40.7 \pm 16.3$  % (Fig. 3 B), when immunoprecipitated with pSMAD2 and  $\alpha$ SMA antibodies, respectively. The influence of knocking-down SMAD2 on the protein complex is more prominent since it induces a  $60.8 \pm 8.6$  % (Fig. 3 C) and  $52.4 \pm 16.1$  % (Fig. 3 D) diminution of  $\alpha$ SMA and TRPC1 association, using TRPC1 and  $\alpha$ SMA immunoprecipitation (IP) antibodies, respectively. Contrary to SMAD2, the effect of  $\alpha$ SMA inhibition is less pronounced, leading to  $38.8 \pm 12.8$  % (Fig. 3 E, with pSMAD2 IP antibody) and  $22 \pm 4.1$  % (Fig. 3 F, with TRPC1 IP antibody) decrease of TRPC1-pSMAD2 interplay. This heterogeneous influence of each partner on the complex constitution shows that TRPC1,  $\alpha$ SMA and pSMAD2 participate at different degrees in the complex assembly, in pre-activated human PSCs. In parallel, we assessed the 72h siRNA transfection efficiency of each protein by Western blotting. TRPC1 protein expression was diminished by  $84.3 \pm 5.4$  % (Supplementary Figure 1 B-C), SMAD2 expression by  $61.9 \pm 9.4$  % (Supplementary Figure 2 A), and  $\alpha$ SMA by  $98.6 \pm 0.6$  % (Supplementary Figure 2 B). Thus, the decrease in the complex formation is not directly proportional to the degree of knock-down of any of the three proteins which argues for a more complex interaction of them. Taken together these data reveal a strong regulatory link between TRPC1,  $\alpha$ SMA and pSMAD2 within the formed protein complex.

### 2.4. Elevated external pressure increases TRPC1 channel function in pre-activated human PSCs

We have previously demonstrated that elevated pressure drives  $\text{Ca}^{2+}$  influx through TRPC1 channel activation in mouse PSCs [19]. According to these findings, we wondered whether an elevated external pressure would rise  $\alpha$ SMA and TRPC1 expression in pre-activated human PSCs. This would then lead to an increased TRPC1-mediated  $\text{Ca}^{2+}$  influx and to an extended PSC activation. To investigate this hypothesis, we

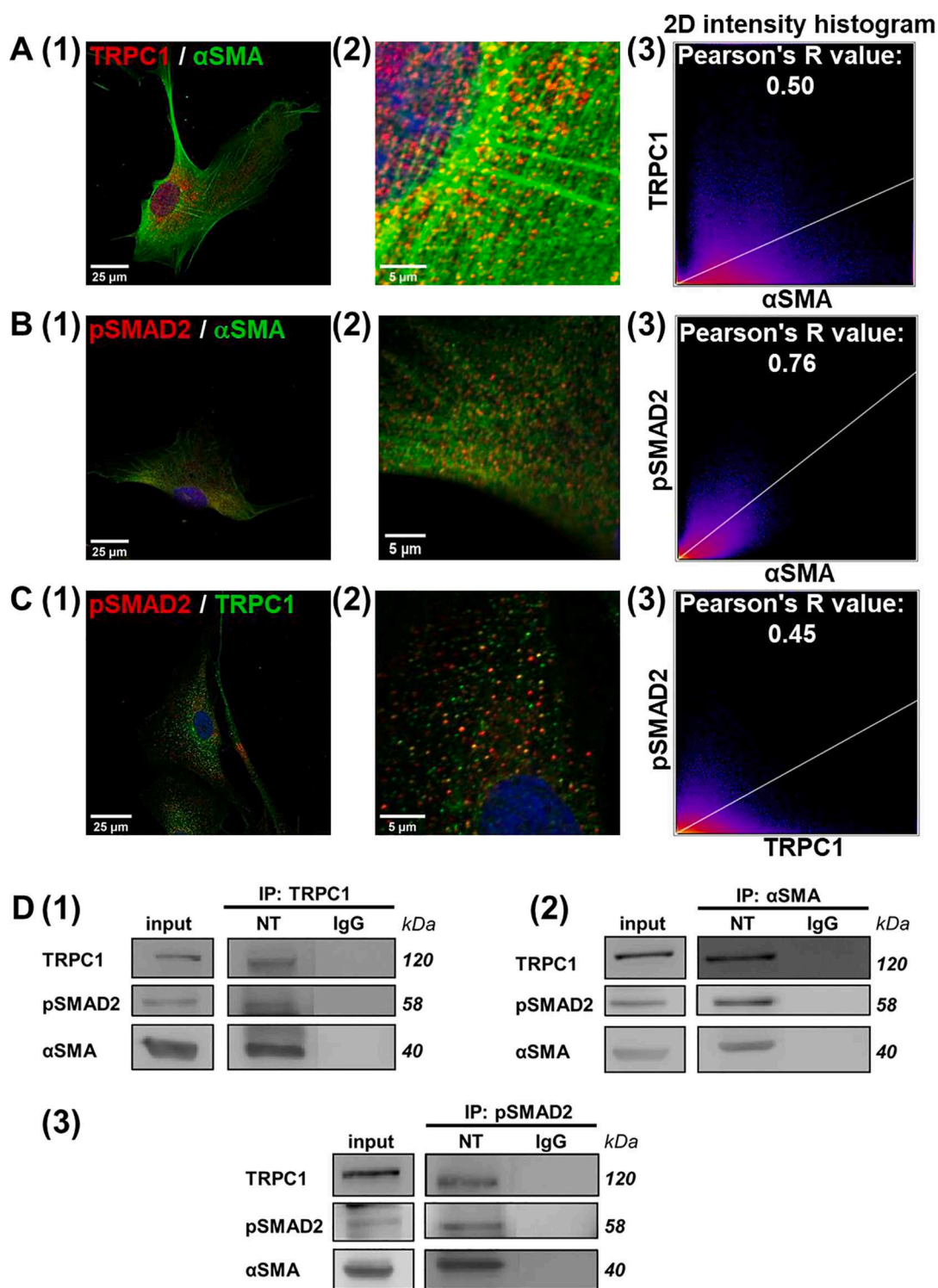


**Fig. 2.** TRPC1 co-localizes and interacts with  $\alpha$ SMA and the phosphorylated form of SMAD2 (pSMAD2) in pre-activated human PSCs. A1-2) Immunofluorescence staining of TRPC1 (red),  $\alpha$ SMA (green) and their merge in PS-1 cells. A3) The colocalization intensity was measured using Pearson's correlation coefficient with Fiji ImageJ software. Each immunofluorescence image was displayed as an intensity-scatter plot, where the x-axis represents the green labeled protein and the y-axis the red labeled protein, both related by the white linear regression line in the scatter plot. The closer Pearson's R value is to 1, the stronger the positive linear relationship, and thus the colocalization between the two proteins is. B1-3) The same experiments were performed to visualize pSMAD2 (red) and  $\alpha$ SMA (green) colocalization as well as C1-3) TRPC1 (green) and pSMAD2 (red) colocalization. All image acquisitions were performed by confocal microscopy. D) Representative Western blot of TRPC1, pSMAD2 and  $\alpha$ SMA expression after immunoprecipitation with D1) anti-pSMAD2, D2) anti- $\alpha$ SMA and D3) anti-TRPC1 antibodies (NT: no-treated cells, at least N=3).

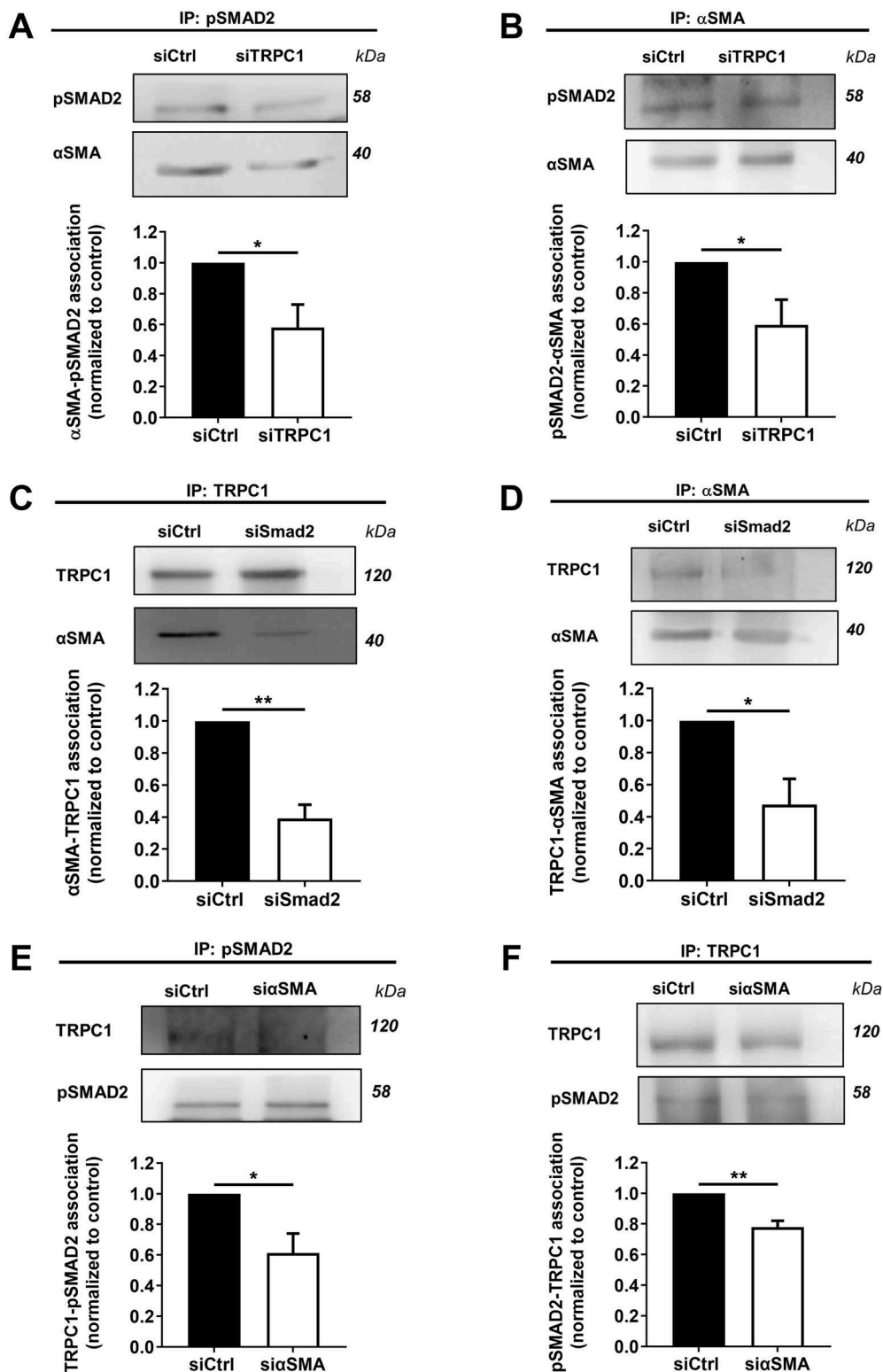


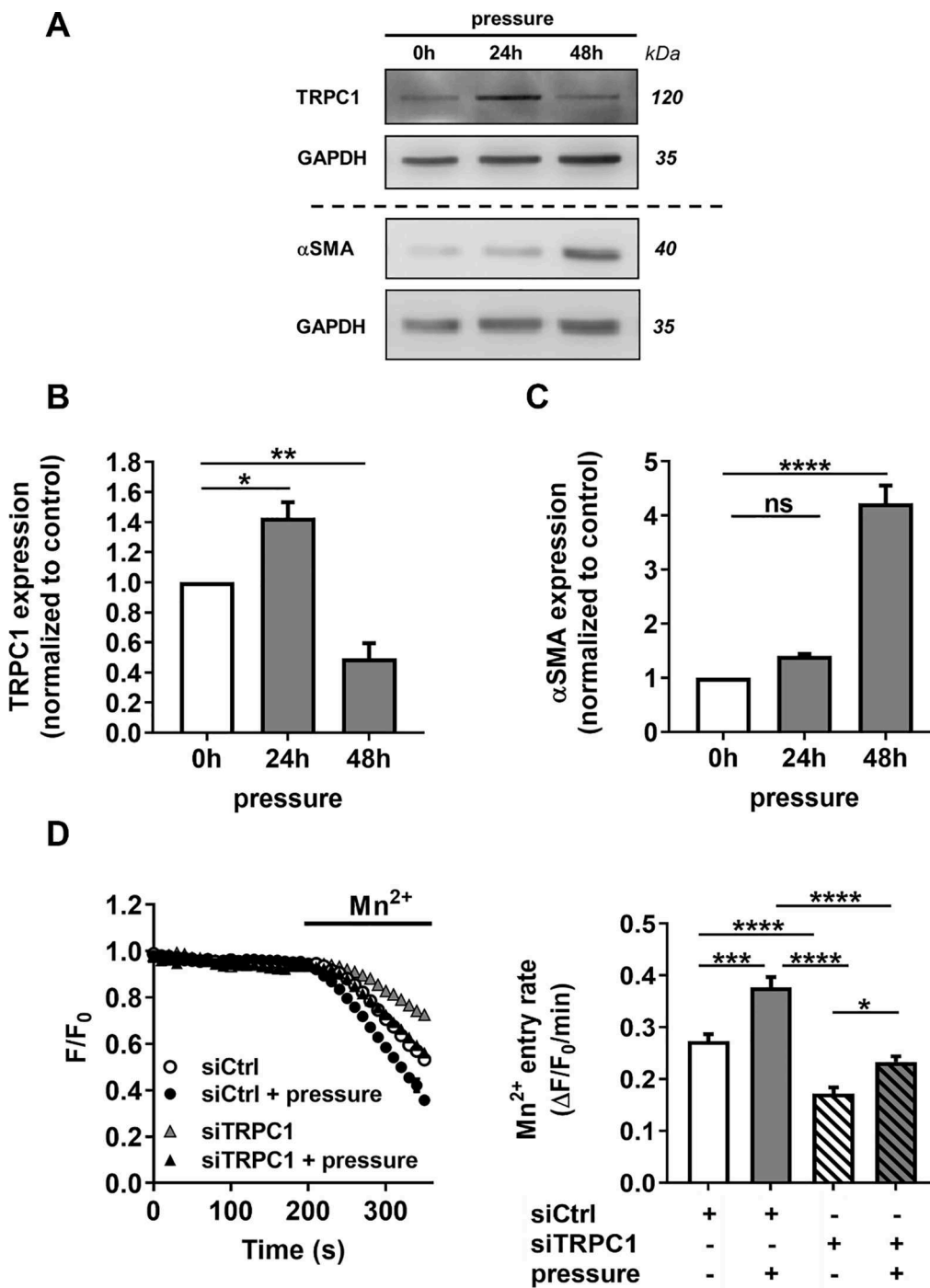
**Fig. 3.** Silencing one of the partners disrupts the protein complex interaction within pre-activated human PSCs. A-B) TRPC1 knock-down impairs the αSMA-pSMAD2 interaction. A) Representative Western blot of αSMA-pSMAD2 interaction after 72h of TRPC1 silencing, using anti-pSMAD2 immunoprecipitation antibody with the quantification. B) Similarly, pSMAD2-αSMA interaction was evaluated in TRPC1 knocked-down PS-1 cells using anti-αSMA immunoprecipitation antibody as illustrated by the representative Western blot and quantification. C-D) SMAD2 knock-down perturbs the interaction between αSMA and TRPC1. C) Representative Western blot of αSMA-TRPC1 interaction after 72h of SMAD2 knock-down using anti-TRPC1 immunoprecipitation antibody with the quantification. D) TRPC1-αSMA interaction was also quantified using anti-αSMA immunoprecipitation antibody as demonstrated in 3 D. E-F) αSMA knocking down disrupts the TRPC1-pSMAD2 complex. Representative Western blot illustrating the effect of 72h αSMA knock-down on TRPC1-pSMAD2 interaction, using E) anti-pSMAD2 and F) anti-TRPC1 immunoprecipitation antibodies, respectively. All values were normalized to the siCtrl condition and reported as mean ± SEM (\* $p < 0.05$ , \*\* $p < 0.01$ , at least  $N = 3$ , Student's  $t$ -test).

pre-incubated PS-1 cells under high pressure ( $\Delta +100$  mmHg) for 24 and 48 hours and evaluated TRPC1 and αSMA expression by Western blotting. 24h of elevated pressure raises TRPC1 protein level  $1.4 \pm 0.1$ -fold (Fig. 4 A-B). However, after 48h of stimulation, pressurization drastically reduces TRPC1 expression by  $0.5 \pm 0.1$ -fold (Fig. 4 A-B), suggesting the existence of an autoprotective cellular mechanism. Simultaneously, we noticed a trend of αSMA expression to rise at 24h post-pressurization ( $1.4 \pm 0.03$ -fold) which becomes significant at 48h

( $4.2 \pm 0.3$ -fold, Fig. 4 A/C). Interestingly, the rise of αSMA expression occurs only after that of TRPC1 (Fig. 4 A/C).

We next sought to know whether the pressure-induced increase of TRPC1 expression is correlated with an augmentation of its channel activity. As TRPC1 proteins are non-selective  $\text{Ca}^{2+}$ -permeable cation channels, we performed  $\text{Mn}^{2+}$  quenching experiments to measure the  $\text{Ca}^{2+}$  influx after TRPC1 silencing. We compared  $\text{Ca}^{2+}$  influx under control conditions with that following pressurization ( $\Delta +100$  mmHg).





Under control conditions the  $Mn^{2+}$  entry rate is reduced from  $0.27 \pm 0.01 \Delta F/F_0/\text{min}$  in siCtrl transfected cells to  $0.17 \pm 0.01 \Delta F/F_0/\text{min}$  in siTRPC1 transfected cells (Fig. 4 D). Elevated external pressure enhances  $Ca^{2+}$  influx in siCtrl cells inducing an increase of  $Mn^{2+}$  entry rate to  $0.38 \pm 0.02 \Delta F/F_0/\text{min}$  (Fig. 4 D). However, the  $Mn^{2+}$  entry rate of pressurized siTRPC1 PSCs is at the same low level ( $0.23 \pm 0.01 \Delta F/F_0/\text{min}$ , Fig. 4 D) as in non-pressurized siCtrl cells under control conditions. These results suggest that TRPC1 channels contribute to the pressure-induced  $Ca^{2+}$  entry into pre-activated human PSCs.

Based on these results, we can conclude that elevated external pressure increases the functional expression of TRPC1 channels, which in turn stimulates TRPC1-dependent  $\alpha$ SMA expression and leads to an enhanced TRPC1-dependent  $Ca^{2+}$  entry.

Fig. 4. Elevated pressure stimulates the functional expression of TRPC1 channels as well as  $\alpha$ SMA expression in pre-activated human PSCs. A-C) 24h and 48h of pressurization ( $\Delta+100$  mmHg) increase both TRPC1 and  $\alpha$ SMA expression, respectively in PS-1 cells. A) Representative Western blot of the effect of pressurization and its quantification for B) TRPC1 and C)  $\alpha$ SMA expression, respectively (\* $p < 0.05$ , \*\* $p < 0.01$ , \*\*\*\* $p < 0.0001$ , ns: no significant, at least  $N = 3$ , one-way ANOVA followed by Bonferroni multiple comparison test). All values were first normalized to the reference protein GAPDH and then to the non-pressurized control condition (0h) and reported as mean  $\pm$  SEM. D) Pressurization for 24h promotes TRPC1-mediated  $Ca^{2+}$  influx, which was measured by  $Mn^{2+}$  quenching of the fluorescent  $Ca^{2+}$  indicator Fura-2 AM in siCtrl and siTRPC1 transfected PS-1 cells. Representative  $Mn^{2+}$  quench traces and the quantification of  $Mn^{2+}$  entry in siCtrl and siTRPC1 cells under control and pressurized conditions (siCtrl:  $n = 64$ , siCtrl + pressure:  $n = 46$ , siTRPC1:  $n = 46$ , siTRPC1 + pressure:  $n = 52$ ,  $N = 3$ , \* $p < 0.05$ , \*\* $p < 0.001$ , \*\*\*\* $p < 0.0001$ , one-way ANOVA followed by Kruskal-Wallis multiple comparison test,  $n$ : number of cells,  $N$ : number of passage). All values were reported as mean  $\pm$  SEM.

#### 2.5. TRPC1 mediates the activation of SMAD2 and ERK1/2 pathways in pre-activated human PSCs

PSC activation is a dynamic mechanism that is coordinated and triggered by several intracellular signaling pathways [28]. Hence, we speculated that except being involved in  $\alpha$ SMA and pSMAD2 interplay, TRPC1 might increase  $\alpha$ SMA expression through the activation of one of these signaling pathways in pre-activated human PSCs. We therefore investigated whether the phosphorylation of ERK1/2 and SMAD2 modulates human PSC activation through the regulation of the main activation marker  $\alpha$ SMA. We treated PS-1 cells with an inhibitor of ERK1/2 (U 0126; 10  $\mu$ M) or SMAD2 (SB 431542; 80  $\mu$ M) activity for 72h. We first evaluated the efficiency of the inhibitors by Western blot.

Treatment with U 0126 reduces ERK1/2 phosphorylation by  $31.9 \pm 6\%$  (Supplementary Figure 3 A), whereas SB 431542 treatment induces a  $37.4 \pm 9.3\%$  decrease of SMAD2 phosphorylation (Supplementary Figure 3 B). We revealed that SMAD2 inhibition with SB 431542 reduces  $\alpha$ SMA protein expression by  $76.9 \pm 5.5\%$  (Fig. 5 B). In contrast, the inhibition of ERK1/2 phosphorylation with U 0126 fails to affect  $\alpha$ SMA expression (Fig. 5 A).

We then wanted to know whether TRPC1 is able to activate one of the above-cited signaling pathways in order to regulate  $\alpha$ SMA expression. We therefore inhibited TRPC1 expression for 72h and assessed SMAD2, ERK1/2 as well as AKT phosphorylation levels by Western blotting. PS-1 cells were kept in FBS(Fetal Bovine Serum)-free media

overnight and then stimulated with 10 % FBS for 10 min. As expected, TRPC1 silencing leads to a decrease of SMAD2 phosphorylation by 57.8 % (siCtrl + 10 min FBS:  $1.6 \pm 0.1$ -fold, siTRPC1 + 10 min FBS:  $0.7 \pm 0.2$ -fold, Fig. 5 C), suggesting that TRPC1 might be involved in this process through its interaction with pSMAD2. Interestingly, knocking-down TRPC1 channels also induces a diminution of ERK1/2 activation by 38.7 % (siCtrl + 10 min FBS:  $6.4 \pm 0.4$ -fold, siTRPC1 + 10 min FBS:  $4.0 \pm 0.7$ -fold, Fig. 5 D). However, it fails to affect AKT phosphorylation (Fig. 5 E). Importantly, for none of the three signaling pathways, TRPC1 silencing influences the total amount of the respective unphosphorylated protein (Fig. 5 C, D & E, right panels).

These results demonstrate that TRPC1 channels stimulate the

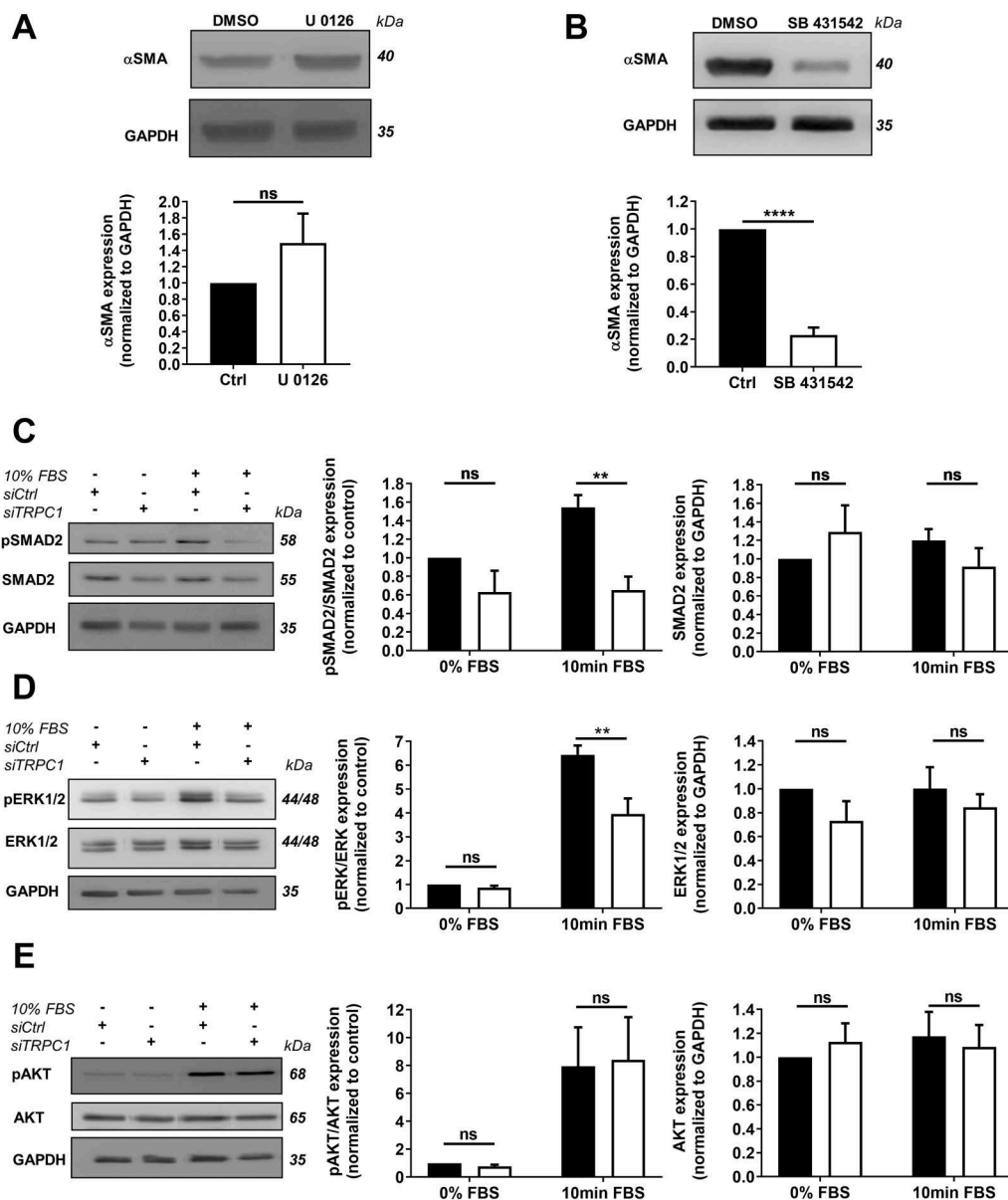


**Fig. 5.** TRPC1 channels drive human PSC activation through the phosphorylation of SMAD2 and ERK1/2 pathways. A-B)  $\alpha$ SMA expression is regulated by the SMAD2 pathway but not ERK1/2 pathway in pre-activated human PSCs. A) Pharmacological inhibition of the ERK1/2 pathway with U 0126 (10  $\mu$ M) for 72h does not affect  $\alpha$ SMA expression and its quantification. B) SMAD2 pathway inhibition with the SB 431542 (80  $\mu$ M) decreases  $\alpha$ SMA expression. Representative Western blot of  $\alpha$ SMA after SB 431542 treatment for 72h and its quantification. All values were firstly normalized to the reference protein (GAPDH) and then to the control condition, reported as mean  $\pm$  SEM (\*\* $p < 0.001$ , \*\* $p < 0.01$ , ns: no significant, at least N = 3, Student's t-test). C-E) TRPC1 channels promote SMAD2 and ERK1/2 activation but not AKT phosphorylation in pre-activated human PSCs. C) Involvement of TRPC1 in SMAD2 phosphorylation in PS-1 cells. Representative Western blot showing the effect of TRPC1 silencing after overnight FBS(Fetal Bovine Serum) starvation of transfected cells. Cells were then stimulated with FBS for 10 min to evaluate the effect of TRPC1 on SMAD2 phosphorylation which was quantified by the ratio of phosphorylated SMAD2 / total SMAD2 protein. In parallel, the impact of TRPC1 silencing on total SMAD2 protein expression was also evaluated. D) Assessment of ERK1/2 activation after TRPC1 knock-down in PS-1 cells. Representative Western blot showing the effect of TRPC1 knock-down using the phosphorylation protocol described above. ERK1/2 phosphorylation was quantified by the ratio of phosphorylated ERK1/2 / total ERK1/2 protein. E) Impact of TRPC1 knock-down on AKT phosphorylation. Representative Western blot showing the effect of TRPC1 knock-down on AKT phosphorylation using the protocol described above. AKT phosphorylation was quantified by the ratio of phosphorylated AKT / total AKT protein. All

values were firstly normalized to the reference protein (GAPDH) and then to the 0 % FBS control condition. siCtrl conditions are represented in black and siTRPC1 conditions are represented in white. All the experiments were performed 72h post-transfection. Values were reported as mean  $\pm$  SEM (\* $p < 0.05$ , ns: no significant, at least N = 3, two-way ANOVA followed by Bonferroni post hoc test).

activation of SMAD2 and ERK1/2 signaling pathways, and that they probably mediate  $\alpha$ SMA expression through the SMAD2 pathway in pre-activated human PSCs.

## 2.6. TRPC1 channels regulate pre-activated human PSC proliferation through an ERK1/2- and SMAD2- dependent pathway

We next sought to know whether TRPC1 channels are involved in typical features of activated PSCs, namely in the proliferation and secretion of growth factors and cytokines [4,5]. We found that TRPC1 silencing inhibits cell proliferation by ~60% (siCtrl:  $100 \pm 2.3$  %, siTRPC1:  $43 \pm 1.5$  %, Fig. 6 A). We then assessed in which cell cycle phase TRPC1 channels are mostly involved in order to modulate PSC proliferation. Using flow cytometry we noted an increase of cells in G0/G1 phase (siCtrl:  $77.2 \pm 0.7$  %, siTRPC1:  $86.1 \pm 0.6$  %) and a decrease of cells in S phase (siCtrl:  $8.4 \pm 0.4$  %, siTRPC1:  $3.9 \pm 0.6$  %) as well as G2/M phase of the cell cycle phases (siCtrl:  $14.4 \pm 0.6$  %, siTRPC1:  $10 \pm 0.6$  %, Fig. 6 B-C). This points to a cell cycle arrest in

G0/G1 phase. To rule out an effect of silencing TRPC1 channels on cell death, we used Trypan Blue colorimetric assay and an Annexin V / Propidium Iodide apoptosis assay. Both techniques reveal no significant effect of TRPC1 silencing on cell death (siCtrl:  $100.0 \pm 13.9$  %, siTRPC1:  $87.2 \pm 19$  %, Supplementary Figure 4 A) or apoptosis (siCtrl:  $3.3 \pm 0.5$  %, siTRPC1:  $6.5 \pm 1.8$  %, Supplementary Figure 4 B-C).

In parallel we evaluated whether one of the TRPC1-mediated signaling pathways, namely SMAD2 and ERK1/2 is involved in the regulation of PSC proliferation. Inhibition of either ERK1/2 or SMAD2 pathways using the pharmacological inhibitors U 0216 and SB 431542, respectively, produces a comparable effect on PS-1 cell proliferation. Blocking ERK1/2 or SMAD2 activity decreases the proliferation rate by approximately one third (ERK1/2: Ctrl:  $100 \pm 4.6$  %, U 0126:  $66.3 \pm 2.2$  %, Fig. 6 D, and SMAD2: Ctrl:  $100 \pm 4.7$  %, SB 431542:  $61.2 \pm 1.2$  %, Fig. 6 E).

Taken together, these data show the involvement of TRPC1 in the modulation of pre-activated human PSC proliferation by driving the cell cycle progression in G1 phase and G1/S transition, probably through

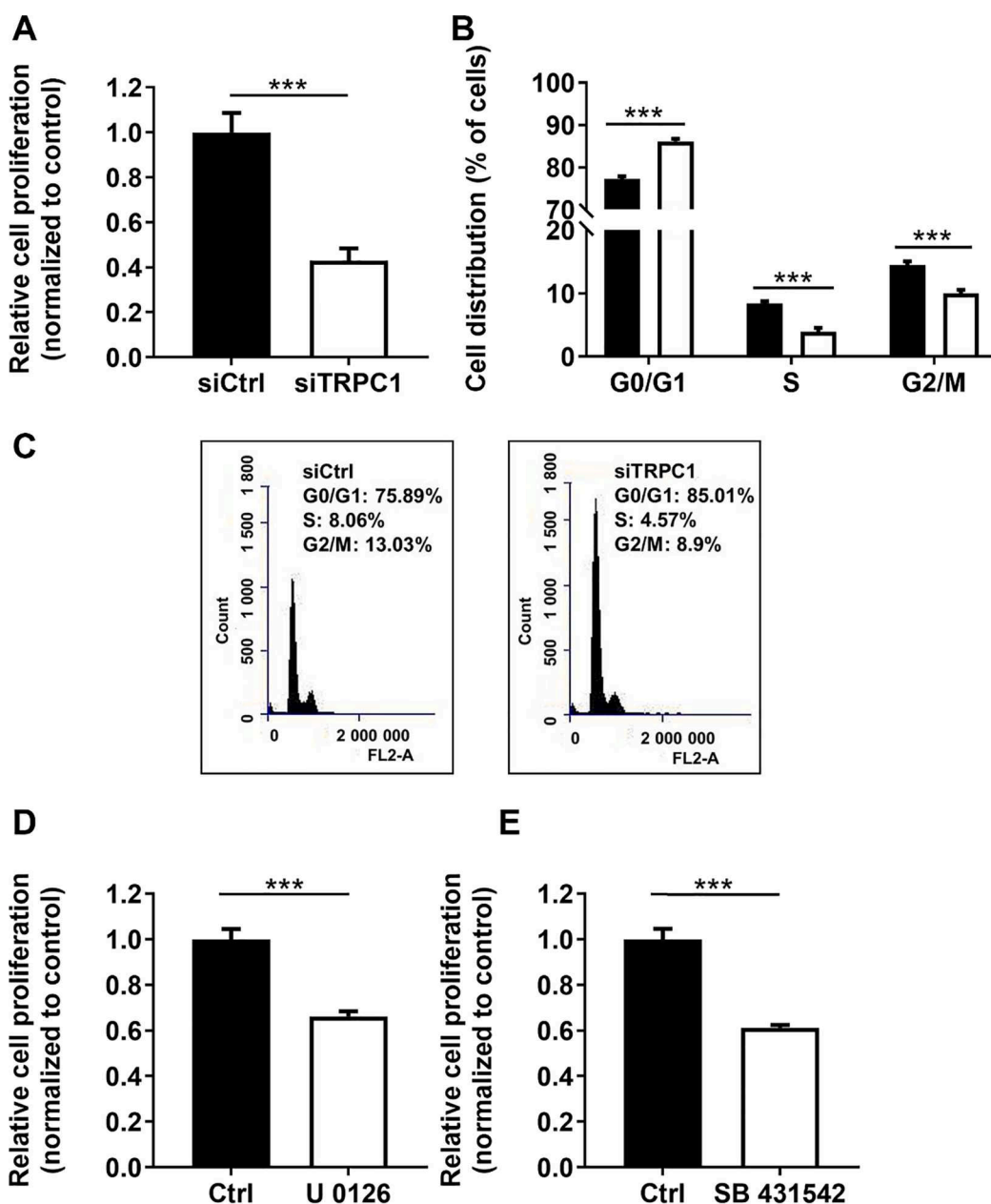


**Fig. 6.** Role of TRPC1 channels, ERK1/2 and SMAD2 pathways in the regulation of pre-activated human PSC proliferation. A-C) TRPC1 channels regulate pre-activated human PSC proliferation. A) Effect of TRPC1 knock-down on PS-1 cell proliferation, assessed 72h post-transfection by MTT assay (\*\**p*<0.001, N = 4, Student's *t*-test). B) Impact of TRPC1 on PS-1 cell cycle progression. Cell cycle distribution (G0/G1, S and G2/M) was examined by flow cytometry with propidium iodide staining 72h after transfection (\*\**p*<0.001, N = 3, two-way ANOVA followed by Bonferroni *post hoc* test). C) Illustrative representation of cell cycle profile 72h after TRPC1 inhibition. Values are reported as mean  $\pm$  SEM, each experiment was performed in triplicate. D-E) Both ERK1/2 and SMAD2 pathways are involved in regulating the proliferation of human PSCs. D) Role of ERK1/2 pathway in PS-1 cell proliferation. Cells were treated with the ERK1/2 inhibitor U 0126 (10  $\mu$ M) for 72h. The inhibition of ERK1/2 pathway decreases PS-1 proliferation which was assessed with an MTT assay. E) Involvement of SMAD2 pathway in PS-1 cell proliferation. Cells were treated with the SMAD2 inhibitor SB 431542 (80  $\mu$ M) for 72h. The impact of SMAD2 inhibition on PS-1 proliferation was evaluated with an MTT assay. All values were normalized to the respective control values after 72h and reported as mean  $\pm$  SEM (\*\**p*<0.001, N = 3 and all MTT experiments were performed in triplicate for each passage, Student's *t*-test).

both ERK1/2 and SMAD2 pathways.

### 2.7. TRPC1 channels regulate IL-6 secretion through the ERK1/2 and SMAD2 pathways in pre-activated human PSCs

We focused on IL-6 which is one of the most abundantly secreted cytokines by activated PSCs [29]. We measured the cytokine secretion by ELISA assay after 72h of TRPC1 silencing. TRPC1 knock-down causes a diminution of IL-6 secretion by more than 50 % (siCtrl:  $100.0 \pm 13.5$

%, siTRPC1:  $42.6 \pm 4.7$  %, Fig. 7 A).

Subsequently, we also studied the impact of ERK1/2 and SMAD2 inhibition on IL-6 secretion. Inhibition of the two pathways independently elicits similar effects on IL-6 secretion. PS-1 treatment with the ERK1/2 blocker U 0126 leads to 40.1 % diminution of IL-6 secretion (Ctrl:  $100.0 \pm 15.7$  %, U 0126:  $59.9 \pm 5.7$  %, Fig. 7 B), and the SMAD2 blocker SB 431542 elicits a decrease of IL-6 secretion by 67.9 % (Ctrl:  $100.0 \pm 12.4$  %, SB 431542:  $32.1 \pm 10.6$  %, Fig. 7 C).

Together these data suggest that TRPC1 channels regulate IL-6

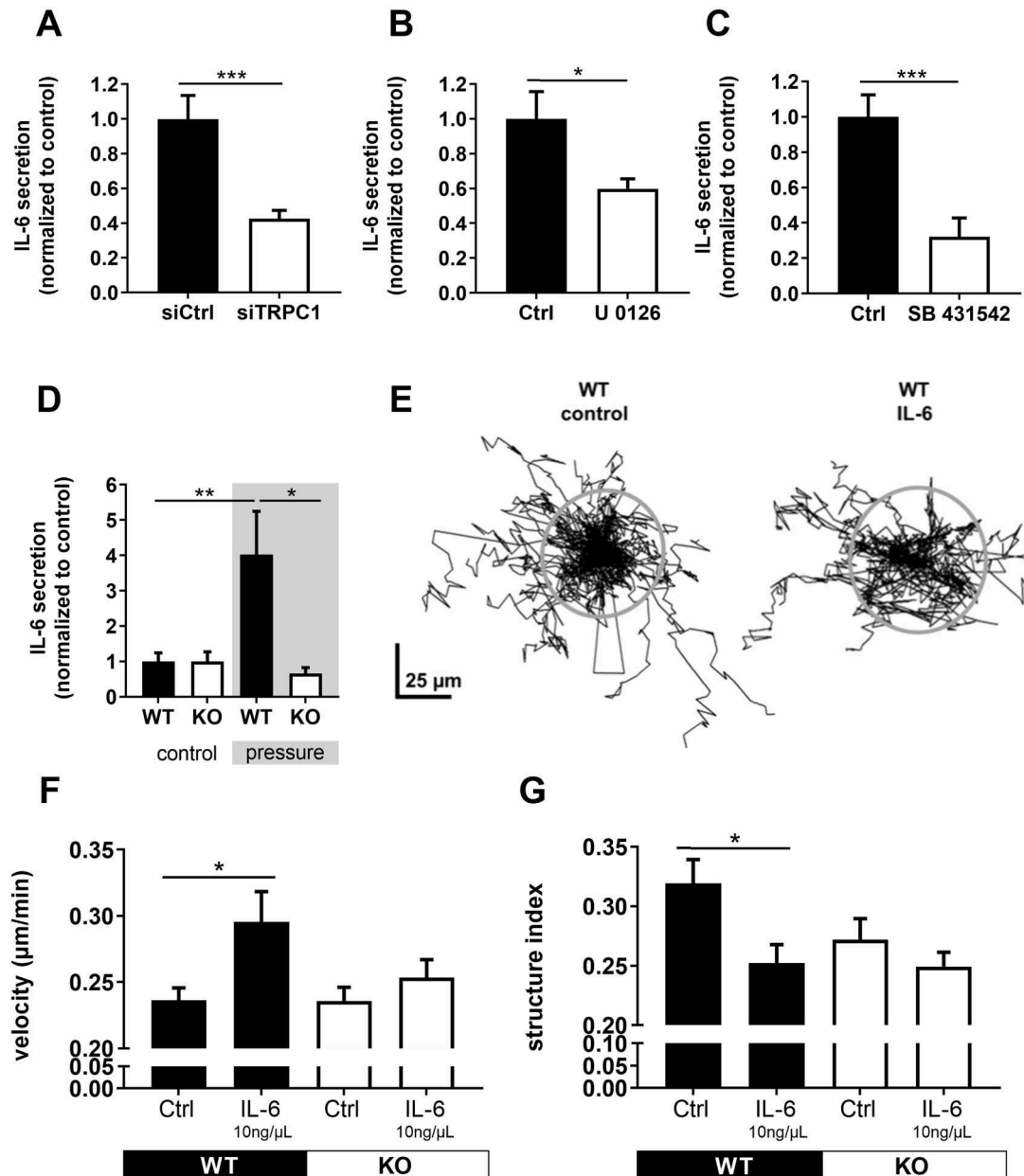


**Fig. 7.** TRPC1 channels regulate IL-6 secretion probably through both ERK1/2- and SMAD2-dependent pathways. In turn, the secreted IL-6 promotes PSC migration via an autocrine feedback loop. A) Silencing of TRPC1 decreases IL-6 secretion. Pharmacological inhibition of B) ERK1/2 pathway with U 0126 (10 μM) and of C) SMAD2 activity using the SB 431542 inhibitor (80 μM) decreases IL-6 secretion. All values were normalized to the control condition and reported as mean ± SEM (\*\*p<0.001, \*p<0.05, N = 3, each experiment was performed at least in triplicate, Student's t-test). D-E) Pressurizing PSCs stimulates TRPC1-dependent IL-6 secretion. D) IL-6 secretion was analyzed after PSCs were cultured at increased ambient pressure (Δ+100 mmHg) for 24h. IL-6 secretion was normalized to the respective control groups. Secretion of IL-6 is markedly increased in pressurized WT PSCs. In contrast, TRPC1-KO PSCs do not respond to increased pressure with elevated cytokine secretion (N = 6; \*p<0.05 WT vs. TRPC1-KO, control vs. pressure). E) Autocrine effects of IL-6 on PSCs migration were analyzed in the absence (control) or presence of IL-6 for a 6h period. Trajectories of individual WT PSCs normalized to common starting points are shown. The grey circles represent the mean translocation of the cells covered during the course of the experiment. F) IL-6 (10 ng/μL) increases the migration velocity of WT PSCs, but not of TRPC1-KO PSCs. G) Structure index of WT but not of TRPC1-KO PSCs is reduced after stimulation with IL-6 indicating a more extended morphology of the PSCs (N = 4, n = 50-63; \*p<0.05, control vs. cytokine).

secretion of pre-activated human PSCs probably through both, ERK1/2 and SMAD2 signaling pathways.

## 2.8. Autocrine effects of IL-6 on murine PSC migration

We next studied whether pressure-induced activation of PSCs also leads to altered secretion of the pro-inflammatory cytokine IL-6 in a TRPC1-dependent way. IL-6 secretion of WT PSCs increases following 24h of pressurization. Notably, TRPC1-KO PSCs do not respond to the pressure treatment with an increased cytokine secretion (Fig. 7 D). Thus, IL-6 secretion of pressurized WT PSCs is significantly higher than that of the PSCs from TRPC1-KO littermates.

To evaluate the autocrine effect of pressure-induced cytokine secretion on PSCs, we performed migration experiments in the absence and presence of IL-6 (10 ng/ $\mu$ L). Stimulation with IL-6 leads to increased PSC migration. The trajectories of individual PSCs are depicted in Fig. 7 E. IL-6 accelerates the migration velocity of WT PSCs (Ctrl:  $0.23 \pm 0.01$   $\mu$ m/min vs. IL-6:  $0.29 \pm 0.02$   $\mu$ m/min), but not of TRPC1-KO PSCs (Ctrl:  $0.24 \pm 0.01$   $\mu$ m/min vs. IL-6:  $0.25 \pm 0.01$   $\mu$ m/min, Fig. 7 F). Accelerated migration is accompanied by changes of PSC morphology. IL-6-treated WT PSCs acquire a more elongated shape as evidenced by a decrease

of the structure index (Ctrl:  $0.32 \pm 0.02$  vs. IL-6:  $0.25 \pm 0.02$ ). This is not the case in TRPC1-KO PSCs (Ctrl:  $0.27 \pm 0.02$  vs. IL-6:  $0.25 \pm 0.01$ , Fig. 7 G).

## 2.9. Impact of TRPC1 channels on murine PSC function under pressure

Finally, we determined the mechanical properties of PSCs themselves and analyzed the elasticity of PSC lamellipodia using the nano-indentation method (Fig. 8 A). Bulk stiffness of WT PSCs rises upon pressure treatment from  $1.25 \pm 0.12$  kPa to  $1.75 \pm 0.15$  kPa (Fig. 8 A-B). In TRPC1-KO cells there is no change in bulk stiffness following pressurization ( $1.38 \pm 0.11$  vs.  $1.1 \pm 0.09$  kPa). Thus, WT PSCs are  $\sim 30\%$  stiffer ( $\Delta +0.68$  kPa) than TRPC1-KO PSCs after culturing them at an elevated pressure.

Increase in cell stiffness of pressurized WT PSCs is accompanied by an increased traction force exerted onto the surrounding matrix. We analyzed this by traction force microscopy (Fig. 8 C). Pressure leads to an increase of force exerted by each PSC by 61.5% (WT Ctrl  $179.4 \pm 17.3$  pPa per cell; pressure  $291.5 \pm 25.9$  pPa per cell). This effect cannot be observed in TRPC1-KO PSCs (Fig. 8 D; Ctrl:  $212.0 \pm 22.8$  pPa per cell; pressure  $153.0 \pm 27.6$  pPa per cell).

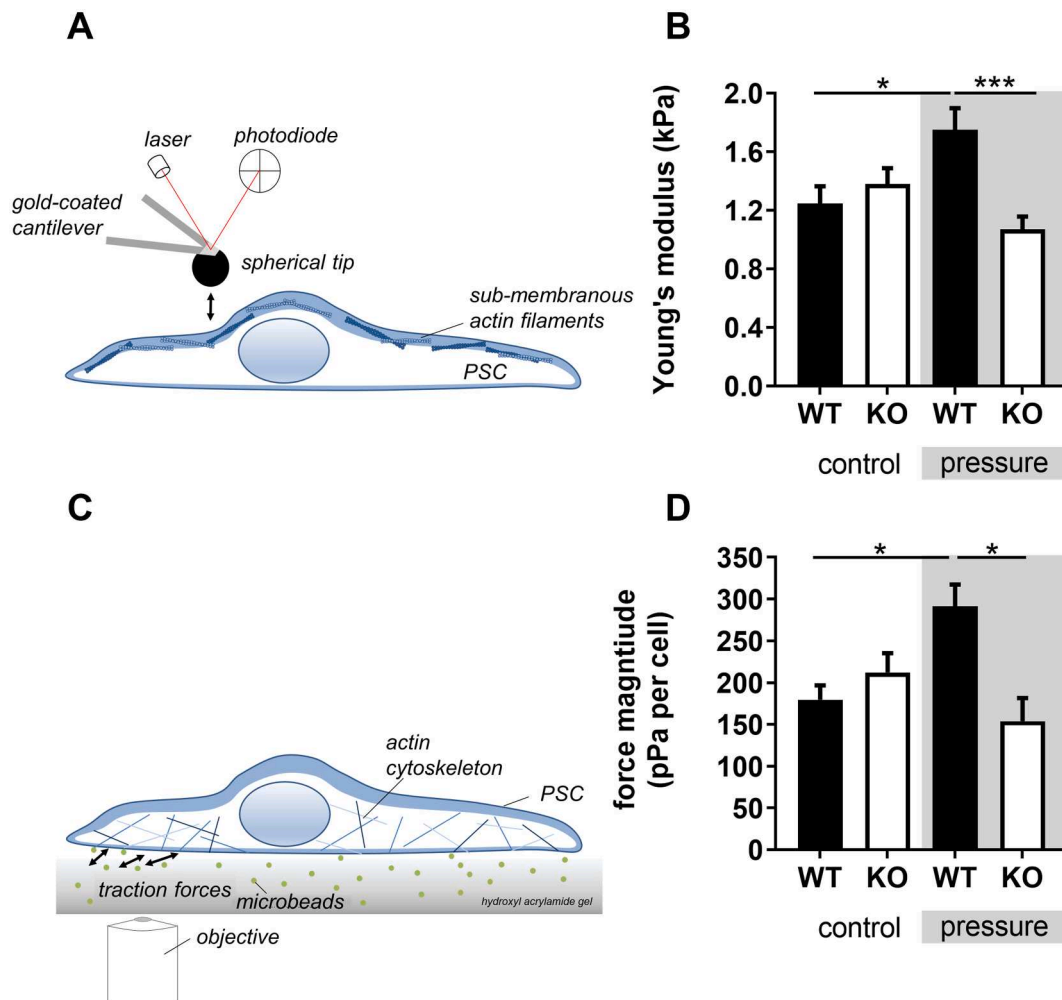


**Fig. 8.** Pressure incubation increases stiffness and traction forces TRPC1-dependently. A) Scheme of AFM measurements. After approaching the cell surface the flexible cantilever encounters the cortical actin layer. The bending of the cantilever is detected by a reflected laser beam on a photodiode. Analysis of force-distance curves evaluates distinct slopes, indicating actin cell mechanics. B) AFM-based measurements of cell stiffness reveal increased cortical stiffness in pressure-treated WT PSCs, but not in TRPC1-KO cells ( $N = 4-5$ ,  $n = 45-60$ ,  $*p < 0.05$ , WT vs. TRPC1-KO). C) Scheme of traction force microscopy. Traction forces are measured by quantifying the displacement of microbeads embedded in the underlying hydrogel. Cell traction on the gel is assessed by acquiring images of the gel/microbeads before and after removing the cell. D) Pressure-stimulated WT cells exert higher forces onto the underlying matrix than under control conditions. Traction forces of TRPC1-KO PSCs are not affected by pressurization ( $N = 3$ ,  $n = 8-11$ ,  $*p < 0.05$ , WT vs. TRPC1-KO).

The results shown in Fig. 8 clearly demonstrate that TRPC1 channels do not only contribute to sensing mechanical cues from the microenvironment. They also modulate the mechanical output of PSCs.

### 3. Discussion

PSC activation plays a crucial role in PDAC development and progression since the dense PSC-derived fibrotic stroma encloses the cancer cells and provides them with essential cytokines, growth factors, and nutrients indispensable for their early spreading [6,30]. This PSC-driven encapsulation is in part responsible for the 10-fold increased tissue pressure observed in PDAC which in turn activates and/or maintains PSC activation through a positive mechanical feedback cycle [31]. Therefore, it seems that interrupting the mechanical activation of PSCs might be a potential route in the battle against PDAC.

In the current study we highlighted the importance of TRPC1 channels in PSC activation and function. We focused especially on the impact of an elevated pressure which is a characteristic mechanical feature of PDAC microenvironment. We showed that TRPC1 channels mediate in part PSC activation under high pressure by promoting  $\alpha$ SMA expression in mouse and human PSCs (Figs. 1 & 4). In turn, the elevated pressure changes the mechanical behavior of PSCs themselves by increasing their stiffness and the emitted traction forces in a TRPC1-dependent manner (Fig. 8). We also reported for the first time that TRPC1 channels regulate  $\alpha$ SMA expression by cooperating with the phosphorylated form of SMAD2 (Figs. 2 & 3). Moreover, we demonstrated that TRPC1 modulates i) PSC proliferation via the G1/S and S/G2 cell cycle phase transition, and ii) IL-6 secretion, through an ERK1/2- and SMAD2-dependent pathway (Figs. 5, 6 & 7).

TRPC1 channels belong to the large family of TRP channels. They are non-selective cation channels that play among others a significant role in  $Ca^{2+}$  homeostasis, notably by regulating the Store-Operated Calcium Entry (SOCE) in association with Orai1 and STIM1 proteins, and they are relevant in the metastatic cascade in cancer [32–34]. However controversial debate evidence shows that TRPC1 mediates  $Ca^{2+}$  influx not only following an endoplasmic reticulum  $Ca^{2+}$  depletion promoting SOCE but also in response to mechanical stimulation in several cell types [35–39]. Indeed, more recently we showed that SOCE through Orai1 channels plays a crucial role in the modulation of PSC activation in PDAC [40]. In addition, we previously demonstrated that TRPC1 drives  $Ca^{2+}$  influx into murine PSCs in response to an elevated ambient pressure supporting the evidence that TRPC1 is involved in mechanosensation [19]. We confirmed these data for pre-activated human PSCs, showing the increased functional expression of TRPC1 under elevated pressure conditions (Fig. 4). Nevertheless, it will be interesting to evaluate in future studies whether TRPC1 channels could have a dual role in PSC by participating also in the SOCE through their interaction with Orai1 and/or STIM1 proteins leading to the regulation of PSC activation.

More importantly, we revealed that TRPC1 channels contribute to the altered cell functions in response to the pressure stimulus. The increased hydrostatic pressure renders WT-PSCs stiffer in a TRPC1-dependent manner. Such cell stiffening in response to elevated hydrostatic pressure has also been shown in endothelial cells. This was linked to  $Ca^{2+}$ -mediated myosin activation and increased actin polymerization driven by mechanosensitive ion channels. The molecular nature of these channels, however, remained elusive [41]. Furthermore, we demonstrated that this TRPC1-mediated PSC stiffening following pressurization is accompanied by higher tension forces exerted by PSCs to the surrounding extracellular matrix (ECM) (Fig. 8). These changes of PSC mechanics might lead to mechanical reorganization of the PDAC microenvironment, and thus further promote PDAC progression. This idea is supported by previous observations from our laboratory. Activation of Piezo1, a mechanosensitive channel, leads also to increased PSC-induced tension on the surrounding ECM that facilitates PSC migration and detachment [42]. Our present study provides mechanistic

insight into how TRPC1 channels mediate these cellular mechanical changes in PSCs in response to pressure.

We observed that the increasing hydrostatic pressure clearly accelerates the initial activation of murine PSCs within the first 48h as evidenced by the increasing expression of  $\alpha$ SMA, which is considered as the main activation marker of PSCs [6]. At later time points the effect of elevated pressure levels off so that control and pressurized PSCs reach the same level of activation (Fig. 1). This can be explained by the *ex vivo* activation of freshly isolated PSCs that is triggered by the stiff substrate of cell culture dishes and the ensuing positive autocrine feedback stimulation of activated PSCs [26,43]. Notably, the pressure-induced acceleration of the activation is absent in TRPC1-KO PSCs. So far, there is few evidence of which mechanosensory proteins play a role in the activation of quiescent PSCs [44]. Based on our results, TRPC1 channels are also one of the mechanosensory proteins driving at least in part the transdifferentiation of quiescent to activated PSCs in response to altered mechanical conditions. Moreover, TRPC1-mediated PSC activation through the expression of  $\alpha$ SMA might also participate in the reorganization of  $\alpha$ SMA into stress fibers, which could explain in part how TRPC1 channels mediate PSC stiffening and -increased traction forces in response to pressurization.

TRPC1 channels regulate  $\alpha$ SMA expression in human PSCs by physically interacting with  $\alpha$ SMA. This protein network is supported by the phosphorylated (= active) form of SMAD2 that colocalizes and physically associates with both TRPC1 and  $\alpha$ SMA. Interestingly, the knock-down of one of these three proteins each has a varying effect on the interaction of the remaining 2 partners. This argues for a different degree of participation of each partner within the complex. Consequently, TRPC1 silencing leads to a reduction of SMAD2 phosphorylation as well, suggesting that it acts as a positive upstream regulator of the SMAD2 pathway (Fig. 2 & 3). This latter is one of the major signaling pathways that control PSC activation, mainly through the regulation of  $\alpha$ SMA expression [25]. Thus, we revealed for the first time that TRPC1 mediates/maintains PSC activation by regulating  $\alpha$ SMA expression through its interaction with the TRPC1-dependently phosphorylated form of SMAD2.

Besides the high  $\alpha$ SMA expression, activated PSCs are characterized by an increased proliferative and secretory potential [1,3]. In the present work, we revealed that inhibition of TRPC1 channels results in a decrease of PSC proliferation. The involvement of TRPC1 in the regulation of cancer cell proliferation is well described [45,46]. Knowledge on its role in cancer-associated fibroblasts, i.e. also in PSCs has been missing so far. We showed that TRPC1 channels regulate the proliferation of PSCs by controlling the cell cycle progression in G1 and G2 phases (Fig. 6).

Furthermore, we noted that TRPC1 knock-down in human PSCs decreases IL-6 secretion. The impact on IL-6 secretion by TRPC1 channels is even more pronounced when mouse PSCs are exposed to increased pressure. IL-6 is a very important pro-inflammatory cytokine in PDAC. High IL-6 concentrations have been found in PDAC cell lines but also in the serum of patients with PDAC. The elevated IL-6 serum level is correlated with PDAC severity [16,47,48]. In addition, secretion of IL-6 by the activated PSCs promotes pancreatic cancer cell migration and epithelial-mesenchymal transition [49,50]. Here, we showed that the secreted IL-6 can also impact PSC activation through an IL-6-mediated positive autocrine feedback loop. Treatment with IL-6 augments TRPC1-dependently PSC migration velocity which is accompanied by the acquisition of a more elongated cell shape (Fig. 7).

All these PSC activation processes are coordinated and controlled by multiple dynamic intracellular signaling pathways [28]. According to our results, TRPC1 channels are crucial for the activation of two of the major signaling pathways underlying PSC activation: the ERK1/2 and SMAD2 pathways. Our data highlight the involvement of TRPC1 in the regulation of PSC proliferation and IL-6 secretion through the activation of both ERK1/2 and SMAD2 pathways (Fig. 5, 6 & 7). Such a role of TRPC1-mediated ERK1/2 and SMAD2 pathways has not been known in

the modulation of IL-6 secretion.

#### 4. Conclusion

In conclusion, our study discloses the importance of TRPC1 channels through their mechanosensing ability in PSC activation. Many of the TRPC1-dependent effects appear to involve ERK1/2 and SMAD2-dependent pathways. We suppose that TRPC1 might regulate these two pathways in a  $\text{Ca}^{2+}$ -dependent and/or a  $\text{Ca}^{2+}$ -independent manner. The ERK1/2 pathway is often activated by the  $\text{Ca}^{2+}$ /calmodulin complex, whereas the SMAD2 pathway has been shown to be inactivated by this complex [51]. Furthermore, we showed that TRPC1 channels colocalize and interact physically with  $\alpha$ SMA and the phosphorylated active form of SMAD2, resulting in the regulation of  $\alpha$ SMA expression. More importantly, we demonstrated that high pressure increases transiently TRPC1 expression leading to a further promotion of PSC proliferation,  $\alpha$ SMA expression and IL-6 secretion in the sense of a positive feedback. This positive feedback cycle also involves the TRPC1-dependent mechanical output of PSCs (Fig. 9). Although not shown in the current study it is conceivable that increased tension exerted by PSCs onto the extracellular matrix contributes to maintaining their mechanical activation. Finally, the increased tension could ease the migration and invasion of pancreatic cancer cells along the straightened matrix fibers. In such a scenario TRPC1 channels in PSCs would ultimately contribute to PDAC progression.

#### 5. Materials and methods

##### 5.1. Animals

Experiments were performed with primary murine pancreatic stellate cells (PSCs). PSCs were isolated from 8-12 weeks old male/female 129Sv/C57BL/6J WT and TRPC1-KO mice [52]. Experimental protocols

were approved by the local committee for animal care (ref no. 84-02.05.50.15.010).

##### 5.2. Isolation of murine PSCs

Primary murine pancreatic stellate cells were isolated as described previously [19,53]. Mice were anaesthetized with isoflurane and sacrificed by subsequent cervical dislocation. The pancreata were removed and briefly washed in cold balanced salt solution (GBSS, Pan-Biotech GmbH) before homogenization. Homogenates were then transferred to 3 mL GBSS with 0.1 % collagenase P (Roche Applied Science) and incubated at 37°C for 25 min on a shaker. After re-suspending and adding GBSS to a final volume of 8 mL cells were centrifuged (8 min, 220 x g), re-suspended in pre-warmed cell culture media (DMEM/F12, Sigma Aldrich; 10 % Fetal Calf Serum-Gold, GE-Healthcare; 1 % penicillin/streptomycin, Biochrom) and seeded onto a FCS-Gold-coated tissue culture dish. Cells were incubated for 2h in the incubator, with subsequent forceful washing steps with warm culture media. After each washing step cells were observed under the microscope to ensure optimal purity. Freshly isolated PSCs were incubated for 5-6 days until first passaging. Cells were used for experiments after two passages. Experiments analyzing the pressure effect on the initial activation of PSCs were done with freshly isolated PSCs within 6h after the isolation.

##### 5.3. PSC cell lines

Activated human pancreatic stellate cell line, PS-1 was obtained from a healthy donated human pancreas and immortalized as previously described [54]. PS-1 cells were kindly provided by Pr Hemant M. Kocher, from the Queen Mary University of London. Cells were cultured in Dulbecco's Modified Eagle Medium/Nutrient Mixture F-12 (DMEM/F12, Gibco, Thermo Fischer Scientific, France) supplemented with 10 % of Fetal Bovine Serum (FBS, Pan Biotech, Dominique

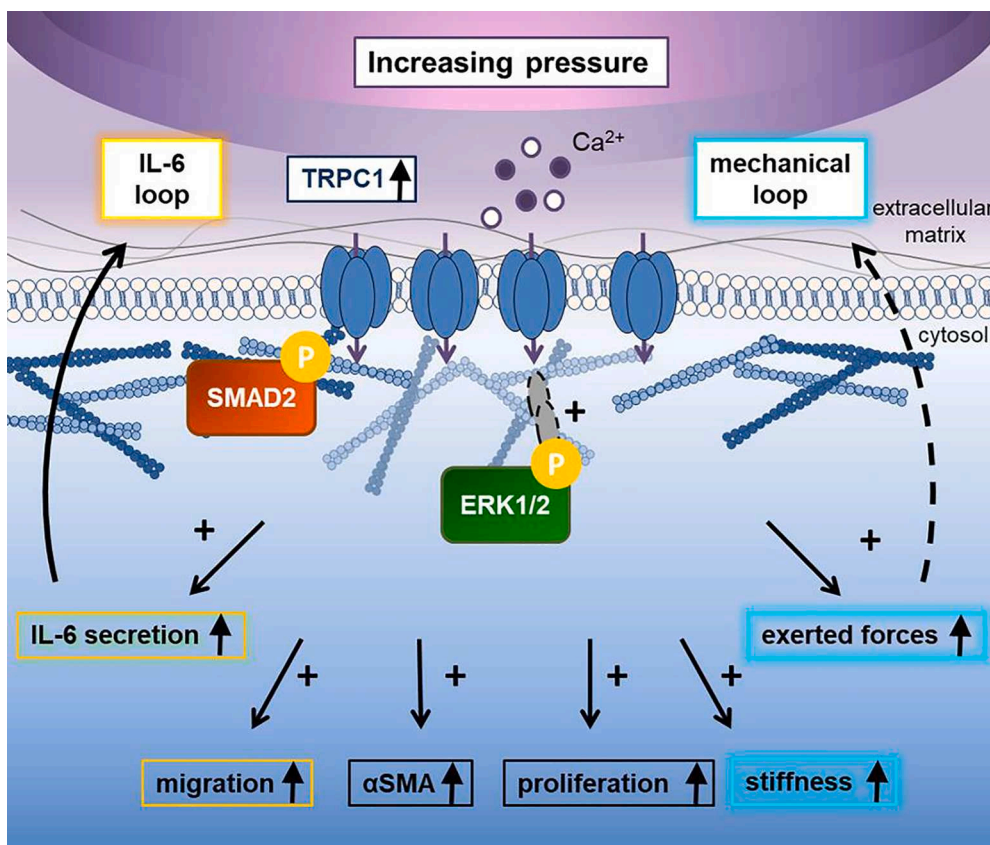


**Fig. 9.** Conclusive scheme: Increased hydrostatic pressure enhances TRPC1 channel expression and activation resulting in an increased  $\text{Ca}^{2+}$  influx into PSCs. Pressure-mediated TRPC1 activation modulates PSC activation by promoting  $\alpha$ SMA expression and PSC proliferation in cooperation with the phosphorylated form of SMAD2. Moreover, the increased pressure promotes TRPC1-mediated IL-6 secretion through an ERK1/2 and SMAD2-dependent pathway, which in turn accelerates PSC migration forming an IL-6 mediated autocrine feedback loop. Furthermore, PSCs increase their cellular stiffness, migratory capacities, and exerted tension forces in response to the elevated pressure in a TRPC1-dependent manner, forming a mechanical feedback loop.

Dutscher, France). PS-1 were kept at 37°C in a humidified atmosphere with 5% CO<sub>2</sub> and cell culture medium was changed every 48 hours.

#### 5.4. Cell transfection and RNA interference

Small interfering RNAs (siRNA) were introduced into cells by electroporation, using the nucleofection technology (Amaxa Biosystems, Lonza, Aubergenville, France). 10<sup>6</sup> cells were transfected according to the manufacturer's protocol with 4 µg of scrambled siRNA as control (*siCtrl*: duplex negative control, Eurogentec), or with siRNA directed against *TRPC1* (*siTRPC1*, ON-TARGET plus SMART pool siRNA, Dharmacon Research, Chicago, IL), *α-SMA* (*siaSMA*: 5'-GGGCU-GUUUCCCAUCCAU-3', Eurogentec) or *Smad2* (*siSmad2*: 5'-GUCCCAUGAAAAGACUAAA-3', Eurogentec). Cells were used for the experiments 72h after the siRNA transfection.

#### 5.5. Chemical reagents

Pharmacological inhibitors used to study the signaling pathways, after 72h of treatment, were the following: U 0126 monoethanolate (10 µM, 72h, Sigma-Aldrich) and SB 431542 (80 µM, 72h, Sigma-Aldrich).

#### 5.6. Pressure incubation

Pressure incubation of WT and TRPC1-KO PSCs was performed in a custom-made pressure chamber at +100 mmHg / +13.3 kPa above ambient atmospheric pressure (760 mmHg / 101.3 kPa) for at least 24h and up to 120h. A 29lexiglas chamber, fitting into a standard cell culture incubator, was pressurized with a humidified atmosphere using an air pump system and monitored continuously with a digital barometer. For control experiments, cells were incubated in the same chambers at atmospheric pressure (760 mmHg / 101.3 kPa). Increasing the ambient pressure in the chamber by 13 % (with respect to the atmospheric pressure) produces no measurable changes of the medium pH [19].

#### 5.7. Cell proliferation assay

MTT colorimetric assay was used to assess the cell proliferation using 6-well plates (8 × 10<sup>4</sup> seeded PS-1 cells per well), 72 hours post siRNA transfection or post pharmacological treatment with inhibitors. The 3-(4,5-dimethylthiazol-2-yl)-2,5-diphenyltetrazolium bromide (MTT, Sigma-Aldrich, Inc.) was solubilized in culture medium (0.5 mg/mL), before cell incubation at 37°C in the dark for 45 min. Once entered in the cells, MTT is converted to formazan crystals, which are thereafter dissolved by culture medium replacement with dimethyl sulfoxide (DMSO, Sigma-Aldrich, Inc.) giving a violet staining. The absorbance was read at 550 nm using the Infinite® 200 Pro reader (Tecan Trading AG).

#### 5.8. Cell cycle analysis

Cell cycle evaluation was performed by quantifying the cellular DNA content by means of flow cytometry. 72h siTRPC1 or siCtrl transfected cells (1 × 10<sup>6</sup>) were fixed with cold absolute ethanol (≥ 99.8%, Sigma-Aldrich) at 4°C for a minimum of 6h. Then they were pelleted, resuspended in 5 mM EDTA / PBS, treated with 20 mg/mL RNase A (Sigma-Aldrich) at room temperature for 30 min, and stained with propidium iodide (50 mg/mL, Sigma-Aldrich). Thereafter, samples were directly analyzed by flow cytometer (Accuri®) and the cell percentage in each cell cycle phase was determined using the Cyflog software.

#### 5.9. Cell mortality

Trypan Blue exclusion assay was used to evaluate PS-1 cell death. Cells were seeded in 35 mm petri-dishes (8 × 10<sup>4</sup> cells) for 72h after siRNA transfection. Then they were trypsinized, diluted in Trypan Blue solution (Sigma-Aldrich) and counted six times using Malassez's cell

counting method. Cell mortality was determined using the formula below: rate of cell death = number of dead cells / number of total cells, normalized to each control condition.

#### 5.10. Apoptosis analysis

The cell surface exposure of phosphatidylserine on the outer leaflet of the plasma membrane was utilized to assess apoptosis, since this is an early marker of apoptotic cell death. Cells (detached and adherent cells) were collected 72h after the siRNA transfection, pelleted, washed twice with ice-cold PBS and resuspended in 1 × binding buffer (BD Biosciences Pharmingen). Following the PE Annexin V Apoptosis Detection Kit staining protocol (BD, Biosciences Pharmingen), we added FITC Annexin V and propidium iodide (PI) to the cell preparations and incubated them at 25°C in the dark for 15 min. Binding buffer was then added to each tube and samples were directly analyzed by the flow cytometer (Accuri®) in order to determine the percentage of apoptotic cells. The following controls were used to set up the compensation and quadrants: unstained cells, cells stained only with FITC Annexin V and cells stained only with PI.

#### 5.11. Migration assay

In order to evaluate whether the cytokine secretion of PSCs causes their autocrine activation, we performed live-cell imaging experiments to monitor PSC migration as described previously [19]. PSCs were seeded in coated tissue culture flasks (~27.000 cells per flasks, 12.5 cm<sup>2</sup>) as described before [55]. The matrix coating mimics desmoplastic regions in PDAC. Polymerization of the desmoplastic matrix was done overnight in the tissue culture incubator prior to seeding PSCs. Prior to the experiment, culture medium was changed to HEPES-buffered RPMI (Sigma-Aldrich) without or with addition of IL-6 (10 ng/µL), flasks were sealed and transferred to preheated (37°C) microscopy chambers. Cell migration was recorded over 6h in 5 min intervals using time-lapse video microscopy. Afterward cell outlines were segmented with the Amira Imaging Software Version 2.2 (Template Graphics Software, Mercury Communication Systems, Carlsbad, US), a self-made Java program and the National Institutes of Health Image J Software (<http://rsb.info.nih.gov/ij/>). Based on segmented cell contours, migratory velocity (in µm/min) was calculated as the movement of the cell center as a function of time. To evaluate the effect on cell morphology, structure index was calculated. More circular PSCs have an index close to 1 and more elongated, star-shaped cells tend towards 0.

#### 5.12. Western blot and Co-immunoprecipitation

RIPA buffer (1% Triton X-100, 0.1% sodium deoxycholate, 150 mM NaCl, 10 mM PO<sub>4</sub>Na<sub>2</sub>/K, pH=7.4) supplemented with protease inhibitor cocktail (Sigma-Aldrich), 5 mM sodium orthovanadate and 2 mM EDTA, was added to lyse the cells. Thereafter, the Bicinchoninic Acid protein assay (Bio-Rad) was utilized to determine the protein concentration of the sample. Each sample was loaded (30µg of protein lysate were used for standard Western blotting) and separated by the denaturing SDS-PAGE, and then transferred onto nitrocellulose membrane (Hybond, GE Healthcare). Blocking of the nonspecific binding sites was done with 3% bovine serum albumin at room temperature for at least 1h, followed by overnight incubation of the membranes with the primary antibody at 4°C. The primary antibodies used were anti-TRPC1 (1:1000, Abcam, #ab51255), anti-αSMA (1:1000, Abcam, #ab7817), anti-GAPDH (1:4000, Abcam, #ab8245), anti-SMAD2 (1:1000, Abcam, #ab40855), anti-p-SMAD2 (phospho S255) (1:1000, Abcam, #ab188334), anti-ERK1/2 (1:500, Cell Signaling, #9102), anti-p-ERK1/2 (Thr202/Tyr204) (1:500, Cell Signaling, #9101), anti-Akt (1:500, Cell Signaling, #9272) and anti-p-Akt (Ser473) (1:500, Cell Signaling, #9271). The secondary antibodies used, were coupled to horseradish peroxidase, leading to protein band detection through an enhanced



chemiluminescence kit (Ozyme). The Bio-Rad image acquisition software (Quantity One) was used for the quantification of protein bands via a densitometric analysis option, and all the results were normalized to GAPDH as reference protein.

For co-immunoprecipitation experiments, precleared protein A sepharose magnetic beads (Millipore, PureProteome™) were incubated with 500 µg of protein lysate (per condition) at 4°C for 90 min. The beads were then removed, and the samples were incubated with the primary antibody at 4°C overnight. The dilutions of primary antibodies used for the co-immunoprecipitation experiments were anti-TRPC1 and anti-p-SMAD2 (phospho S255) 1 :100 (Abcam) and for anti- $\alpha$ SMA 1 :200 (Abcam). The next day the antigen-antibody complex was precipitated with protein A sepharose magnetic beads (Millipore, PureProteome™) at 4°C for 1h. After denaturation, proteins were used as for standard Western blot.

### 5.13. Immunostainings

**Primary murine PSCs:** Directly after isolation PSCs were seeded onto poly-L-lysine coated coverslips (30.000 cells on 20 mm coverslips). They were given a 2h time period for adhesion. This time point, in total 6h after the isolation of pancreata, marked the starting point ( $t = 0$ h) of the experiments which examined the time course of PSC activation. PSCs fixed at  $t = 0$ h were considered as quiescent PSCs. Samples from the control group (ambient pressure) and the pressurized group were collected at  $t = 24$ h, 48h, 72h and 120h.

PSCs were washed twice with PBS and fixed with 3.5 % paraformaldehyde at room temperature for 1h. Fixation was stopped with 0.1 mM glycine for 10 min. For Vitamin A stainings, cells were incubated with 25 µM Nile Red in a wet chamber for 15 min as described earlier [53]. After washing with PBS, cell nuclei were stained with DAPI (1 µg/mL), and coverslips were mounted on glass slides.

For  $\alpha$ SMA stainings, fixed PSCs were rinsed with PBS and permeabilized using 0.5 % Triton-X100 in PBS for 10 min. PSCs were blocked with 10 % normal goat serum for 1h and subsequently incubated with the primary antibody against  $\alpha$ SMA (anti-mouse, 1:400 in blocking solution, Sigma Aldrich, #A2547) overnight at 4°C. The coverslips were then washed with PBS and incubated with appropriate secondary Alexa488-conjugated antibody (1:400 in blocking solution for 1h). Cell nuclei were stained with DAPI (1 µg/mL), and coverslips were mounted on glass slides. For image acquisition we used an Axiovert 200 microscope (40 x) connected to a RT-SE-Spot camera (Visitron Systems) and controlled by Metaview software.

**PS-1 cells:** They were first gently washed twice with PBS solution (pH=7.4, Sigma-Aldrich) and then fixed using 4 % paraformaldehyde diluted in PBS at room temperature for 20 min. Cells were after permeabilized with 0.1 % of saponin diluted in PBS for 10 min, washed three times with PBS, blocked with 5 % bovine serum albumin diluted in PBS (blocking solution) for 45 min and then incubated with the primary antibody at 4°C overnight. We used the following primary antibodies: anti-TRPC1 (1:200; Alomone Labs - anti-rabbit, #ACC-010) and anti-TRPC1 (1:50; Santa Cruz – anti-mouse, #sc-133076), anti-p-SMAD2 (phospho S255; 1:200; Abcam, #ab188334) and anti- $\alpha$ SMA (1:1000; Abcam, #ab7817). Thereafter, the coverslips were incubated at room temperature with the secondary antibody for 45 min. For TRPC1 (anti-rabbit) and p-SMAD2 detection, a secondary AlexaFluor® 550 conjugated antibody (1:200; IgG DyLight, Thermo Fischer Scientific, # 84541) was used, and for  $\alpha$ SMA and TRPC1 (anti-mouse) detection, a secondary AlexaFluor® 488 conjugated antibody (Invitrogen, # A-11029) was used at 1:1000 and 1:50 dilution, respectively. Both, primary and secondary antibodies were diluted in the blocking solution. The immunofluorescence staining was made in a sequential way for the double labeling. At the end DAPI (1 µg/ml, Sigma-Aldrich) staining was used to mark the nucleus, before mounting coverslips on glass slides. The fluorescence image acquisition was made with a confocal microscope LSM710 and ZEN software (Carl Zeiss Microimaging) and images were

analyzed with Fiji Image J software.

### 5.14. Cytokine quantification

For quantification of cytokine secretion, cell culture supernatants of pressurized and control WT and TRPC1-KO PSCs (pre-activated, passage 2 after isolation) were collected after 24h of stimulation. The concentration of the pro-inflammatory cytokine interleukin-6 (IL-6) was measured with the LEGENDplex Kit (Biolegend) according to the manufacturer's instructions as described before [56].

PS-1 cell culture supernatants were collected 72h after siRNA transfection or treatment with the pharmacological inhibitors and used for enzyme-linked immunosorbent assay (ELISA) to quantify IL-6. IL-6 supernatant concentration was measured based on the technical protocol provided by the suppliers (Invitrogen, # 88-7066-86). The absorbance obtained by the colorimetric reaction revealing IL-6 quantity in the supernatant was measured at 450 nm.

### 5.15. $Ca^{2+}$ influx measurements

$Ca^{2+}$  influx into the cells was quantified using the  $Mn^{2+}$  quench technique as described before [19,42,55,57].  $Mn^{2+}$  influx largely mimics  $Ca^{2+}$  entry as it enters cells via similar pathways. In contrast to  $Ca^{2+}$  ions,  $Mn^{2+}$  ions quench the fluorescence emission of the  $Ca^{2+}$  sensitive dye Fura-2 AM which we employed for these experiments. The  $Mn^{2+}$ -induced decrease of the Fura-2 AM fluorescence intensity is largely proportional to the transmembrane influx of  $Ca^{2+}$ .

PS-1 cells were stained with 6 µM of the  $Ca^{2+}$  indicator Fura-2-AM (#F1221, Thermo Fisher Scientific, Inc., Waltham, US) at 37°C in HEPES buffered solution for 20 min. PS-1 were visualized using an ionic imaging setup consisting of a fluorescence microscope, a high-speed shutter and a polychromator (Visitron Systems, Puchheim, Germany). The proper isosbestic excitation wavelength, at which the emission is  $Ca^{2+}$  independent, was determined in pilot experiments to be 357 nm and fluorescence emission was recorded at 510 nm. Images were acquired in 10 sec intervals. Each experiment started with an initial 3 min incubation in Ringer's solution, followed by another 3 min incubation in a  $Ca^{2+}$ -free,  $Mn^{2+}$  supplemented Ringer's solution ( $Mn^{2+}$  Ringer's). The  $Mn^{2+}$  concentration in  $Mn^{2+}$  Ringer's was 400 µM.

Data analysis was performed by measuring fluorescence intensities over the whole cell area and correcting it for background fluorescence. The extracted fluorescence intensity  $F$  was normalized to the initial fluorescence intensity  $F_0$  determined under control conditions in the presence of Ringer's solution ( $F/F_0$ ). For each cell, the slope of linear regression ( $\Delta F/F_0/\text{min}$ ) was calculated before and after  $Mn^{2+}$  application over intervals of 30 sec. Subsequently, the slope after  $Mn^{2+}$  application was subtracted by the slope in the presence of Ringer's solution to correct for potential photobleaching. The inverse value of the  $Mn^{2+}$  quench was determined which directly correlates with  $Ca^{2+}$  influx.

### 5.16. Atomic force microscopy (AFM)

AFM measurements were performed using a Nanowizard III microscope (JPK Instruments) equipped with the SmallCell™ closed liquid cell (JPK Instruments). The elasticity of PSCs was measured by nano-indentation spectroscopy [58]. We used silicon nitride gold-coated cantilevers (Novascan Technologies) with 10 µm polystyrene spherical probes (0.03 N/m nominal spring constant) for all experiments. Cantilevers were manually calibrated prior to each measurement.

Force-distance curves were obtained with a tip velocity of 1 µm/s and loading forces of 300 pN. We analyzed the first 100 nm strain of the force-indentation curve, as this part is known to correspond to the cortical actin cytoskeleton [59,60]. Eight to ten force-distance curves were obtained for each cell, and 15 cells were measured in each experiment (4 to 5 repeated experiments). Elasticity values were calculated from force-distance curves with the Protein Unfolding and

Nano-Indentation Analysis Software PUNIAS3D version 1.0 release 2.3 and data were presented as absolute data values ('Young's modulus').

### 5.17. Traction Force Microscopy

Traction Force Microscopy (TFM) quantifies the forces imposed by the cells onto the surrounding matrix. PSCs were seeded on hydroxyl acrylamide gels with a calculated stiffness of 10 kPa. The hydroxyl acrylamide gels contained  $2 \times 10^7$  microbeads per mL (FluoSpheres 1  $\mu$ m, Invitrogen, Carlsbad, USA) to monitor matrix traction. Gels were crosslinked to Poly-L-Lysin by using the UV-light activated Sulfo-SANPAH (0.5 mg/mL, Sigma Aldrich). After seeding, PSCs were incubated in a humidified pressure chamber for 24h, as described [19]. Fluorescence images of the embedded microbeads were taken with a Zeiss Axiovert 25 microscope. The traction force can be measured by deformations caused by adherent stellate cells which are recorded by taking images of the gel/microbeads before and after removing the cell with 0.05 % trypsin. Image analysis quantifies the beads displacement using the particle image velocimetry (PIV) method as described [61].

### 5.18. Statistical analysis

All data are presented as mean values ( $\pm$  S.E.M), with n corresponding to the number of cells and N referring to the number of cell passages or mice. All experiments were realized at least with three different cell passages or with cells from at least three mice. Tests for normality (unpaired Student's *t* test), one-way ANOVA or two-way ANOVA performed with Tukey's or Bonferroni post hoc test, for multiple comparisons, depending to the compared conditions, were applied using GraphPad Prism version 5 or 7. Statistical significance was assumed when  $p < 0.05$ .

### Author contributions

**Silviya Radoslavova:** Conceptualization, Performing experiments and data analysis, Investigation, Writing-original draft preparation, Writing-review and editing

**Benedikt Fels:** Conceptualization, Performing experiments and data analysis, Investigation, Writing-original draft preparation, Writing-review and editing

**Zoltan Pethő:** Conceptualization, Performing experiments and data analysis, Investigation

**Matthias Gruner:** Performing experiments and data analysis

**Tobias Ruck:** Performing experiments and data analysis

**Sven G. Meuth:** Performing experiments and data analysis

**Natalia Prevarskaya:** Conceptualization, Investigation, Writing-review and editing, Study supervision

**Albrecht Schwab:** Conceptualization, Investigation, Writing-review and editing, Study supervision

**Halima Ouadid-Ahidouch:** Conceptualization, Investigation, Writing-review and editing, Study supervision

### Conflicts of Interest Statement

Manuscript title: TRPC1 channels regulate the activation of pancreatic stellate cells through ERK1/2 and SMAD2 pathways and perpetuate their pressure-mediated activation

The authors whose names are listed immediately below certify that they have NO affiliations with or involvement in any organization or entity with any financial interest (such as honoraria; educational grants; participation in speakers' bureaus; membership, employment, consultancies, stock ownership, or other equity interest; and expert testimony or patent-licensing arrangements), or non-financial interest (such as personal or professional relationships, affiliations, knowledge or beliefs) in the subject matter or materials discussed in this manuscript.

### Author names

Silviya Radoslavova, Benedikt Fels, Zoltan Pethő, Matthias Gruner, Tobias Ruck, Sven G. Meuth, Antoine Folcher, Natalia Prevarskaya, Albrecht Schwab and Halima Ouadid-Ahidouch. The authors declare that they have no interest of any kind affecting this study.

### Author contributions

Conceptualization: S.R, B.F, Z.P, N.P, A.S and H.O-A, performing experiments and data analysis: S.R, B.F, Z.P, M.G, T.R, and S.M, investigation: S.R, B.F, Z.P, N.P, A.S and H.O-A, writing-original draft preparation: S.R and B.F, writing-review and editing: S.R, B.F, N.P, A.S and H.O-A, study supervision: N.P, A.S and H.O-A. All authors have read and agreed to the published version of the manuscript.

### Declaration of Competing Interest

The authors declare that they have no interest of any kind affecting this study.

### Data Availability

Data are contained within the article and supplementary materials

### Acknowledgments

We acknowledge the Région Hauts-de-France (Picardie), the FEDER (Fonds Européen de Développement Économique Régional), the Université de Picardie Jules Verne, the Ministère de l'Enseignement Supérieur et de la Recherche, the Cancéropôle Nord-Ouest (CNO) and the Ligue contre le cancer (SEPTENTRION) for supporting this study. We thank the Pr H.M. Kocher and his laboratory members from the Queen Mary University of London, for kindly providing us the PS-1 cell line, used for this study. A.S acknowledges support from IZKF Münster (Schw2/020/18) and Deutsche Forschungsgemeinschaft SCHW 407/22-1.

### Supplementary materials

Supplementary material associated with this article can be found, in the online version, at [doi:10.1016/j.ceca.2022.102621](https://doi.org/10.1016/j.ceca.2022.102621).

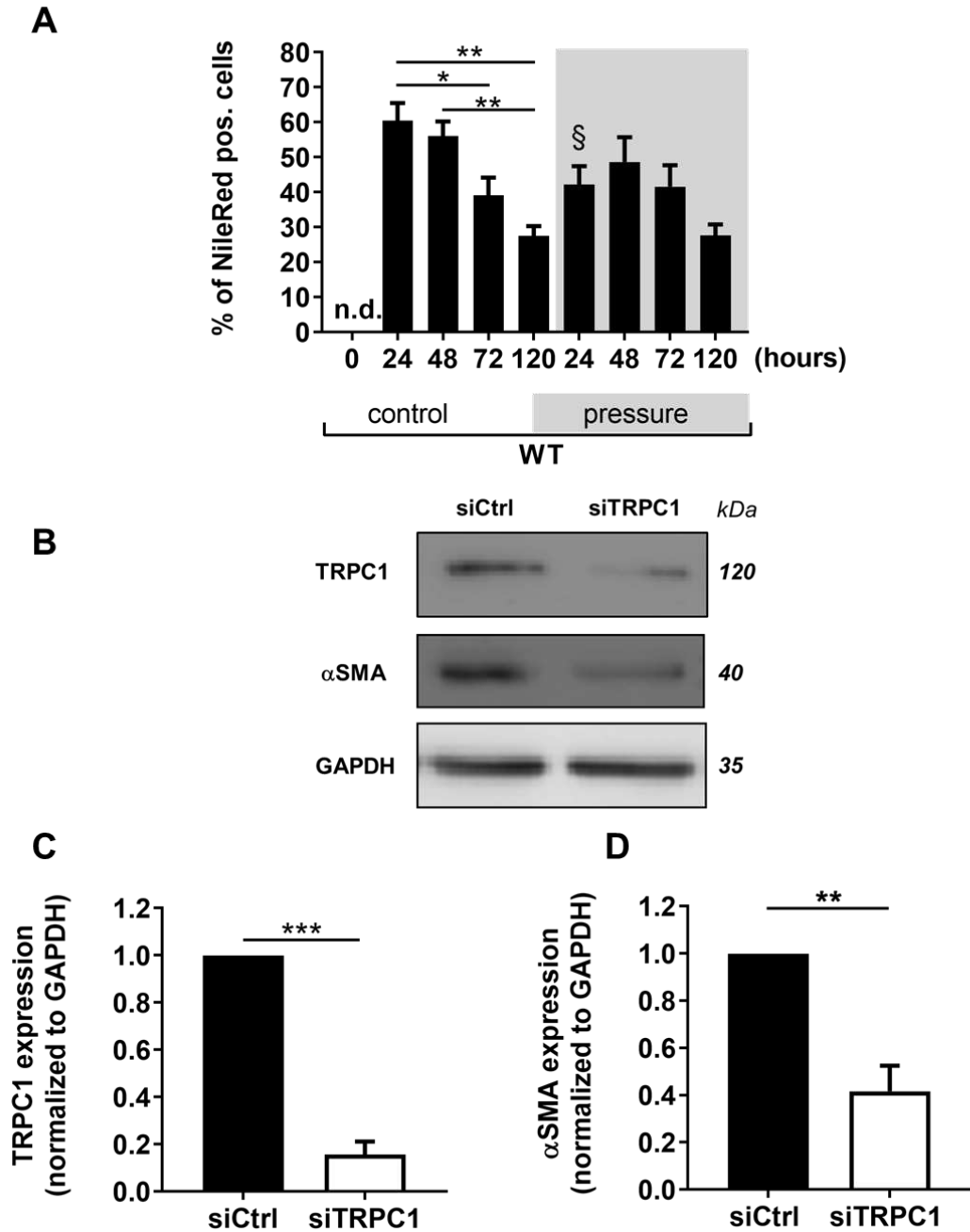
### References

- [1] M.V. Apte, R.C. Pirola, J.S. Wilson, Pancreatic stellate cells: a starring role in normal and diseased pancreas, *Front Physiol* 3 (2012), <https://doi.org/10.3389/fphys.2012.00344>.
- [2] R. Jaster, J. Emmrich, Crucial role of fibrogenesis in pancreatic diseases, *Best Pract Res Clin Gastroenterol* 22 (2008) 17–29, <https://doi.org/10.1016/j.bpg.2007.10.004>.
- [3] D. Thomas, P. Radhakrishnan, Pancreatic Stellate Cells: The Key Orchestrator of The Pancreatic Tumor Microenvironment, in: A. Birbrair (Ed.), *Tumor Microenvironment: Non-Hematopoietic Cells*, Springer International Publishing, Cham, 2020, pp. 57–70, [https://doi.org/10.1007/978-3-030-37184-5\\_5](https://doi.org/10.1007/978-3-030-37184-5_5).
- [4] A. Masamune, T. Shimosegawa, Pancreatic stellate cells – Multi-functional cells in the pancreas, *Pancreatol* 13 (2013) 102–105, <https://doi.org/10.1016/j.pan.2012.12.058>.
- [5] P.E. Ferdek, M.A. Jakubowska, Biology of pancreatic stellate cells-more than just pancreatic cancer, *Pflugers Arch* (2017), <https://doi.org/10.1007/s00424-017-1968-0>.
- [6] M.V. Apte, J.S. Wilson, A. Lugea, S.J. Pandol, A starring role for stellate cells in the pancreatic cancer microenvironment, *Gastroenterology* 144 (2013) 1210–1219, <https://doi.org/10.1053/j.gastro.2012.11.037>.
- [7] R.R. Bynigeri, A. Jakkampudi, R. Jangala, C. Subramanyam, M. Sasikala, G.V. Rao, D.N. Reddy, R. Talukdar, Pancreatic stellate cell: Pandora's box for pancreatic disease biology, *World J Gastroenterol* 23 (2017) 382–405, <https://doi.org/10.3748/wjg.v23.i3.382>.
- [8] H. Aoki, H. Ohnishi, K. Hama, S. Shinozaki, H. Kita, H. Yamamoto, H. Osawa, K. Sato, K. Tamada, K. Sugano, Existence of autocrine loop between interleukin-6

- and transforming growth factor-beta1 in activated rat pancreatic stellate cells, *J Cell Biochem* 99 (2006) 221–228, <https://doi.org/10.1002/jcb.20906>.
- [9] H. Aoki, H. Ohnishi, K. Hama, T. Ishijima, Y. Satoh, K. Hanatsuka, A. Ohashi, S. Wada, T. Miyata, H. Kita, H. Yamamoto, H. Osawa, K. Sato, K. Tamada, H. Yasuda, H. Mashima, K. Sugano, Autocrine loop between TGF-beta1 and IL-1beta through Smad3- and ERK-dependent pathways in rat pancreatic stellate cells, *Am J Physiol Cell Physiol* 290 (2006) C1100–C1108, <https://doi.org/10.1152/ajpcell.00465.2005>.
- [10] A. Allam, A.R. Thomsen, M. Gothwal, D. Saha, J. Maurer, T.B. Brunner, Pancreatic stellate cells in pancreatic cancer: In focus, *Pancreatol* 17 (2017) 514–522, <https://doi.org/10.1016/j.pan.2017.05.390>.
- [11] A. Neesse, S. Krug, T.M. Gress, D.A. Tuveson, P. Michl, Emerging concepts in pancreatic cancer medicine: targeting the tumor stroma, *Onco Targets Ther* 7 (2013) 33–43, <https://doi.org/10.2147/OTT.S38111>.
- [12] M.V. Apte, P.S. Haber, S.J. Darby, S.C. Rodgers, G.W. McCaughan, M.A. Korsten, R.C. Pirola, J.S. Wilson, Pancreatic stellate cells are activated by proinflammatory cytokines: implications for pancreatic fibrogenesis, *Gut* 44 (1999) 534–541, <https://doi.org/10.1136/gut.44.4.534>.
- [13] P. Mews, P. Phillips, R. Fahmy, M. Korsten, R. Pirola, J. Wilson, M. Apte, Pancreatic stellate cells respond to inflammatory cytokines: potential role in chronic pancreatitis, *Gut* 50 (2002) 535–541, <https://doi.org/10.1136/gut.50.4.535>.
- [14] E. Schneider, A. Schmid-Kotsas, J. Zhao, H. Weidenbach, R.M. Schmid, A. Menke, G. Adler, J. Waltenberger, A. Grünert, M.G. Bachem, Identification of mediators stimulating proliferation and matrix synthesis of rat pancreatic stellate cells, *American Journal of Physiology-Cell Physiology* 281 (2001) C532–C543, <https://doi.org/10.1152/ajpcell.2001.281.2.C532>.
- [15] G. van Duijneveldt, M.D.W. Griffin, T.L. Putoczki, Emerging roles for the IL-6 family of cytokines in pancreatic cancer, *Clin Sci (Lond)* 134 (2020) 2091–2115, <https://doi.org/10.1042/CS20191211>.
- [16] S. Okada, T. Okusaka, H. Ishii, A. Kyogoku, M. Yoshimori, N. Kajimura, K. Yamaguchi, T. Kakizoe, Elevated serum interleukin-6 levels in patients with pancreatic cancer, *Jpn J Clin Oncol* 28 (1998) 12–15, <https://doi.org/10.1093/jjco/28.1.12>.
- [17] S. Watanabe, Y. Nagashio, H. Asami, Y. Nomiya, M. Taguchi, M. Tashiro, Y. Kihara, H. Nakamura, M. Otsuki, Pressure activates rat pancreatic stellate cells, *Am J Physiol Gastrointest Liver Physiol* 287 (2004) G1175–G1181, <https://doi.org/10.1152/ajpgi.00339.2004>.
- [18] P.P. Provenzano, S.R. Hingorani, Hyaluronan, fluid pressure, and stromal resistance in pancreas cancer, *Br J Cancer* 108 (2013) 1–8, <https://doi.org/10.1038/bjc.2012.569>.
- [19] B. Fels, N. Nielsen, A. Schwab, Role of TRPC1 channels in pressure-mediated activation of murine pancreatic stellate cells, *Eur Biophys J* (2016) 1–14, <https://doi.org/10.1007/s00249-016-1176-4>.
- [20] Z. Pethő, K. Najder, E. Bulk, A. Schwab, Mechanosensitive ion channels push cancer progression, *Cell Calcium* 80 (2019) 79–90, <https://doi.org/10.1016/j.ceca.2019.03.007>.
- [21] B. Martinac, Mechanosensitive ion channels: molecules of mechanotransduction, *Journal of Cell Science* 117 (2004) 2449–2460, <https://doi.org/10.1242/jcs.01232>.
- [22] G. Mesquita, N. Prevarskaya, A. Schwab, V. Lehen'kyi, Role of the TRP Channels in Pancreatic Ductal Adenocarcinoma Development and Progression, *Cells* 10 (2021) 1021, <https://doi.org/10.3390/cells10051021>.
- [23] R. Jaster, G. Sparmann, J. Emmrich, S. Liebe, Extracellular signal regulated kinases are key mediators of mitogenic signals in rat pancreatic stellate cells, *Gut* 51 (2002) 579–584, <https://doi.org/10.1136/gut.51.4.579>.
- [24] A.A. Kusiak, M.D. Szopa, M.A. Jakubowska, P.E. Ferdek, Signaling in the Physiology and Pathophysiology of Pancreatic Stellate Cells – a Brief Review of Recent Advances, *Front Physiol* 11 (2020), <https://doi.org/10.3389/fphys.2020.00078>.
- [25] H. Ohnishi, T. Miyata, H. Yasuda, Y. Satoh, K. Hanatsuka, H. Kita, A. Ohashi, K. Tamada, N. Makita, T. Iiri, N. Ueda, H. Mashima, K. Sugano, Distinct roles of Smad2-, Smad3-, and ERK-dependent pathways in transforming growth factor-beta1 regulation of pancreatic stellate cellular functions, *J Biol Chem* 279 (2004) 8873–8878, <https://doi.org/10.1074/jbc.M309698200>.
- [26] D. Lachowski, E. Cortes, D. Pink, A. Chronopoulos, S.A. Karim, J. Morton, A.E. del Río Hernández, Substrate Rigidity Controls Activation and Durotaxis in Pancreatic Stellate Cells, *Scientific Reports* 7 (2017) 2506, <https://doi.org/10.1038/s41598-017-02689-x>.
- [27] B.M. MacCurtain, N.P. Quirke, S.D. Thorpe, T.K. Gallagher, Pancreatic Ductal Adenocarcinoma: Relating Biomechanics and Prognosis, *J Clin Med* 10 (2021) 2711, <https://doi.org/10.3390/jcm10122711>.
- [28] A. Masamune, T. Shimosegawa, Signal transduction in pancreatic stellate cells, *J Gastroenterol* 44 (2009) 249–260, <https://doi.org/10.1007/s00535-009-0013-2>.
- [29] M. Shimada, A. Andoh, K. Hata, K. Tasaki, Y. Araki, Y. Fujiyama, T. Bamba, IL-6 secretion by human pancreatic periacinar myofibroblasts in response to inflammatory mediators, *J Immunol* 168 (2002) 861–868, <https://doi.org/10.4049/jimmunol.168.2.861>.
- [30] M.V. Apte, J.S. Wilson, Dangerous liaisons: pancreatic stellate cells and pancreatic cancer cells, *J Gastroenterol. Hepatol.* 27 (2) (2012) 69–74, <https://doi.org/10.1111/j.1440-1746.2011.07000.x>. Suppl.
- [31] P.P. Provenzano, C. Cuevas, A.E. Chang, V.K. Goel, D.D. Von Hoff, S.R. Hingorani, Enzymatic targeting of the stroma ablates physical barriers to treatment of pancreatic ductal adenocarcinoma, *Cancer Cell* 21 (2012) 418–429, <https://doi.org/10.1016/j.ccr.2012.01.007>.
- [32] B. Fels, E. Bulk, Z. Pethő, A. Schwab, The Role of TRP Channels in the Metastatic Cascade, *Pharmaceuticals (Basel)* 11 (2018) E48, <https://doi.org/10.3390/ph11020048>.
- [33] K.T. Cheng, H.L. Ong, X. Liu, I.S. Ambudkar, Chapter Seven - Contribution and Regulation of TRPC Channels in Store-Operated Ca<sup>2+</sup> Entry, in: M. Prakriya (Ed.), *Current Topics in Membranes*, Academic Press, 2013, pp. 149–179, <https://doi.org/10.1016/B978-0-12-407870-3.00007-X>.
- [34] O.M. Elzamazzy, R. Penner, L.A. Hazlehurst, The Role of TRPC1 in Modulating Cancer Progression, *Cells* 9 (2020) 388, <https://doi.org/10.3390/cells9020388>.
- [35] J.E. Camacho Londoño, V. Kuryshv, A. Raso, T.G. Wood, A. Kurosky, C. Bowman, P. Nawroth, A. Dietrich, L. Birnbaumer, P. Lipp, C. Dieterich, M. Freichel, Transcriptional signatures regulated by TRPC1/CA-mediated Background Ca<sup>2+</sup> entry after pressure-overload induced cardiac remodelling, *Progress in Biophysics and Molecular Biology* 159 (2021) 86–104, <https://doi.org/10.1016/j.pbiomolbio.2020.07.006>.
- [36] A. Fabian, J. Bertrand, O. Lindemann, T. Pap, A. Schwab, Transient receptor potential canonical channel 1 impacts on mechanosignaling during cell migration, *Pflügers Arch* 464 (2012) 623–630, <https://doi.org/10.1007/s00424-012-1169-9>.
- [37] P. Gottlieb, J. Folgering, R. Maroto, A. Raso, T.G. Wood, A. Kurosky, C. Bowman, D. Bichet, A. Patel, F. Sachs, B. Martinac, O.P. Hamill, E. Honoré, Revisiting TRPC1 and TRPC6 mechanosensitivity, *Pflügers Arch* 455 (2008) 1097–1103, <https://doi.org/10.1007/s00424-007-0359-3>.
- [38] R. Maroto, A. Raso, T.G. Wood, A. Kurosky, B. Martinac, O.P. Hamill, TRPC1 forms the stretch-activated cation channel in vertebrate cells, *Nat. Cell Biol.* 7 (2005) 179–185, <https://doi.org/10.1038/ncb1218>.
- [39] L. Xia, K. Cheung, S.S. Yeung, E.W. Yeung, The involvement of transient receptor potential canonical type 1 in skeletal muscle regrowth after unloading-induced atrophy, *J Physiol* 594 (2016) 3111–3126, <https://doi.org/10.1113/JP271705>.
- [40] S. Radoslavova, A. Folcher, T. Lefebvre, K. Kondratska, S. Guénin, I. Dhennin-Duthille, M. Gautier, N. Prevarskaya, H. Ouadid-Ahidouch, Orail1 Channel Regulates Human-Activated Pancreatic Stellate Cell Proliferation and TGFβ1 Secretion through the AKT Signaling Pathway, *Cancers* 13 (2021) 2395, <https://doi.org/10.3390/cancers13102395>.
- [41] V. Prystopiuk, B. Fels, C.S. Simon, I. Liashkovich, D. Pasrednik, C. Kronlage, R. Wedlich-Söldner, H. Oberleithner, J. Fels, A two-phase response of endothelial cells to hydrostatic pressure, *J Cell Sci* 131 (2018), <https://doi.org/10.1242/jcs.206920>.
- [42] A. Kuntze, O. Goetsch, B. Fels, K. Najder, A. Unger, M. Wilhelm, S. Sargin, S. Schimmelpfennig, I. Neumann, A. Schwab, Z. Pethő, Protonation of Piezo1 Impairs Cell-Matrix Interactions of Pancreatic Stellate Cells, *Front Physiol* 11 (2020) 89, <https://doi.org/10.3389/fphys.2020.00089>.
- [43] C. Dou, Z. Liu, K. Tu, H. Zhang, C. Chen, U. Yaqoob, Y. Wang, J. Wen, J. van Deursen, D. Sicard, D. Tschumperlin, H. Zou, W.-C. Huang, R. Urrutia, V.H. Shah, N. Kang, P300 Acetyltransferase Mediates Stiffness-Induced Activation of Hepatic Stellate Cells Into Tumor-Promoting Myofibroblasts, *Gastroenterology* 154 (2018) 2209–2221, <https://doi.org/10.1053/j.gastro.2018.02.015>, e14.
- [44] Y. Xiao, H. Zhang, Q. Ma, R. Huang, J. Lu, X. Liang, X. Liu, Z. Zhang, L. Yu, J. Pang, L. Zhou, T. Liu, H. Wu, Z. Liang, YAP1-mediated pancreatic stellate cell activation inhibits pancreatic cancer cell proliferation, *Cancer Letters* 462 (2019) 51–60, <https://doi.org/10.1016/j.canlet.2019.07.015>.
- [45] M. Faouzi, F. Hague, D. Geerts, A.-S. Ay, M. Potier-Cartereau, A. Ahidouch, H. Ouadid-Ahidouch, Functional cooperation between KCa3.1 and TRPC1 channels in human breast cancer: Role in cell proliferation and patient prognosis, *Oncotarget* 7 (2016) 36419–36435, <https://doi.org/10.18632/oncotarget.9261>.
- [46] C. Selli, Y. Erac, B. Kosova, E.S. Erdal, M. Tosun, Silencing of TRPC1 regulates store-operated calcium entry and proliferation in Huh7 hepatocellular carcinoma cells, *Biomed Pharmacother* 71 (2015) 194–200, <https://doi.org/10.1016/j.biopha.2015.02.024>.
- [47] M.S.S. Alhaddani, M. Youns, M. Buchholz, T.M. Gress, M.-C. Beckers, D. Maréchal, A. Bauer, C. Schröder, J.D. Hoheisel, Immunoassay-based proteome profiling of 24 pancreatic cancer cell lines, *J Proteomics* 75 (2012) 3747–3759, <https://doi.org/10.1016/j.jprot.2012.04.042>.
- [48] R. Li, J. Hou, Q. Xu, Q.-J. Liu, Y.-J. Shen, G. Rodin, M. Li, High level interleukin-6 in the medium of human pancreatic cancer cell culture suppresses production of neurotransmitters by PC12 cell line, *Metab Brain Dis* 27 (2012) 91–100, <https://doi.org/10.1007/s11011-011-9270-x>.
- [49] L. Magri, R. Bouazzi, H. Heredero Olmedilla, P.S.S. Petersen, M. Tozzi, I. Novak, The P2X7 Receptor Stimulates IL-6 Release from Pancreatic Stellate Cells and Tocilizumab Prevents Activation of STAT3 in Pancreatic Cancer Cells, *Cells* 10 (2021) 1928, <https://doi.org/10.3390/cells10081928>.
- [50] Y.S. Wu, I. Chung, W.F. Wong, A. Masamune, M.S. Sim, C.Y. Looi, Paracrine IL-6 signaling mediates the effects of pancreatic stellate cells on epithelial-mesenchymal transition via Stat3/Nrf2 pathway in pancreatic cancer cells, *Biochimica et Biophysica Acta (BBA) - General Subjects* 1861 (2017) 296–306, <https://doi.org/10.1016/j.bbagen.2016.10.006>.
- [51] S.J. Wicks, S. Lui, N. Abdel-Wahab, R.M. Mason, A. Chantry, Inactivation of smad-transforming growth factor beta signaling by Ca(2+)-calmodulin-dependent protein kinase II, *Mol Cell Biol* 20 (2000) 8103–8111, <https://doi.org/10.1128/mcb.20.21.8103-8111.2000>.
- [52] A. Dietrich, H. Kalwa, U. Storch, M. Mederos y Schnitzler, B. Salanova, O. Pinkenburg, G. Dubrovskaya, K. Essin, M.-L. Gollasch, L. Birnbaumer, T. Gudermann, Pressure-induced and store-operated cation influx in vascular smooth muscle cells is independent of TRPC1, *Pflügers Arch* 455 (2007) 465–477, <https://doi.org/10.1007/s00424-007-0314-3>.

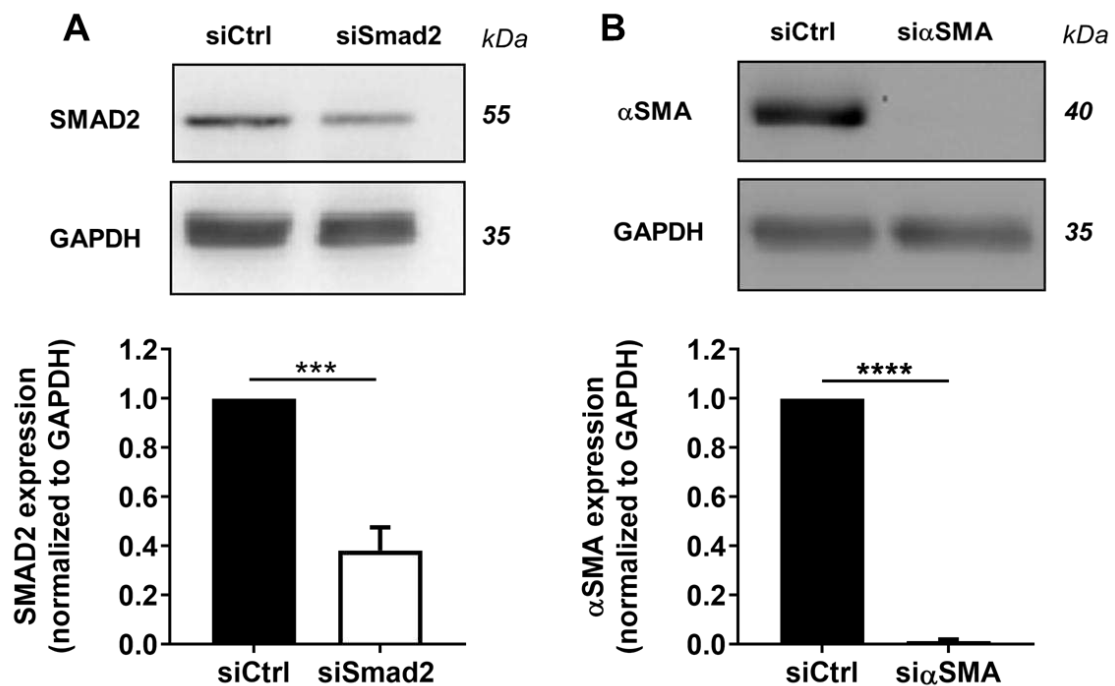
- [53] K.A. Haanes, A. Schwab, I. Novak, The P2X7 Receptor Supports Both Life and Death in Fibrogenic Pancreatic Stellate Cells, *PLoS One* 7 (2012), <https://doi.org/10.1371/journal.pone.0051164>.
- [54] F.E.M. Froeling, T.A. Mirza, R.M. Feakins, A. Seedhar, G. Elia, I.R. Hart, H. M. Kocher, Organotypic culture model of pancreatic cancer demonstrates that stromal cells modulate E-cadherin, beta-catenin, and Ezrin expression in tumor cells, *Am J Pathol* 175 (2009) 636–648, <https://doi.org/10.2353/ajpath.2009.090131>.
- [55] N. Nielsen, K. Kondratska, T. Ruck, B. Hild, I. Kovalenko, S. Schimmelpennig, J. Welzig, S. Sargin, O. Lindemann, S. Christian, S.G. Meuth, N. Prevarskaya, A. Schwab, TRPC6 channels modulate the response of pancreatic stellate cells to hypoxia, *Pflügers Arch* 469 (2017) 1567–1577, <https://doi.org/10.1007/s00424-017-2057-0>.
- [56] K. Göbel, S. Pankratz, C.-M. Asaridou, A.M. Herrmann, S. Bittner, M. Merker, T. Ruck, S. Glumm, F. Langhauser, P. Kraft, T.F. Krug, J. Breuer, M. Herold, C. C. Gross, D. Beckmann, A. Korb-Pap, M.K. Schuhmann, S. Kuerten, I. Mitroulis, C. Ruppert, M.W. Nolte, C. Panousis, L. Klotz, B. Kehrel, T. Korn, H.F. Langer, T. Pap, B. Nieswandt, H. Wiendl, T. Chavakis, C. Kleinschnitz, S.G. Meuth, Blood coagulation factor XII drives adaptive immunity during neuroinflammation via CD87-mediated modulation of dendritic cells, *Nat Commun* 7 (2016) 11626, <https://doi.org/10.1038/ncomms11626>.
- [57] J.E. Merritt, R. Jacob, T.J. Hallam, Use of manganese to discriminate between calcium influx and mobilization from internal stores in stimulated human neutrophils, *J Biol Chem* 264 (1989) 1522–1527.
- [58] P. Carl, H. Schillers, Elasticity measurement of living cells with an atomic force microscope: data acquisition and processing, *Pflügers Arch* 457 (2008) 551–559, <https://doi.org/10.1007/s00424-008-0524-3>.
- [59] J. Fels, P. Jeggle, K. Kusche-Vihrog, H. Oberleithner, Cortical actin nanodynamics determines nitric oxide release in vascular endothelium, *PLoS ONE* 7 (2012) e41520, <https://doi.org/10.1371/journal.pone.0041520>.
- [60] H. Oberleithner, C. Callies, K. Kusche-Vihrog, H. Schillers, V. Shahin, C. Riethmüller, G.A. Macgregor, H.E. de Wardener, Potassium softens vascular endothelium and increases nitric oxide release, *Proc. Natl. Acad. Sci. U.S.A.* 106 (2009) 2829–2834, <https://doi.org/10.1073/pnas.0813069106>.
- [61] J.-L. Martiel, A. Leal, L. Kurzawa, M. Balland, I. Wang, T. Vignaud, Q. Tseng, M. Théry, Chapter 15 - Measurement of cell traction forces with ImageJ, in: E. K. Paluch (Ed.), *Methods in Cell Biology*, Academic Press, 2015, pp. 269–287, <https://doi.org/10.1016/bs.mcb.2014.10.008>.

SUPPLEMENTARY FIGURES

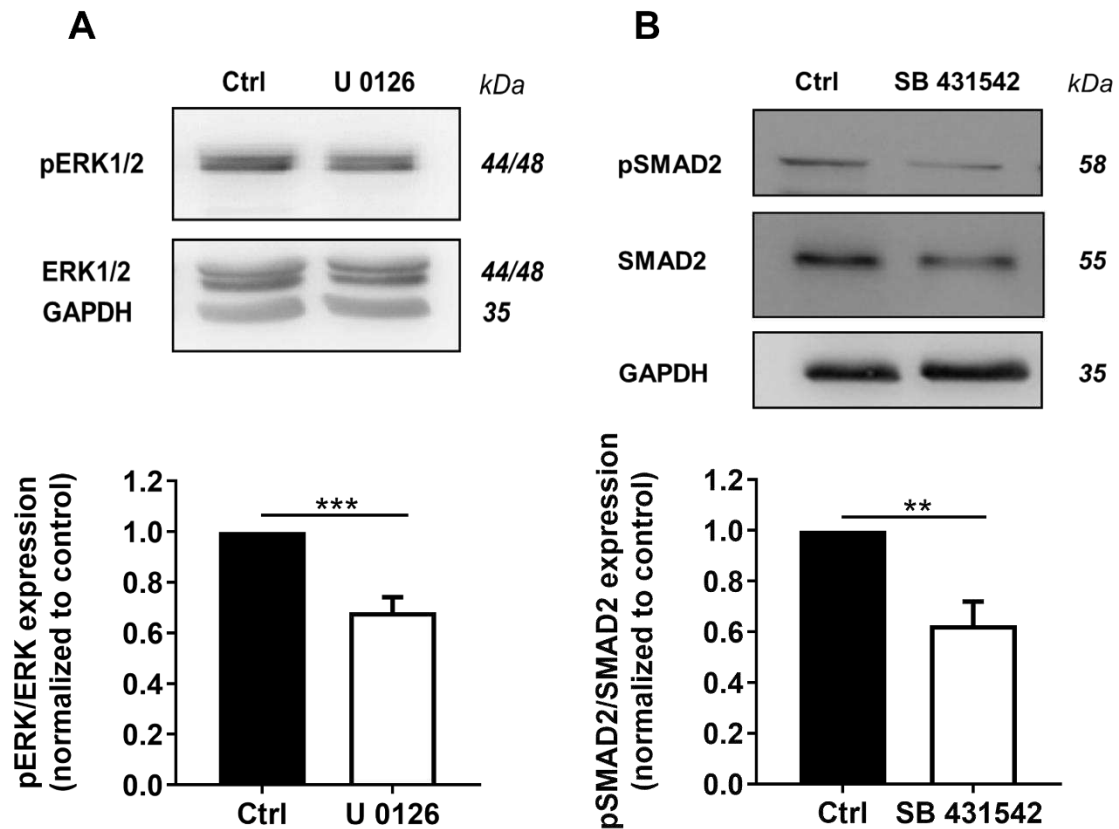


**Supplementary Figure 1: A) Quantification of lipid droplets in mouse PSCs using the Nile Red labelling.** Time course of lipid droplets staining from 24h to 120h after isolation. Under control conditions the percentage of Nile Red-positive PSCs steadily decreases as they become activated. Pressure incubation (grey shading) accelerates this activation after 24h (N=4-5, n=5-9, \*\* $p < 0.01$ , \* $p = 0.05$  (timepoints), § $p < 0.05$  (control vs. pressure) Student's *t*-test). **B-D) TRPC1 knock-down efficiency and its impact on  $\alpha$ SMA expression in pre-activated human PSCs.** B/C) Evaluation of TRPC1 siRNA efficiency in PS-1 cells 72h post-transfection

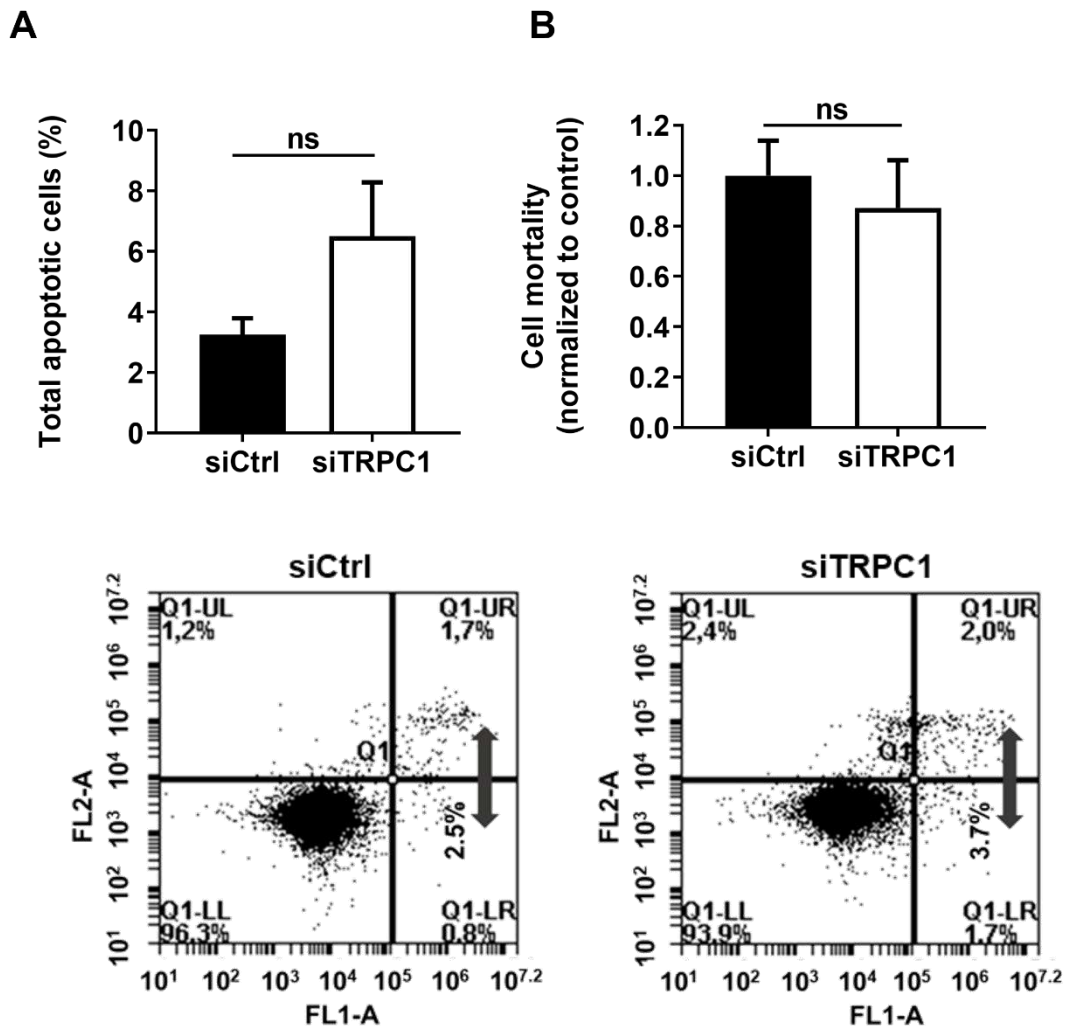
by Western blot. Illustrative Western blot of TRPC1 protein knock-down in PS-1 cells with the quantification. B/D) Assessment of TRPC1 silencing on  $\alpha$ SMA protein expression after 72h of transfection by Western blot. Illustrative Western blot of  $\alpha$ SMA expression following TRPC1 knock-down in PS-1 cells. All results of Western blotting were first normalized to the reference protein GAPDH and then to the siCtrl condition, reported as mean  $\pm$  SEM (N=4, \*\*\*\*p<0.0001, \*\*p = 0.0017, Student's *t*-test).



**Supplementary Figure 2: SMAD2 and  $\alpha$ SMA siRNA efficiency 72h post-transfection in pre-activated human PSCs.** A) Protein expression of SMAD2 72h after siSmad2 transfection quantified by Western blot in PS-1 cells. Illustrative Western blot of SMAD2 protein knock-down with the quantification. B) Evaluation of si $\alpha$ SMA efficiency in PS-1 cells 72h post-transfection by Western blot. Illustrative Western blot of  $\alpha$ SMA protein knock-down with the quantification. All results of Western blotting were first normalized to the reference protein GAPDH and then to the siCtrl condition, reported as mean  $\pm$  SEM (N=5 for siSmad2, N=3 for si $\alpha$ SMA, \*\*\*\*p<0.0001, \*\*\*p = 0.0002, Student's *t*-test).



**Supplementary Figure 3: Pharmacological inhibition of ERK1/2 and SMAD2 activation in PS-1 cells after 72h cell treatment with the U 0126 and SB 431542 inhibitors, respectively.** A) Assessment of ERK1/2 phosphorylation following 72h treatment of PS-1 cells with the U 0126 (10  $\mu$ M) inhibitor by Western blot. Representative Western blot of reduced ERK1/2 phosphorylation by U 0126 treatment and the quantification as described above in this article. B) Evaluation of the reduction of SMAD2 activation after 72h treatment of PS-1 cells with the SB 431542 (80  $\mu$ M) inhibitor by Western blot. Illustrative Western blot of inhibited SMAD2 phosphorylation by SB 431542 treatment with the quantification as described above. All values were first normalized to the reference protein GAPDH and then to the control condition, reported as mean  $\pm$  SEM (N=5 for U 0126, N=4 for SB 431542, \*\*\*p = 0.0007, \*\*p = 0.0069, Student's *t*-test).



**Supplementary Figure 4: TRPC1 channels do not affect PS-1 cell survival.** A) Evaluation of cell mortality after TRPC1 knock-down for 72h by Trypan blue assay in PS-1 cells. B) Total apoptosis rate was measured by flow cytometry using annexin V / propidium iodide staining 72h after TRPC1 knock-down. C) Representative flow cytometric histograms showing Annexin V-FITC fluorescence collected by the emission FL1 filter (represented in the x-axis) and the Propidium Iodide fluorescence collected by the emission FL2 filter (represented in the y-axis). Values were normalized to the siCtrl condition and reported as mean  $\pm$  SEM (N=3, each experiment was performed at least in triplicate, NS: no significant, Student *t*-test).



## Complementary Results in PS-1 cells:

### 1) TRPC1- $\alpha$ SMA-pSMAD2 cooperation

#### 1.1) Physical interaction between TRPC1, $\alpha$ SMA, and SMAD2

We have shown in the above work that TRPC1 can directly or indirectly interact with  $\alpha$ SMA and the phosphorylated active form of SMAD2 (pSMAD2), maintaining PS-1's activation, and that each partner is involved with a different participation degree in the formed complex. However, before determining that pSMAD2 was implicated in this protein network, we first checked whether the non-phosphorylated form of SMAD2 could participate and influence this association. Indeed, previous studies have shown that TRPC (1,4,6) channels can regulate  $\alpha$ SMA expression, in hepatic stellate cells, intestinal myofibroblasts and murine fibroblasts (Iyer et al., 2015; Kurahara et al., 2015; Sassoli et al., 2016). Moreover, in intestinal myofibroblasts, TRPC6 is also able to interact and form a complex with  $\alpha$ SMA, participating in the maintenance of myofibroblast's activation (Kurahara et al., 2015). Additionally, myofibroblast activation has been reported to be mediated by the SMAD2/3 signalling pathway, and ion channels including TRPC1 have been shown to activate this pathway (Roach et al., 2014; Sassoli et al., 2016; Um et al., 2020). However, Ohnishi *et al.* have demonstrated that SMAD2 transcription factor but not SMAD3 mediates rodent PSC's activation through the modulation of  $\alpha$ SMA expression (Ohnishi et al., 2004). We, thereby, knocked down  $\alpha$ SMA and TRPC1 independently, and we evaluated the association of SMAD2-TRPC1 and SMAD2- $\alpha$ SMA, respectively, by co-immunoprecipitation experiments. The silencing of  $\alpha$ SMA diminished by  $36.40 \pm 8.79\%$  the interaction between SMAD2 and TRPC1 (N=2, **Figure 38 A**) whereas TRPC1 invalidation decreased by  $41.90 \pm 14.20\%$  the association between SMAD2 and  $\alpha$ SMA (N=2, **Figure 38 B**). SMAD2 seems to associate approximatively with the same affinity to TRPC1 and  $\alpha$ SMA, even though more co-immunoprecipitation experiments are needed to be performed to confirm these results, especially using SMAD2 as immunoprecipitation antibody. These data show that both the non-phosphorylated inactive and phosphorylated active form of SMAD2 can form a complex with TRPC1 and  $\alpha$ SMA.

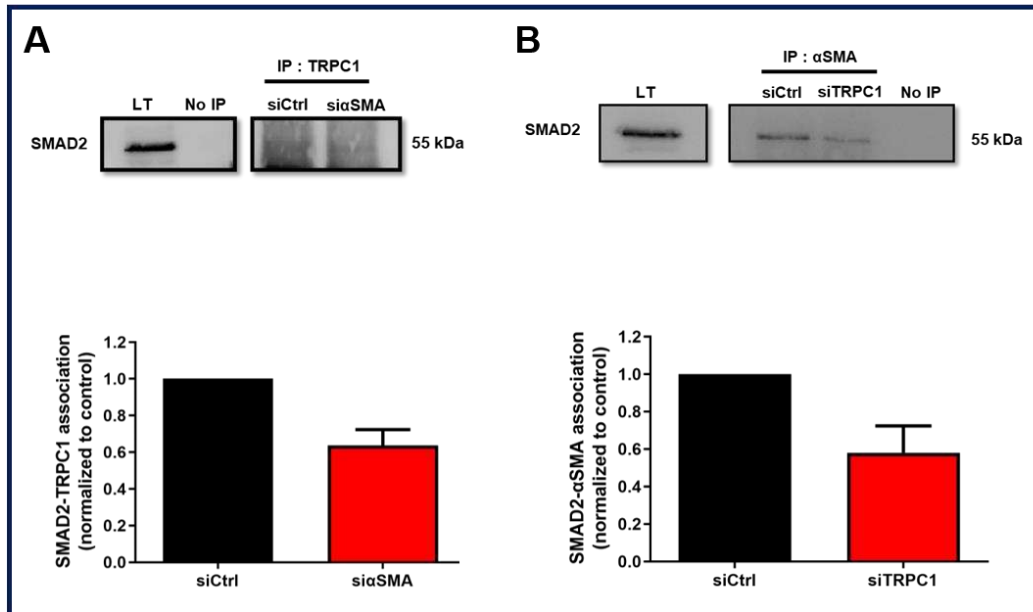


**Figure 38: TRPC1, αSMA and SMAD2 form a complex, and their interaction is disrupted when TRPC1 or αSMA are inhibited, in PS-1 cells.** A) Effect of 72h αSMA knocking down on the interaction between SMAD2 and TRPC1, using an anti-TRPC1 immunoprecipitation antibody (N=2). B) Impact of 72h TRPC1 silencing on SMAD2-αSMA association using anti-αSMA immunoprecipitation antibody (N=2). All values were normalized to the control condition and reported as mean ±SEM.

### 1.2) TRPC1, αSMA, and pSMAD2 form a complex in the lipid rafts

Thereafter, we kept focusing on the active pSMAD2 form, and we sought to know whether the physical interaction between the three partners takes place, at least partially, in the lipid rafts. It is known now that TRPC1 can be localized in cholesterol-rich membrane microdomains called lipid rafts and participate in the maintenance of lipid rafts 'integrity regulating phosphatidylserine transmembrane distribution (Kunzelmann-Marche et al., 2002). We thus hypothesized that its interaction with αSMA and pSMAD2 might occur, at least in part, within the lipid rafts. To assess this hypothesis, we treated PS-1 cells for 24h with the plasma membrane cholesterol destabilizer MβCD, and 72h post proliferation, we evaluated TRPC1-αSMA-pSMAD2 association by co-immunoprecipitation experiments using the pSMAD2 immunoprecipitation antibody. We noted that under MβCD treatment, the interaction between TRPC1 and pSMAD2 was decreased by  $48.05 \pm 16.68\%$  (N=2, **Figure 39 A-B**), while the impact on αSMA-pSMAD2 association was more important, reducing their interaction by

63.02 ± 11.71% (p=0.0058, N=3, Figure 39 A-C). Although these data remain yet preliminary and require validation, they give evidence that the complex formation between TRPC1, αSMA, and pSMAD2 takes partially place in the lipid rafts and confirms that each partner participates with a different degree to form the complex.

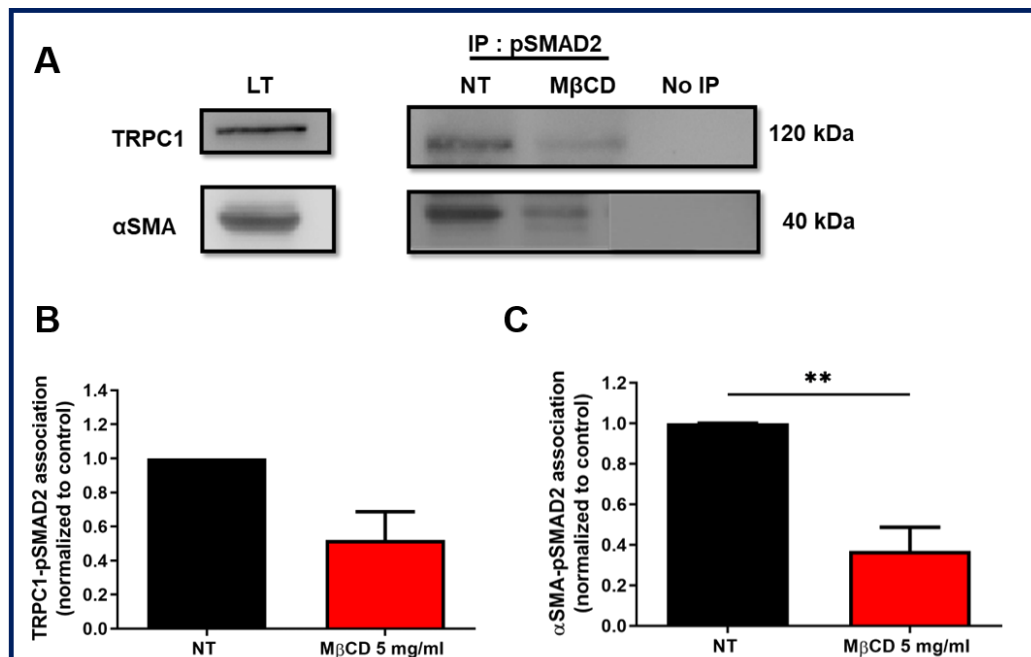


**Figure 39: TRPC1 and αSMA interacts with the active phosphorylated form of SMAD2 (pSMAD2), and their interaction partially occurs in the lipid rafts, in PS-1 cells.** A-C) 24h treatment of non-transfected PS-1 cells with 5 ng/ml of MβCD, used for destabilizing the plasma membrane cholesterol, partially interrupted TRPC1-pSMAD2 (B) (N=2) and αSMA-pSMAD2 (C) (p=0.0058, N=3, Student's *t*-test) interaction in the lipid rafts, as quantified using anti-pSMAD2 immunoprecipitation antibody and revealed subsequently by Western blot. All values were normalized to the control condition and reported as mean ±SEM.

## 2) TRPC1 modulates IL-6 and IL-11 but not TGF-β1 mRNA expression

Another role of TRPC1 in the activation processes of PSCs revealed by our current report is its involvement in the regulation of IL-6 secretion. Supplementary to this finding, we quantified whether TRPC1 can also modulate the synthesis of this proinflammatory cytokine, evaluating IL-6 mRNA expression. 72h TRPC1 silencing led to 63.63% reduction of IL-6

mRNAs (siCtrl:  $100 \pm 9.63\%$ , siTRPC1:  $36.37 \pm 9.88\%$ ,  $p=0.0027$ ,  $N=3$ , **Figure 40 A**), indicating TRPC1's role in IL-6 production as well. Simultaneously, we assessed the impact of TRPC1 knocking down in the modulation of IL-11 synthesis, which is a member of the IL-6 cytokine family, shown to have a fibrogenic activity (Ng et al., 2020; Schafer et al., 2017; Widjaja et al., 2019), additional to its pro-inflammatory potential. We noted that TRPC1 invalidation diminished by 44.24% the mRNA expression of IL-11 (siCtrl:  $100 \pm 1.58\%$ , siTRPC1:  $55.76 \pm 11.53\%$ ,  $p<0.05$ ,  $N=3$ , **Figure 40 B**), suggesting that TRPC1 plays a role in activated PSC's inflammatory cytokines synthesis. Moreover, it would be interesting to investigate whether TRPC1-induced IL-6 and IL-11 production participate in perpetuating PSC's activation through an autocrine positive feedback loop. However, we have established in the above report that TRPC1 regulates also  $\alpha$ SMA expression in PS-1 cells. Could it be possible that this channel drives simultaneously PS-1's inflammatory and myofibroblastic phenotype acquisition? The two main PSC subpopulations described by Öhlund *et al.* are characterized from the one side by an elevated IL-6 and IL-11 synthesis and secretion, and a low  $\alpha$ SMA expression, corresponding to the inflammatory PSC subpopulation located in distantly from the PCCs. From the other side, the second subtype is characterized by a high  $\alpha$ SMA expression and low inflammatory cytokine secretion (IL-6 and IL-11) located in a close proximity to PCCs, corresponding to the myofibroblastic PSC subpopulation (Öhlund et al., 2017). Additionally, the authors have showed that each subpopulation can revert to the other subpopulation according to the microenvironmental factors or their interaction with the PCCs. To answer this question, it would be better to overexpress TRPC1 channel in PS-1 cells and then compared the ratio of  $\alpha$ SMA/IL-6 and  $\alpha$ SMA/IL-11 expression to determine whether TRPC1 mediates mostly PS-1 myofibroblastic or inflammatory phenotype acquisition. To further investigate this aspect, it would be interesting to inhibit and conversely overexpress TRPC1 channel in PS-1 cells and co-culture them with PCCs. Besides, even though we have shown that TRPC1 does not regulate TGF- $\beta$ 1 secretion in PS-1 cells, we checked whether it could be involved in the modulation of TGF- $\beta$ 1 mRNA expression. In accordance with our data on TGF- $\beta$ 1 secretion, TRPC1 inhibition failed to affect TGF- $\beta$ 1 synthesis (siCtrl:  $100 \pm 36.23\%$ , siTRPC1:  $72.48 \pm 22.31\%$ ,  $p>0.05$ ,  $N=3$ , **Figure 40 C**).

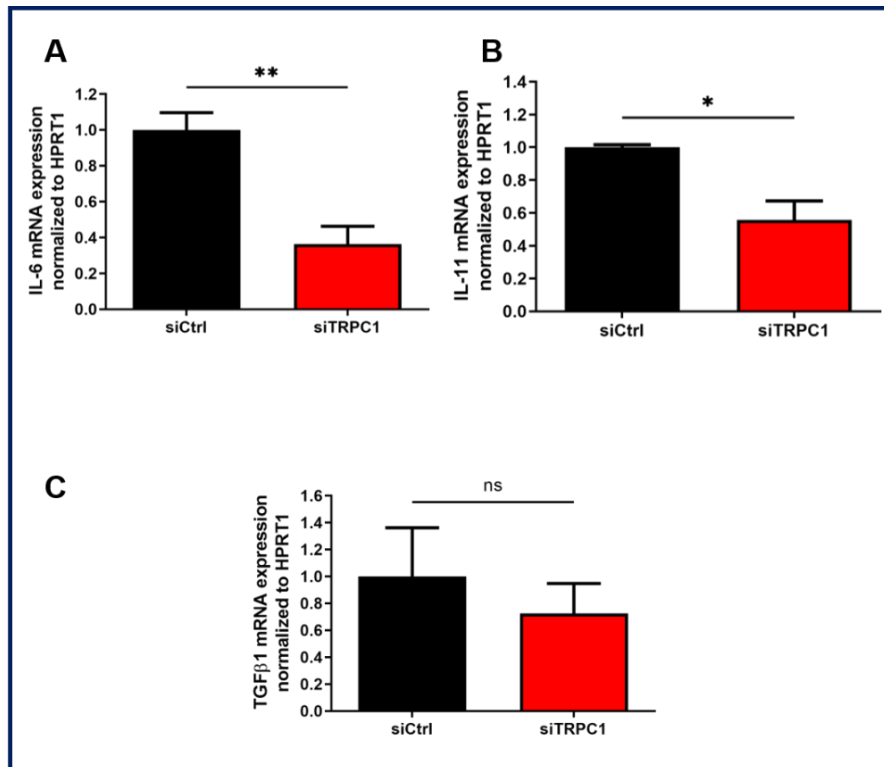


**Figure 40: TRPC1 channel mediates IL-6 and IL-11 mRNA expression in PS-1** Assessment of TRPC1 silencing in IL-6 (A) (\*\* $p=0.0027$ ,  $N=3$ , Student  $t$ -test), IL-11 (B) (\* $p<0.05$ ,  $N=3$ , Student  $t$ -test) and TGF- $\beta$ 1 (C) (NS: no significant, Student  $t$ -test) mRNA expression by qPCR. All values were reported as mean  $\pm$  SEM normalized first to the HPRT1 referent gene and then to the control condition.

### 3) Impact of the other two complex partners, pSMAD2 and $\alpha$ SMA, on TRPC1 expression

#### 3.1) SMAD2 but not ERK1/2 pathway regulates TRPC1 expression

We have established that TRPC1 drives the activation of SMAD2 pathway, probably via its interaction with the phosphorylated active form of SMAD2, and ERK1/2 activation pathway. We, then, wanted to know whether the phosphorylation of SMAD2 could modulate in its turn the protein expression of TRPC1. Therefore, we treated PS-1 cells 72h with the pharmacological inhibitor of SMAD2 pathway, SB 431542, and we observed a  $59.99 \pm 4.95\%$  reduction of TRPC1 expression ( $N=2$ , **Figure 41 A-B**), suggesting the existence of a positive loop between TRPC1 and pSMAD2-mediated protein expression, probable due to their physical interaction. However, the result of pSMAD2 inhibition on TRPC1 expression must be

strengthened with more experiments. Moreover, since TRPC1 has the ability to modulate ERK1/2 pathway too in PS-1 cells, and as we have previously demonstrated that its downstream effector ERK1/2 can mediate TRPC1 expression via a positive feedback loop in MCF7 breast cancer cells (El Hiani et al., 2009), we verified whether this loop could also exist in PS-1 cells. Inhibition of ERK1/2 signalling pathways by 72h PS-1 cells treatment with its pharmacological inhibitor, U 0126, failed to induce any significant difference in TRPC1 protein expression (U 0126:  $68.53 \pm 13.05\%$ ,  $p > 0.05$ ,  $N=3$ , **Figure 41 C-D**), excluding the above hypothesis.

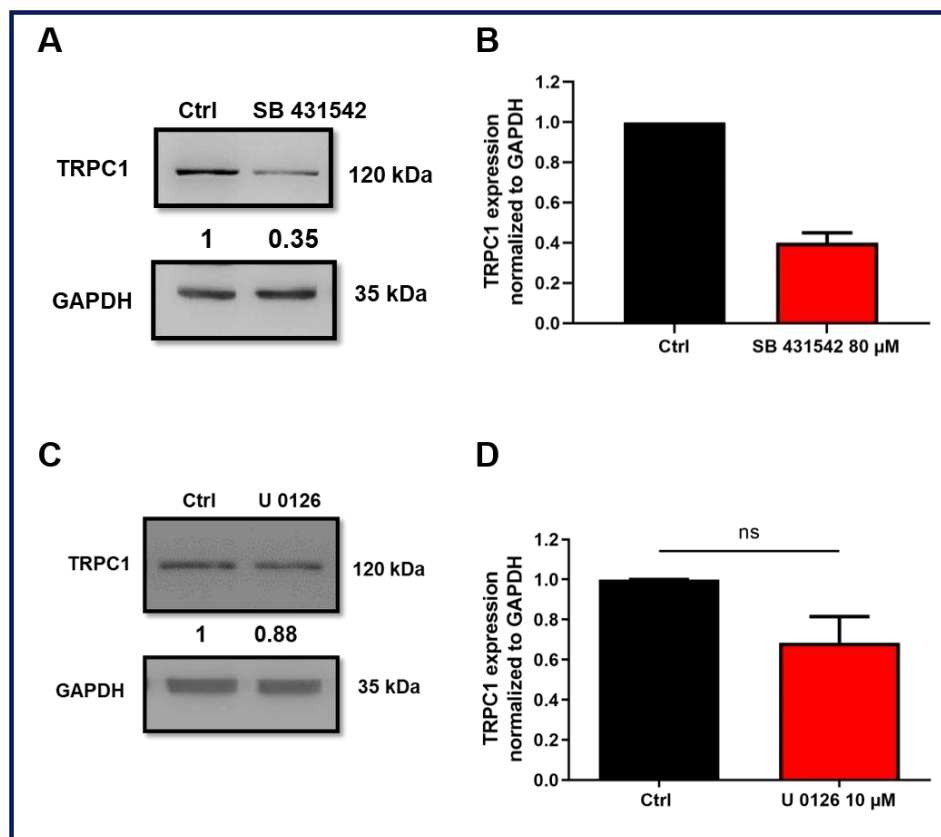


**Figure 41:** A-B) Pharmacological inhibition of SMAD2 pathway with SB 431542 (80  $\mu\text{M}$ ) for 72h seems to decrease TRPC1 expression. Representative Western blot of TRPC1 expression after 72h treatment with SB 431542 (A) and its quantification (B) ( $N=2$ ). C-D) ERK1/2 pathway inhibition with the U 0126 (10  $\mu\text{M}$ ) pharmacological inhibitor did not influence TRPC1 expression. Representative Western blot of TRPC1 expression after U 0126 treatment for 72h (C) and its quantification (D) (NS: no significant,  $N=3$ , Student's *t*-test). All values were firstly normalized to the referent protein (GAPDH) and then to the control condition, reported as mean  $\pm$ SEM.

### 3.2) $\alpha$ SMA modulates TRPC1 expression

Subsequently, we investigated the involvement of the other complex's partner,  $\alpha$ SMA, in the modulation of TRPC1 protein and mRNA expression. After 72h knocking down of  $\alpha$ SMA, we first quantified the transfection efficiency by Western blotting, which almost wholly abolished  $\alpha$ SMA protein expression (si $\alpha$ SMA:  $1.38 \pm 0.62\%$ ,  $p < 0.0001$ ,  $N=3$ , **Figure 42 A-B**). Likewise, to pSMAD2 inhibition,  $\alpha$ SMA silencing decreased the expression of TRPC1 similarly, inducing a  $60.92 \pm 17.41\%$  diminution ( $p < 0.05$ ,  $N=3$ , **Figure 42 A-C**). Additionally, we evaluated if the invalidation of  $\alpha$ SMA affected TRPC1 mRNA expression, without observing any significant impact (siCtrl:  $100 \pm 42.76\%$ , si $\alpha$ SMA:  $108.20 \pm 34.70\%$ ,  $p > 0.05$ ,  $N=3$ , **Figure 42 D**). Together, these data show that each actor mediates the protein expression of the other two partners within the formed complex, highlighting the strong link between TRPC1,  $\alpha$ SMA, and pSMAD2.

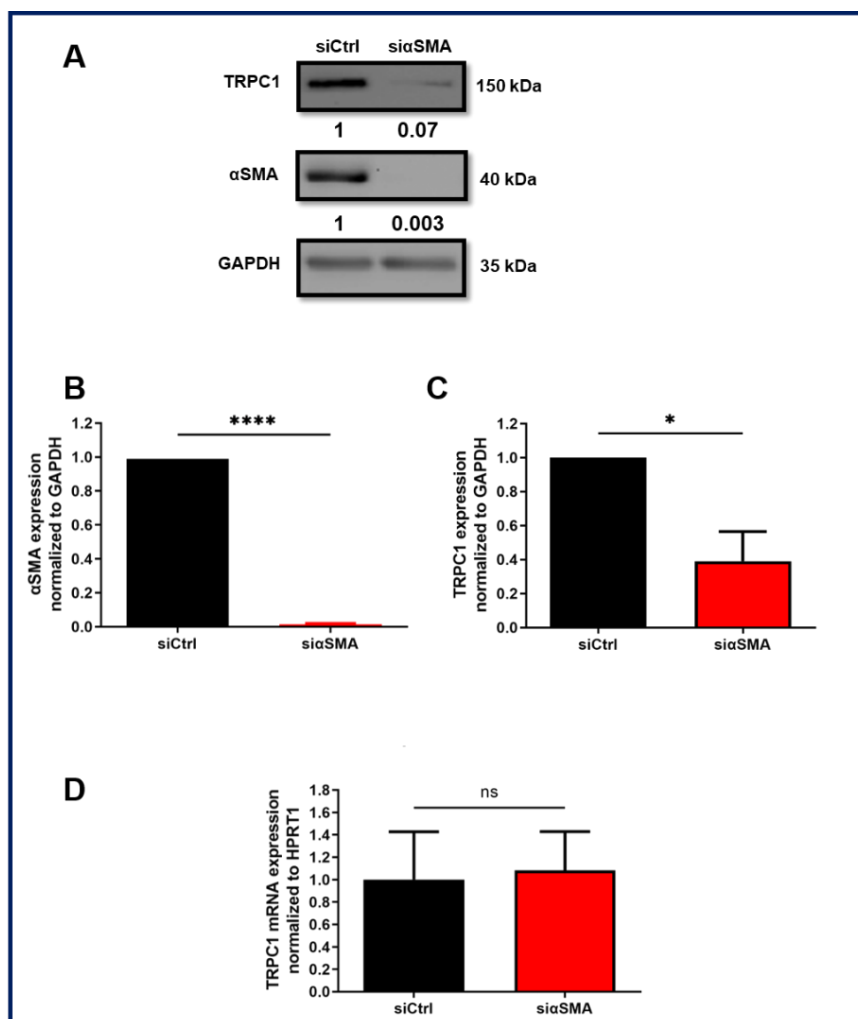


**Figure 42:  $\alpha$ SMA regulates TRPC1 protein expression.** A) Knocking down of  $\alpha$ SMA reduced TRPC1 expression. Representative Western blot of  $\alpha$ SMA inhibition efficiency as well as its effect on TRPC1 expression after 72h of transfection. B) Quantification of  $\alpha$ SMA silencing efficiency (\*\*\*\* $p < 0.0001$ ,  $N=3$ , Student's  $t$ -test) and C) the effect on TRPC1 protein expression (\* $p < 0.05$ ,  $N=3$ , Student's  $t$ -test). D)  $\alpha$ SMA knocking down does not affect TRPC1 mRNA expression, assessed by qPCR (NS: no significant,  $N=3$ , Student's  $t$ -test). All values were firstly normalized to the referent protein (GAPDH) or referent gene (HPRT1), and then to the control condition, reported as mean  $\pm$  SEM.

#### 4) Effect of pSMAD2 and $\alpha$ SMA on TRPC1-mediated cellular activation processes

##### 4.1) SMAD2 but not ERK1/2 pathway mediates IL-6 mRNA expression

As mentioned previously, we have demonstrated that TRPC1 mediates not only IL-6 secretion but also its mRNA expression. Furthermore, in the above work, we showed that both, SMAD2 and ERK1/2 pathways control IL-6 secretion. We, thus, sought to know if one of these signalling pathways or both regulate IL-6 mRNA expression, as it does TRPC1. Indeed, Aoki *et al.* have already demonstrated that IL-6 expression in rodent PSCs is mediated by the SMAD2/3 signalling pathway (Aoki *et al.*, 2006). In consistence with their finding, independent PS-1 72h treatment with the SB 431542 and U 0126 pharmacological inhibitors decreased SMAD2 and ERK1/2 activation, respectively, revealing the implication only of SMAD2 pathway in IL-6 mRNA modulation. Indeed, SB 431542 treatment resulted to 45.32% decrease of IL-6 mRNA expression (Ctrl:  $100 \pm 11.10\%$ , SB 431542:  $54.68 \pm 10.92\%$ ,  $p < 0.05$ ,  $N=4$ , **Figure 43 A**), while U 0126 treatment did not influence its mRNAs (Ctrl:  $100 \pm 20.13\%$ , U 0126:  $86.55 \pm 16.14\%$ ,  $p > 0.05$ ,  $N=4$ , **Figure 43 B**).



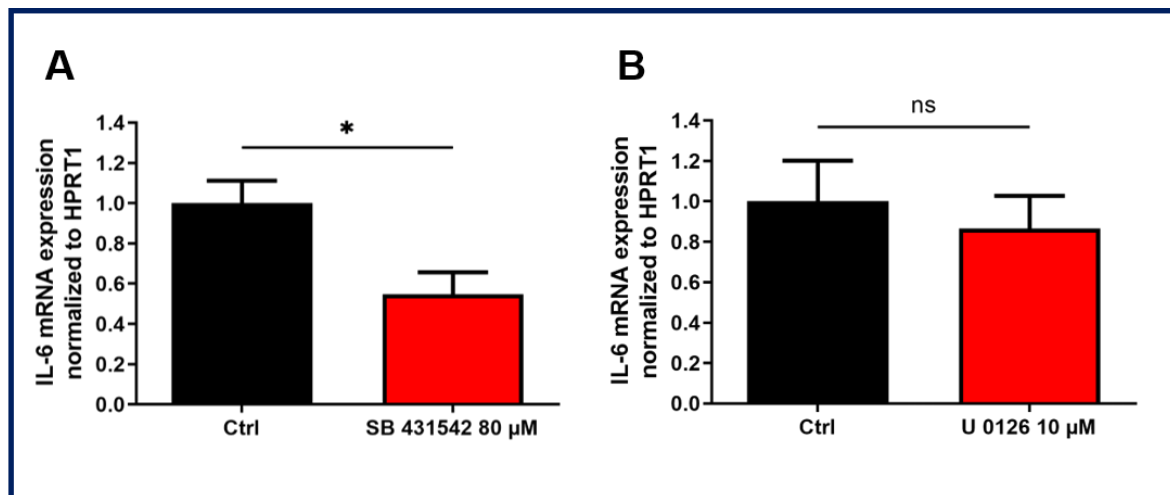


**Figure 43: SMAD2 but not ERK1/2 signalling pathway modulates IL-6 mRNA expression in PS-1.** A) Effect of SMAD2 pathway inhibition on IL-6 mRNA expression, after treating PS-1 cells for 72h with the pharmacological inhibitor SB 4315432 (80 μM), quantified by qPCR (\* $p < 0.05$ ,  $N = 4$ , Student's  $t$ -test. Impact of ERK1/2 decreased activity on PS-1's IL-6 mRNA expression, using the pharmacological inhibitor U 0126 (10 μM) for 72h by qPCR (NS: no significant,  $N = 4$ , Student's  $t$ -test). Values were normalized first normalized to the referent gene HPRT1 and then to the control condition, reported as mean  $\pm$  SEM.

#### 4.2) $\alpha$ SMA drives PS-1's proliferation, survival, and IL-6 secretion

We have displayed so far the role of TRPC1 and its complex partner pSMAD2 in the modulation of PS-1 cell proliferation and IL-6 expression and secretion, but what about the role of the third complex partner in these PSC's activation processes? We, thus, firstly assessed the impact of  $\alpha$ SMA knocking down on PS-1 proliferation by Trypan Blue assay and cell cycle progression by flow cytometry. 72h silencing of  $\alpha$ SMA led to 45.81% reduction of PS-1 proliferation (siCtrl:  $100 \pm 6.89\%$ , si $\alpha$ SMA:  $54.19 \pm 4.43\%$ ,  $p < 0.0001$ ,  $N = 4$ , **Figure 44 A**), inducing a cell arrest in the G0/G1 phase (siCtrl:  $77.18 \pm 0.65\%$ , si $\alpha$ SMA:  $92.11 \pm 0.66\%$ ,  $p < 0.0001$ ,  $N = 3$ , **Figure 44 B-C**), and subsequently an important decrease of S (siCtrl:  $8.37 \pm 0.37\%$ , si $\alpha$ SMA:  $2.21 \pm 0.25\%$ ,  $p < 0.0001$ ) and G2/M (siCtrl:  $14.43 \pm 0.61\%$ , si $\alpha$ SMA:  $5.66 \pm 0.49\%$ ,  $p < 0.0001$ ) phases. Interestingly, during the proliferation rate measurement, we noted a change in si $\alpha$ SMA transfected cell's morphology, resulting in the acquisition of a more circular phenotype, suggesting that cell survival might also be affected (**Figure 44 D**). Consequently, we evaluated by Trypan Blue whether the inhibition of  $\alpha$ SMA diminished in parallel the cell

survival. Indeed, we found a 35.40% augmentation of the mortality rate in si $\alpha$ SMA transfected cells (siCtrl:  $100 \pm 11.50\%$ , si $\alpha$ SMA:  $135.40 \pm 11.07\%$ ,  $p < 0.05$ , N=4, **Figure 44 E**) compared to the siCtrl cells, indicating that  $\alpha$ SMA expression is indispensable for both, cell proliferation and survival of activated PSCs.

Thereafter, we investigated the role of  $\alpha$ SMA in the modulation of IL-6 mRNA expression and secretion. Unfortunately,  $\alpha$ SMA invalidation failed to impact IL-6 expression, although there was a clear tendency of IL-6 mRNA decrease (siCtrl:  $100 \pm 61.18\%$ , si $\alpha$ SMA:  $18.13 \pm 4.61\%$ ,  $p > 0.05$ , N=3, **Figure 45 A**). However, due to the high variability of siCtrl samples, as reflected by the elevated standard error of the mean, these experiments should be repeated since this could induce a bias in the interpretation of the results. On the other side, as TRPC1 and pSMAD2,  $\alpha$ SMA was involved in the mediation of IL-6 secretion too. The silencing of  $\alpha$ SMA reduced by 50.66% the secretion of IL-6 (siCtrl:  $100 \pm 18.95\%$ , si $\alpha$ SMA:  $49.34 \pm 6.99$ ,  $p = 0.0250$ , N=4, **Figure 45 B**), comparably to siTRPC1-induced decrease.

Taken together, these data illustrate the role of  $\alpha$ SMA in the regulation of activated PSC's proliferation, survival, and IL-6 secretion, highlighting one more time the importance of the TRPC1- $\alpha$ SMA-pSMAD2 formed complex in the modulation of PSC's activation processes.

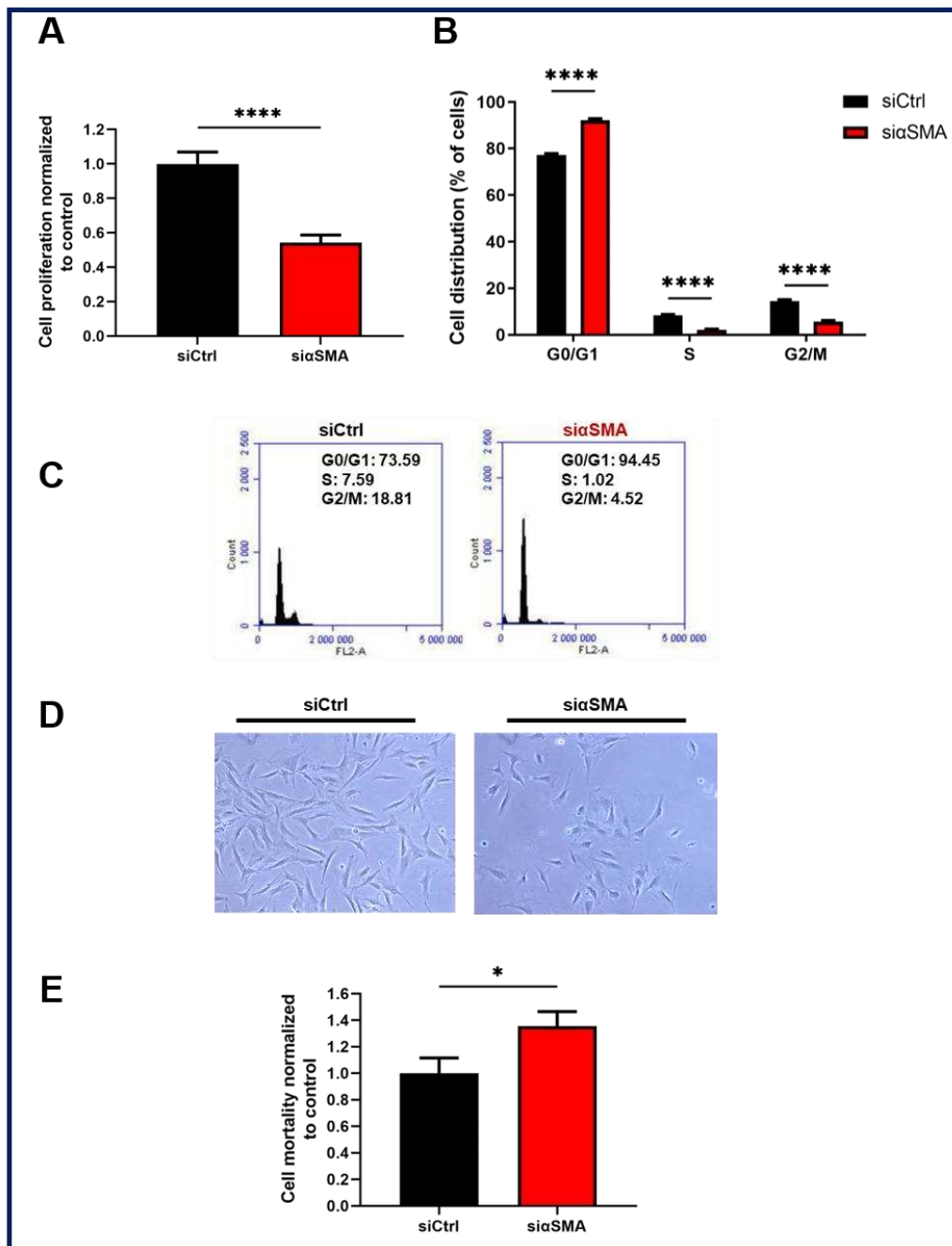


**Figure 44:  $\alpha$ SMA mediates PS-1 cell proliferation and survival.** A) Effect of  $\alpha$ SMA silencing on PS-1 cell proliferation, assessed 72h post-transfection by Trypan blue assay (\*\*\*\* $p < 0.0001$ ,  $N=4$ , Student's  $t$ -test). B) Assessment of  $\alpha$ SMA knocking down in PS-1 cell cycle progression. Cell distribution (G0/G1, S and G2/M phase) was examined by flow cytometry 72h after transfection, with propidium iodide staining (\*\*\*\* $p < 0.0001$ ,  $N=3$ , two-way ANOVA followed by Bonferroni *post hoc* test). C) Illustrative representation of cell cycle profile 72h after Orail inhibition. D) Decrease of  $\alpha$ SMA expression modifies PS-1 cell morphology. E) Impact of  $\alpha$ SMA knocking down on PS-1 survival measured by Trypan blue

assay (\* $p < 0.05$ ,  $N = 4$ , Student's  $t$ -test). Values were normalized to control and reported as mean  $\pm$  SEM.

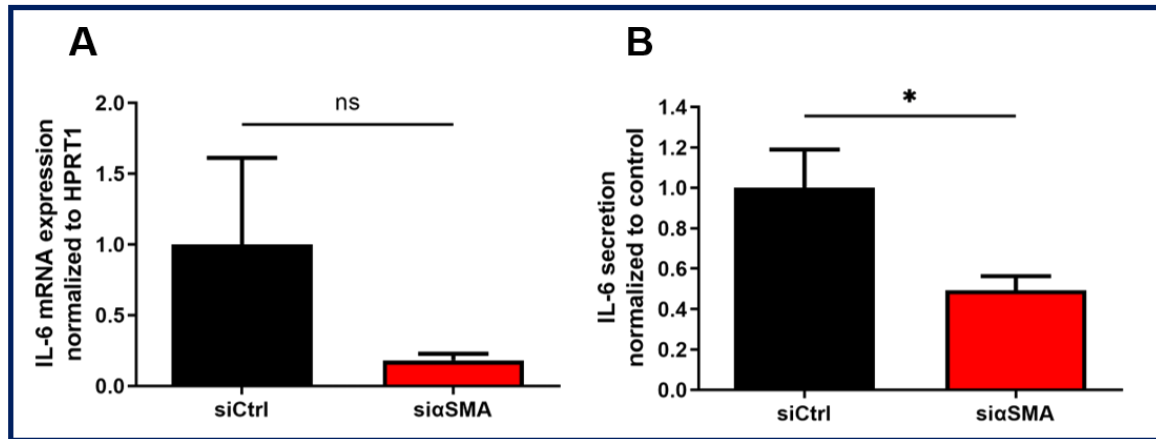


**Figure 45:  $\alpha$ SMA modulates IL-6 secretion but not mRNA expression in PS-1 cells.** Evaluation of  $\alpha$ SMA silencing in IL-6 mRNA expression by qPCR (A) (NS: no significant,  $N = 3$ , Student  $t$ -test) and IL-6 secretion measured by Elisa assay (B) (\* $p = 0.0250$ ,  $N = 4$ , Student  $t$ -test). All values were reported as mean  $\pm$  SEM normalized to the control condition. qPCR values were first normalized to the HPRT1 referent gene and then to the control condition.

## 5) Identification of a $\text{Ca}^{2+}$ -dependent and -independent mechanisms

Furthermore, we have demonstrated that PS-1 proliferation and IL-6 secretion are controlled by the ERK1/2 pathway as well, whereas only SMAD2 pathway drives  $\alpha$ SMA expression, suggesting that the two signalling pathways might act through two different or complementary mechanisms.

### 5.1) ERK1/2 activation is $\text{Ca}^{2+}$ /calmodulin-dependent while SMAD2 phosphorylation is $\text{Ca}^{2+}$ -independent

Knowing that  $\text{Ca}^{2+}$  and its downstream target effectors activate multiple signalling pathways to trigger the cellular responses, we sought to know whether SMAD2 and ERK1/2 activation require  $\text{Ca}^{2+}$  stimulation in PS-1 cells. We cultured non-treated PS-1 cells for 72h and then stimulated them for 10 min with 10% FBS culture medium containing physiological (1.4 mM) or low (0.1 mM)  $\text{Ca}^{2+}$  concentrations. The day before the experiment, cells were FBS

starved overnight. Interestingly, we noticed that the reduced extracellular  $\text{Ca}^{2+}$  concentration impacted just the activation of ERK1/2 pathway, diminishing by 3.26-fold its phosphorylation, compared to the physiological  $\text{Ca}^{2+}$  conditions (10% FBS+1.4 mM  $\text{Ca}^{2+}$ :  $8.77 \pm 0.88$ -fold, 10% FBS+ 0.1 mM  $\text{Ca}^{2+}$ :  $5.50 \pm 0.47$ -fold,  $p=0.0023$ ,  $N=3$ , **Figure 46 A-B**). Whereas SMAD2 phosphorylation was not influenced by the extracellular  $\text{Ca}^{2+}$  concentration decrease (10% FBS+1.4 mM  $\text{Ca}^{2+}$ :  $1.46 \pm 0.47$ -fold, 10% FBS+ 0.1 mM  $\text{Ca}^{2+}$ :  $1.4 \pm 0.34$ -fold,  $p>0.05$ ,  $N=3$ , **Figure 46 C-D**). These data exhibited that ERK1/2 pathway is activated through a  $\text{Ca}^{2+}$ -dependent mechanism, while SMAD2 via a  $\text{Ca}^{2+}$ -independent mechanism.

To further elucidate these findings, we studied the involvement of calmodulin (CaM), known to be one of the most common  $\text{Ca}^{2+}$ -activated downstream effectors, using the pharmacological calmodulin antagonist W 7. Following the previous results, we observed that 72h treatment of PS-1 cells with W 7 decreased by  $51.80 \pm 15.64\%$  ERK1/2 phosphorylation ( $p=0.0296$ ,  $N=3$ , **Figure 47 A-B**). Surprisingly, W 7 treatment promoted SMAD2 activation, augmenting by  $12.30 \pm 2.51\%$  its phosphorylation ( $p=0.0082$ ,  $N=3$ , **Figure 47 C-D**). In fact, Zimmerman *et al.* have found that SMAD2 transcription factor contains a CaM binding domain to its N-terminal region, and Wicks and workers supported the link between SMAD2 and CaM association showing that the downstream effector of CaM, the CaM dependent protein kinase II phosphorylates SMAD2 factor (Wicks et al., 2000; Zimmerman et al., 1998). Wicks et al. have additionally identified that SMAD2 factor possess putative RXXS and SXD consensus CaM kinase II binding sites, where CaM kinase II binds triggering SMAD2 phosphorylation and blocking its nuclear accumulation, and consequently promoting SMAD2 activity independently to TGF- $\beta$ 1 (Wicks et al., 2000), in human embryonic kidney fibroblasts (HEK-293 cells). Therefore, these finding could justify our observed effect on SMAD2 phosphorylation after treating PS-1 cells with the CaM inhibitor, W7, supporting simultaneously the existence of a similar mechanism in human activated PSCs. Moreover, it is well know that TRPC1 activation is inhibited by CaM binding to its C-terminal region, in the presence of high intracellular  $\text{Ca}^{2+}$  concentration (Rosado et al., 2002; Singh et al., 2002; Tang et al., 2001; Vaca and Sampieri, 2002). We could then hypothesize that TRPC1 channel mediates both ERK1/2 and SMAD2 phosphorylation to regulate PSC's proliferation and IL-6 secretion, using two antagonistic mechanisms. For instance, we suggest that when intracellular  $\text{Ca}^{2+}$  concentration is low, TRPC1-mediated  $\text{Ca}^{2+}$  influx activates the ERK1/2 pathway through a CaM-dependent pathway. Whereas, when the intracellular  $\text{Ca}^{2+}$  concentration becomes higher, TRPC1 uses an alternative CaM-dependent mechanism, independently to TRPC1-

mediated  $\text{Ca}^{2+}$  influx to modulate PSC's proliferation and IL-6 secretion, passing through its association with SMAD2 factor and thus its activation. However to investigate this hypothesis, simultaneous TRPC1 silencing using ERK1/2, SMAD2, CaM inhibitors, independently, is required, assessing the impact on PSC's proliferation and IL-6 secretion when using siTRPC1 transfected cells in the presence of ERK1/2 or SMAD2 inhibitors, and respectively the impact on ERK1/2 and SMAD2 phosphorylation when TRPC1 is knocked down in the presence of CaM inhibitors.

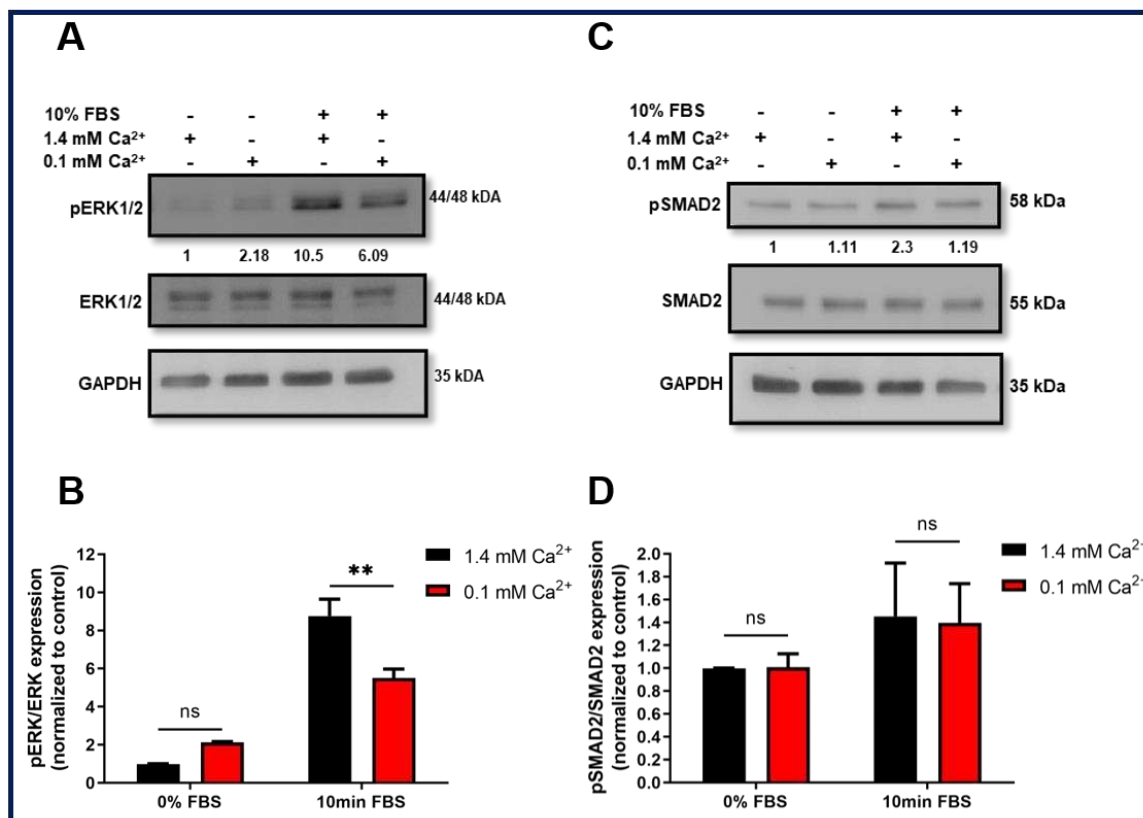


**Figure 46: TRPC1 regulates ERK1/2 and SMAD2 phosphorylation through a calcium dependent / independent manner, respectively.** A-D) Effect of  $\text{Ca}^{2+}$  on ERK1/2 and SMAD2 activation, after a FBS starvation of no transfected PS-1 cells, over-night. Then PS-1 cells were pre-treated for 30 min with 1.3 mM EGTA to reduce the extracellular calcium concentration (0.1 mM  $\text{Ca}^{2+}$ ) with and without 10% FBS or 10 more minutes. Representative western blot of extracellular  $\text{Ca}^{2+}$  concentration decrease on ERK1/2 (A) and SMAD2 (C) phosphorylation. The ratio of phosphorylated protein form/ total protein expression was used to quantify ERK1/2 (B) and SMAD2 (D) activation. All the experiments were performed 72h post-proliferation. (\*\* $p=0.0023$ , NS: no significant,  $N=3$ , two-way ANOVA followed by

Bonferroni *post hoc* test). All values were firstly normalized to the referent protein (GAPDH) and then to the 0% FBS control condition, reported as mean  $\pm$ SEM.

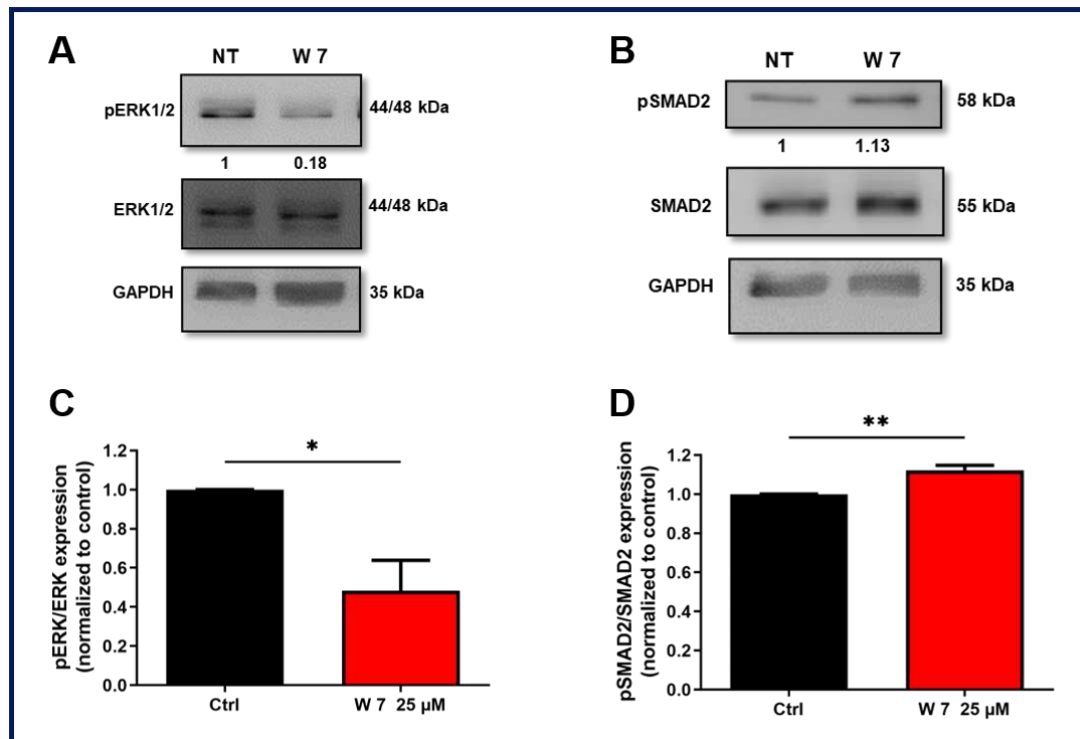


**Figure 47: Activation of ERK1/2 but not SMAD2 by calmodulin, after 72h cell treatment with the calmodulin pharmacological inhibitor W 7 (25  $\mu$ M).** Representative Western blot of ERK1/2(A) and SMAD2 (B) phosphorylation and its quantification as described above, for ERK1/2 (C) and SMAD2 (D), respectively. (\*\* $p < 0.01$ , \* $p < 0.05$ ,  $N = 3$ , Student's *t*-test). All values were firstly normalized to the referent protein (GAPDH) and then to the control condition, reported as mean  $\pm$ SEM.

## 5.2) ERK1/2 pharmacological inhibition increases SMAD2 mRNA expression

We then thought that ERK1/2 and SMAD2 pathways might compete or modulate each other to mediate PS-1's proliferation and IL-6 secretion. Indeed, as mentioned in the introduction part, in several cell types, ERK1/2 can directly phosphorylate Smad2, inhibiting its activity (Zhang, 2017). This possible direct crosstalk between the two pathways could partially justify the observed effect with W 7 on Smad2 phosphorylation, probably due to the inhibition of the calmodulin-mediated ERK1/2 activation, supporting our above emitted

hypothesis. Additionally, we found that ERK1/2 pharmacological inhibition with U 0126 increased SMAD2 mRNA expression by 30.40% (Ctrl:  $100 \pm 4.71\%$ , U 0126:  $130.40 \pm 10.19\%$ ,  $p=0.0220$ ,  $N=3$ , **Figure 48**), suggesting that ERK1/2 might negatively regulate SMAD2 expression, and consequently its activation. However, to verify this hypothesis, we should evaluate the activation of SMAD2 under U 0126 treatment and reversibly the phosphorylation of ERK1/2 under SB 431542 treatment to determine whether each pathway negatively regulates the other one.

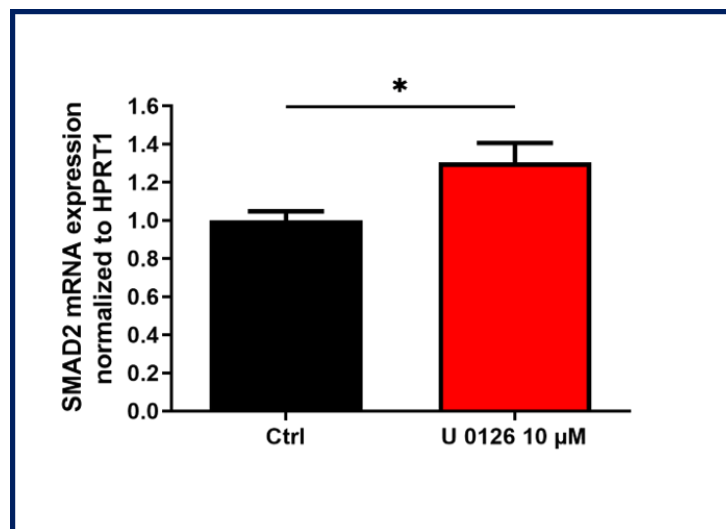


**Figure 48: Pharmacological inhibition of ERK1/2 pathway using the U 0126 inhibitor increase SMAD2 mRNA expression, quantified by qPCR ( $p<0.05$ ,  $N=3$ , Student *t*-test). All values were reported as mean  $\pm$  SEM normalized first to the HPRT1 referent gene and then to the control condition.**

### **5.3) $\alpha$ SMA functional expression is $Ca^{2+}$ and SOCE independent**

According to the above results, indicating the presence of a SMAD2- $Ca^{2+}$  independent mechanism and the fact that the SMAD2 pathway mediates  $\alpha$ SMA expression in PS-1 cells, we wanted to determine whether its expression was also  $Ca^{2+}$ -independent. We, so, reduced the extracellular  $Ca^{2+}$  concentration to 0.1 mM using the EGTA and treated PS-1 cells under this condition for 72h. As expected, the low  $Ca^{2+}$  conditions did not reveal any significant effect on  $\alpha$ SMA expression compared to the physiological conditions (1.4 mM  $Ca^{2+}$ ), although we



remarked a slight tendency to its expression increase (0.1 mM Ca<sup>2+</sup>: 1.33 ± 0.22-fold, p>0.05, N=3, **Figure 49 A-B**).

To support this data, we used the SKF 96365 SOCE inhibitor to decrease the cellular Ca<sup>2+</sup> influx, as we have already demonstrated that the Ca<sup>2+</sup> influx in PS-1 cells is mainly modulated by the Orai1-mediated SOCE and by the mechanosensitive TRPC1 channel, and evaluated the impact on αSMA expression. 72h treatment of PS-1 with SKF 96365 failed to induce any significant difference (SKF 96365: 0.83 ± 0.11-fold, p>0.05, N=3, **Figure 49 C-D**), confirming that αSMA expression is Ca<sup>2+</sup> and SOCE independent. These findings provide evidence that TRPC1 and SMAD2 pathway regulates αSMA expression through a Ca<sup>2+</sup> independent mechanism. However, using a mechanosensitive TRPC1 channel inhibitor, such as GsMTx4, would strengthen and clarify the idea that TRPC1 modulates αSMA expression independently to its Ca<sup>2+</sup> channel function. Moreover, to elucidate whether TRPC1-mediated SMAD2 pathway is responsible for the regulation of αSMA expression, probably due to their physical interaction within the formed complex, experiments using siTRPC1 transfected cells treated with SB 431542 should be performed.

Besides αSMA SOCE-independent expression, we tested in parallel whether its expression is indispensable for the SOCE-mediated Ca<sup>2+</sup> influx. After silencing αSMA for 72h, we measured the SOCE response following the previous described protocol, and we noted a minimal decrease of 10.54% in SOCE (siCtrl: 100 ± 2.50%, siαSMA: 89.46 ± 3.92%, p=0.0183, N=5, **Figure 49 E-F**), suggesting that αSMA expression is not essential for the SOCE-mediated Ca<sup>2+</sup> influx.

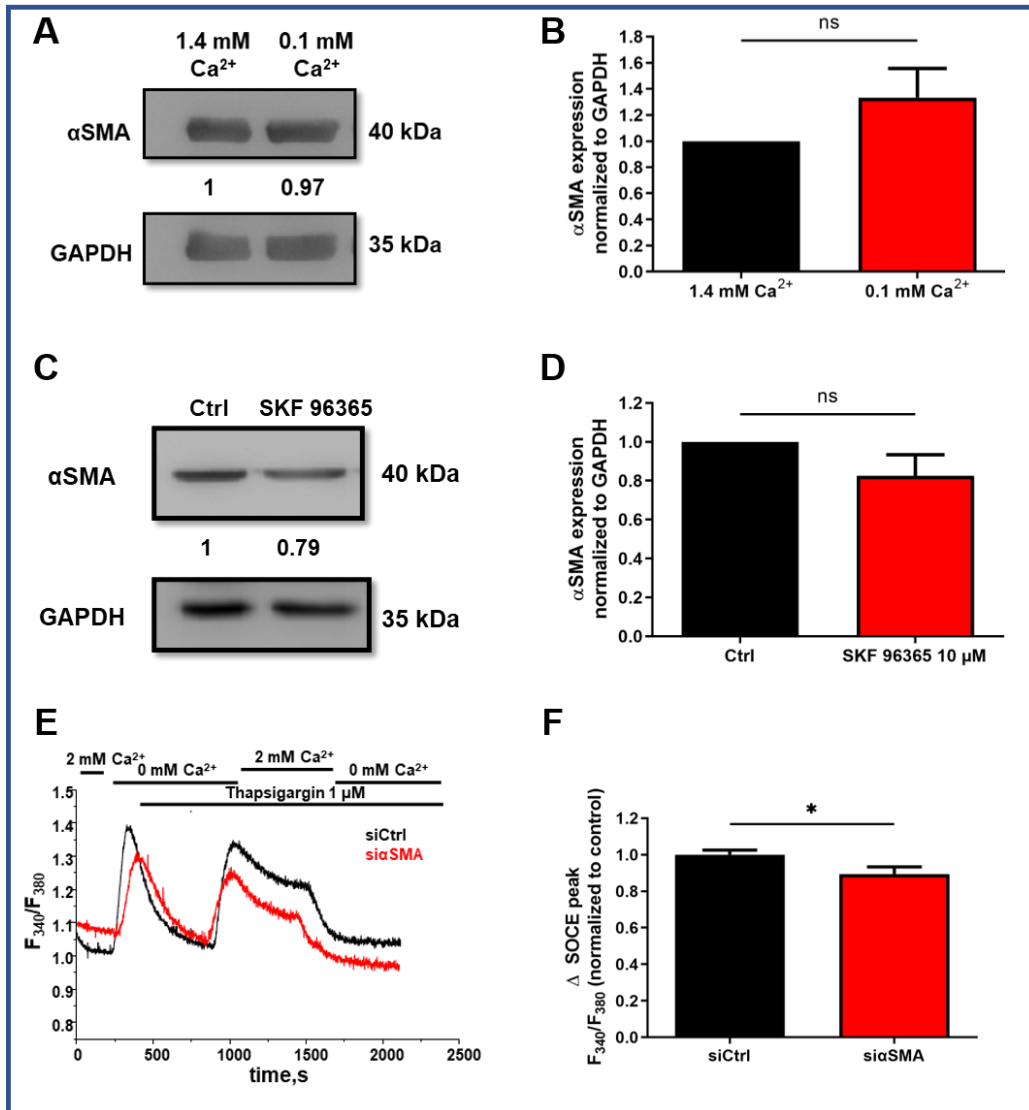


**Figure 49:  $\alpha$ SMA expression is  $\text{Ca}^{2+}$ - and SOCE- independent in PS-1 cells.** A-B) Decrease of extracellular calcium concentration (0.1 mM) using 1.3 mM EGTA for 72h, did not impact  $\alpha$ SMA expression. Representative Western blot of  $\alpha$ SMA expression after treating the cells with EGTA (A) and its quantification (B). C-D) 72h treatment of  $\alpha$ SMA with the SOCE pharmacological inhibitor SKF 96365 (10  $\mu\text{M}$ ) did not affect  $\alpha$ SMA expression protein expression, as illustrated by representative Western blot (C) and the quantification (D). All values were firstly normalized to the referent protein (GAPDH) and then to the control condition, reported as mean  $\pm$ SEM. (NS : no significant, N=3, Student's *t*-test). E-F) Impact of  $\alpha$ SMA in SOCE, evaluated using 72h si $\alpha$ SMA transfected PS-1 cells. SOCE was measured as described previously. Representative traces of SOCE measurements (E) and SOCE quantification (F) (siCtrl: n=249, si $\alpha$ SMA: n=139, N=5, p=0.0183, Student *t*-test). All values

were reported as mean  $\pm$  SEM normalized to the control (n: number of cells, N: number of passage).

## 6) TRPC1 channel mediates SOCE

Nevertheless, albeit the minor role of  $\alpha$ SMA in the SOCE-mediated  $\text{Ca}^{2+}$  influx, we assessed whether its complex partner TRPC1 could play an important role in this process. In addition, it is well known from the literature that except its function as a mechanosensitive channel, TRPC1 can also drive the  $\text{Ca}^{2+}$  influx through a SOCE mechanism, in part by its interaction to STIM1 (Ambudkar et al., 2017; Cheng et al., 2011). We, hence, measured the SOCE response in 72h siTRPC1 transfected cells, and interestingly we detected a 37.72% reduction of the SOCE compared to the siCtrl transfected cells (siCtrl:  $100 \pm 2.80\%$ , siTRPC1:  $62.28 \pm 1.73\%$ ,  $p < 0.0001$ , N=4, **Figure 50 A-B**). Furthermore, TRPC1 knocking down feebly affected the ER- $\text{Ca}^{2+}$  depletion, reflected by the measurement of Tg response, inducing a 12.99% diminution of this response compared to the control condition (siCtrl:  $100 \pm 3.87\%$ , siTRPC1:  $87.01 \pm 3.27\%$ ,  $p = 0.0152$ , N=4, **Figure 50 A-C**). These results exposed an additional potential function of the TRPC1 channel in SOC-mediated  $\text{Ca}^{2+}$  entry through a mechanism that remains to be defined. It would be also worth to assess whether TRPC1 interacts physically with STIM1 in order to support our hypothesis of TRPC1 being a component of the SOCE in PS-1 cells as well.

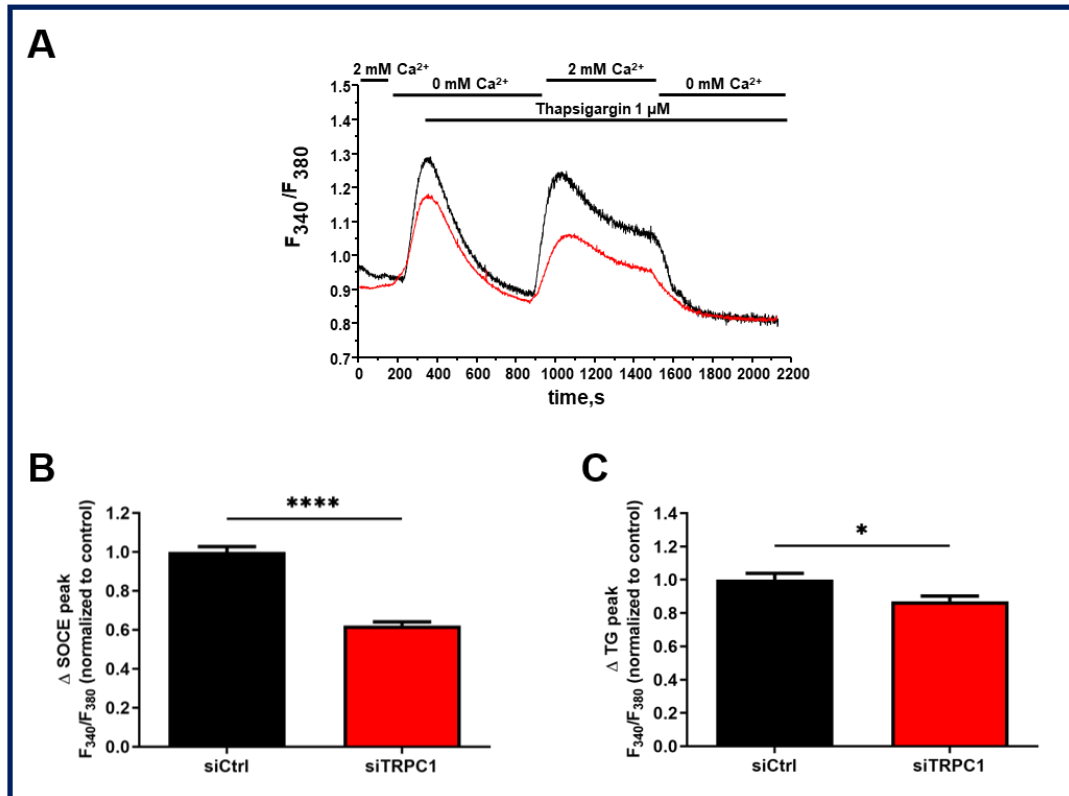


**Figure 50: TRPC1 channel regulates the Store-Operated Calcium Entry (SOCE) and Thapsigargin-induced ER-Ca<sup>2+</sup> depletion in PS-1 cells.** A) Representative traces of SOCE measurements by Ca<sup>2+</sup> imaging. Measurements were performed 72h after siCtrl or siTRPC1 transfection. B-C) SOCE (B) (siCtrl : n=141, siTRPC1 : n=112, N=3) and ER Ca<sup>2+</sup> release induced by 1 μM Thapsigargin (C) (siCtrl : n=92, siTRPC1 : n= 69, N=3) (\*p<0.05, \*\*\*p<0.001, NS: no significant, Student's *t*-test) values are respectively represented as histograms of averages ± SEM normalized the siCtrl condition (n: number of cells, N: number of passage).



---

# **CONCLUSION AND PERSPECTIVES**

---



This thesis work represents one of the first studies of both laboratories (LPCM UR-UPJV 4667 and Inserm U1003- PhyCell) on the assessment of Orai1 and TRPC1 channels' involvement in human PSC's activation processes. We could determine through this work the importance of  $\text{Ca}^{2+}$  entry, mediated via two different  $\text{Ca}^{2+}$  channels, namely Orai1 and TRPC1, in two major PSC's activation processes, including cell proliferation and cytokine secretion.

We have demonstrated on the one side that Orai1 channels mediate  $\text{Ca}^{2+}$  entry in human activated PSC through a SOCE process, triggered by the interaction of Orai1 with STIM1, in part within the lipid rafts. The increased intracellular  $\text{Ca}^{2+}$  concentration, followed the SOCE, activates then the AKT pathway by promoting AKT phosphorylation. Once activated, the AKT pathway stimulates PSC's proliferation through the cell cycle progression in G1/S phase, and TGF- $\beta$ 1 mRNA expression and secretion. However, the downstream effectors of AKT pathway implicated in these two processes remain to be investigated. Additionally, Orai1 mediates in part IL-6 secretion but not expression through a mechanism that needs to be identified. Interestingly, the secreted TGF- $\beta$ 1 enters in a positive feedback loop, enhancing in its turn Orai1 mRNA et protein expression, and also STIM1 mRNA expression, which is reflected by an increase of Orai1/STIM1-mediated SOCE. TGF- $\beta$ 1-promoted SOCE rises intracellular  $\text{Ca}^{2+}$  concentration activating the AKT pathway and hence stimulating even more PSC's proliferation creating a vicious circle, which perpetuates PSC's activation.

One the other side we have shown that  $\text{Ca}^{2+}$  entry through TRPC1 channels is mainly mediated via a SOCE-independent mechanism, involving the mechanosensitive channel component of TRPC1. Indeed, in response to elevated external pressure, one of pancreatic fibrosis' feature, TRPC1 becomes further activated triggering a more important  $\text{Ca}^{2+}$  influx, partly explained by the observed increase of its expression under pressurization. We have suggested that TRPC1-mediated  $\text{Ca}^{2+}$  influx activates ERK1/2 pathway through a calmodulin-dependent mechanism stimulating PSC's proliferation and IL-6 secretion. In parallel, TRPC1 is able to activate another important signalling pathway in PSC's activation, the SMAD2 pathway through its interaction with SMAD2. We speculate that the association of SMAD2 to TRPC1 induces SMAD2 phosphorylation and thereby activation. Interestingly, we have established that TRPC1 not only forms a complex with the active phosphorylated form of SMAD2 (pSMAD2) but also with  $\alpha$ SMA, the principal activation marker of PSCs, and that the three actors are involved in protein network constituting a TRPC1- $\alpha$ SMA-pSMAD2 complex. Importantly, within this complex, each partner regulates the expression of the other partners, suggesting the establishment of a dynamic communication between the three proteins. Showing

that inhibition of SMAD2 pathway and  $\alpha$ SMA knocking down diminish IL-6 secretion and PSC's proliferation, as TRPC1 invalidation does, we could propose that the TRPC1- $\alpha$ SMA-pSMAD2 complex mediates these two processes. To confirm this hypothesis, more experiments are required, inhibiting at least two actors of the complex simultaneously and evaluating the effect on IL-6 secretion and PSC's proliferation. Moreover, our data demonstrated that ERK1/2 inhibition upregulated SMAD2 mRNA expression, implying a role of ERK1/2 as a negative regulator of SMAD2 activation. This hypothesis could also explain the observed increase SMAD2 phosphorylation when treating the cells with a CaM inhibitor, suggesting that CaM-ERK1/2 pathway modulates negatively SMAD2 activation. Indeed, Wicks *et al.* have previously demonstrated that CaM-kinase II inhibits SMAD2 activation by blocking its accumulation in the nucleus and thus its effect. The same authors have reported that SMAD2 contains CaM-kinase II binding sites, which supports partly our data, even though more experiments are needed to clarify this aspect (Wicks *et al.*, 2000). Furthermore, except IL-6 secretion, TRPC1 also modulates IL-6 and IL-11 mRNA expression, which is another member of the IL-6 inflammatory cytokines family, suggesting that TRPC1 might mostly drive the inflammatory phenotype of PSCs, as these two cytokines are characteristic markers of the iCAFs PSC phenotype, as defined by Öhlund *et al.* (Öhlund *et al.*, 2017) (**Figure 51**).

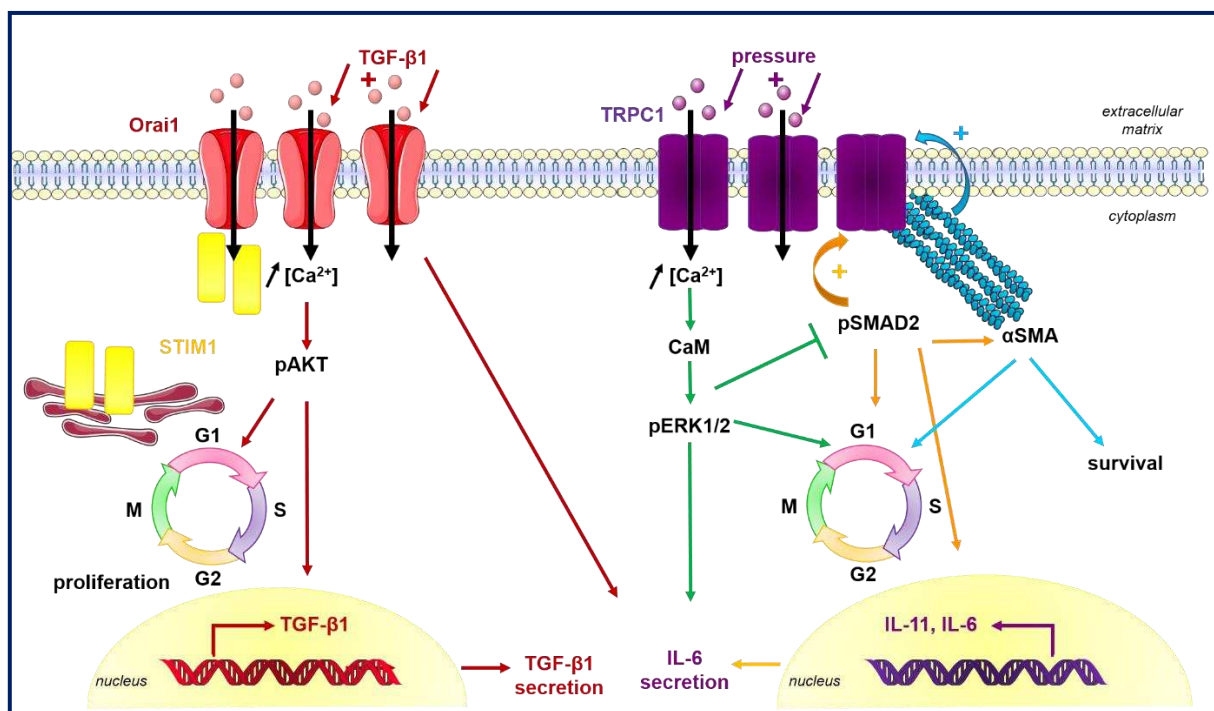


**Figure 51: Conclusive scheme of Orai1 and TRPC1 involvement in PSC's activation processes.**

During our work, we have also been interested in the other two Orai isoforms, Orai2 and Orai3. We have demonstrated that both Orai2 and Orai3 increase SOCE when they are invalidated independently, without impacting the mRNA expression of the other isoforms. However from these finding we cannot conclude whether Orai2 and Orai3 act as negative regulators of Orai1, whether they interact with Orai1 to form heterohexamers or whether they are involved in  $\text{Ca}^{2+}$  entry through a SOCE- independent mechanism (Yoast et al., 2020). To answer these questions, double inhibition of the Orai isoforms will need to be perform, or even using double Orai isoform mutants, evaluating their interaction by co-immunoprecipitation experiments, proximity ligation assay, and effect on SOCE by  $\text{Ca}^{2+}$  imaging or patch clamp experiments. Furthermore, we have observed that Orai3 silencing influences PSC's proliferation and morphology suggesting a potential role also in PSC's migration, by a mechanism that requires more experiments to be identified. Since Orai3 impacts PSC's proliferation, it will be worth to verify the effect of Orai2 as well in this process in order to investigate whether Orai isoforms' stoichiometries could have an impact on the regulation of PSC's proliferation. In parallel, it would be interesting to evaluate whether Orai2 and Orai3 could play a role in TGF- $\beta$ 1 expression and secretion, as it does their homologue, Orai1 (**Figure 52**).

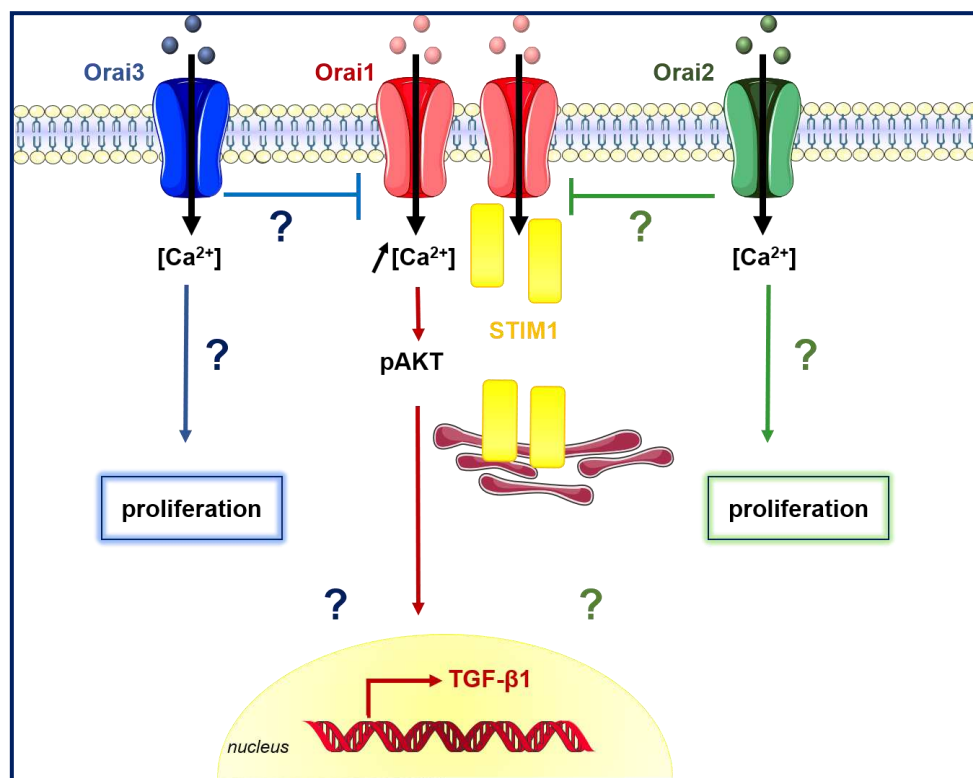


**Figure 52: Role of Orai isoforms in PSC's proliferation and TGF- $\beta$ 1 expression and secretion.**



Besides clarifying the above-cited points, the next step will be to study the role of these channels, namely Orai1 and TRPC1 in the interaction between activated PSC and PCC. As demonstrated by numerous reports, activated PSC plays a primordial role in the development and progression of PDAC, mainly through their dynamic dialogue with the PCCs. Better understanding the molecular mechanisms involved in this communication might permit to identify new and more efficient therapeutic targets. Therefore, disrupting this dynamic dialogue might be the key for improving patient's prognosis.

We have started by investigating whether  $\text{Ca}^{2+}$  could play a role in activated PSCs and PCCs inter-communication, using conditioned medium (CM) from activated PSCs. We cultivated independently PS-1 and RLT-PSCs during 48h in physiological  $\text{Ca}^{2+}$  (1.8 mM)/FBS-free DMEM medium, which is the basic medium we use for MIA PaCa-2 culture in the laboratory, the pancreatic cancer cell line we utilized during these preliminary experiments. Simultaneously, we also cultivated PS-1 and RLT-PSCs in low  $\text{Ca}^{2+}$  (0.2 mM)/ FBS-free DMEM medium. After 48h of culture, the PS-1 and RLT-PSC CM was collected and filtered. We then, replaced in parallel the classic culture medium of MIA PaCa-2 with the collected physiological  $\text{Ca}^{2+}$  and low- $\text{Ca}^{2+}$  PS-1 and RLT-PSC CM, letting MiaPaCa-2 growing in these media for 48h and 72h. Afterwards, we assessed the effect on their viability by MTT colorimetric assay. As expected, we observed an augmentation of MIA PaCa-2 viability in the presence of both PS-1 and RLT-PSC CM, but interestingly we noted a time-lapse between the two PSC cell lines' CM effect. PS-1 CM increases MIA PaCa-2 after 48h of culture whereas RLT-PSCs effect occurs lately, at 72h of culture (MIA PaCa-2+1.8 mM  $\text{Ca}^{2+}$ :  $100 \pm 5.07\%$ , MIA PaCa-2+0.2 mM  $\text{Ca}^{2+}$ :  $72.54 \pm 4.96\%$ , MIA PaCa-2+ RLT CM 1.8 mM  $\text{Ca}^{2+}$ :  $147.50 \pm 15.68\%$ , MIA PaCa-2+ RLT CM 0.2 mM  $\text{Ca}^{2+}$ :  $142.70 \pm 1.45\%$ , N=3, **Figure 53 D**). More importantly, it seems that the low  $\text{Ca}^{2+}$  CM from PS-1 and RLT-PSCs does not have the same influence. PS-1 low  $\text{Ca}^{2+}$  CM induces a decrease of MIA PaCa-2 viability after 48h ( MIA PaCa-2 +1.8 mM  $\text{Ca}^{2+}$ :  $100 \pm 4.60\%$ , MIA PaCa-2 + 0.2 mM  $\text{Ca}^{2+}$ :  $68.33 \pm 7.13\%$ , MIA PaCa-2 + PS-1 CM 1.8 mM  $\text{Ca}^{2+}$ :  $142.70 \pm 8.09\%$ , MIA PaCa-2 + PS-1 CM 0.2 mM  $\text{Ca}^{2+}$ :  $107.30 \pm 7.80\%$ , N=3, **Figure 53 A**) and 72h of culture (MIA PaCa-2 +1.8 mM  $\text{Ca}^{2+}$ :  $100 \pm 4.28\%$ , MIA PaCa-2 +0.2 mM  $\text{Ca}^{2+}$ :  $81.82 \pm 6.56\%$ , MIA PaCa-2 + PS-1 CM 1.8 mM  $\text{Ca}^{2+}$ :  $189.60 \pm 5.39\%$ , MIA PaCa-2 + PS-1 CM 0.2 mM  $\text{Ca}^{2+}$ :  $144.80 \pm 3.19\%$ , N=3, **Figure 53 C**). Whereas RLT low  $\text{Ca}^{2+}$  does not affect MIA PaCa-2 viability (MIA PaCa-2 +1.8 mM  $\text{Ca}^{2+}$ :  $100 \pm 4.47\%$ , MIA PaCa-2+0.2 mM  $\text{Ca}^{2+}$ :  $64.64 \pm 6.81\%$ , MIA PaCa-2 + RLT CM 1.8 mM  $\text{Ca}^{2+}$ :  $121.30 \pm 14.19\%$ , MIA PaCa-2 + RLT CM 0.2 mM  $\text{Ca}^{2+}$ :  $170.40 \pm 3.10\%$ , N=3, one-way ANOVA followed by

Bonferroni multiple comparison test, **Figure 53 B**). This data indicates that PS-1-MIA PaCa-2 interaction is partially  $\text{Ca}^{2+}$ -depend, while RTL-PSC-MIA PaCa-2 interaction is  $\text{Ca}^{2+}$ -independent. This finding highlights the existence of more than one PSC subpopulation, supporting that different PSC's subpopulation have a different impact on PCCs' behavior, and thus on PDAC prognosis.

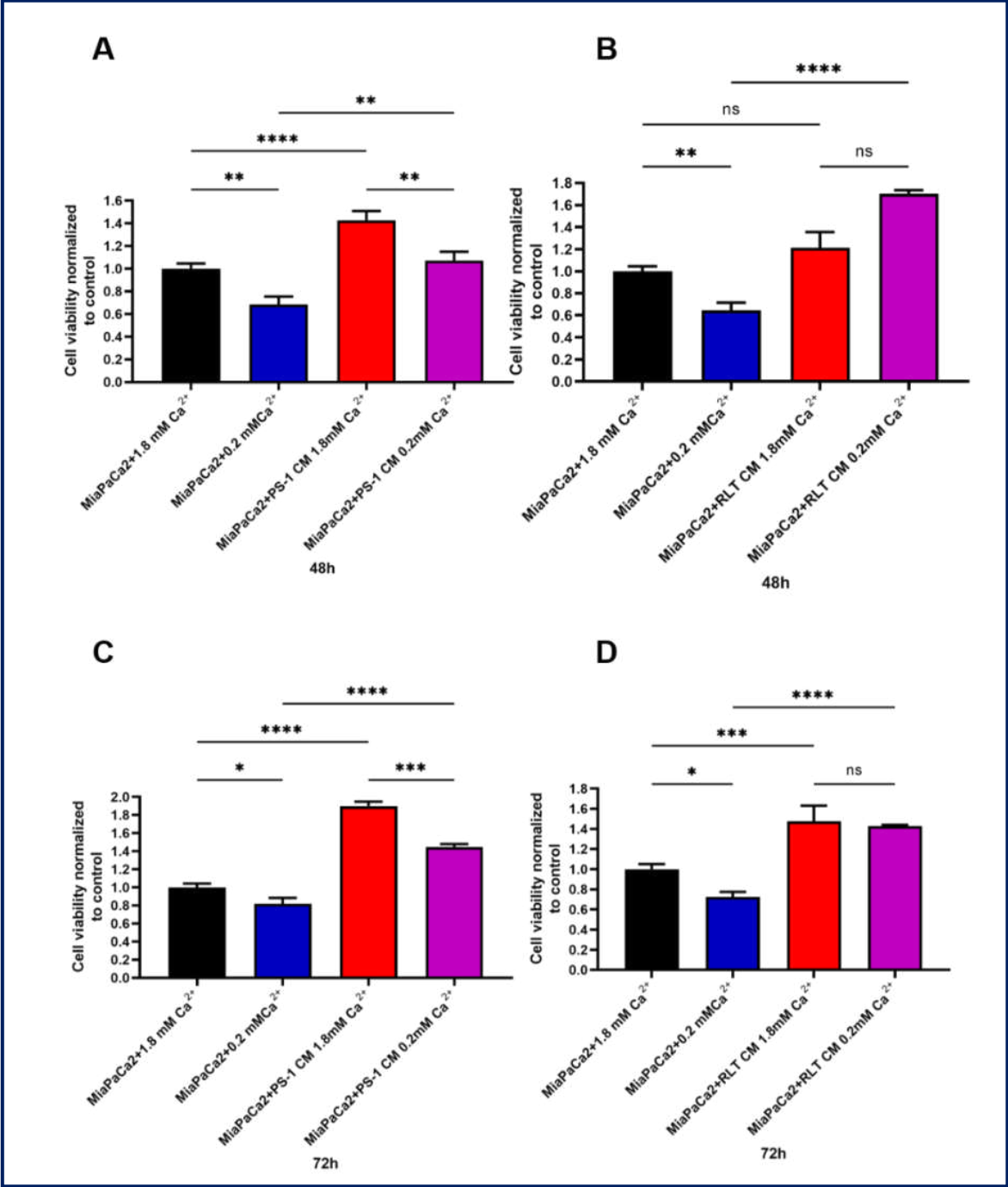


**Figure 53: The interaction between PCC and PSCs is partly Ca<sup>2+</sup>-dependent.** A/C) Evaluation of MIA PaCa-2 viability by MTT colorimetric assay 48h (A) (\*\*p<0.005, \*\*\*\*p<0.0001, N=3) et 72h (C) (\*p=0.0446, \*\*\*p=0.0002, \*\*\*\*p<0.0001, N=3) post-incubation with PS-1 physiological Ca<sup>2+</sup> CM (1.8 mM Ca<sup>2+</sup>) and low Ca<sup>2+</sup> CM (0.2 mM), respectively. PS-1 and RLT-PSCs CM was obtained by 48h culture in FBS-free DMEM medium supplemented or not with the Ca<sup>2+</sup> chelator EGTA (1.6 mM), used for decreasing PSCs' CM Ca<sup>2+</sup> concentration. B/D) Assessment of MIA PaCa-2 viability after 48h (B) (\*\*p=0.0052, \*\*\*\*p<0.0001, N=3) et 72h (D) (\*p=0.0290, \*\*\*p=0.0002, \*\*\*\*p<0.0001, N=3) of culture with RLT-PSC physiological Ca<sup>2+</sup> CM and low Ca<sup>2+</sup> CM, respectively. All values were normalized to the MIA PaCa-2 + 1.8 mM Ca<sup>2+</sup> control condition and reported as mean ± sem. Statistical analysis was performed using one-way ANOVA followed by Turkey multiple comparison test.

Since it seems that MIA PaCa-2 and PS-1 interaction is partially Ca<sup>2+</sup> dependent, we wondered whether the inhibition of one of the SOCE major actors could influence this dialogue. We started by assessing the involvement of STIM1. We so invalidated STIM1 expression in MIA PaCa-2 cells and 24h post-transfection we incubated the cell with PS-1 CM. Interestingly, we observed that STIM1 knocking down in MIA PaCa-2 diminished the efficiency of PS-1 CM on MIA PaCa-2 (MIA PaCa-2 siCtrl: 100 ± 0.50, MIA PaCa-2 siSTIM1: 97.84 ± 5.30%, MIA PaCa-2 siCtrl+ PS-1 CM: 178.90 ± 8.19%, MIA PaCa-2 siSTIM1 + PS-1 CM: 150.10 ± 1.20%, N=3, one-way ANOVA followed by Bonferroni multiple comparison test, **Figure 54 C**), implying that STIM1 might be in part involved in the inter-communication between MIA PaCa-2 and PS-1.

However, given that the utilization of CM implies an indirect communication between the two cell types (PSCs and PCCs), it would be more interesting to use culture models permitting a direct communication study. For instance, using 3D culture models of organoids from PCCs in a direct co-culture with PSCs could strengthen more our future data. Even though, these data remain preliminary, they are promising for evaluating Orai1 and TRPC1 role in the communication between PCCs and PSCs. Even more interesting would be to investigate the impact of each channel's-mediated cytokine (Orai1-mediated TGF-β1 secretion and TRPC1-mediated IL-6 secretion) from PSCs to PCCs, and vice-versa, since their interaction is bidirectional. These future experiments could answer the question whether modulating Orai1 and/or TRPC1 expression and/or activity either only in PSCs or PCCs either in both cell types

or their proposed downstream effectors can be used as a novel therapeutic target for improving PDAC patient's care.

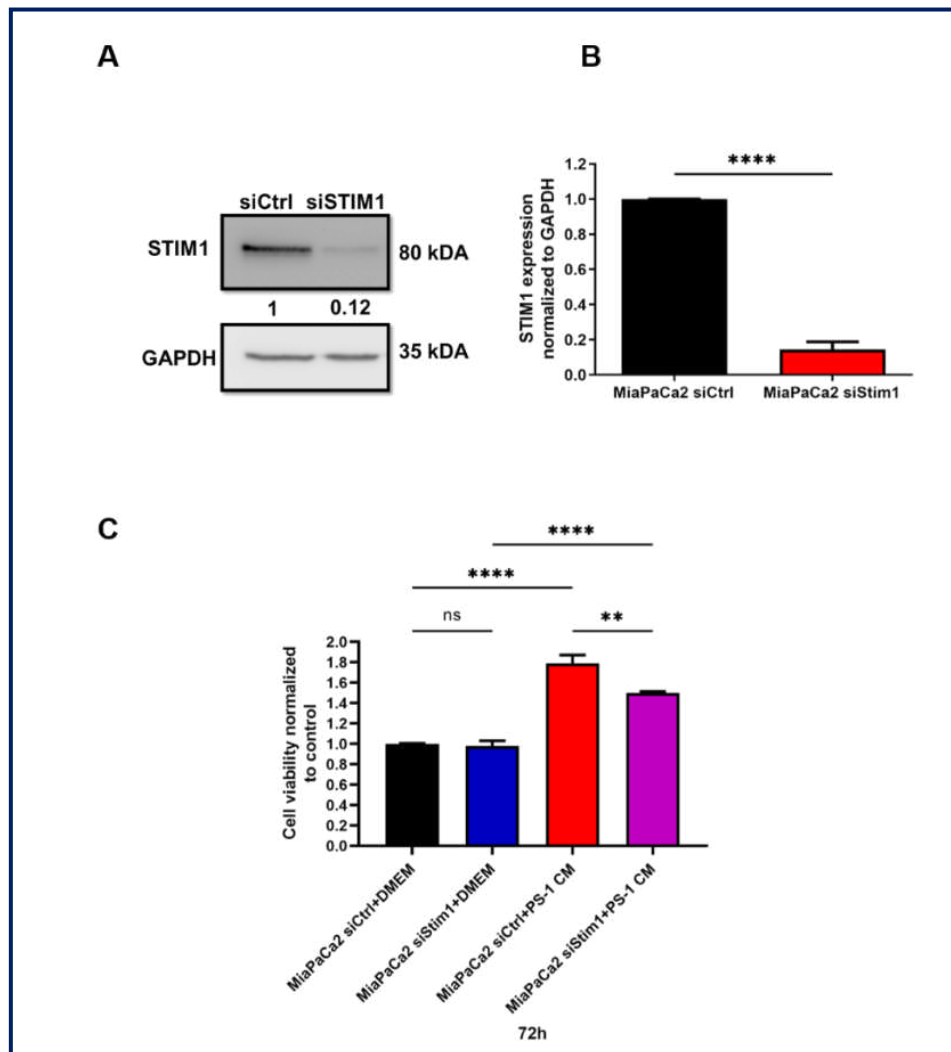


**Figure 54: STIM1 plays a role in the interaction between PCCs and PSCs.** A/B) Evaluation of STIM1 knocking down efficiency in MIA PaCa-2 cells after 96h of transfection. Representative Western blot of STIM1 silencing (A) with the quantification (B) (\*\*\*\* $p < 0.0001$ ,  $N = 3$ , Student  $t$ -test). Values were first normalized to the referent protein GAPDH and then to the siCtrl condition, reported as mean  $\pm$  SEM. C) Investigation of PS-1 CM impact on siSTIM1 transfected MIA PaCa-2 cells' viability. MIA PaCa-2 cells were transfected with siCtrl and siSTIM1, and 24h post-transfection they were cultivated in PS-1 CM for 72h, before quantifying the effect on their viability by MTT colorimetric assay (\*\* $p = 0.0016$ , \*\*\*\* $p < 0.0001$ ,  $N = 3$ , one-way ANOVA followed by Turkey multiple comparison test). All values were normalized to the MIA PaCa-2 siCtrl condition and reported as mean  $\pm$  SEM.



---

# Résumé de Thèse

---



## **Introduction**

La persistance de la fibrose est une caractéristique majeure de la pancréatite chronique (PC) et du cancer du pancréas (CP). Elle provoque une altération des fonctions du pancréas, entraînant une grave détérioration de la qualité de vie des patients. Biologiquement, cette fibrose est principalement médiée par les cellules stellaires pancréatiques activées (CSP) (Apte et al., 2012; Jaster et Emmrich, 2008; Klöppel et al., 2004). En effet, l'activation exacerbée des CSP s'accompagne par un dépôt important de matrice extracellulaire (MEC) conduisant au développement de la fibrose pancréatique (FP). Par conséquent, les CSP sont devenues l'objet de recherches intensives en tant que cible thérapeutique potentielle pour le traitement de la fibrose pancréatique, ainsi que pour le traitement de la PC et CP.

Dans des conditions physiologiques, les CSP se trouvent dans un état quiescent et permettent le stockage de gouttelettes lipidiques de vitamine A. Les CSP représentent 4-7% des cellules qui constituent le pancréas et sont impliquées dans le maintien de l'architecture du pancréas en régulant le renouvellement de la MEC. Cependant, lors d'une lésion pancréatique ou d'une inflammation, les CSP s'activent en acquérant un phénotype myofibroblastique. Elles expriment fortement l'alpha actine du muscle lisse ( $\alpha$ SMA) et perdent en revanche leur gouttelettes lipidiques. Les CSP activées sont également caractérisées par des capacités accrues de prolifération, de migration, de sécrétion des cytokines et des protéines de la MEC (Apte et al., 2013; Bynigeri et al., 2017; Ferdek et Jakubowska, 2017; Masamune et Shimosegawa, 2013; Masamune et al., 2009). Une fois activées, les CSP maintiennent et perpétuent leur propre activation par des sécrétions autocrines mais également paracrines provenant des cellules voisines (Ferdek and Jakubowska, 2017; Shimada et al., 2002). Ceci est dû à la communication étroite des CSP activées avec les cellules voisines, y compris les cellules acineuses pancréatiques lors de la pancréatite (Gryshchenko et al., 2018) et les cellules cancéreuses (Allam et al., 2017) lors du CP, favorisant ainsi le développement d'un tissu fibreux dense. Au cours du CP, par exemple, le dialogue permanent et dynamique entre les CSP activées et les cellules cancéreuses favorise la formation d'un stroma fibreux dense entourant la tumeur, qui peut représenter plus de 80% de la masse tumorale totale (Neesse et al., 2013; Thomas et Radhakrishnan, 2020). Ceci empêche, par conséquent, l'arrivée d'agents chimiothérapeutiques au niveau de la tumeur, tout en augmentant la chimiorésistance du CP.

Les CSP peuvent également être activées par différentes cytokines et facteurs de croissance, sécrétés par les cellules acineuses pancréatiques, les cellules cancéreuses, ou encore les CSP elles-mêmes (Apte et al., 1999; Mews et al., 2002; Schneider et al., 2001). Parmi ces

cytokines et facteurs de croissance, le TGF- $\beta$ 1 (transforming growth factor-beta 1) est bien connu pour être le régulateur majeur de la fibrose pancréatique, notamment par son effet sur l'activation des CSP. En effet, le TGF- $\beta$ 1 stimule l'expression de l' $\alpha$ SMA (marqueur principal d'activation des CSP), leur prolifération ainsi que la production des protéines de l'MEC, notamment le collagène de type I (Kim et al., 2018; Omary et al., 2007). Une autre cytokine d'importance majeure est l'IL-6 (interleukine-6) qui est sécrétée lors de la PC et le CP, et associée à une survie courte de patients (van Duijneveldt et al., 2020). Cette cytokine favorise l'expression de l' $\alpha$ SMA, la sécrétion du collagène de type I mais également celle du TGF- $\beta$ 1. Les CSP activées secrètent elles-mêmes du TGF- $\beta$ 1 et d'IL-6, leur permettant de maintenir ainsi leur propre activation *via* cette positive boucle autocrine (Aoki et al., 2006; Mews et al., 2002). En outre, la modification des propriétés mécaniques du microenvironnement survenue lors de la PC et le CP, contribue aussi à l'activation des CSP. En effet, lors de la fibrose pancréatique, la pression de la tumeur canalaire pancréatique et de son environnement tumoral augmente jusqu'à 10 fois plus que dans le pancréas sain. L'augmentation de cette pression active les CSP en stimulant leur prolifération, l'expression de l' $\alpha$ SMA et la sécrétion du collagène de type I (Fels et al., 2016 ; Provenzano et Hingorani, 2013 ; Watanabe et al., 2004).

Par ailleurs, une grande partie des processus biologiques, tels que la prolifération, la migration, la survie cellulaire, l'expression des gènes ou encore la sécrétion des différentes protéines, sont connus pour être régulés par un second messager universel qui est le calcium ( $\text{Ca}^{2+}$ ) intracellulaire (Radoslavova et al., 2020). L'entrée du  $\text{Ca}^{2+}$  dans la cellule est assurée par la présence des canaux calciques au niveau de la membrane plasmique. Les canaux calciques de type SOC (*Store-Operated Channels*), autrement connus sous le nom des canaux CRAC (*Calcium Release-Activated Channels*), constituent l'une des principales voies d'entrée du  $\text{Ca}^{2+}$  dans les cellules non excitables. Ces canaux SOC sont principalement constitués de la protéine Orai1, qui forme le pore du canal, et de la protéine réticulaire STIM1 (*STromal Interaction Molecule 1*), et ils s'activent à la suite d'une déplétion des stocks calciques du réticulum endoplasmique (Son et al., 2016). Le  $\text{Ca}^{2+}$  semble être également crucial pour la régulation des processus biologiques dans les CSP. Won *et al.* ont été les premiers à démontrer en 2010 que les CSP activées ont une signature calcique différente des CSP quiescentes. En effet les CSP activées présentent des élévations transitoires du  $\text{Ca}^{2+}$  intracellulaire en réponse à la thrombine ou à la trypsine, qui sont absentes dans les CSP quiescentes (Won et al., 2011). En outre, une autre étude menée en 2016, a suggéré la présence des canaux CRAC dans les CSP murines en utilisant des inhibiteurs pharmacologiques (Gryshchenko et al., 2016). Ces données ont

récemment été confirmé par Waldron *et al*, qui ont clairement démontré l'expression d'Orai1 et STIM1 dans les CSP murines (Waldron et al., 2019). Néanmoins, jusqu'à présent, l'importance de l'entrée du  $Ca^{2+}$  *via* les canaux SOC dans la régulation de processus d'activation des CSP humaines, n'a pas encore été élucidée.

Le  $Ca^{2+}$  peut également entrer dans les cellules *via* des canaux calciques mécanosensibles qui agissent comme des capteurs de la force mécanique en la convertissant, ensuite, en signaux biochimiques intracellulaires par la conduction des ions calciques. Ceci résulte à des différents processus cellulaires, tels que la prolifération et migration cellulaire, l'apoptose ou encore l'expression et sécrétion des protéines. Ces canaux calciques impliqués dans la mécanotransduction semblent jouer également un rôle important dans la activation des CSP (Kuntze et al., 2020). L'un des canaux calciques impliqués dans la mécanotransduction est le canal calcique TRPC1 qui fait partie de la grande famille des canaux TRP (*Transient Receptor Potential*). En effet, il a précédemment été démontré par nos collaborateurs en Allemagne, que les forces mécaniques générées par l'augmentation de la pression interstitielle du microenvironnement fibrotique lors de la PC ou du CP, sont détectées par le canal TRPC1 en induisant son activation. L'activation de TRPC1 va ensuite permettre l'influx du  $Ca^{2+}$  à l'intérieur des CSP murines et aura pour conséquence la modulation de leur migration (Fels et al., 2016). Cependant, l'implication du canal TRPC1 dans les CSP humaines reste jusqu'à présent non connue.

### **Objectifs**

Jusqu'à présent le rôle du  $Ca^{2+}$  et des canaux calciques dans la régulation des mécanismes moléculaires et cellulaires modulant l'activation des CSP reste très peu connu en raison de la quantité limitée des études existantes. Par conséquent, les objectifs de ce projet de thèse ont été divisés en deux grands axes :

- 1) Évaluer le rôle des canaux calciques de type SOC et en particulier du canal Orai1 dans les processus d'activation des cellules stellaires pancréatiques humaines, en se focalisant sur la prolifération cellulaire, la survie et la sécrétion de cytokines, tout en explorant les voies de signalisation associées.



Article publié: **Orai1 Channel Regulates Human-Activated Pancreatic Stellate Cell Proliferation and TGFβ1 Secretion through the AKT Signaling Pathway.** *Cancers*, 2021.

Silviya Radoslavova, Antoine Folcher, Thibaut Lefebvre, Kateryna Kondratska, Stéphanie Guénin, Isabelle Dhennin-Duthille, Mathieu Gautier, Natalia Prevarskaya and Halima Ouadid-Ahidouch

- 2) Mieux appréhender le rôle du canal calcique TRPC1, connue pour être impliqué dans la mécanotransduction, dans les processus d'activation des CSP humaines.

Article publié: **TRPC1 channels regulate the activation of pancreatic stellate cells through ERK1/2 and SMAD2 pathways and perpetuate their pressure-mediated activation.** *Cell Calcium*, 2022

Silviya Radoslavova\*, Benedikt Fels\*, Zoltan Pethö, Matthias Gruner, Tobias Ruck, Sven G. Meuth, Antoine Folcher, Natalia Prevarskaya, Albrecht Schwab and Halima Ouadid-Ahidouch

## **Résultats et Discussion**

### **Partie 1 : Le canal calcique Orai1 régule la prolifération et la sécrétion de TGF-β1 des CSP humaines activées *via* la voie de signalisation dépendante d'AKT**

Nous nous sommes focalisés, au cours de cette première partie de la thèse, sur le rôle de l'un des acteurs principaux de SOC, qui est le canal Orai1, dans quelques processus majeurs de l'activation de CSP, à savoir leur prolifération et survie ainsi que l'expression et sécrétion du TGF-β1 par les CSP. Cette première partie a alors été réalisée sur deux lignées cellulaires immortalisées des CSP humaines activées d'origine différente. La lignée PS-1 isolée à partir d'un pancréas humain sain (Froeling et al., 2009), tandis que la lignée RLT-PSCs obtenue suite à une résection pancréatique d'un patient atteint de pancréatite chronique (Jesnowski et al., 2005).

L'expression fonctionnelle du canal Orai1 ainsi que son extinction *via* l'ARN interférence (siRNAs, siCtrl vs siOrai1) ont été étudiées en qPCR (niveau d'ARNm) et en Western Blot (niveau protéique). L'entrée du Ca<sup>2+</sup> médiée par Orai1 a été mesurée en imagerie calcique grâce à la sonde fluorescente et ratiométrique Fura2-AM, et en utilisant la thapsigargine (Tg) qui est inhibiteur irréversible de la pompe sarco/réticulo-endoplasmique

Ca<sup>2+</sup>-ATPase (SERCA). Ce protocole expérimental a pour conséquence la déplétion des stocks calciques du réticulum endoplasmique permettant ainsi la translocation de la protéine STIM1 à la membrane plasmique où elle va interagir avec le canal Orai1 afin de l'activer permettant l'influx du Ca<sup>2+</sup>. L'inhibition d'Orai1 a de ce fait induit une diminution de l'entrée du Ca<sup>2+</sup> mesurée en imagerie calcique dans les deux lignées de CSP humaines. De plus, nous avons constaté que les CSP transfectées avec siOrai1 présentent une concentration basale en Ca<sup>2+</sup> (reflétée par le ratio de la fluorescence basale) moins importante que les CSP transfectées avec siCtrl, suggérant qu'Orai1 module également la concentration basale en Ca<sup>2+</sup> dans les CSP humaines.

Nous avons ensuite cherché à savoir si l'expression fonctionnelle d'Orai1 joue un rôle important dans l'activation de CSP humaines, en évaluant d'abord leur prolifération suite à l'inhibition d'Orai1. La prolifération cellulaire a été étudiée dans un premier temps par le test colorimétrique au MTT après l'inactivation génique d'Orai1 dans les deux lignées de CSP pendant 72h. Nous avons observé que cette inactivation entraîne un effet similaire dans les PS-1 et RLT-PSCs en diminuant le taux de leur prolifération de 37,12% et de 31,39% respectivement. Par la suite, nous avons réalisé des expériences de cytométrie en flux afin de déterminer dans quelles phases du cycle cellulaire Orai1 est impliqué. Les CSP transfectées avec siOrai1 ont montré une accumulation des cellules en phase G0/G1 et une diminution du pourcentage cellulaire en phase S sans modification du nombre de cellules dans la phase G2/M du cycle cellulaire. Simultanément, nous avons vérifié si l'effet observé sur la prolifération n'est pas aussi dû à un effet d'Orai1 sur la survie des CPS. Nous avons évalué la mortalité cellulaire par le test d'exclusion au Bleu de Trypan et en cytométrie en flux par l'analyse du taux de cellules apoptotiques grâce au marquage avec l'Annexine V et l'Iodure de Propidium. L'inhibition d'Orai1 n'a révélé aucun effet significatif sur la mortalité de PS-1 et RLT-PSCs montrant que Orai1 impact uniquement la prolifération des CSP.

L'activation des CSP est également caractérisée par l'acquisition d'une capacité accrue de production et de sécrétion de nombreuses cytokines afin de maintenir leur propre activation et participer au dialogue avec les cellules acineuses lors de la PC et cancéreuses lors du CP. Parmi ces cytokines, nous avons choisi de nous focaliser sur l'étude de l'expression et sécrétion du TGF-β1 (*transforming growth factor*), connu pour être la principale cytokine pro-fibrotique impliquée dans le développement de la fibrose pancréatique ainsi que dans l'activation de CSP et leur communication avec les cellules cancéreuses (Ferdek and Jakubowska, 2017). Nous avons donc quantifié l'expression d'ARN messager (ARNm) du TGF-β1 par qPCR, 72h après

l'invalidation génique d'Orai1 dans les CSP, et nous avons constaté une diminution de ces transcrits. Afin de voir si cette diminution de l'expression de TGF- $\beta$ 1 est corrélée avec une diminution de sa sécrétion par les CSP, nous avons mesuré le TGF- $\beta$ 1 secrété par dosage d'immunoabsorption enzymatique (ELISA). Cependant, nous avons observé une diminution de sa sécrétion 96h après l'inhibition d'Orai1, indiquant qu'Orai1 module l'expression et la sécrétion de TGF- $\beta$ 1 dans les CSP.

Nous nous sommes ensuite intéressés aux voies de signalisation activées par Orai1. Les voies de signalisation impliquées dans l'activation des CSP ont été bien définies (Masamune and Shimosegawa, 2009). Parmi celles-ci, nous avons choisi d'étudier les voies de signalisation d'AKT, d'ERK1/2 et de SMAD2 (Jaster et al., 2002; Masamune et al., 2003; Ohnishi et al., 2004). Nous avons alors évalué la phosphorylation de chacune de ces protéines, par Western Blot, et avons observé une diminution de la phosphorylation uniquement de la protéine AKT dans les CSP transfectées avec siOrai1 comparées à celles transfectées avec siCtrl. Ceci suggère qu'Orai1 module probablement la prolifération ainsi que l'expression et sécrétion de TGF- $\beta$ 1 par la voie AKT. Nous avons voulu valider cette hypothèse en utilisant un inhibiteur pharmacologique de la voie AKT, le LY 294002, car jusqu'à présent aucune étude n'avait montré l'implication directe de cette voie dans la régulation de la prolifération de CSP. Le traitement, de 72h, avec cet inhibiteur a révélé une réduction de la prolifération des CSP, ainsi que de l'expression et sécrétion de TGF- $\beta$ 1, confirmant l'implication de la voie AKT dans ces processus.

Cependant, afin de déterminer si c'est le  $\text{Ca}^{2+}$  entrant *via* le canal Orai1 qui contrôle tous ces processus et non pas Orai1 en tant que protéine, nous avons réduit la concentration physiologique extracellulaire en  $\text{Ca}^{2+}$  dans le milieu de culture des CSP, et avons évalué l'impact sur la voie AKT. Cela a induit une diminution de l'activation d'AKT traduite par la réduction de sa phosphorylation dans les conditions de faible concentration en  $\text{Ca}^{2+}$  (0,1 mM) comparées aux conditions physiologiques en  $\text{Ca}^{2+}$  (1,4 mM), et une diminution de la prolifération. Par la suite, nous avons voulu établir si c'est l'influx calcique médié par Orai1 qui est impliqué dans la régulation de la prolifération des CSP et la sécrétion de TGF- $\beta$ 1. Nous avons alors cultivé des CSP transfectées avec siCtrl et siOrai1 dans un milieu de culture contenant 1,4 mM et 0,1 mM  $\text{Ca}^{2+}$  pendant 72h. Nous avons observé une prolifération plus faible des cellules transfectées avec siOrai1 et cultivées en 0,1 mM  $\text{Ca}^{2+}$  par rapport à la prolifération des CSP cultivées en 1,4 mM  $\text{Ca}^{2+}$ . Cet effet additif sur la prolifération pourrait être expliqué par une augmentation significative de la mortalité cellulaire des CSP transfectées

avec siOrai1 et cultivées en 0,1 mM  $\text{Ca}^{2+}$ . En parallèle, nous avons quantifié la sécrétion de TGF- $\beta$ 1 et nous n'avons pas observé de différences significatives dans la réduction de sa sécrétion par les CSP transfectées avec siOrai1 en 1,4 mM  $\text{Ca}^{2+}$  et en 0,1 mM  $\text{Ca}^{2+}$ . Ces résultats suggèrent que l'entrée du  $\text{Ca}^{2+}$ , médiée par Orai1, régule la prolifération de CSP humaines ainsi que la sécrétion de TGF- $\beta$ 1 *via* l'activation de la voie AKT.

La sécrétion de TGF- $\beta$ 1 par les CSP activées a également été rapportée pour jouer un rôle essentiel dans le maintien de leur activation *via* des boucles de régulation autocrines (Apte et al., 1999). De plus, un lien entre le TGF- $\beta$ 1 et le canal Orai1 a précédemment été montré dans les cellules musculaires lisses des voies aériennes. Dans cette étude, les auteurs ont montré que le traitement par TGF- $\beta$ 1 induit une augmentation des ARNm d'Orai1, ce qui a pour conséquence l'augmentation de l'entrée du  $\text{Ca}^{2+}$  *via* Orai1 (Gao et al., 2013). Nous nous sommes par conséquent demandé si le TGF- $\beta$ 1 secrétée par les CSP activées pourrait à son tour moduler l'entrée du  $\text{Ca}^{2+}$  *via* Orai1. Afin d'investiguer cette hypothèse, des CSP transfectées avec siCtrl et siOrai1 pendant 72h, ont été prétraitées pendant 10 minutes avec de la thapsigargine pour dépléter les stocks calciques du réticulum endoplasmique. Par la suite, l'entrée du  $\text{Ca}^{2+}$  médiée par Orai1 a été mesurée en perfusant du TGF- $\beta$ 1. La perfusion du TGF- $\beta$ 1 a induit une augmentation significative (de 14%) de l'entrée du  $\text{Ca}^{2+}$  dans les CSP transfectées avec siCtrl. Cette augmentation n'était plus observée dans les CSP transfectées avec siOrai1. Ce résultat indique que le TGF- $\beta$ 1 stimule l'entrée du  $\text{Ca}^{2+}$  *via* Orai1. Nous avons alors supposé que l'effet observé à court terme du TGF- $\beta$ 1 sur l'entrée du  $\text{Ca}^{2+}$  *via* Orai1 pourrait être lié à un effet à long terme de cette cytokine au niveau d'ARNm et de la protéine d'Orai1. Nous avons ainsi traité les CSP avec du TGF- $\beta$ 1 pendant 48h en réduisant le sérum du milieu de culture (1% SVF), et nous avons constaté une augmentation importante de l'expression d'Orai1 au niveau transcriptionnel et protéique.

Le TGF- $\beta$ 1 est connu pour avoir un double rôle dans la régulation de la prolifération cellulaire. En effet, selon le type cellulaire il peut induire soit une inhibition soit une stimulation de la prolifération. Cependant, son rôle dans la prolifération des CSP ainsi que dans les voies de signalisation associées, reste peu connu. Nous avons, de ce fait, commencé par étudier l'implication du TGF- $\beta$ 1 dans l'activation de la voie AKT médiée par Orai1. Après 72h de transfection, les CSP transfectées avec siCtrl et siOrai1 ont été stimulées pendant 30 minutes avec du TGF- $\beta$ 1 et ensuite la phosphorylation de l'AKT a été quantifiée par Western Blot. Comme attendu, nous avons constaté une augmentation de l'activation d'AKT dans les CSP transfectées avec siCtrl et stimulées avec du TGF- $\beta$ 1 comparées aux non stimulées. Toutefois,

aucun effet additif n'a été observé dans la réduction de la phosphorylation d'AKT dans les CSP transfectées avec siOrai1 stimulées et non stimulées avec du TGF- $\beta$ 1. Ces résultats montrent l'implication du TGF- $\beta$ 1 dans l'activation de la voie AKT médiée par Orai1.

Nous avons ainsi voulu savoir si la stimulation de la voie AKT par le TGF- $\beta$ 1 est liée à un effet sur la prolifération des CSP. Pour cela nous avons traité les CSP transfectées avec siCtrl et siOrai1, avec du TGF- $\beta$ 1 pendant 48h, et nous avons remarqué une augmentation de la prolifération des CSP transfectées avec siCtrl et traitées avec du TGF- $\beta$ 1 comparées aux non traitées. Cette augmentation de la prolifération par le TGF- $\beta$ 1 n'est plus observée sur des CSP transfectées avec siOrai1.

L'ensemble de ces résultats met en évidence, pour la première fois, le rôle du canal Orai1 ainsi que de l'entrée calcique médiée par Orai1 dans la régulation de processus d'activation des CSP, et notamment dans la modulation de leur prolifération et de la sécrétion de TGF- $\beta$ 1. Ces données révèlent également que le TGF- $\beta$ 1 sécrété par les CSP, *via* une boucle de rétrocontrôle positive, favorise encore plus la prolifération médiée par Orai1. Cet effet autocrine de TGF- $\beta$ 1 est traduit par une augmentation de l'expression fonctionnelle d'Orai1, ce qui stimule encore plus la phosphorylation d'AKT et par conséquent la prolifération des CSP.

## **Partie 2 : Rôle du canal calcique TRPC1 dans l'activation des CSPs**

La deuxième partie de ce travail de thèse a été dédiée à mieux appréhender le rôle du canal calcique TRPC1 dans l'activation des CSP, notamment en réponse à des conditions de pression élevée. En effet, l'augmentation de la pression tissulaire pancréatique est un évènement caractéristique qui survient lors de la fibrose pancréatique sévère présente dans la PC et le CP. Cette pression est 10 fois plus élevée que dans le pancréas sain (Provenzano and Hingorani, 2013). En outre, il a précédemment été démontré par l'équipe du Pr Albrecht Schwab en Allemagne que les forces mécaniques créées par l'élévation de cette pression tissulaire pancréatique sont détectées par le canal calcique TRPC1 en induisant son activation. L'activation de TRPC1 va ensuite permettre l'influx du Ca<sup>2+</sup> à l'intérieur des CSP murines et aura pour conséquence la modulation de leur migration (Fels et al., 2016). Cependant, le rôle du canal TRPC1 dans les CSP humaines reste jusqu'à présent inconnu. Par conséquent, en collaboration avec l'équipe du Pr Schwab nous avons cherché à mieux comprendre l'importance de ce canal dans les processus d'activation de CSP. Pour réaliser cette étude, des CSP primaires murines dont lesquelles le gène de TRPC1 a été inactivé (TRPC1-KO) ainsi que

la lignée cellulaire des CSP humaines PS-1 dont lesquelles le canal TRPC1 a été inhibé de manière transitoire par siRNA (siCtrl vs siTRPC1) ont été utilisées.

Il a été démontré que la pression élevée présente dans le microenvironnement fibrotique de la PC et du CP, stimule l'activation des CSP (Watanabe et al., 2004). Nous avons alors, dans un premier temps, cherché à savoir si l'expression de TRPC1 est indispensable pour l'activation des CSP induite par des conditions de pression élevée. En utilisant des CSP primaires murines sauvages (WT) et TRPC1-KO cultivées dans des conditions contrôle et de pressurisation ( $\Delta+100$  mmHg), nous avons quantifié par immunofluorescence le niveau d'expression de l' $\alpha$ SMA, connue pour être le principal marqueur d'activation des CSP. Nous avons constaté que les CSP-WT présentent une accélération de l'augmentation de l'expression d' $\alpha$ SMA dans des conditions de pression élevée comparées à celles en condition contrôle. Cependant cette accélération de l'activation traduite par l'augmentation d' $\alpha$ SMA est absente dans les CSP TRPC1-KO en conditions de pression élevée, suggérant que l'activation des CSP induite par la pressurisation est, en partie, modulée par le canal TRPC1. Cette partie d'expériences a été réalisée par nos collaborateurs en Allemagne.

L'élévation de la pression tissulaire durant la fibrose pancréatique est entre autres provoquée par l'augmentation de la rigidité tissulaire, elle-même induite par le dépôt excessif de protéines de la matrice extracellulaire (MacCurtain et al., 2021). Une telle rigidité élevée est également observée sur le support plastique de boîtes de pétri de culture cellulaire (Lachowski et al., 2017), ce qui induit et maintient l'activation des CSP. Afin de mieux comprendre le rôle de TRPC1 dans l'activation des CSP, nous avons par la suite utilisé la lignée des CSP humaines pré-activées, la lignée PS-1, lorsqu'elles sont cultivées sur le support plastique de boîtes de pétri de culture cellulaire. Nous avons alors inhibé l'expression de TRPC1 pendant 72h par transfection de siRNA (siCtrl vs siTRPC1) dans les PS-1 et nous avons regardé l'expression protéique d' $\alpha$ SMA en Western Blot. L'invalidation de TRPC1 a induit une diminution importante (de 58,4%) de l'expression d' $\alpha$ SMA dans les CSP humaines pré-activées, suggérant que son expression est en partie dépendante de la présence du canal TRPC1.

Après avoir montré qu'il y a un lien entre l'expression de TRPC1 et l'expression d' $\alpha$ SMA dans CSP murines cultivées dans des conditions de pression élevée et les CSP humaines pré-activées, nous nous sommes demandés si TRPC1 pourrait être colocalisé avec l' $\alpha$ SMA. Par ailleurs, comme l'expression d' $\alpha$ SMA est connue pour être modulée par la voie de signalisation de SMAD2 dans les CSP de rat (Ohnishi et al., 2004), nous avons cherché à savoir si le canal TRPC1 pourrait être lié à la protéine  $\alpha$ SMA *via* la forme active/phosphorylée

de SMAD2 (pSMAD2). Pour répondre à ces questions, nous avons évalué la colocalisation de TRPC1, d' $\alpha$ SMA et de pSMAD2 en immunofluorescence par microscopie confocale en utilisant la lignée de CSP pré-activées PS-1. Nous avons pu quantifier la colocalisation entre ces trois acteurs en utilisant le coefficient de corrélation de Pearson qui a révélé une colocalisation partielle entre TRPC1,  $\alpha$ SMA et pSMAD2, indiquant qu'il y a peut-être aussi une interaction physique entre ces trois protéines. Afin de vérifier cette hypothèse, nous avons réalisé des expériences de Co-immunoprécipitation en utilisant des anticorps contre TRPC1,  $\alpha$ SMA et pSMAD2 qui nous ont permis de mettre en évidence une interaction physique directe ou indirecte entre les trois acteurs dans les CSP humaines pré-activées. Nous avons ensuite voulu évaluer l'importance de la présence de chaque acteur au sein du complexe protéique formé. Pour cela nous avons invalidé indépendamment chaque protéine pendant 72h (siCtrl vs siTRPC1 vs si $\alpha$ SMA vs siSmad2) et nous avons quantifié son interaction avec les deux autres protéines par Co-immunoprécipitation et en Western Blot. Ces expériences ont révélé que les trois acteurs ensemble (TRPC1,  $\alpha$ SMA et pSMAD2) sont indispensables pour la formation du complexe protéique car l'absence d'un acteur, interrompt l'interaction entre les deux autres protéines.

Simultanément, nous avons complété nos données en étudiant l'expression fonctionnelle de TRPC1 dans les CSP humaines pré-activées dans des conditions de pression élevée, car jusqu'à présent celle-ci a été évaluée uniquement dans les CSP murines (Fels et al., 2016). Nous avons alors cultivé les PS-1 dans des conditions de pression élevée ( $\Delta+100$  mmHg) pendant 24h et 48h, et nous avons quantifié, en premier lieu, l'expression de TRPC1 mais également d' $\alpha$ SMA, en Western Blot. Cette pressurisation a induit une augmentation de l'expression protéique de TRPC1 et d' $\alpha$ SMA dans les PS-1. Afin de voir si cette augmentation protéique de TRPC1 est corrélée à une stimulation plus importante de sa fonction canal, nous avons mesuré l'influx calcique en imagerie calcique. Nous avons cultivé des CSP humaines transfectées avec siCtrl et siTRPC1 dans des conditions de pression élevée et contrôle pendant 24h, et ensuite nous avons mesuré l'influx calcique en appliquant un protocole de quench manganèse. Nous avons constaté une augmentation importante de l'influx calcique dans les CSP transfectées avec siCtrl en condition de pressurisation comparées à celles en condition contrôle. Cependant, cet influx calcique a été fortement réduit dans les CSP transfectées avec siTRPC1 en condition de pressurisation mais également en condition contrôle. Ces résultats suggèrent que le canal TRPC1 a une activité basale dans des conditions physiologiques dans les CSP humaines pré-activées, et que cette activité devient encore plus importante dans des

conditions de pression élevée. Cette partie du travail a été réalisée en collaboration avec l'équipe du Pr Schwab en Allemagne.

Nous avons, par la suite, cherché à savoir si TRPC1 module l'activation des CSP, notamment par la régulation de l'expression d' $\alpha$ SMA (le principal marqueur d'activation des CSP) *via* l'une de voies de signalisation impliquées dans l'activation des CSP. Parmi ces voies, il a été démontré que les voies d'ERK1/2 et de SMAD2 favorisent l'activation des CSP en réponse à de stimuli environnementaux (Jaster et al., 2002; Ohnishi et al., 2004; Watanabe et al., 2004). Nous avons alors examiné si la phosphorylation d'ERK1/2 et de SMAD2 peut moduler l'activation des CSP humaines pré-activées *via* la régulation de l'expression d' $\alpha$ SMA. Pour cela nous avons inhibé chaque voie indépendamment en traitant les CSP humaines avec des inhibiteurs pharmacologiques pendant 72h et avons observé que seule l'inhibition de la voie SMAD2 induit une réduction de l'expression d' $\alpha$ SMA. En parallèle, nous avons remarqué, de manière intéressante, que l'inhibition de TRPC1 induit une réduction de la phosphorylation de la protéine SMAD2 mais aussi de la protéine ERK1/2.

Une fois que nous avons établi les voies de signalisation modulées par TRPC1, nous nous sommes demandés si TRPC1 pourrait être impliqué dans la régulation d'autres processus d'activation de CSP. Nous avons alors choisi de se focaliser sur deux processus majeurs, à savoir la prolifération des CSP et la sécrétion de cytokines. Après avoir inhibé TRPC1 pendant 72h, nous avons observé une réduction de 60% de la prolifération des CSP humaines, mesurée par le test colorimétrique au MTT. Cette diminution était associée à une accumulation des CSP transfectées avec siTRPC1 dans la phase G0/G1, et une réduction du pourcentage de cellules dans les phases S et G2/M du cycle cellulaire. Simultanément, nous avons regardé si l'une des voies de signalisation médiées par TRPC1, les voies ERK1/2 et SMAD2, sont également impliquées dans la modulation de la prolifération des CSP humaines. En inhibant pharmacologiquement et indépendamment chacune de voies pendant 72h, nous avons remarqué un effet inhibiteur de la prolifération des CSP similaire. Ces données montrent l'implication du canal TRPC1 dans la régulation de la prolifération des CSP probablement *via* l'activation des voies de signalisation d'ERK1/2 et de SMAD2.

Nous avons également étudié le rôle du TRPC1 dans la modulation de la sécrétion de cytokines par les CSP, en se focalisant en particulier sur la sécrétion de l'interleukine-6 (IL-6). En effet, l'IL-6 représente l'une des cytokines pro-inflammatoires les plus secrétées par les CSP activées et elle joue un rôle très important dans le microenvironnement fibrotique du pancréas. Il a été démontré que la concentration d'IL-6 dans le sérum des patients atteints de PC ou de



CP est très élevée, et que cette augmentation corrélée avec la sévérité de la pathologie chez les patients (Biffi et al., 1996; Okada et al., 1998). Nous avons alors inhibé l'expression de TRPC1 pendant 72h et nous avons mesuré, par dosage ELISA, le taux de sécrétion d'IL-6 par les CSP. L'inactivation de TRPC1 a induit une diminution, supérieure à 50%, de la sécrétion d'IL-6. En parallèle, nous avons vérifié si les deux voies de signalisation modulées par TRPC1 sont également impliquées dans la modulation de la sécrétion d'IL-6, en les bloquant pharmacologiquement. L'inhibition de la voie ERK1/2 a réduit la sécrétion d'IL-6 de 40% alors que celle de SMAD2 a induit une diminution de 68%. De plus, nous avons constaté, par des expériences réalisées par nos collaborateurs, que la sécrétion d'IL-6 par les CSP-WT murines en conditions de pressurisation est de 4 fois plus importante que celle des CSP-WT en conditions contrôle. De même, comme pour les CSP humaines transfectées avec siTRPC1, les CSP TRPC1-KO murines en conditions de pression élevée secrètent beaucoup moins d'IL-6 comparées aux CSP-WT dans les mêmes conditions. Ces résultats montrent l'implication du TRPC1 dans la régulation de la sécrétion d'IL-6, probablement *via* l'activation des voies ERK1/2 et SMAD2.

Ensemble, tous ces données apportent des nouvelles connaissances sur le rôle du canal TRPC1 dans les processus d'activation des CSP dans des conditions qui miment le microenvironnement pathologique.

### **Conclusion**

Ce travail de thèse, réalisé en co-direction entre le laboratoire LPCM UR-UPJV 4667 à Amiens et le laboratoire PhyCell-Inserm U1003 à Lille, représente la première étude effectuée sur l'implication des canaux calciques Orai1 et TRPC1 dans les processus d'activation des CSP humaines. Au cours de ce travail, nous avons pu déterminer l'importance de ces deux canaux calciques dans la physiopathologie des CSP, et notamment dans les processus de prolifération cellulaire et de sécrétion des cytokines.

Nous montrons, d'une part, que le canal Orai1 est exprimé et fonctionnel dans les CSP humaines, en modulant l'influx du  $Ca^{2+}$  dans les CSP. Cette entrée du  $Ca^{2+}$  induit une augmentation de la concentration intracellulaire en  $Ca^{2+}$  participant à la phosphorylation et ainsi à l'activation de la voie de signalisation AKT. Une fois activée, la voie AKT stimule la

prolifération de CSP, en régulant la transition de la phase G1/S du cycle cellulaire, et elle stimule également l'expression et sécrétion de TGF- $\beta$ 1 par les CSP. Cependant, les effecteurs impliqués en aval de la voie AKT et qui participent à la régulation de ces processus d'activation de CSP restent à être élucidés.

De manière intéressante, nous avons mis en évidence que le TGF- $\beta$ 1 secrété par les CSP, module à son tour l'activation des CSP, *via* une boucle de rétrocontrôle positive. En effet, une fois secrété, le TGF- $\beta$ 1 induit une augmentation de l'expression du canal Orai1 au niveau transcriptomique et protéique, ce qui favorise l'entrée du Ca<sup>2+</sup> *via* ce canal dans les CSP. Ceci a pour conséquence une augmentation plus importante de la concentration intracellulaire en Ca<sup>2+</sup>, ce qui favorise la phosphorylation d'AKT et la prolifération des CSP, formant un cercle vicieux qui maintient l'activation des CSP (**schéma récapitulatif**).

D'autre part, nous montrons une augmentation de l'influx du Ca<sup>2+</sup> *via* TRPC1 par des forces mécaniques qui découlent de la pression élevée présente dans le microenvironnement fibrotique du pancréas. En effet, la pressurisation induit une augmentation de l'expression protéique de TRPC1, ce qui favorise une entrée calcique importante *via* les canaux TRPC1. Nos résultats montrent que cet influx calcique médié par TRPC1 active ERK1/2 et stimule la prolifération et la sécrétion d'IL-6 par les CSP.

Par ailleurs, TRPC1 forme un complexe protéique avec la forme phosphorylée de SMAD2 (pSMAD2). De plus, au sein de ce complexe, chaque acteur module l'expression protéique des autres partenaires suggérant la présence d'une communication dynamique entre les trois protéines. Nous supposons alors que TRPC1 *via* la formation de ce complexe protéique TRPC1- $\alpha$ SMA-pSMAD2 régule également la prolifération des CSP et la sécrétion d'IL-6 par les CSP (**schéma récapitulatif**). Cependant, cette hypothèse nécessite d'être confirmée par d'autres expériences, notamment en inhibant simultanément l'expression de deux acteurs du complexe et en évaluant l'effet sur la prolifération et la sécrétion d'IL-6.

En conclusion générale, l'ensemble de ces travaux a permis de mieux comprendre le rôle de canaux calciques et notamment des canaux Orai1 et TRPC1 dans l'activation des CSP. Les connaissances acquises pourront permettre d'étudier l'implication de ces canaux dans l'interaction des CSP avec les cellules cancéreuses pancréatiques lors du CP ou encore les cellules acineuses lors de la PC.

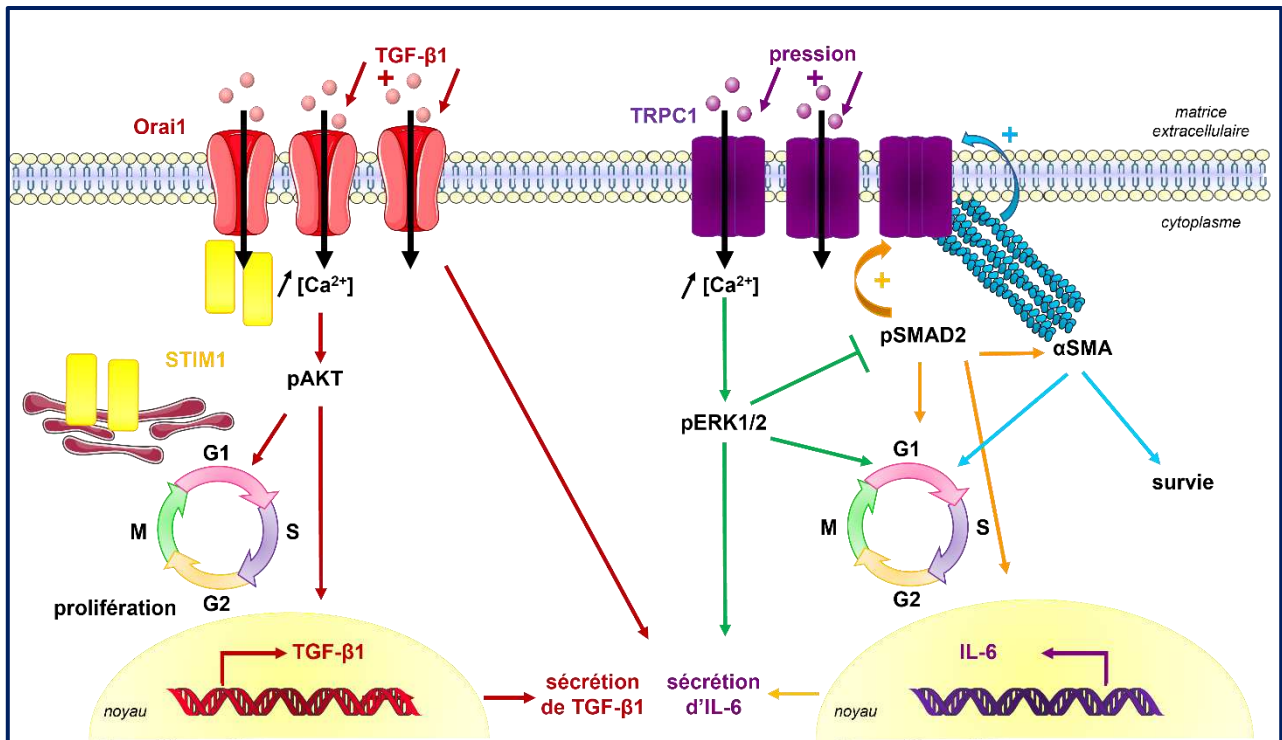


Schéma récapitulatif du rôle des canaux Orai1 et TRPC1 dans les processus d'activation des CSP.

## Valorization

### Articles and Reviews:

**TRPC1 channels regulate pancreatic stellate cell activation through ERK1/2 and SMAD2 pathways and perpetuate their pressure-mediated activation.** *Cell Calcium* (Cell Calcium, Volume 106, 2022, 102621, <https://doi.org/10.1016/j.ceca.2022.102621>).

Silviya Radoslavova\*, Benedikt Fels\*, Zoltan Pethö, Matthias Gruner, Tobias Ruck, Sven Meuth, Antoine Folcher, Natalia Prevarskaya, Albrecht Schwab, Halima Ouadid-Ahidouch.

**TRPM7 Modulates Human Pancreatic Stellate Cell Activation.** *Cells* (*Cells* 2022, 11(14), 2255; <https://doi.org/10.3390/cells11142255>).

Julie Auwercx\*, Philippe Kischel\*, Thibaut Lefebvre\*, Nicolas Jonckheere, Alison Vanlaeys, Stéphanie Guénin, **Silviya Radoslavova**, Isabelle Van Seuning, Halima Ouadid-Ahidouch, Hemant M Kocher, Isabelle Dhennin-Duthille, Mathieu Gautier.

**Orai1 Channel Regulates Human-Activated Pancreatic Stellate Cell Proliferation and TGF $\beta$ <sub>1</sub> Secretion through the AKT Signaling Pathway.** *Cancers* 2021 (*Cancers* 2021, 13, 2395. <https://doi.org/10.3390/cancers13102395>).

Silviya Radoslavova, Antoine Folcher, Thibaut Lefebvre, Kateryna Kondratska, Stéphanie Guénin, Isabelle Dhennin-Duthille, Mathieu Gautier, Natalia Prevarskaya, Halima Ouadid-Ahidouch.

**Ca<sup>2+</sup> signaling is critical for pancreatic stellate cell's pathophysiology: from fibrosis to cancer hallmarks.** *Current Opinion in Physiology* 2020 (*Current Opinion in Physiology* 2020, 17:255–260, <https://doi.org/10.1016/j.cophys.2020.08.018>).

Silviya Radoslavova, Halima Ouadid-Ahidouch and Natalia Prevarskaya.

**Mammary SLAMF3 Regulates Store-Operated Ca<sup>2+</sup> Entry and Migration Through STIM1 in Breast Cancer Cells and Cell Lines.** *Journal of Cancer Science and Clinical Therapeutic* 2020 (*J Cancer Sci Clin Ther* 2020; 4 (4): 462-479 DOI: 10.26502/jcsct.5079087).

Grégory Fouquet, Constance Marié, Mehdi Badaoui, Baptiste Demey, Sylviya Radoslavova, Marie-Sophie Telliez, Isabelle Dhennin-Duthille, Jagadeesh Bayry, Henri Sevestre, Halima Ouadid-Ahidouch, Ingrid Marcq, Hicham Bouhlal.

**Ion Channels: New Actors Playing in Chemotherapeutic Resistance.** *Cancers* 2019 (*Cancers* 2019, 11, 376;doi:10.3390/cancers11030376).

Philippe Kischel\*, Alban Girault\*, Lise Rodat-Desoix, Mohamed Chamlali, Silviya Radoslavova, Hiba Abou Daya, Thibaut Lefebvre, Arthur Foulon, Pierre Rybarczyk, Frédéric Hague, Isabelle Dhennin-Duthille, Mathieu Gautier and Halima Ouadid-Ahidouch.

**Oral communications:**

**Calcium entry through TRPC1 and ORAI1 regulates activated pancreatic stellate cells proliferation.**

S. Radoslavova, T. Lefebvre, MS. Telliez, A. Vanlaeys, I. Dhennin-Duthille, M. Gautier, N. Prevarskaya, H. Ouadid-Ahidouch.

Conference: Physiology 2019, Aberdeen, Scotland, United-Kingdom, 8-9 July 2019

**Calcium is crucial for activated pancreatic stellate cells and for their interaction with pancreatic cancer cells.**

S. Radoslavova, K. Kondratska, A. Kondratskyi, T. Lefebvre, MS. Telliez, A. Vanlaeys, I. Dhennin-Duthille, M. Gautier, N. Prevarskaya, H. Ouadid-Ahidouch.

Conference: Journée Amiénoise de Recherche en Santé (JARS), Amiens, France, 17 January 2019

**Regulation of constitutive cation entry and proliferation by TRPM7 channel in human pancreatic stellate cells.**

T. Lefebvre, A. Vanlaeys, S. Radoslavova, H. Ouadid-Ahidouch, I. Dhennin-Duthille, M. Gautier.

Conference: Europhysiology 2018, London, England, United-Kingdom, 14-16 September 2018

**Poster communications:**

**Regulation of human activated pancreatic stellate cells proliferation by TRPM7 channels.**

T.Lefebvre, S. Radoslavova, H. Ouadid-Ahidouch, I. Dhennin-Duthille, M. Gautier.

Conference: Physiology 2019, Aberdeen, Scotland, United-Kingdom, 8-9 July 2019

**ORAI1 and STIM1 are overexpressed in activated pancreatic stellate cells and regulate cell proliferation and survival.**

**S. Radoslavova**, K. Kondratska, A. Kondratskyi, T. Lefebvre, MS. Telliez, A. Vanlaeys, I. Dhennin-Duthille, M. Gautier, N. Prevarskaya, H. Ouadid-Ahidouch.

Conference : 1<sup>ère</sup> Journée de Recherche: Signalisation oncogéniques et canaux ioniques, Amiens, France, 27 November 2018

**ORAI1 and STIM1 are overexpressed in activated pancreatic stellate cells and regulate cell proliferation and survival.**

S. Radoslavova, K. Kondratska, A. Kondratskyi, T. Lefebvre, MS. Telliez, A. Vanlaeys, I. Dhennin-Duthille, M. Gautier, N. Prevarskaya, H. Ouadid-Ahidouch.

Conference : 2<sup>ème</sup> Journée Nationale Canaux Ioniques et Cancer, Poitiers, France, 7 July 2018



---

# REFERENCES

---



Ambudkar, I.S., de Souza, L.B., Ong, H.L., 2017. TRPC1, Orai1, and STIM1 in SOCE: Friends in tight spaces. *Cell Calcium* 63, 33–39. <https://doi.org/10.1016/j.ceca.2016.12.009>

*Anatomy and Histology of the Pancreas*, n.d. <https://doi.org/10.3998/panc.2014.3>

Andoh, A., Takaya, H., Saotome, T., Shimada, M., Hata, K., Araki, Y., Nakamura, F., Shintani, Y., Fujiyama, Y., Bamba, T., 2000. Cytokine regulation of chemokine (IL-8, MCP-1, and RANTES) gene expression in human pancreatic periacinar myofibroblasts. *Gastroenterology* 119, 211–219. <https://doi.org/10.1053/gast.2000.8538>

Aoki, H., Ohnishi, H., Hama, K., Ishijima, T., Satoh, Y., Hanatsuka, K., Ohashi, A., Wada, S., Miyata, T., Kita, H., Yamamoto, H., Osawa, H., Sato, K., Tamada, K., Yasuda, H., Mashima, H., Sugano, K., 2006a. Autocrine loop between TGF-beta1 and IL-1beta through Smad3- and ERK-dependent pathways in rat pancreatic stellate cells. *Am J Physiol Cell Physiol* 290, C1100-1108. <https://doi.org/10.1152/ajpcell.00465.2005>

Aoki, H., Ohnishi, H., Hama, K., Shinozaki, S., Kita, H., Osawa, H., Yamamoto, H., Sato, K., Tamada, K., Sugano, K., 2007. Cyclooxygenase-2 is required for activated pancreatic stellate cells to respond to proinflammatory cytokines. *Am J Physiol Cell Physiol* 292, C259-268. <https://doi.org/10.1152/ajpcell.00030.2006>

Aoki, H., Ohnishi, H., Hama, K., Shinozaki, S., Kita, H., Yamamoto, H., Osawa, H., Sato, K., Tamada, K., Sugano, K., 2006c. Existence of autocrine loop between interleukin-6 and transforming growth factor-beta1 in activated rat pancreatic stellate cells. *J Cell Biochem* 99, 221–228. <https://doi.org/10.1002/jcb.20906>

Apte, M., McCarroll, J., Pirola, R., Wilson, J., 2007. Pancreatic MAP kinase pathways and acetaldehyde. *Novartis Found Symp* 285, 200–211; discussion 211-216. <https://doi.org/10.1002/9780470511848.ch15>

Apte, M., Pirola, R., Wilson, J., 2011. The fibrosis of chronic pancreatitis: new insights into the role of pancreatic stellate cells. *Antioxid Redox Signal* 15, 2711–2722. <https://doi.org/10.1089/ars.2011.4079>

Apte, M.V., Haber, P.S., Applegate, T.L., Norton, I.D., McCaughan, G.W., Korsten, M.A., Pirola, R.C., Wilson, J.S., 1998. Periacinar stellate shaped cells in rat pancreas: identification, isolation, and culture. *Gut* 43, 128–133. <https://doi.org/10.1136/gut.43.1.128>

Apte, M.V., Haber, P.S., Darby, S.J., Rodgers, S.C., McCaughan, G.W., Korsten, M.A., Pirola, R.C., Wilson, J.S., 1999. Pancreatic stellate cells are activated by proinflammatory cytokines: implications for pancreatic fibrogenesis. *Gut* 44, 534–541. <https://doi.org/10.1136/gut.44.4.534>

Apte, M.V., Park, S., Phillips, P.A., Santucci, N., Goldstein, D., Kumar, R.K., Ramm, G.A., Buchler, M., Friess, H., McCarroll, J.A., Keogh, G., Merrett, N., Pirola, R., Wilson, J.S., 2004. Desmoplastic reaction in pancreatic cancer: role of pancreatic stellate cells. *Pancreas* 29, 179–187. <https://doi.org/10.1097/00006676-200410000-00002>

Apte, M.V., Phillips, P.A., Fahmy, R.G., Darby, S.J., Rodgers, S.C., McCaughan, G.W., Korsten, M.A., Pirola, R.C., Naidoo, D., Wilson, J.S., 2000. Does alcohol directly stimulate pancreatic fibrogenesis? Studies with rat pancreatic stellate cells. *Gastroenterology* 118, 780–794. [https://doi.org/10.1016/s0016-5085\(00\)70148-x](https://doi.org/10.1016/s0016-5085(00)70148-x)



- Apte, M.V., Pirola, R.C., Wilson, J.S., 2016. Alcohol and the Pancreas. *Pancreapedia: The Exocrine Pancreas Knowledge Base*. <https://doi.org/10.3998/panc.2016.17>
- Apte, M.V., Pirola, R.C., Wilson, J.S., 2012. Pancreatic stellate cells: a starring role in normal and diseased pancreas. *Front Physiol* 3, 344. <https://doi.org/10.3389/fphys.2012.00344>
- Apte, M.V., Wilson, J.S., 2012. Dangerous liaisons: pancreatic stellate cells and pancreatic cancer cells. *J Gastroenterol Hepatol* 27 Suppl 2, 69–74. <https://doi.org/10.1111/j.1440-1746.2011.07000.x>
- Apte, M.V., Wilson, J.S., Lugea, A., Pandol, S.J., 2013. A starring role for stellate cells in the pancreatic cancer microenvironment. *Gastroenterology* 144, 1210–1219. <https://doi.org/10.1053/j.gastro.2012.11.037>
- Apte, M.V., Xu, Z., Pothula, S., Goldstein, D., Pirola, R.C., Wilson, J.S., 2015. Pancreatic cancer: The microenvironment needs attention too! *Pancreatology* 15, S32-38. <https://doi.org/10.1016/j.pan.2015.02.013>
- Arnaudeau, S., Kelley, W.L., Walsh, J.V., Demaurex, N., 2001. Mitochondria recycle Ca(2+) to the endoplasmic reticulum and prevent the depletion of neighboring endoplasmic reticulum regions. *J Biol Chem* 276, 29430–29439. <https://doi.org/10.1074/jbc.M103274200>
- Asaumi, H., Watanabe, S., Taguchi, M., Tashiro, M., Otsuki, M., 2007. Externally applied pressure activates pancreatic stellate cells through the generation of intracellular reactive oxygen species. *Am J Physiol Gastrointest Liver Physiol* 293, G972-978. <https://doi.org/10.1152/ajpgi.00018.2007>
- Ashkenazi, A., 2008. Directing cancer cells to self-destruct with pro-apoptotic receptor agonists. *Nat Rev Drug Discov* 7, 1001–1012. <https://doi.org/10.1038/nrd2637>
- Ay, A.-S., Benzerdjeb, N., Sevestre, H., Ahidouch, A., Ouadid-Ahidouch, H., 2013. Orai3 Constitutes a Native Store-Operated Calcium Entry That Regulates Non Small Cell Lung Adenocarcinoma Cell Proliferation. *PLoS One* 8. <https://doi.org/10.1371/journal.pone.0072889>
- B, P., S, B., Bb, S., 2012. The TR (i)P to Ca<sup>2+</sup> signaling just got STIMy: an update on STIM1 activated TRPC channels. *Front Biosci (Landmark Ed)* 17, 805–823. <https://doi.org/10.2741/3958>
- Bachem, M.G., Schneider, E., Gross, H., Weidenbach, H., Schmid, R.M., Menke, A., Siech, M., Beger, H., Grünert, A., Adler, G., 1998. Identification, culture, and characterization of pancreatic stellate cells in rats and humans. *Gastroenterology* 115, 421–432. [https://doi.org/10.1016/s0016-5085\(98\)70209-4](https://doi.org/10.1016/s0016-5085(98)70209-4)
- Bachem, M.G., Schünemann, M., Ramadani, M., Siech, M., Beger, H., Buck, A., Zhou, S., Schmid-Kotsas, A., Adler, G., 2005. Pancreatic carcinoma cells induce fibrosis by stimulating proliferation and matrix synthesis of stellate cells. *Gastroenterology* 128, 907–921. <https://doi.org/10.1053/j.gastro.2004.12.036>
- Barnum, K.J., O'Connell, M.J., 2014. Cell Cycle Regulation by Checkpoints. *Methods Mol Biol* 1170, 29–40. [https://doi.org/10.1007/978-1-4939-0888-2\\_2](https://doi.org/10.1007/978-1-4939-0888-2_2)
- Bateman, A.C., Turner, S.M., Thomas, K.S.A., McCrudden, P.R., Fine, D.R., Johnson, P.A., Johnson, C.D., Iredale, J.P., 2002. Apoptosis and proliferation of acinar and islet cells in chronic

pancreatitis: evidence for differential cell loss mediating preservation of islet function. *Gut* 50, 542–548. <https://doi.org/10.1136/gut.50.4.542>

Bhattacharya, A., Kumar, J., Hermanson, K., Sun, Y., Qureshi, H., Perley, D., Scheidegger, A., Singh, B.B., Dhasarathy, A., 2018. The calcium channel proteins ORAI3 and STIM1 mediate TGF- $\beta$  induced Snail expression. *Oncotarget* 9, 29468–29483. <https://doi.org/10.18632/oncotarget.25672>

Brandman, O., Liou, J., Park, W.S., Meyer, T., 2007. STIM2 is a feedback regulator that stabilizes basal cytosolic and endoplasmic reticulum Ca<sup>2+</sup> levels. *Cell* 131, 1327–1339. <https://doi.org/10.1016/j.cell.2007.11.039>

Beaugé, L., DiPolo, R., 2005. SEA-0400, a potent inhibitor of the Na<sup>+</sup>/Ca<sup>2+</sup> exchanger, as a tool to study exchanger ionic and metabolic regulation. *Am J Physiol Cell Physiol* 288, C1374–1380. <https://doi.org/10.1152/ajpcell.00492.2004>

Beech, D.J., 2005. TRPC1: store-operated channel and more. *Pflugers Arch* 451, 53–60. <https://doi.org/10.1007/s00424-005-1441-3>

Bergdahl, A., Gomez, M.F., Dreja, K., Xu, S.-Z., Adner, M., Beech, D.J., Broman, J., Hellstrand, P., Swärd, K., 2003. Cholesterol depletion impairs vascular reactivity to endothelin-1 by reducing store-operated Ca<sup>2+</sup> entry dependent on TRPC1. *Circ Res* 93, 839–847. <https://doi.org/10.1161/01.RES.0000100367.45446.A3>

Berna, M.J., Seiz, O., Nast, J.F., Benten, D., Bläker, M., Koch, J., Lohse, A.W., Pace, A., 2010. CCK1 and CCK2 Receptors Are Expressed on Pancreatic Stellate Cells and Induce Collagen Production. *J Biol Chem* 285, 38905–38914. <https://doi.org/10.1074/jbc.M110.125534>

Bernard, V., Semaan, A., Huang, J., San Lucas, F.A., Mulu, F.C., Stephens, B.M., Guerrero, P.A., Huang, Y., Zhao, J., Kamyabi, N., Sen, S., Scheet, P.A., Taniguchi, C.M., Kim, M.P., Tzeng, C.-W., Katz, M.H., Singhi, A.D., Maitra, A., Alvarez, H.A., 2019. Single-Cell Transcriptomics of Pancreatic Cancer Precursors Demonstrates Epithelial and Microenvironmental Heterogeneity as an Early Event in Neoplastic Progression. *Clin Cancer Res* 25, 2194–2205. <https://doi.org/10.1158/1078-0432.CCR-18-1955>

Berridge, M.J., 2003. Cardiac calcium signalling. *Biochem Soc Trans* 31, 930–933. <https://doi.org/10.1042/bst0310930>

Berridge, M.J., Bootman, M.D., Lipp, P., 1998. Calcium - a life and death signal. *Nature* 395, 645–648. <https://doi.org/10.1038/27094>

Berridge, M.J., Irvine, R.F., 1984. Inositol trisphosphate, a novel second messenger in cellular signal transduction. *Nature* 312, 315–321. <https://doi.org/10.1038/312315a0>

Biffi, W.L., Moore, E.E., Moore, F.A., Peterson, V.M., 1996. Interleukin-6 in the injured patient. Marker of injury or mediator of inflammation? *Ann Surg* 224, 647–664.

Binkley, C.E., Zhang, L., Greenon, J.K., Giordano, T.J., Kuick, R., Misek, D., Hanash, S., Logsdon, C.D., Simeone, D.M., 2004. The molecular basis of pancreatic fibrosis: common stromal gene expression in chronic pancreatitis and pancreatic adenocarcinoma. *Pancreas* 29, 254–263. <https://doi.org/10.1097/00006676-200411000-00003>

- Blaustein, M.P., Lederer, W.J., 1999. Sodium/calcium exchange: its physiological implications. *Physiol Rev* 79, 763–854. <https://doi.org/10.1152/physrev.1999.79.3.763>
- Bober, R., Bredoux, R., Corvazier, E., Lacabaratz-Porret, C., Martin, V., Kovács, T., Enouf, J., 2005. How many Ca<sup>2+</sup>-ATPase isoforms are expressed in a cell type? A growing family of membrane proteins illustrated by studies in platelets. *Platelets* 16, 133–150. <https://doi.org/10.1080/09537100400016847>
- Bockman, D.E., 1992. Functional Anatomy of the Pancreas: The Ductal System, in: Pederzoli, P., Bassi, C., Vesentini, S. (Eds.), *Pancreatic Fistulas*. Springer, Berlin, Heidelberg, pp. 1–9. [https://doi.org/10.1007/978-3-642-77418-8\\_1](https://doi.org/10.1007/978-3-642-77418-8_1)
- Boulay, G., Brown, D.M., Qin, N., Jiang, M., Dietrich, A., Zhu, M.X., Chen, Z., Birnbaumer, M., Mikoshiba, K., Birnbaumer, L., 1999. Modulation of Ca<sup>2+</sup> entry by polypeptides of the inositol 1,4, 5-trisphosphate receptor (IP3R) that bind transient receptor potential (TRP): evidence for roles of TRP and IP3R in store depletion-activated Ca<sup>2+</sup> entry. *Proc Natl Acad Sci U S A* 96, 14955–14960. <https://doi.org/10.1073/pnas.96.26.14955>
- Brandman, O., Liou, J., Park, W.S., Meyer, T., 2007. STIM2 is a feedback regulator that stabilizes basal cytosolic and endoplasmic reticulum Ca<sup>2+</sup> levels. *Cell* 131, 1327–1339. <https://doi.org/10.1016/j.cell.2007.11.039>
- Bray, F., Ferlay, J., Soerjomataram, I., Siegel, R.L., Torre, L.A., Jemal, A., 2018. Global cancer statistics 2018: GLOBOCAN estimates of incidence and mortality worldwide for 36 cancers in 185 countries. *CA Cancer J Clin* 68, 394–424. <https://doi.org/10.3322/caac.21492>
- Brazer, S.-C.W., Singh, B.B., Liu, X., Swaim, W., Ambudkar, I.S., 2003. Caveolin-1 contributes to assembly of store-operated Ca<sup>2+</sup> influx channels by regulating plasma membrane localization of TRPC1. *J Biol Chem* 278, 27208–27215. <https://doi.org/10.1074/jbc.M301118200>
- Brownlow, S.L., Harper, A.G.S., Harper, M.T., Sage, S.O., 2004. A role for hTRPC1 and lipid raft domains in store-mediated calcium entry in human platelets. *Cell Calcium* 35, 107–113. <https://doi.org/10.1016/j.ceca.2003.08.002>
- Brownlow, S.L., Sage, S.O., 2005. Transient receptor potential protein subunit assembly and membrane distribution in human platelets. *Thromb Haemost* 94, 839–845. <https://doi.org/10.1160/TH05-06-0391>
- Buchholz, M., Kestler, H.A., Holzmann, K., Ellenrieder, V., Schneiderhan, W., Siech, M., Adler, G., Bachem, M.G., Gress, T.M., 2005. Transcriptome analysis of human hepatic and pancreatic stellate cells: organ-specific variations of a common transcriptional phenotype. *J Mol Med (Berl)* 83, 795–805. <https://doi.org/10.1007/s00109-005-0680-2>
- Buck, E., Zimanyi, I., Abramson, J.J., Pessah, I.N., 1992. Ryanodine stabilizes multiple conformational states of the skeletal muscle calcium release channel. *J Biol Chem* 267, 23560–23567.
- Bynigeri, R.R., Jakkampudi, A., Jangala, R., Subramanyam, C., Sasikala, M., Rao, G.V., Reddy, D.N., Talukdar, R., 2017. Pancreatic stellate cell: Pandora's box for pancreatic disease biology. *World J Gastroenterol* 23, 382–405. <https://doi.org/10.3748/wjg.v23.i3.382>

Cabrera, M.C., Tilahun, E., Nakles, R., Diaz-Cruz, E.S., Charabaty, A., Suy, S., Jackson, P., Ley, L., Slack, R., Jha, R., Collins, S.P., Haddad, N., Kallakury, B.V.S., Schroeder, T., Pishvaian, M.J., Furth, P.A., 2014. Human Pancreatic Cancer-Associated Stellate Cells Remain Activated after in vivo Chemoradiation. *Front Oncol* 4, 102. <https://doi.org/10.3389/fonc.2014.00102>

Cai, X., Zhou, Y., Nwokonko, R.M., Loktionova, N.A., Wang, X., Xin, P., Trebak, M., Wang, Y., Gill, D.L., 2016. The Orai1 Store-operated Calcium Channel Functions as a Hexamer. *J Biol Chem* 291, 25764–25775. <https://doi.org/10.1074/jbc.M116.758813>

Cancer Facts & Figures 2019 | American Cancer Society [WWW Document], n.d. URL <https://www.cancer.org/research/cancer-facts-statistics/all-cancer-facts-figures/cancer-facts-figures-2019.html> (accessed 4.26.21).

Cánepa, E.T., Scassa, M.E., Ceruti, J.M., Marazita, M.C., Carcagno, A.L., Sirkin, P.F., Ogara, M.F., 2007. INK4 proteins, a family of mammalian CDK inhibitors with novel biological functions. *IUBMB Life* 59, 419–426. <https://doi.org/10.1080/15216540701488358>

Carafoli, E., Genazzani, A., Guerini, D., 1999. Calcium controls the transcription of its own transporters and channels in developing neurons. *Biochem Biophys Res Commun* 266, 624–632. <https://doi.org/10.1006/bbrc.1999.1879>

Carafoli, E., Santella, L., Branca, D., Brini, M., 2001. Generation, control, and processing of cellular calcium signals. *Crit Rev Biochem Mol Biol* 36, 107–260. <https://doi.org/10.1080/20014091074183>

Casini, A., Galli, A., Pignalosa, P., Frulloni, L., Grappone, C., Milani, S., Pederzoli, P., Cavallini, G., Surrenti, C., 2000. Collagen type I synthesized by pancreatic periacinar stellate cells (PSC) co-localizes with lipid peroxidation-derived aldehydes in chronic alcoholic pancreatitis. *J Pathol* 192, 81–89. [https://doi.org/10.1002/1096-9896\(2000\)9999:9999<::AID-PATH675>3.0.CO;2-N](https://doi.org/10.1002/1096-9896(2000)9999:9999<::AID-PATH675>3.0.CO;2-N)

C. Duluc, S. Moatassim-Billah, M. Chalabi-Dchar, A. Perraud, R. Samain, F. Breibach, M. Gayral, P. Cordelier, M.-B. Delisle, M.-P. Bousquet-Dubouch, R. Tomasini, H. Schmid, M. Mathonnet, S. Pyronnet, Y. Martineau, C. Bousquet, Pharmacological targeting of the protein synthesis mTOR/4E-BP1 pathway in cancer-associated fibroblasts abrogates pancreatic tumour chemoresistance, *EMBO Mol Med.* 7 (2015) 735–753. <https://doi.org/10.15252/emmm.201404346>.

Cell Cycle Checkpoints | Biology for Majors I [WWW Document], n.d. URL <https://courses.lumenlearning.com/wmopen-biology1/chapter/cell-cycle-checkpoints/> (accessed 5.27.21).

C. Guerra, M. Collado, C. Navas, A.J. Schuhmacher, I. Hernández-Porras, M. Cañamero, M. Rodríguez-Justo, M. Serrano, M. Barbacid, Pancreatitis-induced inflammation contributes to pancreatic cancer by inhibiting oncogene-induced senescence, *Cancer Cell.* 19 (2011) 728–739. <https://doi.org/10.1016/j.ccr.2011.05.011>.

Chang, L., Karin, M., 2001. Mammalian MAP kinase signalling cascades. *Nature* 410, 37–40. <https://doi.org/10.1038/35065000>

- Chen, J., Barritt, G.J., 2003. Evidence that TRPC1 (transient receptor potential canonical 1) forms a Ca<sup>2+</sup>-permeable channel linked to the regulation of cell volume in liver cells obtained using small interfering RNA targeted against TRPC1. *Biochem J* 373, 327–336. <https://doi.org/10.1042/BJ20021904>
- Cheng, K.T., Liu, X., Ong, H.L., Swaim, W., Ambudkar, I.S., 2011. Local Ca<sup>2+</sup> Entry Via Orai1 Regulates Plasma Membrane Recruitment of TRPC1 and Controls Cytosolic Ca<sup>2+</sup> Signals Required for Specific Cell Functions. *PLOS Biology* 9, e1001025. <https://doi.org/10.1371/journal.pbio.1001025>
- Cicenas, J., Kvederaviciute, K., Meskinyte, I., Meskinyte-Kausiliene, E., Skeberdyte, A., Cicenas, J., 2017. KRAS, TP53, CDKN2A, SMAD4, BRCA1, and BRCA2 Mutations in Pancreatic Cancer. *Cancers (Basel)* 9. <https://doi.org/10.3390/cancers9050042>
- Clapham, D.E., 2007. Calcium signaling. *Cell* 131, 1047–1058. <https://doi.org/10.1016/j.cell.2007.11.028>
- Conery, A.R., Cao, Y., Thompson, E.A., Townsend, C.M., Ko, T.C., Luo, K., 2004. Akt interacts directly with Smad3 to regulate the sensitivity to TGF-beta induced apoptosis. *Nat Cell Biol* 6, 366–372. <https://doi.org/10.1038/ncb1117>
- Cory, S., Adams, J.M., 2002. The Bcl2 family: regulators of the cellular life-or-death switch. *Nat Rev Cancer* 2, 647–656. <https://doi.org/10.1038/nrc883>
- Crompton, M., 2000. Mitochondrial intermembrane junctional complexes and their role in cell death. *J Physiol* 529 Pt 1, 11–21. <https://doi.org/10.1111/j.1469-7793.2000.00011.x>
- Da Silva Xavier, G., 2018. The Cells of the Islets of Langerhans. *J Clin Med* 7. <https://doi.org/10.3390/jcm7030054>
- David, C.J., Huang, Y.-H., Chen, M., Su, J., Zou, Y., Bardeesy, N., Iacobuzio-Donahue, C.A., Massagué, J., 2016. TGF-β Tumor Suppression through a Lethal EMT. *Cell* 164, 1015–1030. <https://doi.org/10.1016/j.cell.2016.01.009>
- Daya, H.A., Kouba, S., Ouled-Haddou, H., Benzerdjeb, N., Telliez, M.-S., Dayen, C., Sevestre, H., Garçon, L., Hague, F., Ouadid-Ahidouch, H., 2021. Orai3-Mediates Cisplatin-Resistance in Non-Small Cell Lung Cancer Cells by Enriching Cancer Stem Cell Population through PI3K/AKT Pathway. *Cancers* 13, 2314. <https://doi.org/10.3390/cancers13102314>
- DeHaven, W.I., Smyth, J.T., Boyles, R.R., Putney, J.W., 2007. Calcium inhibition and calcium potentiation of Orai1, Orai2, and Orai3 calcium release-activated calcium channels. *J Biol Chem* 282, 17548–17556. <https://doi.org/10.1074/jbc.M611374200>
- Dietrich, A., Fahlbusch, M., Gudermann, T., 2014. Classical Transient Receptor Potential 1 (TRPC1): Channel or Channel Regulator? *Cells* 3, 939–962. <https://doi.org/10.3390/cells3040939>
- Ding, Z., Maubach, G., Masamune, A., Zhuo, L., 2009. Glial fibrillary acidic protein promoter targets pancreatic stellate cells. *Dig Liver Dis* 41, 229–236. <https://doi.org/10.1016/j.dld.2008.05.001>
- Dionisio, N., Galán, C., Jardín, I., Salido, G.M., Rosado, Juan.A., 2011. Lipid rafts are essential for the regulation of SOCE by plasma membrane resident STIM1 in human platelets.

Biochimica et Biophysica Acta (BBA) - Molecular Cell Research 1813, 431–437. <https://doi.org/10.1016/j.bbamcr.2011.01.010>

Dohke, Y., Oh, Y.S., Ambudkar, I.S., Turner, R.J., 2004. Biogenesis and topology of the transient receptor potential Ca<sup>2+</sup> channel TRPC1. *J Biol Chem* 279, 12242–12248. <https://doi.org/10.1074/jbc.M312456200>

Dolmetsch, R.E., Lewis, R.S., Goodnow, C.C., Healy, J.I., 1997. Differential activation of transcription factors induced by Ca<sup>2+</sup> response amplitude and duration. *Nature* 386, 855–858. <https://doi.org/10.1038/386855a0>

Drifka, C.R., Loeffler, A.G., Esquibel, C.R., Weber, S.M., Eliceiri, K.W., Kao, W.J., 2016. Human pancreatic stellate cells modulate 3D collagen alignment to promote the migration of pancreatic ductal adenocarcinoma cells. *Biomed Microdevices* 18, 105. <https://doi.org/10.1007/s10544-016-0128-1>

Dubois, C., Kondratska, K., Kondratskyi, A., Morabito, A., Mesilmany, L., Farfariello, V., Toillon, R.-A., Ziental Gelus, N., Laurence, E., Vanden Abeele, F., Lemonnier, L., Prevarskaya, N., 2021. ORAI3 silencing alters cell proliferation and promotes mitotic catastrophe and apoptosis in pancreatic adenocarcinoma. *Biochim Biophys Acta Mol Cell Res* 1868, 119023. <https://doi.org/10.1016/j.bbamcr.2021.119023>

Duronio, R.J., Xiong, Y., 2013. Signaling pathways that control cell proliferation. *Cold Spring Harb Perspect Biol* 5, a008904. <https://doi.org/10.1101/cshperspect.a008904>

Dziadek, M.A., Johnstone, L.S., 2007. Biochemical properties and cellular localisation of STIM proteins. *Cell Calcium* 42, 123–132. <https://doi.org/10.1016/j.ceca.2007.02.006>

El Hiani, Y., Ahidouch, A., Lehen'kyi, V., Hague, F., Gouilleux, F., Mentaverri, R., Kamel, S., Lassoued, K., Brûlé, G., Ouadid-Ahidouch, H., 2009. Extracellular signal-regulated kinases 1 and 2 and TRPC1 channels are required for calcium-sensing receptor-stimulated MCF-7 breast cancer cell proliferation. *Cell Physiol Biochem* 23, 335–346. <https://doi.org/10.1159/000218179>

Ellenrieder, V., Hendler, S.F., Boeck, W., Seufferlein, T., Menke, A., Ruhland, C., Adler, G., Gress, T.M., 2001. Transforming growth factor beta1 treatment leads to an epithelial-mesenchymal transdifferentiation of pancreatic cancer cells requiring extracellular signal-regulated kinase 2 activation. *Cancer Res* 61, 4222–4228.

Ene-Obong, A., Clear, A.J., Watt, J., Wang, J., Fatah, R., Riches, J.C., Marshall, J.F., Chin-Aleong, J., Chelala, C., Gribben, J.G., Ramsay, A.G., Kocher, H.M., 2013. Activated pancreatic stellate cells sequester CD8<sup>+</sup> T cells to reduce their infiltration of the juxtatumoral compartment of pancreatic ductal adenocarcinoma. *Gastroenterology* 145, 1121–1132. <https://doi.org/10.1053/j.gastro.2013.07.025>

Erkan, M., Adler, G., Apte, M.V., Bachem, M.G., Buchholz, M., Detlefsen, S., Esposito, I., Friess, H., Gress, T.M., Habisch, H.-J., Hwang, R.F., Jaster, R., Kleeff, J., Klöppel, G., Kordes, C., Logsdon, C.D., Masamune, A., Michalski, C.W., Oh, J., Phillips, P.A., Pinzani, M., Reiser-Erkan, C., Tsukamoto, H., Wilson, J., 2012. StellaTUM: current consensus and discussion on pancreatic stellate cell research. *Gut* 61, 172–178. <https://doi.org/10.1136/gutjnl-2011-301220>

- Erkan, M., Kleeff, J., Gorbachevski, A., Reiser, C., Mitkus, T., Esposito, I., Giese, T., Büchler, M.W., Giese, N.A., Friess, H., 2007. Periostin creates a tumor-supportive microenvironment in the pancreas by sustaining fibrogenic stellate cell activity. *Gastroenterology* 132, 1447–1464. <https://doi.org/10.1053/j.gastro.2007.01.031>
- Erkan, M., Michalski, C.W., Rieder, S., Reiser-Erkan, C., Abiatari, I., Kolb, A., Giese, N.A., Esposito, I., Friess, H., Kleeff, J., 2008. The activated stroma index is a novel and independent prognostic marker in pancreatic ductal adenocarcinoma. *Clin Gastroenterol Hepatol* 6, 1155–1161. <https://doi.org/10.1016/j.cgh.2008.05.006>
- Erkan, M., Reiser-Erkan, C., Michalski, C.W., Deucker, S., Sauliunaite, D., Streit, S., Esposito, I., Friess, H., Kleeff, J., 2009. Cancer-stellate cell interactions perpetuate the hypoxia-fibrosis cycle in pancreatic ductal adenocarcinoma. *Neoplasia* 11, 497–508. <https://doi.org/10.1593/neo.81618>
- Ertel, E.A., Campbell, K.P., Harpold, M.M., Hofmann, F., Mori, Y., Perez-Reyes, E., Schwartz, A., Snutch, T.P., Tanabe, T., Birnbaumer, L., Tsien, R.W., Catterall, W.A., 2000. Nomenclature of voltage-gated calcium channels. *Neuron* 25, 533–535. [https://doi.org/10.1016/s0896-6273\(00\)81057-0](https://doi.org/10.1016/s0896-6273(00)81057-0)
- Etemad, B., Whitcomb, D.C., 2001. Chronic pancreatitis: diagnosis, classification, and new genetic developments. *Gastroenterology* 120, 682–707. <https://doi.org/10.1053/gast.2001.22586>
- Fabian, A., Bertrand, J., Lindemann, O., Pap, T., Schwab, A., 2012. Transient receptor potential canonical channel 1 impacts on mechanosignaling during cell migration. *Pflugers Arch.* 464, 623–630. <https://doi.org/10.1007/s00424-012-1169-9>
- Fan, J., Yang, M.X., Ouyang, Q., Fu, D., Xu, Z., Liu, X., Mino-Kenudson, M., Geng, J., Tang, F., 2016. Phosphatase PPM1A is a novel prognostic marker in pancreatic ductal adenocarcinoma. *Hum Pathol* 55, 151–158. <https://doi.org/10.1016/j.humpath.2016.05.002>
- Faouzi, M., Hague, F., Geerts, D., Ay, A.-S., Potier-Cartereau, M., Ahidouch, A., Ouadid-Ahidouch, H., 2016. Functional cooperation between KCa3.1 and TRPC1 channels in human breast cancer: Role in cell proliferation and patient prognosis. *Oncotarget* 7, 36419–36435. <https://doi.org/10.18632/oncotarget.9261>
- Feitelson, M.A., Arzumanyan, A., Kulathinal, R.J., Blain, S.W., Holcombe, R.F., Mahajna, J., Marino, M., Martinez-Chantar, M.L., Nawroth, R., Sanchez-Garcia, I., Sharma, D., Saxena, N.K., Singh, N., Vlachostergios, P.J., Guo, S., Honoki, K., Fujii, H., Georgakilas, A.G., Amedei, A., Niccolai, E., Amin, A., Ashraf, S.S., Boosani, C.S., Guha, G., Ciriolo, M.R., Aquilano, K., Chen, S., Mohammed, S.I., Azmi, A.S., Bhakta, D., Halicka, D., Nowsheen, S., 2015. Sustained proliferation in cancer: mechanisms and novel therapeutic targets. *Semin Cancer Biol* 35, S25–S54. <https://doi.org/10.1016/j.semcancer.2015.02.006>
- Fels, B., Nielsen, N., Schwab, A., 2016. Role of TRPC1 channels in pressure-mediated activation of murine pancreatic stellate cells. *Eur Biophys J* 45, 657–670. <https://doi.org/10.1007/s00249-016-1176-4>
- Ferde, P.E., Jakubowska, M.A., 2017. Biology of pancreatic stellate cells—more than just pancreatic cancer. *Pflugers Arch* 469, 1039–1050. <https://doi.org/10.1007/s00424-017-1968-0>

- Feske, S., 2011. Immunodeficiency due to defects in store-operated calcium entry. *Ann N Y Acad Sci* 1238, 74–90. <https://doi.org/10.1111/j.1749-6632.2011.06240.x>
- Feske, S., Gwack, Y., Prakriya, M., Srikanth, S., Puppel, S.-H., Tanasa, B., Hogan, P.G., Lewis, R.S., Daly, M., Rao, A., 2006. A mutation in Orai1 causes immune deficiency by abrogating CRAC channel function. *Nature* 441, 179–185. <https://doi.org/10.1038/nature04702>
- Fill, M., Copello, J.A., 2002. Ryanodine receptor calcium release channels. *Physiol Rev* 82, 893–922. <https://doi.org/10.1152/physrev.00013.2002>
- Finnson, K.W., Almadani, Y., Philip, A., 2020. Non-canonical (non-SMAD2/3) TGF- $\beta$  signaling in fibrosis: Mechanisms and targets. *Semin Cell Dev Biol* 101, 115–122. <https://doi.org/10.1016/j.semcdb.2019.11.013>
- Friess, H., Yamanaka, Y., Büchler, M., Ebert, M., Beger, H.G., Gold, L.I., Korc, M., 1993. Enhanced expression of transforming growth factor beta isoforms in pancreatic cancer correlates with decreased survival. *Gastroenterology* 105, 1846–1856. [https://doi.org/10.1016/0016-5085\(93\)91084-u](https://doi.org/10.1016/0016-5085(93)91084-u)
- Frischauf, I., Schindl, R., Derler, I., Bergsmann, J., Fahrner, M., Romanin, C., 2008. The STIM/Orai coupling machinery. *Channels (Austin)* 2, 261–268. <https://doi.org/10.4161/chan.2.4.6705>
- Froeling, F.E.M., Mirza, T.A., Feakins, R.M., Seedhar, A., Elia, G., Hart, I.R., Kocher, H.M., 2009. Organotypic Culture Model of Pancreatic Cancer Demonstrates that Stromal Cells Modulate E-Cadherin,  $\beta$ -Catenin, and Ezrin Expression in Tumor Cells. *Am J Pathol* 175, 636–648. <https://doi.org/10.2353/ajpath.2009.090131>
- Fukumoto, J., Patil, S., Krishnamurthy, S., Galam, L., Sharma, N., Patel, K., Hooker, R., Dunning, J., Lockey, R.F., Kolliputi, N., 2019. Characterization of cell proliferation in idiopathic pulmonary fibrosis. *Journal of Allergy and Clinical Immunology* 143, AB218. <https://doi.org/10.1016/j.jaci.2018.12.663>
- Fukushima, N., Kikuchi, Y., Nishiyama, T., Kudo, A., Fukayama, M., 2008. Periostin deposition in the stroma of invasive and intraductal neoplasms of the pancreas. *Mod Pathol* 21, 1044–1053. <https://doi.org/10.1038/modpathol.2008.77>
- Fulda, S., Debatin, K.-M., 2006. Extrinsic versus intrinsic apoptosis pathways in anticancer chemotherapy. *Oncogene* 25, 4798–4811. <https://doi.org/10.1038/sj.onc.1209608>
- Iyer, S.C., Kannan, A., Gopal, A., Devaraj, N., Halagowder, D., 2015. Receptor channel TRPC6 orchestrate the activation of human hepatic stellate cell under hypoxia condition. *Experimental Cell Research* 336, 66–75. <https://doi.org/10.1016/j.yexcr.2015.03.023>
- Gao, Z., Wang, X., Wu, K., Zhao, Y., Hu, G., 2010. Pancreatic stellate cells increase the invasion of human pancreatic cancer cells through the stromal cell-derived factor-1/CXCR4 axis. *Pancreatology* 10, 186–193. <https://doi.org/10.1159/000236012>
- Gao, Y.-D., Zheng, J.-W., Li, P., Cheng, M., Yang, J., 2013. Store-operated Ca<sup>2+</sup> entry is involved in transforming growth factor- $\beta$ 1 facilitated proliferation of rat airway smooth muscle cells. *J Asthma* 50, 439–448. <https://doi.org/10.3109/02770903.2013.778275>



- Giorgi, C., Baldassari, F., Bononi, A., Bonora, M., De Marchi, E., Marchi, S., Missiroli, S., Patergnani, S., Rimessi, A., Suski, J.M., Wieckowski, M.R., Pinton, P., 2012. Mitochondrial Ca(2+) and apoptosis. *Cell Calcium* 52, 36–43. <https://doi.org/10.1016/j.ceca.2012.02.008>
- Glazer, E.S., Welsh, E., Pimiento, J.M., Teer, J.K., Malafa, M.P., 2017. TGFβ1 overexpression is associated with improved survival and low tumor cell proliferation in patients with early-stage pancreatic ductal adenocarcinoma. *Oncotarget* 8, 999–1006. <https://doi.org/10.18632/oncotarget.13533>
- Goel, M., Sinkins, W.G., Schilling, W.P., 2002. Selective association of TRPC channel subunits in rat brain synaptosomes. *J Biol Chem* 277, 48303–48310. <https://doi.org/10.1074/jbc.M207882200>
- Goel, M., Sinkins, W.G., Zuo, C.-D., Estacion, M., Schilling, W.P., 2006. Identification and localization of TRPC channels in the rat kidney. *Am J Physiol Renal Physiol* 290, F1241–1252. <https://doi.org/10.1152/ajprenal.00376.2005>
- Golovina, V.A., 2005. Visualization of localized store-operated calcium entry in mouse astrocytes. Close proximity to the endoplasmic reticulum. *J Physiol* 564, 737–749. <https://doi.org/10.1113/jphysiol.2005.085035>
- Gryshchenko, O., Gerasimenko, J.V., Peng, S., Gerasimenko, O.V., Petersen, O.H., 2018. Calcium signalling in the acinar environment of the exocrine pancreas: physiology and pathophysiology. *J Physiol* 596, 2663–2678. <https://doi.org/10.1113/JP275395>
- Gupta, S., Maitra, A., 2016. EMT: Matter of Life or Death? *Cell* 164, 840–842. <https://doi.org/10.1016/j.cell.2016.02.024>
- Guzman, R., Valente, E.G., Pretorius, J., Pacheco, E., Qi, M., Bennett, B.D., Fong, D.H., Lin, F.-F., Bi, V., McBride, H.J., 2014. Expression of ORAI1, a Plasma Membrane Resident Subunit of the CRAC Channel, in Rodent and Non-rodent Species. *J Histochem Cytochem* 62, 864–878. <https://doi.org/10.1369/0022155414554926>
- Gwack, Y., Srikanth, S., Feske, S., Cruz-Guilloty, F., Oh-hora, M., Neems, D.S., Hogan, P.G., Rao, A., 2007. Biochemical and functional characterization of Orai proteins. *J Biol Chem* 282, 16232–16243. <https://doi.org/10.1074/jbc.M609630200>
- Haas, S.L., Fitzner, B., Jaster, R., Wiercinska, E., Gaitantzi, H., Jesnowski, R., Jesenowski, R., Löhr, J.-M., Singer, M.V., Dooley, S., Breitkopf, K., 2009. Transforming growth factor-beta induces nerve growth factor expression in pancreatic stellate cells by activation of the ALK-5 pathway. *Growth Factors* 27, 289–299. <https://doi.org/10.1080/08977190903132273>
- Haber, P.S., Apte, M.V., Moran, C., Applegate, T.L., Pirola, R.C., Korsten, M.A., McCaughan, G.W., Wilson, J.S., 2004. Non-oxidative metabolism of ethanol by rat pancreatic acini. *Pancreatology* 4, 82–89. <https://doi.org/10.1159/000077608>
- Haber, P.S., Keogh, G.W., Apte, M.V., Moran, C.S., Stewart, N.L., Crawford, D.H., Pirola, R.C., McCaughan, G.W., Ramm, G.A., Wilson, J.S., 1999. Activation of pancreatic stellate cells in human and experimental pancreatic fibrosis. *Am J Pathol* 155, 1087–1095. [https://doi.org/10.1016/S0002-9440\(10\)65211-X](https://doi.org/10.1016/S0002-9440(10)65211-X)

- Haber, P.S., Wilson, J.S., Apte, M.V., Pirola, R.C., 1993. Fatty acid ethyl esters increase rat pancreatic lysosomal fragility. *J Lab Clin Med* 121, 759–764.
- Habisch, H., Zhou, S., Siech, M., Bachem, M.G., 2010. Interaction of Stellate Cells with Pancreatic Carcinoma Cells. *Cancers (Basel)* 2, 1661–1682. <https://doi.org/10.3390/cancers2031661>
- Hama, K., Ohnishi, H., Aoki, H., Kita, H., Yamamoto, H., Osawa, H., Sato, K., Tamada, K., Mashima, H., Yasuda, H., Sugano, K., 2006. Angiotensin II promotes the proliferation of activated pancreatic stellate cells by Smad7 induction through a protein kinase C pathway. *Biochem Biophys Res Commun* 340, 742–750. <https://doi.org/10.1016/j.bbrc.2005.12.069>
- Hama, K., Ohnishi, H., Yasuda, H., Ueda, N., Mashima, H., Satoh, Y., Hanatsuka, K., Kita, H., Ohashi, A., Tamada, K., Sugano, K., 2004. Angiotensin II stimulates DNA synthesis of rat pancreatic stellate cells by activating ERK through EGF receptor transactivation. *Biochem Biophys Res Commun* 315, 905–911. <https://doi.org/10.1016/j.bbrc.2004.01.155>
- Hamacher, R., Schmid, R.M., Saur, D., Schneider, G., 2008. Apoptotic pathways in pancreatic ductal adenocarcinoma. *Mol Cancer* 7, 64. <https://doi.org/10.1186/1476-4598-7-64>
- Hamada, S., Masamune, A., Takikawa, T., Suzuki, N., Kikuta, K., Hirota, M., Hamada, H., Kobune, M., Satoh, K., Shimosegawa, T., 2012. Pancreatic stellate cells enhance stem cell-like phenotypes in pancreatic cancer cells. *Biochem Biophys Res Commun* 421, 349–354. <https://doi.org/10.1016/j.bbrc.2012.04.014>
- Hanahan, D., Weinberg, R.A., 2011. Hallmarks of cancer: the next generation. *Cell* 144, 646–674. <https://doi.org/10.1016/j.cell.2011.02.013>
- Harper, J.W., Adami, G.R., Wei, N., Keyomarsi, K., Elledge, S.J., 1993. The p21 Cdk-interacting protein Cip1 is a potent inhibitor of G1 cyclin-dependent kinases. *Cell* 75, 805–816. [https://doi.org/10.1016/0092-8674\(93\)90499-g](https://doi.org/10.1016/0092-8674(93)90499-g)
- He, J., Sun, X., Qian, K.-Q., Liu, X., Wang, Z., Chen, Y., 2009. Protection of cerulein-induced pancreatic fibrosis by pancreas-specific expression of Smad7. *Biochimica et Biophysica Acta (BBA) - Molecular Basis of Disease* 1792, 56–60. <https://doi.org/10.1016/j.bbadis.2008.10.010>
- He, P., Yang, J.W., Yang, V.W., Bialkowska, A.B., 2018. Krüppel-like Factor 5, Increased in Pancreatic Ductal Adenocarcinoma, Promotes Proliferation, Acinar-to-Ductal Metaplasia, Pancreatic Intraepithelial Neoplasia, and Tumor Growth in Mice. *Gastroenterology* 154, 1494–1508.e13. <https://doi.org/10.1053/j.gastro.2017.12.005>
- Hegyí, P., Rakonczay, Z., 2011. The role of nitric oxide in the physiology and pathophysiology of the exocrine pancreas. *Antioxid Redox Signal* 15, 2723–2741. <https://doi.org/10.1089/ars.2011.4063>
- Hengartner, M.O., 2000. The biochemistry of apoptosis. *Nature* 407, 770–776. <https://doi.org/10.1038/35037710>
- Hezel, A.F., Kimmelman, A.C., Stanger, B.Z., Bardeesy, N., Depinho, R.A., 2006. Genetics and biology of pancreatic ductal adenocarcinoma. *Genes Dev* 20, 1218–1249. <https://doi.org/10.1101/gad.1415606>

- Hidalgo, M., 2010. Pancreatic Cancer [WWW Document]. <http://dx.doi.org/10.1056/NEJMra0901557>. <https://doi.org/10.1056/NEJMra0901557>
- Hofmann, T., Schaefer, M., Schultz, G., Gudermann, T., 2002. Subunit composition of mammalian transient receptor potential channels in living cells. *Proc Natl Acad Sci U S A* 99, 7461–7466. <https://doi.org/10.1073/pnas.102596199>
- Hong, O.-K., Lee, S.-H., Rhee, M., Ko, S.-H., Cho, J.-H., Choi, Y.-H., Song, K.-H., Son, H.-Y., Yoon, K.-H., 2007. Hyperglycemia and hyperinsulinemia have additive effects on activation and proliferation of pancreatic stellate cells: possible explanation of islet-specific fibrosis in type 2 diabetes mellitus. *J Cell Biochem* 101, 665–675. <https://doi.org/10.1002/jcb.21222>
- Holmer, R., Goumas, F.A., Waetzig, G.H., Rose-John, S., Kalthoff, H., 2014. Interleukin-6: a villain in the drama of pancreatic cancer development and progression. *Hepatobiliary Pancreat Dis Int* 13, 371–380. [https://doi.org/10.1016/s1499-3872\(14\)60259-9](https://doi.org/10.1016/s1499-3872(14)60259-9)
- Hu, R., Wang, Y.-L., Edderkaoui, M., Lugea, A., Apte, M.V., Pandol, S.J., 2007. Ethanol augments PDGF-induced NADPH oxidase activity and proliferation in rat pancreatic stellate cells. *Pancreatology* 7, 332–340. <https://doi.org/10.1159/000105499>
- Hwang, R.F., Moore, T., Arumugam, T., Ramachandran, V., Amos, K.D., Rivera, A., Ji, B., Evans, D.B., Logsdon, C.D., 2008. Cancer-associated stromal fibroblasts promote pancreatic tumor progression. *Cancer Res* 68, 918–926. <https://doi.org/10.1158/0008-5472.CAN-07-5714>
- Ide, T., Kitajima, Y., Miyoshi, A., Ohtsuka, T., Mitsuno, M., Ohtaka, K., Koga, Y., Miyazaki, K., 2006. Tumor-stromal cell interaction under hypoxia increases the invasiveness of pancreatic cancer cells through the hepatocyte growth factor/c-Met pathway. *Int J Cancer* 119, 2750–2759. <https://doi.org/10.1002/ijc.22178>
- Ikejiri, N., 1990. The vitamin A-storing cells in the human and rat pancreas. *Kurume Med J* 37, 67–81. <https://doi.org/10.2739/kurumemedj.37.67>
- Ino, Y., Yamazaki-Itoh, R., Shimada, K., Iwasaki, M., Kosuge, T., Kanai, Y., Hiraoka, N., 2013. Immune cell infiltration as an indicator of the immune microenvironment of pancreatic cancer. *Br J Cancer* 108, 914–923. <https://doi.org/10.1038/bjc.2013.32>
- Itoh, F., Asao, H., Sugamura, K., Heldin, C.H., ten Dijke, P., Itoh, S., 2001. Promoting bone morphogenetic protein signaling through negative regulation of inhibitory Smads. *EMBO J* 20, 4132–4142. <https://doi.org/10.1093/emboj/20.15.4132>
- Jakubowska, M.A., Ferdek, P.E., Gerasimenko, O.V., Gerasimenko, J.V., Petersen, O.H., 2016. Nitric oxide signals are interlinked with calcium signals in normal pancreatic stellate cells upon oxidative stress and inflammation. *Open Biol* 6. <https://doi.org/10.1098/rsob.160149>
- Jalleh, R.P., Aslam, M., Williamson, R.C., 1991. Pancreatic tissue and ductal pressures in chronic pancreatitis. *Br J Surg* 78, 1235–1237. <https://doi.org/10.1002/bjs.1800781028>
- Jardin, I., Salido, G.M., Rosado, J.A., 2008. Role of lipid rafts in the interaction between hTRPC1, Orail and STIM1. Channels (Austin) 2, 401–403. <https://doi.org/10.4161/chan.2.6.7055>

- Jaster, R., Emmrich, J., 2008. Crucial role of fibrogenesis in pancreatic diseases. *Best Practice & Research Clinical Gastroenterology, Pancreatic Diseases* 22, 17–29. <https://doi.org/10.1016/j.bpg.2007.10.004>
- Jaster, R., Lichte, P., Fitzner, B., Brock, P., Glass, A., Karopka, T., Gierl, L., Koczan, D., Thiesen, H.-J., Sparmann, G., Emmrich, J., Liebe, S., 2005. Peroxisome proliferator-activated receptor gamma overexpression inhibits pro-fibrogenic activities of immortalised rat pancreatic stellate cells. *J Cell Mol Med* 9, 670–682. <https://doi.org/10.1111/j.1582-4934.2005.tb00497.x>
- Jaster, R., Sparmann, G., Emmrich, J., Liebe, S., 2002. Extracellular signal regulated kinases are key mediators of mitogenic signals in rat pancreatic stellate cells. *Gut* 51, 579–584. <https://doi.org/10.1136/gut.51.4.579>
- Javle, M., Li, Y., Tan, D., Dong, X., Chang, P., Kar, S., Li, D., 2014. Biomarkers of TGF- $\beta$  signaling pathway and prognosis of pancreatic cancer. *PLoS One* 9, e85942. <https://doi.org/10.1371/journal.pone.0085942>
- Jesnowski, R., Fürst, D., Ringel, J., Chen, Y., Schrödel, A., Kleeff, J., Kolb, A., Schareck, W.D., Löhr, M., 2005. Immortalization of pancreatic stellate cells as an in vitro model of pancreatic fibrosis: deactivation is induced by matrigel and N-acetylcysteine. *Lab Invest* 85, 1276–1291. <https://doi.org/10.1038/labinvest.3700329>
- Jin, G., Hong, W., Guo, Y., Bai, Y., Chen, B., 2020. Molecular Mechanism of Pancreatic Stellate Cells Activation in Chronic Pancreatitis and Pancreatic Cancer. *J Cancer* 11, 1505–1515. <https://doi.org/10.7150/jca.38616>
- Jin, Z., El-Deiry, W.S., 2005. Overview of cell death signaling pathways. *Cancer Biol Ther* 4, 139–163. <https://doi.org/10.4161/cbt.4.2.1508>
- Johnson, A., DiPietro, L.A., 2013. Apoptosis and angiogenesis: an evolving mechanism for fibrosis. *FASEB J* 27, 3893–3901. <https://doi.org/10.1096/fj.12-214189>
- Johnstone, L.S., Graham, S.J.L., Dziadek, M.A., 2010. STIM proteins: integrators of signalling pathways in development, differentiation and disease. *J Cell Mol Med* 14, 1890–1903. <https://doi.org/10.1111/j.1582-4934.2010.01097.x>
- Jonitz, A., Fitzner, B., Jaster, R., 2009. Molecular determinants of the profibrogenic effects of endothelin-1 in pancreatic stellate cells. *World J Gastroenterol* 15, 4143–4149. <https://doi.org/10.3748/wjg.15.4143>
- J. Yamaguchi, Y. Yokoyama, T. Kokuryo, T. Ebata, M. Nagino, Cells of origin of pancreatic neoplasms, *Surg Today*. 48 (2018) 9–17. <https://doi.org/10.1007/s00595-017-1501-2>
- Kappel, S., Kilch, T., Baur, R., Lochner, M., Peinelt, C., 2020. The Number and Position of Orai3 Units within Heteromeric Store-Operated Ca<sup>2+</sup> Channels Alter the Pharmacology of ICRAC. *Int J Mol Sci* 21. <https://doi.org/10.3390/ijms21072458>
- Kawasaki, T., Ueyama, T., Lange, I., Feske, S., Saito, N., 2010. Protein kinase C-induced phosphorylation of Orai1 regulates the intracellular Ca<sup>2+</sup> level via the store-operated Ca<sup>2+</sup> channel. *J Biol Chem* 285, 25720–25730. <https://doi.org/10.1074/jbc.M109.022996>

- Kikuta, K., Masamune, A., Satoh, M., Suzuki, N., Satoh, K., Shimosegawa, T., 2006. Hydrogen peroxide activates activator protein-1 and mitogen-activated protein kinases in pancreatic stellate cells. *Mol Cell Biochem* 291, 11–20. <https://doi.org/10.1007/s11010-006-9189-4>
- Kikuta, K., Masamune, A., Satoh, M., Suzuki, N., Shimosegawa, T., 2004. 4-hydroxy-2, 3-nonenal activates activator protein-1 and mitogen-activated protein kinases in rat pancreatic stellate cells. *World J Gastroenterol* 10, 2344–2351. <https://doi.org/10.3748/wjg.v10.i16.2344>
- Kikuta, K., Masamune, A., Watanabe, T., Ariga, H., Itoh, H., Hamada, S., Satoh, K., Egawa, S., Unno, M., Shimosegawa, T., 2010. Pancreatic stellate cells promote epithelial-mesenchymal transition in pancreatic cancer cells. *Biochem Biophys Res Commun* 403, 380–384. <https://doi.org/10.1016/j.bbrc.2010.11.040>
- Kim, K.K., Sheppard, D., Chapman, H.A., 2018a. TGF- $\beta$ 1 Signaling and Tissue Fibrosis. *Cold Spring Harb Perspect Biol* 10. <https://doi.org/10.1101/cshperspect.a022293>
- Kim, N., Choi, S., Lim, C., Lee, H., Oh, J., 2010. Albumin mediates PPAR- $\gamma$  or C/EBP- $\alpha$ -induced phenotypic changes in pancreatic stellate cells. *Biochem Biophys Res Commun* 391, 640–644. <https://doi.org/10.1016/j.bbrc.2009.11.112>
- Kim, N., Yoo, W., Lee, J., Kim, H., Lee, H., Kim, Y.-S., Kim, D.-U., Oh, J., 2009. Formation of vitamin A lipid droplets in pancreatic stellate cells requires albumin. *Gut* 58, 1382–1390. <https://doi.org/10.1136/gut.2008.170233>
- Kisseleva, T., Brenner, D.A., 2008. Mechanisms of fibrogenesis. *Exp Biol Med (Maywood)* 233, 109–122. <https://doi.org/10.3181/0707-MR-190>
- Kleeff, J., Korc, M., Apte, M., La Vecchia, C., Johnson, C.D., Biankin, A.V., Neale, R.E., Tempero, M., Tuveson, D.A., Hruban, R.H., Neoptolemos, J.P., 2016. Pancreatic cancer. *Nat Rev Dis Primers* 2, 16022. <https://doi.org/10.1038/nrdp.2016.22>
- Klöppel, G., Detlefsen, S., Feyerabend, B., 2004. Fibrosis of the pancreas: the initial tissue damage and the resulting pattern. *Virchows Arch* 445, 1–8. <https://doi.org/10.1007/s00428-004-1021-5>
- Koikawa, K., Ohuchida, K., Ando, Y., Kibe, S., Nakayama, H., Takesue, S., Endo, S., Abe, T., Okumura, T., Iwamoto, C., Moriyama, T., Nakata, K., Miyasaka, Y., Ohtsuka, T., Nagai, E., Mizumoto, K., Hashizume, M., Nakamura, M., 2018. Basement membrane destruction by pancreatic stellate cells leads to local invasion in pancreatic ductal adenocarcinoma. *Cancer Lett* 425, 65–77. <https://doi.org/10.1016/j.canlet.2018.03.031>
- Königer, J., Giese, T., di Mola, F.F., Wente, M.N., Esposito, I., Bachem, M.G., Giese, N.A., Büchler, M.W., Friess, H., 2004. Pancreatic tumor cells influence the composition of the extracellular matrix. *Biochem Biophys Res Commun* 322, 943–949. <https://doi.org/10.1016/j.bbrc.2004.08.008>
- Koong, A.C., Mehta, V.K., Le, Q.T., Fisher, G.A., Terris, D.J., Brown, J.M., Bastidas, A.J., Vierra, M., 2000. Pancreatic tumors show high levels of hypoxia. *Int J Radiat Oncol Biol Phys* 48, 919–922. [https://doi.org/10.1016/s0360-3016\(00\)00803-8](https://doi.org/10.1016/s0360-3016(00)00803-8)
- Kordes, C., Brookmann, S., Häussinger, D., Klonowski-Stumpe, H., 2005. Differential and Synergistic Effects of Platelet-derived Growth Factor-BB and Transforming Growth Factor- $\beta$ 1

on Activated Pancreatic Stellate Cells. *Pancreas* 31, 156–167. <https://doi.org/10.1097/01.mpa.0000168222.05591.a0>

Kordes, C., Sawitza, I., Götze, S., Häussinger, D., 2012. Stellate cells from rat pancreas are stem cells and can contribute to liver regeneration. *PLoS One* 7, e51878. <https://doi.org/10.1371/journal.pone.0051878>

Kroemer, G., Galluzzi, L., Vandenabeele, P., Abrams, J., Alnemri, E.S., Baehrecke, E.H., Blagosklonny, M.V., El-Deiry, W.S., Golstein, P., Green, D.R., Hengartner, M., Knight, R.A., Kumar, S., Lipton, S.A., Malorni, W., Nuñez, G., Peter, M.E., Tschopp, J., Yuan, J., Piacentini, M., Zhivotovsky, B., Melino, G., Nomenclature Committee on Cell Death 2009, 2009. Classification of cell death: recommendations of the Nomenclature Committee on Cell Death 2009. *Cell Death Differ* 16, 3–11. <https://doi.org/10.1038/cdd.2008.150>

Kruse, M.L., Hildebrand, P.B., Timke, C., Fölsch, U.R., Schmidt, W.E., 2000. TGFbeta1 autocrine growth control in isolated pancreatic fibroblastoid cells/stellate cells in vitro. *Regul Pept* 90, 47–52. [https://doi.org/10.1016/s0167-0115\(00\)00104-x](https://doi.org/10.1016/s0167-0115(00)00104-x)

Kulkarni, A.A., Thatcher, T.H., Olsen, K.C., Maggirwar, S.B., Phipps, R.P., Sime, P.J., 2011. PPAR- $\gamma$  Ligands Repress TGF $\beta$ -Induced Myofibroblast Differentiation by Targeting the PI3K/Akt Pathway: Implications for Therapy of Fibrosis. *PLoS One* 6. <https://doi.org/10.1371/journal.pone.0015909>

Kuntze, A., Goetsch, O., Fels, B., Najder, K., Unger, A., Wilhelmi, M., Sargin, S., Schimmelpfennig, S., Neumann, I., Schwab, A., Pethó, Z., 2020. Protonation of Piezo1 Impairs Cell-Matrix Interactions of Pancreatic Stellate Cells. *Front Physiol* 11, 89. <https://doi.org/10.3389/fphys.2020.00089>

Kunzelmann-Marche, C., Freyssinet, J.-M., Martínez, M.C., 2002. Loss of plasma membrane phospholipid asymmetry requires raft integrity. Role of transient receptor potential channels and ERK pathway. *J Biol Chem* 277, 19876–19881. <https://doi.org/10.1074/jbc.M200324200>

Kurahara, L.H., Sumiyoshi, M., Aoyagi, K., Hiraishi, K., Nakajima, K., Nakagawa, M., Hu, Y., Inoue, R., 2015. Intestinal Myofibroblast TRPC6 Channel May Contribute to Stenotic Fibrosis in Crohn's Disease. *Inflamm Bowel Dis* 21, 496–506. <https://doi.org/10.1097/MIB.0000000000000295>

Kwong, J.Q., Molkenin, J.D., 2015. Physiological and pathological roles of the mitochondrial permeability transition pore in the heart. *Cell Metab* 21, 206–214. <https://doi.org/10.1016/j.cmet.2014.12.001>

Lachowski, D., Cortes, E., Pink, D., Chronopoulos, A., Karim, S.A., P. Morton, J., del Río Hernández, A.E., 2017. Substrate Rigidity Controls Activation and Durotaxis in Pancreatic Stellate Cells. *Sci Rep* 7. <https://doi.org/10.1038/s41598-017-02689-x>

Lanner, J.T., Georgiou, D.K., Joshi, A.D., Hamilton, S.L., 2010. Ryanodine Receptors: Structure, Expression, Molecular Details, and Function in Calcium Release. *Cold Spring Harb Perspect Biol* 2. <https://doi.org/10.1101/cshperspect.a003996>

Lardon, J., Rooman, I., Bouwens, L., 2002. Nestin expression in pancreatic stellate cells and angiogenic endothelial cells. *Histochem Cell Biol* 117, 535–540. <https://doi.org/10.1007/s00418-002-0412-4>

- Lee, E., Ryu, G.R., Ko, S.-H., Ahn, Y.-B., Song, K.-H., 2017. A role of pancreatic stellate cells in islet fibrosis and  $\beta$ -cell dysfunction in type 2 diabetes mellitus. *Biochem Biophys Res Commun* 485, 328–334. <https://doi.org/10.1016/j.bbrc.2017.02.082>
- Lee, Hongsik, Lim, C., Lee, J., Kim, N., Bang, S., Lee, Hojae, Min, B., Park, G., Noda, M., Stetler-Stevenson, W.G., Oh, J., 2008. TGF-beta signaling preserves RECK expression in activated pancreatic stellate cells. *J Cell Biochem* 104, 1065–1074. <https://doi.org/10.1002/jcb.21692>
- Lee, K.P., Choi, S., Hong, J.H., Ahuja, M., Graham, S., Ma, R., So, I., Shin, D.M., Muallem, S., Yuan, J.P., 2014. Molecular determinants mediating gating of Transient Receptor Potential Canonical (TRPC) channels by stromal interaction molecule 1 (STIM1). *J Biol Chem* 289, 6372–6382. <https://doi.org/10.1074/jbc.M113.546556>
- Lee, M.G., Ohana, E., Park, H.W., Yang, D., Muallem, S., 2012. Molecular mechanism of pancreatic and salivary gland fluid and HCO<sub>3</sub> secretion. *Physiol Rev* 92, 39–74. <https://doi.org/10.1152/physrev.00011.2011>
- Lee, M.S., Gu, D., Feng, L., Curriden, S., Arnush, M., Krahl, T., Gurushanthaiah, D., Wilson, C., Loskutoff, D.L., Fox, H., 1995. Accumulation of extracellular matrix and developmental dysregulation in the pancreas by transgenic production of transforming growth factor-beta 1. *Am J Pathol* 147, 42–52.
- Leung, L., Radulovich, N., Zhu, C.-Q., Wang, D., To, C., Ibrahimov, E., Tsao, M.-S., 2013. Loss of canonical Smad4 signaling promotes KRAS driven malignant transformation of human pancreatic duct epithelial cells and metastasis. *PLoS One* 8, e84366. <https://doi.org/10.1371/journal.pone.0084366>
- Li, F., Chen, B., Li, L., Zha, M., Zhou, S., Wu, T., Bachem, M.G., Sun, Z., 2014. INS-1 cells inhibit the production of extracellular matrix from pancreatic stellate cells. *J Mol Histol* 45, 321–327. <https://doi.org/10.1007/s10735-013-9547-y>
- Li, H., Zhu, H., Xu, C.J., Yuan, J., 1998. Cleavage of BID by caspase 8 mediates the mitochondrial damage in the Fas pathway of apoptosis. *Cell* 94, 491–501. [https://doi.org/10.1016/s0092-8674\(00\)81590-1](https://doi.org/10.1016/s0092-8674(00)81590-1)
- Li, J., Yuan, J., 2008. Caspases in apoptosis and beyond. *Oncogene* 27, 6194–6206. <https://doi.org/10.1038/onc.2008.297>
- Li, Z., Lu, J., Xu, P., Xie, X., Chen, L., Xu, T., 2007. Mapping the interacting domains of STIM1 and Orai1 in Ca<sup>2+</sup> release-activated Ca<sup>2+</sup> channel activation. *J Biol Chem* 282, 29448–29456. <https://doi.org/10.1074/jbc.M703573200>
- Liou, J., Kim, M.L., Heo, W.D., Jones, J.T., Myers, J.W., Ferrell, J.E., Meyer, T., 2005. STIM is a Ca<sup>2+</sup> sensor essential for Ca<sup>2+</sup>-store-depletion-triggered Ca<sup>2+</sup> influx. *Curr Biol* 15, 1235–1241. <https://doi.org/10.1016/j.cub.2005.05.055>
- Lis, A., Peinelt, C., Beck, A., Parvez, S., Monteilh-Zoller, M., Fleig, A., Penner, R., 2007. CRACM1, CRACM2, and CRACM3 are store-operated Ca<sup>2+</sup> channels with distinct functional properties. *Curr Biol* 17, 794–800. <https://doi.org/10.1016/j.cub.2007.03.065>

- Liu, S., Chen, S., Zeng, J., 2018. TGF- $\beta$  signaling: A complex role in tumorigenesis (Review). *Molecular Medicine Reports* 17, 699–704. <https://doi.org/10.3892/mmr.2017.7970>
- Liu, W.-B., Wang, X.-P., Wu, K., Zhang, R.-L., 2005. Effects of angiotensin II receptor antagonist, Losartan on the apoptosis, proliferation and migration of the human pancreatic stellate cells. *World J Gastroenterol* 11, 6489–6494. <https://doi.org/10.3748/wjg.v11.i41.6489>
- Liu, X., Singh, B.B., Ambudkar, I.S., 2003. TRPC1 is required for functional store-operated Ca<sup>2+</sup> channels. Role of acidic amino acid residues in the S5-S6 region. *J Biol Chem* 278, 11337–11343. <https://doi.org/10.1074/jbc.M213271200>
- Lockwich, T.P., Liu, X., Singh, B.B., Jadowiec, J., Weiland, S., Ambudkar, I.S., 2000. Assembly of Trp1 in a signaling complex associated with caveolin-scaffolding lipid raft domains. *J Biol Chem* 275, 11934–11942. <https://doi.org/10.1074/jbc.275.16.11934>
- Löhr, M., Schmidt, C., Ringel, J., Kluth, M., Müller, P., Nizze, H., Jesnowski, R., 2001. Transforming growth factor-beta1 induces desmoplasia in an experimental model of human pancreatic carcinoma. *Cancer Res* 61, 550–555.
- Longnecker, D., 2014. Anatomy and Histology of the Pancreas. <https://doi.org/10.3998/PANC.2014.3>
- Lu, J., Zhou, S., Siech, M., Habisch, H., Seufferlein, T., Bachem, M.G., 2014. Pancreatic stellate cells promote hapto-migration of cancer cells through collagen I-mediated signalling pathway. *Br J Cancer* 110, 409–420. <https://doi.org/10.1038/bjc.2013.706>
- Lu, Z., Friess, H., Graber, H.U., Guo, X., Schilling, M., Zimmermann, A., Korc, M., Büchler, M.W., 1997. Presence of two signaling TGF-beta receptors in human pancreatic cancer correlates with advanced tumor stage. *Dig Dis Sci* 42, 2054–2063. <https://doi.org/10.1023/a:1018814416903>
- Luik, R.M., Wang, B., Prakriya, M., Wu, M.M., Lewis, R.S., 2008. Oligomerization of STIM1 couples ER calcium depletion to CRAC channel activation. *Nature* 454, 538–542. <https://doi.org/10.1038/nature07065>
- Lytton, J., Westlin, M., Hanley, M.R., 1991. Thapsigargin inhibits the sarcoplasmic or endoplasmic reticulum Ca-ATPase family of calcium pumps. *J Biol Chem* 266, 17067–17071.
- MacCurtain, B.M., Quirke, N.P., Thorpe, S.D., Gallagher, T.K., 2021. Pancreatic Ductal Adenocarcinoma: Relating Biomechanics and Prognosis. *J Clin Med* 10, 2711. <https://doi.org/10.3390/jcm10122711>
- Mace, T.A., Bloomston, M., Lesinski, G.B., 2013. Pancreatic cancer-associated stellate cells: A viable target for reducing immunosuppression in the tumor microenvironment. *Oncoimmunology* 2, e24891. <https://doi.org/10.4161/onci.24891>
- Malumbres, M., 2014. Cyclin-dependent kinases. *Genome Biology* 15, 122. <https://doi.org/10.1186/gb4184>
- Malumbres, M., Barbacid, M., 2009. Cell cycle, CDKs and cancer: a changing paradigm. *Nat Rev Cancer* 9, 153–166. <https://doi.org/10.1038/nrc2602>



- Manohar, M., Verma, A.K., Venkateshaiah, S.U., Sanders, N.L., Mishra, A., 2017. Pathogenic mechanisms of pancreatitis. *World J Gastrointest Pharmacol Ther* 8, 10–25. <https://doi.org/10.4292/wjgpt.v8.i1.10>
- Mantoni, T.S., Lunardi, S., Al-Assar, O., Masamune, A., Brunner, T.B., 2011. Pancreatic stellate cells radioprotect pancreatic cancer cells through  $\beta$ 1-integrin signaling. *Cancer Res* 71, 3453–3458. <https://doi.org/10.1158/0008-5472.CAN-10-1633>
- Marchi, S., Pinton, P., 2016. Alterations of calcium homeostasis in cancer cells. *Current Opinion in Pharmacology, Cancer • Immunomodulation* 29, 1–6. <https://doi.org/10.1016/j.coph.2016.03.002>
- Maroto, R., Raso, A., Wood, T.G., Kurosky, A., Martinac, B., Hamill, O.P., 2005. TRPC1 forms the stretch-activated cation channel in vertebrate cells. *Nat Cell Biol* 7, 179–185. <https://doi.org/10.1038/ncb1218>
- Martonosi, A.N., Pikula, S., 2003. The structure of the  $\text{Ca}^{2+}$ -ATPase of sarcoplasmic reticulum. *Acta Biochim Pol* 50, 337–365. <https://doi.org/035002337>
- Masamune, A., Kikuta, K., Satoh, M., Kume, K., Shimosegawa, T., 2003. Differential roles of signaling pathways for proliferation and migration of rat pancreatic stellate cells. *Tohoku J Exp Med* 199, 69–84. <https://doi.org/10.1620/tjem.199.69>
- Masamune, A., Kikuta, K., Satoh, M., Sakai, Y., Satoh, A., Shimosegawa, T., 2002a. Ligands of peroxisome proliferator-activated receptor- $\gamma$  block activation of pancreatic stellate cells. *J Biol Chem* 277, 141–147. <https://doi.org/10.1074/jbc.M107582200>
- Masamune, A., Kikuta, K., Satoh, M., Satoh, A., Shimosegawa, T., 2002b. Alcohol activates activator protein-1 and mitogen-activated protein kinases in rat pancreatic stellate cells. *J Pharmacol Exp Ther* 302, 36–42. <https://doi.org/10.1124/jpet.302.1.36>
- Masamune, A., Kikuta, K., Satoh, M., Satoh, K., Shimosegawa, T., 2003b. Rho kinase inhibitors block activation of pancreatic stellate cells. *Br J Pharmacol* 140, 1292–1302. <https://doi.org/10.1038/sj.bjp.0705551>
- Masamune, A., Kikuta, K., Satoh, M., Suzuki, N., Shimosegawa, T., 2005a. Protease-activated receptor-2-mediated proliferation and collagen production of rat pancreatic stellate cells. *J Pharmacol Exp Ther* 312, 651–658. <https://doi.org/10.1124/jpet.104.076232>
- Masamune, A., Kikuta, K., Suzuki, N., Satoh, M., Satoh, K., Shimosegawa, T., 2004. A c-Jun NH2-terminal kinase inhibitor SP600125 (anthra[1,9-cd]pyrazole-6 (2H)-one) blocks activation of pancreatic stellate cells. *J Pharmacol Exp Ther* 310, 520–527. <https://doi.org/10.1124/jpet.104.067280>
- Masamune, A., Kikuta, K., Watanabe, T., Satoh, K., Hirota, M., Shimosegawa, T., 2008a. Hypoxia stimulates pancreatic stellate cells to induce fibrosis and angiogenesis in pancreatic cancer. *Am J Physiol Gastrointest Liver Physiol* 295, G709–717. <https://doi.org/10.1152/ajpgi.90356.2008>
- Masamune, A., Kikuta, K., Watanabe, T., Satoh, K., Satoh, A., Shimosegawa, T., 2008b. Pancreatic stellate cells express Toll-like receptors. *J Gastroenterol* 43, 352–362. <https://doi.org/10.1007/s00535-008-2162-0>

- Masamune, A., Sakai, Y., Kikuta, K., Satoh, M., Satoh, A., Shimosegawa, T., 2002c. Activated rat pancreatic stellate cells express intercellular adhesion molecule-1 (ICAM-1) in vitro. *Pancreas* 25, 78–85. <https://doi.org/10.1097/00006676-200207000-00018>
- Masamune, A., Satoh, A., Watanabe, T., Kikuta, K., Satoh, M., Suzuki, N., Satoh, K., Shimosegawa, T., 2010. Effects of ethanol and its metabolites on human pancreatic stellate cells. *Dig Dis Sci* 55, 204–211. <https://doi.org/10.1007/s10620-008-0695-y>
- Masamune, A., Satoh, M., Hirabayashi, J., Kasai, K., Satoh, K., Shimosegawa, T., 2006. Galectin-1 induces chemokine production and proliferation in pancreatic stellate cells. *Am J Physiol Gastrointest Liver Physiol* 290, G729-736. <https://doi.org/10.1152/ajpgi.00511.2005>
- Masamune, A., Satoh, M., Kikuta, K., Sakai, Y., Satoh, A., Shimosegawa, T., 2003c. Inhibition of p38 Mitogen-Activated Protein Kinase Blocks Activation of Rat Pancreatic Stellate Cells. *J Pharmacol Exp Ther* 304, 8–14. <https://doi.org/10.1124/jpet.102.040287>
- Masamune, A., Satoh, M., Kikuta, K., Suzuki, N., Shimosegawa, T., 2005b. Endothelin-1 stimulates contraction and migration of rat pancreatic stellate cells. *World J Gastroenterol* 11, 6144–6151. <https://doi.org/10.3748/wjg.v11.i39.6144>
- Masamune, A., Satoh, M., Kikuta, K., Suzuki, N., Shimosegawa, T., 2003d. Establishment and characterization of a rat pancreatic stellate cell line by spontaneous immortalization. *World J Gastroenterol* 9, 2751–2758. <https://doi.org/10.3748/wjg.v9.i12.2751>
- Masamune, A., Shimosegawa, T., 2009. Signal transduction in pancreatic stellate cells. *J Gastroenterol* 44, 249–260. <https://doi.org/10.1007/s00535-009-0013-2>
- Masamune, A., Watanabe, T., Kikuta, K., Satoh, K., Shimosegawa, T., 2008c. NADPH oxidase plays a crucial role in the activation of pancreatic stellate cells. *Am J Physiol Gastrointest Liver Physiol* 294, G99–G108. <https://doi.org/10.1152/ajpgi.00272.2007>
- Masamune, A., Watanabe, T., Kikuta, K., Shimosegawa, T., 2009. Roles of pancreatic stellate cells in pancreatic inflammation and fibrosis. *Clin Gastroenterol Hepatol* 7, S48-54. <https://doi.org/10.1016/j.cgh.2009.07.038>
- Massagué, J., 2012. TGF $\beta$  signalling in context. *Nat Rev Mol Cell Biol* 13, 616–630. <https://doi.org/10.1038/nrm3434>
- Mato, E., Lucas, M., Petriz, J., Gomis, R., Novials, A., 2009. Identification of a pancreatic stellate cell population with properties of progenitor cells: new role for stellate cells in the pancreas. *Biochem J* 421, 181–191. <https://doi.org/10.1042/BJ20081466>
- McCarroll, J.A., Naim, S., Sharbeen, G., Russia, N., Lee, J., Kavallaris, M., Goldstein, D., Phillips, P.A., 2014. Role of pancreatic stellate cells in chemoresistance in pancreatic cancer. *Front Physiol* 5, 141. <https://doi.org/10.3389/fphys.2014.00141>
- McCarroll, J.A., Phillips, P.A., Kumar, R.K., Park, S., Pirola, R.C., Wilson, J.S., Apte, M.V., 2004. Pancreatic stellate cell migration: role of the phosphatidylinositol 3-kinase (PI3-kinase) pathway. *Biochem Pharmacol* 67, 1215–1225. <https://doi.org/10.1016/j.bcp.2003.11.013>
- McCarroll, J.A., Phillips, P.A., Park, S., Doherty, E., Pirola, R.C., Wilson, J.S., Apte, M.V., 2003. Pancreatic Stellate Cell Activation by Ethanol and Acetaldehyde: Is it Mediated by the Mitogen-Activated Protein Kinase Signaling Pathway? *Pancreas* 27, 150–160.

- McCarroll, J.A., Phillips, P.A., Santucci, N., Pirola, R.C., Wilson, J.S., Apte, M.V., 2006. Vitamin A inhibits pancreatic stellate cell activation: implications for treatment of pancreatic fibrosis. *Gut* 55, 79–89. <https://doi.org/10.1136/gut.2005.064543>
- McFadzean, I., Gibson, A., 2002. The developing relationship between receptor-operated and store-operated calcium channels in smooth muscle. *Br J Pharmacol* 135, 1–13. <https://doi.org/10.1038/sj.bjp.0704468>
- McNally, B.A., Yamashita, M., Engh, A., Prakriya, M., 2009. Structural determinants of ion permeation in CRAC channels. *Proc Natl Acad Sci U S A* 106, 22516–22521. <https://doi.org/10.1073/pnas.0909574106>
- Mekapogu, A.R., Pothula, S.P., Pirola, R.C., Wilson, J.S., Apte, M.V., 2019. Multifunctional role of pancreatic stellate cells in pancreatic cancer. *Annals of Pancreatic Cancer* 2. <https://doi.org/10.21037/apc.2019.05.02>
- Mercer, J.C., Dehaven, W.I., Smyth, J.T., Wedel, B., Boyles, R.R., Bird, G.S., Putney, J.W., 2006. Large store-operated calcium selective currents due to co-expression of Orai1 or Orai2 with the intracellular calcium sensor, Stim1. *J Biol Chem* 281, 24979–24990. <https://doi.org/10.1074/jbc.M604589200>
- Mews, P., Phillips, P., Fahmy, R., Korsten, M., Pirola, R., Wilson, J., Apte, M., 2002. Pancreatic stellate cells respond to inflammatory cytokines: potential role in chronic pancreatitis. *Gut* 50, 535–541. <https://doi.org/10.1136/gut.50.4.535>
- Michalski, C.W., Gorbachevski, A., Erkan, M., Reiser, C., Deucker, S., Bergmann, F., Giese, T., Weigand, M., Giese, N.A., Friess, H., Kleeff, J., 2007. Mononuclear cells modulate the activity of pancreatic stellate cells which in turn promote fibrosis and inflammation in chronic pancreatitis. *J Transl Med* 5, 63. <https://doi.org/10.1186/1479-5876-5-63>
- Misquitta, C.M., Mack, D.P., Grover, A.K., 1999. Sarco/endoplasmic reticulum Ca<sup>2+</sup> (SERCA)-pumps: link to heart beats and calcium waves. *Cell Calcium* 25, 277–290. <https://doi.org/10.1054/ceca.1999.0032>
- Morikawa, M., Derynck, R., Miyazono, K., 2016. TGF- $\beta$  and the TGF- $\beta$  Family: Context-Dependent Roles in Cell and Tissue Physiology. *Cold Spring Harb Perspect Biol* 8. <https://doi.org/10.1101/cshperspect.a021873>
- Morrison, C.D., Parvani, J.G., Schiemann, W.P., 2013. The relevance of the TGF- $\beta$  Paradox to EMT-MET programs. *Cancer Lett* 341, 30–40. <https://doi.org/10.1016/j.canlet.2013.02.048>
- Motiani, R.K., Abdullaev, I.F., Trebak, M., 2010. A novel native store-operated calcium channel encoded by Orai3: selective requirement of Orai3 versus Orai1 in estrogen receptor-positive versus estrogen receptor-negative breast cancer cells. *J Biol Chem* 285, 19173–19183. <https://doi.org/10.1074/jbc.M110.102582>
- Muik, M., Frischauf, I., Derler, I., Fahrner, M., Bergsmann, J., Eder, P., Schindl, R., Hesch, C., Polzinger, B., Fritsch, R., Kahr, H., Madl, J., Gruber, H., Groschner, K., Romanin, C., 2008. Dynamic coupling of the putative coiled-coil domain of ORAI1 with STIM1 mediates ORAI1 channel activation. *J Biol Chem* 283, 8014–8022. <https://doi.org/10.1074/jbc.M708898200>

- Nakamura, T., Ito, T., Oono, T., Igarashi, H., Fujimori, N., Uchida, M., Niina, Y., Yasuda, M., Suzuki, K., Takayanagi, R., 2011. Bacterial DNA promotes proliferation of rat pancreatic stellate cells through toll-like receptor 9: potential mechanisms for bacterially induced fibrosis. *Pancreas* 40, 823–831. <https://doi.org/10.1097/MPA.0b013e318224a501>
- Neuzillet, C., Tijeras-Raballand, A., Ragulan, C., Cros, J., Patil, Y., Martinet, M., Erkan, M., Kleeff, J., Wilson, J., Apte, M., Tosolini, M., Wilson, A.S., Delvecchio, F.R., Bousquet, C., Paradis, V., Hammel, P., Sadanandam, A., Kocher, H.M., 2019. Inter- and intra-tumoural heterogeneity in cancer-associated fibroblasts of human pancreatic ductal adenocarcinoma. *J Pathol* 248, 51–65. <https://doi.org/10.1002/path.5224>
- Ng, B., Dong, J., Viswanathan, S., Widjaja, A.A., Paleja, B.S., Adami, E., Ko, N.S.J., Wang, M., Lim, S., Tan, J., Chothani, S.P., Albani, S., Schafer, S., Cook, S.A., 2020. Fibroblast-specific IL11 signaling drives chronic inflammation in murine fibrotic lung disease. *The FASEB Journal* 34, 11802–11815. <https://doi.org/10.1096/fj.202001045RR>
- Nielsen, M.F.B., Mortensen, M.B., Detlefsen, S., 2017. Identification of markers for quiescent pancreatic stellate cells in the normal human pancreas. *Histochem Cell Biol* 148, 359–380. <https://doi.org/10.1007/s00418-017-1581-5>
- Nishida, A., Andoh, A., Shioya, M., Kim-Mitsuyama, S., Takayanagi, A., Fujiyama, Y., 2008. Phosphatidylinositol 3-kinase/Akt signaling mediates interleukin-32 $\alpha$  induction in human pancreatic periacinar myofibroblasts. *Am J Physiol Gastrointest Liver Physiol* 294, G831–838. <https://doi.org/10.1152/ajpgi.00535.2007>
- Nomiyama, Y., Tashiro, M., Yamaguchi, T., Watanabe, S., Taguchi, M., Asaumi, H., Nakamura, H., Otsuki, M., 2007. High glucose activates rat pancreatic stellate cells through protein kinase C and p38 mitogen-activated protein kinase pathway. *Pancreas* 34, 364–372. <https://doi.org/10.1097/MPA.0b013e31802f0531>
- Norbury, C., Nurse, P., 1992. Animal cell cycles and their control. *Annu Rev Biochem* 61, 441–470. <https://doi.org/10.1146/annurev.bi.61.070192.002301>
- Norton, J., Foster, D., Chinta, M., Titan, A., Longaker, M., 2020. Pancreatic Cancer Associated Fibroblasts (CAF): Under-Explored Target for Pancreatic Cancer Treatment. *Cancers (Basel)* 12. <https://doi.org/10.3390/cancers12051347>
- Novák, B., Sible, J.C., Tyson, J.J., 2003. Checkpoints in the Cell Cycle, in: ELS. American Cancer Society. <https://doi.org/10.1038/npg.els.0001355>
- Oettle, H., 2014. Progress in the knowledge and treatment of advanced pancreatic cancer: from benchside to bedside. *Cancer Treat Rev* 40, 1039–1047. <https://doi.org/10.1016/j.ctrv.2014.07.003>
- Ogami, Y., Otsuki, M., 1998. Exocrine pancreatic physiology: overview. *Pancreas* 16, 265–272. <https://doi.org/10.1097/00006676-199804000-00010>
- Öhlund, D., Handly-Santana, A., Biffi, G., Elyada, E., Almeida, A.S., Ponz-Sarvisé, M., Corbo, V., Oni, T.E., Hearn, S.A., Lee, E.J., Chio, I.I.C., Hwang, C.-I., Tiriác, H., Baker, L.A., Engle, D.D., Feig, C., Kultti, A., Egeblad, M., Fearon, D.T., Crawford, J.M., Clevers, H., Park, Y., Tuveson, D.A., 2017. Distinct populations of inflammatory fibroblasts and myofibroblasts in pancreatic cancer. *J Exp Med* 214, 579–596. <https://doi.org/10.1084/jem.20162024>

- Ohnishi, H., Miyata, T., Yasuda, H., Satoh, Y., Hanatsuka, K., Kita, H., Ohashi, A., Tamada, K., Makita, N., Iiri, T., Ueda, N., Mashima, H., Sugano, K., 2004. Distinct roles of Smad2-, Smad3-, and ERK-dependent pathways in transforming growth factor-beta1 regulation of pancreatic stellate cellular functions. *J Biol Chem* 279, 8873–8878. <https://doi.org/10.1074/jbc.M309698200>
- Ohnishi, N., Miyata, T., Ohnishi, H., Yasuda, H., Tamada, K., Ueda, N., Mashima, H., Sugano, K., 2003. Activin A is an autocrine activator of rat pancreatic stellate cells: potential therapeutic role of follistatin for pancreatic fibrosis. *Gut* 52, 1487–1493. <https://doi.org/10.1136/gut.52.10.1487>
- Okada, S., Okusaka, T., Ishii, H., Kyogoku, A., Yoshimori, M., Kajimura, N., Yamaguchi, K., Kakizoe, T., 1998. Elevated serum interleukin-6 levels in patients with pancreatic cancer. *Jpn J Clin Oncol* 28, 12–15. <https://doi.org/10.1093/jjco/28.1.12>
- Omary, M.B., Lugea, A., Lowe, A.W., Pandol, S.J., 2007. The pancreatic stellate cell: a star on the rise in pancreatic diseases [WWW Document]. <https://doi.org/10.1172/JCI30082>
- Ong, H.L., de Souza, L.B., Zheng, C., Cheng, K.T., Liu, X., Goldsmith, C.M., Feske, S., Ambudkar, I.S., 2015. STIM2 enhances receptor-stimulated Ca<sup>2+</sup> signaling by promoting recruitment of STIM1 to the endoplasmic reticulum-plasma membrane junctions. *Sci Signal* 8, ra3. <https://doi.org/10.1126/scisignal.2005748>
- Pande, G., Kumar, N.A., Manogaran, P.S., 1996. Flow cytometric study of changes in the intracellular free calcium during the cell cycle. *Cytometry* 24, 55–63. [https://doi.org/10.1002/\(SICI\)1097-0320\(19960501\)24:1<55::AID-CYTO7>3.0.CO;2-H](https://doi.org/10.1002/(SICI)1097-0320(19960501)24:1<55::AID-CYTO7>3.0.CO;2-H)
- Pandol, S., Gukovskaya, A., Edderkaoui, M., Edderkoui, M., Dawson, D., Eibl, G., Lugea, A., 2012. Epidemiology, risk factors, and the promotion of pancreatic cancer: role of the stellate cell. *J Gastroenterol Hepatol* 27 Suppl 2, 127–134. <https://doi.org/10.1111/j.1440-1746.2011.07013.x>
- Pandol, S.J., 2015. Normal Pancreatic Function. *Pancreapedia: The Exocrine Pancreas Knowledge Base*. <https://doi.org/10.3998/panc.2015.17>
- Pandol, S.J., 2010. *Anatomy, The Exocrine Pancreas*. Morgan & Claypool Life Sciences.
- Pardee, A.B., 1974. A restriction point for control of normal animal cell proliferation. *Proc Natl Acad Sci U S A* 71, 1286–1290. <https://doi.org/10.1073/pnas.71.4.1286>
- Parekh, A.B., Putney, J.W., 2005. Store-operated calcium channels. *Physiol Rev* 85, 757–810. <https://doi.org/10.1152/physrev.00057.2003>
- Park, H., Bang, J., Nam, A., Park, J.E., Jin, M.H., Bang, Y., Oh, D., 2019. The prognostic role of soluble TGF-beta and its dynamics in unresectable pancreatic cancer treated with chemotherapy. *Cancer Med* 9, 43–51. <https://doi.org/10.1002/cam4.2677>
- Parkash, J., Asotra, K., 2010. Calcium wave signaling in cancer cells. *Life Sci* 87, 587–595. <https://doi.org/10.1016/j.lfs.2010.09.013>
- Patel, A.G., Toyama, M.T., Alvarez, C., Nguyen, T.N., Reber, P.U., Ashley, S.W., Reber, H.A., 1995. Pancreatic interstitial pH in human and feline chronic pancreatitis. *Gastroenterology* 109, 1639–1645. [https://doi.org/10.1016/0016-5085\(95\)90654-1](https://doi.org/10.1016/0016-5085(95)90654-1)

- Patel, M.B., Pothula, S.P., Xu, Z., Lee, A.K., Goldstein, D., Pirola, R.C., Apte, M.V., Wilson, J.S., 2014. The role of the hepatocyte growth factor/c-MET pathway in pancreatic stellate cell-endothelial cell interactions: antiangiogenic implications in pancreatic cancer. *Carcinogenesis* 35, 1891–1900. <https://doi.org/10.1093/carcin/bgu122>
- Patergnani, S., Danese, A., Bouhamida, E., Aguiari, G., Previati, M., Pinton, P., Giorgi, C., 2020. Various Aspects of Calcium Signaling in the Regulation of Apoptosis, Autophagy, Cell Proliferation, and Cancer. *Int J Mol Sci* 21. <https://doi.org/10.3390/ijms21218323>
- Patron, M., Checchetto, V., Raffaello, A., Teardo, E., Vecellio Reane, D., Mantoan, M., Granatiero, V., Szabò, I., De Stefani, D., Rizzuto, R., 2014. MICU1 and MICU2 finely tune the mitochondrial Ca<sup>2+</sup> uniporter by exerting opposite effects on MCU activity. *Mol Cell* 53, 726–737. <https://doi.org/10.1016/j.molcel.2014.01.013>
- Paulo, J.A., Kadiyala, V., Banks, P.A., Conwell, D.L., Steen, H., 2013. Mass spectrometry-based quantitative proteomic profiling of human pancreatic and hepatic stellate cell lines. *Genomics Proteomics Bioinformatics* 11, 105–113. <https://doi.org/10.1016/j.gpb.2013.01.009>
- Pereira, B.A., Vennin, C., Papanicolaou, M., Chambers, C.R., Herrmann, D., Morton, J.P., Cox, T.R., Timpson, P., 2019. CAF Subpopulations: A New Reservoir of Stromal Targets in Pancreatic Cancer. *Trends Cancer* 5, 724–741. <https://doi.org/10.1016/j.trecan.2019.09.010>
- Petersen, O.H., 2002. Calcium signal compartmentalization. *Biol Res* 35, 177–182. <https://doi.org/10.4067/s0716-97602002000200008>
- Pfaffl, M.W., Horgan, G.W., Dempfle, L., 2002. Relative expression software tool (REST) for group-wise comparison and statistical analysis of relative expression results in real-time PCR. *Nucleic Acids Res* 30, e36. <https://doi.org/10.1093/nar/30.9.e36>
- Philipson, K.D., Nicoll, D.A., 2000. Sodium-calcium exchange: a molecular perspective. *Annu Rev Physiol* 62, 111–133. <https://doi.org/10.1146/annurev.physiol.62.1.111>
- Phillips, P.A., McCarroll, J.A., Park, S., Wu, M.-J., Pirola, R., Korsten, M., Wilson, J.S., Apte, M.V., 2003. Rat pancreatic stellate cells secrete matrix metalloproteinases: implications for extracellular matrix turnover. *Gut* 52, 275–282. <https://doi.org/10.1136/gut.52.2.275>
- Phillips, P.A., Yang, L., Shulkes, A., Vonlaufen, A., Poljak, A., Bustamante, S., Warren, A., Xu, Z., Guilhaus, M., Pirola, R., Apte, M.V., Wilson, J.S., 2010. Pancreatic stellate cells produce acetylcholine and may play a role in pancreatic exocrine secretion. *Proc Natl Acad Sci U S A* 107, 17397–17402. <https://doi.org/10.1073/pnas.1000359107>
- Pickup, M., Novitskiy, S., Moses, H.L., 2013. The roles of TGFβ in the tumour microenvironment. *Nat Rev Cancer* 13, 788–799. <https://doi.org/10.1038/nrc3603>
- Piro, S., Urbano, F., Folli, F., Finzi, G., Marselli, L., Marchetti, P., 2018. The Endocrine Pancreas, in: Belfiore, A., LeRoith, D. (Eds.), *Principles of Endocrinology and Hormone Action, Endocrinology*. Springer International Publishing, Cham, pp. 423–454. [https://doi.org/10.1007/978-3-319-44675-2\\_31](https://doi.org/10.1007/978-3-319-44675-2_31)
- P.K. Mazur, J.T. Siveke, Genetically engineered mouse models of pancreatic cancer: unravelling tumour biology and progressing translational oncology, *Gut*. 61 (2012) 1488–1500. <https://doi.org/10.1136/gutjnl-2011-300756>.

- Porter, V.A., Bonev, A.D., Knot, H.J., Heppner, T.J., Stevenson, A.S., Kleppisch, T., Lederer, W.J., Nelson, M.T., 1998. Frequency modulation of Ca<sup>2+</sup> sparks is involved in regulation of arterial diameter by cyclic nucleotides. *Am J Physiol* 274, C1346-1355. <https://doi.org/10.1152/ajpcell.1998.274.5.C1346>
- Prakriya, M., Lewis, R.S., 2015. Store-Operated Calcium Channels. *Physiol Rev* 95, 1383–1436. <https://doi.org/10.1152/physrev.00020.2014>
- Prevarskaya, N., Ouadid-Ahidouch, H., Skryma, R., Shuba, Y., 2014. Remodelling of Ca<sup>2+</sup> transport in cancer: how it contributes to cancer hallmarks? *Philos Trans R Soc Lond B Biol Sci* 369, 20130097. <https://doi.org/10.1098/rstb.2013.0097>
- Provenzano, P.P., Hingorani, S.R., 2013. Hyaluronan, fluid pressure, and stromal resistance in pancreas cancer. *Br J Cancer* 108, 1–8. <https://doi.org/10.1038/bjc.2012.569>
- Qian, Z.-Y., Peng, Q., Zhang, Z.-W., Zhou, L.-A., Miao, Y., 2010. Roles of Smad3 and Smad7 in rat pancreatic stellate cells activated by transforming growth factor-beta 1. *Hepatobiliary Pancreat Dis Int* 9, 531–536.
- R, T.-W., A, G., B, S., H, R.-M., A, K., E, M.-P., 2008. Clinical significance of interleukin-6 (IL-6) gene polymorphism and IL-6 serum level in pancreatic adenocarcinoma and chronic pancreatitis. *Dig Dis Sci* 54, 683–689. <https://doi.org/10.1007/s10620-008-0390-z>
- Radoslavova, S., Ouadid-Ahidouch, H., Prevarskaya, N., 2020. Ca<sup>2+</sup> signaling is critical for pancreatic stellate cell's pathophysiology : from fibrosis to cancer hallmarks. *Current Opinion in Physiology, Calcium Signaling* 17, 255–260. <https://doi.org/10.1016/j.cophys.2020.08.018>
- Raimondi, S., Lowenfels, A.B., Morselli-Labate, A.M., Maisonneuve, P., Pezzilli, R., 2010. Pancreatic cancer in chronic pancreatitis; aetiology, incidence, and early detection. *Best Pract Res Clin Gastroenterol* 24, 349–358. <https://doi.org/10.1016/j.bpg.2010.02.007>
- Ramsey, I.S., Delling, M., Clapham, D.E., 2006. An introduction to TRP channels. *Annu Rev Physiol* 68, 619–647. <https://doi.org/10.1146/annurev.physiol.68.040204.100431>
- Rao, A., 2009. Signaling to gene expression: calcium, calcineurin and NFAT. *Nat Immunol* 10, 3–5. <https://doi.org/10.1038/ni0109-3>
- Rees, D.D., Palmer, R.M., Moncada, S., 1989. Role of endothelium-derived nitric oxide in the regulation of blood pressure. *Proc Natl Acad Sci U S A* 86, 3375–3378. <https://doi.org/10.1073/pnas.86.9.3375>
- Reinehr, R., Zoller, S., Klonowski-Stumpe, H., Kordes, C., Häussinger, D., 2004. Effects of angiotensin II on rat pancreatic stellate cells. *Pancreas* 28, 129–137. <https://doi.org/10.1097/00006676-200403000-00003>
- Remy, I., Montmarquette, A., Michnick, S.W., 2004. PKB/Akt modulates TGF-beta signalling through a direct interaction with Smad3. *Nat Cell Biol* 6, 358–365. <https://doi.org/10.1038/ncb1113>
- Roach, K.M., Wulff, H., Feghali-Bostwick, C., Amrani, Y., Bradding, P., 2014. Increased constitutive  $\alpha$ SMA and Smad2/3 expression in idiopathic pulmonary fibrosis myofibroblasts is KCa<sub>3.1</sub>-dependent. *Respir Res* 15, 155. <https://doi.org/10.1186/s12931-014-0155-5>

- Roderick, H.L., Cook, S.J., 2008. Ca<sup>2+</sup> signalling checkpoints in cancer: remodelling Ca<sup>2+</sup> for cancer cell proliferation and survival. *Nat Rev Cancer* 8, 361–375. <https://doi.org/10.1038/nrc2374>
- Rosado, J.A., Brownlow, S.L., Sage, S.O., 2002. Endogenously expressed Trp1 is involved in store-mediated Ca<sup>2+</sup> entry by conformational coupling in human platelets. *J Biol Chem* 277, 42157–42163. <https://doi.org/10.1074/jbc.M207320200>
- Rosado, J.A., Sage, S.O., 2001. Activation of store-mediated calcium entry by secretion-like coupling between the inositol 1,4,5-trisphosphate receptor type II and human transient receptor potential (hTrp1) channels in human platelets. *Biochem J* 356, 191–198. <https://doi.org/10.1042/0264-6021:3560191>
- Rosado, J.A., Sage, S.O., 2000. Coupling between inositol 1,4,5-trisphosphate receptors and human transient receptor potential channel 1 when intracellular Ca<sup>2+</sup> stores are depleted. *Biochem J* 350 Pt 3, 631–635.
- Rychkov, G., Barritt, G.J., 2007. TRPC1 Ca(2+)-permeable channels in animal cells. *Handb Exp Pharmacol* 23–52. [https://doi.org/10.1007/978-3-540-34891-7\\_2](https://doi.org/10.1007/978-3-540-34891-7_2)
- Sahin, I.H., Iacobuzio-Donahue, C.A., O'Reilly, E.M., 2016. Molecular signature of pancreatic adenocarcinoma: an insight from genotype to phenotype and challenges for targeted therapy. *Expert Opin Ther Targets* 20, 341–359. <https://doi.org/10.1517/14728222.2016.1094057>
- Sárközi, S., Komáromi, I., Jóna, I., Almássy, J., 2017. Lanthanides Report Calcium Sensor in the Vestibule of Ryanodine Receptor. *Biophysical Journal* 112, 2127–2137. <https://doi.org/10.1016/j.bpj.2017.03.023>
- Sassoli, C., Chellini, F., Squecco, R., Tani, A., Idrizaj, E., Nosi, D., Giannelli, M., Zecchi-Orlandini, S., 2016. Low intensity 635 nm diode laser irradiation inhibits fibroblast-myofibroblast transition reducing TRPC1 channel expression/activity: New perspectives for tissue fibrosis treatment. *Lasers Surg Med* 48, 318–332. <https://doi.org/10.1002/lsm.22441>
- Satoh, K., Shimosegawa, T., Hirota, M., Koizumi, M., Toyota, T., 1998. Expression of transforming growth factor beta1 (TGFbeta1) and its receptors in pancreatic duct cell carcinoma and in chronic pancreatitis. *Pancreas* 16, 468–474. <https://doi.org/10.1097/00006676-199805000-00002>
- Scarlett, C.J., Colvin, E.K., Pinese, M., Chang, D.K., Morey, A.L., Musgrove, E.A., Pajic, M., Apte, M., Henshall, S.M., Sutherland, R.L., Kench, J.G., Biankin, A.V., 2011. Recruitment and activation of pancreatic stellate cells from the bone marrow in pancreatic cancer: a model of tumor-host interaction. *PLoS One* 6, e26088. <https://doi.org/10.1371/journal.pone.0026088>
- Schafer, S., Viswanathan, S., Widjaja, A.A., Lim, W.-W., Moreno-Moral, A., DeLaughter, D.M., Ng, B., Patone, G., Chow, K., Khin, E., Tan, J., Chothani, S.P., Ye, L., Rackham, O.J.L., Ko, N.S.J., Sahib, N.E., Pua, C.J., Zhen, N.T.G., Xie, C., Wang, M., Maatz, H., Lim, S., Saar, K., Blachut, S., Petretto, E., Schmidt, S., Putoczki, T., Guimarães-Camboa, N., Wakimoto, H., van Heesch, S., Sigmundsson, K., Lim, S.L., Soon, J.L., Chao, V.T.T., Chua, Y.L., Tan, T.E., Evans, S.M., Loh, Y.J., Jamal, M.H., Ong, K.K., Chua, K.C., Ong, B.-H., Chakaramakkil, M.J., Seidman, J.G., Seidman, C.E., Hubner, N., Sin, K.Y.K., Cook, S.A., 2017. IL-11 is a crucial



determinant of cardiovascular fibrosis. *Nature* 552, 110–115. <https://doi.org/10.1038/nature24676>

Schneider, A., Löhr, J.M., Singer, M.V., 2007. The M-ANNHEIM classification of chronic pancreatitis: introduction of a unifying classification system based on a review of previous classifications of the disease. *J Gastroenterol* 42, 101–119. <https://doi.org/10.1007/s00535-006-1945-4>

Schneider, E., Schmid-Kotsas, A., Zhao, J., Weidenbach, H., Schmid, R.M., Menke, A., Adler, G., Waltenberger, J., Grünert, A., Bachem, M.G., 2001. Identification of mediators stimulating proliferation and matrix synthesis of rat pancreatic stellate cells. *Am J Physiol Cell Physiol* 281, C532–543. <https://doi.org/10.1152/ajpcell.2001.281.2.C532>

Schneider, Eric, Schmid-Kotsas, A., Zhao, J., Weidenbach, H., Schmid, R.M., Menke, A., Adler, G., Waltenberger, J., Grünert, A., Bachem, M.G., 2001. Identification of mediators stimulating proliferation and matrix synthesis of rat pancreatic stellate cells. *American Journal of Physiology-Cell Physiology* 281, C532–C543. <https://doi.org/10.1152/ajpcell.2001.281.2.C532>

Schwer, C.I., Stoll, P., Rospert, S., Fitzke, E., Schallner, N., Bürkle, H., Schmidt, R., Humar, M., 2013. Carbon monoxide releasing molecule-2 CORM-2 represses global protein synthesis by inhibition of eukaryotic elongation factor eEF2. *The International Journal of Biochemistry & Cell Biology* 45, 201–212. <https://doi.org/10.1016/j.biocel.2012.09.020>

Seidel, M., Lai, F.A., Zissimopoulos, S., 2015. Structural and functional interactions within ryanodine receptor. *Biochemical Society Transactions* 43, 377–383. <https://doi.org/10.1042/BST20140292>

Shao, S., Qin, T., Qian, W., Yue, Y., Xiao, Y., Li, X., Zhang, D., Wang, Z., Ma, Q., Lei, J., 2020. Positive feedback in Cav-1-ROS signalling in PSCs mediates metabolic coupling between PSCs and tumour cells. *J Cell Mol Med* 24, 9397–9408. <https://doi.org/10.1111/jcmm.15596>

Shek, F.W.-T., Benyon, R.C., Walker, F.M., McCrudden, P.R., Pender, S.L.F., Williams, E.J., Johnson, P.A., Johnson, C.D., Bateman, A.C., Fine, D.R., Iredale, J.P., 2002. Expression of transforming growth factor-beta 1 by pancreatic stellate cells and its implications for matrix secretion and turnover in chronic pancreatitis. *Am J Pathol* 160, 1787–1798. [https://doi.org/10.1016/s0002-9440\(10\)61125-x](https://doi.org/10.1016/s0002-9440(10)61125-x)

Shen, H., Huang, G.-J., Gong, Y.-W., 2003. Effect of transforming growth factor beta and bone morphogenetic proteins on rat hepatic stellate cell proliferation and trans-differentiation. *World J Gastroenterol* 9, 784–787. <https://doi.org/10.3748/wjg.v9.i4.784>

Sherr, C.J., Roberts, J.M., 1995. Inhibitors of mammalian G1 cyclin-dependent kinases. *Genes Dev* 9, 1149–1163. <https://doi.org/10.1101/gad.9.10.1149>

Shi, J., Miralles, F., Birnbaumer, L., Large, W.A., Albert, A.P., 2017. Store-operated interactions between plasmalemmal STIM1 and TRPC1 proteins stimulate PLC $\beta$ 1 to induce TRPC1 channel activation in vascular smooth muscle cells. *J Physiol* 595, 1039–1058. <https://doi.org/10.1113/JP273302>

Shi, Y., Hata, A., Lo, R.S., Massagué, J., Pavletich, N.P., 1997. A structural basis for mutational inactivation of the tumour suppressor Smad4. *Nature* 388, 87–93. <https://doi.org/10.1038/40431>

Shimada, M., Andoh, A., Hata, K., Tasaki, K., Araki, Y., Fujiyama, Y., Bamba, T., 2002. IL-6 secretion by human pancreatic periacinar myofibroblasts in response to inflammatory mediators. *J Immunol* 168, 861–868. <https://doi.org/10.4049/jimmunol.168.2.861>

Shimizu, K., Hashimoto, K., Tahara, J., Imaeda, H., Andoh, A., Shiratori, K., 2012. Pancreatic stellate cells do not exhibit features of antigen-presenting cells. *Pancreas* 41, 422–427. <https://doi.org/10.1097/MPA.0b013e31822e673b>

Shimizu, K., Kobayashi, M., Tahara, J., Shiratori, K., 2005. Cytokines and peroxisome proliferator-activated receptor gamma ligand regulate phagocytosis by pancreatic stellate cells. *Gastroenterology* 128, 2105–2118. <https://doi.org/10.1053/j.gastro.2005.03.025>

Shimizu, K., Shiratori, K., Hayashi, N., Kobayashi, M., Fujiwara, T., Horikoshi, H., 2002. Thiazolidinedione derivatives as novel therapeutic agents to prevent the development of chronic pancreatitis. *Pancreas* 24, 184–190. <https://doi.org/10.1097/00006676-200203000-00010>

Shinozaki, S., Ohnishi, H., Hama, K., Kita, H., Yamamoto, H., Osawa, H., Sato, K., Tamada, K., Mashima, H., Sugano, K., 2008. Indian hedgehog promotes the migration of rat activated pancreatic stellate cells by increasing membrane type-1 matrix metalloproteinase on the plasma membrane. *Journal of Cellular Physiology* 216, 38–46. <https://doi.org/10.1002/jcp.21372>

Simms, B.A., Zamponi, G.W., 2014. Neuronal voltage-gated calcium channels: structure, function, and dysfunction. *Neuron* 82, 24–45. <https://doi.org/10.1016/j.neuron.2014.03.016>

Singh, B.B., Liu, X., Tang, J., Zhu, M.X., Ambudkar, I.S., 2002. Calmodulin regulates Ca(2+)-dependent feedback inhibition of store-operated Ca(2+) influx by interaction with a site in the C terminus of TrpC1. *Mol Cell* 9, 739–750. [https://doi.org/10.1016/s1097-2765\(02\)00506-3](https://doi.org/10.1016/s1097-2765(02)00506-3)

Soboloff, J., Spassova, M.A., Tang, X.D., Hewavitharana, T., Xu, W., Gill, D.L., 2006. Orai1 and STIM reconstitute store-operated calcium channel function. *J Biol Chem* 281, 20661–20665. <https://doi.org/10.1074/jbc.C600126200>

Soboloff, J., Spassova, M.A., Hewavitharana, T., He, L.-P., Xu, W., Johnstone, L.S., Dziadek, M.A., Gill, D.L., 2006. STIM2 Is an Inhibitor of STIM1-Mediated Store-Operated Ca<sup>2+</sup> Entry. *Current Biology* 16, 1465–1470. <https://doi.org/10.1016/j.cub.2006.05.051>

Son, A., Park, S., Shin, D.M., Muallem, S., 2016. Orai1 and STIM1 in ER/PM junctions: roles in pancreatic cell function and dysfunction. *Am J Physiol Cell Physiol* 310, C414–422. <https://doi.org/10.1152/ajpcell.00349.2015>

Spanier, B.W.M., Dijkgraaf, M.G.W., Bruno, M.J., 2008. Epidemiology, aetiology and outcome of acute and chronic pancreatitis: An update. *Best Practice & Research Clinical Gastroenterology, Pancreatic Diseases* 22, 45–63. <https://doi.org/10.1016/j.bpg.2007.10.007>

Sparmann, G., Kruse, M.-L., Hofmeister-Mielke, N., Koczan, D., Jaster, R., Liebe, S., Wolff, D., Emmrich, J., 2010. Bone marrow-derived pancreatic stellate cells in rats. *Cell Res* 20, 288–298. <https://doi.org/10.1038/cr.2010.10>

- Spassova, M.A., Soboloff, J., He, L.-P., Xu, W., Dziadek, M.A., Gill, D.L., 2006. STIM1 has a plasma membrane role in the activation of store-operated Ca(2+) channels. *Proc Natl Acad Sci U S A* 103, 4040–4045. <https://doi.org/10.1073/pnas.0510050103>
- Srikanth, S., Gwack, Y., 2012. Orai1, STIM1, and their associating partners. *J Physiol* 590, 4169–4177. <https://doi.org/10.1113/jphysiol.2012.231522>
- Stanisz, H., Saul, S., Müller, C.S.L., Kappl, R., Niemeyer, B.A., Vogt, T., Hoth, M., Roesch, A., Bogeski, I., 2014. Inverse regulation of melanoma growth and migration by Orai1/STIM2-dependent calcium entry. *Pigment Cell Melanoma Res* 27, 442–453. <https://doi.org/10.1111/pcmr.12222>
- Stewart, T.A., Yapa, K.T.D.S., Monteith, G.R., 2015. Altered calcium signaling in cancer cells. *Biochim Biophys Acta* 1848, 2502–2511. <https://doi.org/10.1016/j.bbamem.2014.08.016>
- Strauss, R., Hamerlik, P., Lieber, A., Bartek, J., 2012. Regulation of stem cell plasticity: mechanisms and relevance to tissue biology and cancer. *Mol Ther* 20, 887–897. <https://doi.org/10.1038/mt.2012.2>
- Strehler, E.E., Filoteo, A.G., Penniston, J.T., Caride, A.J., 2007. Plasma-membrane Ca(2+) pumps: structural diversity as the basis for functional versatility. *Biochem Soc Trans* 35, 919–922. <https://doi.org/10.1042/BST0350919>
- Strehler, E.E., Zacharias, D.A., 2001. Role of alternative splicing in generating isoform diversity among plasma membrane calcium pumps. *Physiol Rev* 81, 21–50. <https://doi.org/10.1152/physrev.2001.81.1.21>
- Strübing, C., Krapivinsky, G., Krapivinsky, L., Clapham, D.E., 2001. TRPC1 and TRPC5 form a novel cation channel in mammalian brain. *Neuron* 29, 645–655. [https://doi.org/10.1016/s0896-6273\(01\)00240-9](https://doi.org/10.1016/s0896-6273(01)00240-9)
- Subedi, K.P., Ong, H.L., Son, G.-Y., Liu, X., Ambudkar, I.S., 2018. STIM2 Induces Activated Conformation of STIM1 to Control Orai1 Function in ER-PM Junctions. *Cell Rep* 23, 522–534. <https://doi.org/10.1016/j.celrep.2018.03.065>
- Subramanian, G., Schwarz, R.E., Higgins, L., McEnroe, G., Chakravarty, S., Dugar, S., Reiss, M., 2004. Targeting endogenous transforming growth factor beta receptor signaling in SMAD4-deficient human pancreatic carcinoma cells inhibits their invasive phenotype1. *Cancer Res* 64, 5200–5211. <https://doi.org/10.1158/0008-5472.CAN-04-0018>
- Suetsugu, A., Katz, M., Fleming, J., Truty, M., Thomas, R., Saji, S., Moriwaki, H., Bouvet, M., Hoffman, R.M., 2012. Imageable fluorescent metastasis resulting in transgenic GFP mice orthotopically implanted with human-patient primary pancreatic cancer specimens. *Anticancer Res* 32, 1175–1180.
- Suetsugu, A., Snyder, C.S., Moriwaki, H., Saji, S., Bouvet, M., Hoffman, R.M., 2015. Imaging the Interaction of Pancreatic Cancer and Stellate Cells in the Tumor Microenvironment during Metastasis. *Anticancer Res* 35, 2545–2551.
- Suhaili, S.H., Karimian, H., Stellato, M., Lee, T.-H., Aguilar, M.-I., 2017. Mitochondrial outer membrane permeabilization: a focus on the role of mitochondrial membrane structural organization. *Biophys Rev* 9, 443–457. <https://doi.org/10.1007/s12551-017-0308-0>

- Takai, Y., Sasaki, T., Tanaka, K., Nakanishi, H., 1995. Rho as a regulator of the cytoskeleton. *Trends Biochem Sci* 20, 227–231. [https://doi.org/10.1016/s0968-0004\(00\)89022-2](https://doi.org/10.1016/s0968-0004(00)89022-2)
- Talathi, S.S., Zimmerman, R., Young, M., 2021. *Anatomy, Abdomen and Pelvis, Pancreas*, in: StatPearls. StatPearls Publishing, Treasure Island (FL).
- Tang, D., Gao, J., Wang, S., Yuan, Z., Ye, N., Chong, Y., Xu, C., Jiang, X., Li, B., Yin, W., Miao, Y., Wang, D., Jiang, K., 2015. Apoptosis and anergy of T cell induced by pancreatic stellate cells-derived galectin-1 in pancreatic cancer. *Tumour Biol* 36, 5617–5626. <https://doi.org/10.1007/s13277-015-3233-5>
- Tang, D., Wang, D., Yuan, Z., Xue, X., Zhang, Y., An, Y., Chen, J., Tu, M., Lu, Z., Wei, J., Jiang, K., Miao, Y., 2013. Persistent activation of pancreatic stellate cells creates a microenvironment favorable for the malignant behavior of pancreatic ductal adenocarcinoma. *Int J Cancer* 132, 993–1003. <https://doi.org/10.1002/ijc.27715>
- Tang, J., Lin, Y., Zhang, Z., Tikunova, S., Birnbaumer, L., Zhu, M.X., 2001. Identification of common binding sites for calmodulin and inositol 1,4,5-trisphosphate receptors on the carboxyl termini of trp channels. *J Biol Chem* 276, 21303–21310. <https://doi.org/10.1074/jbc.M102316200>
- Tasaki, K., Shintani, Y., Saotome, T., Andoh, A., Fujiyama, Y., Hozawa, S., Bamba, T., 2003. Pro-inflammatory cytokine-induced matrix metalloproteinase-1 (MMP-1) secretion in human pancreatic periacinar myofibroblasts. *Pancreatology* 3, 414–421. <https://doi.org/10.1159/000073889>
- Thiery, J.P., Acloque, H., Huang, R.Y.J., Nieto, M.A., 2009. Epithelial-mesenchymal transitions in development and disease. *Cell* 139, 871–890. <https://doi.org/10.1016/j.cell.2009.11.007>
- Thomas, D., Radhakrishnan, P., 2020. Pancreatic Stellate Cells: The Key Orchestrator of The Pancreatic Tumor Microenvironment, in: Birbrair, A. (Ed.), *Tumor Microenvironment: Non-Hematopoietic Cells*, *Advances in Experimental Medicine and Biology*. Springer International Publishing, Cham, pp. 57–70. [https://doi.org/10.1007/978-3-030-37184-5\\_5](https://doi.org/10.1007/978-3-030-37184-5_5)
- Tian, L., Lu, Z.-P., Cai, B.-B., Zhao, L.-T., Qian, D., Xu, Q.-C., Wu, P.-F., Zhu, Y., Zhang, J.-J., Du, Q., Miao, Y., Jiang, K.-R., 2016. Activation of pancreatic stellate cells involves an EMT-like process. *Int J Oncol* 48, 783–792. <https://doi.org/10.3892/ijo.2015.3282>
- Tjomsland, V., Pomianowska, E., Aasrum, M., Sandnes, D., Verbeke, C.S., Gladhaug, I.P., 2016. Profile of MMP and TIMP Expression in Human Pancreatic Stellate Cells: Regulation by IL-1 $\alpha$  and TGF $\beta$  and Implications for Migration of Pancreatic Cancer Cells. *Neoplasia* 18, 447–456. <https://doi.org/10.1016/j.neo.2016.06.003>
- Tontonoz, P., Spiegelman, B.M., 2008. Fat and beyond: the diverse biology of PPAR $\gamma$ . *Annu Rev Biochem* 77, 289–312. <https://doi.org/10.1146/annurev.biochem.77.061307.091829>
- Truty, M.J., Urrutia, R., 2007. Basics of TGF-beta and pancreatic cancer. *Pancreatology* 7, 423–435. <https://doi.org/10.1159/000108959>
- Tsien, R.W., Tsien, R.Y., 1990. Calcium Channels, Stores, and Oscillations. *Annual Review of Cell Biology* 6, 715–760. <https://doi.org/10.1146/annurev.cb.06.110190.003435>

- Tsujimoto, T., Kawaratani, H., Yoshiji, H., Uemura, M., Fukui, H., 2008. Recent developments in the treatment of alcoholic chronic pancreatitis. *Curr Drug Abuse Rev* 1, 197–202. <https://doi.org/10.2174/1874473710801020197>
- Tsvilovskyy, V., Solís-López, A., Schumacher, D., Medert, R., Roers, A., Kriebbs, U., Freichel, M., 2018. Deletion of *Orai2* augments endogenous CRAC currents and degranulation in mast cells leading to enhanced anaphylaxis. *Cell Calcium* 71, 24–33. <https://doi.org/10.1016/j.ceca.2017.11.004>
- Uehara, K., 2005. Localization of TRPC1 channel in the sinus endothelial cells of rat spleen. *Histochem Cell Biol* 123, 347–356. <https://doi.org/10.1007/s00418-004-0741-6>
- Um, J.-Y., Kang, S.Y., Kim, H.J., Chung, B.Y., Park, C.W., Kim, H.O., 2020. Transient receptor potential vanilloid-3 (TRPV3) channel induces dermal fibrosis via the TRPV3/TSLP/Smad2/3 pathways in dermal fibroblasts. *J Dermatol Sci* 97, 117–124. <https://doi.org/10.1016/j.jdermsci.2019.12.011>
- Vaca, L., Sampieri, A., 2002. Calmodulin modulates the delay period between release of calcium from internal stores and activation of calcium influx via endogenous TRP1 channels. *J Biol Chem* 277, 42178–42187. <https://doi.org/10.1074/jbc.M204531200>
- van Westerloo, D.J., Florquin, S., de Boer, A.M., Daalhuisen, J., de Vos, A.F., Bruno, M.J., van der Poll, T., 2005. Therapeutic effects of troglitazone in experimental chronic pancreatitis in mice. *Am J Pathol* 166, 721–728. [https://doi.org/10.1016/S0002-9440\(10\)62293-6](https://doi.org/10.1016/S0002-9440(10)62293-6)
- Vennin, C., Murphy, K.J., Morton, J.P., Cox, T.R., Pajic, M., Timpson, P., 2018. Reshaping the Tumor Stroma for Treatment of Pancreatic Cancer. *Gastroenterology* 154, 820–838. <https://doi.org/10.1053/j.gastro.2017.11.280>
- Vig, M., DeHaven, W.I., Bird, G.S., Billingsley, J.M., Wang, H., Rao, P.E., Hutchings, A.B., Jouvin, M.-H., Putney, J.W., Kinet, J.-P., 2008. Defective mast cell effector functions in mice lacking the CRACM1 pore subunit of store-operated calcium release-activated calcium channels. *Nat Immunol* 9, 89–96. <https://doi.org/10.1038/ni1550>
- Vogelmann, R., Ruf, D., Wagner, M., Adler, G., Menke, A., 2001. Effects of fibrogenic mediators on the development of pancreatic fibrosis in a TGF-beta1 transgenic mouse model. *Am J Physiol Gastrointest Liver Physiol* 280, G164-172. <https://doi.org/10.1152/ajpgi.2001.280.1.G164>
- von Ahrens, D., Bhagat, T.D., Nagrath, D., Maitra, A., Verma, A., 2017. The role of stromal cancer-associated fibroblasts in pancreatic cancer. *J Hematol Oncol* 10, 76. <https://doi.org/10.1186/s13045-017-0448-5>
- Vonlaufen, A., Joshi, S., Qu, C., Phillips, P.A., Xu, Z., Parker, N.R., Toi, C.S., Pirola, R.C., Wilson, J.S., Goldstein, D., Apte, M.V., 2008a. Pancreatic stellate cells: partners in crime with pancreatic cancer cells. *Cancer Res* 68, 2085–2093. <https://doi.org/10.1158/0008-5472.CAN-07-2477>
- Vonlaufen, A., Phillips, P.A., Xu, Z., Goldstein, D., Pirola, R.C., Wilson, J.S., Apte, M.V., 2008b. Pancreatic Stellate Cells and Pancreatic Cancer Cells: An Unholy Alliance. *Cancer Res* 68, 7707–7710. <https://doi.org/10.1158/0008-5472.CAN-08-1132>

- Vonlaufen, A., Phillips, P.A., Xu, Z., Zhang, X., Yang, L., Pirola, R.C., Wilson, J.S., Apte, M.V., 2011. Withdrawal of alcohol promotes regression while continued alcohol intake promotes persistence of LPS-induced pancreatic injury in alcohol-fed rats. *Gut* 60, 238–246. <https://doi.org/10.1136/gut.2010.211250>
- Vonlaufen, A., Xu, Z., Daniel, B., Kumar, R.K., Pirola, R., Wilson, J., Apte, M.V., 2007. Bacterial endotoxin: a trigger factor for alcoholic pancreatitis? Evidence from a novel, physiologically relevant animal model. *Gastroenterology* 133, 1293–1303. <https://doi.org/10.1053/j.gastro.2007.06.062>
- Wagner, M., Kleeff, J., Lopez, M.E., Bockman, I., Massaqué, J., Korc, M., 1998. Transfection of the type I TGF-beta receptor restores TGF-beta responsiveness in pancreatic cancer. *Int J Cancer* 78, 255–260. [https://doi.org/10.1002/\(sici\)1097-0215\(19981005\)78:2<255::aid-ijc21>3.0.co;2-8](https://doi.org/10.1002/(sici)1097-0215(19981005)78:2<255::aid-ijc21>3.0.co;2-8)
- Wake, K., 1971. “Sternzellen” in the liver: perisinusoidal cells with special reference to storage of vitamin A. *Am J Anat* 132, 429–462. <https://doi.org/10.1002/aja.1001320404>
- Wakefield, L.M., Hill, C.S., 2013. Beyond TGFβ: roles of other TGFβ superfamily members in cancer. *Nat Rev Cancer* 13, 328–341. <https://doi.org/10.1038/nrc3500>
- Waldron, R.T., Chen, Y., Pham, H., Go, A., Su, H.-Y., Hu, C., Wen, L., Husain, S.Z., Sugar, C.A., Roos, J., Ramos, S., Lugea, A., Dunn, M., Stauderman, K., Pandol, S.J., 2019. The Orai Ca<sup>2+</sup> channel inhibitor CM4620 targets both parenchymal and immune cells to reduce inflammation in experimental acute pancreatitis. *J Physiol* 597, 3085–3105. <https://doi.org/10.1113/JP277856>
- Wang, L.M., Silva, M.A., D’Costa, Z., Bockelmann, R., Soonawalla, Z., Liu, S., O’Neill, E., Mukherjee, S., McKenna, W.G., Muschel, R., Fokas, E., 2016. The prognostic role of desmoplastic stroma in pancreatic ductal adenocarcinoma. *Oncotarget* 7, 4183–4194. <https://doi.org/10.18632/oncotarget.6770>
- Wang, W., O’Connell, B., Dykeman, R., Sakai, T., Delporte, C., Swaim, W., Zhu, X., Birnbaumer, L., Ambudkar, I.S., 1999. Cloning of Trp1beta isoform from rat brain: immunodetection and localization of the endogenous Trp1 protein. *Am J Physiol* 276, C969–979. <https://doi.org/10.1152/ajpcell.1999.276.4.C969>
- Wang, Y., Deng, X., Gill, D.L., 2010. Calcium signaling by STIM and Orai: intimate coupling details revealed. *Sci Signal* 3, pe42. <https://doi.org/10.1126/scisignal.3148pe42>
- Watanabe, S., Nagashio, Y., Asaumi, H., Nomiyama, Y., Taguchi, M., Tashiro, M., Kihara, Y., Nakamura, H., Otsuki, M., 2004. Pressure activates rat pancreatic stellate cells. *Am J Physiol Gastrointest Liver Physiol* 287, G1175–1181. <https://doi.org/10.1152/ajpgi.00339.2004>
- Watanabe, T., Masamune, A., Kikuta, K., Hirota, M., Kume, K., Satoh, K., Shimosegawa, T., 2009. Bone marrow contributes to the population of pancreatic stellate cells in mice. *Am J Physiol Gastrointest Liver Physiol* 297, G1138–1146. <https://doi.org/10.1152/ajpgi.00123.2009>
- Watari, N., Hotta, Y., Mabuchi, Y., 1982. Morphological studies on a vitamin A-storing cell and its complex with macrophage observed in mouse pancreatic tissues following excess vitamin A administration. *Okajimas Folia Anat Jpn* 58, 837–858. [https://doi.org/10.2535/ofaj1936.58.4-6\\_837](https://doi.org/10.2535/ofaj1936.58.4-6_837)

- Wei, L., Ye, H., Li, G., Lu, Y., Zhou, Q., Zheng, S., Lin, Q., Liu, Y., Li, Z., Chen, R., 2018. Cancer-associated fibroblasts promote progression and gemcitabine resistance via the SDF-1/SATB-1 pathway in pancreatic cancer. *Cell Death Dis* 9, 1065. <https://doi.org/10.1038/s41419-018-1104-x>
- Wei, M.C., Zong, W.X., Cheng, E.H., Lindsten, T., Panoutsakopoulou, V., Ross, A.J., Roth, K.A., MacGregor, G.R., Thompson, C.B., Korsmeyer, S.J., 2001. Proapoptotic BAX and BAK: a requisite gateway to mitochondrial dysfunction and death. *Science* 292, 727–730. <https://doi.org/10.1126/science.1059108>
- Wes, P.D., Chevesich, J., Jeromin, A., Rosenberg, C., Stetten, G., Montell, C., 1995. TRPC1, a human homolog of a Drosophila store-operated channel. *Proc Natl Acad Sci U S A* 92, 9652–9656. <https://doi.org/10.1073/pnas.92.21.9652>
- Wicks, S.J., Lui, S., Abdel-Wahab, N., Mason, R.M., Chantry, A., 2000. Inactivation of smad-transforming growth factor beta signaling by Ca(2+)-calmodulin-dependent protein kinase II. *Mol Cell Biol* 20, 8103–8111. <https://doi.org/10.1128/mcb.20.21.8103-8111.2000>
- Whittaker, S.R., Mallinger, A., Workman, P., Clarke, P.A., 2017. Inhibitors of Cyclin-Dependent Kinases as Cancer Therapeutics. *Pharmacol Ther* 173, 83–105. <https://doi.org/10.1016/j.pharmthera.2017.02.008>
- Widjaja, A.A., Singh, B.K., Adami, E., Viswanathan, S., Dong, J., D'Agostino, G.A., Ng, B., Lim, W.W., Tan, J., Paleja, B.S., Tripathi, M., Lim, S.Y., Shekeran, S.G., Chothani, S.P., Rabes, A., Sombetzki, M., Bruinstroop, E., Min, L.P., Sinha, R.A., Albani, S., Yen, P.M., Schafer, S., Cook, S.A., 2019. Inhibiting Interleukin 11 Signaling Reduces Hepatocyte Death and Liver Fibrosis, Inflammation, and Steatosis in Mouse Models of Nonalcoholic Steatohepatitis. *Gastroenterology* 157, 777-792.e14. <https://doi.org/10.1053/j.gastro.2019.05.002>
- Won, J.H., Zhang, Y., Ji, B., Logsdon, C.D., Yule, D.I., 2011. Phenotypic changes in mouse pancreatic stellate cell Ca<sup>2+</sup> signaling events following activation in culture and in a disease model of pancreatitis. *Mol Biol Cell* 22, 421–436. <https://doi.org/10.1091/mbc.E10-10-0807>
- Worley, P.F., Zeng, W., Huang, G.N., Yuan, J.P., Kim, J.Y., Lee, M.G., Muallem, S., 2007. TRPC channels as STIM1-regulated store-operated channels. *Cell Calcium* 42, 205–211. <https://doi.org/10.1016/j.ceca.2007.03.004>
- Wright, F.A., Wojcikiewicz, R.J.H., 2016. Chapter 4 - Inositol 1,4,5-Trisphosphate Receptor Ubiquitination. *Prog Mol Biol Transl Sci* 141, 141–159. <https://doi.org/10.1016/bs.pmbts.2016.02.004>
- Wu, J.W., Hu, M., Chai, J., Seoane, J., Huse, M., Li, C., Rigotti, D.J., Kyin, S., Muir, T.W., Fairman, R., Massagué, J., Shi, Y., 2001. Crystal structure of a phosphorylated Smad2. Recognition of phosphoserine by the MH2 domain and insights on Smad function in TGF-beta signaling. *Mol Cell* 8, 1277–1289. [https://doi.org/10.1016/s1097-2765\(01\)00421-x](https://doi.org/10.1016/s1097-2765(01)00421-x)
- Wyllie, A.H., Morris, R.G., Smith, A.L., Dunlop, D., 1984. Chromatin cleavage in apoptosis: association with condensed chromatin morphology and dependence on macromolecular synthesis. *J Pathol* 142, 67–77. <https://doi.org/10.1002/path.1711420112>

- Xiong, Y., Hannon, G.J., Zhang, H., Casso, D., Kobayashi, R., Beach, D., 1993. p21 is a universal inhibitor of cyclin kinases. *Nature* 366, 701–704. <https://doi.org/10.1038/366701a0>
- Xu, S.Z., Beech, D.J., 2001. TrpC1 is a membrane-spanning subunit of store-operated Ca(2+) channels in native vascular smooth muscle cells. *Circ Res* 88, 84–87. <https://doi.org/10.1161/01.res.88.1.84>
- Xu, X.-F., Liu, F., Xin, J.-Q., Fan, J.-W., Wu, N., Zhu, L.-J., Duan, L.-F., Li, Y.-Y., Zhang, H., 2018. Respective roles of the mitogen-activated protein kinase (MAPK) family members in pancreatic stellate cell activation induced by transforming growth factor- $\beta$ 1 (TGF- $\beta$ 1). *Biochemical and Biophysical Research Communications* 501, 365–373. <https://doi.org/10.1016/j.bbrc.2018.04.176>
- Xu, Z., Vonlaufen, A., Phillips, P.A., Fiala-Beer, E., Zhang, X., Yang, L., Biankin, A.V., Goldstein, D., Pirola, R.C., Wilson, J.S., Apte, M.V., 2010. Role of pancreatic stellate cells in pancreatic cancer metastasis. *Am J Pathol* 177, 2585–2596. <https://doi.org/10.2353/ajpath.2010.090899>
- Yana, I., Seiki, M., 2002. MT-MMPs play pivotal roles in cancer dissemination. *Clin Exp Metastasis* 19, 209–215. <https://doi.org/10.1023/a:1015527220537>
- Yoast, R.E., Emrich, S.M., Trebak, M., 2020a. The anatomy of native CRAC channel(s). *Curr Opin Physiol* 17, 89–95.
- Yoast, R.E., Emrich, S.M., Zhang, X., Xin, P., Johnson, M.T., Fike, A.J., Walter, V., Hempel, N., Yule, D.I., Sneyd, J., Gill, D.L., Trebak, M., 2020b. The native ORAI channel trio underlies the diversity of Ca<sup>2+</sup> signaling events. *Nat Commun* 11, 2444. <https://doi.org/10.1038/s41467-020-16232-6>
- Yoo, B.-M., Oh, T.-Y., Kim, Y.-B., Yeo, M., Lee, J.-S., Surh, Y.J., Ahn, B.-O., Kim, W.-H., Sohn, S., Kim, J.-H., Hahn, K.-B., 2005. Novel antioxidant ameliorates the fibrosis and inflammation of cerulein-induced chronic pancreatitis in a mouse model. *Pancreatology* 5, 165–176. <https://doi.org/10.1159/000085268>
- Yoshida, S., Ujiki, M., Ding, X.-Z., Pelham, C., Talamonti, M.S., Bell, R.H., Denham, W., Adrian, T.E., 2005. Pancreatic stellate cells (PSCs) express cyclooxygenase-2 (COX-2) and pancreatic cancer stimulates COX-2 in PSCs. *Mol Cancer* 4, 27. <https://doi.org/10.1186/1476-4598-4-27>
- Yoshida, S., Yokota, T., Ujiki, M., Ding, X.-Z., Pelham, C., Adrian, T.E., Talamonti, M.S., Bell, R.H., Denham, W., 2004. Pancreatic cancer stimulates pancreatic stellate cell proliferation and TIMP-1 production through the MAP kinase pathway. *Biochem Biophys Res Commun* 323, 1241–1245. <https://doi.org/10.1016/j.bbrc.2004.08.229>
- Yuan, J.P., Kiselyov, K., Shin, D.M., Chen, J., Shcheynikov, N., Kang, S.H., Dehoff, M.H., Schwarz, M.K., Seeburg, P.H., Muallem, S., Worley, P.F., 2003. Homer binds TRPC family channels and is required for gating of TRPC1 by IP<sub>3</sub> receptors. *Cell* 114, 777–789. [https://doi.org/10.1016/s0092-8674\(03\)00716-5](https://doi.org/10.1016/s0092-8674(03)00716-5)
- Yuan, J.P., Zeng, W., Huang, G.N., Worley, P.F., Muallem, S., 2007. STIM1 heteromultimerizes TRPC channels to determine their function as store-operated channels. *Nat Cell Biol* 9, 636–645. <https://doi.org/10.1038/ncb1590>



- Yunis, A.A., Arimura, G.K., Russin, D.J., 1977. Human pancreatic carcinoma (MIA PaCa-2) in continuous culture: sensitivity to asparaginase. *Int J Cancer* 19, 128–135. <https://doi.org/10.1002/ijc.2910190118>
- Zang, G., Sandberg, M., Carlsson, P.-O., Welsh, N., Jansson, L., Barbu, A., 2015. Activated pancreatic stellate cells can impair pancreatic islet function in mice. *Ups J Med Sci* 120, 169–180. <https://doi.org/10.3109/03009734.2015.1032453>
- Zha, M., Li, F., Xu, W., Chen, B., Sun, Z., 2014a. Isolation and characterization of islet stellate cells in rat. *Islets* 6, e28701. <https://doi.org/10.4161/isl.28701>
- Zha, M., Xu, W., Jones, P.M., Sun, Z., 2016. Isolation and characterization of human islet stellate cells. *Exp Cell Res* 341, 61–66. <https://doi.org/10.1016/j.yexcr.2015.11.002>
- Zha, M., Xu, W., Zhai, Q., Li, F., Chen, B., Sun, Z., 2014b. High glucose aggravates the detrimental effects of pancreatic stellate cells on Beta-cell function. *Int J Endocrinol* 2014, 165612. <https://doi.org/10.1155/2014/165612>
- Zhang, H., Wu, H., Guan, J., Wang, L., Ren, X., Shi, X., Liang, Z., Liu, T., 2015. Paracrine SDF-1 $\alpha$  signaling mediates the effects of PSCs on GEM chemoresistance through an IL-6 autocrine loop in pancreatic cancer cells. *Oncotarget* 6, 3085–3097. <https://doi.org/10.18632/oncotarget.3099>
- Zhang, S.L., Yu, Y., Roos, J., Kozak, J.A., Deerinck, T.J., Ellisman, M.H., Stauderman, K.A., Cahalan, M.D., 2005. STIM1 is a Ca<sup>2+</sup> sensor that activates CRAC channels and migrates from the Ca<sup>2+</sup> store to the plasma membrane. *Nature* 437, 902–905. <https://doi.org/10.1038/nature04147>
- Zhang, X., Jin, T., Huang, X., Liu, X., Liu, Z., Jia, Y., Hao, J., 2018. Effects of the tumor suppressor PTEN on biological behaviors of activated pancreatic stellate cells in pancreatic fibrosis. *Exp. Cell Res.* 373, 132–144. <https://doi.org/10.1016/j.yexcr.2018.10.005>
- Zhang, Y., Alexander, P.B., Wang, X.-F., 2017. TGF- $\beta$  Family Signaling in the Control of Cell Proliferation and Survival. *Cold Spring Harb Perspect Biol* 9. <https://doi.org/10.1101/cshperspect.a022145>
- Zhang, Y.E., 2017. Non-Smad Signaling Pathways of the TGF- $\beta$  Family. *Cold Spring Harb Perspect Biol* 9. <https://doi.org/10.1101/cshperspect.a022129>
- Zhang, Y.E., 2009. Non-Smad pathways in TGF-beta signaling. *Cell Res* 19, 128–139. <https://doi.org/10.1038/cr.2008.328>
- Zheng, M., Li, H., Sun, L., Brigstock, D.R., Gao, R., 2021. Interleukin-6 participates in human pancreatic stellate cell activation and collagen I production via TGF- $\beta$ 1/Smad pathway. *Cytokine* 143, 155536. <https://doi.org/10.1016/j.cyto.2021.155536>
- Zhou, Y., Sun, B., Li, W., Zhou, J., Gao, F., Wang, X., Cai, M., Sun, Z., 2019. Pancreatic Stellate Cells: A Rising Translational Physiology Star as a Potential Stem Cell Type for Beta Cell Neogenesis. *Front. Physiol.* 10. <https://doi.org/10.3389/fphys.2019.00218>
- Zhu, X., Chu, P.B., Peyton, M., Birnbaumer, L., 1995. Molecular cloning of a widely expressed human homologue for the *Drosophila* trp gene. *FEBS Lett* 373, 193–198. [https://doi.org/10.1016/0014-5793\(95\)01038-g](https://doi.org/10.1016/0014-5793(95)01038-g)

Zimmerman, C.M., Kariapper, M.S., Mathews, L.S., 1998. Smad proteins physically interact with calmodulin. *J Biol Chem* 273, 677–680. <https://doi.org/10.1074/jbc.273.2.677>



---




# ANNEXES

---



Review

# Ion Channels: New Actors Playing in Chemotherapeutic Resistance

Philippe Kischel <sup>1,\*†</sup>, Alban Girault <sup>1,†</sup> , Lise Rodat-Despoix <sup>1</sup>, Mohamed Chamli <sup>1</sup>,  
Silviya Radoslavova <sup>1</sup>, Hiba Abou Daya <sup>1</sup>, Thibaut Lefebvre <sup>1</sup>, Arthur Foulon <sup>1,2</sup> ,  
Pierre Rybarczyk <sup>1,3</sup>, Frédéric Hague <sup>1</sup>, Isabelle Dhennin-Duthille <sup>1</sup>, Mathieu Gautier <sup>1</sup>   
and Halima Oquadid-Ahidouch <sup>1</sup>

<sup>1</sup> Laboratoire de Physiologie Cellulaire et Moléculaire (EA 4667), Université de Picardie Jules Verne, UFR des Sciences, 33 Rue St Leu, 80039 Amiens, France; alban.girault@u-picardie.fr (A.G.); lise.despoix@u-picardie.fr (L.R.-D.); mohamed.chamli@etud.u-picardie.fr (M.C.); silviya.radoslavova@u-picardie.fr (S.R.); hiba.abou.day@etud.u-picardie.fr (H.A.D.); thibaut.lefebvre@u-picardie.fr (T.L.); arthfoulon@gmail.com (A.F.); rybarczyk pierre@hotmail.com (P.R.); fh-lnc@u-picardie.fr (F.H.); isabelle.dhennin@u-picardie.fr (I.D.-D.); mathieu.gautier@u-picardie.fr (M.G.); halima.ahidouch-ouadid@u-picardie.fr (H.O.-A.)

<sup>2</sup> Service de Gynécologie Obstétrique, CHU Amiens Picardie, 80000 Amiens, France

<sup>3</sup> Laboratoire d'Anatomie et Cytologie Pathologiques, CHU Amiens Picardie, 80000 Amiens, France

\* Correspondence: Philippe.Kischel@u-picardie.fr; Tel.: +33-3-2282-7643; Fax: +33-3-2282-7550

† These authors contributed equally to this work.

Received: 1 February 2019; Accepted: 12 March 2019; Published: 16 March 2019



**Abstract:** In the battle against cancer cells, therapeutic modalities are drastically limited by intrinsic or acquired drug resistance. Resistance to therapy is not only common, but expected: if systemic agents used for cancer treatment are usually active at the beginning of therapy (i.e., 90% of primary breast cancers and 50% of metastases), about 30% of patients with early-stage breast cancer will have recurrent disease. Altered expression of ion channels is now considered as one of the hallmarks of cancer, and several ion channels have been linked to cancer cell resistance. While ion channels have been associated with cell death, apoptosis and even chemoresistance since the late 80s, the molecular mechanisms linking ion channel expression and/or function with chemotherapy have mostly emerged in the last ten years. In this review, we will highlight the relationships between ion channels and resistance to chemotherapy, with a special emphasis on the underlying molecular mechanisms.

**Keywords:** ion channels; cancer; chemoresistance

## 1. Introduction

Cancers cells have the ability to develop resistance to traditional therapies. Drug resistance may be intrinsic (i.e., present before chemotherapy exposure), but tumor cells can also acquire drug resistance. Indeed, although systemic agents used for cancer treatment (cytotoxic, hormonal, and immunotherapeutic agents) are usually active at the beginning of therapy (90% of primary breast cancers and 50% of metastases for instance), about 30% of patients with early-stage breast cancer will have recurrent disease. Resistance to therapy is not only common, but expected [1]. Tumor cells from recurrent tumors exhibit increased resistance to chemotherapeutic drugs [2], and exposure to chemotherapeutic drugs can promote development of drug resistance in tumor cells, leading to subsequent failure of the chemotherapeutic treatment [3], thus drastically limiting effective therapeutic modalities. Residual tumor cells are detected post-treatment in most cancer patients, and these cells are thought to remain in a quiescent state for years before resuming growth, resulting in tumor recurrence. Deciphering molecular mechanisms of this acquired cellular resistance is therefore mandatory for

predicting tumor resistance and to allow discovery of new treatments. Several mechanisms underlying cell resistance have been identified so far. Among those, membrane transporters and ion channels have been shown to play key roles in chemosensitivity. These include [4]:

- Decreased activity of the uptake transporters, or alternatively enhanced efflux for water-soluble drugs (such as cisplatin)
- Increased drug efflux mediated by energy-dependent transporters. For hydrophobic drugs (such as vinblastine, doxorubicin, and paclitaxel), entry occurs largely by diffusion across the membrane, although this process can also be critically enhanced by transport proteins
- Indirect mechanisms by which transporters and channels affect chemosensitivity by modulating apoptosis pathways or the efficiency of drug diffusion along electrochemical gradients into cells

This review will more specifically focus on ion channels. Altered expression of ion channels is now considered as one of the hallmarks of cancer [5], and several ion channels have been linked to cancer cell resistance. While some ion channels have been associated with chemoresistance since the 80s [6], extensive description of molecular mechanisms involved in chemoresistance is more recent (early 2000s [7], with the vast majority of scientific articles being published after 2010). In this review, we will highlight the relationships between channels (calcium, potassium, magnesium and chloride channels) and resistance to chemotherapy, with special emphasis on the underlying molecular mechanisms.

## 2. Calcium Channels

### 2.1. Plasma Membrane $Ca^{2+}$ Channels

Calcium ( $Ca^{2+}$ ) is a well-known ubiquitous second messenger regulating a wide variety of physiological functions [8,9], including cell death [10]. Disruption of  $Ca^{2+}$  homeostasis was reported in many pathological conditions, including cancer [11,12]. There is a ~10,000-fold concentration gradient for  $Ca^{2+}$  across the plasma membrane, and three major classes of membrane-associated proteins directly involved in  $Ca^{2+}$  regulation: channels, pumps (ATP-ases), and exchangers. These proteins have different cellular and tissue distribution and their regulation occurs through multiple signalling pathways ([13] for review). Extracellular  $Ca^{2+}$  can enter cells by several classes of channels, including:

- Voltage-operated channels, activated by membrane depolarization
- Second messenger-operated channels, activated by small messenger molecules such as inositol phosphates, cyclic nucleotides, and lipid-derived messengers (diacyl-glycerol, arachidonic acid and its metabolites)
- Receptor-operated channels, activated by direct binding of a neurotransmitter or hormone agonist
- Store-operated channels (SOC), activated by depletion of intracellular  $Ca^{2+}$  stores [14]

SOC Entry (SOCE) is one of the main calcium entries in non-excitabile cells, and typically allows calcium influx through the plasma membrane, subsequently to endoplasmic reticulum depletion. This ubiquitous SOCE pathway is not only necessary to refill internal calcium stores, but also to activate downstream signalling cascades [15,16]. Apoptosis is also potentially triggered when a large and sustained rise in cytosolic calcium occurs through SOCE (mediated by store-operated channels SOCs [17–19]). Actors of this mechanism include depletion sensors (STIM reticular proteins, the STIM1 and STIM2 isoforms), as well as plasma membrane channels. Among these, Orai channels represent highly selective calcium channels (with 3 distinct Orai isoforms described to date, Orai1, Orai2 and Orai3), while TRP (Transient Receptor Potential) channels are non-selective calcium channels.

$Ca^{2+}$  entries can also occur without any stimulation, suggesting that some  $Ca^{2+}$  channels are constitutively active in resting conditions. Interestingly, these basal  $Ca^{2+}$  influxes are linked to malignant transformation, but the underlying molecular mechanisms are far from being understood ([20], for review).

In addition, under certain conditions,  $\text{Ca}^{2+}$  can enter cells via the  $\text{Na}^+/\text{Ca}^{2+}$  exchanger (NCX) operating in reverse mode. Cytosolic calcium concentration can also rise following endoplasmic reticulum depletion (see Section 2.2. Intracellular Calcium Stores below).

Chemoresistance has been first associated with  $\text{Ca}^{2+}$  channel activity in the 80s. Blockade of  $\text{Ca}^{2+}$  channels was associated with the enhancement of anticancer drug cytotoxicity ([21], for review). It was notably demonstrated that combination of verapamil (a calcium channel blocker) with antineoplastic agents was able to potentiate the efficacy of chemotherapeutic agents in drug-sensitive malignancies, and was also able to confer chemosensitivity in resistant tumor cells [22]. However, there was inconclusive evidence for the role of  $\text{Ca}^{2+}$  ions and  $\text{Ca}^{2+}$  channels in the modulation of chemoresistance, and furthermore, there was no evidence that  $\text{Ca}^{2+}$  channels blocking activity per se was necessary for the reversal of drug resistance [21]. Although  $\text{Ca}^{2+}$  channels blockers have been studied in combination with chemotherapeutic drugs for several decades, it is noteworthy that the mechanism of action for these  $\text{Ca}^{2+}$  blockers in inhibiting the growth of some drug-resistant tumors was entirely independent of  $\text{Ca}^{2+}$  channels modulation, and instead appeared to be related to non-specific interactions with the MultiDrug Resistance-1 (MDR1) protein ([23] for review). For instance, Kiwit et al. have shown that calcium antagonists did not influence chemoresistance in gliomas that do not express MDR1. On the other hand, addition of calcium antagonists to the adjuvant chemotherapy could overcome primary chemoresistance only in tumors expressing the multidrug-resistant phenotype [24].

Since the beginning of the 2010s, a growing number of studies have shown a clear link between  $\text{Ca}^{2+}$  channels expression (and/or function) and sensitivity to chemotherapeutic drugs. Many calcium channels are involved in chemoresistance, against a number of chemotherapeutic drugs, in a large variety of cancers. We will more specifically focus on the main calcium entry, SOCE, and its key actors, the Orai and TRP channels.

#### 2.1.1. Orai/Stim Mediated SOCE and Chemoresistance

Depending on cancer cell lines and chemotherapeutic drugs, SOCE can lead to increased or decreased resistance. First, because each cell line differentially express Orai and Stim proteins. Second because both Orai1 and Stim1 were shown to regulate the activity of a number of intracellular effectors including PKC  $\beta$ 2 [25], PKC  $\delta$  [26], extracellular signal-related kinases ERK1/2 [27], and both cytoplasmic kinase Pyk2 and calpain [28]. Third, both Orai1 and Stim1 were shown to have SOCE independent functions. For instance, the Secretory Pathway  $\text{Ca}^{2+}$ -ATPase SPCA2 can activate Orai1 independently of ER calcium stores or Stim proteins [29]. Within such a complex regulatory network and the role of Orai1/Stim1 downstream targets in both pro-survival and pro-apoptotic processes, the resistance of each cell line is likely to depend on the activated signalling pathway [30].

#### Increased Resistance Conferred by the Overexpression of Stim and Orai Proteins

Numerous studies have now established a clear link between the Orai/Stim complex and cell resistance, although the mechanisms are not always accurately described. For instance, Stim1-mediated SOCE protects osteosarcoma cells from undergoing cisplatin-induced apoptosis. Knockdown of Stim1 effectively sensitizes cells to cisplatin via promoting Endoplasmic Reticulum (ER) stress-mediated apoptosis [31]. In pancreatic adenocarcinoma, both Stim1 and Orai1 mediate SOCE and have a pro-survival anti-apoptotic role, as Orai1 and/or Stim1 silencing by siRNA enhance 5-Fluoro-Uracile (5-FU) and gemcitabine induced apoptosis [30]. Mechanisms by which the Orai/Stim complex affects chemoresistance include MDR transporters and intracellular signalling pathways (Figure 1). The overexpression of the transporter MDR1 is one of the best known mechanisms by which breast cancers cells develop chemoresistance [32]. It has notably been shown that high salts were able to induce MDR1 mediated treatment resistance in breast cancer cells through SOCE [33]. It has also been shown that Orai1 and Stim1 expression are increased in chemoresistant ovarian carcinoma cells, associated to an increase of SOCE. During the acquisition of the chemoresistant phenotype, Orai1 expression is upregulated by the Akt signalling pathway, leading to an increase of SOCE [34].

Furthermore, Orai1 expression is also elevated in hepatocellular carcinoma (HCC) tissues, and contributes to a chemoresistant phenotype. Orai1-mediated  $\text{Ca}^{2+}$  entry is able to block 5-FU-induced autophagic cell death in HepG2 cells via activation of the PI3K/Akt/mTOR signalling pathway [35]. In human gastrointestinal stromal tumors, Orai1 is able to mediate tumor-promoting SOCE via c-KIT and the ERK pathway [36]. Whilst far less studied than its sibling Orai1, Orai3 protein deserves special attention, because of (i) its exclusive presence in mammals [37], (ii) its receptivity to pharmacological modulation [38], and (iii) its recent emergence in the cancer field, especially in breast cancer. Many data establish now a clear link between Orai3 and chemoresistance (Figure 1). Orai3 was primarily described as involved in proliferation, cell cycle progression, and Estrogen Receptor positive (ER<sup>+</sup>) breast cancer cells survival [39]. In these cells, SOCE is dependent on Orai3 expression, whereas Estrogen Receptor negative (ER<sup>-</sup>) cells depends on Orai1 [40]. In such ER<sup>-</sup> cells, Bhattacharya et al. [41] have shown that Orai3 and Stim1 were able to mediate TGF- $\beta$  induced expression of Snai1, a transcriptional repressor protein known to mediate Epithelial to Mesenchymal Transition (EMT), a cell state transition process implicated in drug resistance [32]. This process was AKT and NF- $\kappa$ B (p65)-dependent [41]. In ER<sup>+</sup> breast cancer cells, Orai3-dependent survival was found to be transduced—at least in part—via the ERK and c-myc pathway [42]. Overexpression of Orai3 protein in ER<sup>+</sup> breast cancer cells revealed consistent chemoresistance against cisplatin, 5-FU and paclitaxel treatments. The main effect of Orai3 upregulation was a SOCE-induced downregulation of the tumor suppressor protein p53, leading to reduced apoptosis [43]. The complete pathway leading to p53 downregulation was extensively deciphered: increased SOCE is able to activate PI3K, but not Akt. Instead, the Sgk1 pathway is specifically activated, leading to Mdm2 activation and p53 downregulation. Sgk1 activation is also responsible for the inactivation of the Sek-1 kinase, and therefore to an hypo-phosphorylated and thus activated Nedd4.2 ubiquitin ligase, able to decrease p53 protein expression [43]. All these results are summarized in Figure 1 and in Table S1.

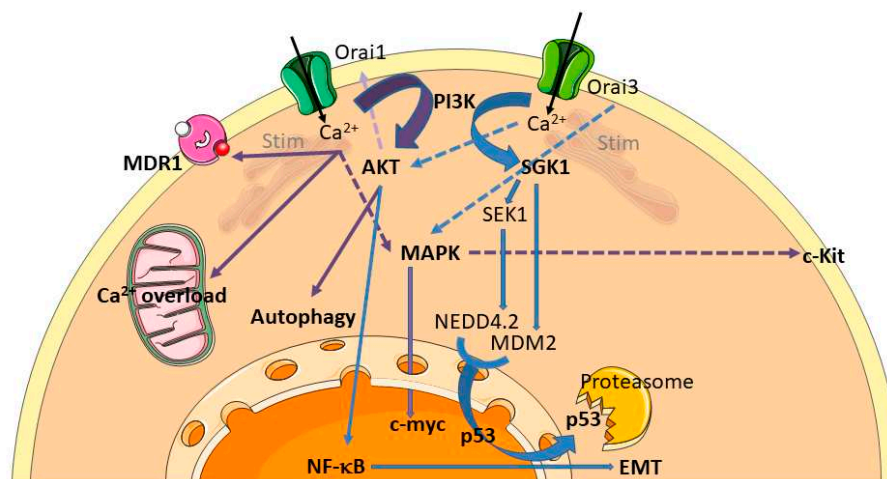


**Figure 1.** Chemoresistance pathways involving Orai calcium channels. Orai calcium channels are able to modulate sensitivity to chemotherapy. Processes known to alter chemoresistance are highlighted in bold. These include calcium overload, MultiDrug Resistance (MDR), autophagy, modulation of signalling pathways (MAPK and PI3K-Akt/Sgk), transcription factors (NF- $\kappa$ B, c-myc, p53), and EMT (Epithelial to Mesenchymal Transition). Processes initiated by Orai1 and Orai3 are summarized by purple and blue arrows, respectively. The dashed arrows are not different from plain arrows, except that they cross other arrows.

#### Reduced Resistance Conferred by the Overexpression of Stim and Orai Proteins

Resistance to apoptosis can also be acquired through a remodeling of the  $\text{Ca}^{2+}$  protein network that will reduce the likelihood of cytosolic  $\text{Ca}^{2+}$  overload. In androgen-independent, apoptosis-resistant prostate cancer cells, such remodeling was shown to involve reduced SOCE via downregulation

of Orai1 or Stim1 proteins, and adaptation of the ER to the conditions of reduced  $\text{Ca}^{2+}$  storage and uptake [18,44]. In prostate cancer cells, low Orai1 expression was shown to contribute to the establishment of an apoptosis-resistant phenotype, irrespective of the apoptosis-inducing stimulus [17]. Orai3 overexpression in prostate cancer cells is able to impair the Orai1-mediated SOCE and causes prostate cancer cell resistance [45].

### 2.1.2. Transient Receptor Potential (TRP) Channels

Transient Receptor Potential (TRP) channels are non-selective cation channels that can allow  $\text{Ca}^{2+}$  influx. The major groups of TRP channels include, among others, TRPM (Melastatin), TRPV (Vanilloid), and TRPC (Canonical). These channels have been associated with chemoresistance in many cancers since a decade [46,47].

TRPV—It has recently been shown that 5-FU induced breast cancer cell death was up-regulated by TRPV1 activation [48]:  $\text{Ca}^{2+}$  entry through TRPV1 is able to decrease chemoresistance. Nabissi et al. have shown that treatment with the TRPV2 agonist cannabidiol, by enhancing TRPV2 expression and activation, increased the chemosensitivity of human glioblastoma cells to the cytotoxic effects of various chemotherapeutic agents commonly used in the treatment of glioblastoma (temozolomide, carmustine and doxorubicin). Abrogation of chemoresistance was obtained by increased calcium influx through TRPV2 channel leading to a calcium-dependant cell death [49]. Moreover, cannabidiol and the proteasome inhibitor bortezomib synergise to increase cytotoxicity in multiple myeloma cell lines through TRPV2 activation [50]. Taken together, these data suggest that TRPV2 activation can potentiate the effects of cytotoxic drugs in various cancer types.

TRPM—In gastric cancer, Almasi et al. have shown that TRPM2 channel expression is negatively correlated with overall patient survival. Moreover, TRPM2 downregulation sensitized gastric cancer cells to paclitaxel and doxorubicin. Indeed, TRPM2, by activating both Akt and JNK signalling pathways, promote gastric cancer cell survival [51]. It has been shown that TRPM2 knockdown activates alternative pathway of cell death in breast cancer cells, leading to enhanced cytotoxicity after treatment with doxorubicin or *N*-methyl-*N'*-nitro-*N*-nitrosoguanidine [52]. In a similar manner, knockdown of TRPM8 was able to enhance epirubicin-induced apoptosis in osteosarcoma cells, and this effect was mediated through impaired regulation of intracellular  $\text{Ca}^{2+}$  concentration and the Akt-GSK-3 $\beta$  pathway [53].

TRPC—Downregulation of TRPC1 was shown to contribute to drug resistance in ovarian cancer, possibly by regulating autophagy [54]. Autophagy can be also mediated by TRPC5 and promotes drug resistance via CaMKK $\beta$ /AMPK $\alpha$ /mTOR pathway in breast cancer cells [55]. The TRPC5 channel has been largely associated with drug resistance in several cancers. TRPC5 can regulate  $\text{Ca}^{2+}$  homeostasis by forming a store-operated channel or a store independent channel. In addition, TRPC5-mediated  $\text{Ca}^{2+}$  entry is elicited by several physiological messengers, including reduced thioredoxin, protons, sphingosine-1-phosphate, lysophospholipids, NO and  $\text{Ca}^{2+}$  itself (see [56] for review). TRPC5 can confer chemoresistance to anticancer drugs in breast cancer. It has been shown that TRPC5 was essential for MDR1 induction in drug-resistant cancer cells [57], notably through activation of the transcription factor NFATc3 [58]. TRPC5 might even act as a non-invasive chemoresistance marker, since increasing circulating exosomes-carrying TRPC5 predicts chemoresistance in metastatic breast cancer patients [59]. In colorectal cancer, TRPC5 overexpression induces the Wnt/ $\beta$ -catenin signalling pathway and the up-regulation of MDR1 [60]. The same team demonstrated the essential role of glycolysis in TRPC5 induced chemoresistance in human colorectal cancer cells by maintaining  $\text{Ca}^{2+}$  homeostasis [61].

In HCC cells, inhibiting TRPC6 enhanced the efficacy of doxorubicin. Moreover,  $\text{Ca}^{2+}$  was found to be essential in mediating mechanisms of EMT, HIF-1 $\alpha$  signalling and DNA damage repair, conferring multidrug resistance in HCC cells. Multidrug resistance was attributed to the sustained accumulation of intracellular free  $\text{Ca}^{2+}$  induced by TRPC6 overexpression. The pathway by which TRPC6 is able to induce multidrug resistance in these cells was demonstrated to be STAT3-dependent [62]. In a



variety of other cancer cell lines (breast, prostate, bone, skin, lung), TRPC6 expression was on the contrary shown to lead to  $\text{Ca}^{2+}$ -dependent apoptotic death and activation of apoptotic genes. Using the antineoplastic drug GaQ3 (an organic derivative of gallium), Madan et al. demonstrated that these apoptotic pathways were activated by the transcriptional upregulation of TRPC6 (and hence intracellular calcium) by p53 [63].

Mechanisms concerning the involvement of TRP channel in chemoresistance are provided in Table S1.

### 2.1.3. Voltage-Gated Calcium Channels and Chemotherapy

Voltage-gated calcium channels (VGCC) are expressed throughout the body and perform several key physiological functions. In small cell lung cancer (SCLC), cells expressing the voltage-dependent calcium channel  $\alpha 2\delta 1$  subunit (isolated from SCLC cell lines or patient-derived xenograft models) exhibit cancer stem cells characteristics and chemotherapeutic resistance. Treatment with etoposide enhanced the cell populations expressing  $\alpha 2\delta 1$  in vitro and in vivo. Chemoresistance in these SCLC cell lines was shown to be mediated by the ERK pathway [64]. Moreover, the suppression of expression or activity of T-type  $\text{Ca}^{2+}$  channel induce apoptosis and hence allow resistance of ovarian cancer cells to chemotherapeutic treatments [65]. Apoptosis was accompanied by decreased Akt phosphorylation and alterations in FOXO and FOXM1 expression. Table S1 succinctly summarizes this information.

## 2.2. Intracellular Calcium Stores

Like extracellular calcium, intracellular calcium plays a decisive role in chemoresistance processes. Several intracellular organelles are implicated in such mechanisms, notably endoplasmic reticulum (ER) and mitochondria. Due to its closed proximity to the mitochondria,  $\text{Ca}^{2+}$  transport mechanisms from the ER to the mitochondria are allowed by the interaction of inositol 1,4,5-trisphosphate receptor ( $\text{IP}_3\text{R}$ ), the Glucose-Regulated Protein 75 and the Voltage-Dependent Anion Channel (VDAC) and the Mitochondrial Calcium Uniport (MCU). Since the MCU is the primary mediator of the mitochondrial  $\text{Ca}^{2+}$  uptake, its expression and function in cancer processes have been extensively investigated over the last ten years. Overexpression of MCU has been correlated to breast cancer progression [66], but its role in chemoresistance processes remains poorly understood. The amount of  $\text{Ca}^{2+}$  transferred from the ER to mitochondria impacts the sensitivity of cells to apoptotic stimuli and their resistance to apoptosis [67]. Moreover, it has been demonstrated that cancer cells escape cell death by lowering the ER  $\text{Ca}^{2+}$ -store, due to a  $\text{Ca}^{2+}$  transfer between ER and mitochondria [68].

### 2.2.1. Intracellular $\text{Ca}^{2+}$ Channels Expression Is Associated to Chemoresistance

Due to the close interaction with mitochondria, and its role in the regulation of mitochondrial  $\text{Ca}^{2+}$  load,  $\text{IP}_3\text{R}$  expression and/or activation have been associated to cancer cell survival and chemoresistance [69]. In bladder cancer cells,  $\text{IP}_3\text{R}1$  expression level has been inversely correlated to cisplatin-resistance: resistant cells express reduced  $\text{IP}_3\text{R}1$  level, and  $\text{IP}_3\text{R}1$ -knockdown prevents apoptosis, leading to cisplatin resistance. On the other hand,  $\text{IP}_3\text{R}1$  overexpression in resistant cells induces apoptosis and increases sensitivity to cisplatin [70]. Conversely, high  $\text{IP}_3\text{R}$  expression levels were associated to low resistance of epithelial pulmonary lung cancer cells to cisplatin treatment [71].

As a key regulator of the ER-mitochondrial interaction, the anti-apoptotic Bcl-2 protein is the subject of utmost attention. The Bcl-2-family members, which are generally divided into three categories (anti-apoptotic proteins, pro-apoptotic executioners and pro-apoptotic BH3-only proteins), act at two different intracellular compartments: the mitochondria and the ER [72]. Mechanistically, anti-apoptotic family members prevent cell death by sequestering the BH3 domains and by preventing their interaction with pro-apoptotic Bax/Bak proteins [73,74]. Small molecules (like BH3 mimetics) can disrupt this interaction, resulting in apoptotic cell death of cancer cells. Bcl-2 expression has been correlated to tumor growth enhancement and to chemoresistance [75] by increasing the passive  $\text{Ca}^{2+}$  leak from the ER [76]. Interestingly, the anti-apoptotic protein Bcl-2 expression level seems

to be a determinant for cancer cell sensitivity to cisplatin [77]. In non-small cell lung cancer and bladder cancer, cisplatin sensitivity could be enhanced by downregulating Bcl-2 [78,79]. In addition, Bcl-2 downregulation in SK-OV-3 ovarian cancer cells increases  $\text{Ca}^{2+}$  levels in the cytosol and in the mitochondria, as well as the number of ER–mitochondrial contact points after cisplatin treatment, thereby increasing the sensitivity to the chemotherapeutic agent [80].

### 2.2.2. Chemotherapy Modulates Intracellular $\text{Ca}^{2+}$ Channels Activity

Numerous studies have demonstrated that intracellular channels/transporters/pumps expression is altered in cancers, leading to intracellular  $\text{Ca}^{2+}$  homeostasis perturbation. However, the impact of chemotherapeutic agents on the activity of these intracellular  $\text{Ca}^{2+}$  channels is less described. Zhang et al. established that paclitaxel accelerates spontaneous  $\text{Ca}^{2+}$  oscillations by increasing the  $\text{IP}_3\text{R}$  opening frequency in the presence of Neuronal Calcium Sensor-1, a  $\text{Ca}^{2+}$  binding protein [81]. Moreover, Boutin et al. have demonstrated that PKA-induced  $\text{IP}_3\text{R1}$  over-activation triggers  $[\text{Ca}^{2+}]_{\text{ER}}$  decrease: this mechanism allows the prostate cancer cell line LNCAP to survive androgen deprivation [82]. Recently, Kang et al. demonstrated that Trifluoperazine, a well-known antipsychotic drug with anticancer effects [83–86], inhibits glioblastoma invasion by binding to the  $\text{Ca}^{2+}$ -binding protein, calmodulin subtype 2 (CaM2). This binding dissociates CaM2 from  $\text{IP}_3\text{R1}$  and  $\text{IP}_3\text{R2}$  leading to massive and irreversible  $\text{Ca}^{2+}$  release from intracellular stores by  $\text{IP}_3\text{R1}$  and  $\text{IP}_3\text{R2}$  subsequent opening [87].

### 2.2.3. Signalling Pathways Involved in Chemoresistance Related to Intracellular $\text{Ca}^{2+}$ Channels

Mechanisms of intracellular  $\text{Ca}^{2+}$  pathways involved in chemoresistance are poorly understood, but few teams have succeeded in deciphering the communication between ER and mitochondria in such processes. In ovarian cancer cells, TAT-fused inositol 1,4,5-trisphosphate receptor-derived peptide (TAT-IDP<sup>5</sup>), which targets the BH4 domain of Bcl-2, enhances the cytotoxicity of cisplatin by stimulating  $\text{Ca}^{2+}$  efflux from the endoplasmic reticulum (ER) into the cytosol and the mitochondria, which further increased cisplatin-induced ER stress-mediated apoptosis by enhancing calpain-1 expression and by activating the mitochondrial apoptotic pathway [88]. Conversely, Bcl-2 attenuates cisplatin-induced  $\text{Ca}^{2+}$  release from the ER into the cytosol and the mitochondria, thus inhibiting cisplatin-induced ER stress-mediated apoptosis and activation of the mitochondrial apoptosis pathway. In this context, decreased ER mitochondrial crosstalk is responsible for Bcl-2 attenuation of cisplatin-induced mitochondrial  $\text{Ca}^{2+}$  accumulation in SKOV3 cells [89]. All these results are summarized in Figure 2 and compiled in Table S1.

Chemoresistance mechanisms have thus been described through phosphorylations inducing overactivation of  $\text{IP}_3\text{R1}$ . Various pharmacological strategies by blocking Bcl-2 inhibition (TAT-IDPs or Bad/BH3 mimetics) or PKA inhibitors (such as H89) have already been suggested to counteract such chemoresistance processes [88,89].

### 2.2.4. Intracellular $\text{Ca}^{2+}$ Channels: Targets to Overcome Chemoresistance

Because of their inaccessibility to pharmacological agents, intracellular channels or receptors do not appear as priority target to overcome chemoresistance. Nevertheless, it has been shown that BH3 binding and the amount of Bim scaffolded by anti-apoptotic Bcl-2 proteins can be used as a predictive marker for the apoptotic response of cancer cells to chemotherapy [90]. It is proposed that cancer cells, in which the mitochondria contain high levels of Bcl-2 and Bim, are most sensitive to toxic stimuli, including chemotherapeutic drugs [91,92]. Hence, from these studies, it seems that the mitochondrial apoptotic priming can predict the tumor response to cytotoxic chemotherapy [91,92]. The mitochondrial priming state is thereby not the same in all malignancies [93]. For instance, cancers that are highly primed are those that respond most favorably to chemotherapy (e.g., blood cancers, including Chronic Lymphocytic Leukemia), whereas those that are unprimed respond poorly to

chemotherapy (endometrial and renal cell carcinomas, serous borderline tumors) [90]. In the latter cases, the therapeutic window for using chemotherapy is very limited [72]. The number of studies published on the role of intracellular calcium channels or receptors in tumoral progression has increased over the last ten years, and may lead to them being considered as new targets for chemotherapy.

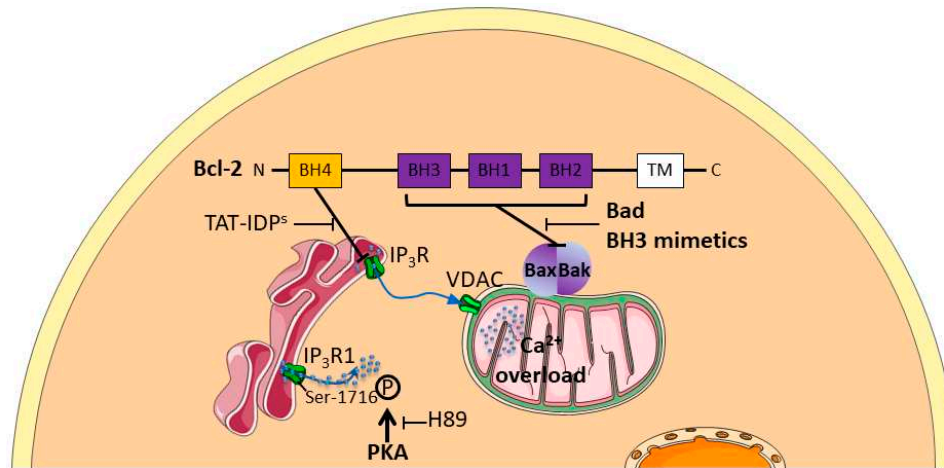


**Figure 2.** Schematic representation of intracellular  $\text{Ca}^{2+}$  pathways involved in chemoresistance. Anti-apoptotic Bcl-2 protein enhances chemoresistance by a dual role at both the Endoplasmic Reticulum (ER), by inhibiting  $\text{Ca}^{2+}$  depletion through Inositol 1,4,5-trisphosphate Receptors ( $\text{IP}_3\text{Rs}$ ), and the mitochondria by inhibiting apoptotic complex Bax/Bak formation. TAT-fused inositol 1,4,5-trisphosphate receptor-derived peptide (TAT-IDP<sup>S</sup>), by inhibiting BH4 domain, enhances  $\text{Ca}^{2+}$  efflux from the ER through  $\text{IP}_3\text{Rs}$  to mitochondrial Voltage-Dependent Anion Channel (VDAC).

### 3. Potassium Channels

Among ion channels, potassium channels compose the largest family, presenting 78 sequences coding for alpha pore forming subunit [94]. Besides regulating many physiological functions (membrane potential, cell volume, excitability . . . ), their involvement in cancer progression is now clearly established (e.g., proliferation, migration or invasiveness capacities, apoptosis resistance and angiogenesis, see [95–97] for review). By using a  $\text{K}^+$  ionophore, amphotericin B, the study reported by Sharp et al., was one of the first showing the importance of  $\text{K}^+$  flux in cisplatin resistance in ovary carcinoma [98]. In the 2000s, Liang et al. showed that cisplatin induced biophysical modifications of the membrane (lipid composition, fluidity), and cisplatin-resistant epidermal carcinoma cells present hyperpolarizing membrane potential compared to the sensitive parental cells [99]. Moreover, Marklund et al. [100,101] reported that both reduction of intracellular  $\text{K}^+$  concentration or addition of  $\text{K}^+$  flux modulators (amphotericin B and bumetanide) regulated cisplatin-induced apoptosis. These early results suggested that the activity of  $\text{K}^+$  channel was associated to therapeutic resistance. Since this demonstration, numerous groups detailed more precise mechanisms involving  $\text{K}^+$  channel in chemoresistance.

#### 3.1. Correlation between the Expression Levels of $\text{K}^+$ Channels and Sensitivity to Chemotherapeutic Drugs

Several studies have reported a correlation between the expression levels of  $\text{K}^+$  channels and the sensitivity to cytotoxic drugs. Both overexpression and reduction of  $\text{K}^+$  channels expression are involved in chemosensitivity. For example, using big data analysis, Liu et al. demonstrated an association between the reduction of *KCNN3* expression (a gene encoding for the SK3  $\text{K}^+$  channel) and drug resistance of ovarian cancer [102]. Similar associations were reported on the classically used cisplatin [103]. Indeed, the decreased *KCNMA1* (also referred to as BKCa—Calcium activated large conductance potassium channel—or maxi K channel) expression (involving potentially miR-31) was described to be associated to less sensitivity to this platinum-based chemotherapy in ovarian

cell lines. In the same way, an association between the reduction of hERG (Kv11.1) expression and increased resistance to vincristine, paclitaxel and hydroxy-camptothecin is reported for different cancer cells [104]. Using similar approaches, Han et al. demonstrated that the voltage activated potassium channel Kv1.5 could participate in the cellular response of gastric cancer cells to adriamycin, and that a downregulation of the channel expression could promote the multidrug phenotype of these cells [105]. Additionally, the Leanza group demonstrated, in several cancer cell lines, a similar relationship between reduced expression of Kv1.1 and Kv1.3 and decreased sensitivity to drugs, provoking mitochondrial-induced apoptotic death [106]. Another study conducted using small cell lung carcinoma cells demonstrated a relation between K<sup>+</sup> channel expression profile and drug resistance [107]. More precisely, authors demonstrated that the expression level of BKCa and Kv channels was inversely correlated to the MRP1 expression levels. They hypothesized that this observation could be a consequence of exposition to doxorubicin, which modulate the transcription factor c-jun (known to affect expression of both MRP1 and Kv channels). In this work, the relationship between K<sup>+</sup> channel repression and chemosensitivity should be an acquired mechanism of resistance.

On the contrary, there are different cases described with association between overexpression and resistance to therapy. For example, an association between an upregulation of hEag1 (Kv10.1) and TWIK-2 channels and an increase of cisplatin resistance was shown by Liang et al. [108]. However, these authors described that channels are overexpressed but they did not obtain mechanistic association between the channel function and the efficiency of cisplatin in the epidermal and liver carcinoma cells tested. Arcangeli's group showed higher levels of KCa3.1 and Kv11.1 channels in cisplatin-resistant colorectal cancer cells compared with their cisplatin-sensitive counterparts. In resistant cells, the treatment by riluzole (an activator of KCa3.1 and also an inhibitor of hERG) overcomes cisplatin resistance in both in vitro and in vivo models [109]. Pardo's group demonstrated also that, depending on the clinical status, acute myeloid leukemia cells could express hEag1 and the inhibition of this channel improves the apoptosis induction by different chemotherapeutic drugs, suggesting the involvement of this channel in basal resistance [110]. hEag1 was also involved in chemoresistance in ovarian cancer cells. By using immunohistochemistry on tissue samples from patients treated with cisplatin-based adjuvant chemotherapy, Hui et al. found that a decreased hEag1 expression was correlated with a favorable prognosis and also predicts higher sensitivity to cisplatin treatment [111]. They also found that hEag1 silencing facilitated the sensitivity of ovarian cancer cells to apoptosis induced by cisplatin through the NF- $\kappa$ B pathway. They thus proposed hEag1 as a potential indicator to predict chemosensitivity.

### 3.2. Chemotherapy Modulates K<sup>+</sup> Channel Activity

Chemotherapy can also alter the activity of K<sup>+</sup> channels without affecting their expression. Chemotherapy drugs may increase or decrease the K<sup>+</sup> channel activity depending on cancer types and drugs nature. In human lung epidermoid cancer cells, cisplatin activates the KCa3.1 channel without affecting its expression levels [112]. This activating effect of cisplatin on KCa3.1 may be due to the increase in intracellular calcium concentration by cisplatin. Results from our laboratory demonstrated similar implication of intracellular calcium concentration on chemoresistance in breast cancer ([43], section Ca<sup>2+</sup> channel). In addition, it has also been observed in human carcinoma HeLa-S3 cells, that Ca<sup>2+</sup> influx through Ca<sup>2+</sup> channels is necessary for cisplatin-induced activation of a Ca<sup>2+</sup>-dependent K<sup>+</sup> channel inhibited by charybdotoxin (BKCa channel) [113]. Also, Jirsch et al. presented in small cell lung cancers cells an increase activity of inwardly rectifying potassium channel associated to increased resistance [114]. The reduction of the activity of KCa3.1 has been demonstrated in both glioma cells (13-06-MG) and colon cancer cells (LoVo) by an oxaliplatin treatment, but not with cisplatin. Indeed, oxaliplatin decreases the KCa3.1 channel open probability [115].

### 3.3. Signalling Pathways Involved in Chemoresistance Related to K<sup>+</sup> Channels

Some groups tried to further detail the cellular mechanisms linking K<sup>+</sup> channels to chemotherapeutic resistance. Chemotherapeutic resistance could be assigned to numerous cellular processes [116]. Among them, links with K<sup>+</sup> channels were reported in the modification of apoptosis regulation, feedback regulation through miRNA or even the relationship between tumour and microenvironment cells.

It is now well known that K<sup>+</sup> channels are involved in the regulation of the apoptosis mechanism through the control of mitochondrial membrane potential, the regulation of cell volume and the availability of K<sup>+</sup> regulating caspase activity [117]. Indeed, different studies report that K<sup>+</sup> channels are located in the mitochondrial membrane where they are involved in mitochondrial functions. Checchetto et al. reviewed the role of the major mitoK<sup>+</sup> channel types described (Kv1.3, Kv1.5, K<sub>ATP</sub>, BKCa, KCa3.1, TASK3) and their involvement in cell death [118]. For example, the calcium-activated potassium channel KCa3.1 has been linked to the melanoma cell response in the presence of vemurafenib [119]. It was previously demonstrated that this BRAF inhibitor promotes apoptosis through a ROS-dependent pathway, which is prevented by the  $\alpha$ -tocopherol. In the study by Bauer et al., it was demonstrated that the combination of TRAM-34 with vemurafenib induced an apoptotic pathway presenting general control through the anti-apoptotic and pro-apoptotic Bcl-2 family. Additionally, to the modification of MMP's functions, they showed that early events are the production of ROS, which is crucial in the apoptotic cascade of this model. TRAIL (TNF-Related Apoptosis-Inducing Ligand) is a recent therapeutic opportunity to treat aggressive melanoma that presents high selectivity to cancer cells but also applicability limitations due to development of resistance. Quast et al. showed that the KCa3.1 inhibition by using TRAM-34 could also overcome the resistance to TRAIL in melanoma cell lines [120]. The same authors also deciphered the apoptotic pathway, which involves activation of caspases 3, 8 and 9, modification of the mitochondrial membrane potential, a dependency to Bax, and the release of mitochondrial factors like cytochrome c, AIF and SMAC (Figure 3). It is worth noting that the cellular response involving K<sup>+</sup> channel is very specific of the cellular type involved. KCa3.1 channel can also be involved in cisplatin sensitivity. Using the epidermoid cancer cell model, Lee et al. demonstrated that the activity of KCa3.1 is necessary to the cisplatin-induced death [112]. In this model, authors showed that the channel participates in the control of the Regulatory Volume Decrease (RVD) and caspase3/7 activity, two processes implicated in the apoptotic mechanism. In the same manner, it has been reported that the activity of the hERG channel is important for cisplatin-induced death of gastric cells [121]. This work demonstrated that cisplatin exposure increases the expression of hERG and that the activity of this channel is necessary in cisplatin-induced death of the different cell lines used. In addition, authors demonstrated that the activity of the channel is important to the caspase dependent apoptotic pathway through the regulation of Bax/Bcl-2 axis and active caspase 3. Their results were confirmed by using animal model where they also demonstrated the involvement of the hERG channels in the cisplatin-induced apoptosis. Using cisplatin-resistant colorectal cancer cell, Pillozzi et al. showed that the combined activation of KCa3.1 and inhibition of Kv11.1 by riluzole reduced the level of p-Akt and p-ERK and increased caspase-3, demonstrating a synergic effect with cisplatin to overcome the resistance to this chemotherapeutic agent [109]. In addition, they demonstrate that the modification of the channel activity allowed an increase in the incorporation of platinum salt in the cell to promote its activity.

To the best of our knowledge, only one report described the implication of K<sup>+</sup> channel in the modulation of the EGFR-Ras-Raf signalling pathway and an association with chemosensitivity (Figure 3). In side population of lung cancer stem cells, Choi et al. demonstrated that the use of different K<sup>+</sup> channel modulators affect the gefitinib efficiency to kill lung cancer cell line [122]. Indeed, application of 4-aminopyridine (Kv blocker), TetraEthylAmmonium (Kv blocker) or flupirtine (Kv7 opener) in combination with gefitinib decreases drastically cell viability compared to the use of the compound alone. This effect is correlated to the reduction of p-EGFR, total Ras, p-Raf and p-ERK1/2, compared to the gefitinib condition alone.

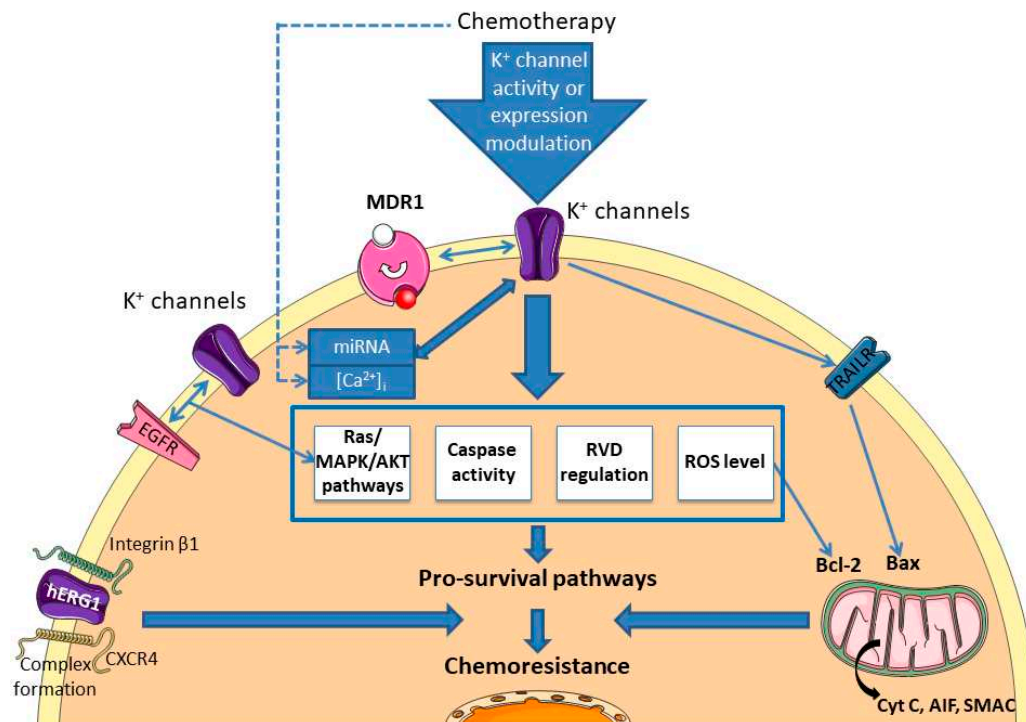


**Figure 3.** Chemoresistance pathways involving  $K^+$  channels.  $K^+$  channels could modulate the sensitivity to different chemotherapies by regulating pro-survival pathways (intrinsic or extrinsic apoptosis pathways, volume regulation, Akt/RAS/MAPK pathways, interacting with receptors or transporters). MDR: Multidrug Resistance Protein; EGFR: Epidermal Growth Factor Receptor; CXCR4: C-X-C Chemokine Receptor type 4; TRAILR: TRAIL Receptor; Cyt C: Cytochrome C; AIF: Apoptosis Inducing Factor; SMAC: Second Mitochondria-derived Activator of Caspases; RVD: Regulatory Volume Decrease.

Among the different molecular mechanisms described in the literature, some articles reported a close link between miRNA,  $K^+$  channel, and chemoresistance (Figure 3). For instance, by using immunohistochemistry, different SCLC cell lines resistant to chemotherapeutic drugs and preclinical in vivo model, Liu et al. demonstrated the involvement of the Kir2.1 channel in drug resistance [123]. First, they described that overexpression of the channel is responsible for the increase of the MRP1/ABCC1 protein in the different cell lines tested and that the level of the channel and of the MDR are correlated with clinical parameters. Second, they evaluated different putative regulators of the channel. They have shown that (i) Kir2.1 expression is modulated by the RAS/MAPK pathway, (ii) Kir2.1 channel is directly regulated by the miR-7, already described in the chemoresistance process. They thus described that miR-7 (downregulated in SCLC) and RAS/MAPK pathway promote directly the expression of Kir2.1, which that is a crucial actor in the resistance to cisplatin, adriamycin and etoposide in the different models used in this study. Similarly, it was described in glioblastoma cell line that reduced expression of miR-296-3p is concurrent to the increase expression of hEag1 and these two modifications are associated to an increased resistance to temozolomide, etoposide, and imatinib [124]. The authors demonstrated here that overexpression of the miRNA drastically decreases the level of hEag1 and restores sensitivity to the drugs. On the contrary, the use of antago-miR to mimic the cancerous conditions promotes resistance in association with an increase of the hEag1 transcription.

A study conducted by Pillozzi et al. reported an interesting relationship between cancer cells and the microenvironment, more precisely acute lymphoblastic leukemia (ALL) cells and bone marrow mesenchymal cells (MSC), involving hERG1 channel and resistance to chemotherapeutic drugs [125]. They demonstrated that the complex involving  $\beta 1$ -integrin subunit, CXCR4 and hERG1 channel is important for interactions between MSC and ALL cells, and regulates protection against drugs of

ALL cells by MSC. They probed deeper into the mechanism by using different hERG1 inhibitors and demonstrated that this channel is crucial for the protection of ALL by microenvironment cells. These results are summarized in Figure 3 and in Table S1.

#### 3.4. $K^+$ Channels: Targets to Overcome Chemoresistance

Evidence reported previously suggest that  $K^+$  channels could be interesting adjuvant targets to fight against the resistance of cancer cells. For instance, astemizole, an inhibitor of Kv10.1, has been evaluated in combination with gefitinib on lung cancer cells [126]. In their models, the authors demonstrated that this association enhances the mortality of cancer cells compared to the application of separate molecules. To pursue these demonstrations, different research teams evaluate this type of combination on preclinical models based on in vivo analyses. For example, the concomitant activation of KCa3.1 and inhibition of hERG1 allow to overcome cisplatin resistance in colorectal cells [109].

Interestingly, some inhibitors of  $K^+$  channels can induce cell death, bypassing the classical mechanisms of chemotherapies. Indeed, Leanza et al. demonstrated that the use of mitoKv1.3 permeant inhibitors could affect this channel at the mitochondrial level, provoking the release of cytochrome C and eliciting the death of cancer cells [127]. This approach could be very interesting to bypass the barrier of the deregulation of the Bax/Bcl-2 pathway.

All elements presented through this state of research about  $K^+$  channel implicated in chemoresistance suggest that it should be interesting to clinically evaluate specific modulators of this class of ion transporters.

## 4. Magnesium Channels

Magnesium ( $Mg^{2+}$ ) is the second most abundant cation in the cell. The main role of  $Mg^{2+}$  is to act as a coenzyme in virtually all the biochemical catalytic reactions [128]. Although  $Mg^{2+}$  status is not systematically assessed in clinical examination, recent epidemiological data suggest that  $Mg^{2+}$  deficiency can be linked to an increase in cancer risk. For example, 100 mg daily decrease of  $Mg^{2+}$  intake is associated with a 24% increase in the incidence of pancreatic cancer [129]. Moreover, increase of  $Mg^{2+}$  intake is also associated with a reduction of colorectal adenoma risk [130].  $Mg^{2+}$  homeostasis of the cell is mainly regulated by the expression of  $Mg^{2+}$  transporters at the plasma membrane. A growing number of studies show that  $Mg^{2+}$  transporters could be involved in cancer progression. Importantly,  $Mg^{2+}$  cytosolic concentration is increased in doxorubicin-resistant colon cancer cells while the  $Mg^{2+}$  influx is reduced when compared to sensitive cancer cells [131]. This lower  $Mg^{2+}$  influx is due to the downregulation of TRPM6 and TRPM7  $Mg^{2+}$  channel expression. Interestingly, TRPM7 silencing in drug sensitive cells shifts their phenotype toward a more resistant one. These data suggest that drug resistance is associated with alteration of  $Mg^{2+}$  homeostasis through TRPM7 regulation in colon cancer cells (Figure 4). However, the role of TRPM7 in cancer cell resistance has never been studied, even if its expression is clearly linked to cancer progression and reduced survival in breast and pancreatic cancer patients [132,133]. It has also been shown that human mitochondrial Mrs2 protein expression is upregulated in a multidrug-resistant gastric cancer cell line compared to its non-resistant counterpart [134]. Mrs2 is located in the mitochondria inner membrane and is responsible for  $Mg^{2+}$  transport in the mitochondria of mammals. Interestingly, Mrs2 expression seems positively correlated with the multidrug resistance of gastric cancer cells in vitro and in vivo. In gastric cancer cells, Mrs2 overexpression inhibits adriamycin-induced apoptosis, probably by suppressing Bax-induced cytochrome-C release by mitochondria. Moreover, p27 is downregulated while cyclin D1 is upregulated following Mrs2 overexpression, leading to gastric cancer cell proliferation enhancement. Although these data suggest that Mrs2 may be a promising target against multidrug resistant gastric cancer, the role of mitochondrial  $Mg^{2+}$  has not been yet elucidated (Figure 4).

The only described mechanism by which magnesium is able to confer resistance was published some 30 years ago:  $Mg^{2+}$  was reported as essential for vincristine binding to the plasma membrane of multidrug-resistant human myelogenous leukemia K562 cells [135]. The binding was observed at

100  $\mu\text{M}$   $\text{Mg}^{2+}$ , and reached a maximum effect in the 5–10 mM  $\text{Mg}^{2+}$  range. The candidate for drug efflux from K62 cells is the ATPase MDR1. The ATPase activity of MDR1 is indeed dependent on  $\text{Mg}^{2+}$ , but can also be modulated by other divalent cations, including manganese ( $\text{Mn}^{2+}$ ) and cobalt ( $\text{Co}^{2+}$ ). On the other hand, calcium ( $\text{Ca}^{2+}$ ), zinc ( $\text{Zn}^{2+}$ ), nickel ( $\text{Ni}^{2+}$ ), cadmium ( $\text{Cd}^{2+}$ ) and copper ( $\text{Cu}^{2+}$ ) inhibit the  $\text{Mg}^{2+}$ -catalyzed ATP hydrolysis [136].

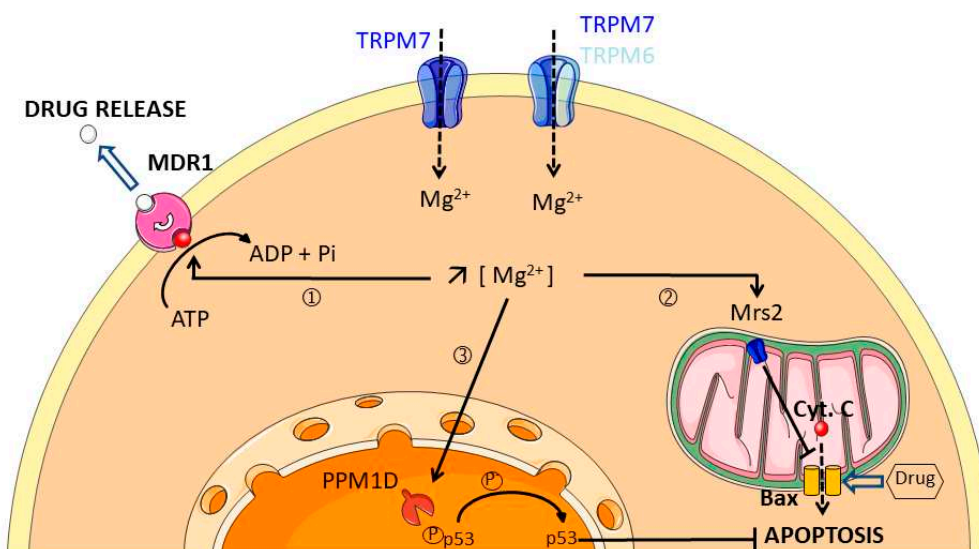


**Figure 4.** Multidrug resistance is associated with an increase of intracellular free  $\text{Mg}^{2+}$ . Intracellular free  $\text{Mg}^{2+}$  could promote multidrug resistance through three main potential mechanisms: ①  $\text{Mg}^{2+}$  binds to MDR1 leading to drug extrusion; ②  $\text{Mg}^{2+}$  enters into the mitochondria through Mrs2 channel leading to Bax inhibition and resistance to apoptosis, ③  $\text{Mg}^{2+}$  activates the nuclear PPM1D phosphatase which alters p53 stabilization and protects cancer cells against apoptosis. Chemoresistant cancer cells have a lower  $\text{Mg}^{2+}$  influx and lower amounts of TRPM6 and TRPM7 channels at the plasma membrane.

Calcium blockers verapamil and nifedipine are able to inhibit both vincristine binding to the plasma membrane of K52 cells and drug efflux in a competitive manner, independently of the surrounding calcium concentration [136,137]. Taken together, these findings confirm that unlike  $\text{Ca}^{2+}$ ,  $\text{Mg}^{2+}$  is essential for active transport of drug outside the cell [137].  $\text{Mg}^{2+}$  is also required for the catalytic activity of the Protein Phosphatase Magnesium-dependent 1D (PPM1D) that confers cisplatin resistance in ovarian and cervical cancer cell cells by deactivating p53 [138]. PPM1D promotes drug resistance in gynecological malignancies by acting as a downstream target of Akt. Moreover, recent studies show that mutations of PPM1D in hematopoietic stem cells confer a selective advantage to resist apoptosis-induced by cytotoxic treatments in a context of clonal hematopoiesis prior to malignancy development [139,140]. On the other hand, clinical data demonstrate that patients treated with cetuximab and panitumumab, monoclonal antibodies targeting the epithelial growth factor receptor (EGFR), develop hypomagnesemia [141–145]. All these results are summarized in Figure 4 and in Table S1. These data suggest that hypomagnesemia is a side-effect of chemotherapy that is associated with better clinical benefits. However, total serum  $\text{Mg}^{2+}$  level is measured for hypomagnesemia assessment in clinical studies and does not necessarily represents the bioactive fraction of  $\text{Mg}^{2+}$  into cells and tissues.

It is tempting to speculate that any modification of the  $\text{Mg}^{2+}$  transporter expression could disturb cytosolic  $\text{Mg}^{2+}$  homeostasis leading to enhanced drug resistance in cancer cells. However, future investigations are needed to better understand how  $\text{Mg}^{2+}$  transporters are expressed and could eventually coordinate during cancer progression from primary tumor to metastatic and multidrug resistant cancer.



## 5. Chloride Channels

The role of selective anion channels, more specifically chloride channels, has been well-described in physiological contexts and their implications in the excitability (neurons, skeletal, cardiac and smooth muscle), the regulation of cell volume, trans-epithelial transport, internal and external acidification, cell cycle progression and apoptosis are the subject of numerous studies ([146] for review). However, anion transporters were initially less studied in the cancer context until the discovery of some structural similarities with the MDR drug transporters involved in chemoresistance. For a decade, the number of reports has grown exponentially and different groups presented reviews about specific class of chloride channels (e.g., CLIC1 [147]; TMEM16A [148]). Although there is no official classification, the chloride channels are subdivided into five classes: CIC family (with 9 members), CFTR, Ca<sup>2+</sup>-activated chloride channels, Maxi-chloride channels and Volume Regulated Chloride (VRAC) channels [149]. Like other ion channels, chloride channels and subsequent signalling pathways are involved in tumor progression and aggressiveness through the regulation of cell motility, cell cycle progression or apoptosis resistance. Additionally, some groups revealed the implication of chloride channels in tumor resistance to chemotherapy. Two major trends have recently emerged: on one hand, expression or activity reductions of VRAC induce resistance to the pro-apoptotic molecules by regulating the apoptotic volume decrease (AVD), and on the other hand, different chloride channels are upregulated and trigger pro-survival pathway or promote different mechanisms to reduce drugs activity.

### 5.1. Volume Regulated Chloride Channel Reduction and Promotion of Chemoresistance

One of the first events at the onset of the apoptosis is a variation of the cell volume due to a modification of the ions (classically K<sup>+</sup> and Cl<sup>-</sup>), solutes and water transports, which precedes caspases activation. Among the different transporters involved in this mechanism, the implication of VRAC has been well established. In addition, it is strictly demonstrated that different chemotherapeutic drugs induce cancer cell apoptosis. The reports of activity or expression reduction of the VRAC molecular support in relation with chemotherapy sensitivity are obvious (Figure 5, left part). For instance, it has been described that doxorubicin could affect VRAC current in MCF-7 cells and the cell response is based on the relationship between MDR1 expression and I<sub>(Cl-swell)</sub> activity [150]. In addition, by using epidermoid cancer cell lines sensitive or resistant to cisplatin, Okada's group demonstrates the involvement of VRAC in the response to this drug [151–153]. The association of this type of current to drug resistance has also been reported in lung, nasopharyngeal carcinoma or anthracyclin MDR cell line [154–156] and was the object of specific reviews to this subject [157,158]. Interestingly, the molecular identification of the VRAC channel, the LRCC8 family [159], occurred recently and new understanding appeared with this highlight. Indeed, it has been shown that the specific subunit composition of the VRAC current affects differentially the sensitivity to chemotherapeutic compounds [160].

### 5.2. Upregulation of Chloride Channels and Chemoresistance

As previously described, chemotherapy resistance is based on the modification of different cellular processes (e.g., apoptosis resistance, autophagy regulation, and MDR modulation). By affecting these processes, chloride channels have also been demonstrated to be major regulators of drug resistance (Figure 5, right part). It has been thus demonstrated that the overexpression of CLIC1 or ANO1 are correlated to the resistance of glioblastoma cancer stem cells, ovarian or breast cancer [161–164]. In another way, Bill et al. demonstrated that ANO1 channel could be functionally linked to the EGFR pathway and its expression level could be used as predictive biomarker to anti-EGFR therapy in head and neck squamous cancer [165].

Chloride channel can be located at the plasma or intracellular membrane level. Weylandt et al. demonstrated that CIC-3 could participate in the acidification of intracellular compartment in order to promote the chelation of the etoposide in neuroendocrine tumor cells and consequently reduce the activity of this compound [166]. Similarly, it was shown that CIC-3 could participate

in cisplatin resistance in erythroleukemia or glioma models by modulating the pH of intracellular compartments, such as lysosome [167,168]. In addition, Fujito et al. demonstrated that CIC-3 and ANO1, by regulating intracellular chloride level, could control the transcription of HER2 in breast cancer cells through the PI3K/Akt/mTOR or STAT3 pathways, depending on the cell/channel type promoting the resistance to anti-HER2 therapies [169]. CIC-3 has also been demonstrated to participate in cisplatin resistance by regulating the Akt pathway and the autophagy process of glioma cells [170] or to promote the decreased answer to different compounds by regulating the overexpression of MDR1 by NF- $\kappa$ B and p65 signalling [171]. CLC-5 has been demonstrated to promote bortezomib resistance in multiple myeloma cell lines by increasing the pro-survival autophagy and inhibiting the Akt-mTOR pathway [172]. In choriocarcinoma models, sensitive or not to methotrexate and floxuridine, CLIC1 channel has been shown to be overexpressed in resistant cells and linked with the upregulation of MRP1 in order to promote drug resistance [173]. All these results are summarized in Figure 5 and Table S1.

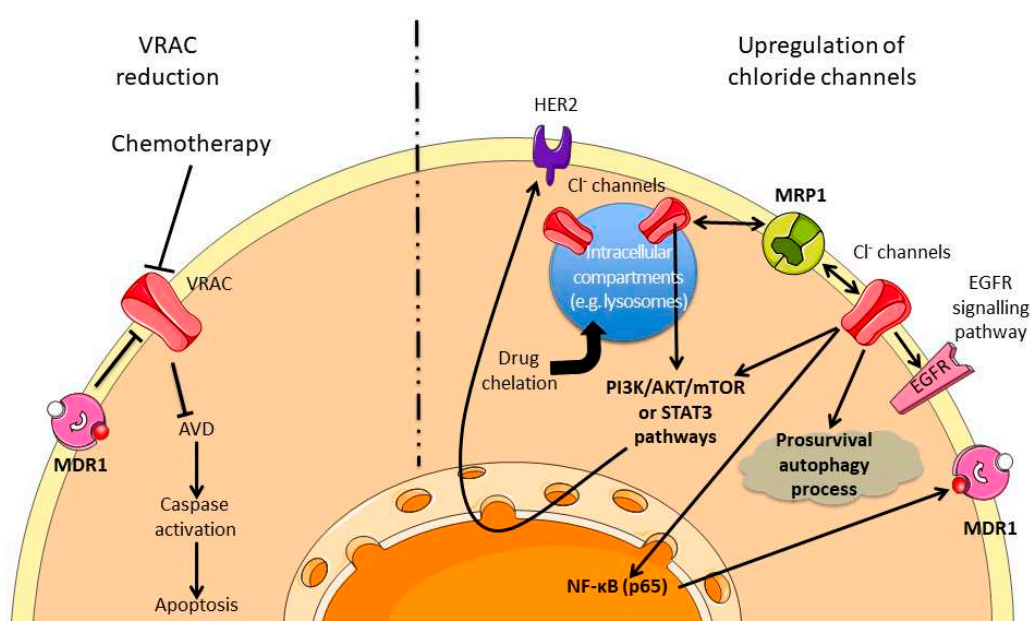


**Figure 5.** Chemoresistance pathways involving  $\text{Cl}^-$  channels.  $\text{Cl}^-$  channels can modulate the sensitivity to different chemotherapies by inhibiting the AVD or by modulating the prosurvival pathways and the drugs availabilities. The dashed line separates two virtual cells presenting either reduction activity of  $\text{Cl}^-$  channels (left part) or an upregulation of  $\text{Cl}^-$  channels (right part). MDR1: Multidrug Resistance 1; VRAC: Volume Regulated Chloride Channel; AVD: Apoptosis Volume Decrease; HER2: Human Epidermal growth factor Receptor 2; MRP1: Multidrug associated Resistance Protein 1; EGFR: Epidermal Growth Factor Receptor.

## 6. Other Ion Channels

As previously described, the associations between  $\text{Ca}^{2+}$ ,  $\text{K}^+$ ,  $\text{Mg}^{2+}$  or  $\text{Cl}^-$  channels with chemoresistance present an increasing number of iterations in the bibliography. However, little information is available regarding the involvement of other channels, water, and solute transporters in the literature. It is however worth mentioning that voltage-gated sodium channels and ASIC channels have been associated with chemoresistance.

### 6.1. Voltage-Gated Sodium Channel in the Chemoresistance Process

This class of ion channel is known to participate in tumor progression by improving cell invasiveness capacity in different tumor types (e.g., breast, colorectal, prostate cancer [174–176]). However, Gerard et al. described that the NG108-15 cells (“neuroblastoma x glioma” hybrid cells),

that are resistant to doxorubicin, show a 1.66-fold increase in  $\text{Na}^+$  conductance when compared to the parental cells [177]. These results are in good agreement with those obtained by Yamashita et al., who showed that leukemia cells expressing a MDR phenotype present a bigger voltage-gated  $\text{Na}^+$  current compared to the sensitive ones [178]. In this study, they confirmed the association between voltage-gated  $\text{Na}^+$  current and MDR phenotype by using revertant cell lines (cell lines that lost the acquired resistance to drug) that did not maintain the  $\text{Na}^+$  conductance.

### 6.2. ASIC Channels in the Chemoresistance Process

It has recently been demonstrated by Zhang et al. that the ASIC1a channel participates in chemotherapy resistance of HCC [179]. ASIC1a is shown to be more expressed in HCC tissues, and the authors have deciphered a pathway involving the channel in the chemoresistance. They notably show that ASIC1a is expressed at the plasma membrane level, where it allows a  $\text{Ca}^{2+}$  influx, which regulates the  $\text{PI}_3\text{K}/\text{Akt}$  pathway, protecting the cells against apoptosis in an extracellular acidic environment.

## 7. Conclusions

Chemoresistance is a major hurdle in cancer treatment leading to recurrence of cancer. Resistance is a complex phenomenon involving multiple mechanisms, including activation of signalling pathways, apoptosis resistance improvement, and increasing extrusion of therapeutic compounds, among others mechanisms. Although many drugs/therapies are now available in oncology, resistance to treatments impedes complete therapeutic successes and is responsible for mid- and long-term recurrence of the disease. Ion fluxes have been reported to modulate the response of cancer cells to several chemotherapeutic drugs [7]. Additionally, apoptosis regulation by ion channels is also well described ([180,181] for review) and consequently, it is interesting to understand their implication in the resistance to therapeutic compounds.

Although many papers report an association between chemoresistance and ion channel expression and/or activity, relatively few studies provide the complete mechanism of resistance. It appears thus necessary to improve knowledge about the different mechanisms involving ion channels, to enable potential new therapeutic associations (including ion channel modulators) to ideally overcome resistance to chemotherapeutic compounds.

Studies reported herein usually describe the implication of one channel in the regulation of chemoresistance processes. However, studies about complexes of ion channels are emerging to explain their involvement in the control of tumour progression. For example, our group demonstrated that the Kv10.1 potassium channel and the Orai1 calcium channel are associated to promote survival of breast cancer cells [182]. It was also demonstrated that the SK3 potassium channel, in association with TRPC1 and Orai1 calcium channels, regulated colon cancer cell migration [183]. Based on data from the literature, and since global ion channel expression is rather dynamically and interdependently regulated, we propose that ion channels-dependant chemoresistance processes are likely to depend on more complex mechanisms than only one channel and only one downstream signalling process (Figure 6). For example,  $\text{K}^+$  channels can be associated with  $\text{Cl}^-$  channels to regulate cell volume and modulate apoptosis resistance. In the same manner, the association of  $\text{K}^+$  channels with  $\text{Ca}^+$  ones could be very important in controlling intracellular signalling pathways or expression/repression of transcription factors. Future research in this field should thus take relationships between ion channels into account, and provide better description of the downstream molecular mechanisms involved in chemoresistance.

To conclude, this emerging field can highlight new targets or new evidence for overriding chemoresistance, but intensive work is still necessary to complete the list of actors involved, the interdependency between some of these actors, and their exact roles in chemoresistance processes by deciphering downstream signalling mechanisms more accurately. Ion channel blockers have been successfully developed over decades by pharmaceutical industries to treat cardiac or psychiatric disorders. Yet, their therapeutic potency has not been extensively investigated in clinical cancer therapy.

Such ion channel blockers could, however, be very useful: for instance, verapamil, a  $\text{Ca}^{2+}$  channel blocker significantly increases the survival of patients with anthracycline-resistant metastatic breast carcinoma when given in association with chemotherapy [184]. Moreover, mibefradil dihydrochloride, a T-type  $\text{Ca}^{2+}$  channel blocker, acts as a radiosensitizer by potentiating the effect of hypofractionated radiation on patients with recurrent glioblastoma [185]. Others  $\text{Na}^{+}$  channel blockers, such as riluzole, have also been described in cancer therapy for patients with brain metastases originating from melanoma [186,187]. Hopefully, accumulating data on chemoresistance conferred by ion channels (most of which are summarized in the present review) will help repurpose ion channels modulators in clinical trials to improve cancer treatment.

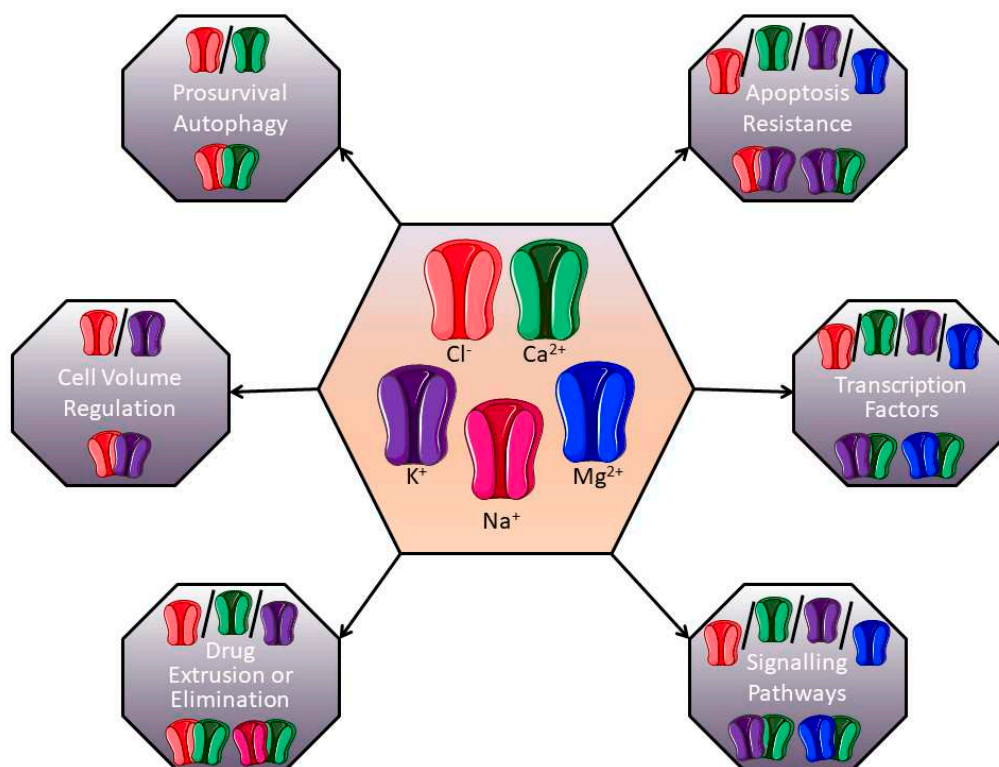


**Figure 6.** Putative channel associations involved in chemoresistance. Different ion channels could form complexes and modulate chemoresistance. In each grey box, the current description of channel associated-chemoresistance is presented in the light part, and examples of putative ion channels associations are suggested in the dark part.

**Supplementary Materials:** The following are available online at <http://www.mdpi.com/2072-6694/11/3/376/s1>, Table S1. Ion channels and associated mechanisms/signalling pathways involved in chemoresistance.

**Funding:** This research received no external funding.

**Acknowledgments:** This work was supported by the UPJV ("Université de Picardie Jules Verne"), the "Ligue Contre le Cancer", the "Région Hauts-de-France" and the CNO ("Cancéropôle Nord-Ouest").

**Conflicts of Interest:** The authors declare that they have no conflict of interest.

## Abbreviations

AIF	Apoptosis-Inducing Factor
ALL	Acute Lymphoblastic Leukemia
ANO1	ANOctamin 1
ASIC	Acid-Sensing Ion Channel
AVD	Apoptosis Volume Decrease
Bax	Bcl-2-Associated X protein

Bcl-2	B-cell lymphoma 2
BKCa	Large conductance, Ca <sup>2+</sup> -activated K <sup>+</sup> channels
CFTR	Cystic Fibrosis Transmembrane conductance Regulator
ClC	Chloride Channel
CLIC1	Chloride Intracellular Channel 1
CXCR4	C-X-C Chemokine Receptor 4
ER	Endoplasmic Reticulum
EMT	Epithelial to Mesenchymal Transition
HCC	HepatoCellular Carcinoma
hEag1	human Ether-à-Go-Go
hERG	human Ether-à-Go-Go-Related Gene
IP <sub>3</sub> R	Inositol 1,4,5-trisphosphate Receptor
MCU	Mitochondrial Calcium Uniport
MDR	MultiDrug Resistance
miRNA	micro-RNA
MMP	Matrix MetalloProteinase
MRP1	Multidrug Resistance-associated Protein 1
MSC	Bone Marrow Mesenchymal Cells
RVD	Regulatory Volume Decrease
SMAC	Second Mitochondria-derived Activator of Caspases
SK3	Small conductance, Ca <sup>2+</sup> activated K <sup>+</sup> channel 3
SOC channels	Store-Operated Calcium channels
SOCE	Store-Operated Calcium Entry
TAT-IDP <sup>s</sup>	TAT-fused inositol 1,4,5-trisphosphate receptor derived peptide
TRAIL	Tumor-necrosis-factor Related Apoptosis Inducing Ligand
VDAC	Voltage-Dependent Anion Channel
VRAC	Volume-Regulated Anion Channel

## References

- Gonzalez-Angulo, A.M.; Morales-Vasquez, F.; Hortobagyi, G.N. Overview of resistance to systemic therapy in patients with breast cancer. *Adv. Exp. Med. Biol.* **2007**, *608*, 1–22.
- Li, S.; Kennedy, M.; Payne, S.; Kennedy, K.; Seewaldt, V.L.; Pizzo, S.V.; Bachelder, R.E. Model of Tumor Dormancy/Recurrence after Short-Term Chemotherapy. *PLoS ONE* **2014**, *9*, e98021. [[CrossRef](#)]
- Ghandadi, M.; Behravan, J.; Abnous, K.; Mosaffa, F. Reactive Oxygen Species Mediate TNF- $\alpha$  Cytotoxic Effects in the Multidrug-Resistant Breast Cancer Cell Line MCF-7/MX. *Oncol. Res. Treat.* **2016**, *39*, 54–59. [[CrossRef](#)] [[PubMed](#)]
- Huang, Y.; Sadée, W. Membrane transporters and channels in chemoresistance and -sensitivity of tumor cells. *Cancer Lett.* **2006**, *239*, 168–182. [[CrossRef](#)] [[PubMed](#)]
- Prevarskaya, N.; Skryma, R.; Shuba, Y. Ion channels and the hallmarks of cancer. *Trends Mol. Med.* **2010**, *16*, 107–121. [[CrossRef](#)] [[PubMed](#)]
- Siesjö, B.K. Historical Overview: Calcium, Ischemia, and Death of Brain Cells. *Ann. N. Y. Acad. Sci.* **1988**, *522*, 638–661. [[CrossRef](#)] [[PubMed](#)]
- Huang, Y.; Anderle, P.; Bussey, K.J.; Barbacioru, C.; Shankavaram, U.; Dai, Z.; Reinhold, W.C.; Papp, A.; Weinstein, J.N.; Sadée, W. Membrane Transporters and Channels: Role of the Transportome in Cancer Chemosensitivity and Chemoresistance. *Cancer Res.* **2004**, *64*, 4294–4301. [[CrossRef](#)]
- Berridge, M.J.; Lipp, P.; Bootman, M.D. The versatility and universality of calcium signalling. *Nat. Rev. Mol. Cell Biol.* **2000**, *1*, 11–21. [[CrossRef](#)]
- Monteith, G.R.; McAndrew, D.; Faddy, H.M.; Roberts-Thomson, S.J. Calcium and cancer: Targeting Ca<sup>2+</sup> transport. *Nat. Rev. Cancer* **2007**, *7*, 519–530. [[CrossRef](#)]
- Berridge, M.J.; Bootman, M.D.; Lipp, P. Calcium—A life and death signal. *Nature* **1998**, *395*, 645–648. [[CrossRef](#)]
- Prevarskaya, N.; Skryma, R.; Shuba, Y. Calcium in tumour metastasis: New roles for known actors. *Nat. Rev. Cancer* **2011**, *11*, 609–618. [[CrossRef](#)] [[PubMed](#)]

12. Roderick, H.L.; Cook, S.J.  $\text{Ca}^{2+}$  signalling checkpoints in cancer: Remodelling  $\text{Ca}^{2+}$  for cancer cell proliferation and survival. *Nat. Rev. Cancer* **2008**, *8*, 361–375. [[CrossRef](#)] [[PubMed](#)]
13. Büsselberg, D.; Florea, A.-M. Targeting Intracellular Calcium Signaling ( $[\text{Ca}^{2+}]_i$ ) to Overcome Acquired Multidrug Resistance of Cancer Cells: A Mini-Overview. *Cancers* **2017**, *9*, 48. [[CrossRef](#)]
14. Parekh, A.B.; Putney, J.W. Store-Operated Calcium Channels. *Physiol. Rev.* **2005**, *85*, 757–810. [[CrossRef](#)] [[PubMed](#)]
15. Putney, J.W. Capacitative calcium entry: From concept to molecules. *Immunol. Rev.* **2009**, *231*, 10–22. [[CrossRef](#)]
16. Hogan, P.G.; Rao, A. Store-operated calcium entry: Mechanisms and modulation. *Biochem. Biophys. Res. Commun.* **2015**, *460*, 40–49. [[CrossRef](#)] [[PubMed](#)]
17. Flourakis, M.; Lehen'kyi, V.; Beck, B.; Raphael, M.; Vandenberghe, M.; Abeele, F.V.; Roudbaraki, M.; Lepage, G.; Mauroy, B.; Romanin, C.; et al. Orai1 contributes to the establishment of an apoptosis-resistant phenotype in prostate cancer cells. *Cell Death Dis.* **2010**, *1*, e75. [[CrossRef](#)] [[PubMed](#)]
18. Abeele, F.V.; Skryma, R.; Shuba, Y.; Van Coppenolle, F.; Slomianny, C.; Roudbaraki, M.; Mauroy, B.; Wuytack, F.; Prevarskaya, N. Bcl-2-dependent modulation of  $\text{Ca}^{2+}$  homeostasis and store-operated channels in prostate cancer cells. *Cancer Cell* **2002**, *1*, 169–179. [[CrossRef](#)]
19. Orrenius, S.; Zhivotovsky, B.; Nicotera, P. Regulation of cell death: The calcium-apoptosis link. *Nat. Rev. Mol. Cell Biol.* **2003**, *4*, 552–565. [[CrossRef](#)]
20. Mignen, O.; Constantin, B.; Potier-Cartereau, M.; Penna, A.; Gautier, M.; Gueguinou, M.; Renaudineau, Y.; Shoji, K.F.; Felix, R.; Bayet, E.; et al. Constitutive calcium entry and cancer: Updated views and insights. *Eur. Biophys. J.* **2017**, *46*, 395–413. [[CrossRef](#)]
21. Helson, L. Calcium Channel Blocker Enhancement of Anticancer Drug Cytotoxicity—A Review. *Cancer Drug Deliv.* **1984**, *1*, 353–361. [[CrossRef](#)]
22. Simpson, W.G. The calcium channel blocker verapamil and cancer chemotherapy. *Cell Calcium* **1985**, *6*, 449–467. [[CrossRef](#)]
23. Mason, R.P. Effects of calcium channel blockers on cellular apoptosis. *Cancer* **1999**, *85*, 2093–2102. [[CrossRef](#)]
24. Kiwit, J.C.; Hertel, A.; Matuschek, A.E. Reversal of chemoresistance in malignant gliomas by calcium antagonists: Correlation with the expression of multidrug-resistant p-glycoprotein. *J. Neurosurg.* **1994**, *81*, 587–594. [[CrossRef](#)] [[PubMed](#)]
25. Khadra, N.; Bresson-Bepoldin, L.; Penna, A.; Chaigne-Delalande, B.; Ségui, B.; Levade, T.; Vacher, A.-M.; Reiffers, J.; Ducret, T.; Moreau, J.-F.; et al. CD95 triggers Orai1-mediated localized  $\text{Ca}^{2+}$  entry, regulates recruitment of protein kinase C (PKC)  $\beta_2$ , and prevents death-inducing signaling complex formation. *Proc. Natl. Acad. Sci. USA* **2011**, *108*, 19072–19077. [[CrossRef](#)] [[PubMed](#)]
26. Limnander, A.; Depeille, P.; Freedman, T.S.; Liou, J.; Leitges, M.; Kurosaki, T.; Roose, J.P.; Weiss, A. STIM1, PKC- $\delta$  and RasGRP set a threshold for proapoptotic Erk signaling during B cell development. *Nat. Immunol.* **2011**, *12*, 425. [[CrossRef](#)] [[PubMed](#)]
27. Soltoff, S.P.; Lannon, W.A. Activation of ERK1/2 by Store-Operated Calcium Entry in Rat Parotid Acinar Cells. *PLoS ONE* **2013**, *8*, e72881. [[CrossRef](#)]
28. Chen, Y.-F.; Chiu, W.-T.; Chen, Y.-T.; Lin, P.-Y.; Huang, H.-J.; Chou, C.-Y.; Chang, H.-C.; Tang, M.-J.; Shen, M.-R. Calcium store sensor stromal-interaction molecule 1-dependent signaling plays an important role in cervical cancer growth, migration, and angiogenesis. *Proc. Natl. Acad. Sci. USA* **2011**, *108*, 15225–15230. [[CrossRef](#)]
29. Feng, M.; Grice, D.M.; Faddy, H.M.; Nguyen, N.; Leitch, S.; Wang, Y.; Muend, S.; Kenny, P.A.; Sukumar, S.; Roberts-Thomson, S.J.; et al. Store-Independent Activation of Orai1 by SPCA2 in Mammary Tumors. *Cell* **2010**, *143*, 84–98. [[CrossRef](#)] [[PubMed](#)]
30. Kondratska, K.; Kondratskyi, A.; Yassine, M.; Lemonnier, L.; Lepage, G.; Morabito, A.; Skryma, R.; Prevarskaya, N. Orai1 and STIM1 mediate SOCE and contribute to apoptotic resistance of pancreatic adenocarcinoma. *Biochim. Biophys. Acta Mol. Cell Res.* **2014**, *1843*, 2263–2269. [[CrossRef](#)]
31. Sun, X.; Wei, Q.; Cheng, J.; Bian, Y.; Tian, C.; Hu, Y.; Li, H. Enhanced Stim1 expression is associated with acquired chemo-resistance of cisplatin in osteosarcoma cells. *Hum. Cell* **2017**, *30*, 216–225. [[CrossRef](#)]
32. Zheng, H.C. The molecular mechanisms of chemoresistance in cancers. *Oncotarget* **2017**, *8*, 59950–59964. [[CrossRef](#)]
33. Babaer, D.; Amara, S.; Ivy, M.; Zhao, Y.; Lammers, P.E.; Titze, J.M.; Tiriveedhi, V. High salt induces P-glycoprotein mediated treatment resistance in breast cancer cells through store operated calcium influx. *Oncotarget* **2018**, *9*, 25193–25205. [[CrossRef](#)] [[PubMed](#)]

34. Schmidt, S.; Liu, G.; Yang, W.; Honisch, S.; Pantelakos, S.; Stournaras, C.; Honig, A.; Lang, F. Enhanced Orai1 and STIM1 expression as well as store operated  $\text{Ca}^{2+}$  entry in therapy resistant ovary carcinoma cells. *Oncotarget* **2014**, *5*, 4799–4810. [[CrossRef](#)]
35. Tang, B.D.; Xia, X.; Lv, X.F.; Yu, B.X.; Yuan, J.N.; Mai, X.Y.; Shang, J.Y.; Zhou, J.G.; Liang, S.J.; Pang, R.P. Inhibition of Orai1-mediated  $\text{Ca}^{2+}$  entry enhances chemosensitivity of HepG2 hepatocarcinoma cells to 5-fluorouracil. *J. Cell. Mol. Med.* **2017**, *21*, 904–915. [[CrossRef](#)] [[PubMed](#)]
36. Wang, L.; Hao, J.; Zhang, Y.; Yang, Z.; Cao, Y.; Lu, W.; Shu, Y.; Jiang, L.; Hu, Y.; Lv, W.; et al. Orai1 mediates tumor-promoting store-operated  $\text{Ca}^{2+}$  entry in human gastrointestinal stromal tumors via c-KIT and the extracellular signal—Regulated kinase pathway. *Tumor Biol.* **2017**, *39*, 1010428317691426. [[CrossRef](#)]
37. Shuttleworth, T.J. Orai3—The ‘exceptional’ Orai? *J. Physiol.* **2012**, *590*, 241–257. [[CrossRef](#)]
38. Schindl, R.; Bergsmann, J.; Frischauf, I.; Derler, I.; Fahrner, M.; Muik, M.; Fritsch, R.; Groschner, K.; Romanin, C. 2-Aminoethoxydiphenyl Borate Alters Selectivity of Orai3 Channels by Increasing Their Pore Size. *J. Biol. Chem.* **2008**, *283*, 20261–20267. [[CrossRef](#)] [[PubMed](#)]
39. Faouzi, M.; Hague, F.; Potier, M.; Ahidouch, A.; Sevestre, H.; Ouadid-Ahidouch, H. Down-regulation of Orai3 arrests cell-cycle progression and induces apoptosis in breast cancer cells but not in normal breast epithelial cells. *J. Cell. Physiol.* **2011**, *226*, 542–551. [[CrossRef](#)] [[PubMed](#)]
40. Motiani, R.K.; Abdullaev, I.F.; Trebak, M. A novel native store-operated calcium channel encoded by Orai3: Selective requirement of Orai3 versus Orai1 in estrogen receptor-positive versus estrogen receptor-negative breast cancer cells. *J. Biol. Chem.* **2010**, *285*, 19173–19183. [[CrossRef](#)]
41. Bhattacharya, A.; Kumar, J.; Hermanson, K.; Sun, Y.; Qureshi, H.; Perley, D.; Scheidegger, A.; Singh, B.B.; Dhasarathy, A. The calcium channel proteins ORAI3 and STIM1 mediate TGF-beta induced Snai1 expression. *Oncotarget* **2018**, *9*, 29468–29483. [[CrossRef](#)] [[PubMed](#)]
42. Faouzi, M.; Kischel, P.; Hague, F.; Ahidouch, A.; Benzerdjeb, N.; Sevestre, H.; Penner, R.; Ouadid-Ahidouch, H. ORAI3 silencing alters cell proliferation and cell cycle progression via c-myc pathway in breast cancer cells. *Biochim. Biophys. Acta Mol. Cell Res.* **2013**, *1833*, 752–760. [[CrossRef](#)]
43. Hasna, J.; Hague, F.; Rodat-Despoix, L.; Geerts, D.; Leroy, C.; Tulasne, D.; Ouadid-Ahidouch, H.; Kischel, P. Orai3 calcium channel and resistance to chemotherapy in breast cancer cells: The p53 connection. *Cell Death Differ.* **2018**, *25*, 691–705. [[CrossRef](#)] [[PubMed](#)]
44. Vanoverbergh, K.; Vanden Abeele, F.; Mariot, P.; Lepage, G.; Roudbaraki, M.; Bonnal, J.L.; Mauroy, B.; Shuba, Y.; Skryma, R.; Prevarskaya, N.  $\text{Ca}^{2+}$  homeostasis and apoptotic resistance of neuroendocrine-differentiated prostate cancer cells. *Cell Death Differ.* **2004**, *11*, 321. [[CrossRef](#)] [[PubMed](#)]
45. Dubois, C.; Vanden Abeele, F.; Lehen'kyi, V.; Gkika, D.; Guarmit, B.; Lepage, G.; Slomianny, C.; Borowiec, A.S.; Bidaux, G.; Benahmed, M.; et al. Remodeling of Channel-Forming ORAI Proteins Determines an Oncogenic Switch in Prostate Cancer. *Cancer Cell* **2014**, *26*, 19–32. [[CrossRef](#)]
46. Nilius, B.; Owsianik, G.; Voets, T.; Peters, J.A. Transient receptor potential cation channels in disease. *Physiol. Rev.* **2007**, *87*, 165–217. [[CrossRef](#)] [[PubMed](#)]
47. Lehen'kyi, V.; Prevarskaya, N. Oncogenic TRP channels. *Adv. Exp. Med. Biol.* **2011**, *704*, 929–945. [[PubMed](#)]
48. Deveci, H.A.; Nazıroğlu, M.; Nur, G. 5-Fluorouracil-induced mitochondrial oxidative cytotoxicity and apoptosis are increased in MCF-7 human breast cancer cells by TRPV1 channel activation but not Hypericum perforatum treatment. *Mol. Cell. Biochem.* **2018**, *439*, 189–198. [[CrossRef](#)] [[PubMed](#)]
49. Nabissi, M.; Morelli, M.B.; Santoni, M.; Santoni, G. Triggering of the TRPV2 channel by cannabidiol sensitizes glioblastoma cells to cytotoxic chemotherapeutic agents. *Carcinogenesis* **2013**, *34*, 48–57. [[CrossRef](#)]
50. Morelli, M.B.; Offidani, M.; Alesiani, F.; Discepoli, G.; Liberati, S.; Olivieri, A.; Santoni, M.; Santoni, G.; Leoni, P.; Nabissi, M. The effects of cannabidiol and its synergism with bortezomib in multiple myeloma cell lines. A role for transient receptor potential vanilloid type-2. *Int. J. Cancer* **2014**, *134*, 2534–2546. [[CrossRef](#)]
51. Almasi, S.; Kennedy, B.E.; El-Aghil, M.; Sterea, A.M.; Gujar, S.; Partida-Sanchez, S.; El Hiani, Y. TRPM2 channel-mediated regulation of autophagy maintains mitochondrial function and promotes gastric cancer cell survival via the JNK-signaling pathway. *J. Biol. Chem.* **2018**, *293*, 3637–3650. [[CrossRef](#)] [[PubMed](#)]
52. Koh, D.W.; Powell, D.P.; Blake, S.D.; Hoffman, J.L.; Hopkins, M.M.; Feng, X. Enhanced cytotoxicity in triple-negative and estrogen receptorpositive breast adenocarcinoma cells due to inhibition of the transient receptor potential melastatin-2 channel. *Oncol. Rep.* **2015**, *34*, 1589–1598. [[CrossRef](#)]

53. Wang, Y.; Yang, Z.; Meng, Z.; Cao, H.; Zhu, G.; Liu, T.; Wang, X. Knockdown of TRPM8 suppresses cancer malignancy and enhances epirubicin-induced apoptosis in human osteosarcoma cells. *Int. J. Biol. Sci.* **2013**, *10*, 90–102. [[CrossRef](#)]
54. Liu, X.; Zou, J.; Su, J.; Lu, Y.; Zhang, J.; Li, L.; Yin, F. Downregulation of transient receptor potential cation channel, subfamily C, member 1 contributes to drug resistance and high histological grade in ovarian cancer. *Int. J. Oncol.* **2016**, *48*, 243–252. [[CrossRef](#)] [[PubMed](#)]
55. Zhang, P.; Liu, X.; Li, H.; Chen, Z.; Yao, X.; Jin, J.; Ma, X. TRPC5-induced autophagy promotes drug resistance in breast carcinoma via CaMKK $\beta$ /AMPK $\alpha$ /mTOR pathway. *Sci. Rep.* **2017**, *7*, 3158. [[CrossRef](#)] [[PubMed](#)]
56. Moccia, F. Endothelial Ca<sup>2+</sup> Signaling and the Resistance to Anticancer Treatments: Partners in Crime. *Int. J. Mol. Sci.* **2018**, *19*, 217. [[CrossRef](#)]
57. Ma, X.; Cai, Y.; He, D.; Zou, C.; Zhang, P.; Lo, C.Y.; Xu, Z.; Chan, F.L.; Yu, S.; Chen, Y.; et al. Transient receptor potential channel TRPC5 is essential for P-glycoprotein induction in drug-resistant cancer cells. *Proc. Natl. Acad. Sci. USA* **2012**, *109*, 16282–16287. [[CrossRef](#)] [[PubMed](#)]
58. Dong, Y.; Pan, Q.; Jiang, L.; Chen, Z.; Zhang, F.; Liu, Y.; Xing, H.; Shi, M.; Li, J.; Li, X.; et al. Tumor endothelial expression of P-glycoprotein upon microvesicular transfer of TrpC5 derived from adriamycin-resistant breast cancer cells. *Biochem. Biophys. Res. Commun.* **2014**, *446*, 85–90. [[CrossRef](#)] [[PubMed](#)]
59. Wang, T.; Ning, K.; Lu, T.X.; Sun, X.; Jin, L.; Qi, X.; Jin, J.; Hua, D. Increasing circulating exosomes-carrying TRPC5 predicts chemoresistance in metastatic breast cancer patients. *Cancer Sci.* **2017**, *108*, 448–454. [[CrossRef](#)] [[PubMed](#)]
60. Wang, T.; Chen, Z.; Zhu, Y.; Pan, Q.; Liu, Y.; Qi, X.; Jin, L.; Jin, J.; Ma, X.; Hua, D. Inhibition of transient receptor potential channel 5 reverses 5-Fluorouracil resistance in human colorectal cancer cells. *J. Biol. Chem.* **2015**, *290*, 448–456. [[CrossRef](#)]
61. Wang, T.; Ning, K.; Sun, X.; Zhang, C.; Jin, L.F.; Hua, D. Glycolysis is essential for chemoresistance induced by transient receptor potential channel C5 in colorectal cancer. *BMC Cancer* **2018**, *18*, 207. [[CrossRef](#)]
62. Wen, L.; Liang, C.; Chen, E.; Chen, W.; Liang, F.; Zhi, X.; Wei, T.; Xue, F.; Li, G.; Yang, Q.; et al. Regulation of Multi-drug Resistance in hepatocellular carcinoma cells is TRPC6/Calcium Dependent. *Sci. Rep.* **2016**, *6*, 23269. [[CrossRef](#)] [[PubMed](#)]
63. Madan, E.; Gogna, R.; Keppler, B.; Pati, U. p53 Increases Intra-Cellular Calcium Release by Transcriptional Regulation of Calcium Channel TRPC6 in GaQ3-Treated Cancer Cells. *PLoS ONE* **2013**, *8*, e71016. [[CrossRef](#)] [[PubMed](#)]
64. Yu, J.; Wang, S.; Zhao, W.; Duan, J.; Wang, Z.; Chen, H.; Tian, Y.; Wang, D.; Zhao, J.; An, T.; et al. Mechanistic Exploration of Cancer Stem Cell Marker Voltage-Dependent Calcium Channel  $\alpha$ 2delta1 Subunit-mediated Chemotherapy Resistance in Small-Cell Lung Cancer. *Clin. Cancer Res. Off. J. Am. Assoc. Cancer Res.* **2018**, *24*, 2148–2158. [[CrossRef](#)]
65. Dziegielewska, B.; Casarez, E.V.; Yang, W.Z.; Gray, L.S.; Dziegielewski, J.; Slack-Davis, J.K. T-Type Ca<sup>2+</sup> Channel Inhibition Sensitizes Ovarian Cancer to Carboplatin. *Mol. Cancer Ther.* **2016**, *15*, 460–470. [[CrossRef](#)]
66. Tosatto, A.; Sommaggio, R.; Kummerow, C.; Bentham, R.B.; Blacker, T.S.; Berecz, T.; Duchon, M.R.; Rosato, A.; Bogeski, I.; Szabadkai, G.; et al. The mitochondrial calcium uniporter regulates breast cancer progression via HIF-1 $\alpha$ . *EMBO Mol. Med.* **2016**, *8*, 569–585. [[CrossRef](#)]
67. Akl, H.; Bultynck, G. Altered Ca<sup>2+</sup> signaling in cancer cells: Proto-oncogenes and tumor suppressors targeting IP3 receptors. *Biochim. Biophys. Acta* **2013**, *1835*, 180–193. [[CrossRef](#)]
68. Giorgi, C.; De Stefani, D.; Bononi, A.; Rizzuto, R.; Pinton, P. Structural and functional link between the mitochondrial network and the endoplasmic reticulum. *Int. J. Biochem. Cell Biol.* **2009**, *41*, 1817–1827. [[CrossRef](#)]
69. Prevarskaya, N.; Skryma, R.; Shuba, Y. Ion Channels in Cancer: Are Cancer Hallmarks Oncochannelopathies? *Physiol. Rev.* **2018**, *98*, 559–621. [[CrossRef](#)]
70. Tsunoda, T.; Koga, H.; Yokomizo, A.; Tatsugami, K.; Eto, M.; Inokuchi, J.; Hirata, A.; Masuda, K.; Okumura, K.; Naito, S. Inositol 1,4,5-trisphosphate (IP3) receptor type1 (IP3R1) modulates the acquisition of cisplatin resistance in bladder cancer cell lines. *Oncogene* **2005**, *24*, 1396–1402. [[CrossRef](#)]
71. Schrod, K.; Oelmez, H.; Edelmann, M.; Huber, R.M.; Bergner, A. Altered Ca<sup>2+</sup>-homeostasis of cisplatin-treated and low level resistant non-small-cell and small-cell lung cancer cells. *Cell Oncol.* **2009**, *31*, 301–315. [[PubMed](#)]



72. Akl, H.; Vervloessem, T.; Kiviluoto, S.; Bittremieux, M.; Parys, J.B.; De Smedt, H.; Bultynck, G. A dual role for the anti-apoptotic Bcl-2 protein in cancer: Mitochondria versus endoplasmic reticulum. *Biochim. Biophys. Acta* **2014**, *1843*, 2240–2252. [[CrossRef](#)] [[PubMed](#)]
73. Cheng, E.H.; Levine, B.; Boise, L.H.; Thompson, C.B.; Hardwick, J.M. Bax-independent inhibition of apoptosis by Bcl-XL. *Nature* **1996**, *379*, 554–556. [[CrossRef](#)] [[PubMed](#)]
74. Letai, A.; Bassik, M.C.; Walensky, L.D.; Sorcinelli, M.D.; Weiler, S.; Korsmeyer, S.J. Distinct BH3 domains either sensitize or activate mitochondrial apoptosis, serving as prototype cancer therapeutics. *Cancer Cell* **2002**, *2*, 183–192. [[CrossRef](#)]
75. Maji, S.; Panda, S.; Samal, S.K.; Shriwas, O.; Rath, R.; Pellicchia, M.; Emdad, L.; Das, S.K.; Fisher, P.B.; Dash, R. Bcl-2 Antiapoptotic Family Proteins and Chemoresistance in Cancer. *Adv. Cancer Res.* **2018**, *137*, 37–75. [[PubMed](#)]
76. Padar, S.; van Breemen, C.; Thomas, D.W.; Uchizono, J.A.; Livesey, J.C.; Rahimian, R. Differential regulation of calcium homeostasis in adenocarcinoma cell line A549 and its Taxol-resistant subclone. *Br. J. Pharm.* **2004**, *142*, 305–316. [[CrossRef](#)] [[PubMed](#)]
77. Kerkhofs, M.; Bittremieux, M.; Morciano, G.; Giorgi, C.; Pinton, P.; Parys, J.B.; Bultynck, G. Emerging molecular mechanisms in chemotherapy: Ca<sup>2+</sup> signaling at the mitochondria-associated endoplasmic reticulum membranes. *Cell Death Dis.* **2018**, *9*, 334. [[CrossRef](#)]
78. Huang, Z.; Lei, X.; Zhong, M.; Zhu, B.; Tang, S.; Liao, D. Bcl-2 small interfering RNA sensitizes cisplatin-resistant human lung adenocarcinoma A549/DDP cell to cisplatin and diallyl disulfide. *Acta Biochim. Biophys. Sin.* **2007**, *39*, 835–843. [[CrossRef](#)]
79. Schaaf, A.; Sagi, S.; Langbein, S.; Trojan, L.; Alken, P.; Michel, M.S. Cytotoxicity of cisplatin in bladder cancer is significantly enhanced by application of bcl-2 antisense oligonucleotides. *Urol. Oncol.* **2004**, *22*, 188–192. [[CrossRef](#)]
80. Xie, Q.; Su, J.; Jiao, B.; Shen, L.; Ma, L.; Qu, X.; Yu, C.; Jiang, X.; Xu, Y.; Sun, L. ABT737 reverses cisplatin resistance by regulating ER-mitochondria Ca<sup>2+</sup> signal transduction in human ovarian cancer cells. *Int. J. Oncol.* **2016**, *49*, 2507–2519. [[CrossRef](#)]
81. Zhang, K.; Heidrich, F.M.; DeGray, B.; Boehmerle, W.; Ehrlich, B.E. Paclitaxel accelerates spontaneous calcium oscillations in cardiomyocytes by interacting with NCS-1 and the InsP3R. *J. Mol. Cell. Cardiol.* **2010**, *49*, 829–835. [[CrossRef](#)] [[PubMed](#)]
82. Boutin, B.; Tajeddine, N.; Monaco, G.; Molgo, J.; Vertommen, D.; Rider, M.; Parys, J.B.; Bultynck, G.; Gailly, P. Endoplasmic reticulum Ca<sup>2+</sup> content decrease by PKA-dependent hyperphosphorylation of type 1 IP3 receptor contributes to prostate cancer cell resistance to androgen deprivation. *Cell Calcium* **2015**, *57*, 312–320. [[CrossRef](#)] [[PubMed](#)]
83. Chen, M.H.; Lin, K.J.; Yang, W.L.; Kao, Y.W.; Chen, T.W.; Chao, S.C.; Chang, P.M.; Liu, C.Y.; Tzeng, C.H.; Chao, Y.; et al. Gene expression-based chemical genomics identifies heat-shock protein 90 inhibitors as potential therapeutic drugs in cholangiocarcinoma. *Cancer* **2013**, *119*, 293–303. [[CrossRef](#)] [[PubMed](#)]
84. Murren, J.R.; Durivage, H.J.; Buzaid, A.C.; Reiss, M.; Flynn, S.D.; Carter, D.; Hait, W.N. Trifluoperazine as a modulator of multidrug resistance in refractory breast cancer. *Cancer Chemother. Pharm.* **1996**, *38*, 65–70. [[CrossRef](#)] [[PubMed](#)]
85. Schleuning, M.; Brumme, V.; Wilmanns, W. Growth inhibition of human leukemic cell lines by the phenothiazine derivative fluphenazine. *Anticancer Res.* **1993**, *13*, 599–602.
86. Yeh, C.T.; Wu, A.T.; Chang, P.M.; Chen, K.Y.; Yang, C.N.; Yang, S.C.; Ho, C.C.; Chen, C.C.; Kuo, Y.L.; Lee, P.Y.; et al. Trifluoperazine, an antipsychotic agent, inhibits cancer stem cell growth and overcomes drug resistance of lung cancer. *Am. J. Respir. Crit. Care Med.* **2012**, *186*, 1180–1188. [[CrossRef](#)] [[PubMed](#)]
87. Kang, S.; Hong, J.; Lee, J.M.; Moon, H.E.; Jeon, B.; Choi, J.; Yoon, N.A.; Paek, S.H.; Roh, E.J.; Lee, C.J.; et al. Trifluoperazine, a Well-Known Antipsychotic, Inhibits Glioblastoma Invasion by Binding to Calmodulin and Disinhibiting Calcium Release Channel IP3R. *Mol. Cancer* **2017**, *16*, 217–227. [[CrossRef](#)]
88. Xie, Q.; Xu, Y.; Gao, W.; Zhang, Y.; Su, J.; Liu, Y.; Guo, Y.; Dou, M.; Hu, K.; Sun, L. TAT-fused IP3R-derived peptide enhances cisplatin sensitivity of ovarian cancer cells by increasing ER Ca<sup>2+</sup> release. *Int. J. Mol. Med.* **2017**, *41*, 809–817. [[CrossRef](#)]
89. Xu, L.; Xie, Q.; Qi, L.; Wang, C.; Xu, N.; Liu, W.; Yu, Y.; Li, S.; Xu, Y. Bcl-2 overexpression reduces cisplatin cytotoxicity by decreasing ER-mitochondrial Ca<sup>2+</sup> signaling in SKOV3 cells. *Oncol. Rep.* **2018**, *39*, 985–992. [[CrossRef](#)]

90. Sarosiek, K.A.; Ni Chonghaile, T.; Letai, A. Mitochondria: Gatekeepers of response to chemotherapy. *Trends Cell Biol.* **2013**, *23*, 612–619. [CrossRef]
91. Vo, T.T.; Ryan, J.; Carrasco, R.; Neuberg, D.; Rossi, D.J.; Stone, R.M.; Deangelo, D.J.; Frattini, M.G.; Letai, A. Relative mitochondrial priming of myeloblasts and normal HSCs determines chemotherapeutic success in AML. *Cell* **2012**, *151*, 344–355. [CrossRef]
92. Ni Chonghaile, T.; Sarosiek, K.A.; Vo, T.T.; Ryan, J.A.; Tammareddi, A.; Moore Vdel, G.; Deng, J.; Anderson, K.C.; Richardson, P.; Tai, Y.T.; et al. Pretreatment mitochondrial priming correlates with clinical response to cytotoxic chemotherapy. *Science* **2011**, *334*, 1129–1133. [CrossRef]
93. Davids, M.S.; Letai, A. Targeting the B-cell lymphoma/leukemia 2 family in cancer. *J. Clin. Oncol.* **2012**, *30*, 3127–3135. [CrossRef]
94. Attali, B.; Chandy, K.G.; Giese, M.H.; Grissmer, S.; Gutman, G.A.; Jan, L.Y.; Lazdunski, M.; Mckinnon, D.; Nerbonne, J.; Pardo, L.A.; et al. Voltage-Gated Potassium Channels. Available online: <http://www.guidetopharmacology.org/GRAC/FamilyDisplayForward?familyId=81> (accessed on 1 February 2019).
95. Ouadid-Ahidouch, H.; Ahidouch, A.; Pardo, L.A. Kv10.1 K<sup>+</sup> channel: From physiology to cancer. *Pflügers Arch. Eur. J. Physiol.* **2016**, *468*, 751–762. [CrossRef]
96. Comes, N.; Serrano-Albarrás, A.; Capera, J.; Serrano-Novillo, C.; Condom, E.; Ramón y Cajal, S.; Ferreres, J.C.; Felipe, A. Involvement of potassium channels in the progression of cancer to a more malignant phenotype. *Biochim. Biophys. Acta Biomembr.* **2015**, *1848*, 2477–2492. [CrossRef] [PubMed]
97. D’Amico, M.; Gasparoli, L.; Arcangeli, A. Potassium channels: Novel emerging biomarkers and targets for therapy in cancer. *Recent Pat. Anticancer Drug Discov.* **2013**, *8*, 53–65. [CrossRef]
98. Sharp, S.Y.; Mistry, P.; Valenti, M.R.; Bryant, A.P.; Kelland, L.R. Selective potentiation of platinum drug cytotoxicity in cisplatin-sensitive and -resistant human ovarian carcinoma cell lines by amphotericin B. *Cancer Chemother. Pharmacol.* **1994**, *35*, 137–143. [CrossRef]
99. Liang, X.-J.; Yin, J.-J.; Zhou, J.-W.; Wang, P.C.; Taylor, B.; Cardarelli, C.; Kozar, M.; Forte, R.; Aszalos, A.; Gottesman, M.M. Changes in biophysical parameters of plasma membranes influence cisplatin resistance of sensitive and resistant epidermal carcinoma cells. *Exp. Cell Res.* **2004**, *293*, 283–291. [CrossRef]
100. Marklund, L.; Andersson, B.; Behnam-Motlagh, P.; Sandstrom, P.E.; Henriksson, R.; Grankvist, K. Cellular potassium ion deprivation enhances apoptosis induced by cisplatin. *Basic Clin. Pharmacol. Toxicol.* **2004**, *94*, 245–251. [CrossRef]
101. Marklund, L.; Henriksson, R.; Grankvist, K. Cisplatin-induced apoptosis of mesothelioma cells is affected by potassium ion flux modulator amphotericin B and bumetanide. *Int. J. Cancer* **2001**, *93*, 577–583. [CrossRef]
102. Liu, X.; Wei, L.; Zhao, B.; Cai, X.; Dong, C.; Yin, F. Low expression of KCNN3 may affect drug resistance in ovarian cancer. *Mol. Med. Rep.* **2018**, *18*, 1377–1386. [CrossRef] [PubMed]
103. Samuel, P.; Pink, R.C.; Caley, D.P.; Currie, J.M.; Brooks, S.A.; Carter, D.R. Over-expression of miR-31 or loss of KCNMA1 leads to increased cisplatin resistance in ovarian cancer cells. *Tumour Biol. J. Int. Soc. Oncodev. Biol. Med.* **2016**, *37*, 2565–2573. [CrossRef]
104. Chen, S.Z.; Jiang, M.; Zhen, Y.S. HERG K<sup>+</sup> channel expression-related chemosensitivity in cancer cells and its modulation by erythromycin. *Cancer Chemother. Pharmacol.* **2005**, *56*, 212–220. [CrossRef]
105. Han, Y.; Shi, Y.; Han, Z.; Sun, L.; Fan, D. Detection of potassium currents and regulation of multidrug resistance by potassium channels in human gastric cancer cells. *Cell Biol. Int.* **2007**, *31*, 741–747. [CrossRef]
106. Leanza, L.; O’Reilly, P.; Doyle, A.; Venturini, E.; Zoratti, M.; Szegezdi, E.; Szabo, I. Correlation between potassium channel expression and sensitivity to drug-induced cell death in tumor cell lines. *Curr. Pharm. Des.* **2014**, *20*, 189–200. [CrossRef]
107. Lam, H.D.; Lemay, A.M.; Kelly, J.; Hill, C.E. Loss of Kv and MaxiK currents associated with increased MRP1 expression in small cell lung carcinoma. *J. Cell. Physiol.* **2006**, *209*, 535–541. [CrossRef] [PubMed]
108. Liang, X.J.; Taylor, B.; Cardarelli, C.; Yin, J.J.; Annereau, J.P.; Garfield, S.; Wincovitch, S.; Szakacs, G.; Gottesman, M.M.; Aszalos, A. Different roles for K<sup>+</sup> channels in cisplatin-resistant cell lines argue against a critical role for these channels in cisplatin resistance. *Anticancer Res.* **2005**, *25*, 4113–4122. [PubMed]
109. Pillozzi, S.; D’Amico, M.; Bartoli, G.; Gasparoli, L.; Petroni, G.; Crociani, O.; Marzo, T.; Guerriero, A.; Messori, L.; Severi, M.; et al. The combined activation of KCa3.1 and inhibition of Kv11.1/hERG1 currents contribute to overcome Cisplatin resistance in colorectal cancer cells. *Br. J. Cancer* **2018**, *118*, 200–212. [CrossRef]

110. Agarwal, J.R.; Griesinger, F.; Stuhmer, W.; Pardo, L.A. The potassium channel Ether a go-go is a novel prognostic factor with functional relevance in acute myeloid leukemia. *Mol. Cancer* **2010**, *9*, 18. [[CrossRef](#)] [[PubMed](#)]
111. Hui, C.; Lan, Z.; Yue-li, L.; Li-lin, H. Knockdown of Eag1 Expression by RNA Interference Increases Chemosensitivity to Cisplatin in Ovarian Cancer Cells. *Reprod. Sci.* **2015**, *22*, 1618–1626. [[CrossRef](#)] [[PubMed](#)]
112. Lee, E.L.; Hasegawa, Y.; Shimizu, T.; Okada, Y. IK1 channel activity contributes to cisplatin sensitivity of human epidermoid cancer cells. *Am. J. Physiol. Cell Physiol.* **2008**, *294*, C1398–C1406. [[CrossRef](#)]
113. Spletstoeser, F.; Florea, A.M.; Busseberg, D. IP(3) receptor antagonist, 2-APB, attenuates cisplatin induced Ca<sup>2+</sup>-influx in HeLa-S3 cells and prevents activation of calpain and induction of apoptosis. *Br. J. Pharmacol.* **2007**, *151*, 1176–1186. [[CrossRef](#)] [[PubMed](#)]
114. Jirsch, J.; Deeley, R.G.; Cole, S.P.; Stewart, A.J.; Fedida, D. Inwardly rectifying K<sup>+</sup> channels and volume-regulated anion channels in multidrug-resistant small cell lung cancer cells. *Cancer Res.* **1993**, *53*, 4156–4160.
115. Huang, M.H.; Huang, Y.M.; Wu, S.N. The Inhibition by Oxaliplatin, a Platinum-Based Anti-Neoplastic Agent, of the Activity of Intermediate-Conductance Ca<sup>2+</sup>-Activated K<sup>+</sup> Channels in Human Glioma Cells. *Cell. Physiol. Biochem. Int. J. Exp. Cell. Physiol. Biochem. Pharmacol.* **2015**, *37*, 1390–1406. [[CrossRef](#)]
116. Pan, S.T.; Li, Z.L.; He, Z.X.; Qiu, J.X.; Zhou, S.F. Molecular mechanisms for tumour resistance to chemotherapy. *Clin. Exp. Pharmacol. Physiol.* **2016**, *43*, 723–737. [[CrossRef](#)] [[PubMed](#)]
117. Burg, E.D.; Remillard, C.V.; Yuan, J.X. K<sup>+</sup> channels in apoptosis. *J. Membr. Biol.* **2006**, *209*, 3–20. [[CrossRef](#)] [[PubMed](#)]
118. Checchetto, V.; Azzolini, M.; Peruzzo, R.; Capitanio, P.; Leanza, L. Mitochondrial potassium channels in cell death. *Biochem. Biophys. Res. Commun.* **2018**, *500*, 51–58. [[CrossRef](#)]
119. Bauer, D.; Werth, F.; Nguyen, H.A.; Kiecker, F.; Eberle, J. Critical role of reactive oxygen species (ROS) for synergistic enhancement of apoptosis by vemurafenib and the potassium channel inhibitor TRAM-34 in melanoma cells. *Cell Death Dis.* **2017**, *8*, e2594. [[CrossRef](#)] [[PubMed](#)]
120. Quast, S.A.; Berger, A.; Buttstadt, N.; Friebel, K.; Schonherr, R.; Eberle, J. General Sensitization of melanoma cells for TRAIL-induced apoptosis by the potassium channel inhibitor TRAM-34 depends on release of SMAC. *PLoS ONE* **2012**, *7*, e39290. [[CrossRef](#)]
121. Zhang, R.; Tian, P.; Chi, Q.; Wang, J.; Wang, Y.; Sun, L.; Liu, Y.; Tian, S.; Zhang, Q. Human ether-a-go-go-related gene expression is essential for cisplatin to induce apoptosis in human gastric cancer. *Oncol. Rep.* **2012**, *27*, 433–440.
122. Choi, S.Y.; Kim, H.R.; Ryu, P.D.; Lee, S.Y. Regulation of voltage-gated potassium channels attenuates resistance of side-population cells to gefitinib in the human lung cancer cell line NCI-H460. *BMC Pharmacol. Toxicol.* **2017**, *18*, 14. [[CrossRef](#)] [[PubMed](#)]
123. Liu, H.; Huang, J.; Peng, J.; Wu, X.; Zhang, Y.; Zhu, W.; Guo, L. Upregulation of the inwardly rectifying potassium channel Kir2.1 (KCNJ2) modulates multidrug resistance of small-cell lung cancer under the regulation of miR-7 and the Ras/MAPK pathway. *Mol. Cancer* **2015**, *14*, 59. [[CrossRef](#)] [[PubMed](#)]
124. Bai, Y.; Liao, H.; Liu, T.; Zeng, X.; Xiao, F.; Luo, L.; Guo, H.; Guo, L. MiR-296-3p regulates cell growth and multi-drug resistance of human glioblastoma by targeting ether-a-go-go (EAG1). *Eur. J. Cancer* **2013**, *49*, 710–724. [[CrossRef](#)] [[PubMed](#)]
125. Pillozzi, S.; Masselli, M.; De Lorenzo, E.; Accordi, B.; Cilia, E.; Crociani, O.; Amedei, A.; Veltroni, M.; D'Amico, M.; Basso, G.; et al. Chemotherapy resistance in acute lymphoblastic leukemia requires hERG1 channels and is overcome by hERG1 blockers. *Blood* **2011**, *117*, 902–914. [[CrossRef](#)] [[PubMed](#)]
126. Chavez-Lopez, M.G.; Zuniga-Garcia, V.; Hernandez-Gallegos, E.; Vera, E.; Chasiquiza-Anchatuna, C.A.; Viteri-Yanez, M.; Sanchez-Ramos, J.; Garrido, E.; Camacho, J. The combination astemizole-gefitinib as a potential therapy for human lung cancer. *Oncotargets Ther.* **2017**, *10*, 5795–5803. [[CrossRef](#)]
127. Leanza, L.; Henry, B.; Sassi, N.; Zoratti, M.; Chandy, K.G.; Gulbins, E.; Szabo, I. Inhibitors of mitochondrial Kv1.3 channels induce Bax/Bak-independent death of cancer cells. *EMBO Mol. Med.* **2012**, *4*, 577–593. [[CrossRef](#)]
128. de Baaij, J.H.; Hoenderop, J.G.; Bindels, R.J. Magnesium in man: Implications for health and disease. *Physiol. Rev.* **2015**, *95*, 1–46. [[CrossRef](#)]

129. Dibaba, D.; Xun, P.; Yokota, K.; White, E.; He, K. Magnesium intake and incidence of pancreatic cancer: The VITamins and Lifestyle study. *Br. J. Cancer* **2015**, *113*, 1615–1621. [[CrossRef](#)] [[PubMed](#)]
130. Zhu, X.; Shrubsole, M.J.; Ness, R.M.; Hibler, E.A.; Cai, Q.; Long, J.; Chen, Z.; Li, G.; Jiang, M.; Hou, L.; et al. Calcium/magnesium intake ratio, but not magnesium intake, interacts with genetic polymorphism in relation to colorectal neoplasia in a two-phase study. *Mol. Carcinog.* **2016**, *55*, 1449–1457. [[CrossRef](#)]
131. Castiglioni, S.; Cazzaniga, A.; Trapani, V.; Cappadone, C.; Farruggia, G.; Merolle, L.; Wolf, F.I.; Iotti, S.; Maier, J.A. Magnesium homeostasis in colon carcinoma LoVo cells sensitive or resistant to doxorubicin. *Sci. Rep.* **2015**, *5*, 16538. [[CrossRef](#)]
132. Middelbeek, J.; Kuipers, A.J.; Henneman, L.; Visser, D.; Eidhof, I.; van Horsen, R.; Wieringa, B.; Canisius, S.V.; Zwart, W.; Wessels, L.F.; et al. TRPM7 is required for breast tumor cell metastasis. *Cancer Res.* **2012**, *72*, 4250–4261. [[CrossRef](#)]
133. Rybarczyk, P.; Gautier, M.; Hague, F.; Dhennin-Duthille, I.; Chatelain, D.; Kerr-Conte, J.; Pattou, F.; Regimbeau, J.M.; Sevestre, H.; Ouadid-Ahidouch, H. Transient receptor potential melastatin-related 7 channel is overexpressed in human pancreatic ductal adenocarcinomas and regulates human pancreatic cancer cell migration. *Int. J. Cancer* **2012**, *131*, E851–E861. [[CrossRef](#)] [[PubMed](#)]
134. Chen, Y.; Wei, X.; Yan, P.; Han, Y.; Sun, S.; Wu, K.; Fan, D. Human mitochondrial Mrs2 protein promotes multidrug resistance in gastric cancer cells by regulating p27, cyclin D1 expression and cytochrome C release. *Cancer Biol. Ther.* **2009**, *8*, 607–614. [[CrossRef](#)] [[PubMed](#)]
135. Naito, M.; Hamada, H.; Tsuruo, T. ATP/Mg<sup>2+</sup>-dependent binding of vincristine to the plasma membrane of multidrug-resistant K562 cells. *J. Biol. Chem.* **1988**, *263*, 11887–11891. [[PubMed](#)]
136. Hamada, H.; Tsuruo, T. Characterization of the ATPase activity of the Mr 170,000 to 180,000 membrane glycoprotein (P-glycoprotein) associated with multidrug resistance in K562/ADM cells. *Cancer Res.* **1988**, *48*, 4926–4932. [[PubMed](#)]
137. Naito, M.; Tsuruo, T. Competitive inhibition by verapamil of ATP-dependent high affinity vincristine binding to the plasma membrane of multidrug-resistant K562 cells without calcium ion involvement. *Cancer Res.* **1989**, *49*, 1452–1455.
138. Ali, A.Y.; Kim, J.Y.; Pelletier, J.F.; Vanderhyden, B.C.; Bachvarov, D.R.; Tsang, B.K. Akt confers cisplatin chemoresistance in human gynecological carcinoma cells by modulating PPM1D stability. *Mol. Carcinog.* **2015**, *54*, 1301–1314. [[CrossRef](#)] [[PubMed](#)]
139. Kahn, J.D.; Miller, P.G.; Silver, A.J.; Sellar, R.S.; Bhatt, S.; Gibson, C.; McConkey, M.; Adams, D.; Mar, B.; Mertins, P.; et al. PPM1D-truncating mutations confer resistance to chemotherapy and sensitivity to PPM1D inhibition in hematopoietic cells. *Blood* **2018**, *132*, 1095–1105. [[CrossRef](#)] [[PubMed](#)]
140. Hsu, J.I.; Dayaram, T.; Tovy, A.; De Braekeleer, E.; Jeong, M.; Wang, F.; Zhang, J.; Heffernan, T.P.; Gera, S.; Kovacs, J.J.; et al. PPM1D Mutations Drive Clonal Hematopoiesis in Response to Cytotoxic Chemotherapy. *Cell Stem Cell* **2018**, *23*, 700–713 e706. [[CrossRef](#)]
141. Cao, Y.; Liao, C.; Tan, A.; Liu, L.; Gao, F. Meta-analysis of incidence and risk of hypomagnesemia with cetuximab for advanced cancer. *Chemotherapy* **2010**, *56*, 459–465. [[CrossRef](#)]
142. Petrelli, F.; Borgonovo, K.; Cabiddu, M.; Ghilardi, M.; Barni, S. Risk of anti-EGFR monoclonal antibody-related hypomagnesemia: Systematic review and pooled analysis of randomized studies. *Expert Opin. Drug Saf.* **2012**, *11* (Suppl. 1), S9–S19. [[CrossRef](#)] [[PubMed](#)]
143. Chen, P.; Wang, L.; Li, H.; Liu, B.; Zou, Z. Incidence and risk of hypomagnesemia in advanced cancer patients treated with cetuximab: A meta-analysis. *Oncol. Lett.* **2013**, *5*, 1915–1920. [[CrossRef](#)] [[PubMed](#)]
144. Wang, Q.; Qi, Y.; Zhang, D.; Gong, C.; Yao, A.; Xiao, Y.; Yang, J.; Zhou, F.; Zhou, Y. Electrolyte disorders assessment in solid tumor patients treated with anti-EGFR monoclonal antibodies: A pooled analysis of 25 randomized clinical trials. *Tumour Biol. J. Int. Soc. Oncodev. Biol. Med.* **2015**, *36*, 3471–3482. [[CrossRef](#)] [[PubMed](#)]
145. Hsieh, M.C.; Wu, C.F.; Chen, C.W.; Shi, C.S.; Huang, W.S.; Kuan, F.C. Hypomagnesemia and clinical benefits of anti-EGFR monoclonal antibodies in wild-type KRAS metastatic colorectal cancer: A systematic review and meta-analysis. *Sci. Rep.* **2018**, *8*, 2047. [[CrossRef](#)]
146. Duran, C.; Thompson, C.H.; Xiao, Q.; Hartzell, H.C. Chloride channels: Often enigmatic, rarely predictable. *Annu. Rev. Physiol.* **2010**, *72*, 95–121. [[CrossRef](#)]

147. Peretti, M.; Angelini, M.; Savalli, N.; Florio, T.; Yuspa, S.H.; Mazzanti, M. Chloride channels in cancer: Focus on chloride intracellular channel 1 and 4 (CLIC1 AND CLIC4) proteins in tumor development and as novel therapeutic targets. *Biochim. Biophys. Acta Mol. Cell Res.* **2015**, *1848*, 2523–2531. [[CrossRef](#)]
148. Wang, H.; Zou, L.; Ma, K.; Yu, J.; Wu, H.; Wei, M.; Xiao, Q. Cell-specific mechanisms of TMEM16A Ca<sup>2+</sup>-activated chloride channel in cancer. *Mol. Cancer* **2017**, *16*, 152. [[CrossRef](#)] [[PubMed](#)]
149. Alexander, S.P.; Kelly, E.; Marrion, N.V.; Peters, J.A.; Faccenda, E.; Harding, S.D.; Pawson, A.J.; Sharman, J.L.; Southan, C.; Davies, J.A.; et al. THE CONCISE GUIDE TO PHARMACOLOGY 2017/18: Other ion channels. *Br. J. Pharmacol.* **2017**, *174* (Suppl. 1), S195–S207. [[CrossRef](#)]
150. Marin, M.; Poret, A.; Maillet, G.; Le Boulenger, F.; Le Foll, F. Regulation of volume-sensitive Cl<sup>-</sup> channels in multi-drug resistant MCF7 cells. *Biochem. Biophys. Res. Commun.* **2005**, *334*, 1266–1278. [[CrossRef](#)]
151. Ise, T.; Shimizu, T.; Lee, E.L.; Inoue, H.; Kohno, K.; Okada, Y. Roles of volume-sensitive Cl<sup>-</sup> channel in cisplatin-induced apoptosis in human epidermoid cancer cells. *J. Membr. Biol.* **2005**, *205*, 139–145. [[CrossRef](#)] [[PubMed](#)]
152. Lee, E.L.; Shimizu, T.; Ise, T.; Numata, T.; Kohno, K.; Okada, Y. Impaired activity of volume-sensitive Cl<sup>-</sup> channel is involved in cisplatin resistance of cancer cells. *J. Cell. Physiol.* **2007**, *211*, 513–521. [[CrossRef](#)] [[PubMed](#)]
153. Okada, Y.; Sato, K.; Numata, T. Pathophysiology and puzzles of the volume-sensitive outwardly rectifying anion channel. *J. Physiol.* **2009**, *587*, 2141–2149.
154. Min, X.J.; Li, H.; Hou, S.C.; He, W.; Liu, J.; Hu, B.; Wang, J. Dysfunction of volume-sensitive chloride channels contributes to cisplatin resistance in human lung adenocarcinoma cells. *Exp. Biol. Med.* **2011**, *236*, 483–491. [[CrossRef](#)] [[PubMed](#)]
155. Poulsen, K.A.; Andersen, E.C.; Hansen, C.F.; Klausen, T.K.; Hougaard, C.; Lambert, I.H.; Hoffmann, E.K. Deregulation of apoptotic volume decrease and ionic movements in multidrug-resistant tumor cells: Role of chloride channels. *Am. J. Physiol. Cell Physiol.* **2010**, *298*, C14–C25. [[CrossRef](#)] [[PubMed](#)]
156. Yang, X.; Zhu, L.; Lin, J.; Liu, S.; Luo, H.; Mao, J.; Nie, S.; Chen, L.; Wang, L. Cisplatin activates volume-sensitive like chloride channels via purinergic receptor pathways in nasopharyngeal carcinoma cells. *J. Membr. Biol.* **2015**, *248*, 19–29. [[CrossRef](#)] [[PubMed](#)]
157. Hoffmann, E.K.; Sorensen, B.H.; Sauter, D.P.; Lambert, I.H. Role of volume-regulated and calcium-activated anion channels in cell volume homeostasis, cancer and drug resistance. *Channels* **2015**, *9*, 380–396. [[CrossRef](#)]
158. Shimizu, T.; Lee, E.L.; Ise, T.; Okada, Y. Volume-sensitive Cl<sup>-</sup> channel as a regulator of acquired cisplatin resistance. *Anticancer Res.* **2008**, *28*, 75–83.
159. Voss, F.K.; Ullrich, F.; Munch, J.; Lazarow, K.; Lutter, D.; Mah, N.; Andrade-Navarro, M.A.; von Kries, J.P.; Stauber, T.; Jentsch, T.J. Identification of LRRC8 heteromers as an essential component of the volume-regulated anion channel VRAC. *Science* **2014**, *344*, 634–638. [[CrossRef](#)]
160. Planells-Cases, R.; Lutter, D.; Guyader, C.; Gerhards, N.M.; Ullrich, F.; Elger, D.A.; Kucukosmanoglu, A.; Xu, G.; Voss, F.K.; Reincke, S.M.; et al. Subunit composition of VRAC channels determines substrate specificity and cellular resistance to Pt-based anti-cancer drugs. *EMBO J.* **2015**, *34*, 2993–3008. [[CrossRef](#)]
161. Fujimoto, M.; Inoue, T.; Kito, H.; Niwa, S.; Suzuki, T.; Muraki, K.; Ohya, S. Transcriptional repression of HER2 by ANO1 Cl<sup>-</sup> channel inhibition in human breast cancer cells with resistance to trastuzumab. *Biochem. Biophys. Res. Commun.* **2017**, *482*, 188–194. [[CrossRef](#)]
162. Kang, M.K.; Kang, S.K. Pharmacologic blockade of chloride channel synergistically enhances apoptosis of chemotherapeutic drug-resistant cancer stem cells. *Biochem. Biophys. Res. Commun.* **2008**, *373*, 539–544. [[CrossRef](#)] [[PubMed](#)]
163. Qu, H.; Chen, Y.; Cao, G.; Liu, C.; Xu, J.; Deng, H.; Zhang, Z. Identification and validation of differentially expressed proteins in epithelial ovarian cancers using quantitative proteomics. *Oncotarget* **2016**, *7*, 83187–83199. [[CrossRef](#)] [[PubMed](#)]
164. Yu, W.; Cui, R.; Qu, H.; Liu, C.; Deng, H.; Zhang, Z. Expression and prognostic value of CLIC1 in epithelial ovarian cancer. *Exp. Ther. Med.* **2018**, *15*, 4943–4949. [[CrossRef](#)] [[PubMed](#)]
165. Bill, A.; Gutierrez, A.; Kulkarni, S.; Kemp, C.; Bonenfant, D.; Voshol, H.; Duvvuri, U.; Gaither, L.A. ANO1/TMEM16A interacts with EGFR and correlates with sensitivity to EGFR-targeting therapy in head and neck cancer. *Oncotarget* **2015**, *6*, 9173–9188. [[CrossRef](#)]

166. Weylandt, K.H.; Nebrig, M.; Jansen-Rosseck, N.; Amey, J.S.; Carmena, D.; Wiedenmann, B.; Higgins, C.F.; Sardini, A. CIC-3 expression enhances etoposide resistance by increasing acidification of the late endocytic compartment. *Mol. Cancer Ther.* **2007**, *6*, 979–986. [[CrossRef](#)]
167. Xu, Y.; Zheng, H.; Kang, J.S.; Zhang, L.; Su, J.; Li, H.Y.; Sun, L.K. 5-Nitro-2-(3-phenylpropylamino) benzoic acid induced drug resistance to cisplatin in human erythroleukemia cell lines. *Anat. Rec.* **2011**, *294*, 945–952. [[CrossRef](#)]
168. Zhang, Y.; Zhou, L.; Zhang, J.; Zhang, L.; Yan, X.; Su, J. Suppression of chloride voltage-gated channel 3 expression increases sensitivity of human glioma U251 cells to cisplatin through lysosomal dysfunction. *Oncol. Lett.* **2018**, *16*, 835–842. [[CrossRef](#)]
169. Fujimoto, M.; Kito, H.; Kajikuri, J.; Ohya, S. Transcriptional repression of human epidermal growth factor receptor 2 by CIC-3 Cl<sup>-</sup> /H<sup>+</sup> transporter inhibition in human breast cancer cells. *Cancer Sci.* **2018**, *109*, 2781–2791. [[CrossRef](#)]
170. Su, J.; Xu, Y.; Zhou, L.; Yu, H.M.; Kang, J.S.; Liu, N.; Quan, C.S.; Sun, L.K. Suppression of chloride channel 3 expression facilitates sensitivity of human glioma U251 cells to cisplatin through concomitant inhibition of Akt and autophagy. *Anat. Rec.* **2013**, *296*, 595–603. [[CrossRef](#)]
171. Chen, Q.; Liu, X.; Luo, Z.; Wang, S.; Lin, J.; Xie, Z.; Li, M.; Li, C.; Cao, H.; Huang, Q.; et al. Chloride channel-3 mediates multidrug resistance of cancer by upregulating P-glycoprotein expression. *J. Cell. Physiol.* **2018**, *234*, 6611–6623. [[CrossRef](#)]
172. Zhang, H.; Pang, Y.; Ma, C.; Li, J.; Wang, H.; Shao, Z. CIC5 Decreases the Sensitivity of Multiple Myeloma Cells to Bortezomib via Promoting Prosurvival Autophagy. *Oncol. Res.* **2018**, *26*, 421–429. [[CrossRef](#)] [[PubMed](#)]
173. Wu, J.; Wang, D. CLIC1 Induces Drug Resistance in Human Choriocarcinoma Through Positive Regulation of MRP1. *Oncol. Res.* **2017**, *25*, 863–871. [[CrossRef](#)]
174. House, C.D.; Wang, B.D.; Ceniccola, K.; Williams, R.; Simaan, M.; Olender, J.; Patel, V.; Baptista-Hon, D.T.; Annunziata, C.M.; Gutkind, J.S.; et al. Voltage-gated Na<sup>+</sup> Channel Activity Increases Colon Cancer Transcriptional Activity and Invasion Via Persistent MAPK Signaling. *Sci. Rep.* **2015**, *5*, 11541. [[CrossRef](#)] [[PubMed](#)]
175. Nelson, M.; Yang, M.; Millican-Slater, R.; Brackenbury, W.J. Nav1.5 regulates breast tumor growth and metastatic dissemination in vivo. *Oncotarget* **2015**, *6*, 32914–32929. [[CrossRef](#)] [[PubMed](#)]
176. Yildirim, S.; Altun, S.; Gumushan, H.; Patel, A.; Djamgoz, M.B. Voltage-gated sodium channel activity promotes prostate cancer metastasis in vivo. *Cancer Lett.* **2012**, *323*, 58–61. [[CrossRef](#)] [[PubMed](#)]
177. Gerard, V.; Rouzaire-Dubois, B.; Dilda, P.; Dubois, J.M. Alterations of ionic membrane permeabilities in multidrug-resistant neuroblastoma x glioma hybrid cells. *J. Exp. Biol.* **1998**, *201*, 21–31.
178. Yamashita, N.; Hamada, H.; Tsuruo, T.; Ogata, E. Enhancement of voltage-gated Na<sup>+</sup> channel current associated with multidrug resistance in human leukemia cells. *Cancer Res.* **1987**, *47*, 3736–3741.
179. Zhang, Y.; Zhang, T.; Wu, C.; Xia, Q.; Xu, D. ASIC1a mediates the drug resistance of human hepatocellular carcinoma via the Ca<sup>2+</sup> /PI3-kinase/AKT signaling pathway. *Lab. Investig. A J. Tech. Methods Pathol.* **2017**, *97*, 53–69. [[CrossRef](#)]
180. Kondratskyi, A.; Kondratska, K.; Skryma, R.; Prevarskaya, N. Ion channels in the regulation of apoptosis. *Biochim. Biophys. Acta Mol. Cell Res.* **2015**, *1848*, 2532–2546. [[CrossRef](#)]
181. Kunzelmann, K. Ion channels in regulated cell death. *Cell. Mol. Life Sci.* **2016**, *73*, 2387–2403. [[CrossRef](#)]
182. Badaoui, M.; Mimsy-Julienne, C.; Saby, C.; Van Gulick, L.; Peretti, M.; Jeannesson, P.; Morjani, H.; Ouadid-Ahidouch, H. Collagen type 1 promotes survival of human breast cancer cells by overexpressing Kv10.1 potassium and Orai1 calcium channels through DDR1-dependent pathway. *Oncotarget* **2018**, *9*, 24653–24671. [[CrossRef](#)] [[PubMed](#)]
183. Gueguinou, M.; Harnois, T.; Crottes, D.; Uguen, A.; Deliot, N.; Gambade, A.; Chantome, A.; Haelters, J.P.; Jaffres, P.A.; Jourdan, M.L.; et al. SK3/TRPC1/Orai1 complex regulates SOCE-dependent colon cancer cell migration: A novel opportunity to modulate anti-EGFR mAb action by the alkyl-lipid Ohmlin. *Oncotarget* **2016**, *7*, 36168–36184. [[CrossRef](#)] [[PubMed](#)]
184. Belpomme, D.; Gauthier, S.; Pujade-Lauraine, E.; Facchini, T.; Goudier, M.J.; Krakowski, I.; Netter-Pinon, G.; Frenay, M.; Gousset, C.; Marie, F.N.; et al. Verapamil increases the survival of patients with anthracycline-resistant metastatic breast carcinoma. *Ann. Oncol.* **2000**, *11*, 1471–1476. [[CrossRef](#)] [[PubMed](#)]

185. Lester-Coll, N.H.; Supko, J.G.; Kluytenaar, J.; Pavlik, K.F.; Yu, J.B.; Moliterno, J.; Piepmeier, J.; Becker, K.; Baehring, J.M.; Huttner, A.; et al. Mibefradil dihydrochloride with hypofractionated radiation for recurrent glioblastoma: A phase I dose expansion trial. *J. Clin. Oncol.* **2018**, *36*, e14046. [[CrossRef](#)]
186. Yu, L.J.; Wall, B.A.; Chen, S. The current management of brain metastasis in melanoma: A focus on riluzole. *Expert Rev. Neurother.* **2015**, *15*, 779–792. [[CrossRef](#)] [[PubMed](#)]
187. Mehnert, J.M.; Silk, A.W.; Lee, J.H.; Dudek, L.; Jeong, B.S.; Li, J.; Schenkel, J.M.; Sadimin, E.; Kane, M.; Lin, H.; et al. A phase II trial of riluzole, an antagonist of metabotropic glutamate receptor 1 (GRM1) signaling, in patients with advanced melanoma. *Pigment Cell Melanoma Res.* **2018**, *31*, 534–540. [[CrossRef](#)] [[PubMed](#)]



© 2019 by the authors. Licensee MDPI, Basel, Switzerland. This article is an open access article distributed under the terms and conditions of the Creative Commons Attribution (CC BY) license (<http://creativecommons.org/licenses/by/4.0/>).



Review Article

## Mammary SLAMF3 Regulates Store-Operated Ca<sup>2+</sup> Entry and Migration Through STIM1 in Breast Cancer Cells and Cell Lines

Grégory Fouquet<sup>1</sup>, Constance Marié<sup>1#</sup>, Mehdi Badaoui<sup>2#</sup>, Baptiste Demey<sup>1#</sup>, Sylviya Radoslavova<sup>2</sup>, Marie-Sophie Telliez<sup>2</sup>, Isabelle Dhennin-Duthille<sup>2</sup>, Jagadeesh Bayry<sup>3</sup>, Henri Sevestre<sup>2,4</sup>, Halima Ouadid-Ahidouch<sup>2\*</sup>, Ingrid Marcq<sup>1\*</sup>, Hicham Bouhlal<sup>1\*</sup>

#Authors contributed equally

<sup>1</sup>INSERM 1247-GRAP, Centre Universitaire de Recherche en Santé CURS, Université de Picardie Jules Verne, CHU Sud, Amiens, France

<sup>2</sup>Laboratoire de Physiologie Cellulaire et Moléculaire, LPCM UR-4667-UPJV, Université de Picardie Jules Verne, UFR Sciences, 80000, Amiens, France

<sup>3</sup>INSERM, Centre de Recherche des Cordeliers-Equipe Immunopathologie et immune-intervention thérapeutique, Sorbonne Université, Université de Paris, Paris, France

<sup>4</sup>Service Anatomie pathologie, Centre Hospitalier Universitaire Nord, Amiens, France

\***Corresponding Authors:** Dr. Hicham Bouhlal, INSERM 1247-GRAP, Centre Universitaire de Recherche en Santé CURS, Université de Picardie Jules Verne, CHU Sud, Amiens, France, Tel: + 33 3 22 82 79 13; Fax: + 33 3 22 82 79 07; E-mail: [hicham.bouhlal@u-picardie.fr](mailto:hicham.bouhlal@u-picardie.fr)

Dr. Ingrid Marcq, INSERM 1247-GRAP, Centre Universitaire de Recherche en Santé CURS, Université de Picardie Jules Verne, CHU Sud, Amiens, France, Tel: + 33 3 22 82 79 13; Fax: + 33 3 22 82 79 07; E-mail: [ingrid.marcq@u-picardie.fr](mailto:ingrid.marcq@u-picardie.fr)

**Received:** 02 July 2020; **Accepted:** 03 August 2020; **Published:** 09 October 2020

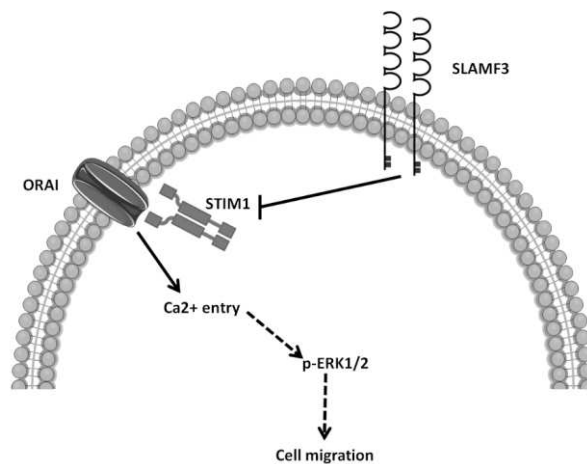
**Citation:** Grégory Fouquet, Constance Marié, Mehdi Badaoui, Baptiste Demey, Sylviya Radoslavova, Marie-Sophie Telliez, Isabelle Dhennin-Duthille, Jagadeesh Bayry, Henri Sevestre, Halima Ouadid-Ahidouch, Ingrid Marcq, Hicham Bouhlal. Mammary SLAMF3 Regulates Store-Operated Ca<sup>2+</sup> Entry and Migration Through STIM1 in Breast Cancer Cells and Cell Lines. Journal of Cancer Science and Clinical Therapeutics 4 (2020): 462-479.



**Abstract**

Abstract: Store Operated Calcium Entry (SOCE) is the main route for calcium entry in breast cells. After its activation by STromal Interaction Molecule (STIM) during endoplasmic reticulum store depletion, membrane channels ORAI are the main actors of this cell calcium entry. STIM, ORAI and SOCE alterations might contribute to Breast Cancer (BC) carcinogenesis. Recently, we reported the tumor suppressor role of Signaling Lymphocytic Activation Molecule Family member 3 (SLAMF3) on HepatoCellular Carcinoma (HCC) progression. SLAMF3 has been shown to regulate the activity of immune cells by modulating the calcium influx. In this report, we aimed at exploring the role of SLAMF3 in regulating SOCE and migration of BC cells. We quantified and compared the expression of SLAMF3 and STIM1 by quantitative RT-PCR in tumor and healthy resections of 14 patients followed at the University Hospital of Amiens. The expressions of SLAMF3 and STIM1 were also quantified and compared in non-invasive T47D and invasive MDA-MB-231 cell lines by quantitative

RT-PCR, Western blot and flow cytometry. We determined the Ca<sup>2+</sup> basal entry as well as SOCE by Mn<sup>2+</sup> quenching and calcium imaging, respectively, in T47D and MDA-MB-231 cells overexpressing SLAMF3 ectopically. The cell proliferation and migration/invasion were investigated by MTT, wound healing assay and Boyden chambers tests, respectively. First, we report the expression of SLAMF3 in mammary epithelial cells. We highlight the complete loss of SLAMF3 expression in invasive BC cell lines compared to non-invasive cells. In addition, we show that the forced expression of SLAMF3 in invasive cells down-regulate specifically the STIM1 expression in invasive compared to non-invasive mammary cell lines. Interestingly, an inverse correlation is observed between the low expression of SLAMF3 and the high expression of STIM1 in primary human BC tissues. Our results indicate that SLAMF3 reduces SOCE and therefore restricts BC cell migration by decreasing STIM1 expression. Therefore, SLAMF3 might be used as a predictive marker of BC evolution and aggressiveness.



Proposed model of SLAMF3 implication in the regulation of Ca<sup>2+</sup> entry through its action on STIM1/ORAI pathway. The STIM1-dependent action of SLAMF3 decreases SOCE, controls ERK1/2 expression and activation, and BC cell migration.

**Keywords:** SLAMF3; Breast cancer; Calcium influx; SOCE; STIM1; Migration; Aggressiveness marker

**Abbreviation:** SLAMF3: Signaling Lymphocytic Activation Molecules Family 3; STIM1: STromal Interaction Molecule; SOCE: Store Operated Calcium Entry; BC: Breast Cancer; ERK1/2: Extracellular signal-Regulated Kinases 1/2; HCC: HepatoCellular Carcinoma; RTqPCR: Real Time quantitative Polymerase Chain Reaction; 5 mRNA: messenger RiboNucleic Acid; WB: Western Blot; MTT: Methylthiazolyldiphenyl-tetrazolium bromide; mTOR: mammalian Target Of Rapamycin; RB: RetinoBlastoma; PLK-1: Polo-Like Kinase-1; IFN- $\gamma$ : InterFeroN- $\gamma$ ; NK: Natural Killer; EAT-2: Ewing's sarcoma-associated transcript 2; MAPK: Mitogen-Activated Protein Kinase

## 1. Introduction

Breast cancer (BC) is one of the most common malignancies, which caused almost 627,000 deaths worldwide in 2018 [1]. Despite advancement in the treatment options, this disease remains lethal, especially when it turns invasive. Eight out of ten BC cases are diagnosed as invasive and presence of metastasis reduces the overall survival [2]. Understanding the regulatory mechanisms and main actors implicated in the pathogenesis of BC is essential to develop new targeted therapies, predictive or diagnostic markers, and optimized patient care. Over the past years, ion channels have emerged as important players in cell proliferation, survival and migration of BC cells [3]. Calcium (Ca<sup>2+</sup>) is one of the major second messengers and its cytoplasmic concentration ([Ca<sup>2+</sup>]<sub>i</sub>) regulates many cell properties [4] including metastatic mechanisms [5]. In unexcitable cells including mammary cells, store-operated calcium entry (SOCE) is the main way of calcium entry. During calcium store depletion of endoplasmic reticulum in BC cells, SOCE is mediated by the Ca<sup>2+</sup> sensor STIM1 (STromal Interaction Molecule 1), which is localized on reticular membrane [6-8], and the

pore-forming proteins ORAI1/3 (Ca<sup>2+</sup> channels) situated on the plasma membrane [9-12]. STIM1 is known to promote Ca<sup>2+</sup>-dependent proliferation [13-17] and migration [17-20] in many cancers including BC.

We have recently identified Signaling Lymphocytic Activation Molecule (SLAM) family member, the SLAMF3 receptor, as a key factor, which controls the proliferation and apoptosis of cancer cells, and the progression of tumor masses in liver tissue [21]. We have also reported the loss of SLAMF3 expression in HepatoCellular Carcinoma (HCC) cells, and that induction of SLAMF3 expression inhibited the proliferation and blocked the cell cycle at the G2/M stage by suppressing the MAPK ERK1/2/JNK, mTOR and RB/PLK-1 pathways [21, 22]. SLAMF3 is also expressed in immune cells [23] where it triggers both activatory and inhibitory signals [24]. Indeed, in CD3-activated T cells, SLAMF3 activation decreases the phosphorylation of ERK1/2 and production of IFN- $\gamma$  [25]. In 3 of 17 parallel, defects in T cell activation and IL-2 production in Ly9 (SLAMF-3)-deficient mice (Ly9<sup>-/-</sup>) suggests a crucial role of Ly9 in T cell functions [26]. Besides, SLAM family members are also involved in the regulation of immune response through the regulation of Ca<sup>2+</sup> influx. In Natural Killer cells (NK), SLAM, via Ewing's sarcoma-associated transcript 2 (EAT-2), a SLAM intracellular adaptor protein, induces activation of MAPK ERK1/2 by recruitment of PLC- $\gamma$  that evokes Ca<sup>2+</sup> influxes [27].

In the present work, we investigated the link between SLAMF3 expression and SOCE modulation in BC. We show a low expression of SLAMF3 in breast tumor tissues compared to the healthy ones. Moreover, in BC cell lines, we highlighted the specific regulatory effect of SLAMF3 on the expression of STIM1 and on SOCE. In addition, high

expression of SLAMF3 reduced the migratory potential of invasive cell lines, which is Ca<sup>2+</sup>-dependent. Taken together, our results provide evidence on the implication of SLAMF3 receptor in the regulation of SOCE through STIM1 pathway in mammary tissue. We also propose high expression of SLAMF3 in cancerous tissue as a therapeutic strategy to control the progression and invasiveness of cancerous mass.

## 2. Results

### 2.1. Inverse correlation between SLAMF3 and STIM1 expression in human breast cancer tissues

We have previously described that in HCC tissues [21], the expression of SLAMF3 is lost in tumor tissues compared to

peri-tumor tissues. Here, we observed a significantly reduced expression of SLAMF3 mRNA in eight of fourteen (60%) breast tumor tissues compared to peri-tumor tissues (n=14; p<0.01; Figure 1A). Moreover, STIM1 expression was not significantly modified in tumor tissues (n=14; Figure 1B). We highlight a weak but significant, inverse correlation between SLAMF3 and STIM1 expression (n=14; R<sup>2</sup>=0.356; p<0.05; Figure 1C). Given the limited number of patients, SLAMF3 and STIM1 expression did not reach significance when patients were grouped according to either tumor grade or metastasis.

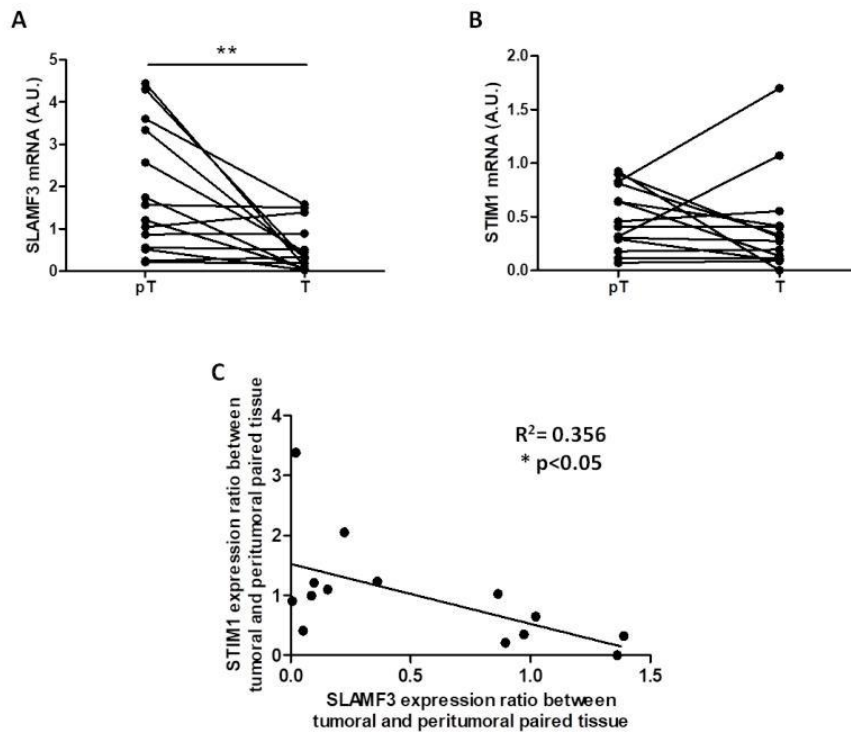


**Figure 1:** Inverse correlation between SLAMF3 and STIM1 expression in primary human breast cancer tissue samples. SLAMF3 (A) and STIM1 (B) mRNA expressions were quantified by quantitative RT-PCR in same extracts of resected breast cancer tissues. The mRNA expression was compared between peritumor (pT) and tumor (T) tissues (n=14; \*\*p<0.01, ns: non-significant). (C) The correlation curve between SLAMF3 and STIM1 expression (R<sup>2</sup>=0.356; \*p<0.05).

## 2.2. SLAMF3 is expressed in human breast epithelial cells

The results obtained with breast tumor tissues prompted us to confirm the expression of SLAMF3 in BC cell lines. Until now, SLAMF3 is known to be expressed in lymphocytes [23] and in hepatocytes [21] but not in epithelial breast cells. We investigated SLAMF3 expression in human breast epithelial cancer cell lines by flow cytometry and western blot. In cancerous cells, the cell surface phenotype analysis showed that SLAMF3 is weakly expressed on the cell surface ( $7.64 \pm 1.80\%$  and  $0.92 \pm 0.07\%$  on non-invasive T47D and invasive MDA-MB-231

triple negative cells, respectively; Figure 2A). Despite this low expression, SLAMF3 expression appears to be significantly lower in invasive human BC cell lines (MDA-MB-231) compared to non-invasive cell lines (T47D) (Figure 2B,  $N=3$ ,  $p<0.01$ ). Western blot analysis confirmed the expression of SLAMF3 in human breast epithelial cells. We found a lower SLAMF3 expression in invasive MDA-MB-231 cells (Figure 2C). Indeed, semi-quantitative analysis of proteins showed a reduction of SLAMF3 protein level by  $37 \pm 7.8\%$  in MDA-MB-231 compared to non-invasive T47D cells (Figure 2D,  $N=3$ ;  $p<0.01$ ).

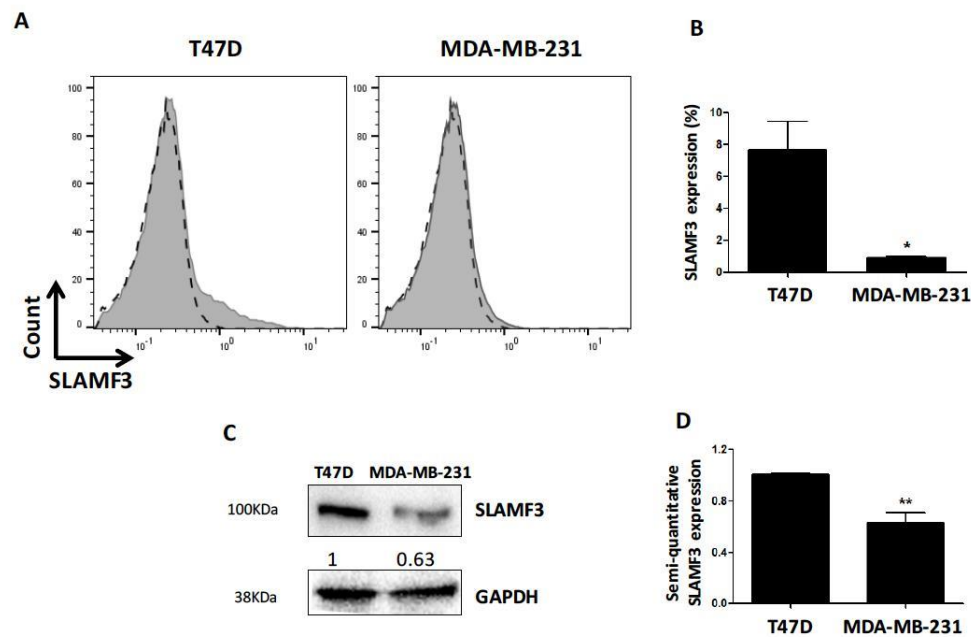


**Figure 2:** Expression of SLAMF3 in human breast epithelial cells. (A) Analysis of SLAMF3 expression by flow cytometry in T47D and MDA-MB-231 human BC cell lines. SLAMF3 staining (in grey) is overlaid by the negative control (in dashed lines). Representative of three independent experiments. SLAMF3 expression (mean  $\pm$  SEM) as percent positive cells (%). ( $N=3$ ;  $*p<0.05$ ). (C) Western blot analysis of proteins extracted from T47D and MDA-MB-231 cells stained with specific antibody directed against SLAMF3 (mAb K12) or an anti-GAPDH antibody. Representative blots of three independent experiments. The density as measured by semi-quantitative analysis of bands is also presented. (D) SLAMF3 expression (mean  $\pm$  SEM) from three independent experiments ( $N=3$ ;  $**p<0.01$ ).

### 2.3. SLAMF3 decreases basal Ca<sup>2+</sup> influx only in invasive breast cancer cells

Previous studies have demonstrated that SLAMF3 is a regulator of Ca<sup>2+</sup> entry in immune cells [27]. Moreover, Ca<sup>2+</sup> homeostasis has been shown to regulate various cellular processes [4] and in particular, metastatic mechanisms [5]. Identification of SLAMF3 expression by human BC cells encouraged us to investigate whether SLAMF3 regulates Ca<sup>2+</sup> influx in human BC cells. We determined the Ca<sup>2+</sup> basal entry by Mn<sup>2+</sup> quenching with Fura Red in both T47D and MDA-MB-231 cell lines overexpressing SLAMF3 ectopically. First, we confirmed that forced expression of SLAMF3 resulted in higher level

of SLAMF3 mRNA and protein than mock plasmid in T47D (increase by  $29 \pm 1375.508$  fold) and MDA-MB-231 cells (increase by  $43.733 \pm 15.102$  fold) (Figure 3A-B-C). We found that the ectopic SLAMF3 expression reduced Mn<sup>2+</sup> quenching slope significantly from  $-0.3345 \pm 0.0299$  to  $-0.1665 \pm 0.0213$  (n=74 and 81 cells respectively; p<0.001) only in invasive MDA-MB-231 cells (Figure 3E). In contrast, SLAMF3 overexpression failed to modify Mn<sup>2+</sup> slope quenching in non-invasive T47D cells (from  $-0.3914 \pm 0.0355$  to  $-0.4059 \pm 0.0387$ ; n=97 and 118 cells respectively; p>0.05; Figure 3D). Our data suggest that SLAMF3 controls basal Ca<sup>2+</sup> influx only in invasive breast cancer cells.

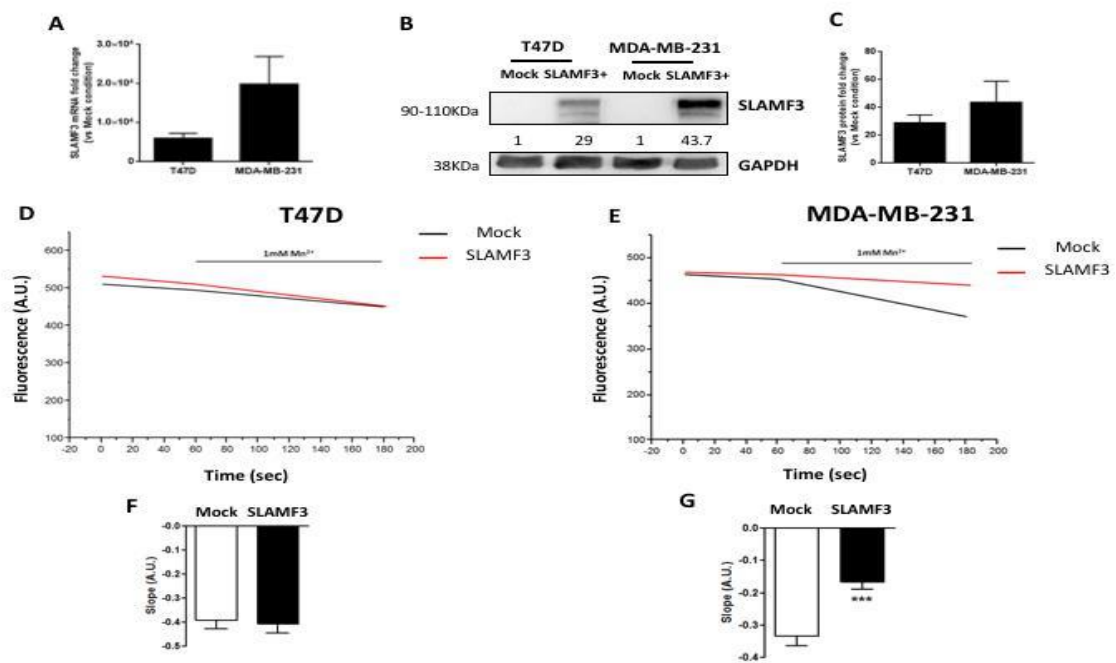


**Figure 3:** Effect of SLAMF3 overexpression on basal Ca<sup>2+</sup> entry in human breast epithelial cells. (A-C) Confirmation of induction of SLAMF3 overexpression by quantitative RT-PCR (A) and Western blot (B-C), in T47D and MDA-MB-231 cell lines. For quantitative RT-PCR experiments, results (mean ± SEM) from three independent experiments are presented. For Western blot, representative of two independent experiments (B), and fold changes (mean ± SEM, N=2 independent experiments) in SLAMF3 expression (C) are presented (Mock: free-plasmid transfected cells; SLAMF3+: SLAMF3- plasmid transfected cells, GAPDH: protein loading control). (D-G) Mean traces and quantification of Mn<sup>2+</sup> quenching in T47D (D, F) and MDA-MB-231 (E, G) cells transfected with SLAMF3 plasmid (SLAMF3: n=97; n=74, respectively) or free plasmid (Mock; n=118; n=81, respectively). Representative data (D-E) and mean ± SEM (F-G) values from three independent experiments are presented. \*\*\* p<0.001.

#### 2.4. SLAMF3 decreases the cell motility but not cell proliferation only in MDA-MB-231 cells

Ion channels and in particular Ca<sup>2+</sup> are known to be altered in numerous cancers and play an essential role in cell proliferation and migration [29]. Moreover, SLAMF3 has been demonstrated as an inhibitor of cell proliferation and migration in HCC [21, 22]. Interestingly, SLAMF3 overexpression significantly reduced the cell motility (Figure 4A). Indeed, wound-healing area is larger in SLAMF3-over expressed condition at 24 hours (from 69.54 ± 3.84% to 82.85 ± 2.93% in Mock and SLAMF3 conditions, respectively) and at 48 hours (from 33.17 ± 7.25% to 56.36 ± 3.69% respectively; N=3; p<0.05; Figure 4B). Migration assays were performed by using transwell

system 48 hours post transfection of SLAMF3 and confirmed the lower cell motility of MDA-MB-231 cells overexpressing SLAMF3 (Figure 4C). In fact, migrating cell number was significantly decreased by 44.91 ± 5.77% in SLAMF3 overexpressing conditions (N=3; p<0.001) compared to mock (Figure 4D). As increased cell migration could be also attributed to proliferative capacity of cells, transfected cells were subjected to colorimetric MTT test assay. MTT assay confirmed that cell proliferation was similar in both the conditions 48 hours post transfection of SLAMF3 (Figure 4E), as well as at 24, 72 and 96 hours (supplementary figure). Our results thus suggest that SLAMF3 represses cell migration in invasive BC cells without affecting cell proliferation.

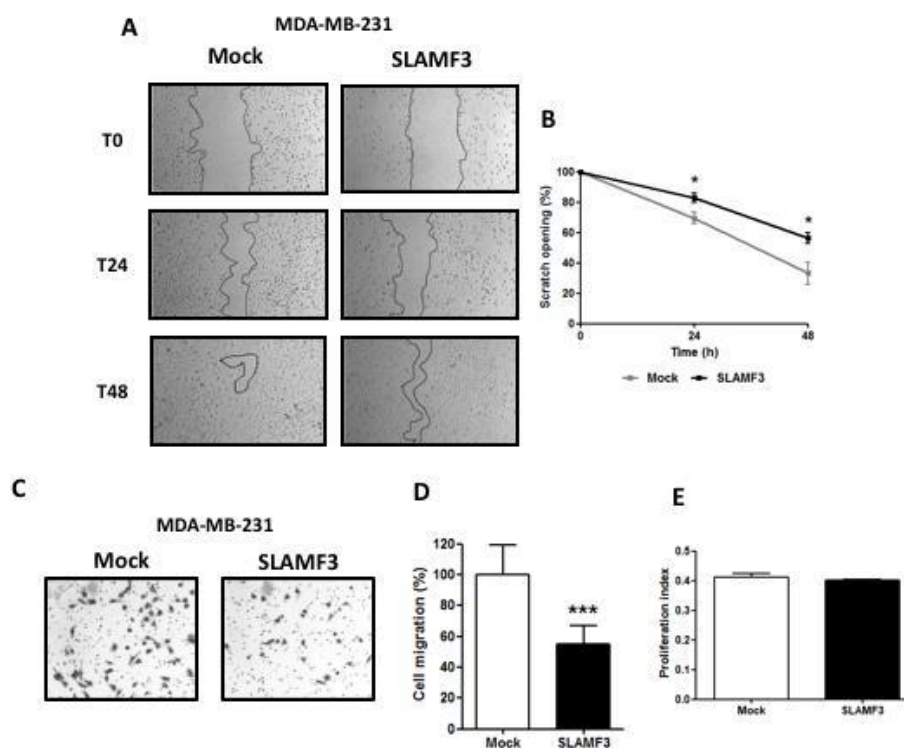


**Figure 4:** SLAMF3 decreases MDA-MB-231 cell motility but not proliferation. Migratory capacity of SLAMF3 overexpressing MDA-MB-231 cells compared to Mock transfected cells in wound healing (A and B) and transwell migration assays (C and D): (A) photographs of same areas performed at 0 (T0), 24 and 48 hours; (B) The migratory index corresponding

to the normalization of the area scratched. Values are presented as percentage compared to T0 and presented as the mean  $\pm$  SEM (N=3; \* $p$ <0.05); (C) Transwell migration assays were performed in MDA-MB-231 cells 48 hours post transfection of SLAMF3. Photographs of one of the three experiments (C) and (D) quantification (mean  $\pm$  SEM) of cell migration (n=180; N=3; \*\*\* $p$ <0.001). (E) No effect of seeding was observed on cell proliferation as analyzed by MTT test in MDA-MB-231 cells transfected with SLAMF3 plasmid (SLAMF3) or free plasmid (Mock), N=3. Associated Supplementary figure: analysis of cell proliferation by MTT assays in MDA-MB-231 cells at 24, 48, 72 and 96 hours post transfection with SLAMF3 plasmid (SLAMF3) or free plasmid (Mock) Results presented as the mean  $\pm$  SEM (N=3; ns:  $p$ >0.05).

### 2.5. SLAMF3 decreases store-operated Ca<sup>2+</sup> entry through STIM1 expression in invasive MDA-MB-231 breast cancer cells

We demonstrated that the ectopic expression of SLAMF3 reduces basal Ca<sup>2+</sup> entry and cell migration in invasive BC cells. ORAI1 and STIM1 regulate store-operated Ca<sup>2+</sup> entry and are essential for BC cell migration and metastasis [20], while ORAI3 and STIM1 are essential for non-invasive BC cell proliferation [30]. First, we determined the effect of SLAMF3 overexpression on STIM1 expression by quantitative RT-PCR in non-invasive T47D and in invasive MDA-MB-231 cell lines, respectively (Figure 5A-B). We observed that overexpression of SLAMF3 led to significant decrease in STIM1 expression (by  $48 \pm 14.5\%$ ) only in MDA-MB-231 (N=5;  $p$ <0.05) but not in T47D cells (STIM1 expression changed from  $1 \pm 0.252\%$  to  $1.204 \pm 0.248\%$ ; N=5; NS). Moreover, neither ORAI1 nor ORAI3 expression was modified in our conditions in T47D cells (N=5;  $p$ >0.05; Figure 5C) or MDA-MB-231 cells (N=5;  $p$ >0.05; Figure 5D). These observations prompted us to quantify the protein level of STIM1 by western blot. The overexpression of SLAMF3 decreased STIM1 proteins level by  $37.25 \pm 9.55\%$  (N=4;  $p$ <0.05; Figure 5E). We then

recorded SOCE in invasive MDA-MB-231 cells 48 hours post transfection with SLAMF3 plasmid by using Ca<sup>2+</sup> imaging assays. We exposed cells to thapsigargin (1  $\mu$ M) in a Ca<sup>2+</sup>-free solution to deplete intracellular Ca<sup>2+</sup> stores and activated store-operated Ca<sup>2+</sup> channels. SOCE-dependent influx was then measured in the presence of 10 mM extracellular Ca<sup>2+</sup>. We observed a reduction in SOCE ( $31.03 \pm 6.86\%$  reduction) in SLAMF3 overexpressed cells compared to Mock ones (SOCE changed from  $15.18 \pm 0.66\%$  to  $10.47 \pm 1.04\%$ ; n=40 and n=39 respectively; N=3;  $p$ <0.001; Figure 5F-G).

SLAMF3 activation negatively controls MAPK ERK 1/2 and JNK activation as reported in HCC [21]. Constitutive activity of MAPK has been reported in aggressive triple-negative BC. To explore the possible link between the SLAMF3 over-expression, SOCE and MAPK pathway, we analyzed ERK1/2 expression and activity in SLAMF3 over-expressing invasive MDA-MB-231 cell lines. We found that SLAMF3 decreased the expression (reduction up to  $18 \pm 3\%$ ,  $p$ <0.05) and phosphorylation of ERK1/2 (reduction up to  $24 \pm 1.76\%$ ; N=3;  $p$ <0.05; Figure 5 H-I).

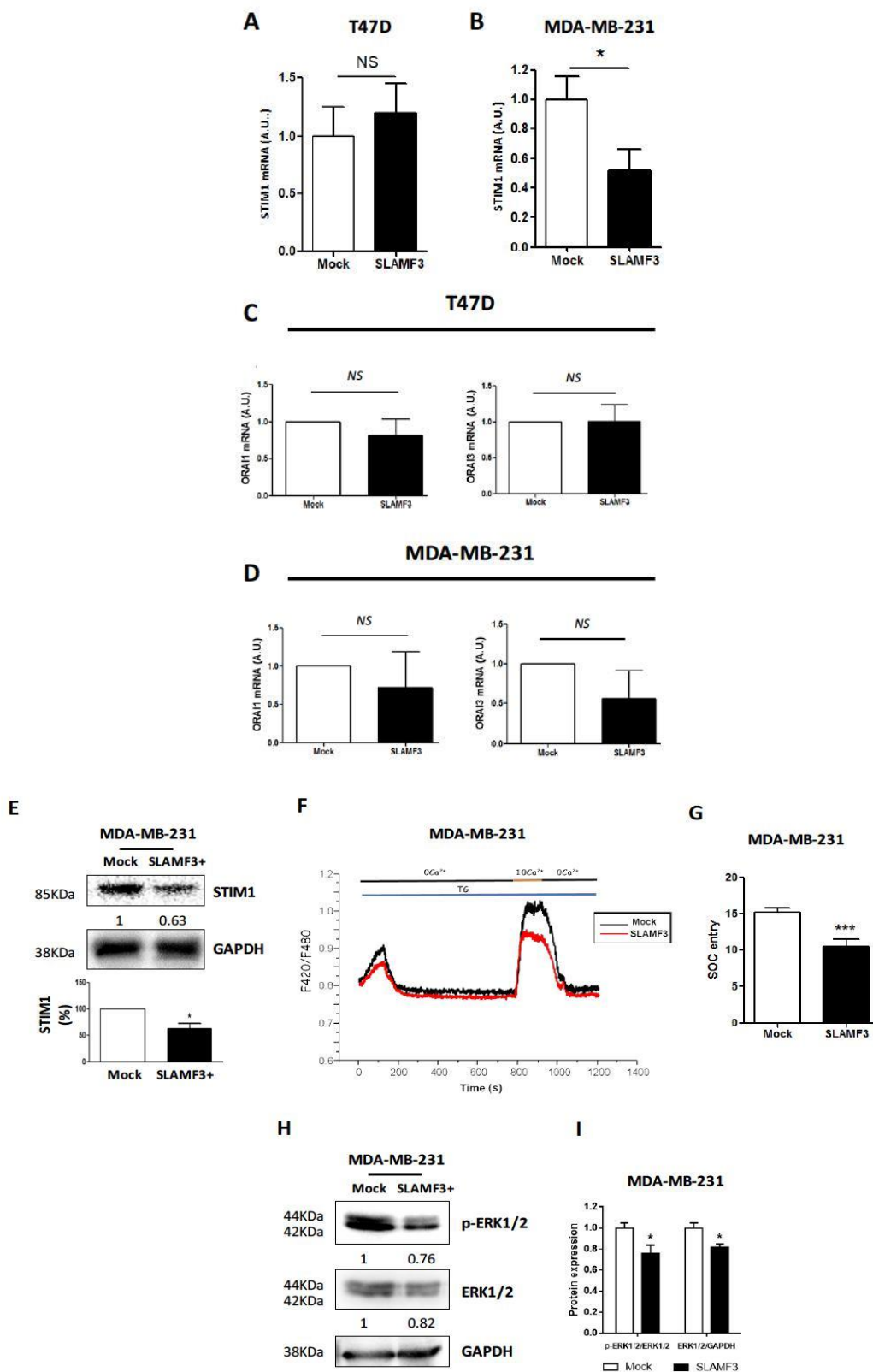




**Figure 5:** SLAMF3 decreases store-operated Ca<sup>2+</sup> entry (SOCE) through STIM1 expression in invasive MDA-MB-231 breast cancer cells. (A-B) Effect of SLAMF3 overexpression on STIM1 expression as analyzed by quantitative RT-PCR in T47D (A) and MDA-MB-231 (B) cells transfected with SLAMF3 plasmid (SLAMF3) or free plasmid (Mock). The results are presented as the mean  $\pm$  SEM from five independent experiments (N=5; ns:  $p > 0.05$  for T47D and  $*p < 0.05$  for MDA-MB-231). (C-D) Expression of ORAI1 and ORAI3 mRNA in T47D (C) and MDA-MB-231 (D) cells transfected with SLAMF3 plasmid (SLAMF3) or free plasmid (Mock) (mean  $\pm$  SEM, N=5, ns:  $p > 0.05$ ). (E) Western blot analysis of STIM1 in protein extracts from MDA-MB-231 cells transfected with SLAMF3 plasmid (SLAMF3+) or free plasmid (Mock). GAPDH was used as a protein loading control. Representative blot and % reduction in STIM1 expression (mean  $\pm$  SEM, N=4 independent experiments,  $*p < 0.05$ ). (F) Mean traces of SOCE in SLAMF3-transfected cells (SLAMF3) or free plasmid (Mock) transfected cells and (G) quantification of the Ca<sup>2+</sup>-bound Fura Red fluorescence showing thapsigargin-activated (TG) SOCE in MDA-MB-231 cells transfected with SLAMF3 plasmid (SLAMF3; n=39 analyzed cells) or free plasmid (Mock; n=40 analyzed cells) in three independent experiment (N=3;  $*** p < 0.001$ ). (H) Western blot and semi-quantitative, analysis of protein extracts from MDA-MB-231 cells transfected with SLAMF3 plasmid (SLAMF3+) or free plasmid (Mock). Membranes were probed with mAbs against ERK1/2 and phospho-ERK1/2. GAPDH was used as a protein loading control. Data from one of three independent experiments is presented. (I) The calculated ratio of phospho-ERK1/2/ERK1/2 and ERK1/2/GAPDH (mean  $\pm$  SEM, N=3 independent experiments,  $*p < 0.05$ ).

### 3. Discussion

Recently, we identified the expression of SLAMF3 in hepatocytes. We highlighted its implication in controlling the proliferation, apoptosis and migration of HCC [21]. The re-introduced expression of SLAMF3 in HCC cells reduced the proliferative index and motility, induced apoptosis by a caspases-dependent manner and blocked the cell cycle [21, 22]. These effects were also confirmed in vivo in mice where neither tumor appearance nor tumor progression were observed when HCC cells overexpressing SLAMF3 were xenografted. The potential tumor suppressive role of SLAMF3 obtained in HCC prompted us to check the implication of this receptor in other solid tumors. In the present pilot study realized on 14 BC patients, we evidenced, for the first time, the expression of SLAMF3 in epithelial BC cells.

BC cells originate as epithelial cells to form the primary tumor, which might acquire cellular motility and form a

more invasive secondary tumor [31]. Several mechanisms and factors have been reported to explain the invasiveness behavior of cancerous cells. In the present work, we show that SLAMF3 is expressed at very low level at cancerous cell surface compared to the total SLAMF3 protein at intracellular level. This result suggests possible regulatory factors in cancerous cells that prevent the membrane expression of SLAMF3 and its tumor suppressive effect. This mechanism might explain, in part, the immune escape behavior of cancerous cells against the processes that control cell proliferation and apoptosis. In addition, the baseline expression of SLAMF3 is different in invasive and non-invasive BC cells. SLAMF3 expression appears to be significantly lower in invasive MDA-MB-231 cells compared to non-invasive T47D cells. It has been reported that SLAMF3 activation through homophilic interactions controls negatively MAPK ERK 1/2 and JNK activation [21]. The MAPK Ras-ERK pathway is dysregulated in approximately one third of human cancers, particularly

those of epithelial origin. In aggressive triple-negative BC, most tumors display increased constitutive phosphorylation of MEK1/2 and ERK1/2 [32]. Taken together, our results suggest that reduced membrane expression of SLAMF3 in cancerous breast cells might prevent SLAMF3 homophilic interactions and its ability to control MAPK pathway. In this sense, we checked the ERK1/2 activation state in SLAMF3 overexpressed BC cells. Ectopic introduction of high SLAMF3 expression decreased ERK protein expression and its activation. Considering the fact that STIM1 regulates Ca<sup>2+</sup> entry in mammary cells, our results highlight a new pathway by which SLAMF3 controls ERK1/2 activation by controlling SOCE (see graphical abstract).

During carcinogenesis, Ca<sup>2+</sup> signaling in some malignant cells is significantly remodeled in a way that compromises normal physiological functions. Various studies strongly suggest the important role of Ca<sup>2+</sup> remodeling in carcinogenesis process [33]. Remodeling of Ca<sup>2+</sup> signaling is the prime reason for such a transformation in cell behavior and is caused by genetic as well as epigenetic factors [4]. In fact, in cancerous cells, Ca<sup>2+</sup> remodeling promotes activation of Ca<sup>2+</sup>-dependent transcription factors such as the Nuclear Factor of Activated T cells (NFAT), c-myc, c-jun and c-fos. All these factors promote hypertrophic growth via induction of G1 and G1/S transition by cyclins (D and E) associated to cyclin-dependent kinases (CDK2 and CDK4) [34]. In addition, this remodeling is implicated in conferring apoptosis resistance to cancerous cells and in promoting cell migration and metastasis. In breast cells, SOCE is mediated by the Ca<sup>2+</sup> sensor STIM1 [6–8] and the pore-forming proteins ORAI1/3 [9–12]. SOCE and its STIM/ORAI constituents have emerged as important regulators of malignant cell migration. Enhanced STIM1-ORAI1-mediated SOCE

promotes higher rate of focal adhesion turnover and fast migration of metastatic BC cells via activation of GTPases Ras and Rac [20]. Here, we provide evidence on the negative regulation of SLAMF3 towards STIM1 expression. On one hand, it is further demonstrated that metastasis potency of MDA-MB231 is drastically reduced upon STIM1 or ORAI1 knockdown [35]. On the other hand, we show that overexpression of SLAMF3 decreases the STIM1 expression selectively in invasive MDA-MB-231 cell line. Taken together, our results strongly support the potential role of SLAMF3 expression in determining the metastatic behavior of BC.

Our results suggest that SLAMF3 controls more efficiently the motility of invasive cells by reducing the STIM1 expression, which is highly expressed in cancerous cells. However, the effect of SLAMF3 on SOCE is weak in non-invasive cells compared to its effect in invasive cells. This result strongly suggests that SLAMF3 might regulate the Ca<sup>2+</sup> remodeling by controlling the STIM1 expression.

Metastatic dissemination from the primary tumor site to multiple tissues is the main cause of mortality in cancer. Tumor cells become invasive by acquiring high migratory potential along with the increased ability to degrade ExtraCellular Matrix (ECM). Ca<sup>2+</sup> signaling is critical for regulating the cell migration and invasion. In malignant cells Ca<sup>2+</sup> signaling is remodeled in such a way that it promotes the turnover of focal adhesions, enhances contractile forces and facilitates proteolysis of ECM components [36]. In our work, we report that high expression of SLAMF3 decreases the motility of the invasive cells and slow down the repopulation of empty spaces in the performed wound test. Similarly, this expression modulates the cell migration through the transwell pores and confers invasive cells a decreased ability to

migrate. However, the links between the expression and function of certain Ca<sup>2+</sup> permeable channels, and cancer cell migration, invasion and metastasis remain unclear [37, 38].

The SOC constituents, STIM1 and ORAI1, are reported to be implicated in the enhanced migration of BC cells [19, 34]. In addition to ORAI channels, it has been reported that high pro-migratory and pro-invasion potentials have been also ascribed to TRPV1, TRPV2, TRPV6 and TRPM8 channels. Higher expression of TRPV2 in prostate cancer cells or TRPM8 in squamous cell carcinoma correlated with the induction of MMP-2, MMP-9 and cathepsin B [39, 40]. Additional analysis is needed to explore the effect of SLAMF3 expression on the expression of metalloproteases and their enzymatic activity, which might explain in part modulatory effect of SLAMF3 on the migratory and motility behavior of BC cells.

Altogether, our results describe, for the first time, the expression of the SLAMF3 in mammary tissues and its potential effect on STIM1/SOCE-dependent Ca<sup>2+</sup> influx and suggests its implication in the regulation of motility and migration in BC cells. More importantly, a pilot study based on resection samples from 14 women with BC was realized by quantifying SLAMF3 and STIM1 mRNA expression. Our results evidenced potential inverse correlation between the expression of SLAMF3 and STIM1 in the same tissue sample. This result suggests reciprocal regulation of SLAMF3 and STIM1 expression, which promotes cancer cell escape, apoptosis resistance, aggressive behavior and metastasis propagation. Additional experiments are required to identify the molecular actors implicated in this negative regulation. Moreover, the present study must be complemented with a

bigger cohort of patients with different stages of BC and thorough analyses of role of SLAMF3-STIM1 according to the cancer stage, treatment and global survival. The present work also suggests that the SLAMF3 loss, combined with the acquired high expression of STIM1 in epithelial mammary cells could be used as a potential diagnosis marker for tumor transformation. Moreover, restoration of high membrane expression of SLAMF3 in cancerous cells, which controls the Ca<sup>2+</sup> influx and prevents, in part, the metastatic cell migration could be exploited for the anti-cancer therapy.

## 4. Material and Methods

### 4.1. Cell lines

Human breast epithelial cancer cell lines T47D and MDA-MB-231 were obtained from ATCC numbers HTB-133 and HTB-26 respectively. T47D and MDA-MB-231 BC cells were maintained in Dulbecco's Modified Eagle's Medium (DMEM) supplemented with 10% Fetal Calf Serum (FCS), 2 mM of L-Glutamine and 100 µg/mL of penicillin/streptomycin (EUROBIO, Les Ulis, France). Cells were grown at 37°C in a humidified incubator with 5% CO<sub>2</sub>.

### 4.2. Patient samples

Fourteen (n=14) pairs of tumor (T) tissues and matched peritumor (pT) tissues were obtained from BC patients undergoing surgical resection at Amiens University Hospital (Amiens, France). Our protocol was approved by the local independent ethics committee (Comité de Protection des Personnes (CPP) Nord-Ouest, Amiens, France) (Table 1). Patients were provided with information on the study procedures and objectives, and all gave their written consent for the participation. Total mRNA was extracted using specific kits and used to test SLAMF3 and STIM1 expression.

Patients	Age	Metastasis	Infiltration	Grade
1	41	Y	Y	II
2	41	N	Y	III
3	70	Y	Y	III
4	49	Y	Y	I
5	50	Y	Y	II
6	50	N	Y	II
7	49	Y	Y	III
8	47	N	Y	II
9	39	N	Y	I
10	31	N	Y	II
11	45	Y	Y	I
12	NC	Y	Y	III
13	NC	Y	Y	III
14	NC	Y	Y	III

Age: Years ; NC: non-communicated ; Y: yes ; N : no.

**Table 1:** The age and characteristics of the the patients whose samples were used in our study.

#### 4.3. Flow cytometry analysis

Cells were collected in cold PBS/0.5% BSA, washed and then incubated with fluorescent- 346 conjugated primary or isotype-matched antibodies for 20 min at 4°C. Following extensive washing (with PBS), cells were fixed (in 1% paraformaldehyde) and 5,000 viable events were analyzed (MACSQuant cytometer running MACSQuantify software; Miltenyi Biotec, Paris, France). Results were expressed as the percentage of positive cells and the MFI ratio (the MFI obtained in the presence of specific antibody divided by the MFI obtained with a non-specific, matched isotype). For SLAMF3 staining, monoclonal FITC-coupled SLAMF3 antibody (clone HLy9.1.25) and the corresponding IgG1-FITC isotype were used (purchased from AbD Serotec) at 1/10 dilution.

#### 4.4. Western blot analysis

Cells ( $3 \times 10^6$  per assay) were lysed in Nonidet P40 (NP40) buffer (1% NP40, 50 mM Tris pH 7.5, 10% glycerol, 150 mM NaCl, 1 mM EDTA, 100 mM Na<sub>3</sub>VO<sub>6</sub>, 0.5 mM phenylmethanesulphonyl fluoride (PMSF), 5 mg/mL aprotinin, 5 mg/ml leupeptin and 2 mg/mL pepstatin) containing protease and phosphatase inhibitors (Roche, Meylan, France). Equal amounts of each (total extracted) protein sample were separated by SDS-PAGE. Proteins were transferred on to PVDF membranes (Bio-Rad, Munich, Germany). Following blockade step, blots were incubated with primary antibodies against SLAMF3 (monoclonal clone K12 or 3H1998; Santa Cruz) used at 1/200; STIM1 (monoclonal anti- STIM1 (clone D88E10) used at 1/1000; ERK1/2 (monoclonal, clone 137F5), phospho-ERK1/2 (monoclonal, Thr202/Tyr204; clone

D13.14.4E) used at 1/1000 and GAPDH (monoclonal, clone D16H11) used at 1/1000 all purchased from Cell Signaling Tech. The secondary antibodies were HRP- coupled anti-mouse and anti-rabbit used at 1/10000 (Santa Cruz Biotechnology). Blots were developed with the Enhanced ChemiLuminescence (ECL) system (Bio-Rad, Munich, Germany).

#### 4.5. RNA extraction, quantitative real time PCR and plasmid construction

Total RNA was extracted using RNeasy kit (Qiagen, Courtaboeuf, France) and 1 µg of total RNA was reverse transcribed into cDNA with multiscribe reverse transcriptase (Applied Biosystems, Villebon-sur-Yvette, France). Quantitative PCR was performed according to the Taqman Gene Expression protocol (Applied Biosystems) using SLAMF3 primers previously described [21]. The transcription of *GAPDH* (*HUMAN GAPDH (DQ) Mix (20x)*, Applied Biosystems®) was measured as an endogenous housekeeping control. For STIM1 quantification, SYBRGreen gene expression protocol was used with the following primers: STIM1 and GAPDH [28]. Transfection of SLAMF3 was performed with pIRES-eGFP-SLAMF3 plasmid in BC cells and with pIRES-eGFP as negative control. The pIRES-eGFP-SLAMF3 plasmid permits both the gene of interest and EGFP gene to be translated from a single bicistronic mRNA.

For SLAMF3 over-expression, 0.3 x 10<sup>6</sup> of T47D or MDA-MB-231 cells were first seeded into six- well plates for 24 hours prior to transfection. Cells were transfected with 0.5 µg of plasmid DNA using the FuGENE HD Transfection Reagent Kit (Promega, Charbonnières-les-bains, France) according to the manufacturer's instructions and were incubated for 48 hours at 37°C before all experiments.

#### 4.6. Calcium imaging

After transfection, 0.1 x 10<sup>6</sup> MDA-MB-231 cells were directly seeded on glass coverslips, and grown for an additional 48 hours. Cells were then incubated in culture medium containing 2 µM Fura Red/AM (Sigma Aldrich) for 45 minutes at 37°C before Ca<sup>2+</sup> measurement. After Fura Red/AM loading, cells were washed and kept in extracellular saline solution containing the Ca<sup>2+</sup>-free solution (in mM): NaCl 145, KCl 5, MgCl<sub>2</sub> 1, HEPES-NaOH 10, glucose 5 and EGTA 1 at pH 7.4 The glass coverslip was mounted in a chamber on a Zeiss (Charly-le-Roi, France) microscope equipped for fluorescence. Fura Red/AM fluorescence was collected upon alternate excitation at 420 nm for the Calcium-bound Fura Red and 480 nm for the Calcium-free Fura Red, using a monochromator (Polychrome IV; TILL Photonics, Planegg, Germany), and captured by a Cool SNAPHQ camera (Princeton Instruments, Evry, France) after filtration through a long-pass filter (660 nm). Metafluor software (version 7.0, Molecular Devices, St. Grégoire, France) was used for acquisition and analysis. The [Ca<sup>2+</sup>]<sub>i</sub> variation is represented as the mean of the fluorescence ratio (F<sub>405</sub>/F<sub>480</sub>). We used classical protocol for measurement of SOCE. Cells were perfused by Thapsigargin at 1 µM in free calcium extracellular medium to induce reticular calcium release, the cells were then perfused by extracellular medium containing 10 mM Ca<sup>2+</sup>. SOCE was quantified by the formula  $\Delta\text{Fluo} = F_{\text{max}} - F_{\text{min}}$  of the measured fluorescence after the excitation at 420 nm for calcium-bound Fura Red, during the perfusion of the 10 mM Ca<sup>2+</sup> (F<sub>Max</sub>) followed by 0 mM Ca<sup>2+</sup> (F<sub>min</sub>). All recordings were performed at room temperature. Cells were continuously perfused with the saline solution and chemicals were added as indicated. Thapsigargin was purchased from CalbioChem. The flow rate of the whole

cell chamber perfusion system was set to 1 mL/min and the chamber volume was 500  $\mu$ L.

#### 4.7. Manganese quenching

To estimate divalent influx through the plasma membrane, we used the Mn<sup>2+</sup>-induced quenching of Fura Red approach. T47D and MDA-MB-231 cells ( $0.1 \times 10^6$ ) were seeded on glass coverslips after transfection. Briefly, cells were loaded with 2  $\mu$ M Fura Red/AM (Sigma-Aldrich Chemie, St Quentin Fallavier, France) in the growth medium at 37°C for 45 minutes. After a period of one minute, the Ca<sup>2+</sup> (2 mM) present in the perfusion medium was replaced with 1 mM Mn<sup>2+</sup>. To measure Mn<sup>2+</sup> flux, cells were excited at 420 nm and the emission signal was recorded at 660 nm at one second intervals. The Mn<sup>2+</sup> influx was estimated from the quenching of 420 nm fluorescence.

#### 4.8. Proliferation assay

The methylthiazole tetrazolium (MTT) salt assay was used to check the anti-proliferative effect of SLAMF3 expression in BC cells. At 24, 48, 72 and 96 hours, transfected cells were rinsed and exposed for 1 hour to a 0.5 mg/mL solution of MTT suspended in culture medium. Reduced purple Formazan crystals were extracted with DMSO: Isopropanol (50:50) and analyzed at a wavelength of 570 nm.

#### 4.9. Migration assays

Cell migration was assessed using a wound healing assay and Boyden chambers test. 24 hours after transfection, MDA-MB-231 cells were scratched with a sterile micropipette tip and then washed to remove floating cells and debris. The cells were cultured in complete medium and wound closure was photographically monitored at 0 hour (T0), 24 hours (T24) and 48 hours (T48) after the scratch. Wound closure analyses were performed by

measuring wound area. Wound area at 24 hours and 48 hours was normalized by the wound opening at T0 for each condition. For the Boyden chambers tests,  $4 \times 10^4$  MDA-MB-231 transfected cells were seeded in the upper side of Boyden chambers (BD Biosciences, 24-wells plates, 8  $\mu$ m pore size) in 200  $\mu$ L of DMEM 10% FCS and the lower were filled with 800  $\mu$ L of DMEM 10% FCS. Cells were incubated for 16 hours at 37°C. Then, cells were washed twice with PBS, fixed with methanol 10min, stained with crystal violet 5 minutes and washed thrice in water. Cells remaining in the upper side were removed using a swab. Migrating cells were observed with an inverted microscope. The number of migrating cells was counted in 20 separate fields for three Boyden chambers per condition. For migration analysis, the number of migrating cells of SLAMF3 condition was normalized by the number of Mock migrating cells.

#### 4.10. Statistical analysis

Independent Student's t-test was used to compare SLAMF3 and STIM1 mRNA expression in T and pT samples. Comparison between STIM1 and SLAMF3 mRNA expressions was performed by the Spearman correlation test. The Mann-Whitney U test was also used to compare STIM1 or SLAMF3 mRNA expression in Mock and overexpressing SLAMF3 cells. Unless otherwise stated, results are expressed as the mean  $\pm$  SEM. Statistical analysis were performed with Sigma Plot software (version 11.0, Systat Software Inc., San Jose, CA, USA). The threshold for statistically significant was set to  $p < 0.05$  for all analysis.

### 5. Conclusions

Our results indicate that SLAMF3 reduces SOCE and therefore migration of BC cells by decreasing the STIM1

expression. SLAMF3 could be used as a predictive marker of BC evolution and aggressiveness.

### Funding

All experiments were financed by Inserm 1247 and LPCM UR-4667-UPJV funds.

### Acknowledgements

We thank Pr Loïc Garçon and Dr Hakim Ouled-Haddou (Hemateam, CURS-UPJV) for analysis and logistic help for flow cytometry as well as ICAP platform (Cytométrie, Centre universitaire de recherché en santé CHU Amiens) for the help.

### Conflicts of Interest

The authors have no financial conflicts of interest.

### Ethical Approval and consent to participate:

Our study was a retrospective essay. Our protocol was approved by the local independent ethics committee (Comité de Protection des Personnes (CPP) Nord-Ouest, Amiens, France) and all patients were provided with information on the study procedures and objectives, and all gave their written consent to participating.

### Consent for publication

All authors of this work have agreed to the publication.

### References

1. Bray F, GLOBOCAN 2012 v1.0 Cancer Incidence and Mortality Worldwide: IARC CancerBase No. 11 (2018).
2. de Boer M, van Dijck J a. a. M, Bult P, et al. Breast cancer prognosis and occult lymph node metastases isolated tumor cells and micrometastases. *J Natl Cancer Inst.* 102 (2010): 410-425.
3. Lastraioli E, Iorio J, Arcangeli A, Ion channel expression as promising cancer biomarker. *Biochim Biophys Acta.* 1848 (2015): 2685-2702.
4. Monteith GR, McAndrew D, Faddy HM, et al. Calcium and cancer: targeting Ca<sup>2+</sup> transport. *Nat Rev Cancer* 7 (2007): 519-30.
5. Chen YF, Chen YT, Chiu WT, et al. Remodeling of calcium signaling in tumor progression. *J Biomed Sci* 20 (2013): 23.
6. Liou J, Kim ML, Heo WD, et al. STIM is a Ca<sup>2+</sup> sensor essential for Ca<sup>2+</sup>-store-depletion-triggered Ca<sup>2+</sup> influx. *Curr Biol CB* 15 (2005): 1235-1241.
7. Roos J, DiGregorio PJ, Yeromin AV, et al. STIM1 an essential and conserved component of store-operated Ca<sup>2+</sup> channel function. *J Cell Biol* 169 (2005): 435-445.
8. Zhang SL, Yu Y, Roos J, Kozak JA et al. STIM1 is a Ca<sup>2+</sup> sensor that activates CRAC channels and migrates from the Ca<sup>2+</sup> store to the plasma membrane. *Nature* 437 (2005): 902-905.
9. Faouzi M, Hague F, Potier M, et al. Down-regulation of Orai3 arrests cell-cycle progression and induces apoptosis in breast cancer cells but not in normal breast epithelial cells. *J Cell Physiol* 226 (2011): 542-51.
10. Feske S, Gwack Y, Prakriya M, et al. A mutation in Orai1 causes immune deficiency by abrogating CRAC channel function. *Nature* 441 (2006): 179-185.
11. Vig M, Peinelt C, Beck A, et al. CRACM1 is a plasma membrane protein essential for store-operated Ca<sup>2+</sup> entry. *Science* 312 (2006): 1220-1223.
12. Zhang SL, Yeromin AV, Zhang XHF, et al. Genome-wide RNAi screen of Ca(2+) influx identifies genes that regulate Ca(2+) release-activated Ca(2+) channel activity. *Proc Natl Acad Sci USA* 103 (2006): 9357-9362.

13. Cheng H, Wang S, Feng R. STIM1 plays an important role in TGF- $\beta$ -induced suppression of breast cancer cell proliferation. *Oncotarget* 7 (2016): 16866-16878.
14. Kim JH, Lkhagvadorj S, Lee MR, et al. Orai1 and STIM1 are critical for cell migration and proliferation of clear cell renal cell carcinoma. *Biochem Biophys Res Commun* 448 (2014): 76-82.
15. Umemura M, Baljinnyam E, Feske S, et al. Store-operated Ca<sup>2+</sup> entry (SOCE) regulates melanoma proliferation and cell migration. *PloS One* 9 (2014): e89292.
16. Wu Z, Qing J, Xia Y, et al. Suppression of stromal interaction molecule 1 inhibits SMMC7721 hepatocellular carcinoma cell proliferation by inducing cell cycle arrest. *Biotechnol Appl Biochem* 62 (2015): 107-111.
17. Xia J, Wang H, Huang H, et al. Elevated Orai1 and STIM1 expressions upregulate MACC1 expression to promote tumor cell proliferation metabolism migration and invasion in human gastric cancer. *Cancer Lett* 381 (2016): 31-40.
18. Zhang Z, Liu X, Feng B, et al. STIM1 a direct target of microRNA-185 promotes tumor metastasis and is associated with poor prognosis in colorectal cancer. *Oncogene* 34 (2015): 4808-4820.
19. Wang Y, Wang H, Pan T, et al. STIM1 silencing inhibits the migration and invasion of A549 cells. *Mol Med Rep* 16 (2017): 3283-3289.
20. Yang S, Zhang JJ, Huang XY. Orai1 and STIM1 are critical for breast tumor cell migration and metastasis. *Cancer Cell* 15 (2009): 124-134.
21. Marcq I, Nyga R, Cartier F, et al. Identification of SLAMF3 (CD229) as an Inhibitor of Hepatocellular Carcinoma Cell Proliferation and Tumor Progression. *PLoS ONE* (2013): 8.
22. Bouhlal H, Ouled-Haddou H, Debuyscher V, et al. RB/PLK1-dependent induced pathway by SLAMF3 expression inhibits mitosis and control hepatocarcinoma cell proliferation. *Oncotarget* 7 (2016): 9832-9843.
23. Calpe S, Wang N, Romero X, et al. The SLAM and SAP Gene Families Control Innate and Adaptive Immune Responses. *Advances in Immunology* (2008): 177-250.
24. Romero X, Zapater N, Calvo M, et al. CD229 (Ly9) lymphocyte cell surface receptor interacts homophilically through its N-terminal domain and relocalizes to the immunological synapse. *J Immunol Baltim Md* 174 (2005): 7033-7042.
25. Martin M, Romero X, de la Fuente MA, et al. CD84 functions as a homophilic adhesion molecule and enhances IFN-gamma secretion: adhesion is mediated by Ig-like domain 1. *J Immunol Baltim Md* 167 (2001): 3668-3676.
26. Graham DB, Bell MP, McCausland MM, et al. Ly9 (CD229)-deficient mice exhibit T cell defects yet do not share several phenotypic characteristics associated with SLAM- and SAP-deficient mice. *J Immunol Baltim Md* 176 (2006): 291-300.
27. Pérez-Quintero LA, Roncagalli R, Guo H, et al. EAT-2 a SAP-like adaptor controls NK cell activation through phospholipase C $\gamma$  Ca<sup>++</sup> and Erk leading to granule polarization. *J Exp Med* 211 (2014): 727-742.
28. Gueder N, Allan G, Telliez MS, et al. sp2 -Iminosugar  $\alpha$ -glucosidase inhibitor 1-C-octyl-2-oxa-3-oxocastanospermine specifically affected breast cancer cell migration through Stim1  $\beta$ 1-integrin and FAK signaling pathways. *J Cell Physiol* 232 (2017): 3631-3640.
29. Déliot N, Constantin B. Plasma membrane calcium channels in cancer: Alterations and consequences for



- cell proliferation and migration. *Biochim Biophys Acta* 1848 (2015): 2512-2522.
30. Motiani RK, Abdullaev IF, Trebak M. A novel native store-operated calcium channel encoded by Orai3: selective requirement of Orai3 versus Orai1 in estrogen receptor-positive versus estrogen receptor-negative breast cancer cells. *J Biol Chem* 285 (2010): 19173-1983.
  31. Roodman GD. Mechanisms of bone metastasis. *N Engl J Med* 350 (2004): 1655-1664.
  32. Donovan JC, Milic A, Slingerland JM. Constitutive MEK/MAPK activation leads to p27(Kip1) deregulation and antiestrogen resistance in human breast cancer cells. *J Biol Chem* 276 (2001): 40888-40895.
  33. Prevarskaya N, Ouadid-Ahidouch H, Skryma R, et al. Remodeling of Ca<sup>2+</sup> transport in cancer: how it contributes to cancer hallmarks? *Philos Trans R Soc Lond B Biol Sci* 369 (2014): 20130097.
  34. Roderick HL, Cook SJ. Ca<sup>2+</sup> signalling checkpoints in cancer: remodeling Ca<sup>2+</sup> for cancer cell proliferation and survival. *Nat Rev Cancer* 8 (2008): 361-375.
  35. Vashisht A, Trebak M, Motiani RK. STIM and Orai proteins as novel targets for cancer therapy. A Review in the Theme: Cell and Molecular Processes in Cancer Metastasis. *Am J Physiol Cell Physiol* 309 (2015): C457-469.
  36. Prevarskaya N, Skryma R, Shuba Y. Calcium in tumor metastasis: new roles for known actors. *Nat Rev Cancer* 11 (2011): 609-618.
  37. Jardin I, Lopez JJ, Salido GM, et al. Store-Operated Ca<sup>2+</sup> Entry in Breast Cancer Cells: Remodeling and Functional Role. *Int. J. Mol. Sci* 19 (2018): 4053.
  38. Latour S, Mahouche I, Cherrier F, et al. Calcium Independent Effect of Orai1 and STIM1 in Non-Hodgkin B Cell Lymphoma Dissemination. *Cancers* 10 (2018): 402.
  39. Okamoto Y, Ohkubo T, Ikebe T, et al. Blockade of TRPM8 activity reduces the invasion potential of oral squamous carcinoma cell lines. *Int J Oncol* 40 (2012): 1431-1440.
  40. Monet M, Lehen'kyi V, Gackiere F, et al. Role of cationic channel TRPV2 in promoting prostate cancer migration and progression to androgen resistance. *Cancer Res* 70 (2010): 1225-1235.



This article is an open access article distributed under the terms and conditions of the [Creative Commons Attribution \(CC-BY\) license 4.0](https://creativecommons.org/licenses/by/4.0/)



ELSEVIER



nanomedjournal.com

# Internal structure and remodeling in dystrophin-deficient cardiomyocytes using second harmonic generation<sup>a</sup>

Béla Varga, PhD<sup>a,1</sup>, Albano C. Meli, PhD<sup>b,1</sup>, Silviya Radoslavova, Master degree<sup>a,b</sup>,  
Mathieu Panel, PhD<sup>b</sup>, Alain Lacampagne, PhD<sup>b</sup>, Csilla Gergely, PhD<sup>a</sup>,  
Olivier Cazorla, PhD<sup>b,\*</sup>,<sup>2</sup>, Thierry Cloitre, PhD<sup>a,\*\*</sup>,<sup>2</sup>

<sup>a</sup>L2C, University of Montpellier, CNRS, Montpellier, France

<sup>b</sup>PhyMedExp, University of Montpellier, CNRS, INSERM, Montpellier, France

Revised 10 August 2020

## Abstract

Duchenne muscular dystrophy (DMD) is a debilitating disorder related to dystrophin encoding gene mutations, often associated with dilated cardiomyopathy. However, it is still unclear how dystrophin deficiency affects cardiac sarcomere remodeling and contractile dysfunction. We employed second harmonic generation (SHG) microscopy, a nonlinear optical imaging technique that allows studying contractile apparatus organization without histologic fixation and immunostaining. Images were acquired on alive DMD (*mdx*) and wild type cardiomyocytes at different ages and at various external calcium concentrations. An automated image processing was developed to identify individual myofibrils and extract data about their organization. We observed a structural aging-dependent remodeling in *mdx* cardiomyocytes affecting sarcomere sinuosity, orientation and length that could not be anticipated from standard optical imaging. These results revealed for the first time the interest of SHG to evaluate the intracellular and sarcomeric remodeling of DMD cardiac tissue in an age-dependent manner that could participate in progressive contractile dysfunction.

© 2020 Elsevier Inc. All rights reserved.

**Key words:** Second harmonic generation; Sarcomeres; Dystrophin; Cardiomyocytes; Duchenne muscular dystrophy

## Introduction

Duchenne muscular dystrophy (DMD) is the worst muscular dystrophy, with an incidence of one in 3500 boys at birth. It affects muscle cell integrity leading to progressive degradation of muscle function with no current therapy available. DMD is associated to mutations silencing the gene encoding dystrophin. Dystrophin acts as a sub-sarcolemmal protein linking the contractile units, namely the sarcomeres, with the extracellular matrix. DMD mutations causing loss-of-function of dystrophin lead to membrane integrity failure, which affects myofiber architecture and has deleterious consequences on the molecular motors and the sarcomeres. Structural changes of the sarcomeres contained in DMD skeletal muscle biopsies have been reported to be linked with muscle weakness and atrophy [1,2]. Ultra-structure analysis of DMD skeletal muscles suggests disruption of sarcomeric anchoring structures in early stage of the disease [3–5]. Even if the major role of dystrophin in maintaining the cardiomyocyte sarcolemma integrity has been revealed, there is still no clear picture on the contractile machinery network remodeling associated with dystrophin deficiency.

Although clinical interest is often related to skeletal muscle wasting and respiratory failure, DMD is often associated with

**Acknowledgments:** We thank Volker Baecker from the “Montpellier Ressources Imagerie” (MRI) platform and Dr. Gerard Subsol from LIRMM-CNRS Montpellier for the scientific discussions.

**Conflict of interest:** The authors declare no conflict of interest.

**Funding:** This work was supported by grants of the French Muscular Dystrophy Association (AFM; project 16073, MNM2 2012 and 20225) and the “Institut National pour la Santé et la Recherche Médicale” (INSERM) and the GDR ImaBio 2588.

\*Correspondence to: O. Cazorla, PhyMedExp, Inserm U1046, CNRS UMR9214, University of Montpellier, CHU Arnaud de Villeneuve, Bâtiment Crastes de Paulet, 34295 Montpellier, Cedex 5, France.

\*\*Correspondence to: T. Cloitre, Laboratoire Charles Coulomb, CNRS–University of Montpellier, Place Eugène Bataillon, CC074, 34095 Montpellier, Cedex 5, France.

**E-mail addresses:** [bela.varga@umontpellier.fr](mailto:bela.varga@umontpellier.fr), (B. Varga), [albano.meli@inserm.fr](mailto:albano.meli@inserm.fr), (A.C. Meli), [sradoslavova.92@gmail.com](mailto:sradoslavova.92@gmail.com), (S. Radoslavova), [mathieu.panel@inserm.fr](mailto:mathieu.panel@inserm.fr), (M. Panel), [alain.lacampagne@inserm.fr](mailto:alain.lacampagne@inserm.fr), (A. Lacampagne), [csilla.gergely@umontpellier.fr](mailto:csilla.gergely@umontpellier.fr), (C. Gergely), [olivier.cazorla@inserm.fr](mailto:olivier.cazorla@inserm.fr), (O. Cazorla), [thierry.cloitre@umontpellier.fr](mailto:thierry.cloitre@umontpellier.fr), (T. Cloitre).

<sup>1</sup> These authors contributed equally to this work.

<sup>2</sup> Both senior co-authors.

progressive development of dilated cardiomyopathy (DCM). While established in skeletal muscle, tissue architecture remodeling in cardiac muscle remains unclear along with the occurrence of DMD-associated DCM. Using DMD dog model, namely golden retriever muscular dystrophy (GRMD), we have also shown that dystrophin deficiency leads to reduced contractility of the cardiac left ventricle [6]. Using synchrotron X-ray diffraction, we evaluated the myofilament lattice spacing and observed that dystrophin deficiency-induced chronic stress causes regional structural changes leading to heart failure [7]. We have also provided evidence in a DMD mouse model (*mdx*) that while overall cardiac dysfunction leading to heart failure appears in mice of 12-month-old, the development of DCM with aging is associated with earlier abnormal contractile properties of the ventricular cardiomyocytes [8].

It should be noted that the majority of the studies investigating DMD repercussion on cardiac muscle remodeling have employed fluorescence microscopy requiring tissue fixation and labeling with antibodies that can skew the results and interpretations. Label-free methods that maintain tissue and cell integrity and viability in a non-destructive manner are of high interest for accurate quantitative evaluation of pathological remodeling occurring in DMD.

Multiphoton microscopy has shown a great potential for *in-vitro* and *in-vivo* label-free imaging [9] of cells and tissues. It has many assets compared to conventional single-photon confocal microscopy for biological applications. The multiphoton excitation is only potent at the focusing volume of the objective (of the order of  $0.1 \mu\text{m}^3$ ), where the intensity is sufficient to generate a nonlinear response. The excitation spatial localization provides a significant photobleaching decrease. In addition, second harmonic generation (SHG) provides useful structural and optical detail of a specimen. SHG emission is at exactly half the wavelength of the light entering the material. SHG requires particular molecular orientation that is available in some highly polarizable and ordered biological systems such as large noncentrosymmetric structures. Hence, SHG microscopy has gained great interest to perform label- and fixation-free imaging of biological structures at the submicron scale [10] such as collagen, microtubules, and muscle myosin [11–13].

SHG-based images of myocytes have revealed that the source of SHG signal in the sarcomeres is not the actin or the myosin heads, but potentially the myosin tails that assemble into a hollow shaped rod structure forming the central core of thick myosin filaments [14]. Some more recent SHG-based studies contributed to the understanding of myofibrillogenesis [15], provided information on subcellular contractions [16], or contributed to evaluate the dystrophic skeletal muscle regeneration with a quantitative morphometry approach [4]. Using 3D SHG microscopy, Friedrich et al have shown that 12-month-old *mdx* skeletal fibers exhibit deranged micromorphology compromising coordinated and aligned contraction [5]. The internal disorganization in the *mdx* skeletal myofibers revealed by SHG has been correlated with altered force generation [17]. However, morphological internal changes have never been explored in DMD cardiomyocytes by SHG microscopy.

In the present study, we employed SHG microscopy to assess the impact of dystrophin deficiency and physiological calcium ( $\text{Ca}^{2+}$ ) concentration on the conformational changes of the myosin filaments and cell characteristics in alive label-free *mdx* cardiomyocytes at early (4-month-old) and later (12-month-old)

stage. Studies reported that at 4 months of age, the cardiac function is normal and that dysfunction of the heart appears later at 12 months old [8]. We developed a computational image analysis process allowing identification of single myofibrils. We extracted fibril-level data on the internal structure of intact cardiomyocytes acquiring details on the organization, orientation and sinuosity of its constituent individual myofibrils in presence or absence of external physiological  $\text{Ca}^{2+}$ .

We observed a structural aging-dependent remodeling in *mdx* cardiomyocytes affecting sarcomere alignment, orientation and length that could not be anticipated from standard optical imaging.

## Methods

### *Animals and myocyte preparation*

C57BL/10-Dmd<sup>*mdx*</sup> mice were obtained from a colony maintained at a local animal facility network (RAM, Montpellier) [18]. C57BL/6 mice were obtained from Janvier Laboratories (Le Genest-Saint-Isle, France). The animals were hosted conventionally in controlled humidity and temperature, operating on 12 h of light and dark cycle with *ad libitum* food and water. All investigations conformed to the European Parliament Directive 2010/63/EU and were validated by the local ethics committee (Comité d'éthique pour l'expérimentation animale Languedoc-Roussillon, no. CEEA-LR-12078). Cardiac ventricular myocytes were enzymatically dissociated using routine procedures [19] (Figure 1, A). In short, we performed cervical dislocation to euthanize the mouse. The heart was then rapidly excised and retrogradely perfused at 37 °C for 6–8 min with a modified Tyrode solution [113 mM NaCl, 4.7 mM KCl, 0.6 mM  $\text{KH}_2\text{PO}_4$ , 0.6 mM  $\text{Na}_2\text{HPO}_4$ , 1.2 mM  $\text{MgSO}_4$ , 12 mM  $\text{NaHCO}_3$ , 10 mM  $\text{KHCO}_3$ , 10 mM Hepes, 30 mM taurine (pH 7.4)] containing  $0.1 \text{ mg}\cdot\text{mL}^{-1}$  of liberase (Roche) [8]. Isolated myocytes were then transferred to the same enzyme-free solution. Cardiomyocytes were maintained in the  $\text{Ca}^{2+}$ -free solution or in solution containing 1.8 mM  $\text{CaCl}_2$ . To avoid cell movement during acquisition, we added before acquisition to the Tyrode solution 15 mM 2,3-butanedione monoxime (BDM, ATPase inhibitor) and 10  $\mu\text{M}$  blebbistatin (myosin II inhibitor) [20]. SHG acquisitions were performed within 2 h to avoid structural changes due to cell degradation after dissociation.

### *Second harmonic generation imaging*

SHG images (Figure 1, B) were recorded using a custom-made multiphoton microscope setup based on a Tsunami tunable Ti:Sapphire laser (Spectra-Physics, Santa Clara, US) and an upright SliceScope microscope (MPSS-1000P) furnished with a multiphoton galvanometer scan head (MP-2000) both from Scientifica, Uckfield, UK. The Ti-Sa laser was operated in pulsed mode configuration for sample excitation, in a 760–900 nm wavelength range, at 80 MHz frequency and  $\sim 100$  fs pulse duration. A Nikon CFI75 LWD-16x-W objective (NA 0.8, water immersion) was used to focus the laser beam on the sample. The SHG signal was recorded by a 1.4-NA oil-immersion condenser (U-AAC, Olympus), through a 482 nm long pass dichroic mirror (86-331, Edmund Optics) and a 447 nm high-performance band-

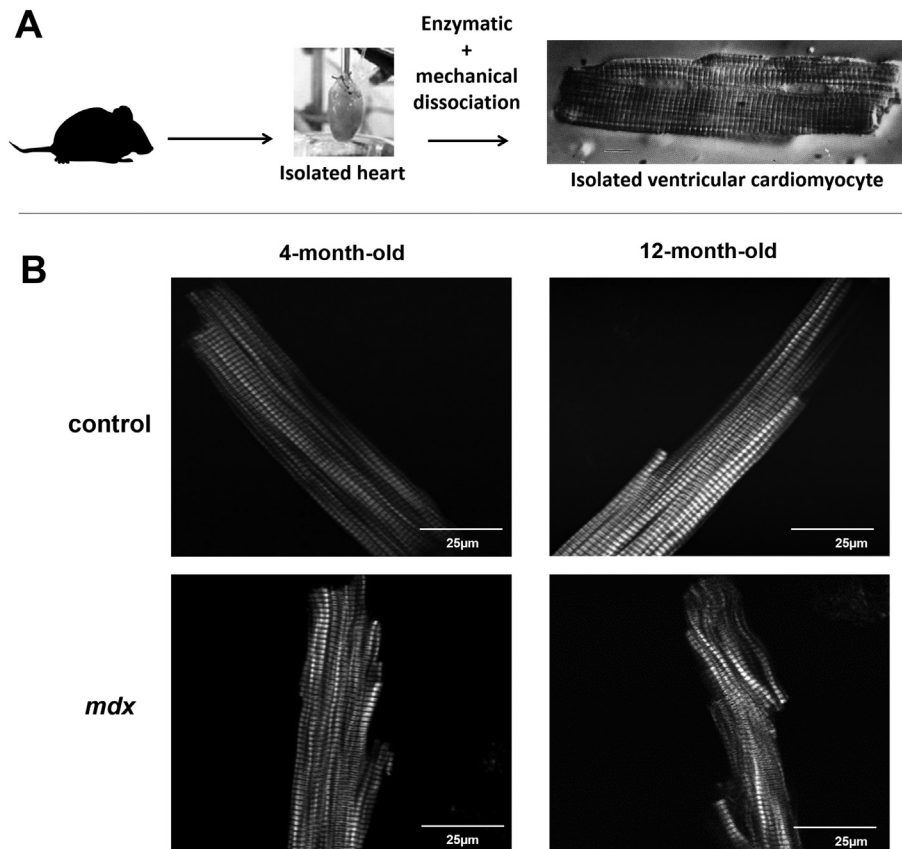


Figure 1. Second harmonic generation (SHG) imaging of intact cardiomyocytes isolated from control and *mdx* mice. (A). Ventricular cardiomyocytes were isolated from the heart of control and *mdx* mice by enzymatic and mechanical dissociation. (B) Representative SHG images on control (top panel) and *mdx* (bottom panel) cardiomyocytes at different ages. Mature *mdx* cardiomyocytes exhibit enhanced disorder in the internal myofibrillar structure.

pass filter (48-074, Edmund Optics) and then detected by a H7422P photomultiplier (Hamamatsu). Intensity images were reconstructed from the SHG signal recorded in transmission. Image acquisitions were done in  $1024 \times 1024$  pixel resolution at 200 line/s scanning rate.

#### Differential interference contrast microscopy

DIC images were recorded using a Nikon Eclipse TE2000-E inverted microscope equipped with a differential interference contrast system, using a CFI Plan 100 $\times$  oil immersion objective having a 1.3 NA and 0.2 mm working distance.

#### Image analysis

The recorded images were subject of a semi-automated image analysis process, as presented in Figure 2. During pre-processing, first a Gaussian blur filter was applied for noise reduction, followed by a step to find and assign all local maxima in the filtered image corresponding to the M-line of the sarcomeres. The detected coordinates of local maxima were then the input of a custom-made automated algorithm aiming to build up a highly connected network by linking every point with each other. This network was afterwards progressively degraded first using maximum distance and then orientation constraints. Distance constraint threshold was defined as 2-fold the average sarcomere length ( $\sim 2 \mu\text{m}$ ), while the orientation constraint was

settled to stay below  $\pm 30^\circ$  compared to the mean orientation of the cell. After resolving the remained over connected nodes (having more than two links) and end point fusions (connected fibrils at their end), the network was clustered into single chains of points corresponding to single fibrils.

The isolated data for every individual fibril allowed the extraction of several fibril-level parameters such as sinuosity, orientation deviation, double-band percentage, double-band rate, or sarcomere length. Sinuosity was defined as the normalized length difference between the total distance (sum of sections between every consecutive point) and the beeline (distance between the start and end points) (Figure 3). Orientation of a fibril was obtained by applying a line fitting and its difference in angle from the mean orientation was defined as its deviation (Figure 3). Every link smaller than  $1.4 \mu\text{m}$  was defined as a double-band. Under double-band percentage we defined the ratio of double-bands in one cell, and the double-band rate is the ratio of fibrils in one cell that contains at least one double-band. The sarcomere length of a fibril was defined as the mean distance between consecutive points, omitting double-bands, while cell width measurements were done manually in ImageJ.

#### Data analysis, statistics and interpretation

Basic image treatment and the pre-processing were done in Fiji (an ImageJ distribution) [21], while the custom-made script

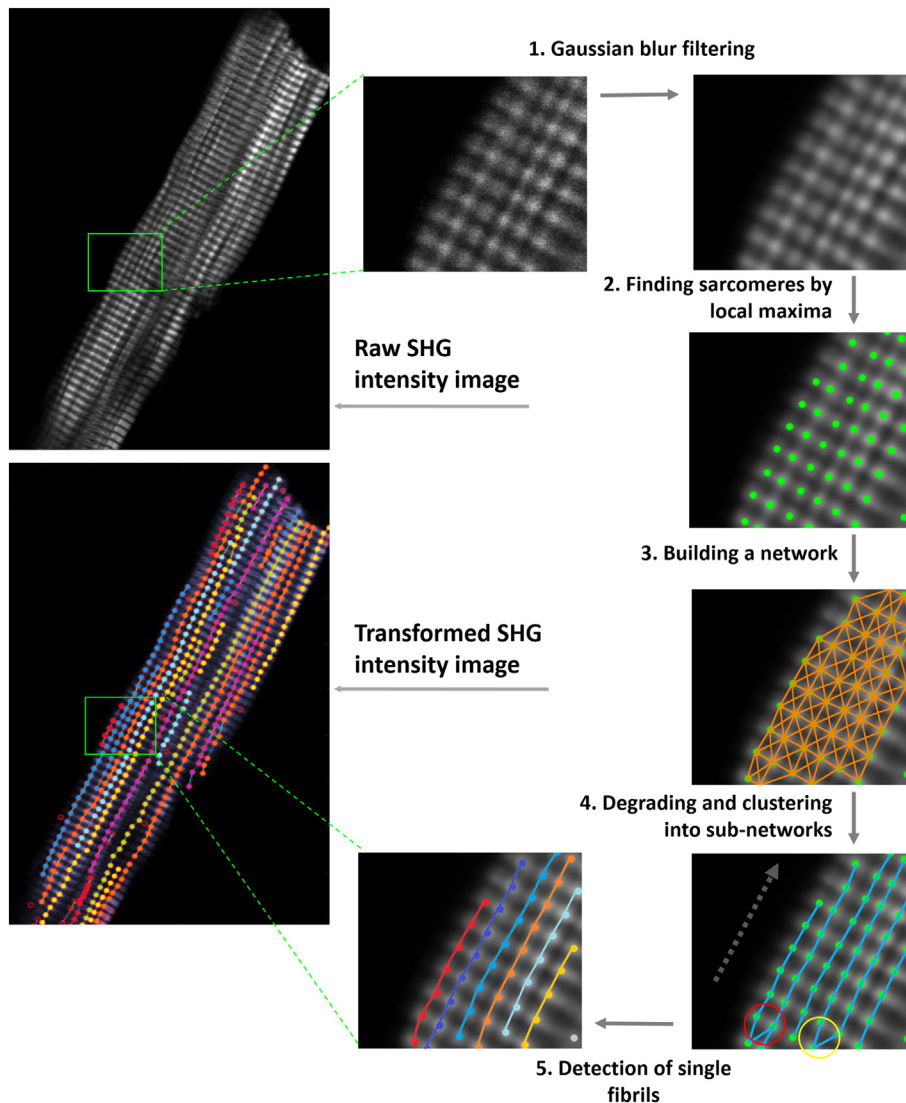


Figure 2. Data processing work flow. After applying a Gaussian filter on the recorded SHG intensity images (step 1), the sarcomeres were detected by finding local maxima (step 2). These were considered as nodes of a network. The obtained highly connected network (step 3) of all sarcomeres was degraded using distance and orientation constraints (step 4) and clustered into single fibrils (step 5). This allowed the extraction of fibril-level parameters, such as orientation dispersion, sinuosity, sarcomere length and double-band related parameters.

for the automated fibril-level data extraction was written in Matlab (MathWorks, Natick, USA).

Statistical analysis was carried out using SigmaPlot (Systat Software, San Jose, USA). The significance was determined by unpaired Student *t* test and two-way ANOVA followed by a Holm-Sidak *post hoc* test, respectively. All data are reported as box plots, with interquartile range from 25% to 75%, where the middle line represents the median, while the red square is the mean of the data. We considered a statistical difference when  $P < 0.05$ .

## Results

### *The SHG signal of control and mdx cardiomyocytes reveals internal structural alterations with aging*

Intact cardiomyocytes were isolated from the hearts of 4- and 12-month-old control and mdx mice by enzymatic digestion

(Figure 1, A). In order to obtain high quality SHG images in alive cardiomyocytes avoiding artifacts induced by spontaneous contractions, the experiments were carried out in presence of the ATP-ase inhibitor butanedione monoxime (BDM) and the myosin inhibitor blebbistatin [20]. During exploratory SHG acquisitions, control and *mdx* cardiomyocytes of young animals (4-month-old) had visually roughly similar internal structure (Figure 1, B, left panels). Interestingly, in older animals (12-month-old), SHG signal of *mdx* cardiomyocytes was noticeably different to control myocytes with curvier myofibrils (Figure 1, B, right panels). This would suggest potential remodeling of the internal structure with aging in *mdx* cardiomyocytes. To quantify those changes, we developed a custom-made automated image analysis algorithm. The process is illustrated in Figure 2 and detailed in Materials and Methods. Briefly, after noise reduction on the recorded SHG intensity images, the sarcomeres were detected by finding local maxima. These points were then considered as nodes of a network.

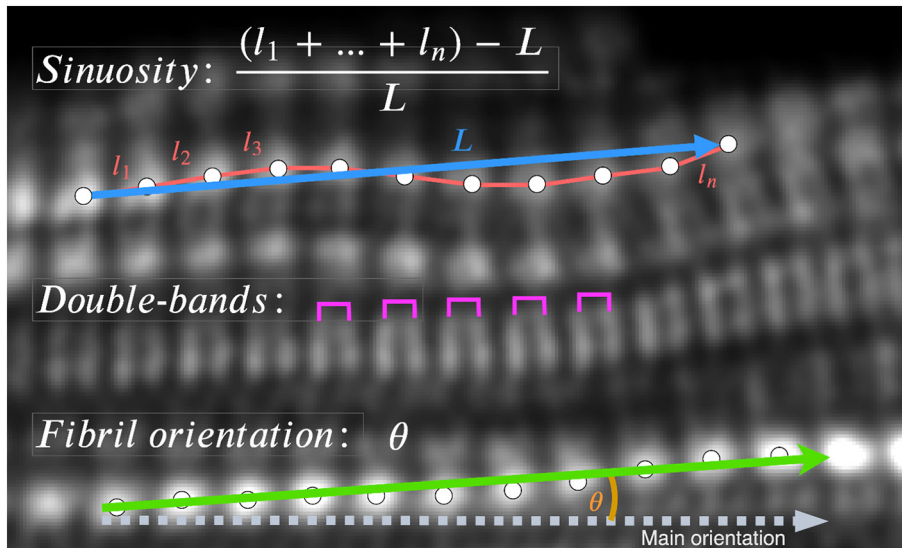


Figure 3. Sinuosity, double-band and fibril orientation. Sinuosity, defined as the difference between the real length of the fibril and the beeline between the two ends of the fibril, normalized with the beeline. **Double-bands**, defined as smaller than 2/3rd of a usual sarcomere length. **Fibril orientation**, defined as the angle between the fitted line on the detected sarcomeres and the mean orientation of all fibrils.

The obtained highly connected network of all sarcomeres was degraded using distance and orientation constraints and clustered into single fibrils. With the algorithm, we could extract different fibril-level structural parameters of the contractile machinery such as fibril orientation, sinuosity, sarcomere length, and, so called, double-bands that characterize the heavy myosin chain organization (for detailed description see Materials and Methods and Figure 3). By fibril orientation we aimed at evaluating the ordering level inside single cardiomyocytes, while sinuosity served to quantify the curviness of the fibrils. From the myosin chain organization, we aimed at quantifying the presence of double-bands in the myocytes. This characteristic was previously associated with multiple factors and considered as an intrinsic characteristic, through relating it to external factors, up to linking them to internal structure disorganization [5,22–24].

#### SHG signal is not affected by the extracellular $Ca^{2+}$ concentration

Intracellular calcium concentration depends on the extracellular calcium concentration. The effect of intracellular calcium content on SHG signal in cardiomyocytes or myocyte in general has never been tested. During the process of cell isolation, the external  $[Ca^{2+}]$  is progressively raised from 0 mM to 1.8 mM  $Ca^{2+}$  that should increase the internal calcium concentration. When released in the cytosol, calcium interacts with troponin C on the actin thin filament. This interaction induces a change of the conformation of the thin filaments to let the myosin head to bind. This change of conformation of the thin filaments still exists in presence of BDM and blebbistatin because both act on the myosin ATPase. Whether this change of thin filament conformation alters SHG signal is unknown. We first tested whether the presence of extracellular  $Ca^{2+}$  at physiological concentration modulates the structure and sarcomere organization visible through SHG microscopy. We hypothesized that the presence of  $Ca^{2+}$  inside the myocyte may affect the conformation

of the thin filaments, number of actin-myosin cross-bridges formed and thus the SHG signal. Freshly dissociated ventricular cardiomyocytes were imaged by SHG microscopy both in normal solution containing 1.8 mM  $Ca^{2+}$  and in external  $Ca^{2+}$ -free solution, which consequently decreases the internal  $Ca^{2+}$  concentration. This test has been performed with old adult control mice. We found that the decrease in extracellular  $Ca^{2+}$  did not change the sarcomere length nor the orientation of the sarcomeres of control myocytes (Figure 4, A and B). Myocytes were perfectly relaxed as indicated by the slack sarcomere length of  $1.97 \pm 0.04$  and  $1.96 \pm 0.04$   $\mu\text{m}$  measured in 1.8 mM  $Ca^{2+}$  and  $Ca^{2+}$ -free respectively (Figure 4, A and B), values consistent with known values published in the literature (see all exact data in Table 1). The sinuosity of the acquired heavy myosin chain signal was unchanged in presence of  $Ca^{2+}$  with no significant difference in double-band percentage and rate (Figure 4, C-E). Similar results on the effect of external  $[Ca^{2+}]$  were obtained with old *mdx* myocytes (Figure 4, F-J). Accordingly, all the following presented results were obtained in physiological conditions in a solution containing 1.8 mM  $Ca^{2+}$ .

#### Aging causes increased sarcomere length and decreased cell width in dystrophin-deficient cardiomyocytes

Using 3D SHG microscopy, Friedrich et al have revealed that dystrophin-deficiency leads to disturbed micromorphology compromising coordinated and aligned contraction in 12-month-old *mdx* skeletal fibers [5]. We next assessed whether aging could similarly affect the structure and sarcomere organization of the *mdx* cardiomyocytes. To that, we compared freshly dissociated intact control and *mdx* cardiomyocytes of 4- and 12-month-old. Aging caused a sarcomere length decrease from 1.99 to 1.96  $\mu\text{m}$  and a cell width increase from 22.6 to 26.7  $\mu\text{m}$  in control cardiomyocytes (Figure 5). Such changes were not observed in dystrophin-deficient cardiomyocytes. Mean

Table 1

Mean  $\pm$  standard deviation of all measured parameters.

	Orientation dispersion ( $^{\circ}$ )	Sinuosity (%)	Double-band percentage (%)	Double-band rate (%)	Sarcomere length ( $\mu\text{m}$ )	Cell width ( $\mu\text{m}$ )
<b>1.8 mM <math>[\text{Ca}^{2+}]_{\text{ext}}</math></b>						
Control 4 mo	<b>3.1 <math>\pm</math> 1.1<sup>a</sup></b>	<b>0.69 <math>\pm</math> 0.26</b>	21.6 $\pm$ 19.2	43.4 $\pm$ 23.7	<b>1.99 <math>\pm</math> 0.04<sup>d</sup></b>	<b>22.3 <math>\pm</math> 5.6<sup>f</sup></b>
Control 12 mo	<b>2.5 <math>\pm</math> 0.8<sup>a,b</sup></b>	<b>0.63 <math>\pm</math> 0.2<sup>c</sup></b>	15.9 $\pm$ 11.3	38.1 $\pm$ 20.0	<b>1.96 <math>\pm</math> 0.04<sup>d,e</sup></b>	<b>25.0 <math>\pm</math> 4.5<sup>f,g</sup></b>
<i>mdx</i> 4 mo	<b>3.0 <math>\pm</math> 1.1</b>	<b>0.75 <math>\pm</math> 0.26</b>	15.7 $\pm$ 11.3	39.0 $\pm$ 18.5	<b>2.00 <math>\pm</math> 0.05</b>	<b>21.1 <math>\pm</math> 6.4</b>
<i>mdx</i> 12 mo	<b>3.5 <math>\pm</math> 1.4<sup>b</sup></b>	<b>0.76 <math>\pm</math> 0.21<sup>c</sup></b>	15.9 $\pm$ 8.9	40.5 $\pm$ 14.5	<b>1.99 <math>\pm</math> 0.06<sup>e</sup></b>	<b>20.3 <math>\pm</math> 3.6<sup>g</sup></b>
<b>0 mM <math>[\text{Ca}^{2+}]_{\text{ext}}</math></b>						
Control 4 mo	3.1 $\pm$ 0.9	0.82 $\pm$ 0.23	12.7 $\pm$ 13.6	34.4 $\pm$ 25.5	2.02 $\pm$ 0.06	20.9 $\pm$ 4.1
Control 12 mo	2.7 $\pm$ 0.7	0.68 $\pm$ 0.14	19.9 $\pm$ 11.2	44.4 $\pm$ 17.9	1.97 $\pm$ 0.04	21.3 $\pm$ 5.7
<i>mdx</i> 4 mo	2.9 $\pm$ 1.0	0.69 $\pm$ 0.14	16.8 $\pm$ 11.5	40.6 $\pm$ 18.5	2.00 $\pm$ 0.07	21.4 $\pm$ 5.4
<i>mdx</i> 12 mo	3.4 $\pm$ 1.2	0.74 $\pm$ 0.19	19.1 $\pm$ 6.9	47.5 $\pm$ 15.7	2.00 $\pm$ 0.04	22.8 $\pm$ 8.1

Bold values correspond to the parameters where significant changes have been observed. Where indicated, identical exponent letters show significant differences between the marked values.

sarcomere lengths for both *mdx* and control cardiomyocytes from young animals were similar, very close to 2  $\mu\text{m}$ , as well as cell width value distributions with mean values around 22  $\mu\text{m}$ . In old animals, sarcomere length was higher in *mdx* cardiomyocytes when compared to age-matched control cells (Figure 5, B). Interestingly, cell width was unchanged with aging in *mdx* cells and was smaller compared to age-matched control cardiomyocytes (Figure 5, C).

#### Aged *mdx* cardiomyocytes exhibit further structural and sarcomere alterations

When exploring the sarcomere organization, sinuosity of the myofibrils of control and *mdx* cardiomyocytes did not differ with aging (Figure 6, B). No statistical difference was observed in the sinuosity between young *mdx* and control population. The orientation dispersion was also identical for both control and *mdx* 4-month-old cardiomyocytes with an average value of about 3.1 $^{\circ}$  (Figure 6, C). In addition, the orientation dispersion decreased with aging only in control cells but not in *mdx* cells. In old animals, *mdx* cardiomyocytes displayed higher percentage of sinuosity and orientation dispersion compared to age-matched control cardiomyocytes (Figure 6, B and C). Aging did not alter the double-band percentage and rate in any group (Figure 6, D and E). The mean and standard deviation values of the extracted parameters (Figures 5 and 6) are gathered in Table 1. We observed no significant difference in any of the extracted parameters when comparing data between *mdx* and control cardiomyocytes, coming from young animals.

Altogether, the SHG data indicate that the cardiomyocytes of old *mdx* mice exhibited longer sarcomere lengths and are thinner by about 30% compared with control myocytes. In addition, their mean fibril sinuosity and orientation dispersion were significantly increased compared to the control cells by about 19% and 44%, respectively, indicative of internal disorganization of the myofibrils.

In order to stress the appropriateness of SHG microscopy for such study and to demonstrate that the alive cardiomyocyte internal structure changes in old *mdx* mice can only be revealed by SHG analysis, we acquired images of the cardiomyocytes from young and old mice with differential interference contrast

(DIC) microscopy (Figure 7). DIC imaging provides a good contrast for the eye. However, as the origin of the contrast is linked to the difference in the optical paths, it does not provide true intensity signal and could not serve for image processing, especially for fibril level data extraction. More importantly, we were unable to detect any structural changes from the images between young and old animals (Figure 7, B). They looked perfectly normal, which contrasts with the images obtained using SHG analysis (Figure 7, A). Altogether, our results indicated the great potential of SHG in evaluating the age-dependent deterioration of myofibrils within alive and intact *mdx* cardiomyocytes.

## Discussion

Our work demonstrates the great potential of nonlinear optics to reveal biological/structural modifications induced by a severe illness. DMD is one of the worst debilitating neuromuscular disorders causing death prior 30 years old due to respiratory and/or cardiac failure. While the skeletal muscle dystrophinopathies have been explored, the consequences of dystrophin deficiency on the cardiac muscle degeneration in link with the lethal development of DCM are unclear. In the present study we revealed, for the first time in cardiac myocytes, the interest in using SHG to evaluate the progressive intracellular and sarcomeric remodeling induced by dystrophin-deficiency with age. Our experimental conditions allowed acquisition of images of the internal structure of intact alive cardiomyocytes, avoiding artifacts associated with cell fixation and antibody binding. Using a custom-made image analysis, we evaluated the cell structure at the single myofibril level.

Considering the key role of  $\text{Ca}^{2+}$  in the cardiac muscle contraction *via* sarcomere shortening, we first tested the impact of physiological  $\text{Ca}^{2+}$  concentration on the myosin SHG signal in control cardiomyocytes. We obtained no conclusive effect of extracellular  $\text{Ca}^{2+}$  concentration on the internal structure, orientation, sinuosity or myosin arrangement. These results suggested that, although we employed experimental conditions to maintain the cardiomyocytes alive, the biophysical properties

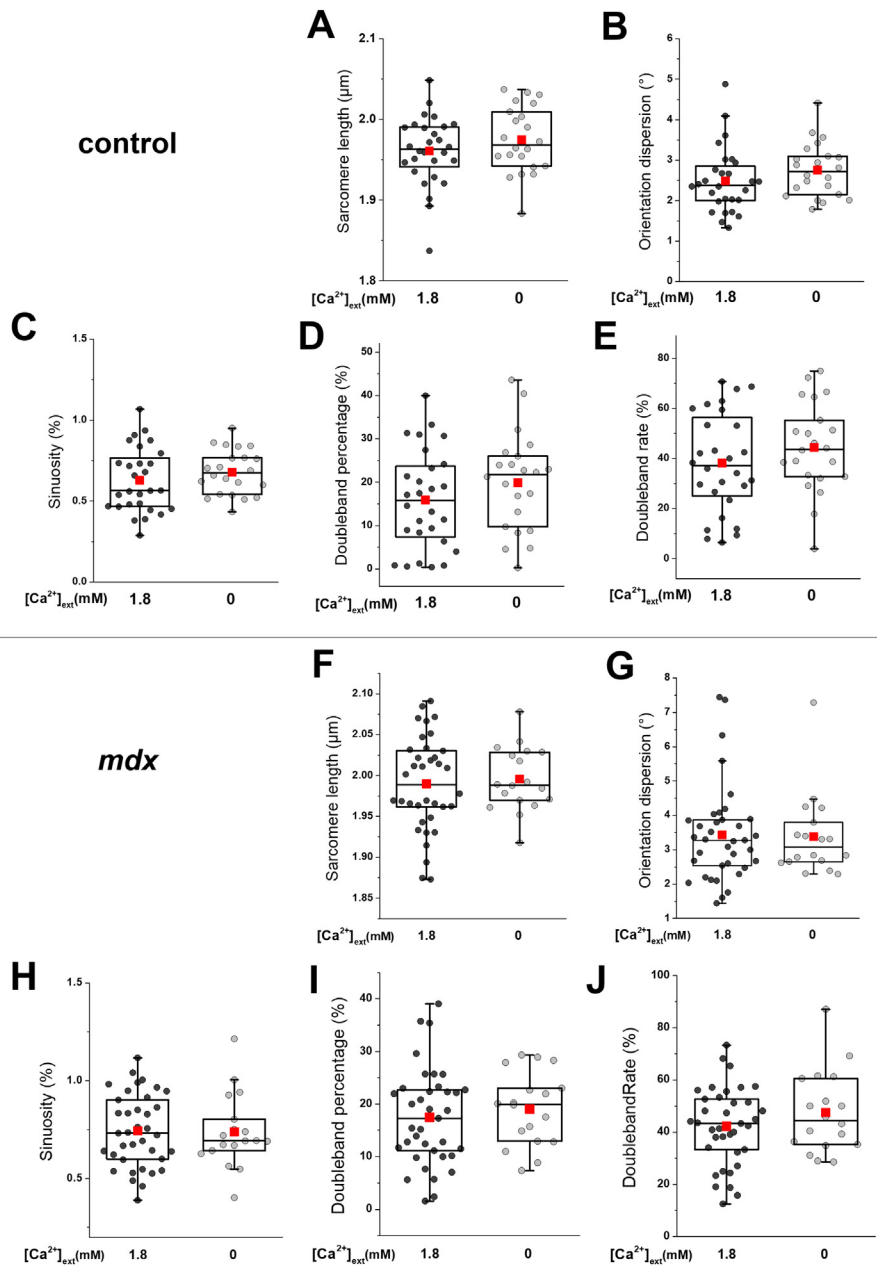


Figure 4. Effect of external  $\text{Ca}^{2+}$  concentration on the extracted parameters from SHG images measured on 12-month-old control/*mdx* cardiomyocytes. SHG images were obtained from cardiomyocytes maintained in 1.8 mM  $\text{Ca}^{2+}$  (black dots) or  $\text{Ca}^{2+}$  free (gray dots) external physiological solution. No significant effect of external  $\text{Ca}^{2+}$  was observed on the extracted parameters ( $n = 28$  myocytes (3 animals) for control with  $\text{Ca}^{2+}$  and  $n = 22$  myocytes (3 animals) for control without  $\text{Ca}^{2+}$ ;  $n = 37$  myocytes (5 animals) for *mdx* with  $\text{Ca}^{2+}$  and  $n = 18$  myocytes (3 animals) for *mdx* without  $\text{Ca}^{2+}$ ).

of the sarcomere resulting from SHG signal are not modulated by the presence of  $\text{Ca}^{2+}$ . We purposely performed these experiments on alive cardiomyocytes, inhibiting spontaneous contraction by BDM and blebbistatin to facilitate acquisition of high quality SHG images. Indeed, by inhibiting acto-myosin interaction, it fully relaxes the myocyte, independently of the amount of diastolic calcium level. Our present experimental conditions are ideal and required to precisely examine sarcomere structure in particular the diastolic sarcomere length and width as we showed previously [25]. Furthermore, Plotnikov et al have demonstrated that only myosin rod domains are responsible for

the SHG signal in skeletal muscle fibers [14]. They also observed that SHG spectroscopy cannot sense muscle contraction as it does not induce any difference in the intensity or polarization of the signal. These features may be similar in cardiac muscle, explaining the unchanged SHG signal recorded on cardiomyocytes obtained in presence or absence of physiological extracellular of  $\text{Ca}^{2+}$ . Here, the increase in intracellular  $\text{Ca}^{2+}$  concentration was expected to further activate the thin-filaments (actin filaments). Indeed,  $\text{Ca}^{2+}$  binds to troponin C, which causes conformational changes of the thin filaments. Our results confirmed that the SHG signal is not altered by any change of



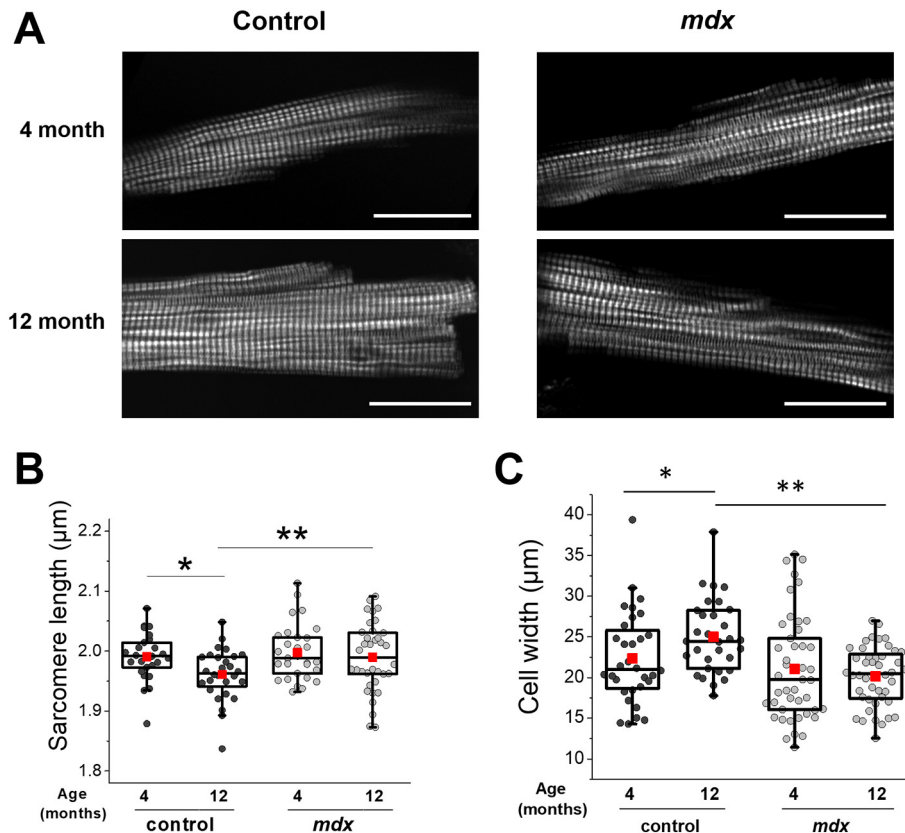


Figure 5. Structural cellular analysis of SHG images from young and old control and *mdx* cardiomyocytes. (A) Representative SHG images of the corresponding conditions. (B) Significant differences in sarcomere length were observed between young and mature control cells, as well as between mature control and mature *mdx* cardiomyocytes ( $n = 26$  myocytes (3 animals) for control at 4 months and  $n = 28$  myocytes (3 animals) for control at 12 months;  $n = 29$  myocytes (5 animals) for *mdx* at 4 months and  $n = 37$  myocytes (5 animals) for *mdx* at 12 months). (C) Significant differences have been observed in cell widths of young and mature control cells, as well as mature control and mature *mdx* cardiomyocytes. In addition, overall significant differences were found between control and *mdx* for both parameters ( $n = 32$  myocytes (3 animals) for control at 4 months and  $n = 31$  myocytes (3 animals) for control at 12 months;  $n = 45$  myocytes (5 animals) for *mdx* at 4 months and  $n = 43$  myocytes (5 animals) for *mdx* at 12 months). \*,  $P < 0.05$ ; \*\*,  $P < 0.01$ , two-way ANOVA.

the thin filaments. These experiments in different external  $\text{Ca}^{2+}$  concentrations confirmed also that the internal structure was not altered by the progressive increase to 1.8 mM  $\text{Ca}^{2+}$  during the process of cell isolation. This was true for both control and *mdx* cardiomyocytes. Indeed, it was previously shown that basal level of calcium concentration is increased in old *mdx* mice [8]. Meantime, like in many cardiomyopathies associated with higher intracellular  $\text{Ca}^{2+}$  concentration, the content and/or activity of intracellular calcium-dependent proteases such as calpains are increased. This has been shown in a utrophin/dystrophin deficiency mouse model, a more severe myopathy model than *mdx* [26]. The absence of SHG signal change in presence or absence of physiological  $\text{Ca}^{2+}$  concentration indicated no  $\text{Ca}^{2+}$ -dependent activation of the proteases leading to structural defaults and ruled out any artifact of the myosin signal change associated to protease activation in both control and *mdx* cardiomyocytes.

Control cardiomyocytes displayed changes between 4- and 12-month-old with regard to sarcomere length, cell width and fibril orientation dispersion. This reflects a physiological adaptation of the cardiomyocytes certainly due to increased workload of the heart [27]. We observed that the cellular internal structure likely becomes more organized at 12 months old,

showing slightly decreased sinuosity and more aligned myofibril structure compared to younger counterparts. Importantly, the shorter sarcomere length and enlarged cell width as well as the decreased orientation dispersion suggest a maturing process towards adult cardiomyocytes. These results on potential maturation of the sarcomeres are supported by previous studies, in which sarcomere lengths of skeletal muscle fibers were used to monitor myofibrils assembly in alive cells [14,28]. The basal sarcomere length shortening observed here with aging in control myocytes could be explained by expression variations in the different isoforms of the sarcomeric elastic protein, titin, during sarcomere development. Titin length is a major contributor of the sarcomere length and of the intracellular stiffness [29]. With aging, the adult normal heart expresses a short titin isoform leading to a decreased sarcomere length and a higher cardiac stiffness [30].

According to our findings, all structural parameters both for control and *mdx* are similar in young animals. Their structural disorganization level, quantified by sinuosity and orientation dispersion, as well as their dimension related characteristics, such as cell width and sarcomere length, is similar. In other words, at early stage, based on the SHG measured parameters, the *mdx* cardiomyocytes are structurally not distinguishable from

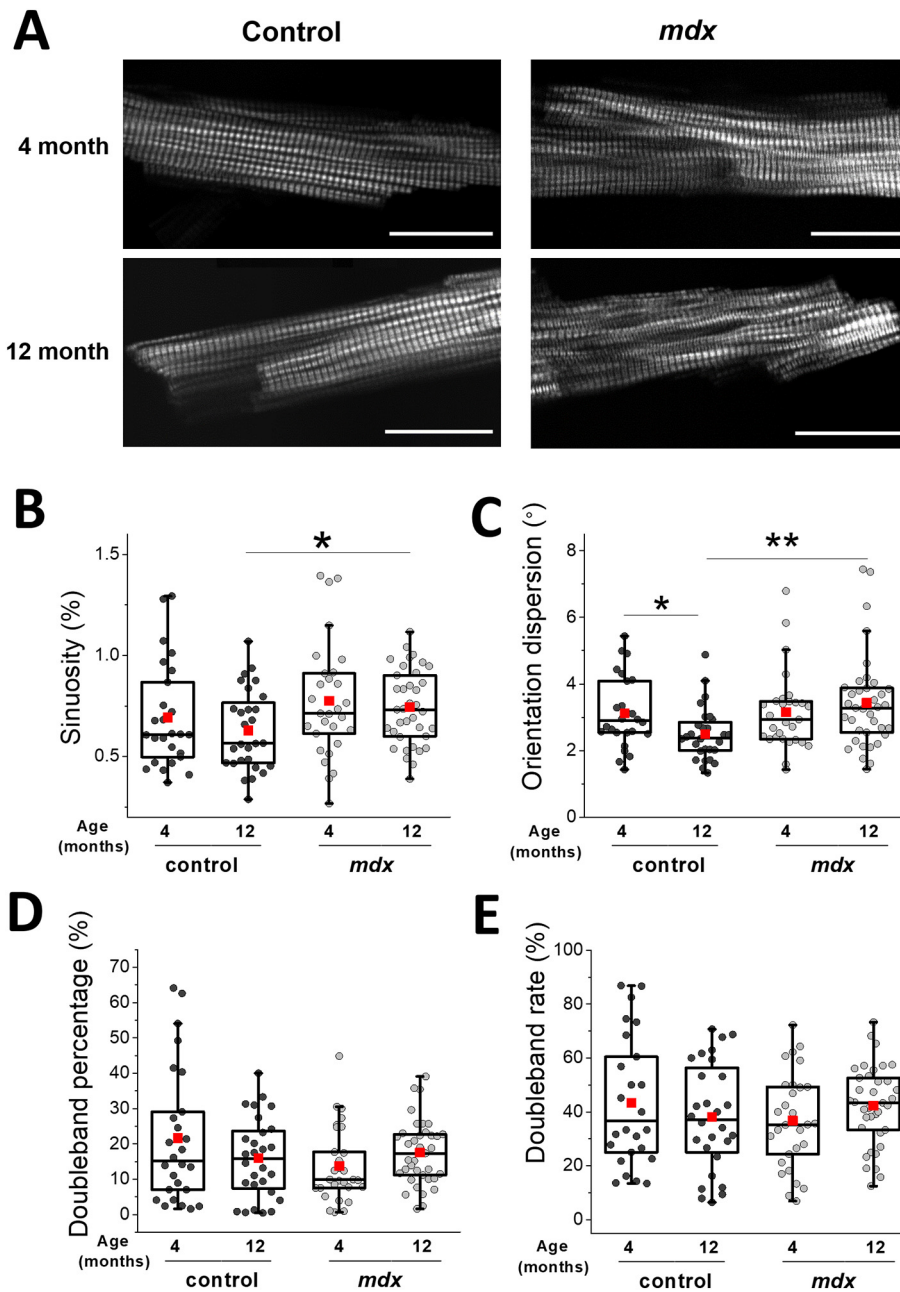


Figure 6. Myofibrillar rearrangement in control and *mdx* cardiomyocytes with aging. (A) Representative SHG images of the corresponding conditions. Average sinuosity (B) and orientation dispersion (C) of myofibrils within each cardiomyocyte, present significant differences between mature control and mature *mdx* cells. Average double-band percentage (D) and rate (E) of the myofibrils within each cardiomyocyte are not significant. In case of sinuosity and orientation dispersion overall significant differences have been also observed between control and *mdx* cardiomyocytes. ( $n = 26$  myocytes (3 animals) for control at 4 months and  $n = 28$  myocytes (3 animals) for control at 12 months;  $n = 29$  myocytes (5 animals) for *mdx* at 4 months and  $n = 37$  myocytes (5 animals) for *mdx* at 12 months). \*,  $P < 0.05$ ; \*\*,  $P < 0.01$ ; two-way ANOVA.

control ones. This does not mean that the *mdx* cardiomyocytes are healthy at this age. Indeed, we have shown defects in the intracellular  $\text{Ca}^{2+}$  cycling in particular an increase in the level of  $\text{Ca}^{2+}$  concentration at rest in 1-month-old *mdx* mouse cardiomyocytes [8]. These early defaults in  $\text{Ca}^{2+}$  homeostasis may trigger intracellular remodeling. Indeed, at the age of 6 months, we observed a decrease in the neuronal nitric oxide synthase (NOS) expression and increase in inducible NOS expression compared with control and 1-month-old *mdx* cardiomyocytes.

The elevation of inducible NOS expression is classically associated with cardiomyopathies.

Our study revealed progressive structural differences between *mdx* compared with control cardiomyocyte at a mature stage (12-month-old) with thinner *mdx* cardiomyocytes displaying longer sarcomeres associated with more tortuous and diversely oriented fibrils. These new findings support the concept that dystrophin-deficiency causes cardiac muscle degeneration at a later stage as a major difference with DMD skeletal muscle loss at early-stage

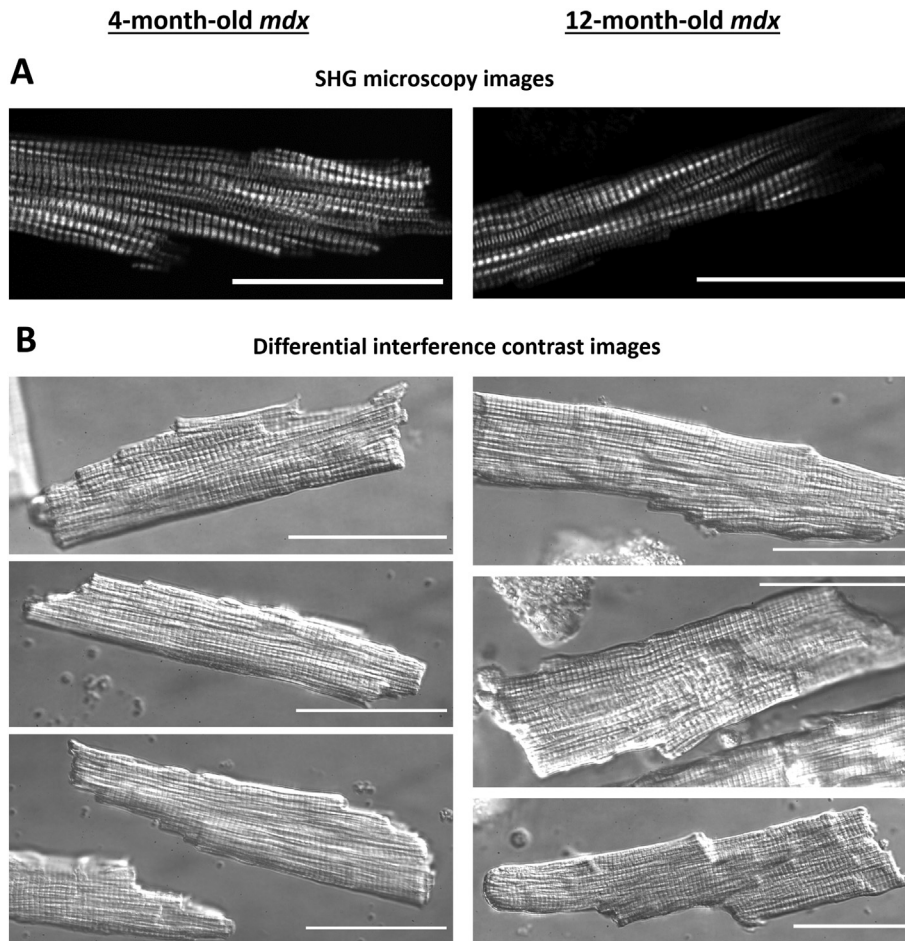


Figure 7. Comparison of SHG and Differential interference contrast (DIC) microscopy images of *mdx* cardiomyocytes. (A) SHG images on 4- and 12-month-old mice cardiomyocytes presenting high background to signal contrast and true myosin intensity signal, being highly appropriate for image processing. (B) DIC images on corresponding cardiomyocytes provide good contrast for the eye; however, as the contrast is linked to optical path difference, it could hardly serve for image processing, especially for fibril level data extraction. All scale bars are 50  $\mu$ m.

[7,31]. They indicate a structural and progressive damage of the myofibrils that was not induced by the procedure of cell dissociation. They also strongly support that the structural disorganization of the myofibrils in *mdx* cardiomyocytes causes an uncoupled and dysfunctional myofibrillar network likely leading to progressive reduced contraction force and eventually hypocontractility as a major feature of the DMD-associated dilated cardiomyopathy. Similar findings, revealed by SHG in *mdx* skeletal muscle fibers, indicated that myofibril tilting and twisting cause a reduced contraction force of at least 20% [5].

The longer sarcomere length in old *mdx* cardiomyocytes could be due to the expression of a longer titin isoform that could reduce the stiffness of the myocytes [32]. This could explain why a previous study reported that old *mdx* mice have a more compliant heart than the age-matched control mice [33]. Our present results indicate that the cardiac sarcomere alignment, orientation and length are progressively affected by the absence of dystrophin with no visible consequences at early-stage (4 months old) compared to a known disease stage (12 months old) related to cardiac dysfunction and progressive DCM as we have previously showed [8].

Furthermore, our findings are also supported by our earlier study showing that the myofilament structure and function are altered in GRMD dogs [7]. Li et al [34] showed that myocyte fractional shortening is higher at 4 months of age in *mdx* compared with control mice being associated with higher calcium release during contraction. This is confirmed by other groups showing that young *mdx* animals have increased calcium current and intracellular calcium transient [36,38,40]. The higher cellular contractility in young animals is supposed to compensate cell death and maintain normal global cardiac contraction. With aging (12 months), the amplitude of cellular contraction of *mdx* cardiomyocytes decreases compared with 4 months of age and reaches similar level than control cardiomyocytes [34]. Thus, at this stage, *mdx* myocytes cannot compensate cell death that occurs at a higher rate (more fibrosis) and thus global contractility is decreased (hypocontractility). This is also in line with reports on myofilament and mitochondrial defects in DCM [35,37] and DMD patient derived cardiomyocytes [39].

The distortion of the myofibrils may be induced by a process of dedifferentiation as observed in myocardial remodeling in heart failure. In fact, morphological rearrangement of cardiomyocytes is

a protective remodeling for adaptation [41]. Loss of features of cell maturity, including de-sarcomerization and myofibril de-organization and re-expression of fetal genes, has been reported in pathophysiological contexts [42,43].

The distortion of the myofibrils may be induced by gradual changes of other intracellular organelles. Interestingly, age dependent changes in mitochondrial morphology were shown in *mdx* hearts [44]. Transmission electron micrographs revealed mitochondrial increased area and loss of normal cristae structure in adult *mdx* cardiac muscle. Meantime, it was shown that changes in mitochondria volume can mechanically affect morphological as well as functional properties of intracellular organelles, including myofilaments and nuclei [45]. Mitochondria are also dynamic structures capable of fission and fusion under stress [46]. Whether those changes in mitochondria morphology are responsible for the myofilament misalignment remains to be determined.

Finally, our study shows a default of coupling between myofibrils. In the cardiomyocytes, intermediate filaments, especially desmin, form an extended scaffold linking the entire contractile apparatus to several membranous compartments (*i.e.*, sarcolemma costameres and desmosomes of the intercalated disks) and organelles (*i.e.*, sarcoplasmic reticulum, mitochondria, nucleus and lysosomes). In dystrophin-deficient mice, desmin expression is increased and may contribute to a compensatory mechanism [47]. The lack of desmin in the heart leads to cardiomyocyte hypertrophy and reduction in active force generation [48]. Whether the intermediate filaments and desmin play a role in the myofibrillar distortion we observed requires further experiments.

We also quantified the SHG signal of double-bands in the cardiomyocytes. As reported previously for DMD fixed and stained skeletal muscle cells [5,49], the appearance of double SHG bands can be related to the internal structural characteristics of myofibers, to disorganization among the fibrils [24] and sarcomere pattern irregularities. Other species such as frog and rabbit also exhibit a double-band signal from their cardiomyocytes and were considered as an intrinsic characteristic of the sarcomeres [22,50]. Nevertheless, other studies reported that occurrence of double-bands can also be the consequence of external factors such as stretching or laser irradiation [23,24]. Although the double-band percentage and rate were considered as promising parameters to reveal structural modifications, our data obtained on alive and intact cardiomyocytes show that the double-band proportion was unaffected by the aging and DCM-induced dystrophin deficiency. Therefore, we concluded that double-band parameters are not relevant indicators to follow structural changes in cardiomyocytes with large scale SHG microscopy, most likely due to the combined ordered- and disordered-state origin of double-band signals together with the highly nonlinear SHG effect.

Altogether, our findings confirmed the great potential for SHG in evaluating the age-dependent deterioration of myofibrils within alive and intact *mdx* cardiomyocytes. For the first time, we provided structural information on the contractile machinery disorganization in alive *mdx* cardiac tissue that could not be detected by other imaging procedures. Further work with non-invasive approaches to directly monitor structural changes in

alive cardiomyocytes is certainly needed to better understand DMD-associated DCM development enabling also to decipher the processes underlying the disease progression. Our work provided valuable quantitative structural parameters to monitor DMD related modifications in alive and intact cardiomyocytes. Overall, our findings may help to identify novel early-stage biomarkers of the DCM progression in DMD patients but also for all other origins of DCM.

### Author contributions

ACM, TC, MP and SR performed the experiments on the mice and cardiomyocytes. BV performed the data and statistical analysis. ACM, OC and AL provided the biological and physiological expertise. BV, CG and TC provided the expertise in physics, microscopy and automated data analysis. BV, ACM, CG and OC wrote the manuscript. ACM, CG, OC and TC designed the study and interpreted the data. All authors provided critical review of the manuscript and approved its submission.

### References

- Cullen MJ, Fulthorpe JJ. Stages in fibre breakdown in Duchenne muscular dystrophy an electron-microscopic study. *J Neurol Sci* 1975;**24**:179-200.
- Matsuda R, Nishikawa A, Tanaka H. Visualization of dystrophic muscle fibers in *mdx* mouse by vital staining with Evans blue: evidence of apoptosis in dystrophin-deficient muscle. *J Biochem* 1995:959-64.
- Brouilly N, Lecroisey C, Martin E, Pierson L, Mariol M, Qadota H, et al. Ultra-structural time-course study in the *C. elegans* model for Duchenne muscular dystrophy highlights a crucial role for sarcomere-anchoring structures and sarcolemma integrity in the earliest steps of the muscle degeneration process. *Hum Mol Genet* 2015;**24**(22):6428-45.
- Buttgereit A, Weber C, Friedrich O. A novel quantitative morphometry approach to assess regeneration in dystrophic skeletal muscle. *Neuromuscul Disord* 2014;**24**(7):596-603.
- Friedrich O, Both M, Weber C, Schrümman S, Teichmann MDH, Wegner F, et al. Microarchitecture is severely compromised but motor protein function is preserved in dystrophic *mdx* skeletal muscle. *Biophys J* 2010;**98**(February):606-16.
- Su JB, Cazorla O, Blot S, Blanchard-Gutton N, Sambin L, Sampedrano CC, et al. Bradykinin restores left ventricular function, sarcomeric protein phosphorylation, and eNOS levels in dogs with Duchenne muscular dystrophy cardiomyopathy. *Cardiovasc Res* 2012;**95**:86-96.
- Ait Mou Y, Lacampagne A, Irving T, Scheuermann V, Blot S, Ghaleb B, et al. Altered myofilament structure and function in dogs with Duchenne muscular dystrophy cardiomyopathy. *J Mol Cell Cardiol* 2018;**114** (November 2017):345-53.
- Fauconnier J, Thireau J, Reiken S, Cassan C, Richard S, Matecki S, et al. Leaky RyR2 trigger ventricular arrhythmias in Duchenne muscular dystrophy. *Proc Natl Acad Sci* 2010;**107**(4):1559-64.
- Zipfel WR, Williams RM, Webb WW. Nonlinear magic: multiphoton microscopy in the biosciences. *Nat Biotechnol* 2003;**21**(11):1369-77.
- Sivaguru M, Kabir MM, Garita MR, Biggs DSC, Sivaguru BS, Sivaguru VA, et al. Application of an advanced maximum likelihood estimation restoration method for enhanced-resolution and contrast in second-harmonic generation microscopy. *J Microsc* 2017;**267**(3):397-408.
- Yuan C, Wang Z, Borg TK, Ye T, Baciu C, Bradshaw A, et al. Changes in the crystallographic structures of cardiac myosin filaments detected by polarization-dependent second harmonic generation microscopy. *Biomed Opt Express* 2019;**10**(7):3183-95.

12. Dubreuil M, Tissier F, Le Roy L, Pennec JP, Rivet S, Giroux-Metges MA, et al. Polarization-resolved second harmonic microscopy of skeletal muscle in sepsis. *Biomed Opt Express* 2018;**9**(12):6350-8.
13. Syverud BC, Mycek MA, Larkin LM. Quantitative, label-free evaluation of tissue-engineered skeletal muscle through multiphoton microscopy. *Tissue Eng - Part C Methods* 2017;**23**(10):616-26.
14. Plotnikov SV, Millard AC, Campagnola PJ, Mohler WA. Characterization of the myosin-based source for second-harmonic generation from muscle sarcomeres. *Biophys J* 2006;**90**(2):693-703.
15. Liu H, Shao Y, Qin W, Runyan RB, Xu M, Ma Z, et al. Myosin filament assembly onto myofibrils in live neonatal cardiomyocytes observed by TPEF-SHG microscopy. *Cardiovasc Res* 2013;**97**:262-70.
16. Awasthi S, Izu LT, Mao Z, Jian Z, Landas T, Lerner A, et al. Multimodal SHG-2PF imaging of microdomain Ca-contraction coupling in live cardiac myocytes. *Circ Res* 2015;**118**(2):19-28.
17. Schneider D, Nübler S, Pröhl G, Reischl B, Schürmann S, Müller OJ, et al. Optical prediction of single muscle fiber force production using a combined biomechanics and second harmonic generation imaging approach. *Light Sci Appl* 2018;**7**(79).
18. de Amancio GCS, Grabe-Guimarães A, Haikel D, Moreau J, Barcellos NMS, Lacampagne A, et al. Effect of pyridostigmine on in vivo and in vitro respiratory muscle of mdx mice. *Respir Physiol Neurobiol* 2017;**243**:107-14.
19. Cazorla O, Szilagy S, Vignier N, Salazar G, Kramer E, Vassort G, et al. Length and protein kinase A modulations of myocytes in cardiac myosin binding protein C-deficient mice. *Cardiovasc Res* 2006;**69**:370-80.
20. Farman GP, Tachampa K, Mateja R, Cazorla O, Lacampagne A, Tombe PP. Blebbistatin: use as inhibitor of muscle contraction. *Pflugers Arch - Eur J Physiol* 2008;**455**:995-1005.
21. Schindelin J, Arganda-Carrera I, Frise E, Kaynig V, Longair M, Pietzch T, et al. Fiji — an open source platform for biological image analysis. *Nat Methods* 2012;**9**(7):241.
22. Boulesteix T, Beaurepaire E, Sauviat M-P, Schanne-Klein M-C. Second-harmonic microscopy of unstained living cardiac myocytes: measurements of sarcomere length with 20-nm accuracy. *Opt Lett* 2004;**29**(17):2031-3.
23. Prent N, Green C, Greenhalgh C, Cisek R, Major A, Stewart B, et al. Intermyofibrillar dynamics of myocytes revealed by second harmonic generation microscopy. *J Biomed Opt* 2008;**13**(4):041318.
24. Recher G, Rouède D, Schaub E, Tiaho F. Skeletal muscle sarcomeric SHG patterns photo-conversion by femtosecond infrared laser. *Biomed Opt Express* 2011;**2**(2):374.
25. Flagg TP, Cazorla O, Remedi MS, Haim TE, Tones MA, Bahinski A, et al. Ca<sup>2+</sup>-independent alterations in diastolic sarcomere length and relaxation kinetics in a mouse model of lipotoxic diabetic cardiomyopathy. *Circ Res* 2009;**104**(1):95-103.
26. Lopez JR, Kolster J, Zhang R, Adams J. Increased constitutive nitric oxide production by whole body periodic acceleration ameliorates alterations in cardiomyocytes associated with utrophin/dystrophin deficiency. *J Mol Cell Cardiol* 2017;**108**:149-57.
27. Piquereau J, Ventura-Clapier R. Maturation of cardiac energy metabolism during perinatal development. *Front Physiol* 2018;**9**:1-10.
28. Sanger JW, Chowrashi P, Shaner NC, Spaltheoff S, Wang J, Freeman NL, et al. Myofibrillogenesis in skeletal muscle cells. *Clin Orthop Relat Res* 2002(403 Suppl):S153-62.
29. Tonino P, Kiss B, Strom J, Methawasin M, Smith JE, Kolb J, et al. The giant protein titin regulates the length of the striated muscle thick filament. *Nat Commun* 2017;**8**(1):1-10.
30. Lahmers S, Wu Y, Call DR, Labeit S, Granzier H. Developmental control of titin isoform expression and passive stiffness in fetal and neonatal myocardium. *Circ Res* 2004;**94**(4):505-13.
31. Amedro P, Vincenti M, De La Villeon G, Lavastre K, Barrea C, Guillaumont S, et al. Speckle-tracking echocardiography in children with Duchenne muscular dystrophy: a prospective multicenter controlled cross-sectional study. *J Am Soc Echocardiogr* 2019;**32**(3):412-22.
32. Cazorla O, Freiburg A, Helmes M, Centner T, McNabb M, Wu Y, et al. Differential expression of cardiac titin isoforms and modulation of cellular stiffness. *Circ Res* 2000;**86**(1):59-67.
33. Meyers TA, Townsend D. Early right ventricular fibrosis and reduction in biventricular cardiac reserve in the dystrophin-deficient mdx heart. *Am J Physiol Heart Circ Physiol* 2015;**308**(4):303-15.
34. Li Y, Zhang S, Zhang X, Li J, Ai X, Zhang L, et al. Blunted cardiac beta-adrenergic response as an early indication of cardiac dysfunction in Duchenne muscular dystrophy. *Cardiovasc Res* 2014;**103**(1):60-71.
35. Saito T, Asai K, Sato S, Hayashi M, Adachi A, Sasaki Y, et al. Autophagic vacuoles in cardiomyocytes of dilated cardiomyopathy with initially decompensated heart failure predict improved prognosis. *Autophagy* 2016;**12**(3):579-87.
36. Williams IA, Allen DG. The role of reactive oxygen species in the hearts of dystrophin-deficient mdx mice. *Am J Physiol - Hear Circ Physiol* 2007;**293**(3):1969-77.
37. Esposito G, Carsana A. Metabolic alterations in cardiomyocytes of patients with Duchenne and Becker muscular dystrophies. *J Clin Med* 2019;**8**:2151.
38. Rubi L, Todt H, Kubista H, Koenig X, Hilber K. Calcium current properties in dystrophin-deficient ventricular cardiomyocytes from aged mdx mice. *Physiol Rep* 2018;**6**(1):1-8.
39. Pioner JM, Guan X, Klaiman JM, Racca AW, Pabon L, Muskheli V, et al. Absence of full-length dystrophin impairs normal maturation and contraction of cardiomyocytes derived from human-induced pluripotent stem cells. *Cardiovasc Res* 2020;**116**(2):368-82, <https://doi.org/10.1093/cvr/cvz109>.
40. Fanchaouy M, Polakova E, Jung C, Ogrodnik J, Shirokova N, Niggli E. Pathways of abnormal stress-induced Ca<sup>2+</sup> influx into dystrophic mdx cardiomyocytes. *Cell Calcium* 2009;**46**(2):114-21.
41. Szibor M, Pöling J, Warnecke H, Kubin T, Braun T. Remodeling and dedifferentiation of adult cardiomyocytes during disease and regeneration. *Cell Mol Life Sci* 2014;**71**(10):1907-16.
42. Bersell K, Arab S, Haring B, Kühn B. Neuregulin1/ErbB4 signaling induces cardiomyocyte proliferation and repair of heart injury. *Cell* 2009;**138**(2):257-70.
43. Kubin T, Pöling J, Kostin S, Gajawada P, Hein S, Rees W, et al. Oncostatin M is a major mediator of cardiomyocyte dedifferentiation and remodeling. *Cell Stem Cell* 2011;**9**(5):420-32.
44. Kyrychenko V, Poláková E, Janicek R, Shirokova N. Mitochondrial dysfunctions during progression of dystrophic cardiomyopathy. *Cell Calcium* 2015;**58**(2):186-95.
45. Kaasik A, Kuum M, Joubert F, Wilding J, Ventura-Clapier R, Veksler V. Mitochondria as a source of mechanical signals in cardiomyocytes. *Cardiovasc Res* 2010;**87**(1):83-91.
46. Youle RJ, Van Der Blik AM. Mitochondrial fission, fusion, and stress. *Science (80- )* 2012;**337**(6098):1062-5.
47. Ferry A, Messéant J, Parlakian A, Lemaitre M, Roy P, Delacroix C, et al. Desmin is a modifier of dystrophic muscle features in Mdx mice. *bioRxiv* 2019;**32**(0):1-32.
48. Balogh J, Merisckay M, Li Z, Paulin D, Arner A. Hearts from mice lacking desmin have a myopathy with impaired active force generation and unaltered wall compliance. *Cardiovasc Res* 2002;**53**(2):439-50.
49. Garbe CS, Buttgerit A, Schurmann S, Friedrich O. Automated multiscale morphometry of muscle disease from second harmonic generation microscopy using tensor-based image processing. *IEEE Trans Biomed Eng* 2012;**59**(1):39-44.
50. Garcia-Canadilla P, Gonzalez-Tendero A, Iruretagoyena I, Crispi F, Torre I, Amat-Roldan I, et al. Automated cardiac sarcomere analysis from second harmonic generation images. *J Biomed Opt* 2014;**19**(5) 056010.

## Résumé:

La fibrose pancréatique est la principale caractéristique de deux pathologies majeures du pancréas, la pancréatite chronique et le cancer du pancréas. Le développement de ce dense tissu conjonctif est essentiellement dû à l'activation des cellules stellaires pancréatiques (CSP). Les CSP activées sont caractérisées, entre autres, par un potentiel prolifératif élevé, une sécrétion abondante de diverses cytokines, ainsi que par une expression importante d' $\alpha$ actine du muscle lisse ( $\alpha$ SMA). Ces processus cellulaires sont connus pour être, parmi d'autres, contrôlés par le  $\text{Ca}^{2+}$  intracellulaire, agissant comme un second messenger universel. Plusieurs types de canaux calciques membranaires assurent l'entrée du  $\text{Ca}^{2+}$  dans les cellules non-excitables notamment les canaux TRPC1 et Orai1. Si le rôle de ces canaux est largement étudié dans les cellules cancéreuses, le rôle du  $\text{Ca}^{2+}$  en général et de ces deux canaux en particulier dans les mécanismes moléculaires et cellulaires des CSP activées reste méconnu. Dans ce travail de thèse, nous avons étudié le rôle des canaux Orai1 et TRPC1 dans la prolifération et la sécrétion de cytokines des CSP activées. En effet, ces derniers sont deux processus majeurs, caractéristiques de leur état d'activation, participant à l'aggravation de la fibrose pancréatique. Nous avons démontré que les canaux Orai1 et TRPC1 sont exprimés et fonctionnels dans les CSP humaines activées. Orai1 est activé par la déplétion des stocks  $\text{Ca}^{2+}$  du réticulum endoplasmique alors que TRPC1 agit comme un canal  $\text{Ca}^{2+}$  mécano-sensible, car il est activé à la suite d'une stimulation par une pression extracellulaire élevée, permettant une augmentation de l'influx  $\text{Ca}^{2+}$  dans les CSP. Orai1 et TRPC1, favorisent tous les deux, la prolifération des CSP en régulant la progression du cycle cellulaire en phase G1, et aussi la sécrétion des cytokines, à travers des voies de signalisation différentes. Nous avons rapporté que Orai1 module la prolifération cellulaire ainsi que la sécrétion de  $\text{TGF}\beta_1$  via la voie de signalisation AKT, tandis que TRPC1 régule la prolifération et la sécrétion d'IL-6 par une voie ERK1/2-dépendante et une voie SMAD2-dépendante. L'un des résultats importants de ce travail est l'identification d'une boucle autocrine positive induite par le  $\text{TGF}\beta_1$  sécrété, qui stimule la prolifération médiée par la voie Orai1/AKT-dépendante via l'augmentation de l'expression d'Orai1 et de l'entrée SOCE médiée par Orai1. En outre, nous avons démontré que TRPC1 peut interagir et former un complexe protéique avec l' $\alpha$ SMA et la forme phosphorylée de SMAD2. En effet, TRPC1 est impliqué dans l'activation de la voie SMAD2 par sa propre liaison au facteur SMAD2, participant ainsi à la régulation de l'expression de l' $\alpha$ SMA. L'ensemble de nos résultats ont mis en évidence le rôle essentiel des canaux Orai1 et TRPC1 dans les processus d'activation de CPS humaines. Ces données suggèrent qu'ils pourraient devenir des cibles thérapeutiques pour le traitement de la fibrose pancréatique, et par conséquent de la pancréatite chronique et/ou du cancer du pancréas.

Mots-clés : cellules stellaires pancréatiques, calcium, Orai1, TRPC1, activation

## Abstract:

Excessive pancreatic fibrosis is the central pathological feature of two major pancreatic diseases, chronic pancreatitis, and pancreatic cancer. The key effectors driving this dense fibrotic tissue development are the well-characterized now activated pancreatic stellate cells (PSCs). Activated PSCs are characterized, among others, by elevated proliferative ability and abundant secretion of various cytokines, as well as increased  $\alpha$ SMA ( $\alpha$ -smooth muscle actin) expression. These cellular processes are known to be triggered by  $\text{Ca}^{2+}$ , acting as an intracellular second messenger. Therefore, several plasma membrane calcium channels allow the  $\text{Ca}^{2+}$  entry in non-excitable cells including store-operated calcium entry (SOCE) and stretch-activated channels. However, until now, the role of  $\text{Ca}^{2+}$  and these  $\text{Ca}^{2+}$  channels in the molecular and cellular mechanisms of PSC's activation remains poorly known. In the current thesis work, we aimed to investigate the role of Orai1 and TRPC1 channels in human-activated PSC's proliferation and cytokine secretion, two main PSC's activation features participating in pancreatic fibrosis exacerbation. We demonstrated that Orai1 and TRPC1 are functionally expressed, and they are mediating the SOCE and stretch-induced  $\text{Ca}^{2+}$  influx, respectively, in human-activated PSCs. Indeed, TRPC1 leads to an increased  $\text{Ca}^{2+}$  influx under pressurization. Both Orai1 and TRPC1 promote PSC's proliferation by regulating the cell cycle progression in the G1 phase, and cytokines secretion, through different signalling pathways. We reported that Orai1 modulates cell proliferation and  $\text{TGF}\beta_1$  secretion through an AKT-dependent pathway, whereas TRPC1 regulates PSC's proliferation and IL-6 secretion via ERK1/2 and SMAD2-dependent pathways. Interestingly, we showed that Orai1-mediated  $\text{TGF}\beta_1$  secretion induces an autocrine positive feedback loop, leading to the stimulation of Orai1/AKT-dependent proliferation via the increase of Orai1 expression and Orai1-mediated SOCE. Another important finding in this work was the identification of a protein network between TRPC1,  $\alpha$ SMA, and the phosphorylated active form of SMAD2. We found that TRPC1 is involved in the activation of SMAD2 via its binding to SMAD2, participating to the regulation of  $\alpha$ SMA expression. Taken together, our data highlighted the crucial role of Orai1 and TRPC1 channels in the activation of human PSCs, suggesting that they could become potential therapeutic targets for pancreatic fibrosis treatment and, thereby, for chronic pancreatitis and pancreatic cancer.

Key words: pancreatic stellate cells, calcium, Orai1, TRPC1, activation